GRAPTOLITE DIVERSITY AND COMMUNITY CHANGES SURROUNDING THE LATE ORDOVICIAN MASS EXTINCTION: HIGH RESOLUTION DATA FROM THE BLACKSTONE RIVER, YUKON

by

Jason David Loxton

Submitted in partial fulfilment of the requirements
for the degree of Doctor of Philosophy

at

Dalhousie University
Halifax, Nova Scotia
August, 2017

TABLE OF CONTENTS

List of Tables iv
List of Figures v
Abstract x
List of Abbreviations and Symbols Used xi
Acknowledgements xii
Chapter 1. Introduction 1
1.1 Background 1
1.2 Motivation 9
1.3 Objectives 13
1.4 Relationship of Project with Recent Studies 17
1.5 Outline 19
1.6 Publications Resulting from this Thesis 21
Chapter 2. Regional Geology and Locality Description 23
2.1 Regional Geology 23
2.2 Locality Description 28
Chapter 3. Methodology 32
3.1 Field Collection 32
3.2 Counting and Density Estimates 40
3.3 Illustration and Descriptions 53
3.4 Biotope Assignment and Environmental Inferences 62
Chapter 4. Biostratigraphy and Correlation 66
4.1 Blackstone River Biostratigraphy 66
4.2 Regional and International Correlation 83
4.2.1 Nevada 84
4.2.2 Arctic Canada 87
4.2.3 Jordan 90
4.2.4 Kurama Range, East Uzbekistan 91
4.2.5 Alaska 93
4.2.6 Dob's Linn, Scotland 96
4.2.7 Southwestern Sweden 100

4.2.8 South China 102
4.2.9 Peri-Gondwanan Europe 105
4.2.9 Southern Kazakhstan 106
4.2.10 Kolyma, Siberia 107
4.3 Biostratigraphic Conclusions and Significance 108
Chapter 5. Faunal Dynamics and Diversity 110
5.1 Diversity Trends 110
5.2 Community Structure, Sampling, and Instability 120
5.3 Extinctions and Environmental Causes 128
Chapter 6. Species Descriptions 144
6.1 Introduction 144
6.2 *Dicellograptus ornatus, Paraorthograptus pacificus*, and *Metabolograptus extraordinarius* zones 147
6.3. Supporting graphs for chapter 6.2 227
6.4 *Metabolograptus persculptus, Akidograptus ascensus* and *Parakidograptus acuminatus* zones 247
6.5 Supporting Graphs for 6.4 362
Chapter 7. Ontogeny and Astogeny of the Graptolite Genus *Appendispinograptus* (Li and Li, 1985) 385
Preamble 385
7.1 Abstract 385
7.2 Introduction 386
7.3 Materials and Methods 389
7.4 *A. supernus* Early Growth 390
7.5 *A. supernus* Parasiculae 393
7.6 *A. leptothecalis* “Membranes” 396
7.7 Discussion 398
7.7.1 Systematics 398
7.7.2 Form and Function 400
7.8 Conclusion 405
7.8 Acknowledgements 406
Chapter 8. Conclusion and Outstanding Issues 407

8.1 Project Overview 407
8.2 Status of Project Objectives 408
8.3 Issues Arising from this Thesis 414
8.4 Future Research 416
Works Cited 418
Plates 439
Appendix A. Sample Descriptions for Counted Samples 553
Appendix B. Graptolite Counts (Tables and Graphs) 563
Appendix C. Binning Methodology 573
Appendix D. Rarefaction Curves 583
Appendix E. Accessory Fauna 587
Appendix F. Comparative Diversity Diagrams 588
Appendix G. Copyright Release 590

List of Tables

Table 3.1 Effect of binning schemes on calculated abundance.....48

Table 3.2 Measured sample area and density.....49

Table 3.3 Sampling completeness.....52

List of Figures

Figure 1.1. Timing and impact of the LOME……2
Figure 1.2. Hypothesized graptolite biotopes……4
Figure 1.3. Distribution of graptolite localities……..9
Figure 2.1. Regional geology of the Blackstone Trough……24
Figure 2.2. Blackstone River section biozone positions……28
Figure 2.3. Blackstone River stratigraphic section……29
Figure 2.4. Calcite content by weight at the Blackstone River……31
Figure 3.1. Geographic location of Blackstone River section……..33
Figure 3.2. Measured and sampled portions of section……..36
Figure 3.3. Latest Ordovician and early Rhuddanian collection locations……40
Figure 4.1. *D. ornatus* Zone to *M. extraordinarius* Zone ranges……68
Figure 4.2. *M. persculptus* Zone ranges……74
Figure 4.3. *A. ascensus* Zone *to A. atavus* Zone ranges……77
Figure 5.1. Katian-early Hirnantian diversity……112
Figure 5.2. Katian-early Hirnantian extinction patterns……114
Figure 5.3. Katian-early Hirnantian origination patterns……..115
Figure 5.4. Latest Katian-early Hirnantian extinction patterns……115
Figure 5.5. Late Katian-early Hirnantian diversity vs. species turnover……116
Figure 5.6. Post-extinction diversity vs. sea level……120
Figure 5.7. *P. pacificus* Zone abundance patterns (Blackstone River)……125
Figure 5.8. *P. pacificus* Zone abundance patterns (Vinini Creek)……126
Figure 5.9. Pre-extinction diversity vs. sea Level……133
Figure 5.10. Sea level relative to community composition……134
Figure 5.11. Rhuddanian extinction patterns (confirmed ranges)……137
Figure 5.12. Rhuddanian extinction patterns (expanded ranges)……137
Figure 6.1. Morphological features used in species descriptions……146
Figure 6.2. Blackstone River *D. ornatus* (A)……227

Figure 6.3. Blackstone River *D. ornatus* (B)……227
Figure 6.4. Proximal vs. distal DVW in *D. ornatus*……228
Figure 6.5. Blackstone River *D.* aff. *mirabilis* vs. *D. minor*……228
Figure 6.6. Blackstone River *Dicellograptus* species……229
Figure 6.7. '*D. turgidus*' specimens……229
Figure 6.8. Large-spined dicellograptids (A)……230
Figure 6.9. Large-spined dicellograptids (B)……230
Figure 6.10. Blackstone '*D. mirabilis*' material……231
Figure 6.11. International specimens of '*D. mirabilis*'……231
Figure 6.12. *Diplograptus* (A)……232
Figure 6.13. *Diplograptus* (B)……232
Figure 6.14: Blackstone River *Paraorthograptus*……233
Figure 6.15. Blackstone River *Paraorthograptus* vs. types of *P. p. kimi* (A)……233
Figure 6.15. Blackstone River *Paraorthograptus* vs. types of *P. p. kimi* (B)……234
Figure 6.17. Widening in *Paraorthograptus*……234
Figure 6.18. Distal DVW vs. 2TRD in *Paraorthograptus*……235
Figure 6.19. Distal DVW/2TRD in non-Blackstone *Paraorthograptus*……235
Figure 6.20. Widening and thecal spacing ratios in *Paraorthograptus*……236
Figure 6.21. Blackstone *Paraorthograptus* vs. *P. affinis* and *P. uniformis*……236
Figure 6.22. Proximal vs. mesial width in *Anticostia uniformis*……237
Figure 6.23. Mesial width vs. 2TRD in *Anticostia uniformis*……237
Figure 6.24. Proximal vs. mesial width in *Parareteograptus*……238
Figure 6.25. Proximal vs. mesial width in global collections of *Parareteograptus*……238
Figure 6.26. Proximal DVW vs. distal 2TRD in global collections of *Parareteograptus*…239
Figure 6.27. Distal vs. mesial width in global collections of *Parareteograptus*……239
Figure 6.28. Distal vs. proximal width in global collections of *Parareteograptus*……240
Figure 6.29. Mesial vs. proximal DVW in Blackstone *Styracograptus*……240
Figure 6.30. Distal vs. proximal DVW in Blackstone *Styracograptus*……241

Figure 6.31. Blackstone *Styracograptus mississippiensis* by stratigraphic level……241
Figure 6.32. Mesial vs. proximal width in global *Styracograptus* specimens……242
Figure 6.33. Distal width vs. distal 2TRD in species of *Appendispinograptus*……242
Figure 6.34. Mesial 2TRD vs. distal DVW in *Appendispinograptus*……243
Figure 6.35. Mesial DVW vs. proximal DVW in *Appendispongraptus*……243
Figure 6.36. *A. supernus* vs. *A. pogrebov*i……244
Figure 6.37. Neograptine species: distal 2TRD vs. Distal DVW……244
Figure 6.38. Neograptine species proximal 2TRD vs. distal DVW……245
Figure 6.39. *Neo. charis* vs. *M. ojsuensis*……245
Figure 6.40. *M. extraordinarius* vs. *Neo charis*……246
Figure 6.41. *N. angustus* vs. *N.* aff. *angustus*……362
Figure 6.42. *Normalograptus*: Mesial 2TRD vs. proximal DVW……362
Figure 6.43. *Normalograptus*: Proximal 2TRD vs. proximal DVW……363
Figure 6.44. *N.*? *minor* vs. *N.? radicatus*: Proximal 2TRD……363
Figure 6.45. *N.*? *radicatus* vs. other *Normalograptus* species……364
Figure 6.46. *N. rectangularis*: Global comparison……364
Figure 6.47. *N.*? *rhizinus* comparison……365
Figure 6.48. Thin "normalograptids"……365
Figure 6.49. *N.*? *transgrediens*……366
Figure 6.50. *N.*? *nanjingensis* comparison……366
Figure 6.51. *N.*? *aff. medius vs. N.*? *trangrediens*……367
Figure 6.52. *N.*? aff*. medius vs. N. rectangularis*……367
Figure 6.53. *N. aff. mirnyensis vs, N. aff. angustus*……368
Figure. 6.54. *N. aff. mirnyensis vs. M.*? *sp*……368
Figure 6.55. *N*. aff. *nanjingensis* vs. *N*. *nanjingensis*……369
Figure 6.56. *N.*? *transgrediens* comparison……369
Figure 6.57: *Normalograptus* sp……370
Figure 6.58. *Metaclimacograptus hughesi* by stratigraphic height……370

Figure 6.59. *Avitograptus avitus* vs. *N.*? *rhizinus*……371
Figure 6.60. *Metabolograptus*? sp. vs. *N.*? aff. *nanjingensis*……371
Figure 6.61. *Neodiplograptus* comparison (A)……372
Figure 6.62. *Neodiplograptus* comparison (B)……372
Figure 6.63. *Neodiplograptus* comparison (C)……373
Figure 6.64. *Neodiplograptus* comparison (D)……373
Figure 6.65. *Neodiplograptus* comparison (E)……374
Figure 6.66. *Neodiplograptus* comparison (F)……374
Figure 6.67. *Glyptograptus*? sp. 2 vs. *K. laciniosus*……375
Figure 6.68. *Korenograptus lanpherei*……375
Figure 6.69. *Korenograptus lanpherei* (Churkin and Carter) types……376
Figure 6.70. *Korenograptus*: Proximal vs. mesial DVW……376
Figure 6.71. *Korenograptus*: Proximal 2TRD vs. distal DVW……377
Figure 6.72. *Korenograptus*: Proximal 2TRD vs. mesial DVW……377
Figure 6.73. *Korenograptus*: Mesial DVW vs. distal DVW……378
Figure 6.74. *K. laciniosus* vs. *K. lungmaensis*……378
Figure 6.75. *K. lanpherei* vs. *K.* sp. 1……379
Figure 6.78. *Korenograptus* sp. 3 vs. *K.* sp. 1……379
Figure 6.77. *Korenograptus* sp. 3……380
Figure 6.78. *Rickardsograptus* comparison (A)……380
Figure 6.79. *Rickardsograptus* comparison (B)……381
Figure 6.80. *Paraclimacograptus*: Th5 vs. Th1 DVW……381
Figure 6.81. *Paraclimacograptus*: Th7 vs. th3 DVW……382
Figure 6.82. *Paramplexograptus*: Mesial DVW vs. proximal DVW……382
Figure 6.83. *Paramplexograptus*: Mesial DVW vs. proximal 2TRD……383
Figure 6.84. *Paramplexograptus*: Distal DVW vs. mesial DVW……383
Figure 6.85. *Glyptograptus*? sp. 1 vs. *Normalograptus*? *radicatus*……384
Figure 6.86. *Glyptograptus* comparison……384

Figure 7.1. Electron micrographs of isolated growth stages of *A. supernus* and *Anticostia* sp……391

Figure 7.2. Comparison of proximal and distal dorsal ventral width (DVW) and thecal height (2TRD) in various populations of three species of *Appendispinograptus*……392

Figure 7.3. Electron micrographs and infrared photographs of an isolated specimen of *A. supernus*……395

Figure 7.4. Comparison of variation in spine length and web development in specimens of *A. leptothecalis* from four global populations……399

Figure 7.5. Examples of extremely mature *A. leptothecalis* with and without basal webs……401

Figure 7.6. Distribution of surface area in three specimens of *A. leptothecalis* with basal webbing……403

Abstract

The Late Ordovician Extinction Event (LOME), the first of the "Big Five" extinction events, decimated marine communities just prior to the end of the period (ca. 444 Ma). Graptolites, the principal index taxon during the interval, and a key proxy for studies of environmental and evolutionary change, were particularly strongly impacted. Studying the extinction event is problematic. A disconformity or abrupt facies change occurs at nearly all global sections, caused by the same mechanism believed to be responsible for the extinction: glacially-induced changes in sea level, ocean temperature, and ocean circulation. Until recently, only South China possessed a well-sampled graptolite record of the LOME and its aftermath. Interpreting Chinese data was complicated by the lack of an equivalently rich and well-sampled comparison section, which made it impossible to distinguish regionally unique patterns from sampling artefacts.

This thesis describes a new global reference section, located along the Blackstone River, which holds North America's only continuous graptolite biozonal record through the interval of extinction and recovery (*ornatus* to *atavus* zones). Intense sampling of a 50 m section identified 106 species of graptolites (described and illustrated with nearly 1000 photos and line drawings), including a number of taxa identified for the first time in Canada. This allowed highly detailed biostratigraphic correlation with China and other regions in the paleotropics. In addition to presence-absence diversity data, all pre- and extinction interval samples were counted (>20,000 specimens). This provided a test of sampling completeness in the present study, as well as quantifying the impacts of sampling on apparent diversity. Abundances also illuminated graptolite population structure, and demonstrated that community-level changes preceded the interval of peak extinction loss, providing support for models of habitat loss and food-web based models of graptolite extinction during the LOME.

Within the post-extinction recovery interval, the Blackstone River section boasts the world's highest levels of graptolite diversity. These post-extinction communities were highly unstable, with dominance fluctuating and high levels of species turnover. In addition to background instability, a second extinction event, previously observed in China, but otherwise very poorly known, occurs at the base of the Silurian, demonstrating its global scale. Geochemical and lithological data tie this second event to sea level fall.

List of Abbreviations and Symbols Used

? = Some uncertainty in attribution

$^{\delta}13C$ = A measure of the ratio of stable isotopes ^{13}C :^{12}C relative to a global standard

Aff. = Latin: 'affinis' (i.e., species is related to, but not the same as, that referenced)

Cf. = Latin: 'confer' (i.e., species should be compared to the one being referenced)

DVW = Dorsal-ventral width

FAD = First appearance datum

HICE = Hirnantian $^{\delta}13C$ excursion

ICE = Image Composite Editor (software)

LAD = Last appearance datum

LOME = Late Ordovician Mass Extinction

NIGP = Nanjing Institute of Geology and Palaeontology

Nd = Neodymium

PAST = Paleontological Statistics (software)

Th = theca

ThX^1/THX^2 = Superscript refers to the first or second thecae in any pair

TOC = Total organic carbon

Sp. = Species (left in open nomenclature)

Acknowledgements

This project was only possible because of the assistance a number of people and organizations:

Funding was provided by the National Science and Engineering Research Council, the National Science Foundation, and the Geological Society of America's Graduate Research Grant program.

Charles Mitchell and Petr Štorch provided access to unpublished data and material, and many hours of feedback and guidance. Chen Xu and Fan Jun-Xuan provided assistance with Chinese material, access to a crucial unpublished manuscript, and deep hospitality as hosts at the NIGP. Lisa Amati provided assistance with trilobite identification. Alf Lenz provided access to material he collected in the Yukon, as well as logisitical assistance with fieldwork planning. Chris Holmden provided access to original geochemical data from the Yukon. My fellow graduate students, Kristi Belescher, Daniel Robinson, Andrew Hawkins, and Daniel LaPorte (who worked on other components of the integrated project this thesis contributes to) generously shared their data and opinions.

Various people offered crucial logistical help: Alison Atkinson served as a field assistant for two seasons under trying conditions; Jillian Baker assisted with density estimates and other monotonous tasks; and Trisha Ang assisted with manuscript preparation. Shawn Ryan and crew facilitated helicopter transport and shipping of material.

I thank my thesis committee members for their guidance and willingness to work on a short timeline to help see this project through to completion. (Martin Gibling and John Gosse are particularly thanked for encouragement and tough love, along with my external examiner, David Loydell, for very detailed comments on a very short time line.)

My supervisor, Michael Melchin, provided years of unhesitating support, patience, and wisdom. Most importantly, he served as an exemplar of how a scientist and scholar behaves, and the expertise hard work can attain. As a student, it was a genuine privilege to have worked with a "master" that I know I can never come close to surpassing.

Finally, I thank my family and friends for continued support. In particular, Alison, Jillian, and Trisha, who collectively stood by me through a decade of struggle, and unfailingly responded to any negativity with a single confident phrase: "Jason, you've got this."

I genuinely could not have done this without all of you.

Chapter 1. Introduction

1.1 Background

The Late Ordovician Mass Extinction[1] (LOME) was the first of the "Big Five" mass extinction events in Earth history (Bond and Grasby, 2017). Species loss was concentrated in two pulses (Brenchley et al., 1994): an initial pulse tied to global sea level fall (ca. 70-100 m), cooling, and increased oceanic mixing; and a second pulse tied to sea level rise and the spread of anoxic or dysoxic ocean conditions (Melchin et al., 2013). Different groups of taxa were differentially affected by each pulse, with the first pulse greatly affecting nektonic and planktonic organisms (especially graptolites) and the second pulse mostly impacting benthic and reef communities (see Fig. 1.1 and overview in Sheehan, 2001, and Bond and Grasby, 2017). The combination of the two pulses eliminated >80% of species on Earth (Sheehan, 2001), ranking the impact on global biodiversity, in terms of species lost, as the second most profound in Earth history, after the end-Permian event (Bambach, 2004).

The LOME was initiated by a dramatic swing in the latest Ordovician from greenhouse to icehouse conditions, and then back to warmer, but unstable conditions in the early Silurian (Finnegan et al., 2011). Convergent lines of supporting evidence come from the widespread presence of tillites (see Sheehan, 2001 for a review); excursions in carbon, oxygen, and neodymium isotopes (Underwood et al., 1997; Melchin and

[1] See stratigraphic column in Chapter 2 (Fig. 2.3) for clarification on the order of graptolite biozones, stages, and other geological units discussed within this thesis.

Holmden, 2006; LaPorte et al., 2009, Finnegan et al., 2011; Holmden et al., 2013); and changes in the distribution of black shales (Melchin et al., 2013). An additional argument in favour of an association with cooling, is the strong latitudinal component to species loss, with those species that had pre-extinction ranges outside of the tropics—and therefore tolerance of cooler conditions—preferentially surviving (Finnegan et al., 2012), a trend that is particularly strong in graptolites (Goldman et al., 2011).

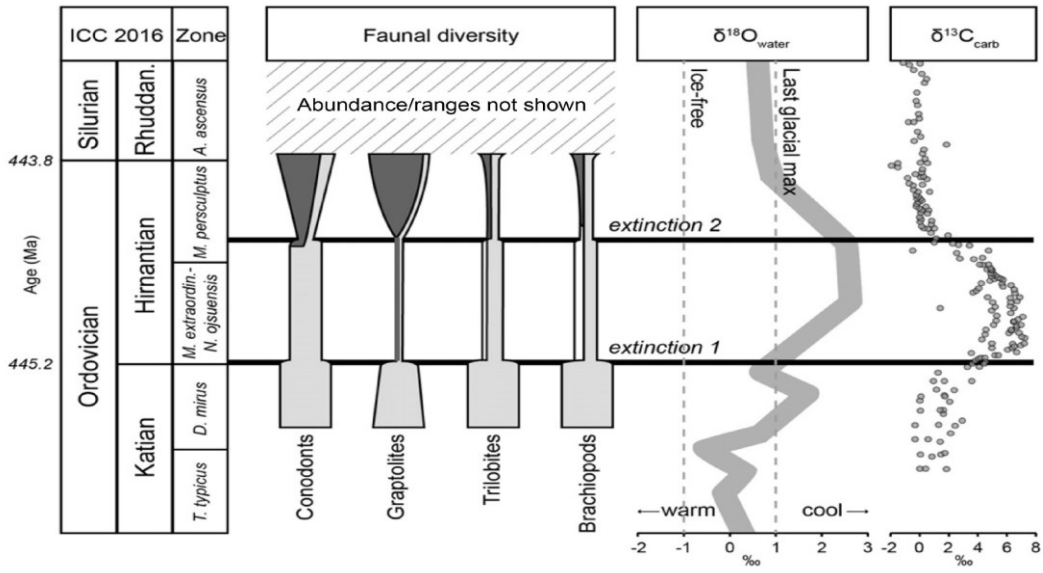

Figure 1.1. Timing and impact of the LOME. Approximate timing of the two pulses of the LOME, plus impact on four key Paleozoic faunas. Oxygen and carbon isotope curves (from carbonates) showing association with shifts in global climate. The *T. typicus* and *D. mirus* Subzones are the upper portions of the *P. pacificus* graptolite Zone. Widening dark portion of graptolite curve shows radiation of neograptines in the late Hirnantian. White portion of brachiopod abundance represents the "Hirnantian fauna". Modified from Bond and Grasby (2017).

Both the ultimate cause of the climate shifts that led to the Late Ordovician glaciation and the specific kill mechanism involved for each group and for each pulse are still poorly understood. Proposed climate forcing agents include enhanced weathering from Late Ordovician mountain building (Kump et al., 1999), marine productivity changes and nutrient input, mediated by the spread of land plants (Lenton et al., 2012),

the eruption of a large igneous province (Lefebvre et al., 2010; Jones et al., 2017), and a gamma ray burst (Melott et al., 2005), likely with secondary orbital effects controlling glacial-interglacial cycles (see references in Melchin et al., 2013). Proposed kill mechanisms include the draining of epicontinental seas, shifts in primary productivity, changes in sea surface temperature (a drop of 6°C: Melchin et al., 2013), anoxia, and enhanced deep-ocean mixing (see review in Bond and Grasby, 2017). Given the range of taxa affected, and the two-step nature of the extinction, it is likely that more than one of these mechanisms played a role, and perhaps all were active at some point during the extinction interval.

Clarifying the patterns and processes of the LOME requires temporally well-constrained records of environmental change, an accurate and globally correlated record of biodiversity changes, and a nuanced understanding of shifts in internal community dynamics. Graptolites, extinct colonial members of the phylum Hemichordata, were a common component of the plankton both before and after the LOME (they are also the principal index taxon for the Ordovician and Silurian: Cooper and Sadler, 2012; Melchin et al., 2012). Because of their high temporal resolution, broad distribution, and the existence of well-correlated, global and regional biozonal schemes, they have been widely employed as a proxy for the studies of the biotic response to the LOME and, more generally, the nature of evolutionary and ecological processes during times of biotic crisis (e.g., Bapst et al., 2012, Sheets et al., 2016, Crampton et al., 2016). Graptolites were most strongly affected by the first wave of the LOME, suffering an

immediate and profound drop in diversity (Chen et al., 2005b). This drop was taxonomically selective, with one group (the diplograptines) experiencing catastrophic species loss during the first pulse of the extinction, while simultaneously ceding ecological dominance to a second, incoming group (the neograptines), which previously had been marginalized to extratropical regions (Melchin and Mitchell, 1991; Chen et al., 2005b; Mitchell et al., 2007c; Goldman et al., 2011).

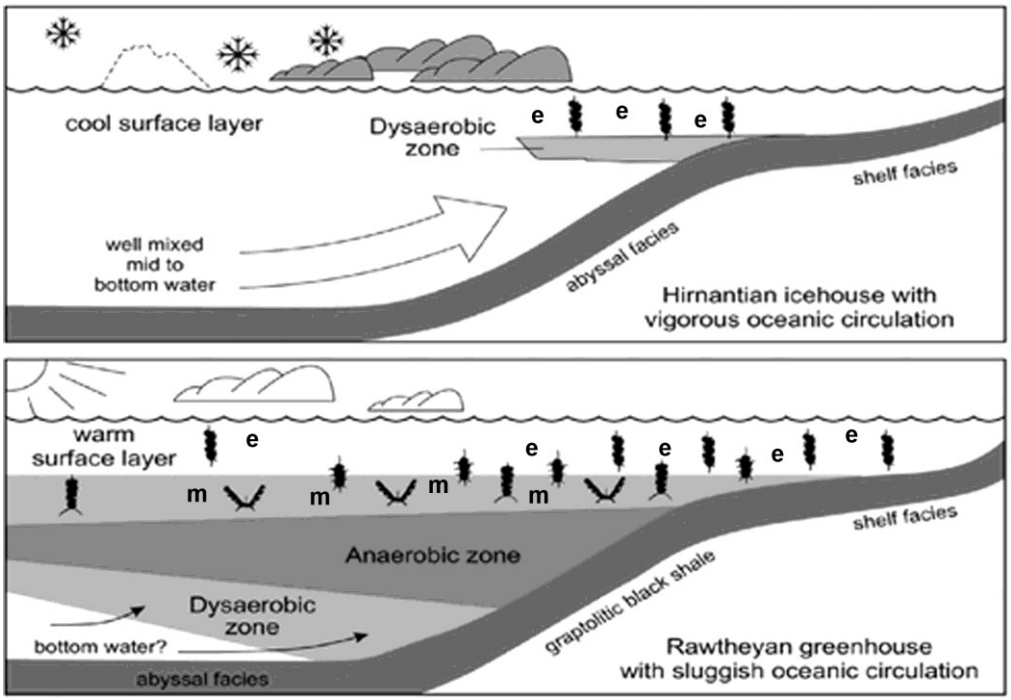

Figure 1.2. Hypothesized graptolite biotopes. Lower image: Idealized distribution of graptolites in a pre-extinction climate regime, possessing warm, well-stratified ocean waters. White upper layer is oxygenated, surface-mixed layer. Grey lower layer is dysoxic/denitrification zone. Note that since graptolites settle to the bottom after death, the resulting death assemblage will be only epipelagic forms (e) in the shelf (right hand side), with the ratio of mesopelagic (m) to epipelagic forms increasing with depth. Upper image: Dysaerobic/dysoxic zones eliminated by enhanced deep-ocean mixing, reducing available habitat for mesopelagic graptolites. Pycnocline is the density boundary between mixed surface layer (white) and underlying dysaerobic layer (grey). Image from Cooper et al. (2012).

Understanding of graptolite ecology remains incomplete, but there is clear evidence of facies preference, with three principal groups resolvable: a rare (and often

endemic) inner shelf community; an epipelagic community that occupied the mixed surface waters; and a mesopelagic community, which occupied the low oxygen, denitrification zone above upwelling zones in the outer shelf and slope (the grey shaed area in Fig. 1.2) (Cooper et al., 2012). Although the graptolite communities occupying the epipelagic and mesopelagic biotopes are thought to have been discrete (separated by the pycnocline), in death they would form aggregated assemblages, as specimens from all positions in the water column settled to the ocean floor (see Fig. 1.2).

This biotope model makes a testable prediction: that the relative abundance of mesopelagic vs. epipelagic species preserved at a locality should change in step with sea level fluctuations, with relatively more mesopelagic species present during intervals of high-stand than low-stand (Sheets et al., 2016). Whereas deep water conditions could support both abundant meso- and epipelagic communities at different water levels, shallower waters could support only an epipelagic community, since there would be no (or a reduced) underlying low oxygen/denitrification zone to support mesopelagic species (Chen et al., 2005b). As the sea level waxed and waned, the relative thickness of the habitable zone in the water column for mesopelagic species would change as well, and with it the abundance of specimens of mesopelagic species preserved in the sediment below, as a percentage of the total death assemblage (Sheets et al., 2016). Because the predicted change involves not just the number of species, but also the relative number of individuals of each species, testing this model requires abundance

data. Such data were collected during this thesis, but are not normally collected in diversity studies.

The biotope model also provides two mechanisms for graptolite diversity loss during Hirnantian cooling. First, enhanced ocean circulation owing to a steeper latitudinal thermal gradient would oxygenate the deeper waters and eliminate the preferred habitat of many graptolite species (Finney et al., 2007). Second, the reduction or elimination of the denitrification zone would result in enhanced delivery of nitrogen to the surface waters, which would provide a competitive advantage to algae over cyanobacteria, leading to a shift in the community of primary producers that would cascade through the food web (LaPorte et al., 2009). (Cyanobacteria fix their own nitrogen, but extracting dissolved atmospheric nitrogen (N_2) is more energy intensive and slower than consuming bioavailable nitrogen.) Conversely, the slow-growing, but nitrogen-fixing cyanobacteria would have an advantage over algae in warmer periods, when a well-developed denitrification zone reduced the abundance of bioavailable nitrogen from upwelling (Melchin et al., 2013).

The taxonomic selectivity of the LOME on graptolite species provides some support for these models of extinction. The group of graptolites that prospered during the LOME (the neograptines) had been excluded from the paleotropics for most of the Katian (Goldman et al., 2011). Reconstruction of their facies preferences suggests that they were epipelagic (Finney et al., 2007), and their pre-extinction biogeography shows that they were cold-tolerant (Goldman et al., 2011), possibly with a preference for algae

as a food source (LaPorte et al., 2009). Thus, the neograptines[2] may have been able to exploit the cooler, more oxygenated, algae-rich waters of the latest Katian and early Hirnantian, either outcompeting the diplograptines in this altered environment or moving into vacated niche space. With the extinction of diplograptines, the neograptines were free to diversify into the mesopelagic biotope in the late Hirnantian and early Silurian, a habitat from which they had previously been excluded[3] (Goldman et al., 2011).

Testing this hypothesis requires confirmation that the neograptines were absent from paleotropics in the pre-extinction interval. Because of their close external similarity to some diplograptine species, numerous false or questionable reports exist in the literature (Štorch et al., 2011; Goldman et al., 2011). It is also possible for rare taxa to be overlooked, producing false absence reports, especially with low sampling effort (as noted by Mitchell et al., 2007c). New, taxonomically-precise data from highly sampled sections during the late Ordovician are required.

[2] Neograptine species are those that belong to the infraorder Neograptina, one of the two large subdivisions of the planktic graptolites in the Late Ordovician (the other is the Diplograptina--often referred to as 'DDO taxa' in the past). The principal species that invaded the paleotropics at the base of the Hirnantian (including the index taxon, *Metabolograptus extraordinarius*) are all neograptines. Specifically, they belong to the paraphyletic family, Neodiplograptidae, a category included within the Neograptina. In the past, many or all of these species were assigned to the genus *Normalograptus* (usage restricted in Melchin et al.'s (2011) revision of the genus). As a result, in discussion of the taxonomic selectivity of the LOME and changes in graptolite biogeography, the terms 'neograptine'/'neograptid', 'neodiplograptine'/'neodiplograptid', 'normalograptid', and '*Normalograptus*' are sometimes used interchangeably. Within this thesis, the term neograptine is used exclusively in discussion of faunal dynamics for clarity, despite the fact that the neograptine species that occur at the Blackstone River section before the *persculptus* Zone are exclusively neodiplograptines. See Štorch et al. (2011) and Melchin et al. (2011) for detailed discussion of higher-level graptolite systematics.

[3] This is referred to as the 'geographic exclusion hypothesis' in subsequent discussions.

In addition to local, depth-related species distributions, graptolites display global geographic occurrence patterns. The clearest of these is a latitudinal division into higher latitude and equatorial provinces, similar to those that define the distributions of modern zooplankton (Vandenbroucke et al., 2009) (Fig.1.3). Sections located in the paleotropics (between ca. 30° north and south) possessed a very different graptolite fauna than localities at higher latitudes (e.g., Legrand, 2003, although see discussion in Chapters 4 and 6 of North African "endemic" species now recorded in the Yukon). Within the paleotropics, additional biogeographic patterns existed, with some areas apparently possessing much higher levels of biodiversity and endemism (Chen et al., 2000), suggesting basin isolation or subtly—but importantly—differing environmental conditions. These patterns possibly became even more pronounced during the LOME (Chen et al., 2003).

Testing these shifts requires a global network of well-sampled sites for comparison. It also requires a common taxonomic approach. In the past, authors working in different regions, in greater isolation than at present and with less ability to visit type collections for comparison, often oversplit lineages or erected duplicate taxa, exaggerating the endemism and obscuring true biogeographic patterns and diversity trends. Recent work has made considerable progress in correcting these misidentifications and removing extraneous species (e.g., Štorch and Loydell, 1996; Chen et al., 2000; Chen et al., 2005a; Loydell, 2007; Štorch et al., 2011), partially due to increased emphasis on more reliable diagnostic features, such as early developmental

patterns (Mitchell, 1987; Melchin, 1998). Considerable work remains to be done, however, especially in the late Katian and earliest Rhuddanian faunas, for which no detailed revised systematic treatise has been published to date on the diverse Chinese fauna (a paper is currently in preparation for the Rhuddanian interval: Fan et al., in prep.).

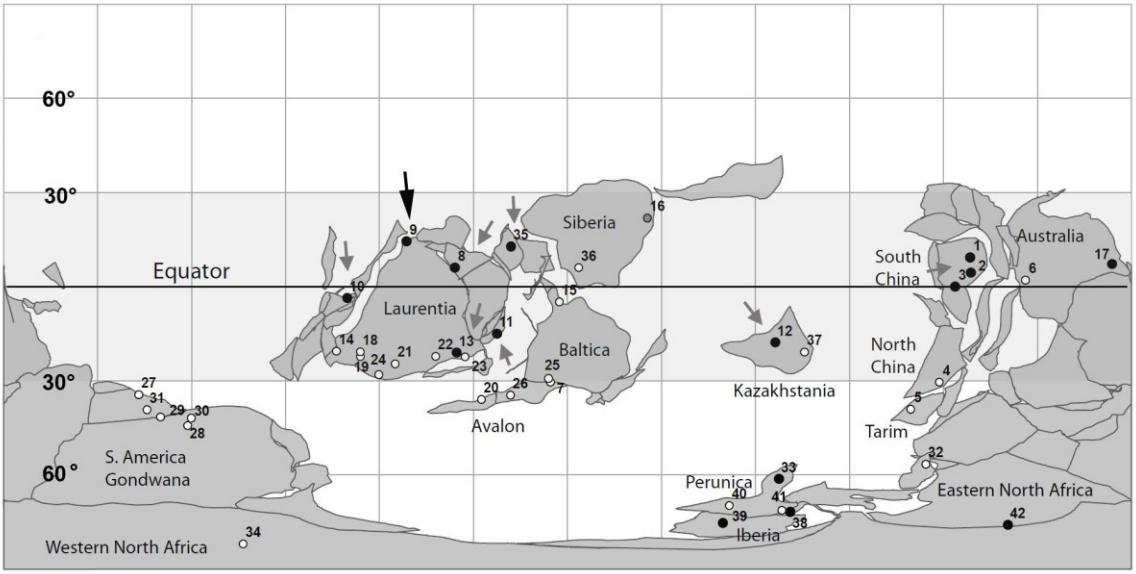

Figure 1.3. Distribution of well-studied graptolite localities. Important sites referenced in this paper shown with arrows. (1-3) South China, (8) Arctic Canada, (9) Blackstone River, (10) Vinini Creek/Monitor Ridge, Nevada, 12. Kazakhstan, (13) Anticosti Island, (11) Dob's Linn, (35) Mirny Creek, (37) Uzbekistan. Locations of (10), (11), and (9) approximate. Additional locations as described in Goldman et al. (2011). Shaded area represents paleotropics. Black, grey, and white circles indicate occurrences of *Normalograptus,* other graptolites, and no graptolites, respectively, during the interval depicted (the *extraordinarius* Zone). Modified from Goldman et al. (2011).

1.2 Motivation

The impetus for this thesis was a provocative paper published by Chinese and North American researchers analyzing graptolite biodiversity patterns in China's Yangtze Platform during the LOME and the subsequent period of post-extinction species radiation (Chen et al., 2005b). Utilizing graphic correlation, a process that combines

multiple sections into a single composite, Chen et al. (2005b), produced an unprecedentedly high-resolution account of graptolite diversity changes in the region during this interval. These occurrence data were then subjected to several levels of statistical analysis to determine trends in rates of origination and extinction. Chen et al.'s (2005b) analysis found that Chinese graptolite diversity followed patterns unlike those seen at any other known locality (higher initial diversity, more protracted response to the extinction, faster recovery from the extinction). This led them to hypothesize that the Yangtze Platform may have possessed environmental conditions uniquely favourable to graptolites, shielding them from the full effects of the extinction, and producing a sort of "nursery" from which biodiversity could expand in the aftermath of the extinction. If correct, this refugium hypothesis has implications that extend well beyond the specific history of graptolites: it points to a generalizable process that may mediate the impacts of mass extinctions broadly.

Refugia had previously been advanced as significant, but difficult to prove, factors in graptolite survivorship (Rickards and Wright, 2002). Since species sometimes disappear from the global record for periods of time, only to reappear later as "Lazarus taxa". Wignall and Benton (1999) have argued that these "resurrected" species do not require a refuge: they are most simply explained by poor preservation and population levels below the minimum detection level of the fossil record. This alternative hypothesis eliminates the need to postulate geographic regions with exceptional environmental conditions, and is more parsimonious.

The problem with the Chen et al. (2005b) data was that they were in a sense too good. The detail of their composite dataset (based on 34 individual sections), while shedding light on the timing of events in South China, actually undermined its comparative value. The number of species expected to be recovered at any given section or in any given sample varies with exposed strata and effort (Boyle et al., 2017). Therefore, the stark differences between both the number of sections and the collecting effort in South China and those for other regions (which are frequently represented by single sections, often sparsely collected) creates the possibility that the apparently anomalous patterns in South China are sampling artifacts.

The null hypothesis to Chen et al.'s refugia hypothesis (H1) then can be stated as:

> H0 - Patterns of diversity and turnover dynamics were uniform throughout the paleotropics and apparent differences are artifacts of preserved record quality and sampling effort.

Testing whether the diversity patterns seen in South China are genuine or spurious requires comparing the data of Chen et al. (2005b) with an equally detailed data set, produced through equally intense sampling, and using the same up-to-date taxonomic scheme. A comparative data set with these properties did not exist when Chen et al. published their paper. Furthermore, it was not clear at the start of this thesis whether it even *could* be produced. The same climate shifts responsible for the LOME also make the LOME very difficult to study. Sea level drop and shifts in marine temperatures and oxygenation resulted in most areas of the world having either truncated records across

the Ordovician-Silurian boundary (an unconformity) or dramatic facies changes, with corresponding shifts in fossils, which make it difficult or impossible to follow any single lineage through the extinction (Delabroye and Vecoli, 2010).

Well-studied, paleotropical candidate sections for comparative work (see Fig. 1.3) all suffer from these or other issues. For example, Dob's Linn, Scotland, the global stratotype for the base of the Silurian System, is only episodically graptolitic during the pre-extinction and main extinction interval; it is also tectonically deformed, complicating species identifications (Williams, 1983; pers. observ.). Similarly, the classic boundary section at Mirny Creek, Siberia, has only sparse graptolite occurrences, making it impossible to collect sufficient material in sufficient quantity and at sufficient resolution for a detailed comparison (Koren' and Sobolevskaya, 2008). Other sections do not continuously record the interval (e.g., Koren' and Melchin, 2000; Melchin, 1987, 1989; Riva, 1988.).

Before the commencement of this thesis, Finney et al. (1999) showed that the Vinini Creek and Monitor Ridge sections in Nevada had much higher levels of diversity than previously believed, making them candidates for resampling. (This was conducted by Belscher, 2007; Štorch et al., 2011; Sheets et al., 2016.) The Nevada sections together only preserve the pre-extinction and extinction intervals, however. Additional potential candidate sections exist in the Yukon. These had been studied in the 1980s by Lenz, McCracken, and others (Lenz, 1979; Lenz, 1982, Lenz and McCracken, 1982; Chen and Lenz, 1984), and while they yielded an excellent record of pre- and post-extinction

graptolites, when this thesis was initiated the crucial extinction interval (upper *pacificus* and *extraordinarius* zones) was believed to be missing regionally. In fact, the *extraordinarius* Zone had never been confidently identified anywhere in Canada.

1.3 Objectives

The following section lays out the main objectives of this thesis, and gives a short overview of how they were accomplished.

Objective 1: Evaluate the suitability of the Blackstone River section as a comparative section for studies of Late Ordovician graptolite biodiversity patterns in China and elsewhere.

Over two field seasons, the Blackstone River section was measured and sampled in detail. The zonal boundaries were identified in the field, and then confirmed in the laboratory through microscope examination of samples and identification of key taxa.. This allowed targeted recollection of crucial intervals to increase the resolution in the subsequent field season. Isotope samples were also collected and analyzed independently by researchers at the Saskatchewan Isotope Laboratory, University of Saskatchewan, to provide chemostratigraphic confirmation of the graptolite correlations and to check for the completeness of the section in non-graptolitic intervals (see LaPorte et al., 2009; Holmden et al., 2013). All the biozones through the LOME and recovery interval were identified at the section, and laboratory analysis showed them to be biodiverse and readily correlated to other global sections, establishing the Blackstone

River section as a globally important reference section for the study of the environmental and ecological changes at the Ordovician-Silurian boundary.

Objective 2: Test the geographic exclusion hypothesis for neograptines during the latest Ordovician (pre-Hirnantian)

All the collections through the pre-extinction interval were systematically searched for neograptines to confidently exclude their presence before the initiation of the LOME. Rarefaction analysis was conducted on samples to increase confidence in sampling completeness. Additionally, the uppermost Katian was sampled at 5 cm resolution, to capture in detail the timing and order of appearance of incoming neograptine species. Data were collected on proxies for environmental change (other fossil taxa, lithology) that would support a shift towards shallower, better oxygenated conditions coinciding with the invasion of neograptines.

Objective 3: Test the impacts of sampling intensity on patterns of apparent species diversity (and establish a collecting standard for future sampling)

Large, consistently-sized samples were collected at a regular interval throughout the section. These were then gridded and counted to produce abundance data that allowed statistical estimates of sampling completeness. All counted samples were then subjected to rarefaction analysis to check for sampling completeness. As a final check, after counts were completed, samples were resplit to expose more surface area to see whether additional material would have boosted species recovery.

Object 4: Test the refugium hypothesis, i.e., determine whether intensive sampling at the Blackstone River section could produce levels and patterns of diversity similar to those in China.

Large, standardized collections were made over two field seasons, with the first season acting as a guide to levels likely to yield better preserved and more abundant samples. This ensured a high probability of sampling most of the species that occurred during the study interval at the section To optimize the comparison with the sections in China specimens were compared to a recently published systematic manuscript for the Hirnantian interval (Chen et al., 2005a), as well as an unpublished manuscript revising Chinese species through the earliest Rhuddanian (Fan et al., in prep.). Additional material from Nevada, Scotland, and Arctic Canada was examined to improve familiarity with species and modes of preservation. Finally, type specimens and samples from a newly collected boundary section in China (Jeiling) were examined in China over several weeks at the Nanjing Institute of Geology and Palaeontology to improve confidence in identifications, with precise measurements taken for comparison with material from the Blackstone River.

Objective 5: Test whether two additional periods of diversity loss in the early Silurian suggested by Chinese data represented additional, global extinction events.

The biodiversity, extinction, and origination curves constructed for the Yangtze Platform by Chen et al. (2005b) showed additional periods of elevated species loss at the end of the *persculptus* and *ascensus* zones. Diversity curves were prepared for this

interval. Additionally, rates of per taxon extinction and origination were calculated to determine whether the controlling agent on diversity patterns, i.e., increased rates of extinction vs. reduced rates of origination (or both), was the same at both sections.

Objective 6: Examine the timing of the Late Ordovician Mass Extinction relative to community structural changes and test whether community changes preceded or followed extinction.

Collections were made at 5 cm intervals just prior to and during the main pulse of extinction to allow any short-duration, gross community compositional changes that preceded the LOME to be observed. In addition, counts were made to rigorously quantify species abundance throughout Katian and early Hirnantian. This allowed for statistical analysis of subtle changes in the character of graptolite communities that might be missed with presence-absence data or less precise estimates of abundance (e.g., “common”, “uncommon”, “abundant”).

Objective 7: Determine the relationship between extinction events seen at the Blackstone River section and environmental changes, specifically their relationship with sea level fall and oxygenation.

Curves of diversity, origination, and extinction were produced for the entire section, and two principal intervals of extinction identified: the LOME, beginning in the latest Katian, and a second, lesser event at the base of the Silurian, after the second pulse of the LOME. These were compared to lithological, paleontological, and geochemical data to indicate changes in water depth and subsurface mixing. These data

were compared with similar data recently collected by colleagues from two sections in Nevada to identify global signals of environmental change from local processes.

1.4 Relationship of Project with Recent Studies

This thesis was conducted as a component of a broader project funded by the National Science and Engineering Research Council and the U.S. National Science Foundation with goal to quantifying global diversity changes relative to environmental changes during the latest Ordovician and early Silurian. Many previous efforts at studying large scale changes graptolite diversity have suffered from difficulties reconciling diversity data sets that were created by different authors, at different times, using differing sampling methodologies and taxonomic approaches (e.g., Melchin and Mitchell, 1991). This project benefited from close working relationships between the broader study particpants, informed by up-to-date data. A number of publications or data sets have arisen arisen out of this project. These publications are heavily referenced within this thesis because they either directly involve data from the Blackstone River (e.g., Sheets et al., 2016; LaPorte et al., 2009; Holmden et al., 2013; Robinson, 2012; Hawkins, 2011; Melchin et al., 2011) or they were conducted in concert with this thesis, with data sharing and communication between the authors and the author of this thesis, making their results more reliably and readily compared (Belscher, 2007; Štorch et al., 2011; Melchin et al., 2013).

Melchin et al. (2011) provided a revision of higher-level graptolite taxonomy utilizing, in part, specimens from the Blackstone River that make up part of this thesis;

this taxonomic scheme is utilized in this thesis. Robinson (2011) conducted a high-resolution morphometric study of species of *Styracograptus,* utilizing Blackstone River material, which was examined in direct cooperation with Loxton in China and Canada; the resulting species determinations inform discussions of the genus in Chapter 6. Belscher (2007) produced abundance data for an equivilant interval at the Vinini Creek section in Nevada. Her raw data were provided during the production of this thesis, and the counting merthodology used here was based upon methodology she utilized. Štorch et al. (2011) provided a detailed systematic treatment of Katian and lower Hirnantian graptolites from Nevada; this analysis was done in concert with this thesis, with morphometic and other data freely shared in both directions. Hawkins (2011) utilized abundance data generated during this for initial studies of graptolite community dynamics. This work was in turn utilized, along with occurrence and abundance data from Vinini Creek (generated by Štorch et al. (2011) and Belscher (2007)) in Sheets et al. (2016), a publication that generated the biotope affiliations used in this thesis. LaPorte et al. (2009) provided a detailed discussion of environmental and depositional conditions in Nevada and the Blackstone River, based largely on geochemical data based on samples collected as part of this thesis, and utilizing biostratigraphic data from this study, alongside preliminary data from Štorch et al. Their study provided the chemostratigraphic correlation for the non-graptolitic portions of the Blackstone River section. Holmden et al. (2013) demonstrated the utility of the Nd isotope proxy for the sea level using isotope samples collected as part of this thesis and biostratigraphic data

data from the Blackstone River (produced as part of this thesis) and Nevada; Nd data generated in the production of that paper was utilized as a secondary or primary indicator of sea level during this thesis (depending on whether lithological indicators were available). Melchin et al. (2013) did not directly use data from the Blackstone River. However, their review of global black shale deposition utilized the same up-to-date biostratigraphic scheme utilized in this thesis, and analyized isotope data from the Vinini Creek section in the context of the correlation developed between the Blackstone River and that section over the course of this study.

Several additional papers, which were not part of the larger project to which this theiss contributes, are also heavily referenced in this thesis because either material or raw data were made available for comparative study during the production of this thesis (Chen et al., 2005; Fan et al., in prep.)

1.5 Outline

This thesis contains eight chapters, seven appendices, and 57 plates. Chapters 2 and 3 provide regional geological context and detailed information on the methodology employed during field sampling, counting, species identification, and illustration. A stratigraphic column, with sample locations indicated, and carbon and neodymium curves for the Blackstone River section is included in Chapter 3. Chapter 4 provides an overview of the biostratigraphic zonation for the section, as well as detailed discussion of correlation with other important global sections. Separate range charts for the *ornatus* to

extraordinarius, persculptus, and *ascensus* to *atavus* zones are presented at the end of the chapter.

Chapter 5 discusses diversity and abundance changes at the Blackstone River section during the study interval, with comparison to patterns seen internationally. Discussion of sampling effects is also included. Graphs showing diversity, extinction, and community structural data are included with this section. The results of the abundance counts are discussed, and the abundance data are presented in Appendix B (in both graph and table form). Chapter 6 provides detailed descriptions of all the species that occur in the studied part of the section. Graphs showing comparative metrics useful for differentiating between species in the section and comparing/contrasting with species identified elsewhere are included. Plates containing both line drawings and digital composite images are located at the end of main chapter section. These high-resolution images are designed to be viewable at magnification. Chapter 7 presents a discussion of the growth, identification, and functional morphology of species of the genus *Appendispinograptus.* This chapter was originally published in the *Proceedings of the Yorkshire Geological Society* (Loxton et al., 2011). A final chapter (Chapter 8) gives a concluding overview of the project and its limitations, and suggests avenues for future research.

Seven appendices are also included. Appendix A gives detailed discussions of the counted samples, including a discussion of evidence for deformation in several of them. Appendix B presents the abundance data for the Katian and early Hirnantian as both

tables and pie graphs. Appendix C provides the sample-by-sample identification and grouping methodology used in the counts. Appendix D provides rarefaction curves for all counted samples. Appendix E provides images and provisional identifications of some accessory fauna that occurs at the Blackstone River section (e.g., trilobites and brachiopods). Appendix F reproduces diversity and/or extinction curves for Ordovician-Silurian boundary sections from China and Nevada for comparative purposes. Appendix G provides a copyright release for Chapter 7.

1.6 Publications Resulting from this Thesis

Chapter 7 reproduces a first-authored paper in its entirety (with minor modification to the published manuscript). Additional peer-reviewed papers arising from this thesis work are noted below, with notes indicating the author's contribution. Conference presentations are not listed (six with published abstracts were produced).

SHEETS, H.D., MITCHELL, C.E., MELCHIN, M.J., LOXTON, J., ŠTORCH, P., CARLUCCI, K.L. and HAWKINS, A.D. 2016. Graptolite community responses to global climate change and the Late Ordovician mass extinction. *Proceedings of the National Academy of Sciences 113***(30)**, 8380–8385.

Contribution: The graptolite abundance counts produced during this thesis comprise the largest component of the dataset analyzed. Loxton also contributed biostratigraphic information, sedimentological, and other paleontological data that contextualized the graptolite counts. Other contributions include working with co-authors to ensure

taxonomic compatibility of the Yukon and Nevada counts and assistance with drafting of text.

LAPORTE, D.F., HOLMDEN, C., PATTERSON, W.P., LOXTON, J.D., MELCHIN, M.J., MITCHELL, C.E., FINNEY, S.C. and SHEETS, H.D. 2009. Local and global perspectives on carbon and nitrogen cycling during the Hirnantian glaciation. *Palaeogeography, Palaeoclimatology, Palaeoecology* **276**(1), 182–195.

Contribution: All of the samples from the Blackstone River used in the geochemical analysis presented in this paper were collected by Loxton during his field work. Loxton provided biostratigraphic and sedimentological information that gave environmental and temporal context to the Blackstone River portion of the isotope results. Loxton also produced the stratigraphic column and provided assistance with the text.

MELCHIN, M.J., MITCHELL, C.E., NACZK-CAMERON, A., FAN, J.X. and LOXTON, J. 2011. Phylogeny and adaptive radiation of the Neograptina (Graptoloida) during the Hirnantian mass extinction and Silurian recovery. *Proceedings of the Yorkshire Geological Society* **58**(4), 281.

Contributions: Loxton provided infrared and light microscope study of Arctic Canadian and Yukon graptolite material that formed part of this analysis. He also coded and provided independent initial cladistic analysis of several taxa that were later integrated into the larger systematic work. Additionally, he provided biostratigraphic control on material (*Glyptograptus*) from the Yukon and editorial feedback on the manuscript.

Chapter 2. Regional Geology and Locality Description

2.1 Regional Geology

The Yukon Territory is divisible roughly into two geologic entities: a younger amalgam of accretionary terranes that comprise the southwest of the territory and extend to the Pacific Ocean and an older complex of sedimentary basins and carbonate platforms that make up the northeastern portion of the territory. These two regions are separated by the Tintina Fault (Cecile et al., 1997). The study section occurs along the Blackstone River, within the Ogilvie Mountains, in northeastern Yukon (Fig. 2.1—see also Chapter 3.1). The strata studied as the bulk of this dissertation were deposited within the Blackstone Trough, an intracratonic basin that was located on the northwestern margin of Laurentia during the study interval (Fig. 2.1), with an approximate paleolatitude of 15°N (LaPorte, 2009; Cocks and Torsvik, 2011). The Blackstone Trough is an east-trending feature, connected to the south end of the larger Richardson Trough, and bounded by carbonate platforms to the east, south, and northwest: respectively, the Mackenzie, Ogilivie, and Porcupine platforms (McCracken and Lenz, 1987; Norford, 1997; Fig. 2.1). Shales, calcareous shales, and dark limestones dominate the Ordovician-Silurian strata at the Blackstone Trough, with rare debris deposits and cherts. Regional lithostratigraphy in the region is coarsely defined. Jackson and Lenz (1962) proposed the Road River Formation for the Ordovician and Silurian—later shown to encompass the Upper Cambrian to Middle Devonian (Norford, 1997)—

sedimentary strata of the Richardson and Blackstone troughs. This term is often, but inconsistently, expanded to the Road River Group, and has since been applied broadly to Devonian and older Paleozoic basinal strata throughout the Cordillera (e.g., Fritz, 1985; Lenz, 1988; Pyle and Barnes, 2001), with local formational division in some areas (e.g., the Selwyn Basin (Gordey, 2013)).

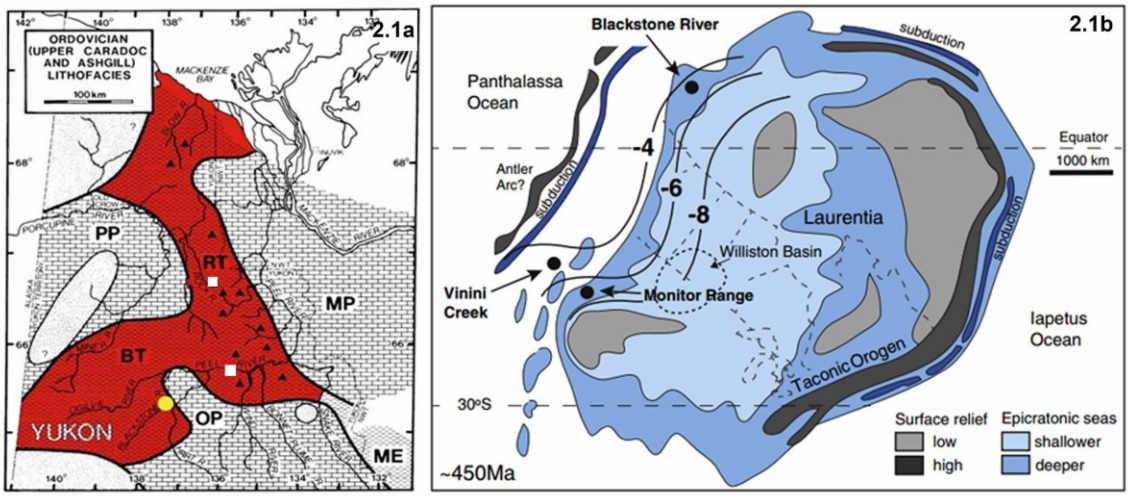

Figure 2.1. Regional geology of the Blackstone Trough. (a.) BT, RT, PP, MP, and OP = Blackstone and Richardson troughs, and Porcupine, Mackenzie, and Ogilivie platforms, respectively. Blackstone River study locality is marked with yellow circle. White squares show other Yukon localities from which graptolite material was examined as part of this thesis. (Modified from McCracken and Lenz, 1987) (b.) Position on Laurentian continent and inferred water depth, based upon εNd values, at Blackstone River during study interval (from Holmden et al., 2013).

Within the northern Yukon, graptolites from several sections (see references in Lenz and Chen, 1985), along with conodonts (Lenz and McCracken, 1982), and trilobites (Lenz and Churkin, 1966) have been studied to provide insight into local environmental conditions and basin connections. Previous authors have suggested, based on conodont (Goodfellow et al., 1992) and graptolite (Lenz and McCracken, 1982) data, that the connection between the Blackstone and Richardson troughs and the wider ocean may

have been restricted by physical or oceanic environmental barriers during the Late Ordovician. However, the synchronous appearance of cosmopolitan fauna at the Blackstone River and elsewhere shown in this study (see Chapter 4.2) indicates that no such barrier existed during any interval where graptolites are preserved during the late Katian through early Rhuddannian. Scarce benthic fauna, and common dark, organic-rich, laminated rocks, indicate mainly quiet, dysoxic to anoxic, relatively deep-water conditions in both the Blackstone and Richardson troughs throughout most of their history (Goodfellow et al., 1992), with the noted exception of the early-mid Hirnantian, where pale carbonates replace shales, and corals, brachiopods, and trilobites are present (Lenz and McCracken, 1982; the present study).

Deposition within the Blackstone Trough began in the Early Ordovician, at which point it was a narrow extension of the Richardson Trough (Norford, 1997), a larger feature interpreted to a failed rift arm (Cecile et al., 1997—see review of rifting models therein). By the Middle Ordovician, the Blackstone Trough was a well-established paleogeographic feature, extending westwards to the current Yukon-Alaska border (Tatonduk River region). Maximum lateral extent was reached in the Late Silurian or early Devonian, when basinal sedimentation overlaid portions of the Porcupine Platform and Oglivie Arch (Norford, 1997). With the exception of the latest Ordovician—much or all of the Hirnantian appears to be missing from well-studied Peel River section, where only 30 cm of strata separate Katian and Rhuddanian horizons (Lenz and McCracken, 1982; Melchin, pers. comm.)—deposition of basinal facies appears to have been more

or less constant in the Richardson and Blackstone Troughs through the Middle Ordovician to Early Devonian, with a trend towards progressive encroachment of deep water sediments onto adjacent platforms (Norford, 1997). The same is not true of the carbonate platforms themselves, where numerous stratigraphic breaks are present locally in the Ordovician and Silurian strata. However, the lack of formal stratigraphic subdivisions within the carbonate facies and a dearth of systematic studies of carbonate-associated fauna make regional correlation difficult (Norford, 1997). On a regional scale, the Road River Formation hosts a diversity of lithologies, indicating moderate to deep water deposition, including argillaceous limestones, cherts, shales, calcarenites, and debris flows. Material was shed from the adjacent carbonate platforms, with (mostly thin) turbidites and debris flows common within many parts of the Richardson and Blackstone troughs, including one prominent and lithostratigraphically useful example from the Early Ordovician, which can be tracked for 70 km in the Richardson Trough, including at the Peel River section (Norford, 1997). Deposition within the Blackstone Trough appears to have ceased by the Middle Devonian (Goodfellow et al., 1992).

The post-depositional history of the study area is complex. A dramatic change in regional sedimentation patterns occurred in the Devonian, when the passive margin of Laurentia became reactivated in a sequence of orogenic events, beginning with the Romanzof Orogeny in the Devonian (Lane, 2007), and continuing through the of Mesozoic collisions that built the Cordilleran region of North America (Norris, 1997).

These events produced the Ogilvie and Richardson mountains, in which the Blackstone River section and nearby Peel River section occur, as well, indirectly, the fault-mediated parallel set of rivers (including the Blackstone), which make up the Peel River watershed, and along which the Blackstone River section is exposed. Folding and faulting regionally manifests at various scales, from the large Richardson Anticlinorium, to the suite of anticlines, synclines, and faults of the Taiga-Nahoni Fold Belt, which includes the Blackstone River section (Norris, 1997; Osadetz et al., 2005). Although the specific strata that make up the study interval at the Blackstone River were largely unaffected by regional deformation[4], deep burial, owing to rapid basinal subsidence (Norford, 1997), and/or subsequent tectonic events resulted in notable diagenetic changes. Conodonts from the uppermost Ordovician and lower Silurian at the Blackstone River have Color Alteration Index values of 4, indicating a maximum burial temperature of 180-190°C (Norford, 1997). This thermal history is also evident in the graptolites, which are preserved principally as silver carbon films, with relatively high reflectance values (Link, 1990; pers. observ.). This mode of preservation commonly obscures internal details and makes them unsuitable for chemical studies of their periderm.

[4] Strata below the study interval at the Blackstone River section are clearly deformed. See discussion in Chapter 3.

2.2 Locality Description

The study section is a cliff face exposed at a sharp northwest bend in the Blackstone River. Strata dip 065/35. The described portion of the exposure is a 50 m interval beginning ca. 0.8 m below the base of the *P. pacificus* Zone and continuing to the lowest horizons of the *A. atavus* Zone. Additional graptolitic exposure exists below and above the described portion, but these strata were not explored or measured in detail during this study. The portion below the studied section becomes deformed and faulted near the base of the exposure, however, at least several meters of strata below the base of the measured section are likely collectable, as is a much thicker interval above the studied portion of the section. (Scree collections confirm that this younger material is both well-preserved and heavily graptolitic.) The outcrop is also exposed at least intermittently east of the camp along a narrow stream, but as this material is younger than the study interval, it was not explored.

Figure 2.2. Blackstone River section biozone positions. Sampled strata extend into area behind green bush in bottom right of fimage. Locations of zonal boundaries approximate. Photograph direction northward.

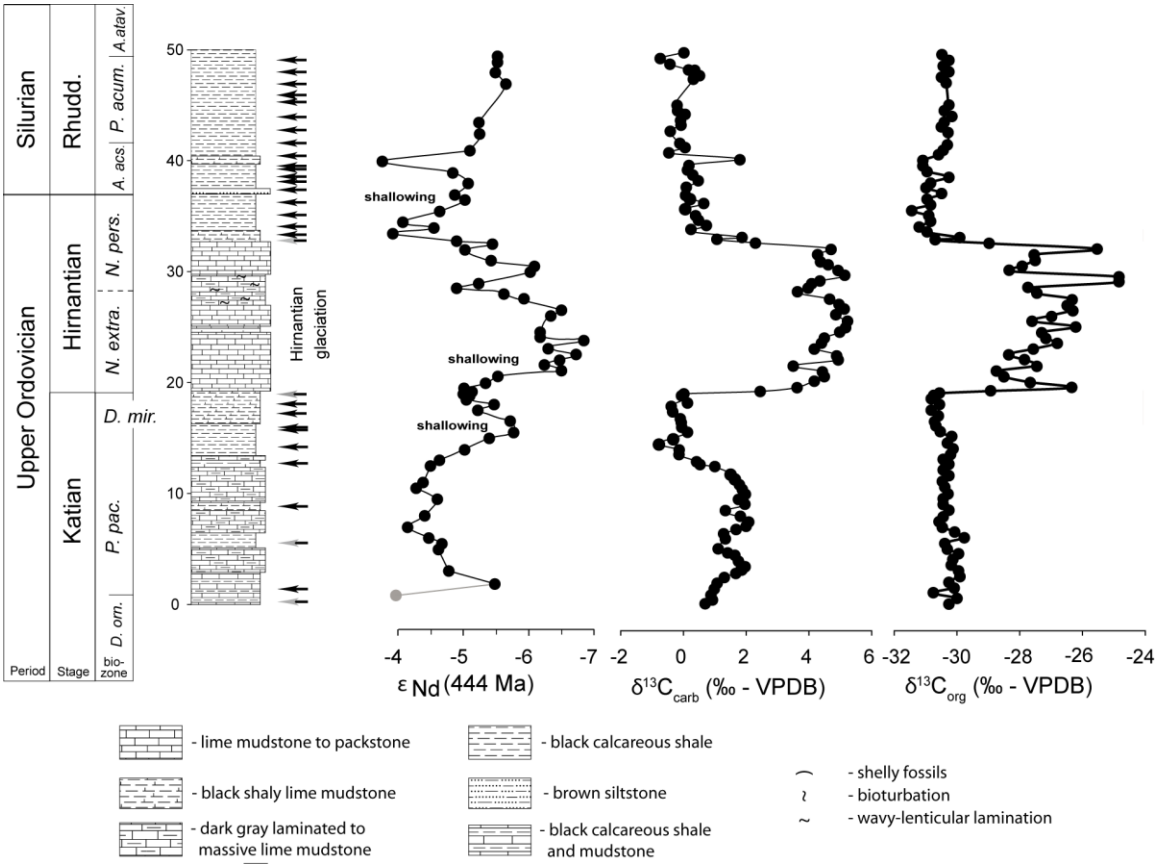

Figure 2.3. Blackstone River stratigraphic section. Measured portion of section shown. Graptolitic strata continue above and below. Black arrows adjacent to the stratigraphic column indicate locations of full graptolite samples. Grey arrows show locations with multiple closely spaced samples. Carbon and neodymium curves from Holmden et al. (2013). Base of the *persculptus* Zone inferred based on comparison with carbon isotope curves at sections that retain graptolites through the lower *persculptus* (LaPorte et al., 2009). Image modified from Holmden et al. (2013).

The lithology for most of the section consists of interbedded black calcareous shale and argillaceous lime mudstones, along with rare siltstones (Fig. 2.3). Within the interval of strata that represent the Hirnantian glacial event (cf. Chapter 4.2 for discussion of correlation), lime mudstone and wackestone dominate. Accompanying this shift in lithology is the appearance of a rare to abundant benthic fauna, consisting of trilobites (numerous at the base of the limestone section and in the strata immediately below the post-glacial return to black shales), isolated corals, brachiopods, and sponge

spicules. These fauna, along with the presence of bioturbation and symmetric(?) ripple cross-lamination, support a transition to shallower-water conditions. Close examination of this interval showed no evidence of subaerial erosion or other hiatuses, and so the section is assumed to be continuous, unlike other regional sections that manifest a hiatus or unconformity during the Hirnantian (Lenz and McCracken, 1982). Above the glacial interval, shales dominate over lime mudstones, whereas in the pre-glacial interval the inverse is true. With the exception of the glacial interval, strata are consistently graptolitic. Average calcite content by weight is 61.4% in the pre-glacial interval, 85% during the glacial interval, and 36.7% in the post-glacial interval[5], but varies substantially within each interval (Fig. 2.4). Based on the shift in facies between black shales and calcareous mudstones during inferred transgressive-regressive cycles, (for geochemical basis of inferred T-R cycles see LaPorte et al., 2009; Holmden et al.,

[5] A glacial interval corresponding to the period of extinction at the end of the Ordovician has long been recognized (e.g., Sheehan, 1973; Brenchley, 1994). Finnegan et al. (2011), however, recently demonstrated that Gondwanan icesheets were present for much of the Late Ordovician and Early Silurian, with a maximum reached in the Hirnantian Stage. Reference to 'pre-glacial', 'glacial', and 'post-glacial' intervals in this thesis refers the Hirnantian glacial maximum. This interval is recognized between ca. 19.30 m and 32.80 m at the Blackstone River section, corresponding to a shift to carbonate deposition and a strong positive carbon isotope excursion (Fig. 2.3).

2013), as well as the periodic presence of benthic fauna, the Blackstone section most likely occupied an outer shelf to upper slope, rather than a deep basinal setting.

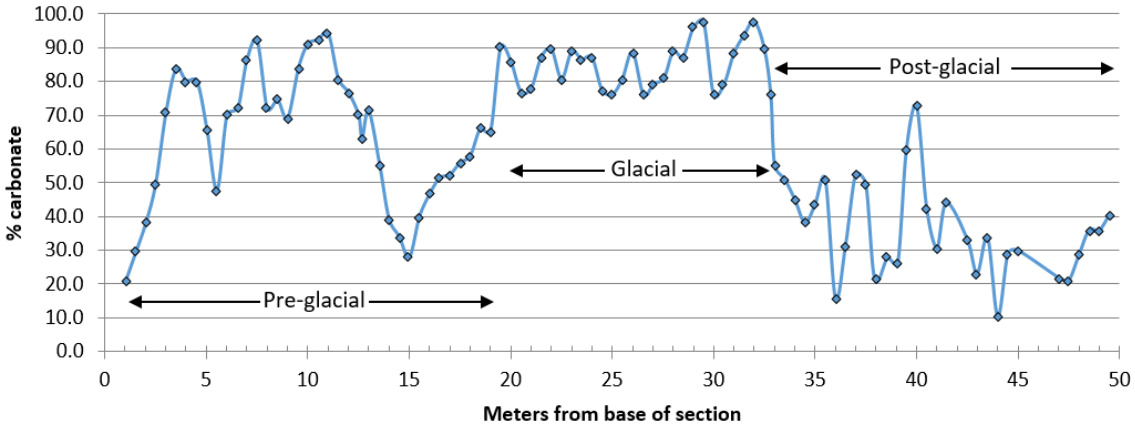

Figure 2.4. Calcite content by weight at the Blackstone River. Note change in carbonate content corresponding from a shift from black shales to limestones and back again at ca. 20 m and 33 m. Data provided by Chris Holmden, University of Saskatchewan, based on samples collected as part of this thesis.

Chapter 3. Methodology

3.1 Field Collection

The Blackstone River locality is located directly on the Blackstone River, about 180 km northeast of Dawson City and 110 km south-southwest of Eagle Plains, Yukon. The coordinates are 8N 0392141 7259301 (WGS 84, +/- 24 m) or Latitude 65.4383 Longitude -137.3258. The locality is about 650 m downriver from the coordinates indicated in Lenz and McCracken (1982). Access to the site is possible either by helicopter or canoe; the Blackstone River is too shallow to allow floatplane landing. The site occurs at a sharp northwest bend in the river, with a large gravel bar immediately in front of the outcrop. This gravel bar was large enough to allow helicopter landing and camp set up during both field seasons. It was also present during visits by Lenz and McCracken in the early 1980s (Lenz, pers. comm.) and therefore appears to be a semi-permanent feature. The nearest point from the section to the Dempster Highway is ca. 40 km by air. Canoe access is possible at Latitude 65.4383°, Longitude -137.3258°, the nearest convergence of the Blackstone River and the Dempster Highway (ca. 60 km upstream from the section). Exiting by canoe requires either proceeding down to the Peel River to a point at which floatplane access is possible or continuing down the Blackstone to the convergence with the Ogilvie River, and then “lining up” river, i.e., pulling the canoe upstream, to the point where the Ogilvie River meets the Dempster Highway (ca. 40 km). Both helicopter and canoe access were used during this study (in 2006 and 2007, respectively).

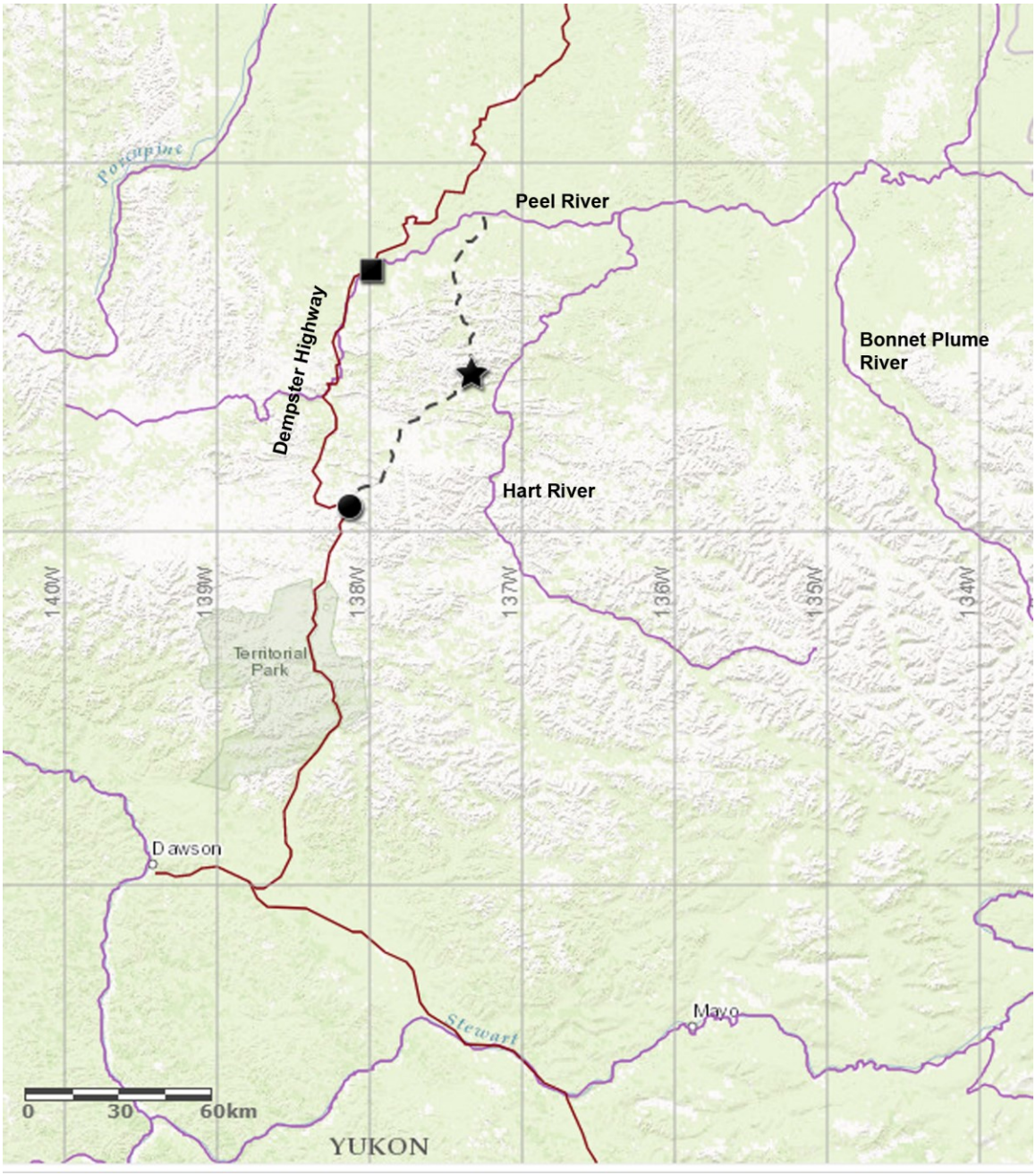

Figure 3.1 Geographic location of Blackstone River section. Dotted line = Blackstone River. Star = Blackstone River section. Black circle = confluence of Blackstone River and Dempster Highway ('put in' location for canoes). Black square = confluence of Oglivie River and Dempster Highway ('line out' location for canoes). Purple lines = rivers. Dark red lines = roads. White circles = towns.

The principal objective of this thesis at the outset was to test the affect of sampling intensity on apparent patterns of extinction and survivorship during the LOME. Study of the Blackstone River section was conducted in concert with restudy of sections in Scotland (Dob's Linn) and Nevada (Vinini Creek and Monitor Range), for comparison with recently restudied sections in China (see Chen et al., 2005b). This context established the temporal interval (latest Ordovician to earliest Silurian) and a methodology for collecting: bulk sampling to allow unbiased species abundance counts, with an emphasis on the period of peak extinction in the latest Katian and earliest Hirnantian. Examination of the site built upon the work of Lenz and McCracken (1982), who identified the presence and approximate stratigraphic position and thicknesses of the *ornatus, pacificus, persculptus,* and *acuminatus* zones. Using this as a guide, the approximate position of the various zones was confirmed by low-frequency sampling through the section.

In order to set a base for the section, examination of strata continued down section below the apparent first appearance of *Paraorthograptus* at a cm-by-cm level over an interval of several days, with slabs examined using a hand lens and field microscope for the presence of *Paraorthograptus*. Its lowest confirmed occurrence was within an interval of calcareous mudstones that were difficult to split (0.83 m) (Fig. 2.3). The base of the section was set at the nearest interval of shale below this level (=*D. ornatus* Zone), and a collection was made from this shale horizon for examination in the lab to ensure that *P. pacificus* was genuinely absent from that level. From this base, the

section was measured and described at centimeter scale. Hand sample-sized lithological samples were collected at half-meter intervals for geochemical analysis, except where horizons were weathered or otherwise questionable (e.g., contaminated by calcite veins), in which case samples were taken as close to the base of each 0.5 m study interval as possible. Lithological samples were taken wherever there was a significant change in lithology. Photographs of each half-meter interval were also taken to allow examination of gross lithology later. Collections were taken sequentially along two sections of the outcrop ('Section A' and 'Section B',Fig. 3.2), correlated using marker beds.

Meterages were marked on the outcrop using a grease pencil during the 2006 field season, and were still visible during the 2007 season, allowing precise correlation of collections taken during each season. Collecting proceeded along Section A from 0 m to 11 m, at which point the outcrop became highly fractured and then scree covered. Higher samples from 11 m and above (geochemical and fossil), except for samples near the base of the *extraordinarius* Zone, were taken from Section B. The majority of graptolite samples were taken during the 2006 field season. These were then examined in the lab and additional samples were taken during the 2007 season to add resolution to key intervals, e.g., base of Hirnantian and base of Silurian, or to substitute for samples with poor preservation. The goal of the sampling was to recover a minimum of 300 identifiable graptolite specimens per sample, a number that would yield a 95% confidence of recovering species present as at least 1% of the population (Phleger,

1960). Based on previous sampling in Nevada (Mitchell, pers. comm.), 0.25 m^2 was determined to be likely to yield the minimum required number of specimens, and was chosen as the standardized collection volume for this project and parallel collections in Scotland. During collecting in Scotland, slabs were laid out to fill a 0.5m x 0.5 m area. This was found to be equivalent to the volume of one 26 x 44 cm cloth sample bag, so one sample bag was used as a proxy for slab area during most collections. Two bags, i.e., 0.5 m^2 of material, were collected from a few horizons, where graptolites were rare or poorly preserved. This approximation was further validated in the lab: the surface area of all but one of the eight Blackstone River samples for which surface area were measured was above 2500 cm^2 (mean = 3084 cm^2).

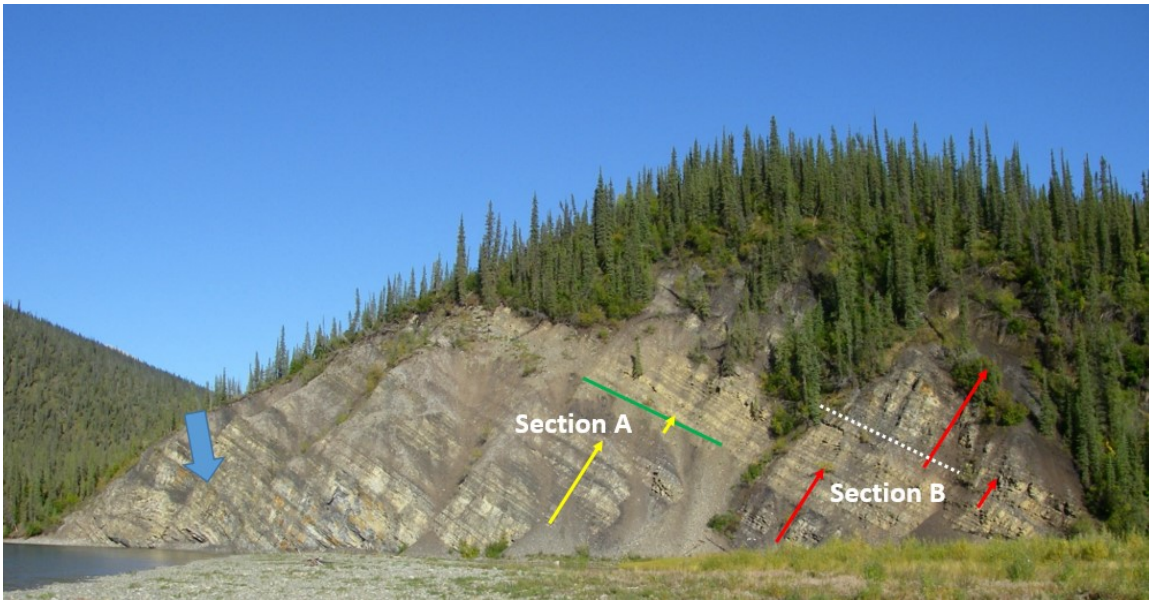

Figure 3.2. Measured and sampled portions of section. Thick blue arrow points to deformed area below the sampled interval. Thin arrows show approximate locations of sampling. Correlation between lines of sampling followed marker beds. Green line shows location of the base of the Hirnantian. Dashed white line shows approximate location of the base of the Silurian. Camera view is northward.

Sampling horizons were determined by graptolite preservation, collectability, and the initial goals of the project, i.e., examination of trends leading up to the LOME. Below 12 m, shales are rare, and the calcareous mudstones, although mostly graptolitic, were extremely difficult to split, making collecting sufficient graptolite material for the planned analysis difficult. Additionally, this interval was of lesser importance to the project as defined at the time of collecting, since it preceded the onset of extinction as determined in other regions. A single collection was taken from the *ornatus* Zone (0.1-0.2 m), and collections were made at 1.32-1.42 m, 5.3-5.4 m, 5.5-5.6 m, and 8.8-8.9 m in the lower *pacificus* Zone (the three intervals where the presence of shale allowed bulk collecting[6]). Two samples were taken near 5 m, at 5.3 m and 5.5 m, as these were graptolite-poor and current aligned, respectively, and therefore deemed to be potentially poorly representative of communities at the time; for the purpose of analysis these two samples were combined. From 12.67 m to 18.95 m, and after the return to shales at 32.84 m and above, samples were taken at ca. 1 to 1.5 m intervals, with precise levels determined by preservation and graptolite abundance. Additional samples through these intervals could easily be collected in the future, especially through the upper Katian. The shales directly below the contact with the Hirnantian limestone (ca. 19.2 m) are highly weathered at Section B, so collection for this interval was conducted at Section A. During the 2007 field season, this interval was resampled at 5 cm resolution from 18.94 m to 19.30 m. Samples of trilobites were collected from the basal

[6] Locations of all full graptolite samples are shown on the stratigraphic column (Fig. 2.3).

meter of limestone (19.3-20.3 m), where they are abundant, for paleoenvironmental and possible biostratigraphic use.

The interval between 19.30 m and 32.80 m is non-graptolitic, but contains rare shelly fauna, including bivalves, brachiopods, crinoid columnals, sponge spicules, trilobites, and isolated corals. Representative examples of this material were collected, but were not studied in detail; images of some fauna are shown in Appendix E, along with preliminary identifications. Several intervals of shales or fissile lime mudstones occur through this part of the section that may represent intervals of deepening. As a return to ecologically diverse graptolitic shales occurs at a similar horizon at Vinini Creek, several days were spent splitting and examining this material in the field to look for the presence of graptolites, without success. Graptolites reappear in abundance with a return to black shales at 32.84 m. Immediately below this is a 3 cm thick interval of orange brown-weathering shale, which contains shelly fragments, including several species of trilobite, as well as very rare, poorly preserved graptolites.

Samples through the *persculptus* Zone and above were difficult to collect. The exposed portion of Section B above 33 m is a near vertical cliff-face, with considerable loose material, making collecting dangerous. Access for collecting was accomplished with the help of a rope, and followed a vertical erosional gap through strata of the upper *acuminatus* Zone (Fig. 3.3a). Material across the basal boundary of the Silurian (ca. 35 m to 38 m) was very poorly preserved. In addition to heavy weathering, which mostly destroyed or obscured graptolites, some strata show localized deformation.

Many days were spent attempting to excavate unweathered, well-preserved material, but sampling through this interval is unavoidably sparse.

At 45.5 m an interval of scree made precise measurements impossible. During the 2006 field season, this interval was estimated at 1.5 m in thickness. Both graptolite and geochemical samples were collected above this scree interval, with meterage assuming a 1.5 m thickness. During the 2007 field season, this interval was excavated and measured. The actual thickness is approximately 1.77 m. As such, the height of all samples from 47 m and above are actually 27 cm higher than indicated, relative to the base of the section. This is uncorrected in LaPorte et al., 2009, and Holmden et al., 2013. The actual base of the *atavus* Zone lies at 49.77 m (=49.50 m in Laporte et al., 2009, and Holmden et al., 2013).

Excavation also uncovered a large scree-filled gap at 47.75 m, approximately 25 cm across, where the lower part of the outcrop has separated from the upper. Lithology, strike, and dip are constant on both sides, so it is assumed that no offset occurred along this fracture. A 22 cm thick, light brown-grey mudstone occurs at 46.43-46.65 m (scree-covered in 2006). This, along with a ca. 40 cm thick mudstone that occurs at 39.85-40.22 m were used to correlate to Section A. The interval between these two marker beds were measured at Section A and compared to the thickness along the sampled interval at Section B. Although there is some minor difference in bed thickness, these two sections appear to correlate well. Measuring down from these markers beds, it appears that the shale is exposed to at least 37 m, before becoming covered in thick

scree. Thus, it is likely that the basal Silurian could be studied at Section A, where the exposure is much less steep, making collecting easier and less dangerous. This correlation was done late in the 2007 field season, however, and no collections were made from Section A above 19.30 m. All collected slabs were individually wrapped in newspaper in the field unsplit, to avoid damage during transportation.

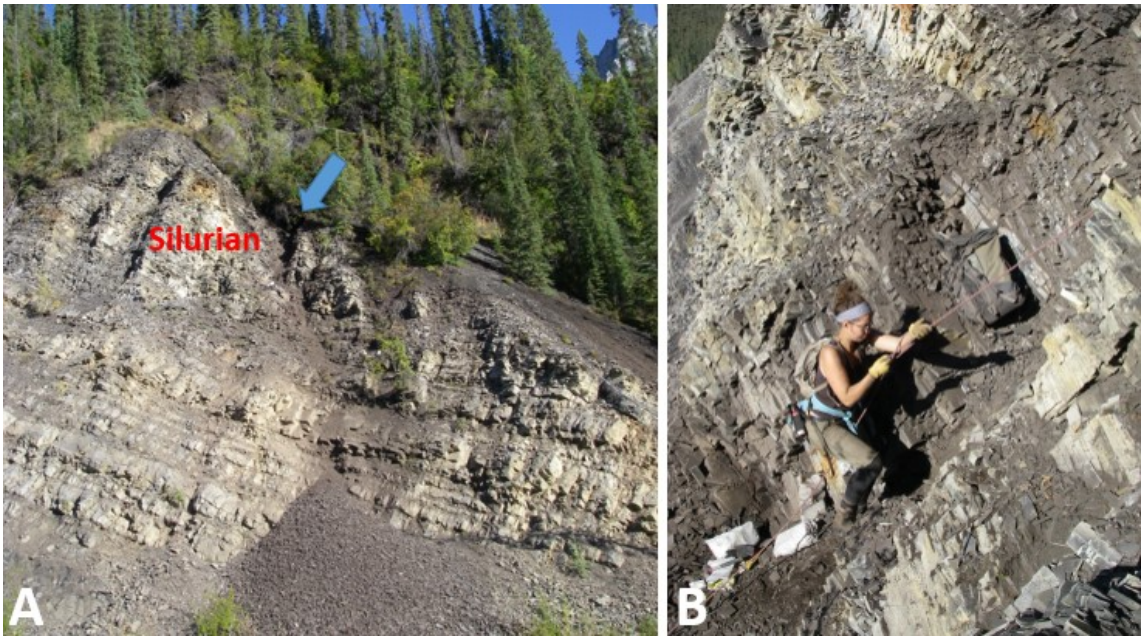

Figure 3.3. Latest Ordovician and early Rhuddanian collection locations. (a.) Outcrop at 'Section B' showing Hirnantian limestone interval (lower half of image) and shales of the latest Ordovician and earliest Silurian (view North). Eroded fracture along which collections were made is indicated by blue arrow. Collections continued into the area obscured by trees. The base of the *atavus* Zone is not visible. Scree pile at the base of photo shows extent of excavation over the course of sampling. (b.) Image showing degree of incline through the Silurian portion of Section B.

3.2 Counting and Density Estimates

Species occurrences and abundances for all samples from the *ornatus* through *extraordinarius* zones were counted. Prior to beginning counts, slabs were washed, split, and labelled with a meterage and slab number. To avoid duplication in the count, care was taken to note parts and counterparts of bedding surfaces, and where they existed

they were given a secondary letter, e.g., 1a and 1b. To add an extra lower *pacificus* Zone sample, a calcareous mudstone sample that had been collected for possible conodont analysis was split and counted late in the production of this thesis. As it was smaller than other collections, this sample did not yield 300 identified specimens.

Before beginning the count, all slabs were scanned and provisional species groups noted. Species bin construction began by consulting the existing systematic literature, especially Chen et al. (2005a), Koren' et al. (1983), Mu et al. (1993), and Williams (1982), as well as a list of identification criteria prepared as part of a parallel MSc thesis on graptolites of an equivalent interval from Nevada (Belscher, 2007). Existing taxonomic schemes mostly described ranges of variation of measurements for species, which often overlap between species. Additionally, many of them describe only well-preserved, mature specimens. Given that the objective of this thesis was to identify all specimens present (including fragmentary and juvenile material), rather than simply identify the presence or absence of a species (possible from one or two well-preserved specimens), a knowledge of the relative frequency of occurrence of specific measurements within a species, such as proximal widths, rather than just total intraspecific variation of these measurements, was required to make binning decisions on questionable material.

Although some more recent papers provide measurements in the form of scatter plots or tables, this is rare in older papers, which usually provide only ranges. As such, a large quantity of metrical data were collected. These data were compared in scatter

plots to attempt to find combinations of measurements that could reliably distinguish between species at various stages of development and with less than ideal preservation. This 'blank slate' approach of collecting measurement data and plotting without preconceptions uncovered criteria that allowed confident identification of many species, even with juvenile and fragmentary specimens. For example, *Apendispinograptus supernus* can be distinguished reliably from *A. leptothecalis* by differences in thecal spacing in individuals only four thecal pairs in length. However, it also called into question a number of species classifications in the existing literature, leading to an expansion of this thesis to include a systematic component (see Chapter 6). The count proceeded by first scanning through each sample to identify the total number of species present. This was used to create a sample-specific set of bins that proceeded from identification (species), to 'either-or' and genus-level categories (e.g., "*Paraorthograptus*" or "*R. abbreviatus* or *D. rarithecatus*"), to general descriptive categories (e.g., "climacograptid thecae[7]"), to completely unidentifiable.

Once categories were created, a series of parallel lines were drawn directly on each slab with a water-soluble pencil crayon, dividing each slab into a series of approximately 1 cm wide "columns". The width of these columns was chosen as it is the field of view of the microscope used for counting at 10x magnification. This level of magnification provided sufficient visual context to avoid losing track of position while scanning, but actual identification of specimens mostly required zooming in briefly to

[7] Placeholder category indicating sharply geniculate thecae parallel to the rhabdosomal axis.

higher power magnification. Counting proceeded by visually scanning from bottom to top of each column, counting all graptolite rhabdosomes that were represented by at least two thecal pairs. Where a specimen overlapped into two columns, the portion of it that fell into the adjacent column was marked with a water-soluble pencil crayon to avoid double counting. Sculae were initially counted as well, but this was abandoned after the first few samples, as difficulty seeing siculae on some slabs meant that abundance data for siculae were likely to be spurious. In addition, siculae could not be reliably assigned to even the genus level, in most cases, so they could not add to the basic count data. Specimens frequently required excavation for identification during the count. This was achieved with a Dremel engraving tool[8], but only after specimens around it were counted to avoid losing data.

Specimens were assigned to a species bin where this could be done with confidence. If not, they were assigned to one of the more general bins, for later distribution into species level bins (as described below). The entire surface of each slab was counted. Counting continued on additional slabs until 300 specimens were assigned confidently to the species-specific bins. If slabs remained uncounted after this threshold was reached, they were gridded and scanned in detail to search for taxa not recovered during the count. In some cases, odd or questionable taxa were noted during the count with a question mark or other notation. Prior to finalizing counts (after the systematic portion of the study was completed), each specimen noted as questionable was

[8]Or an an Air Scribe, on rare occasions where samples were very well-cemented.

rechecked and assigned to a bin. In several instances, the slabs or specimens were lost or destroyed in the interval between counting and final checking. In these rare cases, a conservative approach was adopted: new species were not introduced to a count unless they could be visually confirmed, even if count notes were suggestive, and the questionable individual was assigned to the most parsimonious category. Due to ongoing systematic work (as part of this thesis and in parallel by colleagues; see Štorch et al., 2011), species categorization schemes changed in several instances after counting. Additional, rare taxa were also uncovered during the process of counting subsequent samples, after some samples had already been counted, forcing revision of previous counts. In both cases, previous slabs were all rescanned to ensure that the change was accounted for, and the count updated as required. In one instance, a change in binning schemes necessitated recounting an entire sample. In most cases, however, this taxonomic shift or newly discovered taxon was irrelevant (i.e., after rescanning, the newly discovered taxon was not found to be present in the previously counted sample) or affected a very small number of specimens, which could be tracked down via slab level counts and rebinned individually. Final determination of how many species of *Paraorthograptus* existed in the sample was not resolved until several years after the principal counts. This uncertainty was anticipated during the counting phase, however, and was accommodated by measuring all high quality individuals encountered during the count process. The resulting measurements were in turn used to assign these specimens into species bins once final systematic decisions were made. All poorly

preserved specimens of *Paraorthograptus* (non-measured specimens) were then assigned based on the relative abundance of species identified within the measured collection.

To test reproducibility of counts, slabs were recounted in several instances. In addition, counterparts of slabs were accidentally counted on several occasions, allowing comparison between counts of count and counterpart (which should have been close to identical). In both the full sample and slab recounts there was variation between initial counts and recounts, as the choice of binning into species level or morphological/genus-level categories involves a degree of subjectivity, but the overall pattern of the relative abundance remained constant.

Once counts were completed, specimens in genus-level, 'either/or', or morphological bins (e.g., 'climacograptid thecae') were assigned to species bins based on the relative abundance of identified specimens. Redistribution proceeded in order of increasing generality. For example, specimens in *Appendispinograptus* or *Styracograptus* genus-level bins were first distributed to species bins, then individuals in the "climaco thecae <1.5 mm" bin were divided among the various *Appendispinograptus* species and *Styracograptus tatianae,* and finally "climacograptid" fragments were divided among species of *Appendispinograptus, Styracograptus,* and *Anticostia lata,* based on relative abundance after previous rebinning.

In some cases, rounding effects increased or decreased the apparent number of taxa in a sample, e.g., four unidentified specimens distributed into three species bins

results in a specimen being lost to rounding (each bin receives 1.33 specimens). The total impact of rounding was never more than 1 or 2 specimens per sample. Counts of percent identified, total excluding siculae, and total with siculae are all adjusted to the final number of specimens after distribution, i.e., they incorporate any rounding errors from distribution for consistency.

This redistribution process was problematic in number of ways. Some species are more readily identified based on juvenile or damaged specimens than others, creating an initial bias in the count, which is then amplified at all stages of distribution, since initial identifications determine the ratio of distribution of uncertain material. Additionally, some species, such as *Dicellograptus*, may be more prone to fragmentation, resulting in the artificial inflation of their apparent abundance, since each disarticulated piece is counted as an individual. Binning fragments also impacted estimates of specimen density: since all fragments were counted as specimens, horizons with more broken specimens will record as having higher density than equivalent horizons with better preservation. An alternative would have been to count only intact specimens retaining a proximal end. While this would have avoided the problem of fragmentary specimens inflating apparent species and total abundance, it would also have involved rejecting a large amount of information. Many specimens can be easily identified from distal portions, and proximal ends are often missing in otherwise complete specimens, with the probability of proximal ends being retained intact not equal across species. As such, utilizing only specimens with intact proximal ends would

have led not just to some species being undercounted, but species that were clearly present in a sample not being counted at all. A hybrid solution would have been to count only specimens that could be identified at least to a genus level. However, some genera—*Paraorthograptus, Dicellograptus*, and *Rectograptus* in particular—are easily identifiable from incomplete specimens, whereas others are more cryptic. For the above reasons, the approach of attempting to assign all morphologically distinct fragmentary and complete specimens, despite the noted shortcomings, was adopted.

Sample-specific binning and bin distribution schemes were created based upon species confirmed to be present. The list of schemes used is included as Appendix C. Only taxa that were captured in the count (not taxa that were found during scans of uncounted slabs) were considered when redistributing unassigned specimens, since there was no way of estimating the abundance of scan-captured taxa. This practice inevitably led to these species being underestimated, as at least some of the fragmentary material likely belonged to scan-captured taxa. However, the alternative was to either arbitrarily assign a value to their abundance or to give them an abundance of '1', and neither strategy would likely capture their abundance any more realistically than not including them in the redistribution process.

For several samples, the distribution scheme was revised after binning had already been completed and the process was repeated. For example, a decision was made to change the order in which probable distal specimens of *A. lata* were combined with proximal specimens of *A. lata* from before to after the redistribution of the bin

"climacograptid fragments >1.5 mm." This was done to account for the fact that the presence of lappets on *A. lata*—a feature that is often, but not always visible—meant relatively few of the unidentified large "climaco" fragments actually belonged *A. lata.* This change provided a test of the effects of the distribution scheme on apparent species abundance (Table 3.1). Note that this change only affected three of 16 taxa captured in the count (those with "climacograptid" thecae). Even among these species, while absolute number of individuals assigned to each species changed, the overall pattern of abundance of each species remained very similar.

Table 3.1. Effect of binning schemes on calculated abundance.

Method A			**Method B**		
Species	Specimens	%	Species	Specimens	%
A. lata	**700**	**42.87%**	***A. lata***	**715**	**43.81%**
A. supernus	**82**	**5.02%**	***A. supernus***	**72**	**4.41%**
C. hastatus	**26**	**1.59%**	***C. hastatus***	**20**	**1.23%**

The table above shows post-distribution calculated relative abundance of "climacograptid" taxa in sample 16.03 m using two different binning schemes. The left side (Method A) shows the scheme that was used to produce the final count. The right side (Method B) shows the results of an earlier scheme that combined bins of *Anticostia lata* fragments before the distribution of "climacograptid" fragments. (See discussion below and in Appendix C for further discussion of binning procedure.)

Specimen density was calculated for eight samples by measuring slab surface area and dividing total specimens per slab by slab surface area, where specimens included all complete or fragmentary graptolites that were later assigned to species bins (i.e., including morphological bins such as 'climaco fragment', but excluding siculae and completely unidentifiable fragments). Slab surface area was measured by tracing the outline of each slab on a one centimeter gridded sheet of paper, and then adding the total number of squares covered. Surface area estimates were rounded to 0.25 cm^2.

Average density, minimum, maximum, and standard deviation of specimen density were calculated using Excel. Any slabs that were not completely counted were removed from density calculations. Surface area of non-counted slabs was also calculated, and estimates of total examined specimens were calculated by multiplying the total surface area of all counted and uncounted slabs per sample by the average specimen density on counted samples.

Table 3.2 Measured sample area and density.

Height (m):	0.10	5.50	8.80	14.15	16.03	17.20	18.06	18.84
Total (exc. sic)	884	777	1531	3807	2471	2142	4786	3310
Total ID	712	608	966	1859	1632	1368	3072	2025
PERCENT Ided	81%	78%	63%	49%	66%	64%	64%	61%
Est. total ID exam.	NA	NA	NA	8730	5413	5276	9382	3730
Counted area (cm)	2544	2607[1]	2040[1]	693[1]	1116	944	1196	1046
Uncounted area (cm)	NA	NA	NA	2974	2586	2695	2457	881
Total area (cm)	NA	NA	NA	3667	3702	3639	3653	1926
Density AVG (ID)	0.279	0.224	0.461	2.381	1.462	1.450	2.569	1.937
Density SD ID	0.280	0.222	0.574	1.122	0.737	0.530	1.245	0.907
Density MIN ID	0.021	0.049	0.072	0.364	0.296	0.889	1.051	0.122
Density MAX ID	1.697	1.273	3.857	4.197	2.581	3.200	6.121	4.909
Density AVG T	0.347	0.286	0.724	4.961	2.214	2.619	4.002	3.166
Density SD T	0.347	0.231	0.781	2.414	1.099	0.682	1.820	1.736
Density MIN T	0.021	0.074	0.120	0.939	0.296	1.370	1.729	0.245
Density MAX T	2.000	1.273	5.286	9.056	2.581	3.980	9.911	9.818

Total ID = number from counts after distribution of bins. Percent IDed is percent of specimens assignable to a species after the distribution process. Estimated total examined is calculated by multiplying average density of identified specimens by total sample area. Counted area is total slab area counted (in cm^2), except samples indicated with a superscript '1', where a small number of the counted slabs were misplaced between counting and area measurements; for these samples, all density calculations use only data from measured slabs. Density AVG is average sample density, calculated as specimens/area, using both IDed specimens (ID) and total specimens, excluding siculae (T), and presented as specimens per cm^2. SD, MIN, and MAX = standard deviation, minimum and maximum specimens per slab, and are calculated for both identified specimens (ID) and total specimens excluding siculae (T).

To test for adequacy of sample size, rarefaction analysis was conducted using the paleontological statistics software package, PAST (Paleontological STatistics- Hammer et al. 2007). Rarefaction is a statistical technique developed by Sanders (1968) that provides an estimate of the effect of sampling on apparent species richness. Rarefaction curves are created by resampling fractions of an existing sample, and observing the number of species captured during each resampling effort. The results of the resampling runs are plotted as curves (see Appendix D), comprising a central red line, representing the average of resampling attempts at a particular sample size, and upper and lower blue lines, representing the 95% confidence interval. The curve of the line is an indication of sampling completeness: the degree to which a curve approaches a plateau indicates the likelihood that a larger sample size would change species abundance (plateaued samples are likely reasonably complete). Analysis was conducted on the counted material after the unassigned bins were redistributed. Uncounted material was not included in the analysis, but provided a test of the projection of the rarefaction analysis (Table 3.3).

With the exception of the combined sample 5.3/5.5 m and sample 12.67 m, rarefaction analysis either indicated sampling was already complete as a result of the counting process or additional non-counted material existed to supplement the count (up to three times the counted surface area). Thus, the total number of recovered species (count plus scans) likely represents a close approximation of actual species abundance preserved at each sampled time interval at the Blackstone River. One caveat

with the rarefaction analysis is that because it was run on the count of specimens after distribution of questionable specimens into species bins, it is likely to have been performed with a lower than actual number of rare taxa and inflated abundances of common taxa, in some cases. This is because some of the fragments that were assigned to identified species may actually have represented taxa not encountered in the count, since the binning procedure only assigned questionable specimens to species bins that had been confidently identified in that sample.

For example, in sample 8.8 m *Styracograptus tatianae* is not recorded, but there were 17 specimens in the catagory "climacograptid thecae <1.5 mm." These specimens were all assigned to *A. supernus*, since it is abundant in the sample, but it is possible that some of these may have been *Styracograptus tatianae* since that species occurs in both higher and lower samples. The impact of this is likely to be minimal, however, for two reasons: 1. most of the potentially missed species are sufficiently different from identified species that they are likely to have been identified even as fragments, and 2. most of the potentially confusable/accidently binned species already co-occur in samples.

Table 3.3. Sampling completeness.

Level	Specimens counted	# Taxa (count)	ScaN.?	# Taxa (scan)	Rarefaction completeness
0.1 m	712	10	N	NA	C
0.17 m	248	6	N	NA	C
1.3 m	1556	12	N	NA	C
5.3 + 5.5 m	993	9	N	NA	M
8.8 m	966	12	N	NA	C
12.67 m	123	14	N	NA	M
14.15 m	1861	9	Y	+3 (4)	I
15.65 m	1629	15	Y	0	M
16.03 m	1632	16	Y	+1	I
17.20 m	1368	11	Y	+4 (5)	M
18.06 m	3072	11	Y	+1	M
18.84 m	2025	14	Y	0	M
19.0 m	884	15	Y	0	C
19.05 m	364	6	Y	0	C
19.10 m	306	7	Y	0	M
19.15 m	720	7	Y	0	I
19.20 m	865	6	Y	0	I
19.25 m	329	5	Y	0	I

Columns show, from left: Total specimens counted, number of taxa recovered during count, whether additional uncounted material remained that was scanned for species, number of additional species recovered during scan of uncounted material (numbers in brackets are questionable IDs), and completeness of sampling indicated by rarefaction curve (where C= complete, i.e., flat line; M = moderate, i.e., near flat line; and I = incomplete = line at substantial angle).

3.3 Illustration and Descriptions

The specimens described in this study occur mostly as compressed silver films on black to grey shales, mudstones, and siltstones (see Appendix A for detailed sample descriptions), although samples from the *extraordinarus* Zone contain rare specimens preserved in relief (internal molds) and the basal *ascensus* Zone collection contains high-contrast black specimens on pale weathered siltstone. There is little evidence of any alteration or deformation in most samples (see discussion at end of this section and Appendix A). In general, preservation of the external features of specimens is excellent, however, especially with species possessing thick-walled rhabdosomes, internal features are often obscured, e.g., sicular length, dicalycal level, etc. The large number of slabs collected at each level, combined with infield efforts to collect large slabs where possible, means that the present collections contain many more complete mature rhabodosomes than many collections in previously published studies. This, and possibly the very extensive mechanical excavation of specimens that occurred during this thesis, often resulted in the present collections yielding larger rhabdomsomal lengths, DVW, and longer virgellae and nemata, than other descriptions of the same species from different areas.

Material from the Blackstone River section can be challenging to study, and particularly to measure or illustrate, due to the lack of contrast between specimens and slabs. Over the course of this project, several techniques were developed to deal with low degree of the contrast between the specimens and matrix. First, the use of

overhead illumination (a ring light) greatly increases visibility, and is highly recommended for any future investigation. Second, material is best viewed either wet or immediately after the wetting liquid has evaporated. For wetting, either straight ethanol or a 50/50 mix of ethanol and water produced the best results, with the fast evaporation of the former proving most useful when counting, or in other situations where rapid switching between wet and dry conditions is useful, and the latter best where longer periods of wetting are required, e.g, measuring or illustration. Many samples are best viewed immediately after the surface wetting liquid has evaporated, but before the liquid absorbed into the matrix has evaporated. This state optimizes contrast, and in some collections it is the only way that details of specimens can be seen.

When scanning slabs, the entire slab can be wetted with ethanol or an ethanol solution, and then dabbed dry. This process causes no damage to specimens in most horizons. When a single specimen is viewed or photographed, requiring it to be located and the focus to be precisely adjusted, wetting and dabbing the entire slab is impractical. As the light-source is much closer, the period of optimum wetness is extremely brief at the high-magnification required for illustration and measurement (often only a few seconds), relative to the period required for the majority of the liquid to evaporate after each wetting (often a period of minutes), making illustrating or studying specimens in this state highly inefficient. Two techniques were developed to deal with this. A very small portion of ethanol or ethanol/water soaked sponge can be

used to lightly dab the specimen. This deposits only a very small amount of liquid, wetting the matrix without leaving an excess of liquid that requires evaporation. This method provides only a few seconds of wetting, but also requires only a few seconds between each wetting. Alternately, slabs may be soaked in water for a period of minutes or hours, and then removed and dabbed dry. This is time-consuming in preparation, but produces a much longer period of optimum contrast, which can be useful in photography. In general, the present material is very robust and is not damaged by the processes described above.

Specimens were illustrated principally as digital photomicrograph and camera lucida illustrations, but limited use was also made of infrared photography and scanning electron micrography. Over the course of this thesis, reflected light photographs of material were taken with a number of microscopes and cameras (while examining collections at other institutions), but two instruments were principally used: Nikon SMZ-U microscope with a Nikon DS-5Mc camera system and a Nikon SMZ-10 microscope and Celestron 44421 eyepiece digital imager. All camera lucida illustrations were produced using the latter microscope. To produce high-resolution images of complete rhabdosomes, images of most specimens were produced as digital composites of many high magnification images. A series of individual photographs along the rhabdosomal axis were taken at a photographic resolution of 1280x960. Magnification differed depending on the size of the specimen and the difficulty creating optimum photographic conditions (e.g., in some samples, changes in contrast with drying meant that if

photography continued for more than a brief interval, the image compositing software would not recognize the material as a series, therefore a few, lower magnification images were taken), but was mostly adjusted so that the distal width of the specimen filled at least half of the camera's field of view.

Digital composites were produced using Microsoft's Image Composite Editor, ICE, (numerous iterations of the software were used over the course of the project, up to and including V.2.0.3.0 (2015)). The stitching algorithm in ICE was set so that only planar motion of images was allowed. This ensured that both relative size and angles were of specimens were preserved. Scales were produced for the images in one of two ways. The software associated with the DS-5Mc camera allows a digital scale to be inserted into the image during photography. This imbedded image was preserved during compositing. With the Celestron 44421, images were taken of a microscope calibration scale at the same magnification used for a particular photograph. The image of this scale was then manually inserted into the resulting composite using Adobe Photoshop (version CS2). In both cases, scaling of images was accomplished by measuring the resulting photographic scale in pixels, and then adjusting the image size in Photoshop until 1 mm equaled the desired level of magnification given the resolution of the plates. This usually involved a reduction in size to 25-33% of the original composite image.

This process of manually measuring and adjusting image scales inevitably resulted in some error. To quantify the degree of error, the total length of the rhabdosome of several specimens were measured using an eyepiece micrometer and

compared to the calculated length of those specimens from scaled digital composite photographs. In all examined cases, the difference between these two measurements was ≤3%, which was considered an acceptable level of error. After scaling, digital composite images were retouched in Photoshop to remove superfluous material from composite images and improve image quality. Original photographs were taken in full colour, but colour information was removed for most plates, except where it was necessary to clearly distinguish features. Visual artifacts surrounding the illustrated specimen, e.g., reflection from the wetting fluid, preparation marks, etc., were digitally removed by either cutting and pasting of surrounding matrix (earlier images) or using Photoshop's clone stamp tool (later images). Images of the specimens themselves were altered only to increase or decrease contrast, brightness, and or light levels (in most cases, contrast was substantially increased and brightness decreased), except in rare cases where the burn tool was used to increase the visibility of hard to see features, e.g., spines, or to darken sections of the rhabdosome that showed a gradient of brightness. No other manipulation of the images took place, and original, unaltered copies of the images were retained for reference in all cases.

Camera lucida images were prepared using a Nikon SMZ-10 microscope. Images were drawn at high magnification (mostly ca. 35x), resulting in originals over a metre long in some cases. Some minor distortion of images occurred during illustration owing to spherical aberration or slabs not being completely level, but this was minimized by only illustrating the middle portion of the field of view and then moving the specimen. A

scale was drawn directly onto the image using an eyepiece micrometer. Since physically drawing a scale results in some error, two versions of a scale were drawn on each image; where they disagreed, a mean of the two was used. All drawings were inked at large scale, and then reduced to approximately 10x magnification using a photocopier. Where illustrations were too large to fit on the bed of a photocopier, they were reduced in portions onto several sheets of paper. The portions were then either scanned individually and aligned using ICE, or they were physically cut and pasted together (using a lightbox to ensure alignment of images) to create a composite and then scanned.

Scanned images were processed in Photoshop in the same way as specimen photographs, with the exception that the scale bar produced was in some cases based on an average value of the two scale bars drawn on the image (e.g., where slight differences in length resulted from the width of the pencil lead). Since error can be introduced at a greater number of points in the production of camera lucida images, measurements should be considered more accurate on plates. However, the scale of several random specimens in final illustrations was compared with original micrometer measurements and found to be agree within 2% of each other. In several cases, drawings from other authors were reproduced for comparison with material described in this study. Scale bars were produced based on stated levels of magnification in the original publication.

Species assignments were made by comparing the large collection of material present with published material, as well as to unpublished material graciously provided

by Petr Štorch and Charles Mitchell (and their co-authors) and Fan Jun-Xuan (and co-authors). Where corresponding descriptions were not available in English, they were either checked with colleagues (Chinese language publications) or scanned and translated using online image to text recognition and translation software, e.g., i2OCR, and translated using Google Translate (Russian language publications). Illustrations played a large role in taxonomic decisions. Comparing side-by-side scaled specimens in plates and text-figs allowed subtle differences or similarities between taxa to be seen. To this end, nearly 1000 individual specimens were illustrated as either composite photographs or camera lucida drawings. For comparison with previously published works, plates or figures from those publications were scanned, scaled, and presented side by side with material from the Blackstone River site. Where possible, original material was also examined. This included the figured material previously collected from the Blackstone River site and surrounding areas (Lenz and McCracken, 1982), which was examined in the Geological Survey of Canada types collections in Ottawa; material illustrated in Štorch et al. (2011) from Nevada, which was examined on several occasions at the State University of New York, Buffalo; material from Dob's Linn, Scotland, Williams (1982, 1983), along with additional material from Dob's Linn collected during an earlier part of this thesis; and material described in Mu et al. (1993), as well as in other Chinese publication, which was examined at the Nanjing Institute of Geology and Palaeontology (NIGP).

Original comparative measurements were made of type and other illustrated material from China while at the NIGP. These were supplemented with additional measurements of Chinese, Nevada, and other material, including a wide variety of types, that were provided by Charles Mitchell. These metrical data were compared with a large data set prepared as part of this thesis: detailed width, thecal spacing, and other measurements on over 2000 individual specimens. The gradations of the eyepiece micrometer used for gathering most of the data in this thesis provided a resolution of 0.025 mm, e.g., 1.025 mm, 1.050 mm, and 1.075 mm. Reported measurements were then rounded to the nearest 1/100 mm, e.g., 1.03 mm, 1.05 mm, and 1.08 mm, to better represent actual measurement resolution. Metrical data were analyzed using bivariate scatter plots and plots of changing dimensions along the rhabdosome in a collection of specimens. The principal features used for quantitative analysis were dorsal ventral width (DVW) and thecal spacing (measured as two thecae repeat distance—2TRD; Howe, 1983), as well as axial width (in *Dicellograptus*). Axial angle was measured in a large collection of dicellograptids, but varied strongly as a result of flattening, and so was only used as a second order criterion. Other morphological features were used for comparative purposes qualitatively (e.g., spine present or absent) or semi-quantitatively (e.g., 'strongly inclined' vs. 'weakly inclined'). Figure 6.1 illustrates features measured as part of this thesis.

Given that so many features used in graptolite identification are strongly affected by strain, close attention was paid for evidence of it. Observations of features

that might indicate deformation were made during field collecting, e.g., lateral changes in bed thickness, faulting, and changes in the symmetry of macrofossils, and samples that were highlighted as potentially deformed were examined with particular caution. At extremes, deformation manifests in obvious changes to the symmetry of features such as aperture excavation in specimens oblique to the strain axis. Deformation can be far subtler, however, and can result in bimodal distributions of population-level quantitative measurements without any obvious changes in individual specimens.

To test for the presence of this cryptic deformation, specimens of the same species were sought out at right angles to each other and checked for inverted length-width ratios wherever possible. Additionally, species that are known to show relatively little variation in morphometrical features (e.g., proximal width and 2TRD in *A. supernus*) were monitored continually during counts and scans (even where measurement data were not formally recorded) for departures from expected dimensions. [Note: this is how *Apendispinograptus pogrebovi,* which has 2TRD intermediate between that *A. supernus* and *A. leptothecalis*, was first noticed.] See Appendix A for discussion of samples showing evidence of deformation. In addition to strain, compaction can strongly alter the dimensions and apparent thecal morphology of graptolites (see, for example Williams, 1981). Since, with only rare exceptions, specimens in the present samples were uniformly flattened, the degree of compaction had little effect on within sample comparisons of measurements of width. To avoid

effects on thecal morphology, where possible specimens were compared in profile orientation.

3.4 Biotope Assignment and Environmental Inferences

Chapter 5 discusses diversity and community changes relative to inferred shifts in environmental conditions, particularly water depth and deep-water oxygen levels/the presence of a well-developed denitrification zone. Interpretation of overall depositional environment and shifts in water depth corresponding to inferred glacial ice volume changes were based upon observation of gross lithological characteristics and the presence of accessory fauna, with geochemical (Nd) and graptolite community data supporting sedimentological interpretations.

Strata in the Blackstone River section are interpreted to be of moderate depth (outer shelf to slope), principally deposited under anoxic or dysoxic conditions, based on the following: 1. The presence of generally featureless, unbioturbated dark grey to black shales or calcareous mudstones during the inferred pre- and post-glacial interval. 2. Only intermittent appearance of benthic fauna (rare trilobites and brachiopods, presumably associated with the periodic spread of oxygenated bottom waters or short-lived sea-level fluctuations), and an absence of rich shelly beds or corals during the pre- and post-glacial interval. 3. A clear upward shift to thickly-bedded limestones, along with the appearance of a diverse, if mostly fragmentary benthic fauna, including corals, during the inferred glacial lowstand. 4. The presence of ripples, which appear to be symmetrical, at some levels within the glacial interval, suggesting that deposition

occurred above storm wave base, but absence of any evidence of exposure and subaerial erosion. Given the estimated 70-100 m sea-level fall during glacial maximum (Brenchley et al., 1994), a pre-glacial water depth in excess of 120 m is required to explain this set of observations. This inference is also supported by comparison with two well-studied sections in Nevada. In contrast with the Blackstone River, the Monitor Range section, interpreted to have been deposited in an outer platform setting (Finney et al., 1999; Laporte et al., 2009; Štorch et al., 2011), is non-graptolitic throughout the Hirnantian, and shifts to a rippled sandstone lithology, with an accompanying erosional disconformity, during the lowstand; Vinini Creek is episodically graptolitic throughout the Hirnantian, with short-lived deepening intervals reflected in the deposition of brown mudstones.

Assignment of species to biotopes (epipelagic vs. mesopelagic) was conducted using statistical methods developed by David Sheets (Canisius College, NY) and reported in Sheets et al. (2016). By comparing occurrence data for graptolites species at a number of international sections to published lithofacies data, Sheets et al. (2016) were able to estimate posterior probabilities that species inhabited either a deep or shallow water habitat using a Bayesian technique (see Supporting Information in Sheets et al., 2016 for a detailed discussion of methodology). Only species that could be assigned to a biotope with a 90% confidence were included in the analysis (ca. 50% of species occurring in the Katian to lower Hirnantian strata at the Blackstone River section). The Blackstone River abundance data were not included in the initial biotope assignments.

Because of this, the biotope affiliation of Blackstone River graptolite communities became an additional test of environmental interpretations. Since the Blackstone River section was inferred to be moderate depth, it was predicted to host communities with a stronger epipelagic dominance signal than the relatively deeper water section at Vinini Creek. This was found to be the case (Sheets et al., 2016). Neodymium isotope data were used to support sedimentological interpretations of changes in water depth, as well as to infer smaller shifts in sea level not reflected in lithology. The neodymium proxy is based upon an observed shoreward gradient in εNd values in modern environments, resulting from differing Nd sources in coastal vs. open ocean waters (weathering of continental rocks vs. island arcs, respectively) (Fanton et al., 2002; Homden et al., 2013). This gradient was hypothesized to also be present along the margin of Laurentia during Ordovician and Silurian. That hypothesis was supported by both within-section shifts towards a continental Nd signature during the Hirnantian glacial interval, as well as a gradient of values between the Monitor Range, Vinini Creek, and Blackstone River sections that matched their inferred depositional environments/positions relative to the coastline (Holmden et al., 2013). In addition to matching overall depositional environments and lithologically indicated shifts in water depth associated with the Hirnantian glacial interval, Nd values also correspond to changes in the dominance patterns of epipelagic and mesopelagic species (Fig. 5.10; see also discussion in Sheets et al., 2013). Since biotope assignments were made using only sedimentological characteristics of comparative sections, without input from

geochemical data, this correlation of community dominance and Nd-values cross-validates both.

The inferred sea level shift at the Ordovician-Silurian boundary (see Chapter 5.3) does not have biotope support, as biotope assignments were only made for Katian and lower Hirnantian species by Sheets et al. (2016). Instead, change in sea level is principally supported by changes in lithology, i.e., a shift from black shales to tan siltstones at the boundary, and lighter-coloured shales in the immediately overlying strata. The relationship between black shale deposition and greater water depths/better developed denitrification zones is supported by nitrogen isotope data from sections in Arctic Canada, Nevada, Anticosti Island, and the Prague Basin (see original data and review in Melchin et al., 2013). Nd data provide additional evidence; lithological interpretations of sea level were made independent of that data. In fact, sea level fall was inferred before neodymium data were provided by Holmden (pers. comm.).

Chapter 4. Biostratigraphy and Correlation

4.1 Blackstone River Biostratigraphy

Large, high-diversity collections and detailed field sampling enable high-confidence identification of biostratigraphic zones (seven zones, plus one subzone[9]) and correlation with international sections, especially sections in Nevada, where zonation and systematics were recently conducted in tandem with this thesis (with data and observations mutually exchanged). Correlation with sites in Jordan, Arctic Canada, Scotland, South China (Yangtze Platform), Southern Kazakhstan, Northeastern Siberia, Peri-Gondwanan Europe, Sweden, and Alaska are also discussed below. Over the course of this thesis, all slabs from all levels were examined multiple times, but the intensity and purpose of examination differed between stratigraphic levels, producing differing degrees of confidence in range and biodiversity estimates. All samples from the *ornatus* to *extraordinarius* zones were counted, and underwent a final slab-by-slab rescan after systematics were completed, resulting in very high range confidence (Fig. 4.1). The *persculptus* Zone samples were not counted, but underwent a slab-by-slab rescan once systematics were complete, resulting in high range confidence (Fig. 4.2). For the *acuminatus* and *ascensus* zones (Fig. 4.3), although all slabs were examined multiple times during the thesis, due to time constraints only slabs that had been pulled for systematic work (ca. 25-75% of each sample, depending on level), and those from the

[9] The location of samples relative to lithological divisions and biozones is presented in Fig. 2.3.

upper *acuminatus* Zone, were rescanned after systematic work was completed. As a result, some of the ranges presented for the *ascensus* and *acuminatus* zones are likely incomplete. Confidence varies between species, as index taxa or potential index taxa (e.g., *A. ascensus, P. acuminatus, C. vesiculosus*, species of *Hirsutograptus*, monograptids) were specifically targeted with multiple scans at various points in this thesis. Large or otherwise easily diagnosed species (e.g., *Neodiplograptus* sp. 1, *Korenograptus* sp. 2, *Paramplexograptus kiliani*) are also much less likely to have been missed than species that require metrical assessment (normalograptids). The species *Normalograptus mirnyensis* was used a catch-all bin for small unassignable normalograptids. It questionably occurs from the *persculptus* Zone to the top of the section; its range is not described in detail below.

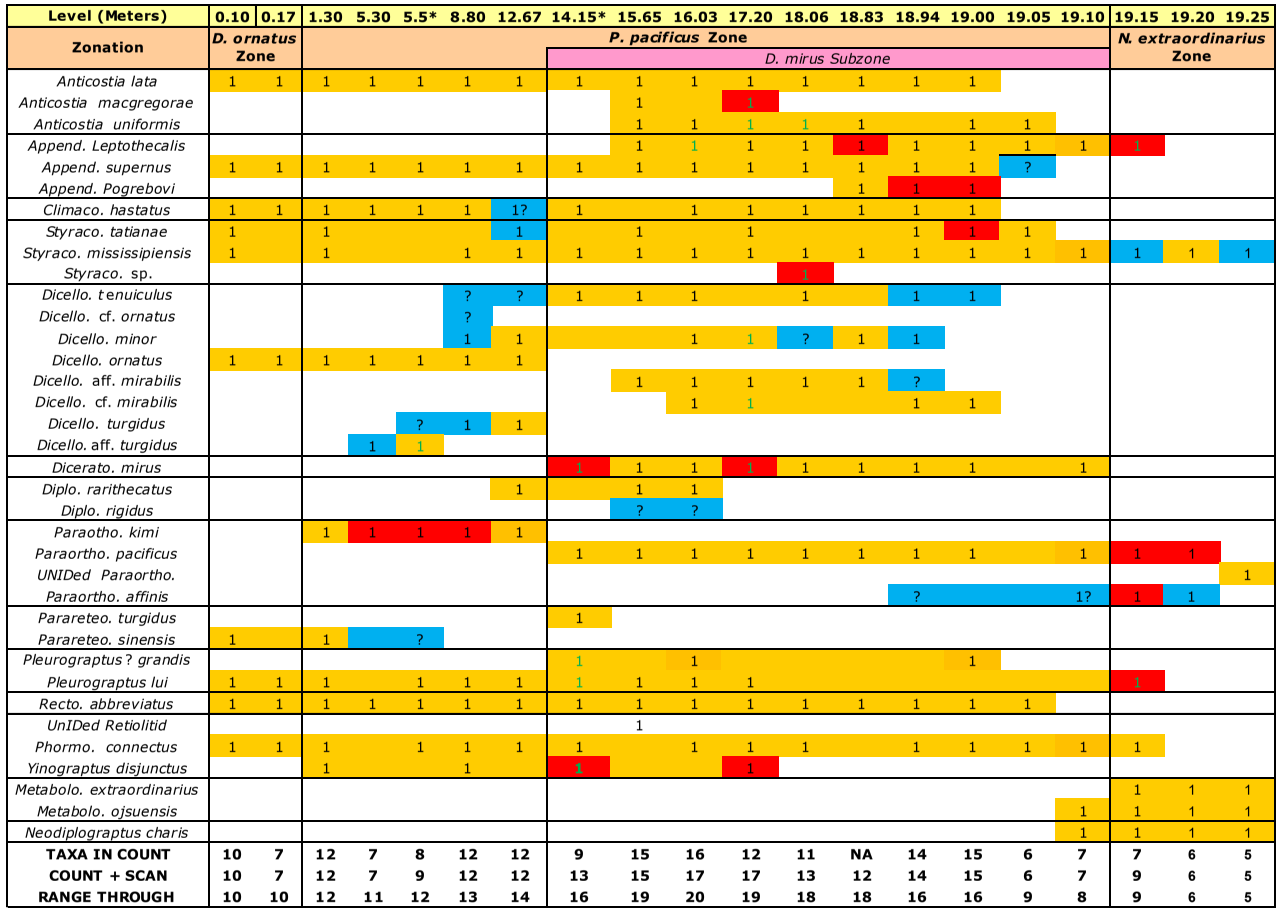

Level (Meters)	0.10	0.17	1.30	5.30	5.5*	8.80	12.67	14.15*	15.65	16.03	17.20	18.06	18.83	18.94	19.00	19.05	19.10	19.15	19.20	19.25
Zonation	*D. ornatus* Zone		*P. pacificus* Zone															*N. extraordinarius* Zone		
								D. mirus Subzone												
Anticostia lata	1	1	1	1	1	1	1	1	1	1	1	1	1	1	1					
Anticostia macgregorae									1		1									
Anticostia uniformis									1	1	1	1	1		1	1				
Append. Leptothecalis									1	1	1	1	1	1	1	1	1	1		
Append. supernus	1	1	1	1	1	1	1	1	1	1	1	1	1	1	1	?				
Append. Pogrebovi													1	1	1					
Climaco. hastatus	1	1	1	1	1	1	1?	1		1	1	1	1	1	1					
Styraco. tatianae	1		1				1		1		1			1	1	1				
Styraco. mississipiensis	1		1			1	1	1	1	1	1	1	1	1	1	1	1	1	1	1
Styraco. sp.												1								
Dicello. tenuiculus						?	?	1	1	1		1		1	1					
Dicello. cf. ornatus						?														
Dicello. minor						1	1			1	1	?	1	1						
Dicello. ornatus	1	1	1	1	1	1	1													
Dicello. aff. mirabilis									1	1	1	1	1	?						
Dicello. cf. mirabilis										1	1			1	1					
Dicello. turgidus					?	1	1													
Dicello. aff. turgidus				1	1															
Dicerato. mirus								1	1	1	1	1	1	1	1		1			
Diplo. rarithecatus							1		1	1										
Diplo. rigidus									?	?										
Paraotho. kimi			1	1	1	1	1													
Paraortho. pacificus								1	1	1	1	1	1	1	1		1	1	1	
UNIDed Paraortho.																				1
Paraortho. affinis														?			1?	1	1	
Pararetteo. turgidus								1												
Pararetteo. sinensis	1		1		?															
Pleurograptus? grandis								1		1					1					
Pleurograptus lui	1	1	1		1	1	1	1	1	1	1							1		
Recto. abbreviatus	1	1	1	1	1	1	1	1	1	1	1	1	1	1	1	1				
UnIDed Retiolitid									1											
Phormo. connectus	1	1	1		1	1	1	1		1	1	1		1	1	1	1	1		
Yinograptus disjunctus			1			1		1			1									
Metabolo. extraordinarius																		1	1	1
Metabolo. ojsuensis																	1	1	1	1
Neodiplograptus charis																	1	1	1	1
TAXA IN COUNT	10	7	12	7	8	12	12	9	15	16	12	11	NA	14	15	6	7	7	6	5
COUNT + SCAN	10	7	12	7	9	12	12	13	15	17	17	13	12	14	15	6	7	9	6	5
RANGE THROUGH	10	10	12	11	12	13	14	16	19	20	19	18	18	16	16	9	8	9	6	5

Confirmed range (specimens that are confirmed as belonging to a taxon)

Possible range (specimens that have been provisionally or questionably assigned to a taxon)

New occurance data 2014 (includes new material from split slabs and reassigned specimens)

1 Confirmed presence (green text = present in scan)

* Samples with additional material added from targeted collection

0.83 m = lowest confirmed Paraorthograptus specimen in the field.

Figure 4.1. D. ornatus Zone to M. extraordinarius Zone ranges

Dicellograptus ornatus Biozone

The *Dicellograptus ornatus* Zone is defined as the interval between the first appearance of *Dicellograptus ornatus* and the first appearance of *Paraorthograptus pacificus* (Štorch et al., 2011). Two samples collected during this thesis are assigned to the upper part of the *ornatus* Zone, since they occur just below the first appearance of *Paraorthograptus* (0.66 m and 0.82 m below, respectively). The total thickness of the *ornatus* Zone at the Blackstone River section is not known, but Lenz and McCracken (1982) recorded three graptolite collections from the *ornatus* Zone at the Blackstone River spanning an interval of ca. 12 m (measurement made by hand from their fig. 2). Ten and seven taxa were recovered from the two *ornatus* Zone samples (Fig. 4.1). The most abundant species are *Appendispinograptus supernus, Styracograptus mississippiensis, Styracograptus tatianae, Rectograptus abbreviatus, Anticostia lata*, and *Climacograptus hastatus. Dicellograptus ornatus, Pleurograptus lui, Phormograptus connectus, Parareteograptus sinensis,* also occur, but never as more than 3% of the population in either sample. All these taxa range into at least the lower *pacificus* Zone. Over the course of this study, material was examined that had been collected from the *ornatus* Zone at the Blackstone River and two nearby localities (Pat Lake and Peel River) that had been described and illustrated in Lenz and McCracken (1982). Those specimens were similar to the material collected for this thesis, with the exception that *Anticostia fastigata* occurs at the Peel River section (a specimen occurs on the same slab as an an illustrated specimen of *D. ornatus*: fig. 3b) and many specimens of *A. supernus*

possessed parasicular thickening of the spines, a feature that is very rare in material from the studied interval at the Blackstone River (see Chapter 7). The specimen assigned to *Glyptograptus tenuissmus* by Lenz and McCracken (1982: fig. 3h) is identified here as a specimen of *Diplograptus*, and the specimen they assigned to *Climacograptus hvalross* (their fig. 3m) is most likely *A. supernus.*

Paraorthograptus pacificus Biozone

The *pacificus* Zone is generally defined as the interval between the first appearance of *Paraorthograptus pacificus* and the first appearance of *Metabolograptus extraordinarius* (Štorch et al., 2011). The base of the *pacificus* Zone in this thesis isplaced at the first appearance of *Paraorthograptus,* specifically material assigned to *Paraorthograptus kimi,* not the material assigned here to *Paraorthograptus pacificus. Pacificograptus kimi* (=*Paraorthograptus*) was erected by Koren' (1979), but has not found widespread usage. The distinction between these two taxa is supported by the large data set of measurements produced for this thesis (see *Paraorthograptus* in Chapter 6.1), and the stratigraphic order of appearance is consistent with that described by Koren' (1979) and Koren' et al. (1979). The types of *Paraorthograptus pacificus* are strongly deformed, making comparison with both the present material and material from other regions difficult. Additionally, authors of regional biostratigraphic papers have tended towards synonymizing all or a large number of previously erected species of *Paraorthograptus* into *P. pacificus* (e.g., Scotland: Williams, 1982; Arctic Canada: Melchin, 1987a; Nevada: Štorch et al., 2011; South China: Chen et al., 2000—although

Chen et al. recognized an unassigned species of *Paraorthograptus* in the *ornatus* Zone), with the effect that the base of the *pacificus* Zone internationally is functionally the first appearance of *Paraorthograptus.* In addition to *Paraorthograptus kimi, Yinograptus disjunctus* makes its first appearance in the lowest parts of the *pacificus* Zone, and *Dicellograptus minor, Dicellograptus* aff. *turgidus, Dicellograptus turgidus, Diplograptus rarithecatus* and questionably *Dicellograptus tenuiculus* all appear below the *mirus* Subzone (Fig. 4.1). All of the species that were present in the *ornatus* Zone continue through the lower *pacificus* Zone, with the exception of *Dicellograptus ornatus* itself, and *Parareteograptus sinensis,* which is only confidently identified in the lowest *pacificus* Zone sample. Per sample diversity is modestly higher in the lower *pacificus* Zone than in the *ornatus* Zone, with nine to 12 species recovered per sample.

Diceratograptus mirus Subzone

Diceratograptus mirus was recognized at the Peel River section in the Yukon by Chen and Lenz (1984), but not at the Blackstone River. In the current Blackstone River collections, it is present as a minor component of all collections between 14.15 m and the level of first appearance of *Metabolograptus extraordinarius* (19.15 m), an interval of consistent black shales and calcareous shales (Fig. 4.1). A specimen recovered from 12.67 m and assigned questionably to *D. turgidus* could possibly be *D. mirus* or a transitional form, but the first confident identification of the species is 14.15 m. The more robust form of *Paraorthograptus*, assigned here to *P. pacificus*, also makes its first appearance at the base of the *mirus* Subzone, as does *Parareteograptus turgidus,* which

is restricted to the basal *mirus* collection, and *Pleurograptus*? g*randis. Dicellograptus tenuiculus* makes its first certain appearance at the base of the subzone. *Anticostia macgregorae, Anticostia uniformis, Appendispinograptus leptothecalis, Dicellograptus* aff. *mirabilis, Dicellograptus* cf. *mirabilis,* and "*Diplograptus rigidus"* [10], also appear in the lower half of the *mirus* Subzone. In addition to *Parareteograptus turgidus* and "*Diplograptus rigidus",* which are restricted to the lower *mirus* Subzone, *Yinograptus disjunctus, Diplograptus rarithecatus,* and *Anticostia macgregorae* make their last appearance in this interval. The upper half of the *mirus* Subzone is marked by the appearance of several distinctive taxa: progressively from 18.06 m, *Styracograptus* sp., *Appendispinograptus pogrebovi,* questionably *Paraorthograptus affinis* (Chapter 6 for discussion of range), and most significantly, in the highest *mirus* Subzone sample, *Neodiplograptus charis* and *Metabolograptus ojsuensis* (Fig. 4.1). This represents the first appearance of neograptine species in the section. Diversity reaches its apex in the lower and middle part of the subzone, with per-sample recovered taxa peaking at 16 species at 16.03 m and range-through counts of 19 to 20 taxa from 15.65 m to 17.20 m. Species diversity declines from 17.20 m upward, with *Anticostia lata, Anticostia uniformis, Appendispinograptus supernus, Appendispinograptus pogrebovi, Climacograptus hastatus, Styracograptus tatianae, Styracograptus* sp., *Dicellograptus tenuiculus, Dicellograptus minor, Dicellograptus* aff. *mirabilis, Dicellograptus* cf.

[10] All specimens of *Diplograptus* are included within *D. rarithecatus* in Chapter 6 and in the 'preferred' category in range and extinction/origination curves, but *D. rigidus* is considered a separate species in Sheets et al. (2016) to ensure data compatibility with the Nevada count data.

mirabilis, Diceratograptus mirus, Pleurograptus? g*randis,* and *Rectograptus abbreviatus* all making their final appearances in the upper *mirus* Subzone (only six and seven taxa were recovered in the uppermost two *mirus* Subzone samples) (Fig. 4.1). In addition to the loss of diversity and the appearance of neograptine species, the uppermost *mirus* samples (highest ca. 15 cm) are distinctive in that they contain abundant small phosphatic brachiopods, which can be more numerous than graptolites in some horizons.

Metabolograptus extraordinarius Zone

The *extraordinarius* Zone is defined by the first appearance of *M. extraordinarius* (Štorch et al., 2011). The transition across the basal boundary of the *extraordinarius* Zone was studied at 5 cm resolution at the Blackstone River (Fig. 2.3[11]). *Metabolograptus extraordinarius* first occurs at 19.15 m, 5 cm above the first appearance of *M. ojsuensis* and *Neo. charis. Metabolograptus extraordinarius* is either the most or second-most abundant taxon in the three *extraordinarius* Zone samples, alternating with *M. ojsuensis* in dominance (Appendix B). In addition to the two species of *Metabolograptus* and *Neodiplogratus charis, Appendispinograptus leptothecalis, Paraorthograptus pacificus, Paraorthograptus affinis, Pleurograptus lui,* and *Phormograptus connectus* occur as minor components of at least one sample (Fig. 4.1).

[11] Individual samples for the high-resolution section cannot be shown at the scale of the stratigraphic column. Instead, the position of all the latest *mirus* Subzone samples are represented collectively with a grey arrow.

The graptolitic interval of the *extraordinarius* Zone is only 15 cm thick, above which there is an abrupt transition to massive limestone. Carbonate-rich rocks continue until a return to graptolitic black shales belonging to the *persculptus* Zone, but the correlation with the *extraordinarius* Zone in the non-graptolitic strata is supported chemostratigraphically (see LaPorte et al., 2009 and Holmden et al., 2013). Both the graptolitic shale portion and the lowest 1 m of the overlying limestone contain abundant trilobite material, including rare articulated specimens, some up to ca. 10 cm in length.

Level (Meters)	32.84	32.97	33.37	34.11	35.15	36.3	Rhud.
Zonation	***persculptus* Zone**						
Avito. avitus	1	1	1	1	1	1	1
Glypto. ? sp 1	?	1	?	1			
Glypto. sp. 1		1	1				
Glypto. ? sp. 2			1				1
Koren. jiangxiensis		1	1	1			
Koren. laciniosus	1	1		1?			
Koren. lungmaensis	1						
Koren. sp.1	?		1	1	1	1	1
Metabolo. parvulus	1	?					
Metabolo. persculptus	1						
Metabolo. ? sp.					1	1	
Norm. aff. *mirnyensis*	1	1	1	1	?	1	1
Norm. ? *transgrediens*	1				1		
Norm. aff. *medius*	1				1		
Norm. ? *minor*	?	?	1	1	?	1?	
Norm. ? *rhizinus*		?	1	1	?		
Neo. xixiangensis		?	1	1		1?	
Neo. clavatus	?	1	1	1			
Neo. shanchongensis	1	1	1	1			
Param. aff. *madernii*		1	1	1	1	1	
Param. madernii		1	1	1	1	1	1
RAW	9	10	13	12	7	6	5
RANGE THROUGH	9	12	16	15	10	9	5

Confirmed range (specimens confirmed as belonging to a taxon)
Possible range (specimens questionably assigned to a taxon)
1 Confirmed presence (1?=likely pressence)

Figure 4.2. M. persculptus Zone ranges

Metabolograptus persculptus Zone

The *persculptus* Zone can be defined, based on graptolite data, as occurring between the first appearance of *Metabolograptus persculptus* and the first appearance of *Akidograptus ascensus* (Rong et al., 2008). This interval is represented by ca. 4 m of graptolitic rocks at the Blackstone River, beginning with a return to black shales at 32.84 m and continuing to 37 m (Fig. 2.3). The base of the *persculptus* Zone is placed lower, however, at approximately 28.5 m, based upon chemostratigraphic correlation with biostratigraphically constrained neodymium and carbon isotope excursions at Vinini Creek (see Laporte et al., 2009; Holmden et al., 2013). This level appears to correspond to a brief interval of deepening at Blackstone River, and possibly at Vinini Creek. Immediately below the return to black shales is a ca. 3 cm thick orange siltstone bed that contains fragmentary shelly material: brachiopods and trilobite fragments tentatively identified as species of *Flexicalymene, Mucronaspis,* and *Odontopleura* or *Anacaenaspis* (Appendix E). This layer also contains very rare fragmentary specimens of unidentifiable neograptine graptolites. The lowest collection containing identifiable graptolites from the *persculptus* Zone contains *Avitograptus avitus, Korenograptus laciniosus, Korenograptus lungmaensis, Metabolograptus persculptus, Metabolograptus parvulus, Normalograptus* aff. *mirnyensis, Normalograptus*? *transgrediens*, *Normalograptus* aff. *medius,* and *Neodiplograptus shanchongensis* (Fig. 4.2). Three additional species present in higher *persculptus* Zone samples are also questionably present in the lowest collection. *Metabolograptus persculptus, K. lungmaensis,* and *M.*

parvulus appear to be restricted to this basal collection. The three collections immediately above this (32.97 m, 33.37 m, and 34.11 m) contain a similar fauna, with the addition of *Glyptograptus* sp., *Glyptograptus*? sp. 1, *Glyptograptus*? sp. 2, *Korenograptus jiangxiensis, Korenograptus* sp. 1, *Normalograptus*? *minor*, *Normalograptus*? *rhizinus, Neodiplograptus xixiangensis, Paramplexograptus madernii*, and *Paramplexograptus* aff. *madernii* in some or all the samples. Samples at 35.15 m and 36.30 m, the highest *persculptus* Zone samples, are markedly different from lower *persculptus* Zone collections. A new taxon appears in 35.15 m that dominates both upper samples: *Metabolograptus*? sp. 1. In addition, diversity drops to approximately half of its peak in lower samples. Only *A. avitus, K.* sp. 1, *N.* sp. 1, *N.* aff. *medius*, *P. madernii, P.* aff. *madernii,* and *Neo. xixiangensis* (and possibly *Normalograptus*? *transgrediens and Normalograptus*? *rhizinus*) extend into the 35.15 m level, and *N.*? *transgrediens* and *N.* aff. *medius* are absent at 36.30 m (Fig. 4.2). *M. persculptus* is present only in the lowest sample at the Blackstone River section, supporting Koren' et al.'s (2003) notion of a post-*persculptus,* pre-*ascensus* interval (see discussion below).

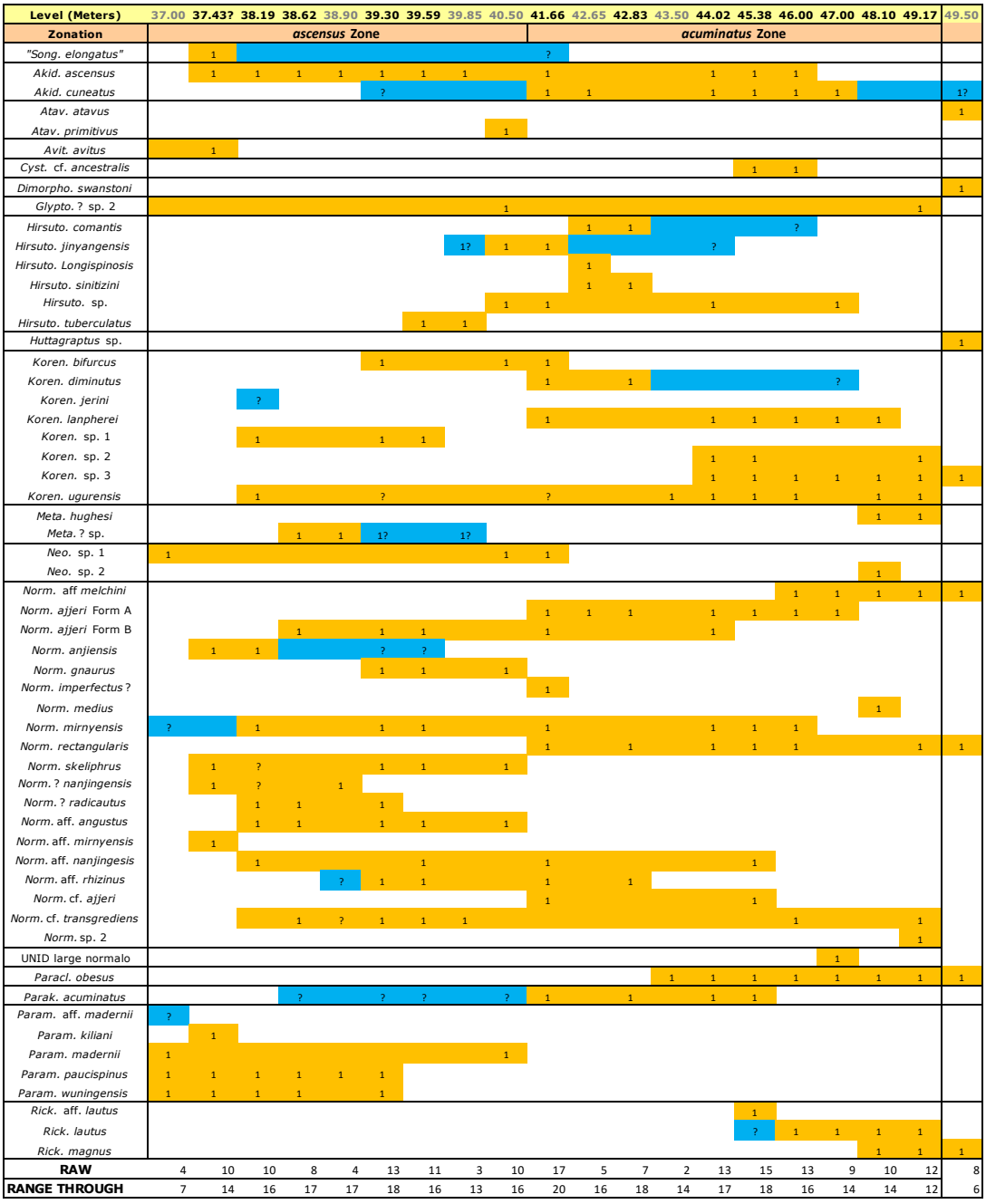

Figure 4.3. A. ascensus Zone to A. atavus Zone ranges

Akidograptus ascensus Zone

The *Akidograptus ascensus* Zone marks the base of the Silurian System and is defined by the first appearance of *A. ascensus* (Rong et al., 2008). Where the eponymous species is absent or its appearance is delayed, e.g., Arctic Canada (Melchin et al., 1991) and Uzbekistan (Koren' and Melchin, 2000), the base of the Silurian System may be recognized by the appearance of some or all of a characteristic suite of earliest Silurian species including *Normalograptus anjiensis, Paramplexograptus kiliani, P. paucispinus* and *P. wuningensis.* At the Blackstone River, the base of the *ascensus* Zone is recognized based on the occurrence of *Normalograptus anjiensis, P. paucispinus,* and *P. wuningensis,* in a small sample collected for geochemical analysis at 37 m; this sample also contains *Paramplexograptus madernii* and a specimen questionably assigned to *Neodiplograptus* sp. 1 (see description). The *ascensus* Zone is 4.66 m thick. The lowest full *ascensus* Zone collection is of somewhat uncertain position due to a labelling error in the field. It is either an amalgam of two samples from 37.03 m and 37.43 m, or entirely of one or the other; it is referred to as 37.43 m? throughout this thesis. This sample contains *A. ascensus, Normalograptus anjiensis, Paramplexograptus kiliani, P. paucispinus* and *P. wuningensis,* as well as *Normalograptus skeliphrus, N.*? *nanjingensis*, *N.*? aff. *mirnyensis, N. anjiensis, Avitograptus avitus,* and the questionable species, "*Songxigraptus elongatus*"(Fig. 4.3). Collections assigned to the *ascensus* Zone above this basal collection include a large number of distinctive new species, many of which are restricted to only one or two samples, but often occur in abundance. In addition to

the species above, the lower half of the *ascensus* Zone contains the first appearance of *Korenograptus ugurensis, Metaclimacograptus*? sp., *Normalograptus* aff. *angustus, Normalograptus ajjeri* Form B, *Normalograptus* cf. *transgrediens, Normalograptus* aff. *nanjingensis,* and questionably *Normalograptus*? *radicatus* and *Normalograptus* aff. *rhizinus.* Holdovers from the *persculptus* Zone are limited to *Avitograptus avitus, Korenograptus* sp. 1, *Glyptograptus*? sp. 2, *Paramplexograptus madernii, Normalograptus* aff. *mirnyensis,* and questionably *Paramplexograptus* aff. *Madernii* (Fig.4.3). The upper half of the *ascensus* Zone sees the appearance of *Normalograptus* cf. *bifurcus, Normalograptus gnaurus, Hirsutograptus tuberculatus, Hirsutograptus jingyangensis, Hirsutograptus* sp., and *Atavograptus primitivus,* and the confirmed appearance of *Normalograptus*? *radicatus* and *N.* aff. *Rhizinus* (Fig. 4.3). Many of these species appear just below the base of the *acuminatus* Zone and are confined to that interval. *Akidograptus cuneatus* is questionably present in the *ascensus* Zone. The species considered to be a proxy for the *ascensus* Zone (*Normalograptus anjiensis, Paramplexograptus kiliani, P. paucispinus* and *P. wuningensis*) are all restricted to the lower half of the zone, with *P. kiliani* restricted to the basal-most full collection (37.43?) m. The only *persculptus* Zone taxon to range through to the *acuminatus* Zone is *Glyptograptus*? sp. 2.

Parakidograptus acuminatus Zone

The base of the *acuminatus* Zone is marked by the first appearance of *Parakidograptus acuminatus* (Schauer, 1971). At the Blackstone River, the base is placed

at 41.66 m, the level of at which the first clearly distinct populations assignable to *Parakidograptus acuminatus* occur (Fig. 2.3). Very rare specimens that possess more inclined thecae and a greater distal width than is typical of *A. ascensus* (max DVW of 1.25 mm or slightly higher) occur lower than this level (samples 39.59 m and 40.5 m, and more questionably 39.30 m and 38.62 m). These ambiguous specimens[12] are a closer match to specimens confidently assigned to *A. ascensus,* which also reach up to 1.2 mm, than they are to later specimens of *P. acuminatus,* so they are are assigned to the former species.

It is possible that some of these borderline specimens should be assigned to *P acuminatus* and that the base of the *acuminatus* Zone has been placed too high[13]. Moving it downwards to include the questionable specimens would cause other biostratigraphic issues, however. It would shift the entire range of *Hirsutograptus tuberculatus* and *Atavograptus primitivus* into the *acuminatus* Zone, and either extend the ranges of *Paramplexograptus wuningensis* and *Paramplexograptus paucispinus* to the base of or into the *acuminatus* Zone, depending on which questionable specimens were included. At Dob's Linn, *H. tuberculatus, Atavograptus ceryx* (questionably=*A. primitivus*), and *P. paucispinus* (and possible *P. wuningensis*--pers. observ.) are all restricted to brief appearances in the middle or lower *ascensus* Zone (Williams, 1983;

[12] In the earliest Silurian strata, distinguishing between the two species is considerably more difficult than higher in the section (see discussion in description of *A. ascensus* in Chapter 6.2), where specimens of *P. acuminatus* have strongly curved rhabdosomes and steeply inclined thecae.

[13] The occurrences of questionable specimens are shown in Fig. 4.3 in the range of *P. acuminatus* with question marks.

Melchin, pers. comm.). In China, the former two species are restricted to the *ascensus* or just range into the *acuminatus* Zone (Fan et al., in prep.). Because of these inconsistencies, as well as uncertainty regarding how to classify the intermediate specimens, the base of the *acuminatus* Zone is placed at 41.66 m, where abundant, confidently identifiable specimens of *P. acuminatus* first occur (Fig. 4.3). Comparison with new material being collected in2017, by M.J. Melchin, from the Peel River, Yukon, should help refine the boundary. All following discussion is based on a 41.66 m base.

The *acuminatus* Zone has a thickness of 8.11 m (adjusting for the change in measured thickness of the covered interval during the 2007 field season; note to avoid confusion with sample labels and previous publications, the 2006 meterage is used for samples 48.10 m, 49.17 m, and the base of the *atavus* Zone, but these collections are actually ca. 27 cm higher than indicated, relative to samples 47 m and below, as discussed in Methodology).

The *acuminatus* Zone witnesses several large turnovers in taxa, with almost no overlap between the assemblage in the basal versus upper portions of the zone. Broadly, the zone can be divided into a series of assemblages: a highly-diverse basal collection (41.66 m), dominated by *Neo.* sp. 1 and various normalograptids; a lower collection (42.65 m and 48.83 m), with abundant spinose species of *Hirsutograptus;* a lower middle (43.50 m and 44.02 m) collection, dominated by the earlier form of *Paraclimacograptus obesus* and *Normalograptus ajjeri* Form A; an upper middle collection (45.38 m and BS06 45.40 m), with abundant *Rickardsograptus* aff. *lautus* and

the first appearance of *Cystograptus* cf. *ancestralis*; a lower upper collection (46 m to 47 m) with abundant typical specimens of *P. obesus* and *Rickardsograptus lautus;* and an upper collection (48.10m and 49.17 m), also dominated by *P. obesus,* but with the addition of *Rickardsograptus magnus, Neodiplograptus* sp. 2, and several other species.

A number of taxa that have been suggested for subzonal division of this interv al elsewhere. *Hirsutograptus sinitzini* (and all spinose hirsutograptids) is restricted to the single interval noted above, with the exception of a single possible fragmentary cross-section of *H. comantis* from 46 m. *Akidograptus cuneatus* is only confidently identified in the upper mid and upper collections, but is likely present from the basal *acuminatus* Zone (and possibly below). *Normalograptus rectangularis* is present throughout the zone, slightly lower than its occurrence elsewhere (e.g., see discussion in Loydell, 2007). *Cystograptus ancestralis* is either absent or only present from the mid *acuminatus* Zone, depending on whether the specimens included here as *C.* cf. *ancestralis* are considered to belong to *C. ancestralis* s.s.. *Normalograptus imperfectus*? appears to be restricted to the basal *acuminatus* Zone. *Akidograptus ascensus* is present at least until the middle of the *acuminatus* Zone (45.38 m). Figure 4.3 shows the known ranges of described taxa from the *ascensus* and *acuminatus* zones. Overall, the fauna of the Blackstone River bears a strong resemblance to that known from other parts of North America, China, and Dob's Linn, Scotland, Southern Kazakhstan, and Siberia, and is less similar to faunas from North Africa and Peri-Gondwanan Europe.

Atavograptus atavus Zone

The *Atavograptus atavus* Zone is defined by the first appearance of *A. atavus* (Zalasiewicz et al., 2009), and its base is equivalent to that of the *vesiculosus* Zone. In addition to the index taxa, the *vesiculosus/atavus* zones correspond with a rapid increase in the diversity of dimorphograptids and monograptids (Zalasiewicz et al., 2009). At the Blackstone River, the base of the *atavus* Zone is placed at 49.50 m (adjusted height=49.77 m), based upon field observation that monograptids are ubiquitous in strata above that horizon and almost absent below, as well as laboratory study of a small collection from that level that yielded *Atavograptus atavus, Huttagraptus* sp., and *Dimorphograptus swanstoni.* In addition to those taxa, there is a continuation of much of the uppermost *acuminatus* Zone fauna, e.g., *R. magnus, P. obesus,* etc. *C. vesiculosus* was not recovered, but it was reported at the section by Lenz (1982), as well as from other regional sections. Many meters of well-exposed strata exist above the base of the *atavus* Zone, but as they were outside of the purview of this study, they were not collected.

4.2 Regional and International Correlation

Detailed discussion of correlation of graptolite biostratigraphy for the interval under study in this thesis has been conducted by Štorch et al. (2011), Loydell (2007), Chen et al. (2000), and Fan et al. (in prep.). The discussion below focuses on taxa that are present in the current samples, relative to those surveys.

4.2.1 Nevada

Ordovician-Silurian boundary sections have recently been restudied in detail (Finney et al., 1999; Štorch et al., 2011) in the Monitor Range (the composite Martin Ridge and Copenhagen Canyon sections) and the Roberts Mountains (Vinini Creek section), Nevada, with the latter section providing a continuous and diverse record of graptolites from the *ornatus* Zone to the lower *persculptus* Zone. Geochemical studies were also recently undertaken at both sections, providing information on local environmental conditions and water depth, and facilitating chemostratigraphic correlation with the Blackstone River section (Finney et al., 1999; LaPorte et al., 2009; Holmden et al., 2013; Melchin et al., 2013)[14]. The upper part of the *ornatus* Zone (the interval studied for this thesis) to the basal *extraordinarius* Zone can be closely correlated biostratigraphically with the Blackstone River. However, the graptolite-bearing portion of the *persculptus* Zone exposed at Vinini Creek sits stratigraphically lower than the graptolitic *persculptus* Zone interval at the Blackstone River section, based on carbon isotope chemostratigraphy (LaPorte et al., 2009). In addition, only the lowest portion of the *extraordinarius* Zone is graptolitic at the Blackstone River, whereas graptolites are present throughout the interval at Vinini Creek.

[14] Fig. 2.3 shows carbon and neodymium curves for the Blackstone River section. Detailed discussion of correlation occurs in LaPorte et al. (2009) and Holmden (2013). The Vinini Creek and Blackstone sections both show a sharp positive carbon isotope excursion that begins at the base of the Hirnantian, as well as a second sharp positive excursion in the lower *persculptus* Zone. Only the second spike is observed at some other sections (see discussion on controversy in the papers cited above).

The graptolite assemblages at the two sections closely agree, with a majority of species occurring at both sections. Species present in Nevada, but absent at the Blackstone River include *Appendispinograptus longispinus, Paraplegmatograptus uniformis, Parareteograptus parvus, Dicellograptus* cf. *anceps, Phormograptus* sp., and *Anticostia fastigata* (*A. fastigata* is present in the *ornatus* Zone at the Peel River section, and is therefore plausibly also present in the unstudied portion of the *ornatus* Zone at the Blackstone River section). Species present at the Blackstone River, but absent in Nevada include *Dicellograptus tenuiculus, Paraorthograptus affinis, Appendispinograptus* pogrebovi*, Pleurograptus*? *grandis,* and *Neodiplograptus charis.* With the exception of *D. tenuiculus* and *Neo. charis,* the species above are rare in the section where they occur, and so their apparent absence from the other section may be due to sampling. The differences in occurrence of *Dicellograptus* cf. *complanatus, Diplograptus rigidus, Dicellograptus tumidus, Dicellograptus* aff. *turgidus, Paraorthograptus kimi,* and *Paraorthograptus uniformis* appear to be largely the result contrasting taxonomic approaches adopted by Štorch et al. (2011) versus this thesis. For example, material that would have been assigned to *D.* cf. *complanatus* by Štorch et al. (2011) occurs at the Blackstone River, but was assigned in this thesis conservatively to *D. ornatus*, and at least some of the material assigned to *Paraorthograptus uniformis* by Štorch et al. would have been assigned to *P. kimi* here. [See discussion of individual species in Chapter 6.1.] Individual species' ranges differ somewhat between the two sections: some taxa that first appear in the *mirus* Subzone at the Blackstone River

section occur lower in the *pacificus* Zone or in the *ornatus* Zone at the Vinini section, e.g., *A. leptothecalis,* and a number of diplograptine species range further into the *extraordinarius* Zone. Both of these patterns are also likely influenced by sampling, since the Vinini section is sampled more heavily through the o*rnatus* and lower *pacificus* zones*,* and retains graptolitic strata further into the *extraordinarius* Zone, with many diplograptine taxa reappearing as Lazarus taxa.

The first appearances of *Paraorthograptus, D. mirus,* and *M. extraordinarius* appear to correlate closely at both sections, corresponding to shifts in $^{\varepsilon}$Nd and/or $^{\delta}$13C (see LaPorte et al., 2009 and Holmden, 2013). Note that the position of the base of the *mirus* Subzone at the Blackstone River in Holmden et al. (2013), is misplaced. It should be lower, at 14.15 m, placing it at the beginning of the steep portion of the falling limb of the $^{\varepsilon}$Nd values corresponding with the regressive phase of the transgressive-regressive cycle 4C, the same position as it is at Vinini. Additionally, the thickness of the *mirus* Subzone as a percent of the total *pacificus* Zone is similar at both sections (ca. 30%). One notable difference is that *M. ojsuensis* and *Neo. charis* occur just below the first appearance of *Metabolograptus extraordinarius* at the Blackstone River, whereas in Nevada no neograptine species occur below *M. extraordinarius.* Peak graptolite diversity also occurs higher at the Blackstone River: in the *mirus* Subzone, rather than the lower *pacificus* Zone.

4.2.2 Arctic Canada

A relatively low diversity fauna from the latest Ordovician and higher diversity fauna from the earliest Silurian have been described from the Canadian Arctic Islands. The Katian material (Melchin, 1987a) and Hirnantian assemblages (Melchin et al., 1991) lack key index fauna, making precise correlation difficult. The Cape Phillips Formation is entirely devoid of dicellograptids, but Melchin (1987a) divided Katian strata there into two sequential zones based on the presence of *Anticostia fastigata* and *Paraorthograptus pacificus,* the former preceding the latter. The lower *fastigata* Zone (*fastigatus* Zone in Melchin, 1987a) was correlated with the *complexus* Subzone in Great Britain, as *A. fastigata* is restricted to that interval there, and tentatively correlated with the *Dicellograptus ornatus* Zone in the Yukon. The range of *A. fastigata* in the Yukon is unknown, but it is absent from the interval of the Blackstone River section studied here (upper *ornatus* and above) and only present in *ornatus* Zone samples in the portions of Lenz and McCracken's (1982) collection reexamined for this thesis. In Nevada, however, *Anticostia fastigata* ranges into the *pacificus* Zone. The *pacificus* Zone in Arctic Canada is readily correlatable to the Yukon and elsewhere due to the cosmopolitan nature of the species, and on Truro Island the uppermost *pacificus* Zone collections also contain *Appendispinograptus pogrebovi,* which is also present at a similar stratigraphic level at Blackstone River. Immediately above this are collections containing *M. ojsuensis* and *N. mirnyensis*, assigned to the *extraordinarius* Zone (Melchin et al., 1991; Melchin and Holmden, 2006), followed by a non-graptolitic interval in all sections.

Graptolites of the *persculptus* Zone (species include *Neo. shangchongensis, Metabolograptus parvulus,* and *Normalograptus wangjiawanensis*) occur in black shales that overlie a dolomitic siltstone (=flooding surface), and correspond to a negative carbon isotope shift. On the basis of all three of these characteristics (lithological, biostratigraphic, and geochemical) these collections appear to correlate well with the lowest Blackstone River *persculptus* Zone collections (=upper *persculptus* Zone). The lowest Silurian in Canadian Arctic is divided into two subzones: the lower *madernii-lubricus* Subzone (*Normalograptus lubricus* = *Normalograptus anjiensis*) and the upper s*initizini* Subzone (Melchin et al., 1991). *Papamplexograptus madernii* occurs in the upper *persculptus* Zone at the Blackstone River (in addition to the lowest *ascensus* Zone), as it does in China (Fan et al., in prep.) and Scotland (pers. observ.); however, *Normalograptus anjiensis* is a reliable indicator of the *ascensus* Zone (Koren' and Melchin, 2000, where it is referred to as *N. lubricus*; Rong et al., 2008; Fan et al., in prep.). In Arctic Canada, *N. anjiensis* appears with *Paramplexograptus wuningensis* (=*P. innotatus* spp. in Melchin et al., 1991; reinterpretation in Fan et al., in prep.). This same association of *N. anjiensis, P. madernii,* and *P. wuningensis* occurs at the Blackstone, at or very close to the same horizon as the first appearance of *Akidograptus ascensus* (see discussion in 4.1 above). Thus, the *madernii-lubricus* Subzone in Arctic Canada is correlatable to the *ascensus* Zone in the Yukon. Melchin (1989) described *Hirsutograptus jinyangensis* as co-occurring with *H. sinitzini*; the former species ranges into the *acinaces* Zone in Arctic Canada (but see discussion of *H. jinyangensis* and

Hirsutograptus sp. in Chapter 6.2). At the Blackstone River, spinose species of *Hirsutograptus* occur only in a thin stratigraphic window. At 42.84 m *H. comantis* is abundant, and a lesser number of specimens of *H. sinitzini* occur in the same collection; *H. longispinosus* occurs slightly lower, at 42.65 m. All of these occurrences are just over a meter above the base of the *acuminatus* Zone. In China, *H. sinitzini* and *H. comantis* both first occur at a similar stratigraphic height as at the Blackstone River: about 1/4 to 1/3 of the way through the *acuminatus* Zone in the composite sequence of Fan et al. (in prep.). Thus, Melchin et al.'s s*initizini* Subzone is likely equivalent to the lower to middle part of the *acuminatus* Zone at the Blackstone River. Melchin (1989, 1987b) described several other species from the *acuminatus* Zone. Most of these are either of unclear affinity (*Climacograptus* n.sp and "*Diplograptus*" cf. "*D*" *angustidens*) or have long stratigraphic ranges (*Normalograptus angustus* and *Normalograptus mirnyensis*), but *Glyptograptus* aff. *G. nanus* appears to be equivalent to the material assigned here to *Korenograptus ugurensis,* and it co-occurs with *P. acuminatus* and just above *P. obesus* at Truro Island (37 m and 38.5 m, respectively). A similar association occurs at the Blackstone River beginning at 46 m. Melchin (1989; 1987b) described several additional species that also occur at the Blackstone River (*Rickardsograptus magnus* (Churkin and Carter), *Metaclimacograptus hughesi* (Nicholson), *Normalograptus rectangularis* (M'Coy)), but whose first appearance is higher in Arctic Canada.

4.2.3 Jordan

Loydell (2007) offered a detailed study of material from 13 Jordanian localities spanning the latest *persculptus* through *vesiculosus* zones. None of the biozones is represented in its entirety within the collections (Loydell, 2007). The combined *ascensus-acuminatus* Zone in Jordan is at least 10.8 m thick (BG-14 core), comparable to its thickness at the Blackstone River (12.8 m); both sections are much thicker than equivalent sections in Peri-Gondwanan Europe (up to 3.5 m: Štorch, 1996) or Dob's Linn, Scotland (ca. 4 m: Melchin and Williams, 2000). Although there are considerable similarities between the present collections and those in Jordan, beyond the eponymous zonal index taxa, most of the shared taxa are of limited stratigraphic use, e.g., *Normalograptus medius*. None of the species of *Neodiplograptus* that are commonly used to correlate within and between Gondwanan and Peri-Gondwanan regions (e.g., *Neo. lanceolatus, Neo. parajanus, Neo. apographon, Neo. africanus*) are present at the Blackstone River section, nor are *Normalograptus targuii* or *Normalograptus trifilis.* If *Neodiplograptus* sp. 3 is equivalent to the material referred here to *N.*? aff. *nanjingensis,* then it has an equivalent range (first appearance in the *ascensus* Zone), supporting Loydell's questioning of it as an index taxon in Libya. Similarly, if the material referred here to *N.*? cf. *transgrediens* is considered to belong to *N. transgrediens* s.s., then its range extends to the base of the *vesiculosus* at least, supporting Loydell's extension of its range. The first appearance of *Normalograptus rectangularis* is somewhat lower at the Blackstone River section than in Jordan,

extending down to the basal *acuminatus* Zone, as is the range of *Metaclimacograptus hughesi,* which first occurs in the uppermost *acuminatus* Zone at the Blackstone River section. Loydell (2007) described one Jordanian specimen of *Neodiplograptus shanchongensis* from the *persculptus* Zone and another that co-occurs with *A. ascensus*. At the Blackstone River, *Neo. shanchongensis* is restricted to the *persculptus* Zone, as it is in China (Chen et al., 2005a, note that it "may range into the Rhuddanian"), in Arctic Canada (Melchin et al., 1991), and at Dob's Linn (Melchin, pers. comm.)

4.2.4 Kurama Range, East Uzbekistan

Koren' and Melchin (2000) assigned a diverse collection of graptolites to a combined *ascensus-acuminatus* Zone, which they subdivided into three subzones: a lower *Normalograptus lubricus* Subzone (=*Normalograptus anjiensis*), a middle *Akidograptus cuneatus* Subzone, and an upper *Hirsutograptus sinitzini* Subzone. *Akidograptus ascensus* makes its first appearance in the *cuneatus* Subzone and *P. acuminatus* makes its first appearance in the *sinitzini* Subzone. *A. cuneatus* is not confidently present in the Blackstone River samples until the middle *acuminatus* Zone, although it likely occurs earlier; in China, its range spans the *ascensus* to *acuminatus* zones (Fan et al., in prep.). The specimens that Koren' and Melchin identified as *"P." kiliani kuramaensis* agree well with the material assigned here to *Paramplexograptus wuningensis* (see Text-fig. 6.83) and the Chinese descriptions of the species. The presence of this species, along with *N. anjiensis*, both of which first appear with *A. ascensus* at the basal Silurian boundary at the Blackstone River (as they do in China: Fan

et al., in prep.), along with *Normalograptus bicaudatus*, another basal *ascensus* Zone species (Chen et al., 2000), support correlating the *lubricus* Subzone to the lower *ascensus* Zone. The upper *sinitzini* Zone appears to correlate to the middle or upper *acuminatus* Zone, based on the presence of *H. sinitzini,* which occurs at that level at the Blackstone River and in China (Fan et al., in prep.). The middle *cuneatus* Zone is harder to correlate with the Blackstone River (as *A. cuneatus* ranges throughout the lowest Silurian in China, and possibly at the Blackstone River as well). *P. wuningensis* is present at that level in Uzbekistan, *N. anjiensis* is questionably present, *Korenograptus ugurensis* (Koren' and Melchin) makes its first appearance, and *P. acuminatus* is not yet present. The absence of *P. acuminatus* suggests that this level is in the *acensus* Zone, and all of the other taxa just described are either restricted to or make their first appearance in the *ascensus* Zone at the Blackstone (although they have longer reported ranges in China: Fan et al., in prep.; Chen et al., 2000; Chen et al., 2005b). Taken together, the *cuneatus* Subzone likely correlates to the middle or upper portion of the *ascensus* Zone at the Blackstone River. [Note: Loydell (2007) questioned whether the specimens identified as *P. acuminatus* by Koren' and Melchin correctly belong to the species, based on lesser proximal elongation, but Fan et al. (in prep.) found them to be consistent with the variation observed in China, and they similarly match specimens in the lower collections at the Blackstone River.]

4.2.5 Alaska

Churkin and Carter (1970) and Churkin et al. (1970) described rich collections of Late Ordovician and early Silurian graptolites from southeast Alaska. The most continuous exposure, at Esquibel Island, was sampled at a reconnaissance level in 1964 (two samples, each covering a ten-foot interval: M1138-SD = *cyphus* Zone and M1139-SD = *acuminatus* and *vesiculosus* zones), and then at a more detailed level (19 samples), extending into the underlying Hirnantian and Katian, in 1967. The six lowest samples (USGS MI036-CO to USGS MI041-CO, a 4.5 m interval) were assigned to the *anceps* Zone. Although only a few of the species were illustrated, and many of those that were not were left in open nomenclature, the collection is still identifiable as a standard late Katian community, containing *Rectograptus abbreviatus, Dicellograptus ornatus, Climacograptus hastatus,* and *Appendispinograptus supernus* (Churkin et al., 1970). The middle two samples in the sequence (MI038 and MI039) contain specimens that Churkin et al. (1970) questionably assigned to *Paraclimacograptus innotatus.* These are not illustrated, but given the stratigraphic context, they are almost certainly *Paraorthograptus pacificus.* The specimens illustrated as *Climacograptus* sp. aff. *C. bicornis* var. *longispina* and *A. supernus* (plate 24 f and g), both from sample USGS MI038-CO, appear actually to be *Appendispinograptus leptothecalis,* based on the large basal web in the former and the thecal inclination in the latter (see Chapter 7); *A. leptothecalis* is restricted to the *pacificus* Zone at the Blackstone River and in Nevada (Štorch et al., 2011), supporting assignment of the middle two collections to the

pacificus Zone. The uppermost sample in the sequence (MI041) does not contain any of the species from lower samples, but exclusively an indeterminate species assigned to *Climacograptus* and "abundant" specimens assigned to *Climacograptus* cf. *sclaris* var. *normalis.* [Note: the occurrence data above is from table 1, but plate 25 (stratigraphic column) and p. 327 list only *Climacograptus* spp. as occurring in MI041.] Neither species is illustrated, but given their stratigraphic position and the biodiversity context (i.e., the preceding loss of other taxa and dominance of the sample by two "climacograptid" species), it is likely that this captures the latest Katian-Hirnantian influx of *Metabolograptus ojsuensis* and/or *Metabolograptus extraordinarius* seen at the Blackstone River and elsewhere. Taken together, it is probable that the Esquibel Island section captures the *ornatus* through to latest *pacificus* or earliest *extraordinarius* zones, and may be an additional section for future study of the Late Ordovician Mass Extinction.

The next sample in the sequence (1.2 m higher) contains *Metabolograptus persculptus*; as Loydell (2007) notes, this species is restricted to its zone, but without additional diagnostic fauna it is unclear how it correlates with the upper *persculptus* material at the Blackstone River. Elsewhere (Sweden: Koren' et al., 2003; China: Chen et al., 2005a; Dob's Linn, Scotland: Melchin, pers. comm.) *M. persculptus* does not occur in the upper portion of the zone. Additionally, sample MI297 contains the same two possible normalograptids that were contained in MI041. All of this suggests that this collection sits stratigraphically lower than the present *persculptus* material. A 5 m thick

interval assigned to the *acuminatus* Zone begins one meter above the *persculptus*-containing sample. The lower of two collections, which sit approximately one meter above the single *persculptus* Zone sample, contains *Parakidograptus acuminatus* and *Normalograptus trifilis.* The former species indicates that the *ascensus* Zone, if it occurs as a separate interval in Alaska, was not sampled, and the latter, occurs in the middle of the combined *ascensus-acuminatus* Zone elsewhere (Štorch, 1996; Zalasiewicz et al., 2009), suggesting that it belongs to the lower part of the *acuminatus* Zone. Several *acuminatus* Zone taxa are shared between the Blackstone River and Alaska, including *Korenograptus diminutus* Elles and Wood and *Normalograptus rectangularis* (=*Climacograptus* cf. *rectangularis* in Churkin and Carter, 1970), but the interval was not collected at sufficient resolution to allow detailed comparison. *Cystograptus vesiculosus* first occurs "five feet" above the last of the two *acuminatus* Zone samples, but dimorphograptids and monograptids do not occurs until significantly higher in the section (five and ten additional feet, respectively). *Paraclimacograptus obesus* and *Rickardsograptus magnus* both first appear in the *cyphus* Zone, considerably higher than their upper *acuminatus* Zone FAD at the Blackstone River section. Several other taxa that are present in the combined *acuminatus-vesiculosus* sample (*K. laciniosus, K. lanpherei, K.* sp. 3=*Glyptograptus* cf. *G. enodis* var. *enodis* in Churkin and Carter, 1970) occur within the *acuminatus* Zone or lower at the Blackstone River. Given the stratigraphic delay in the appearance of monograptids and dimorphograptids, it is possible that their lowest specimens of *C. vesiculosus* are actually *C. ancestralis*, a

misidentification that was common before *C. ancestralis* was recognized as a separate taxon (Štorch, 1985) (the one illustrated specimen of *C. vesiculosus* where the sample number is indicated comes from higher in their section: MI138-SD = *cyphus* Zone); this would better align the Alaskan and Yukon collections.

4.2.6 Dob's Linn, Scotland

Pioneering work on the global Silurian stratotype section by Lapworth, Toghill, and Williams has recently been updated by Melchin and Williams (2000), Melchin et al. (2003), and Rong et al. (2008), as well as an unpublished restudy of Williams' collections by Melchin (pers. comm.). These new studies significantly increased the known diversity at Dob's Linn, while fine-tuning zonal positions. Additionally, large collections were made early in this thesis from both the Long Burn and Linn Branch sections, and samples from the *persculptus, ascensus,* and *acuminatus* zones were examined. The Dob's Linn section is divisible into the lower Upper Hartfell Shale Formation and the upper Birkhill Shale Formation. The former is mostly barren, but contains a series of thin bands of graptolitic black shale (Anceps Bands A-E and the *Extraordinarius* Band). Anceps Bands A-D belong to the *anceps* Zone, with Bands A-B assignable to the *complexus* Subzone and Bands C-D to the *pacificus* Subzone (first appearance of *Paraorthograptus pacificus*—Williams, 1982). Band E includes the first appearance of *Metabolograptus extraordinarius* and the Extraordinarius Band contains the first appearance of *Metabolograptus persculptus*, allowing them to be assigned to the *extraordinarius* and *persculptus* zones, respectively (Melchin et al., 2003). The Extraordinarius Band is

followed by 1.37 m of non-graptolite strata, and then a return to strata of the *persculptus* Zone (Williams, 1983), followed conformably by the *ascensus* and *acuminatus* zones (Rong et al., 2008).

Dicellograptus complexus does not occur in Canada, but the *complexus* Subzone is considered approximately correlative to the upper *ornatus* Zone in North America (Lenz and McCracken, 1988; Štorch et al., 2011). Aside from *D. anceps* and *C. complexus,* the fauna of the lower two Anceps Bands is very similar to that of the two *ornatus* Zone samples at the Blackstone. The *pacificus* and *extraordinarius* zones appear to be closely correlative globally (e.g., Williams, 1982; Melchin, 1987a; Lenz and McCracken, 1988; Chen and Lin, 2000; Koren' and Sobolevskaya, 2008; Štorch et al., 2011). The appearance of graptolites is episodic within the Upper Hartfell Shale, however, and species occurrence is reported at a band level, rather than cm by cm, so precise correlation is problematic.

Diceratograptus mirus has not been reported at Dob's Linn. Chen et al. (2000) noted that *Dicellograptus mirabilis* and *Dicellograptus turgidus* both occur in Band E (*extraordinarius* Zone) at Dob's Linn, whereas they occur in the *Tangyagraptus typicus* Subzone in China (=mid *pacificus* Zone). *D. mirabilis* s.s. does not occur at the Blackstone River, but *Dicellograptus turgidus* is restricted to the pre-*mirus* portion of the *pacificus* Zone; in Nevada, both species are restricted to the pre-*mirus* interval (Štorch et al., 2011). This suggests that Band E contains a portion of the lower or middle *pacificus* Zone, as well as strata equivalent *mirus* Subzone, and the transition to the basal

extraordinarius Zone. If this is the case, then the *mirus*-equivalent interval is highly condensed at Dob's Linn, as it is in many sections in China (Chen et al., 2000). Unpublished observations by M.J. Melchin (pers. comm.) support this: *D. turgidus* is reported only from the lower portion of Band E, while *M. extraordinarius* makes its first appearance in the middle of the band. The graptolitic portion of the *extraordinarius* Zone preserved at the Blackstone River is 15 cm thick, and likely corresponds with the upper portion of Band E, while the portion of the *extraordinarius* Zone recorded in Extraordinarius Band likely correlates to a non-graptolitic interval at the Blackstone. The proposed biostratigraphic interpretation is at odds with global correlation in Melchin et al. (2013), which places the base of the Hirnantian just above Band D and interprets Band E to represent an upper *extraordinarius* Zone interglacial episode (fig. 3). This is based on sedimentological evidence for shallowing above Band D (Armstrong and Coe, 1997), as well as a slight negative carbon isotope excursion at Band E. However, Holmden et al. (2013) and the current thesis provide evidence for sea level oscilations during the *pacificus* Zone, meaning that the biostratigraphic and sedimentological evidence are not necessarily in conflict.

The Extraordinarius Band, in which *Metabolograptus persculptus* has been reported (Melchin et al., 2003), precedes the peak of the Hirnantian carbon isotope excursion (HICE) (Underwood et al., 1997), whereas all of the graptolitic portion of the *persculptus* Zone at the Blackstone River is in the falling limb or post-dates the HICE (Holmden et al., 2013). The lithological shift to black shales at the base of the Birkhill

Shale may predate the return to black shales at the Blackstone River (the inferred post-glacial flooding surface at 32.80 m). At the level of return to black shales, the carbon isotope curve of Underwood et al. (1997) retains strongly positive values, whereas they have returned to near pre-excursion values at the Blackstone (Holmden et al., 2013). Additionally, species that occur at or very close to the base of the black shale at the Blackstone (*Avitograptus avitus, Neodiplograptus shanchongensis, Paramplexograptus madernii,* and *Normalograptus*? *minor*) do not occur at Dob's Linn until ca. 1/3 of the way through the Birkhill Shale portion of the *persculptus* Zone (Melchin, pers. comm.). Notably, many of these species are components of Koren' et al.'s (2003) post-*persculptus,* "a*vitus* Fauna". [Note: *M. persculptus* is present in the lowest *persculptus* Zone collection at the Blackstone River.]

The base of the *ascensus, acuminatus,* and *atavus* zones are all readily correlatable by their index taxa at both sections. The *ascensus* and *acuminatus* zones are both approximately three times as thick at the Blackstone River as at Dob's Linn. As with the *persculptus* Zone, the Blackstone is considerably more diverse, in particular in the *acuminatus* Zone, where taxa are both relatively low diversity and sparse at Dob's Linn (pers. observ.). Melchin has recently conducted a review of material described by Williams (1983) and provided updated, unpublished range data; additionally, large new collections were taken through this interval at Dob's Linn as part of this thesis, and scanned for approximate ranges of taxa. There are a number of similarities that may be biostratigraphically useful. *Normalograptus anjiensis, Paramplexograptus paucisipinus,*

and *Paramplexograptus madernii* all last appear in the lower half of the *ascensus* Zone, as is the case at the Blackstone River. Pre-*atavus* Zone occurrences of *Atavograptus* are restricted to the middle *ascensus* Zone at Dob's Linn (one questionable specimen from the lower *acuminatus* Zone—pers. observ.) and to the upper *ascensus* Zone at the Blackstone River. [Note: *A. primitivus* is reported from the *acuminatus* Zone at some sections in China—Fan et al., in prep.] The distinctive *Hirsutograptus tuberculatus* occurs in the mid-*ascensus* Zone at Dob's Linn (Melchin, pers. comm.) and slightly higher at the Blackstone, but it is absent from the lowest and uppermost *ascensus* Zone strata at both sections. There is little faunal overlap between the two sections within the *acuminatus* Zone, mostly as a result of the low diversity at Dob's Linn in this interval, but the uppermost portion of the *acuminatus* Zone contains *Paraclimacograptus innotatus* and *Metaclimacograptus hughesi* at Dob's Linn (Melchin, pers. comm.). A similar association (*Paraclimacograptus obesus* and *Metaclimacograptus hughesi*) occurs at the Blackstone during this interval.

4.2.7 Southwestern Sweden

Koren et al. (2003) provided a detailed description of a core through the Kallholn Formation, covering the *persculptus* through *acuminatus* zones. They identified four discrete faunas: an upper and lower *persculptus* Zone assemblage, and an assemblage from each of the *ascensus* and *acuminatus* zones. Almost all of the species in the four assemblages are simple "normalograptid"-type species, with climacograptid or glyptograptid thecae, and lacking ornamentation. The present collections contain a

wider array of morphologies and diversity, but the ranges of the taxa identified by Koren' et al. (2003) are similar to those at the Blackstone. The lowest of the current *persculptus* Zone collections contains *Normalograptus*? *minor, Avitograptus avitus, Korenograptus laciniosus,* and *Normalograptus*? *transgrediens,* a collection that makes up almost the entirety of Koren' et al.'s *avitus* Fauna. Additionally, the present collections contain *Paramplexograptus* aff. *madernii,* which is very similar to *Normalograptus skiliphrus,* and may be equivalent to the material Koren' et al. (2003) illustrated as another component of the *avitus* Fauna (note the off-center nema in their fig. 3.19, suggesting that the specimen may be aseptate). *Metabolograptus persculptus* is present in the lowest Blackstone River *persculptus* Zone sample, but is otherwise missing from the *persculptus* Zone at the Blackstone River. The bases of *ascensus* and *acuminatus* zones within the Kallhlon Formation can be correlated with the Yukon by their index taxa, but other species either are absent from the Yukon or have abbreviated ranges. In discussion of their four faunas, Koren' et al. (2003) refer to an additional core from Bornholm, Denmark, which was described by Koren' and Bjerreskov (1997), who subdivided it into *persculptus* through *acuminatus* zones. *M. persculptus* is recorded by Koren' and Bjerreskov (1997) occurring alongside species (*N. trifilis, N. balticus,* and *N. rectangularis*) that are normally associated with the *ascensus* or *acuminatus* Zone (including in Koren' et al., 2003). None of the specimens are illustrated, and therefore cannot be checked, but it seems possible that there is an error in identification.

4.2.8 South China

Research on Ordovician-Silurian graptolites has been conducted in China for nearly one hundred years (Chen et al., 2000). This work has identified a very high-diversity of taxa, represented at several dozen sections (Chen et al., 2003). Over the past two decades, a concerted effort has been made to update and synthesize previous work. Chen et al. (2000) revised species lists for "Ashgillian" graptolites and updated global correlation; Chen et al. (2005b) and Fan and Chen (2007) employed graphic correlation to create a composite section charting regional patterns of graptolite diversity through the Late Ordovician Mass Extinction; Chen et al. (2005a) conducted a detailed revision of Hirnantian ranges and systematics; and Fan et al. (in prep.) are continuing this process for the earliest Silurian.

Globally standard zones from the Katian to early Rhuddanian (*D. complexus, P. pacificus, M. extraordinarius, M. persculptus, A. ascensus, P. acuminatus,* and *C. vesiculosus*) are recognized in China, facilitating correlation with the present section, with a few minor exceptions. *Dicellograptus complexus* does not occur in Canada, but at least the upper portion of the North American *ornatus* Zone appears to correlate well with the *complexus* Zone in China (Chen and Lenz, 1984; Štorch et al., 2011). The *pacificus* Zone in China is divided into three subzones: an unnamed lower zone, a middle *Tangyagraptus typicus* Subzone, and an upper *Diceratograptus mirus* Subzone; the genus *Tangyagraptus* is not known outside of China, but *D. mirus* occurs in the Yukon, allowing subdivision of the zone, and resulting in only slightly lower resolution. The base

of the *pacificus* Zone appears to be closely synchronous globally (see discussion above), but testing this at the Yukon is complicated by the fact that species that co-occur at both sections, and whose FADs coincide with the base of the *pacificus* Zone in the Yukon, range into the underlying *complexus* Zone in China. An additional caveat is required for the *mirus* Subzone, which is considerably thicker in both the Yukon and Nevada (Štorch et al., 2011) than it is in China, raising the possibility that the species appears later in China than it does in North America. Biodiversity also peaks earlier in China: within the *typicus* Subzone, whereas at the Blackstone River it does not reach a maximum until the *mirus* Subzone. *Dicellograptus turgidus* occurs approximately one quarter of the way through the *pacificus* Zone at the Blackstone River, and is common in the *typicus* Subzone in China (Chen et al., 2000); it is located in a similar position within the *pacificus* Zone in Nevada (Štorch et al., 2011). A dramatic drop in diversity occurs in both China and the Yukon during the latest Katian. Correlation of the base of the Hirnantian is further facilitated by the fact that in both sections *Metabolograptus ojsuensis* and *Neodiplograptus charis* occur immediately below the first appearance of *Metabolograptus extraordinarius* (Chen et al., 2005a; note: the specimens referred to *Neo. shanchongensis* in Chen et al., 2000, were reassigned to *Neo. charis* by Chen et al., 2005a).

The majority of the *extraordinarius* Zone and the lower *persculptus* Zone are not graptolitic at the Blackstone River, whereas the graptolite record is more or less continuous in China. The fauna of the upper *persculptus* in China correlates very well

with the *persculptus* Zone at the Blackstone River section (interpreted to be upper *persculptus* Zone), although diversity is lower during the interval in China. Shared taxa include *N.*? *rhizinus, N.*? *minor, A. avitus, M. parvulus, K. lungmaensis, K. laciniosus,* and likely *N. mirnyensis* (Chen et al., 2005a; Fan et al., in prep.). *Metabolograptus persculptus* is absent from the uppermost *persculptus* Zone in both regions, as are all diplograptine taxa. The base of the *ascensus* Zone is very well correlated, with the FADs of *A. ascenus, P. wuningensis, P. kiliani, P. paucispinus,* and *N. anjiensis* all marking the boundary in both regions. The synchronicity of base of the *acuminatus* Zone is supported by *P. acuminatus* and *N. imperfectus* (the latter occurs just above the base of the *acuminatus* Zone in China (Fan et al., in prep.) and at the base of the zone in the Yukon). Other taxa that have FADs at the base of the *acuminatus* Zone at the Blackstone River range into the *asensus* in China or do not occur. Within the *acuminatus* Zone, *H. sinitizini* and *H. comantis* occur simultaneously in the lower third of the zone at both sections.

The ranges of taxa in the composite section created by Fan et al. (in prep.) are generally greater than at the Blackstone River, which is to be expected when comparing a single section to a composite. Interestingly, however, the mid to upper *acuminatus* Zone in China is an interval of low origination, whereas in the Yukon a number of the species occur in this interval, especially towards the base of the *atavus/vesiculosus* Zone. Since *C. vesiculosus* was not recovered, the boundary is roughly correlatable by the appearance of *A. atavus* and dimorphograptids (which occurs slightly above the first

appearance of *C. vesiculosus* in Fan et al.'s composite, and marks the base of the *atavus* Zone in the current research).

4.2.9 Peri-Gondwanan Europe

The Katian and lower Hirnantian graptolite fauna of Peri-Gondwanan Europe correlates poorly with North America (Štorch et al., 2011) and other sections occuring at low paleolatitudes. Although separate *ascensus* and *acuminatus* zones can be recognized at some individual sections within Peri-Gondwanan Europe, Štorch (1996) created a regional scheme for the lower Rhuddanian, subdividing a combined *ascensus-acuminatus* Zone into lower, middle, and upper portions, overlain by the *vesiculosus* Zone. Most of the biostratigraphically useful taxa do not occur in the Yukon (or elsewhere in the paleotropical realm)—see Štorch, 1996, fig. 2: *N. trifilis, Neo. parajanus*, *Neo. lancelatus, N. longifilis,* etc. *Cystograptus ancestralis* questionably does occur (see Chapter 6), but if so, it appears later than it is does in Peri-Gondwanan Europe (Štorch, 1996). *Rickardsograptus lautus* occurs within the mid to upper *acuminatus* Zone at the Blackstone River, and at a similar level in many sections within Peri-Gondwanan Europe (e.g., Štorch, 1996; Štorch and Feist, 2008; Štorch and Schönlaub, 2012). Štorch and Schönlaub (2012) also noted a thinner variant of *N.*? *transgediens* from the *acuminatus* Zone and either the *acuminatus* or *persculptus* zones at two sections in the southern Austrian Alps; a very similar species occurs in the *ascensus* and *acuminatus* zones at the Blackstone River. Additionally, Štorch and Schönlaub (2012) also described material they assigned to *Rickardsograptus*? *bifurcus*

(here: *Korenograptus bifurcus*) from the *acuminatus* Zone; similar material occurs at the Blackstone River in the uppermost *ascensus* and lowest *acuminatus* zones. *Normalograptus trifilis* provides a useful indirect method of correlation between the Yukon and Peri-Gondwanan Europe, since it is present in the Great Britain and in China (Zalasiewicz et al., 2009; Fang et al., 1990). Recent high-resolution biostratigraphy at Dob's Linn (Melchin, unpub. data.) and South China show it to be restricted to the *ascensus* Zone or lowest *acuminatus* Zone, allowing correlation via taxa that co-occur between those sections and the Yukon.

4.2.9 Southern Kazakhstan

Apollonov et al. (1980) recognized a Katian *supernus* Zone, overlain sequentially by a *persculptus* Zone, *acuminatus* Zone, and *vesiculosus* Zone. The upper *supernus* Zone contains a collection of taxa associated with the *ornatus* and *pacificus* zones at the Blackstone River: *C. hastatus, A. supernus, S. tatianae, D. ornatus, A. lata,* and *P. pacificus.* The uppermost *supernus* Zone includes both *P. pacificus* and *M. ojsuensis,* and can be correlated to the latest *pacificus* Zone in the Yukon. *Paraorthograptus affinis* briefly occurs in this interval, above the LAD of *Paraorthograptus pacificus* and alongside *M. ojsuensis,* at the Ojsu Spring section (Koren' et al., 1979), a similar stratigraphic position to its occurrence at the Blackstone River. The lowest "*persculptus* Zone" contains specimens assigned to *Glyptograptus persculptus* forma A, which is actually *M. extraordinarius* (see Chen et al., 2000). Thus, *M. ojsuensis* precedes *M. extraordinarius* in Southern Kazakhstan as in the Yukon. The *persculptus, acuminatus,* and *vesiculosus*

zones can all be roughly correlated with the Blackstone based on the zonally defining taxa, but the paucity of co-occurring taxa make more detailed correlation difficult. Although they do not occur at the Blackstone River, *S. illustris, H. jideliensis,* and *H. acceptus* are indicative of the *ascensus* Zone elsewhere (Koren' and Melchin, 2000; Fan et al., in prep.), and strata where they occur in Kazakhstan are therefore likely correlatable to the *ascensus* Zone in the Yukon.

4.2.10 Kolyma, Siberia

Koren' et al. (1983, 1988) and Koren' and Sobolevskaya (2008) described a series of sections, including the classic Mirny Creek section, in the Omulev Mountains, Siberia. The Ordovician-Silurian boundary sequence there is divisible into a Katian *supernus* Zone (subdivided into lower *A. longispinus* and upper *P. pacificus* subzones), Hirnantian *extraordinarius* and *persculptus* zones, and Rhuddanian *ascenus, acuminatus,* and *vesiculosus* zones (note: Koren' et al., 1983, did not recognize a separate *ascensus* Zone). The fauna of the *pacificus* Subzone correlates well with the *pacificus* Zone at the Blackstone River (e.g., *D. ornatus, P. pacificus, A. lata,* and *C. hastatus*). Notably, *Metabolograptus ojsuensis* and *Appendispinograptus pogrebovi* occur in the uppermost portion of the zone, just below the base of the Hirnantian. Both of these species also appear in the uppermost *pacificus* Zone at the Blackstone River, although the LAD of *A. pogrebovi* is slightly below the FAD of *M. ojsuensis*. Also notable is the occurrence of specimens of *Appendispinograptus leptothecalis* (*Climacograptus longispinus*

longispinus in Koren' et al., 1983) with thick basal webs, a modification of the proximal end also seen in the Yukon (see Chapter 7 for further discussion).

The base of the Hirnantian is defined by the first appearance of *M. extraordinarius,* and coincides with a loss of all but one diplograptine species, an apparently more abrupt turnover than occurs in the Yukon. All recovered Hirnantian diplograptine species at the Blackstone River are exceedingly rare, however so this apparent difference may be the result of more intense sampling at the Blackstone River. The *persculptus* Zone is recognized by the eponymous species, plus a low diversity collection of non-diagnostic normalograptids (Koren' and Sobolevskaya, 2008) that does not allow more precise correlation with the Yukon. The bases of the *ascensus* and *acuminatus* zones are defined by the eponymous species. The interval is low diversity. No taxa occur that allow more precise correlation with the *ascensus* portion of the zone, but *H. sinitzini* first occurs in the middle part of the *acuminatus* Zone, as it does at the Blackstone River and elsewhere. Unlike at the Blackstone River, the species persists until just below the FAD of *C. vesiculosus.* The FAD of the *N. rectangularis* is in the upper *acuminatus* Zone, as it is in many other sections, but unlike the Blackstone River, where it first appears at the base of the zone.

4.3 Biostratigraphic Conclusions and Significance

With the recovery of the zonal index taxa for the *ornatus* to *atavus* zones, the Blackstone River section possesses North America's only biostratigraphically complete graptolite record through the interval of extinction and recovery (*ornatus* to *atavus*

zones). Additionally, the diverse Blackstone River collections contain a number of other biostratigraphically useful taxa that validate previous zonal assignments in several sections lacking the index taxa (e.g., Arctic Canada). The present collections also support the recognition of a distinct latest Ordovician post-*persculptus* interval zone, definable as extending from the last appearance of *Metabolograptus persculptus* to the first appearance of *Akidograptus ascensus,* and supported by the co-occurrence of a distinct suite of taxa including *Avitograptus avitus, Paramplexograptus madernii, Normalograptus*? *minor, Korenograptus laciniosus,* and *Normalograptus*? *rhizinus*. Finally, combined with preliminary data for the Rhuddanian from Dob's Linn and South China (Melchin, pers. comm.; Fan et al., in prep.), the current data suggest that the *ascensus* and *acuminatus* zones are likely divisible into globally useful subzones, with *Hirsutograptus tuberculatus* and/or *Atavograptus primitivus/Atavograptus ceryx* indicating the mid to upper *ascensus* Zone, *Hirsutograptus sinitzini* indicating the mid-*acuminatus* Zone, and *Paraclimacograptus obesus* (and perhaps *Paraclimacograptus innotatus*) indicating the upper *acuminatus* Zone.

Chapter 5. Faunal Dynamics and Diversity

5.1 Diversity Trends

The ca. 50 m interval sampled and examined in this thesis runs from the *ornatus* Zone (one full sample and one partial), through the *pacificus* Zone (14 samples, one a composite of two closely spaced smaller samples), the basal *extraordinarius* Zone (three samples), the upper *persculptus* Zone (six samples), *ascensus* Zone (five full samples, four partial), *acuminatus* Zone (eight full samples, and two partial), and a single partial sample from the *atavus* Zone, collected to confirm field identification of the level of boundary. Sampling intensity varied between zones, but averaged approximately one collection per meter, with the following exceptions: the *ornatus* and early *pacificus* zones, where graptolite-bearing shales were rare; the upper *pacificus* and basal *extraordinarius* zones, which were collected at 5 cm intervals for close study of the LOME; and the lowest *persculptus* Zone, where the basal collections were taken 13 cm and 40 cm apart, to better capture faunal shifts in the inferred post-glacial/flooding interval. According to the most recent global timescale (Cooper and Sadler, 2012; Melchin et al., 2012) the *pacificus* Zone was estimated to represent ca. 1.86 Ma (= to 18.32 m of strata at the Blackstone River); the *extraordinarius* Zone ca. 0.73 Ma; the *persculptus* Zone ca. 0.6 Ma[15]; the *ascensus* Zone ca. 0.43 Ma (=4.67 m of strata at the BlackStone River); and the *acuminatus* Zone ca. 0.93 Ma (=8.11 m of strata at the

[15] Only the lowest *extraordinarius* and upper *persculptus* zone are graptolitic at the Blackstone River.

Blackstone River). This yields an average sampling resolution of ca. 100 ka, with minimum resolution in the lower *pacificus* Zone and maximum resolution at the Katian/Hirnantian boundary[16]. This resolution is comparable to the resolution of Chen et al.'s (2005b) study of biodiversity changes in South China—although the latter is based on a composite section—and is sufficient to test whether diversity changes seen in South China, especially in the later Hirnantian and Rhuddanian, are global or local.

Identifying range lengths, and therefore diversity, is an inherently subjective process. It requires deciding how many taxa exist in a section, as well as how to bin individual specimens into those identified categories. To test and control for the affects of subjective taxonomic decisions on estimates of diversity and of rates of origination and extinction, curves for all three were each plotted several different ways[17]: 1. using the author's preferred identifications, 2. a conservative approach (e.g., all questionable occurrences rejected and morphologically similar species grouped), and 3. a liberal binning scheme (e.g., all questionable occurrences accepted and all 'cf.' occurrences counted as separate species). The results of these varying schemes are shown as 'Preferred', 'Lumper', and 'Splitter', respectively, in Katian and early Hirnantian figures, and as 'confirmed' and 'expanded' ranges in figures for the *persculptus* Zone and Silurian. The resulting curves do not substantially differ, relative to large-scale trends, raising confidence that the observed trends capture actual shifts in diversity, or at least

[16] See Fig. 2.3 and discussion of sampling in Chapter 3.1 and Chapter 4.1.
[17] Uncertainty is also shown on the range charts (Figs. 4.1-4.3) with colour coding (blue=uncertainty) and questions marks. See legends for figures in Chapter 4 for more information.

are not significantly influenced by observer bias (Figs. 5.1 and 5.2). Within-sample diversity is considered in two different ways. Raw diversity is the total number of species recovered in a sample. Range-through diversity, which is presented in the figures and in the discussion below, unless otherwise noted, is the total inferred number of species present in a sample based on ranges, i.e., the species actually recovered in a sample, plus any species that occur in samples both above and below that sample, and are therefore inferred to be extant, but not recovered. Appendix B gives the results of abundance counts as both tables and pie graphs. Text-figures 4.1, 4.2, and 4.3 show individual species ranges.

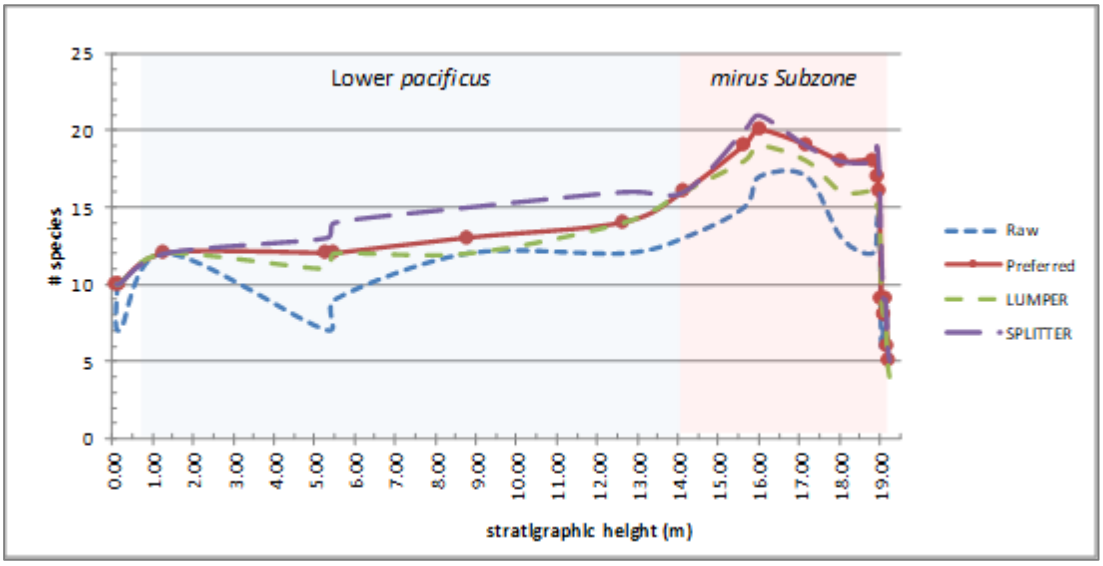

Figure 5.1. Katian-early Hirnantian diversity. Raw = species recovered in each sample during counts and scans. Preferred, LUMPER, and SPLITTER are all range through counts, i.e., taxa are counted as being present in a sample if they occur in a stratigraphically higher sample. Preferred = the binning and taxonomic scheme considered most realistic by the author; LUMPER = groups all morphologically similar taxa and removes any questionable occurrences; SPLITTER = adds all questionable occurrences and elevates cf. species and questionable taxa to species level. Markers in the 'preferred' curve show collection localities, which are the same for all curves. The 15 cm thick non-shaded area on the far right of the graph is the *extraordinarius* Zone. The non-shaded area on the left of the figure is the *ornatus* Zone.

Ten species are present in the two *ornatus* Zone samples, which are dominated by *Appendispinograptus supernus* and *Anticostia lata,* respectively. Species of *Styracograptus* make up 25% of the complete (lower) sample, the only sample in the collections where *Styracograptus* represents a significant proportion of a community. Given the limited sampling resolution, this is likely a substantial underestimation of actual upper *ornatus* Zone diversity at the Blackstone River, but rarefaction curves support completeness of sampling at the levels sampled (see Appendix D). All of the species present in the *ornatus* Zone samples range into the *pacificus* Zone. Diversity rises slightly (to 12 species) at the base of the *pacificus* Zone (1.30 m), and then continues to slowly rise until a maximum diversity of 20 species (raw=17) is reached just below the middle of the *mirus* Subzone. Species turnover increases in the middle *pacificus* Zone, with both origination and extinction rates spiking in the transition to the *mirus* Subzone (see Figs. 5.2-5.5). Immediately after its 16.03 m peak, diversity begins to decline, slowly at first, until just below the base of the *extraordinarius* Zone, at which point there is a rapid drop in diversity (Fig. 5.1 and 5.5), and even more profound shift in community dominance (see subsequent section and graphs in Appendix B).

The highest graptolitic sample of the *extraordinarius* Zone has only four species, a drop of 80% from the *mirus* Subzone peak. The beginning phase of the diversity loss slightly precedes the invasion of neograptine species, and coincides approximately with the first appearance of two short-lived diplograptine species (*Appendispinigraptus pogrebovi* in the upper *mirus* Subzone and *Paraorthograptus affinis* in the upper *mirus*

or basal *extraordinarius* Zone; these short-lived species also appear at a similar stratigraphic position in Siberia and Kazakhstan, respectively (Koren' et al., 1983; Apollonov et al., 1980). These new appearances partially mask the loss of diversity of pre-extinction taxa: the penultimate *extraordinarius* Zone sample contains six species, but only two of them carry over from the *pacificus* Zone, and the final sample contains five species, but perhaps only a single typically Katian species (it contains an unidentifiable species of *Paraorthograptus,* which may be either *P. pacificus* or *P. affinis*). Origination increases near the onset of the main pulse of extinction due to the appearances of neograptines and the two new diplograptines species described above (Fig. 5.4); the dramatic rise in extinction rates more than offsets origination, however.

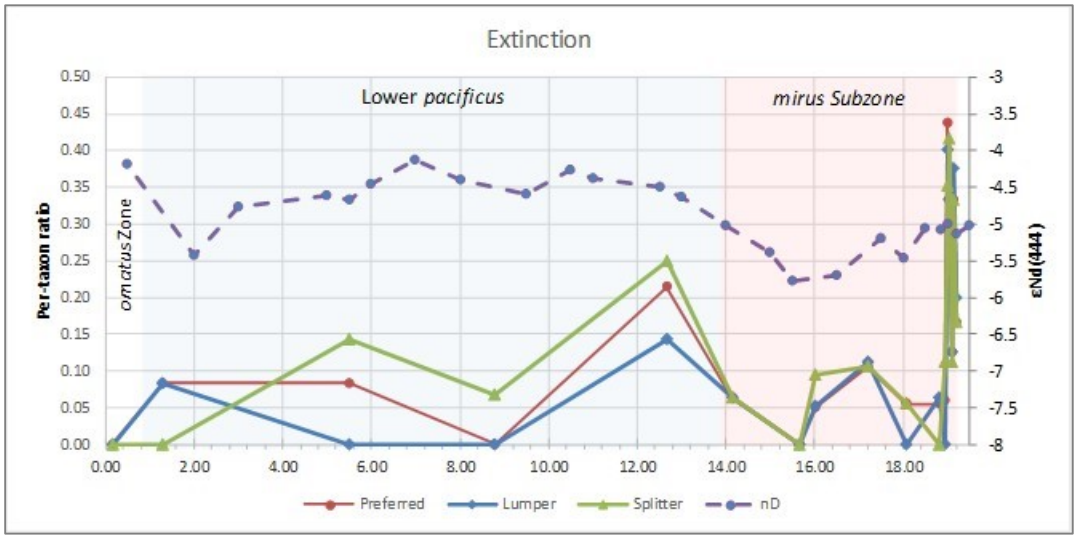

Figure 5.2. Katian-early Hirnantian extinction patterns. Preferred, Lumper, and Splitter curves represent the author's preferred species binning scheme, a conservative approach, and a liberal one. Per-taxon extinction is the ratio of taxa that last appear in a sample by the total number of taxa in that sample. This approach counts extinctions as occurring within a sample, when in reality they occurred at some point between the top of that sample and the next sample. This results in extinction changes appearing slightly prematurely relative to diversity/geochemical data. Nd data was produced by Chris Holmden, University of Saskatchewan. Shifts towards less and more negative values are a rough proxy for sea level rise and fall, respectively (see Holmden et al., 2013, for a discussion of rationale and supporting evidence).

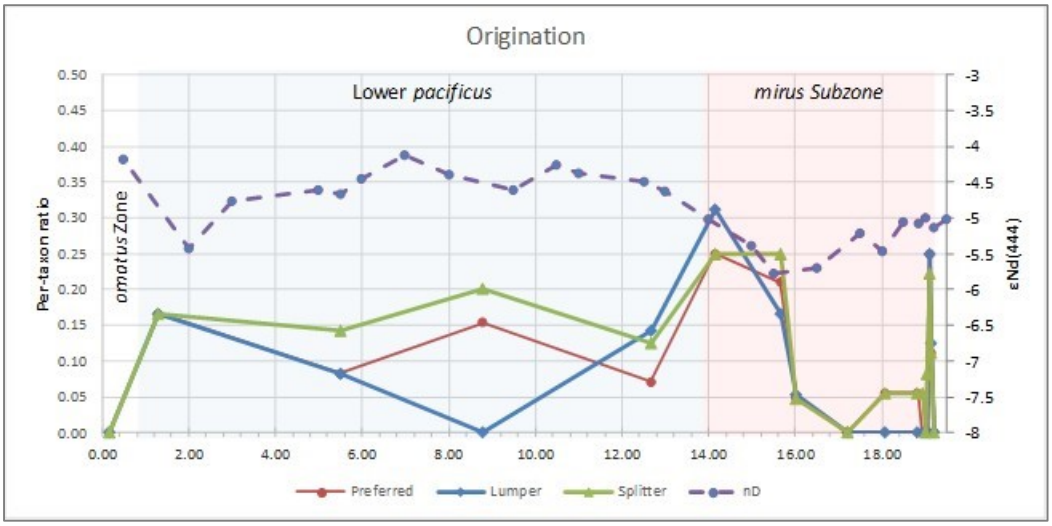

Figure 5.3. Katian-early Hirnantian origination patterns. Origination is calculated as a ratio of taxa that first appear in a sample relative to the total number of taxa that occur in that sample. Origination events are counted as occurring within a sample through this approach, when in reality they occurred at some point between the same at which a new species is observed and the previous sample; this has the effect of shifting origination rates changes up-section. See Figure 5.2 for further explanation of figure labels.

Figure 5.4. Latest Katian-early Hirnantian extinction patterns. Data from Blackstone River. See discussion in captions for Figs. 5.2 and 5.3 for further information.

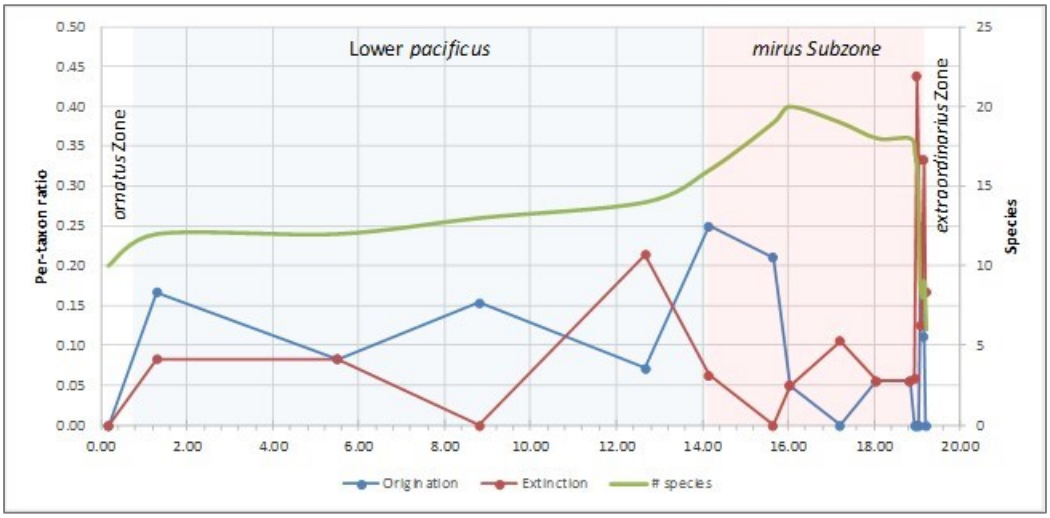

Figure 5.5. Late Katian-early Hirnantian diversity vs. species turnover. Data from Blackstone River. All curves show the 'preferred' ranges. See discussion in captions for Figs. 5.2 and 5.3 for further information.

The late Katian-early Hirnantian loss of diversity at the Blackstone River in many ways mirrors that seen elsewhere, especially the dramatic drop in diversity near the base of the Hirnantian, coincident with a replacement of diplograptine species by neograptine species, but varies in some subtle ways. In Nevada (Štorch et al., 2011; Finney et al., 1999), the upper *pacificus* Zone sees the same accelerating drop in biodiversity, concentrated on diplograptine species, near the base of Hirnantian. However, peak diversity is reached earlier at Vinini Creek than at the Blackstone River (lower *pacificus* Zone vs. *mirus* Subzone), and, apart from *Diceratograptus mirus* itself, no new species originate in the *mirus* Subzone at all. The Vinini Creek section, an inferred deeper water locality, possibly less influenced by sea level change (LaPorte et al., 2009), also retains a higher diversity diplograptine fauna in the basal Hirnantian, followed by the reappearance of diplograptine "Lazarus taxa" in the upper *extraordinarius* Zone and *persculptus* Zone; corresponding upper *extraordinarius* and

lower *persculptus* zone strata at the Blackstone River are barren of graptolites. In China, the patterns of diversity are similar to Nevada[18]: peak diversity in the mid-*pacificus* Zone (*typicus* Subzone), followed by a sharp initial drop in taxa in the upper *pacificus* Zone, and with a subgroup of diplograptines persisting until the upper *extraordinarius* Zone (Chen et al., 2005b). Like the Blackstone River, there is a spike of origination at the base of the *mirus* Subzone (Chen et al., 2005b: fig. 7—reproduced in Appendix F).

At Mirny Creek, Siberia, and neighboring sections, a somewhat different pattern is observed (Koren' et al., 2003; Koren' and Sobolevskaya, 2008). A significant drop in diversity occurs in the transition from the *supernus* (=*ornatus* Zone) to *pacificus* zones, followed by a profound drop in diplogratine diversity at the base of the Hirnantian (only a single species, *P.* cf. *pacificus*, is present in the lowest *extraordinarius* Zone sample, and none beyond; Koren' and Sobolevskaya, 2008). However, there is no significant change in overall species diversity across the basal Hirnantian boundary, a result of the already low levels of diversity in the *pacificus* Zone, which is offset by the origination and/or invasion of neograptine species. This different pattern of diversity turnover is likely due partially to the low abundance of graptolitic horizons and specimens within those horizons (see section description in Koren' and Sobolevskaya, 2008) and partially a result of the fact that Mirny Creek represents a shallower water locality (Sheets et al., 2016).

[18] Diversity curves for Vinini Creek, Nevada, and South China, and extinction and origination curves for South China, are reproduced for ease of comparison in Appendix F.

Graptolitic strata return within the *persculptus* Zone at the Blackstone River. Diversity is relatively high even in the initial collections. The lowest sample (32.84 m), which likely corresponds to the upper *persculptus* Zone (see Chapter 4.1 and Laporte et al., 2009), contains a minimum of nine species, and possibly as many as 13 species, and the second sample, 13 cm higher, contains 10 species. This is equivalent to the levels of diversity seen at the section in the *ornatus* and lower *pacificus* zones. Diversity rises to 16 species by the middle of the graptolitic portion of the *persculptus* interval, close to the pre-extinction maximum diversity, before beginning a drop to nine species in the highest *persculptus* Zone (Fig. 5.6). A minimum of 21 species are present in the *persculptus* Zone (four additional questionable occurrences are discussed in Chapter 6.2). This is considerably higher than diversity levels reported for this interval elsewhere. In comparison, Koren' et al. (2003) reported 14 species from the upper *persculptus* Zone in Scania; Melchin (pers. comm.) reported 13 species during his reexamination of the William's Birkhill Shale collections from Linn Branch, Dob's Linn; Koren' and Sobolevskaya (2008) reported eight species from the entire *persculptus* Zone at Mirny Creek; Sheets et al. (2016: Dataset S04) reported 14 species from Vinini Creek (mid to upper *persculptus* Zone), many of them late persisting diplogratine species; and Chen et al. (2005a) reported 13 species from the upper *persculptus* Zone at Wangjiawan (with 22 species total occurring in the four studied Yangtze sections over the course of the *persculptus* Zone). The high levels of diversity at the Blackstone River section were unexpected, and require further study to determine whether they result from the

intense sampling undertaken or represent genuinely anomalous diversity. The resolution they provide, however, creates an opportunity to examine changes in diversity patterns at the Ordovician-Silurian boundary. These are discussed in section 5.3.

The lowest complete Silurian (*ascensus* Zone) collection contains 14 species (10 raw). This rises to 16 species in the subsequent collection, and then reaches a plateau, with a slight rise in the lowest confirmed *acuminatus* collection (20 species; raw=17), followed by a slow drop in the uppermost *acuminatus* Zone (Fig. 5.6). The Silurian counts are likely underestimates, as range lengths and species identifications are less confident than in the counted lower portions of the sections, but it is notable that diversity levels recovered to at least the same level as pre-extinction highs by the base of the *acuminatus* Zone. While overall diversity is relatively uniform throughout the studied interval of the Silurian, community composition and rates of origination and extinction vary greatly. Each of these is discussed in the sections below.

Total diversity in the *ascensus* Zone is at least 29 species (Fig. 5.6), with all but five species newly appeared within the zone; a minimum of 36 species occur in the *acuminatus* Zone. The total combined diversity of the *ascensus-acuminatus* Zone is at least 56 species. This is almost certainly an underestimate, given the meter interval sampling through most of the interval and the very conservative approach taken to identifying species, especially normalograptids. Presently observed diversity is already

slightly higher than reported for the entire Yangtze region of China (55 species: Fan et al., in prep.), which had previously been recognized as uniquely diverse (Chen et al., 2005b). The Chinese diversity estimate is the result of intensive study of 30 sections (29 different localities), making the level of diversity recorded in this study of a single section in the Yukon even more notable.

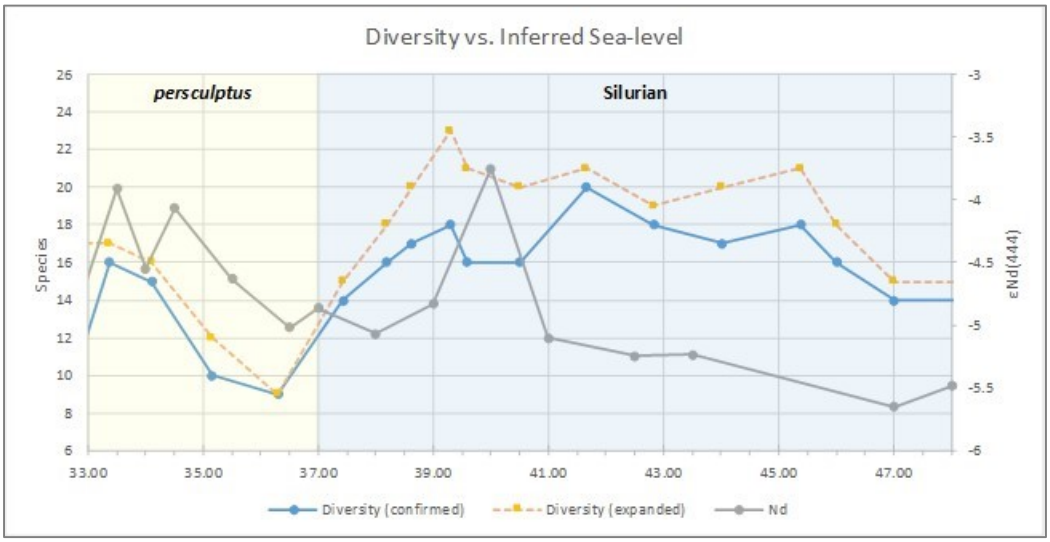

Figure 5.6. Post-extinction diversity vs. sea level. Expanded diversity adds questionable occurrences and species to ranges estimates. See Fig. 5.2 caption for a discussion of the neodymium level proxy.

5.2 Community Structure, Sampling, and Instability

Samples from the Katian and early Hirnantian portion of the section were counted in order to attain species abundance data to address two questions: 1. Did the sampling methodology used produce a reliable estimate of diversity (and is that estimate significantly different from previous estimates produced through lower intensity sampling)? 2. Did graptolite communities change structurally in the lead up to the LOME? These questions are interrelated. If communities shifted towards lower evenness (evenness is a measure of how similar in abundance each species in a

community is) in response to ecological crisis, then estimates of diversity during extinctions and other periods of ecological stress would be even more subject to sampling artifacts[19].

The methodology for counting and binning is outlined in Chapter 3 and Appendix C, and results of counts are presented as tables and graphs in Appendix B. A similar approach to assessing abundance (counting whole slabs) was employed independently by Pannell et al. (2006) on graptolites of the *sedgwickii* Zone (upper Aeronian, Llandovery) at Dob's Linn, as well as by Belscher (2007), on samples from Vinini Creek coeval with the present study, collected and studied specifically for the purpose of generating commensurable data for comparison with the present material.

The structure of communities can be examined and quantified in a number of ways with varying complexity. The simplest metric is diversity, i.e., the total number of taxa present in a community, which can be measured at various taxonomic levels. Other measures include morphological disparity (a proxy for ecological role diversity, e.g., Bapst et al., 2012), evenness, and various metrics of species abundance distribution (SAD), which attempt to determine the complexity of ecological interactions between species in a community. Further discussion of statistical analysis of communities is in the

[19] See Mitchell et al. (2007c) for discussion of the Inverse Signor-Lipps Effect. In uneven communtities a greater percentage of diversity is represented by rare taxa. The probability of recovery is a function of the original abundance and sampling intensity. Therefore, fewer taxa are likely to be recovered from uneven than even communities with the same sampling intensity.

Supporting Information for Sheets et al. (2016), while the body of that paper presents statistical analysis of the Blackstone River abundance data generated during this thesis. Consideration of evenness provides important paleoecological insight, but it also provides a check on sampling completeness. Uneven communities must be sampled much more intensely to accurately reflect their diversity than even ones, since rare taxa are less likely to be captured in a sample than common ones (Boyle et al., 2017). The present abundance counts show that communities become increasingly uneven in the lead up to the LOME, as they do at Vinini Creek (see Sheets et al., 2016, for analysis) and diplograptine taxa become vanishingly rare during the peak pulse of the extinction. In the first two *extraordinarius* Zone samples, 19.15 m and 19.20 m (note: the binning process in the final sample, 19.25 m, likely exaggerated the abundance of *Styracograptus mississippiensis,* so that sample is not discussed here), eight and six species are present, with diplograptines still comprising the majority of species diversity: five and three of those species, respectively. However, in terms of relative abundance, diplogratine species collectively account for <1% (19.15 m) and <0.5% (19.20 m) of specimens present. The rarity of captured diplograptines strongly suggests that residual diplogratine diversity remains underestimated at the Blackstone River section. This is supported by rarefaction analysis, which shows that the sampling of all three *extraordinarius* Zone samples is incomplete (see Appendix D). Additionally, most of the recovered diplogratine specimens are very poorly preserved. (For example, the final specimens of *Parorthograptus* have only a few, indistinct spines intact.) This

combination of rarity and poor preservation makes it very unlikely that they would have been recovered without the active search effort that was employed during this thesis.

Chen et al.'s (2005b) refugium hypothesis for the Yangzte Platform during the LOME was premised on the assumption that sampling at other sections was complete enough that the absence of diplogratines during the Hirnantian outside of China represented a genuine ecological signal, and not a sampling artifact. The present work, as well as recent work in Nevada (Belscher, 2007; Štorch et al., 2011), at the very least minimizes the argument for a refugium[20]. At the Blackstone River, diplograptines are present in all graptolitic lower Hirnantian collections, but graptolites are only known from the basal-most *extraordinarius* Zone. No graptolites have been recorded from any other part of the *extraordinarius* or lower *persculptus* Zone elsewhere in the Yukon, but the present work is the only targeted, intensive effort thus far to identify and recover taxa from this interval. Given how widespread the black shales of the Road River Group are in the Yukon, future work may show younger residual populations diplogratines in the Hirnantian in the Yukon as well.

The discovery of rare diplograptines in the Hirnantian at the Blackstone River section, Nevada (Štorch et al., 2011), and Siberia (Koren' and Sobolevskaya, 2008) has clear implications for the evaluation of previous Late Ordovician diversity estimates.

[20] Diplogratines remain only known from the *persculptus* Zone in South China and Nevada. It is possible that both of these regions functioned as refugia. Additionally, the patterns of early *persculptus* Zone diverification are still poorly known. It is possible that China played a crucial role in early post-extinction recoloniziation.

Mitchell et al. (2007c) referred to the bias created by highly uneven, ecological crisis communities as the 'Inverse Signor-Lipps Effect', after the well-known artifact whereby incomplete collecting results in artificially staggered LADs[21], making extinctions seem more gradual than they actually are. In the Inverse Signore-Lipps Effect, incomplete sampling of ecologically marginalized species has the opposite effect: exaggerating the abruptness of extinctions. The present data supports Mitchell et al.'s assertion that this is a real effect that must be taken into account in studies of extinctions.

The abundance estimates from the Blackstone River (as well as those from Vinini Creek) show that the impact of community unevenness on diversity estimates also extends beyond extinction events (albeit to a lesser degree). For example, in the pre-extinction interval of peak diversity (16.03 m, *mirus* Subzone), 17 taxa were recovered, with an additional three species inferred to be present from range-through data. Of these species, only seven occur as >1% of the population, five species occur as </=0.1% of the population, and two species collectively comprise 81% of the population. Figure 5.7 shows relative species abundance during the pre-extinction portion of *pacificus* Zone at the Blackstone River. This community structure—i.e., one or a handful of species making up more than 50% of a population—is present to varying degrees throughout all the counted samples (*ornatus* to *extraordinarius* Zone), and although not quantified, clearly continues throughout the younger samples at the Blackstone River (*persculptus* through *acuminatus* zones).

[21] Last Appearance Datum.

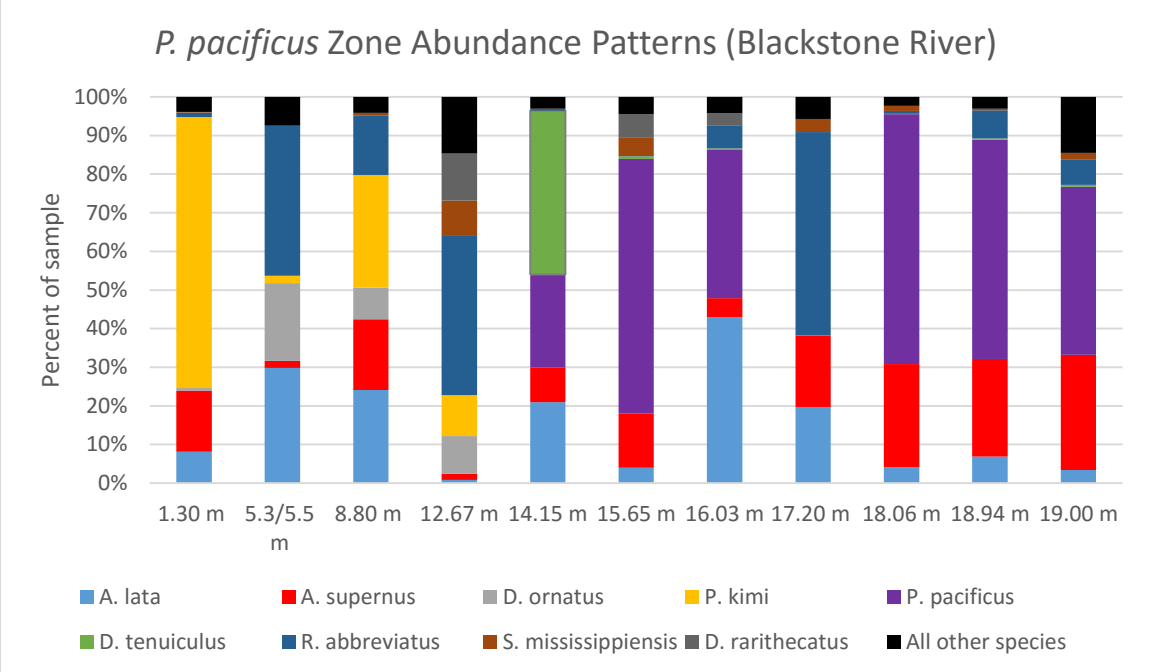

Figure 5.7. *P. pacificus* Zone abundance patterns (Blackstone River). Percentage of samples composed by each of the ten common species indicated. Samples from the interval of peak extinction (19.50 and 19.10 m) are not shown. All data were generated during the current thesis.

Similar abundance patterns occur at Vinini Creek. The precise composition of the Vinini collections differs from those at the Blackstone River, as the Vinini Creek section was deposited in a deeper water environment (LaPorte et al., 2009; Štorch et al., 2011) and therefore has consistently more mesopelagic species, but the overall pattern is similar. Figure 5.8 graphically represents species abundance during the *pacificus* Zone at Vinini Creek: twelve species (48% of total diversity) collectively account for 77-99% of specimens per sample in the interval, with a much smaller number of species accounting for half or more of the population in any given sample. The Vinini Creek data may also underestimate the number of very rare taxa, since many fewer specimens were examined (Sheets et al., 2016, table S04) than at the Blackstone River, the result of much lower specimen density in Vinini Creek section samples (pers. observ.). (Note:

rarefaction curves suggest sampling in most Vinini Creek samples was relatively complete (Belscher, 2007; Sheets et al., 2016)).

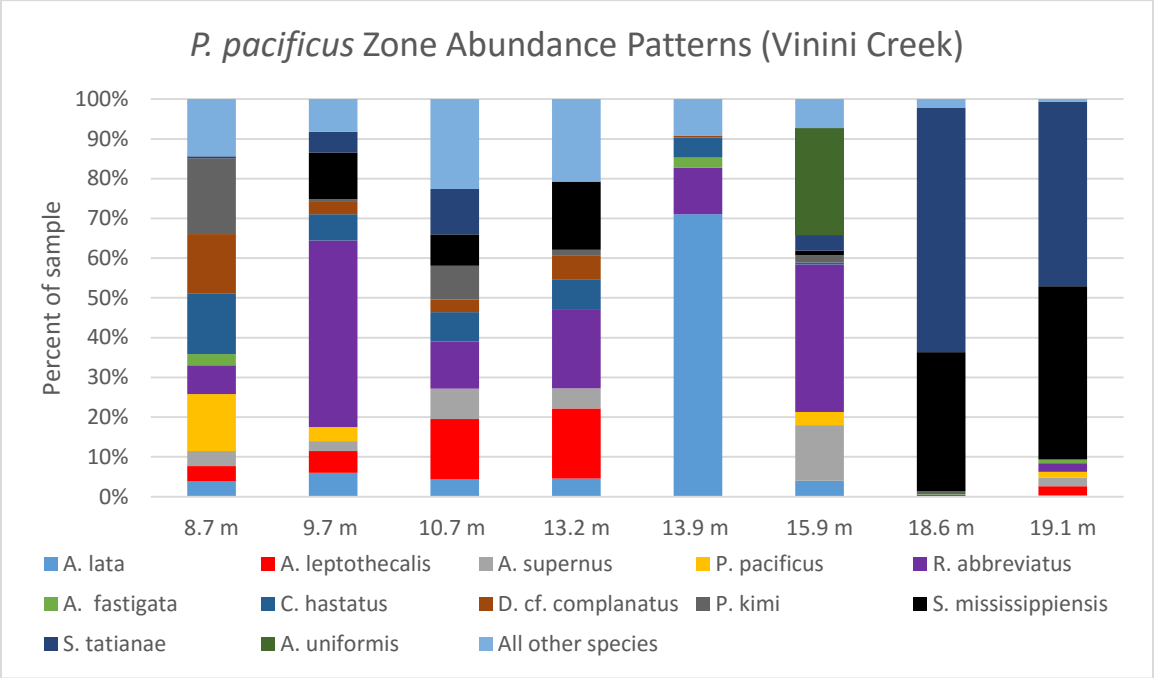

Figure 5.8. P. pacificus Zone abundance patterns (Vinini Creek). Percentage of samples made up of one of twelve common species. All data as presented in SI04a, Sheets et al. (2016).

Beyond the implications for the sampling, the patterns shown in the abundance data have an additional implication for studying the LOME. A small number of species (10) dominate all pre-extinction *pacificus* Zone collections at the Blackstone River (together they make up only 36% of total diversity, but comprise between 85-97% of specimens in each sample) (Fig. 5.7). It is also clear thatfrom that group of ten species there is variation in which specific species or subgroup of species dominates from collection to collection. While there is a stratigraphic component to which species dominate, since some species are restricted to specific intervals (e.g., *P. kimi* and *P. pacificus* are restricted to the lower and upper *pacificus* Zone, respectively) or are only

abundant for short intervals and then become rare (e.g., *D. tenuiculus*), the abundance of common, long-ranging species also varies. Sheets et al. (2016) showed that there was a strong correlation between abundance patterns and sea level, with relative proportions of species and specimens categorized as mesopelagic and epipelagic shifting along with water depth (see also Cooper and Sadler, 2010, and Cooper et al., 2012, for further discussion of graptolite ecology and extinction). Biotope assignment, however, at least in a binary mesopelagic vs. epipelagic biotope sense, fails to account for the gross shifts in dominant species evident in Figure 5.7, since the majority of the taxa that trade positions between samples are categorized as epipelagic species by Sheets et al.'s analysis[22] (*Anticostia lata, Paraorthograptus pacificus, Appendispinograptus supernus,* and *Rectograptus abbreviatus*). The principal model of the graptolite extinction during the LOME invokes the loss of the preferred habitat of mesopelagic biotope species, due to sea level fall and changing patterns of deep ocean circulation (Finney et al., 2007), and stress on epipelagic taxa, as a result of changing water temperatures and phytoplankton community composition (see Goldman et al., 2011; Melchin et al., 2013). Understanding the subtle environmental controls on pre-extinction patterns of community dominance within epipelagic communities has the potential to identify additional mechanisms underlying the loss of the species during the LOME or provide

[22] A brief discussion of biotope assignment occurs in Chapter 1. A detailed discussion is available in the Supplementary Information for Sheets et al. (2016).

greater precision to our understanding of the operation of known mechanisms. This is an avenue for future research.

Pannell et al. (2006) tracked a much smaller number of taxa, at a lower resolution (some taxa counted at the genus level), in their *sedgwickii* Zone abundance study, but they also noted strong variations in dominance and abundance, shifts that were correlatable between two outcrops, and sometimes persisted through several collections. They suggested that these abundance spikes might be responses to short-lived oceanographic changes, and might prove to be biostratigraphically useful (perhaps providing resolution below the zonal level). Sheets et al. (2016) showed that a common signal of community change (percent meso- vs. epipelagic species), correlating with inferred sea level change, could be detected at the Blackstone River and Vinini Creek; but this signal was subtle and overprinted by local conditions (e.g., position relative to the shelf, starting species composition). Additionally, the variation in timing of diversity peaks at the Blackstone River vs. Nevada and China, as well as the differences in species present, dominant species, and evenness, suggest that local conditions play a very strong role in graptolite community structure, and therefore biostratigraphic schemes based on abundance spikes are likely to be useful only on a regional level, or would require strictly comparative enviroments for those biostratigraphic analyses.

5.3 Extinctions and Environmental Causes

As discussed in Chapter 1, the prevailing model for the extinction of graptolites during the initial phase of the LOME invokes a combination of a habitat loss, owing to

the destruction of the oxygen minimum zone, ocean cooling, and a shift in the structure of phytoplankton communities (all linked to shifts in climate and icesheet growth). The selectivity of the mass extinction in regards to graptolites has long been noted (e.g., Melchin and Mitchell, 1991; Chen et al., 2005b). Diplograptine species immediately drop in diversity and lose ecological dominance to newly evolved or invading neograptine species in the latest Katian and earliest Hirnantian, before the clade as a whole gradually becomes extinct over the course of the Hirnantian. Chen et al. (2005b) showed statistically that the apparent taxonomic selectivity in South China was unlikely to have resulted from random extinctions. The reality of this pattern, and its relationship to ecological factors, is further supported by two lines of evidence: its global synchroneity throughout the well-studied sections of the paleotropics (Koren' et al., 2003; Chen et al., 2005b, Štorch et al., 2011; Melchin and Williams, 2000; the present data), as well as a reverse pattern of replacement (neograptines by diplograptines) earlier in the Katian (Goldman et al., 2011) that coincided with a shift to warmer, deeper, and more stratified oceans (Melchin et al., 2013). Understanding the biogeographic distribution of these two clades at a high-resolution clarifies what environmental factors might have limited their distribution during the Katian, as well as how those these factors might have changed, i.e., illuminating the possible environmental causal mechanisms for the LOME. Ordovician neograptines differ morphologically only in very subtle ways from coeval diplograptine genera such as *Styracograptus,* leading to many spurious reports in the literature, which obscure their true geographic distribution (Štorch et al., 2011;

Goldman et al., 2011), and complicates attempts to understand the relationship between shifts in distribution, extinction, and environmental change. Goldman et al. (2011) attempted to expunge false reports of neograptines in the paleotropics in the pre-Hirnantian Ordovician and confirm absences by reexamining specimens and/or published illustrations, but noted that this process could not control for sampling intensity, and therefore false absence data.

The Blackstone River data are uniquely useful towards the goal of clarifying neograptine biogeography for two reasons: first, the process of counting graptolites required that every individual specimen was closely examined and categorized during the Katian and earliest Hirnantian, a degree of effort that does not normally occur in diversity surveys, making it extremely unlikely that species of neograptines, if they occurred, would have been missed. (Testing the neograptine geographic exclusion hypothesis was also a conscious secondary goal of this thesis, so extra effort was expended during counting to check specimens that could potentially belong to the clade.) Second, the very fine scale of sampling across the Katian-Hirnantian boundary (five cm resolution) produced a precise snapshot of the timing of the neograptine invasion and its relationship with both diplograptine diversity and abundance. The present data confidently demonstrate that neograptines were absent from the Blackstone River area during the study interval until the very latest Katian. Close examination confirmed that none of the specimens that were recovered by the sampling were neograptines, and rarefaction analysis suggests that it is unlikely that

neograptines were present at the section but not recovered by sampling—see Appendix D. It also revealed that two species of neograptines (*Metabolograptus ojsuensis* and *Neodiplograptus charis* invade immediately below (19.10 m) the base of the Hirnantian (19.15 m), confirming a pattern observed at some other paleotropical localities (e.g., Siberia), but easily missed at lower resolution.

Although there is no obvious changes in the physical depositional environment (black shales are continuous), several lines of evidence point to environmental changes occurring—and presumably driving—the transition between diplograptine and neograptine community dominance in the latest Katian. First, diversity drops and extinction rates increase immediately prior to the first appearance of neodiplogratines (see Fig. 5.4), suggesting the addition of an environmental stressor of some sort. Second, the highest sample below the appearance of neograptines (19.05 m) is dominated by *Anticostia uniformis* (81% of specimens), a long-ranging species that comprises 3.4% of the preceding sample (19.0 m), and had never been greater than 0.25% of any other sample below that (see Appendix B). This is the highest degree of dominance by a single species in any collection from the Blackstone River, suggesting a fundamental breakdown within the community[23]. Third, the samples from 19.0 m to

[23] Note: *Anticostia uniformis* does not have a clear biotope affiliation in the analysis of Sheets et al. (2016), but it is one of just seven diplograptine species that persist into the *persculptus* Zone in Nevada (four are epis, one is a meso, and two are indeterminate: Štorch et al., 2011; Sheets et al., 2016). It also persists to just below the *persculptus* Zone in China (Chen et al., 2005b), and was the only graptolite recovered from light coloured (olive), presumably well-aerated shales (late Katian to Hirnantian age) within the limestone-dominated Xiazhen Formation (Chen et al., 2016). This suggests that it was preadapted towards tolerance of the cooler, mixed Hirnantian oceans.

19.25 m possess an increasingly diverse accessory fauna, indicating changing water mass properties: abundant small, phosphatic brachiopods just before the first appearance of neograptines; small phosphatic brachiopods, plus several larger species of brachiopods or bivalves, coinciding with the appearance of *M. ojsuensis* and *Neo. charis;* and an abundant, monospecific trilobite fauna in the shales of the basal Hirnantian (synchronous with the first appearance of *Metabolograptus extraordinarius*). The trilobites are mostly disarticulated, but some articulated specimens occur, along with abundant early growth stages (protaspids). Co-occurring graptolites are somewhat current aligned, so the trilobites may have been transported. Nevertheless, the presence of these well-preserved trilobites suggests that well-aerated bottom waters suitable for benthic fauna existed adjacent to the area of deposition by the lowest Hirnantian.

These changes took place within the context of longer-term shifts in diversity and community structure. The lower *pacificus* Zone corresponds with an interval of relatively warm global temperatures (Finnegan et al., 2011; Melchin et al., 2013) and relatively high sea levels (Holmden et al., 2013). Sea level begins to fall nearly coincident with the base of the *mirus* Subzone at the Blackstone River (see Fig. 5.2; note: the base of the *mirus* Subzone is placed too high in Holmden et al., 2013, fig. 4) and the percent of mesopelagic species and evenness both fall correspondingly (Fig. 5.10; see also Sheets et al., 2016). Surprisingly, diversity actually rises within the early *mirus* Subzone interval (Fig. 5.1 and Fig. 5.9), the opposite of what is seen higher in the section (Fig. 5.6)

and what might be predicted from the biotope model of extinction. Given the low number of samples within the lower *pacificus* Zone it is not clear that the apparent increase in diversity in the *mirus* Subzone is genuine. Even if it is, however, Finnegan et al. (2011) demonstrated that glacial ice volume (and therefore sea level) and sea surface temperature (and presumably deep ocean circulation and phytoplankton composition), are not always coupled during the Ordovician and Silurian. Therefore, it is possible for sea level to fall without triggering an extinction scenario, based on the model of LOME graptolite habitat change. The fact that evenness and percent mesopelagic species do fall during the *mirus* Subzone, in step with sea level (Fig. 5.10), supports the general biotope/ stratification model of graptolite ecology.

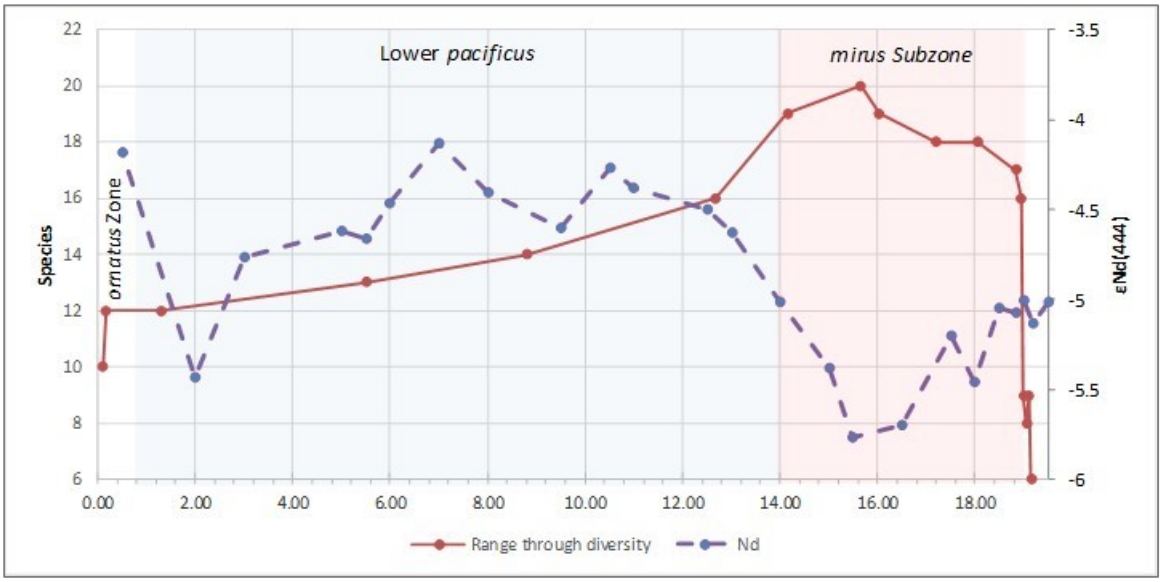

Figure 5.9. Pre-extinction diversity vs. sea Level. Neodymium proxy for sea level versus range through diversity data. εNd provides a proxy for sea level change: highly negative εNd values correspond to low sea level. Data as presented in Sheet et al. (2016), supplemental documents. Neodymium values provided by Chris Holmden (c.f. Holmden et al., 2013).

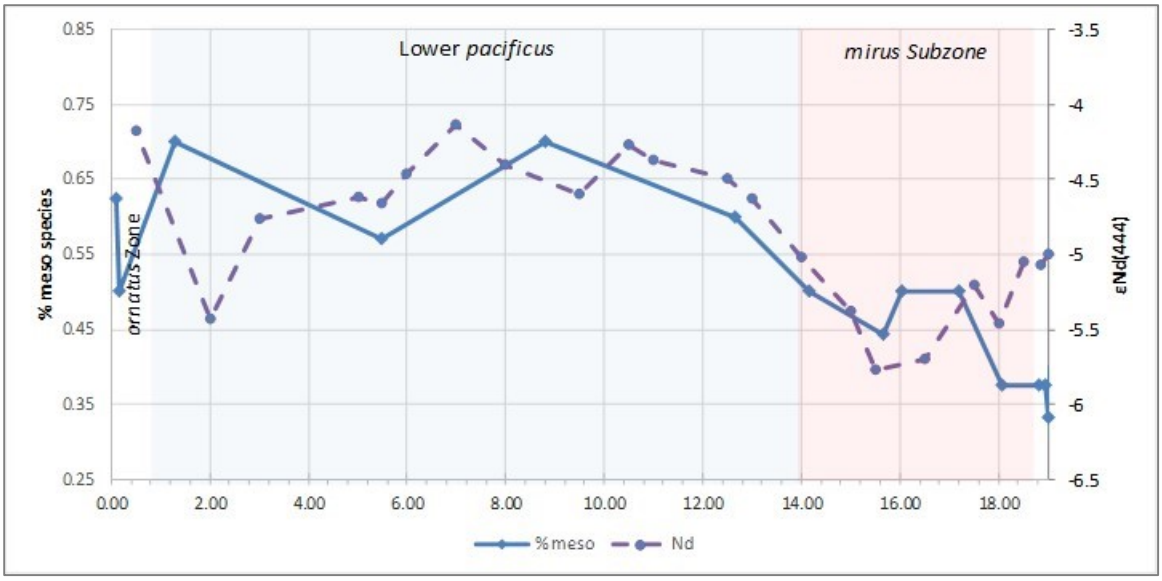

Figure 5.10. Sea level relative to community composition. "% meso species" is the ratio of species assigned to the mesopelagic biotope vs. epipelagic biotope. Data as presented in Sheet et al. (2016), Supporting Information. Nd data as explained in Fig. 5.9.

Shortly above the *mirus* Subzone peak, diversity at the Blackstone River begins to decline (Fig. 5.9), due mostly to a drop in origination (Fig. 5.3). Sea level rises slightly in the upper *mirus* Subzone, but without a corresponding shift towards more mesopelagic species or more even communities (Fig. 5.10; Sheets et al., 2016). This implies that the return of higher sea level did not bring a corresponding return of the preferred dysoxic habitat of mesopelagic graptolites (Fig. 5.10), supporting increased mixing of deeper waters during the latest Katian.

Whereas the LOME has been studied extensively, little work has been done on the biodiversity patterns of graptolites in the latest Hirnantian and early Silurian. The LOME is recognized to be stepwise, with an initial pulse that strongly affected the graptolites, followed by a second pulse, corresponding to a return to pre-glacial conditions, and a spread of black shales, that primarily affected reef and benthic communities, but

apparently had less affect on the graptolites (e.g., Sheehan, 2001; Melchin et al., 2013). Chen et al.'s (2005b) detailed study of graptolite diversity patterns in South China focused on the timing and and potential mechanisms underlying the LOME, but their analysis also suggested a number of interesting patterns in the post-extinction interval in South China. Until now, no detailed comparative biodiversity data has existed from other regions to test whether these post-extinction biodiversity shifts represent local or global events. Providing tests and confirmation of these patterns is a major contribution of this thesis.

As previously discussed, diversity and range data at the Blackstone River were gathered from 20 large samples, at approximately one-meter intervals, from the inferred post-glacial flooding surface (upper *persculptus* Zone) to the base of the *atavus* Zone. Additional material originally collected for other purposes (lithological, conodont, and isotope samples) was examined around the *persculptus-ascensus* and *ascensus-acuminatus* zonal boundaries to provide better resolution around intervals of apparent species loss. This sampling was less intensive than at the base of the Hirnantian, but nonetheless clear patterns of diversity change emerge. The lowest *persculptus* Zone collections already possess a diverse community of graptolites (exclusively neograptines), which reaches a peak in the middle of the preserved portion of the *persculptus* Zone, before dropping steadily across the *persculptus-ascensus* boundary (to a third of peak diversity). This interval shows strongly elevated extinction risks, as well as a drop in origination (see Figs. 5.11 and 5.12). Extinction progresses over three samples, with a larger drop in the uppermost *persculptus* Zone sample, a similar pattern (though less

dramatic) to that seen in the latest Katian. The same pattern occurs in China (Chen et al., 2005b: figure 7), where origination drops to nearly zero in the latest *persculptus* and extinction peaks. The lowest *ascensus* Zone at both the Blackstone River section and in the Chinese composite both show strong spikes of origination, completing the turnover in taxa.

Corresponding with the shifts in diversity at the Blackstone River are lithological and geochemical (Nd) signals that suggest shallowing and an increase in aeration. Lithology shifts from dark, thinly bedded shales associated with peak *persculptus* Zone diversity, to paler, well-cemented, somewhat thicker bedded mudstones in the uppermost two *persculptus* collections, and then to tan siltstones in the basal *ascensus* Zone. Subsequent *ascensus* Zone collections return to shales, but the lower ones remain lighter in colour than those closest to the base of the *acuminatus* Zone. These shifts in lithology correspond with drops in total organic carbon (TOC, see LaPorte et al., 2009), as well as a shift to more negative εNd, supporting shallowing (see Fig. 5.6). Neodymium values support sea level remaining low throughout most of the *ascensus* Zone (*ascensus* Zone = 37.0-41.66 m), before rising and hitting a peak at the base of the *acuminatus* Zone, followed by an apparently sustained fall for the remainder of the *acuminatus* (sampling resolution is low for the mid and upper *acuminatus* Zone).

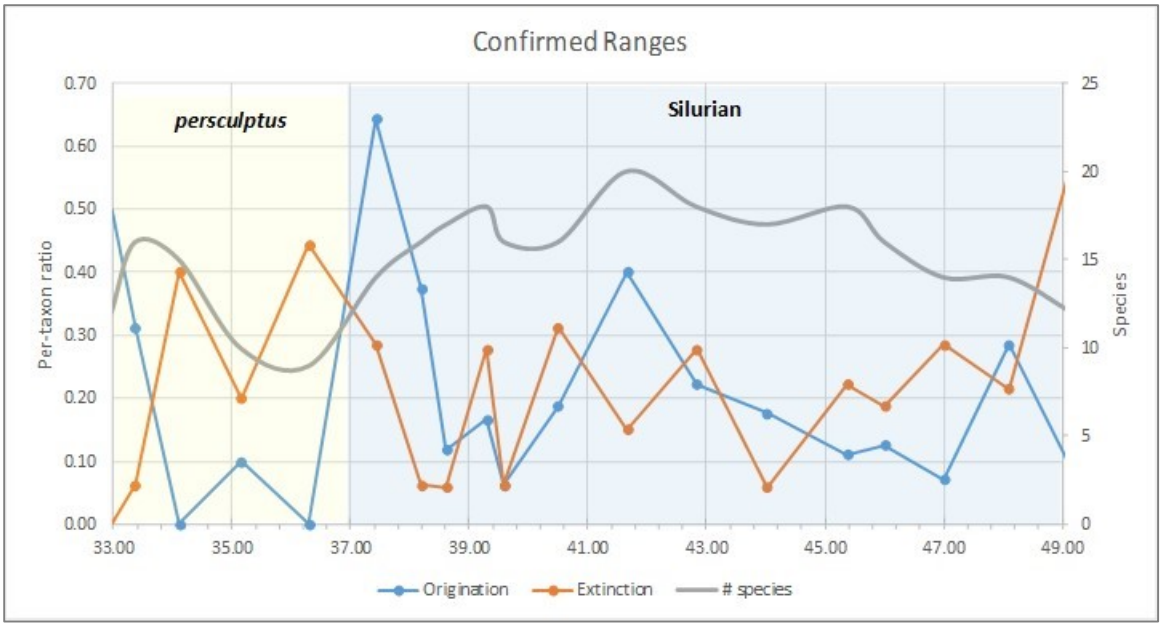

Figure 5.11. Rhuddanian extinction patterns (confirmed ranges). The *acuminatus* Zone boundary is placed at 41.66 m, but may plausibly actually be at 39.59 m—see Chapter 5.1. See discussion of the effects on per-taxon extinction and origination rates in Figs. 5.2 and 5.3.

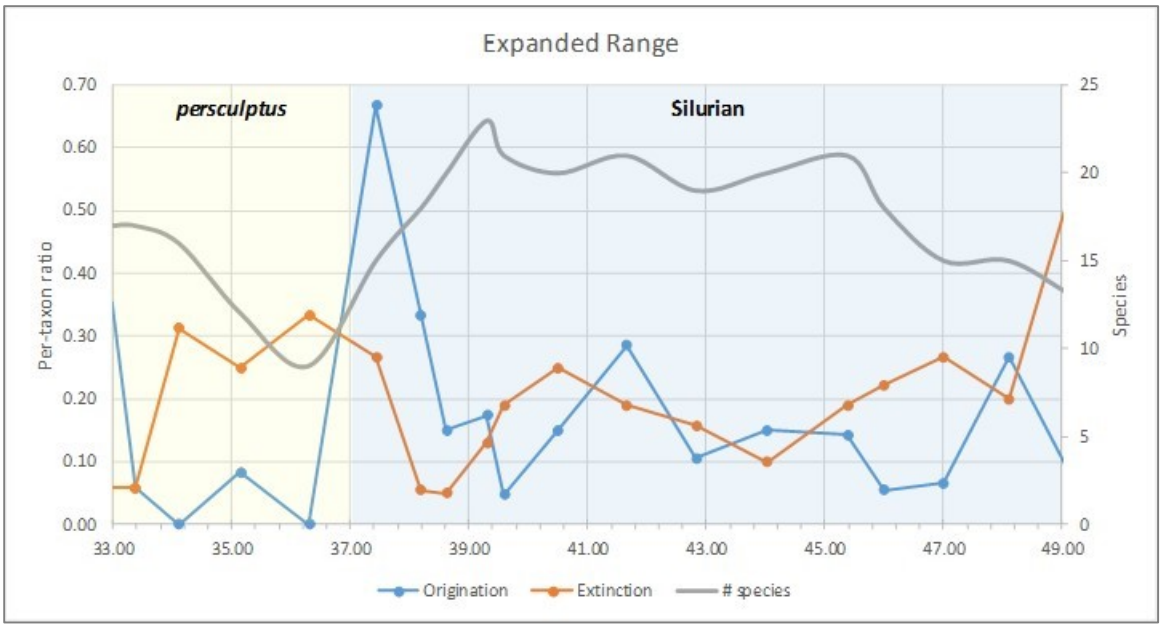

Figure 5.12. Rhuddanian extinction patterns (expanded ranges). Expanded ranges includes questionable species and occurrences in calculation of species' ranges lengths. The base of the *acuminatus* Zone is not shown. It is placed at 41.66 m, but may plausibly be at 39.59 m—see Chapter 5.1. See discussion of the effects on per-taxon extinction and origination rates in Figs. 5.2 and 5.3.

Because of its association with the LOME, sedimentary characteristics of early to mid-Hirnantian strata have been studied more intensively than those of the latest Hirnantian and earliest Rhuddanian. Black shale deposition is constant across the Ordovician-Silurian boundary at Dob's Linn (Williams, 1983; pers. observ.) and in Scania, Sweden (Koren' et al., 2003). Melchin et al. (2013) showed that black shales were more widespread and persistant during the Silurian than during the Ordovician, perhaps due to shifts in nutrient flux from plant-mediated weathering, changes in salinity-based ocean stratification due changes in precipitation, or some combination of those and other factors (Melchin et al., 2013). Given this, it is possible that the Rhuddanian sedimentological record does not record sea levels shifts as readily as the Katian and Hirnantian. That said, there is some support for sea level fall at the base of the Rhuddanian. Haq and Schutter's (2008) synthesis of Paleozoic global sea level data shows a Rhuddanian boundary drop, although given the coarse resolution of the analysis, it is possible that this actually represents one of the earlier Hirnantian glacial advances. Similarly, Lui et al. (2017), in a recent sequence stratigraphic study of the Lungmachio Formation, South China, showed a small and larger sea level fall in the lower and middle Rhuddanian, respectively. The Ordovician-Silurian boundary is poorly constrained biostratigraphically in their study, however, so it is possible that one or both of these events occurred earlier.

Diversity patterns across the *ascensus-acuminatus* zonal boundary at the Blackstone River less clearly parallel those in China than those at the *persculptus-ascensus*

boundary. This is partially because there is some uncertainty as to the position of the base of the *acuminatus* Zone (see discussion in Chapter 6.1), and because this interval was studied less intensively than other intervals in the section (making range lengths and diversity counts less robust), but also because background rates of extinction and origination appear to be consistently higher, making peaks harder to detect. There is a spike of origination at the base of the *acuminatus* Zone, which is also seen in China, and extinction rates are elevated around the boundary, but less so than at the base of the Silurian. The truncation of sampling at the base of the *atavus* Zone means that upper *acuminatus* Zone extinction and diversity patterns are likely to be affected by edge effects (Foote, 2000). Nevertheless, it is worth noting that there appears to be another interval of species turnover in this interval, which globally corresponds to a dramatic shift in the typical morphology of graptolites (abundant dimoprhograptids and monograptids). Abundant material exists above the end of the collected area of the section at the Blackstone River for future workers to investigate the nature and timing of this shift.

A final pattern worth discussing is community structure and dominance. As noted previously, the pattern of one or a small number of species dominating each sample seen in the pre-extinction interval continued throughout the upper portion of the section, as did the tendency for the specific species that dominate any given samples to vary even in stratigraphically close collections. No counts were made on samples from the *persculptus* Zone or above, so the degree of evenness and any

stratigraphic trends in evenness could not be quantified[24], but the strong dominance of all samples by a handful of species is readily observed. The *persculptus* Zone and Silurian samples differ from the older ones, however, in that the taxa that are dominant in one sample rarely retain or regain that position in subsequent samples. In contrast to Katian species, such *Rectograptus abbreviatus, Appendispinograptus supernus,* and *Paraorthograptus pacificus*, which dominated samples, at least intermittently, for all or most of the *pacificus* Zone interval, dominant Silurian species are either restricted to short intervals at the Blackstone River section (e.g., *Hirsutograptus comantis, Metabolograptus*? sp., *Paramplexograptus kiliani*) or dominate for only a short interval and are rare before and/or after (e.g., *Korenograptus laciniosus , Neodiplograptus* sp. 1). Thus, communities in the post-extinction interval appear to be considerably less stable than those existing prior to the extinction, and taxa, especially taxa that dominate samples, appear to be much shorter-lived. The exception to this is *Paraclimacograptus obesus,* which dominates almost all samples from the mid *acuminatus* to at least the base of the *atavus* Zone (44.04 m to 49.50 m). Whether this represents a shift to stabler communities in the upper half of the *acuminatus* Zone or whether *P. obesus* is simply a long-lived exception to a rule requires more data to establish (note: secondarily dominant taxa still appear be unstable within the upper *acuminatus* Zone, but without abundance data this is difficult to confirm). In their analysis of the global graptolite

[24] Species abundance was recorded semi-quanitatively, i.e., taxa were ranked as 'rare', 'uncommon', or 'abundant'.

composite, Crampton et al. (2016) identified a broader version of the pattern described here: Late Ordovician and Silurian species appear to be particularly short-lived in comparison with pre-Katian species, with rapid species turnover, which is the background condition for most of the Silurian.

Having identified a common interval of extinction in China and the Yukon at the Ordovician-Silurian boundary (and possibly at the base of the *acuminatus* Zone), the next step is to consider causes—specifically whether the models applied to the LOME have explanatory power in the late Hirnantian and Silurian. Chen et al. (2005b) considered whether the late *persculptus* Zone extinction corresponds to the well-studied second wave of the LOME (which strongly affected benthic communities during the *persculptus* Zone). They concluded that this was unlikely because the end *persculptus* extinction post-dates the main phase of post-glacial sea level rise and return to stratified ocean conditions. Additionally, the shift in environmental conditions that decimated Hirnantian benthic communities (at the level of the post-glacial sea level rise) corresponds to a level of high graptolite diversity. Instead, Chen et al. speculated that the extinction event may have resulted from internal ecological dynamics, as destabilized ecosystems restabilized in the post-extinction interval (i.e., the second pulse of graptolite extinctions may have required no external forcing agent). The present data support the suggestion of unstable post-extinction communities, especially in the early Rhuddanian (fluctuating dominance and elevated extinction rates), but whether this was the result of internal ecosystem

dynamics, or because the climate system remained unstable in this interval, or both, is unclear.

Some aspects of post-extinction graptolites dynamics are readily correlatable to climate. From the *persculptus* to lower *acuminatus* Zone sea level tracks diversity (Fig. 5.6), with high diversity associated with high sea levels. Additionally, the *persculptus-ascensus* extinction closely correlates with evidence for sea-level fall and increased aeration (drop in TOC, shift from shales to siltstone), and corresponds roughly with an interval of sea surface cooling (Finnegan et al., 2011). These observations are all compatible with the hypothesized mechanisms for graptolite diversity loss during the LOME. That is, some combination of cooler water, the loss of preferred habitat (dysoxic deep shelf and slope waters), and a shift in the phytoplankton community (e.g., Finney and Berry, 2007; LaPorte et al., 2009; Goldman et al., 2011; Melchin et al., 2013; Rohrssen et al., 2013). For these mechanisms to impact neograptines in the manner in which they impacted diplograptines, the former would have had to transition into the niche/ecospace vacated by diplograptines. This implies that the failure of the neograptines to occupy this space during most of the Katian (Goldman et al., 2011) was the result of competitive exclusion, not some fundamental aspect of neograptine physiology.

Several observations made during this thesis are difficult to explain with the mesopelagic habitat loss model, however. Assuming that it is not an artifact, why would graptolites diversify during the early *mirus* Subzone interval of sea level drop, as they

appear to at the Blackstone River? Further, what explains the strong spike in origination at the base of the *ascensus* Zone, an interval of continued low sea level and apparently increased mixing (and correspondingly, why do the taxa that originate in this interval of lower sea level appear to disappear from the section with the rise of sea level before the base of the *acuminatus* Zone)? Studies of shifts in phytoplankton communities via geochemical proxies or direct observation of fossils have yielded intriguing data for the Katian and early Hirnantian extinction (LaPorte et al., 2009; Delabroye et al., 2011; Melchin et al., 2013; Rohrssen et al., 2013), suggesting that species extinction patterns may be to due to food preference, as phytoplankton communities shifted in dominance between cyanobacteria and algae. In this perspective, sea level and water mass properties (e.g., temperature, salinity, nutrient and oxygen content), may have exercised only indirect control on graptolite diversity and abundance, through their control on the primary producers. The thick exposure, consistent record through the latest *persculptus* Zone and early Rhuddanian, and tight biostratigraphic control make the Blackstone River an ideal location for future efforts along this vein.

Chapter 6. Species Descriptions

6.1 Introduction

This chapter follows the higher-level taxonomy proposed by Štorch et al. (2011) and Melchin et al. (2011). As there is no overlap in species' ranges, taxa from the pre-glacial (*ornatus* to *extraordinarius* zones) and post-glacial (*persculptus* to *acuminatus* zones) intervals are presented in separate sub-chapters for ease of navigation. Plates (photographic and line drawings) are binned in temporal sequence (Plates 1-26: *ornatus* to *extraordinarius*; Plates 27-38: *persculptus* Zone; and Plates 39-57: *ascensus* to *atavus* zones) to facilitate visual searching for taxa while reading this thesis and by future investigators doing comparative work. To aid comparison, family and genera are presented in the same order used by Štorch et al. (2011) in the section covering the *ornatus* to *extraordinarius* zones, and follow Melchin et al. (2011) for the upper zones.

The state of Late Ordovician-early Silurian species-level systematics is in flux. In many cases, lengthy synonymy lists have recently been published (e.g., Štorch et al., 2011 or Loydell, 2007) or are in preparation (Fan et al., in prep.), and including them here would be duplicative. In other cases, species are poorly known and/or poorly described and illustrated, with primary descriptions often not available in English. Synonymizing this material is best done by authors working in these regions with access to type collections. This work is currently underway. For these reasons, only incomplete synonymies are given within the systematic section, mostly within the 'remarks' section

for each species, and many species are left in open nomenclature. References are given to detailed published synonymies where they exist, along with regionally relevant papers and/or papers where confident identification can be made based on illustrations, or where it is judged that comparative observations will be of use to future intensive revision efforts.

Figure 6.1 shows morpholgical features used in this thesis for species identifications. Discussion of some other relevant terminology is presented in the Glossary. 2TRD was used in this paper in a manner different from that intended by Howe (1983). Howe defined 2TRD as the distance in millimeters between two equivalent points on thecae *n*-1 and *n*+1, with the intermediate thecae *n* used as the reference point. For example, in Howe's definition, 2TRD th2 is the distance between the apertures of thecae th1 and th3. In gathering data for this thesis, 2TRD was measured with the reference thecae being the first aperture in the series, not the middle, e.g., the distance between the aperture of th1 and th3 is here referred to as 2TRD th1. This approach was also used by Melchin in the data set of Chinese material and types that he provided (pers. comm.), as well as by Mitchell, both in earlier published work (e.g., Mitchell et al., 2009) and in some data he provided early in the production of this thesis. In contrast, Štorch used the definition of 2TRD intended by Howe in producing the majority of the measurement data for Vinini Creek, which were presented in Štorch et al. (2011) and provided in raw form for use in producing this thesis. This inconsistency in use was not discovered until all of the data in this thesis was

gathered and analysis completed, making normalizing measurements logistically unfeasible. The result is that the reference position for 2TRDs as measured in this thesis is one place off of measurements provided for the Vinini material. Since 2TRD stabilizes distally in most species, this difference in definition should have little effect on comparisons of th10 and beyond. For comparisons of th2 and th5, however, values measured in this thesis will be marginally higher than values measured using Howe's intended methodology (th2 and th5 as measured for this thesis = th1 and th4 as intended by Howe). For the purpose of this thesis, all references to 2TRD follow the alternative definition of 2TRD, rather than Howe's usage, except where noted. Where data is compared that were collected using Howe's definition (e.g., Vinini Creek measurements) it is indicated in graph captions.

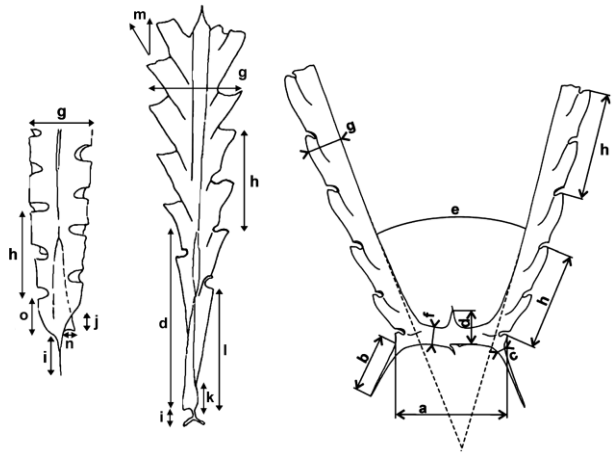

Figure 6.1. Morphological features used in species descriptions. (a) axial width; (b) spine length; (c) basal spine width; (d) length of sicula; (e) axial angle; (f) stipe width at th1[1] (dicellograptids); (g) dorsal ventral width (DVW); (h) two theca repeat distance (2TRD); (i) length of virgella; (j) sicular exposure below th1[2]; (k) distance between sicular aperture and upward-grown portion of th1[1]; (l) distance between the sicula to th1[1] aperture; (m) thecal angle/angle of supragenicular wall; (n) width of the sicular aperture; (o) upward-grown portion of th1[1]. Figures modified from Loydell (2007) and Štorch et al. (2011).

6.2 *Dicellograptus ornatus, Paraorthograptus pacificus*, and *Metabolograptus extraordinarius* zones

Suborder Axonophora

Infraorder Diplograptina

Superfamily Dicranograptoidea

Genus *Dicellograptus*

Genus *Diceratograptus*

Genus *Pleurograptus*

Superfamily Diplograpoidea

Family Diplograptidae

Genus *Diplograptus*

Genus *Rectograptus*

Genus *Paraorthograptus*

Genus *Anticostia*

Genus *Parareteograptus*

Family Lasiograptidae

Genus *Phormograptus*

Genus *Yinograptus*

Superfamily Climacograptoidea

Genus *Climacograptus*

Genus *Styracograptus*

Genus *Appendispinograptus*

Infraorder Neograptina

Family Normalograptidae

Genus *Normalograptus*

Family Neodiplograptidae

Genus *Neodiplograptus*

Genus *Metabolograptus*

SUPERFAMILY Dicranograptoidea, Lapworth, 1873; emend Mitchell et al., 2007b

GENUS *Dicellograptus* Hopkinson, 1871

Type species. *Didymograptus elegans* Carruthers, 1867, subsequently designated by Gurley 1896.

Remarks: With their divergent stipes, common rhabdosomal coiling, and stipe torsion, species of *Dicellograptus* are particularly susceptible to artifacts of preservation. Depending on the nature and angle of compression, flattened specimens of the same species may manifest a wide variety of apparent thecal morphologies, thecal widths, axial forms, and stipe forms upon compaction (e.g., Williams et al., 1982). Further, many species produce features that have been considered diagnostic only late in astogeny, e.g., large basal spines and axial “membranes”, making identification of juvenile specimens difficult. As a result, a considerable number of likely redundant species exist in the literature, along with a large number of collections of unassigned specimens. Many of the species described below are left in open nomenclature in light of this. Revision of the genus would form a very useful future project.

***Dicellograptus ornatus* Elles and Wood, 1904**

Plates: (Photos) 19.1-7, 20.5, 20.8-10, 22.5;

(Line drawings) 5.6?, 5.8?, 6.4?, 6.1-3, 9.2-7

Material and stratigraphical range: Common from the upper *ornatus* and lower *pacificus* zones. 29 specimens measured in detail, plus 5 specimens questionably assigned.

Description: Robust species with square axial region and initially upright stipes, which diverge at ca. 30-50 degrees, and gently curve dorsally, producing an ovoid form in mature specimens. Stipes sometimes cross distally. Maximum stipe length to 110 mm. DVW at th2 is 0.4-0.58 (mostly ca. 0.45-0.5 mm), 0.45-0.65 mm at th3 (mostly 0.5-0.58 mm), 0.58-0.83 mm at th5 (mostly 0.6-0.7 mm), 0.68-0.9 mm at th7, 0.65-0.9 mm at th10 (mostly >0.75 mm), and 0.75-1.2 mm distally (mean is 1 mm for the spiraling morph). 2TRD is 1.35-1.7 mm at th2, 1.7-1.9 mm at th5, 1.65-2.2 at th7, and 1.9-2.15 mm distally (1 specimen is 2.6 mm). Axial width is variable: 1.5-1.9 mm (1 specimen is 1.35 mm). Each theca in the first pair bears a robust subapertural spine that is up to 4 mm long and 0.18-0.13 mm wide (up to 0.5 mm, where secondarily thickened). Thecae are straight to moderately inclined, depending on orientation upon compression, with slightly convex supragenicular walls. Thecal apertures are introverted. Interthecal septa are inclined at ca. 45 degrees. Several specimens possess a basal interstipe membrane that extends up to the fourth thecal pair along the dorsal margin of each stipe, and up to the third thecal pair at its midpoint (see Plate 19.1b and 19.5b). Specimens with developed membranes also possess a parathecal-like thickening of the spines (see Plate

19.5a). The sicula is normally not preserved, but it is 1.8 mm long in one 5.5 mm long specimen.

Remarks: *Dicellograptus ornatus* is distinguished from contemporary dicellograptids by the presence of long and robust subapertural spines, slightly convex and introverted thecae, a square proximal region, and, in most specimens, straight stipes with a moderate axial angle. Most illustrated material matches this description, although, as Štorch et al. (2011) noted, examples of specimens with distally curved stipes are known from the literature. For example, Ross and Berry (1963) illustrated (pl. 6, fig. 13 and 19) examples of specimens that match the two morphs identified in this collection. The type specimens of *D. ornatus* (two specimens illustrated by Elles and Wood, 1904, and assigned by Toghill, 1970) are immature, but possess a maximum DVW of 0.6-0.7 mm. Other authors report maximum distal widths at somewhat higher values: for example, 0.7-0.8 mm (Williams, 1982: a collection that includes specimens of the larger *Dicellograptus mirabilis*); up to 0.9 mm (Apollonov et al., 1980); 0.8 mm (Mu et al., 1993); 0.8-0.9 mm (Mu et al., 2002); up to 1 mm (Ross and Berry, 1963). Štorch et al. (2011), reported extreme values of up to 0.9 mm, but all their illustrated specimens fall well below this (maximum of 0.55-0.65 mm). Mu and Chen (in Li, 1984) described a long-spined dicellograptid, *Dicellograptus magnus*, occurring below the *mirus* Zone, with a rapidly attained DVW of 1.2 mm, which Mu et al. (1993) considered to be a junior synonym of *D. ornatus*. Spine length in *D. ornatus* is variable and generally increases

with maturity, but some specimens described by Štorch et al. (2011) with maximum DVWs of <0.6 mm possess spines in excess of 3 mm long [data provided by authors]. Within the present collection, two apparent morphs occur: those from the *ornatus* Zone and lowest *pacificus* Zone have straight, upright stipes, a somewhat lower DVW (mean of 0.75 mm vs. 0.85 mm at th10), and less stipe torsion compared to higher collections. [See Plate 6.2 and 6.3 for comparisons of DVWs and 2TRD.] The upper collection mostly contains very mature specimens (three with maximum stipe lengths over 85 mm), the result of targeted collection of a rich horizon of mature current-aligned specimens. All large specimens have curved stipes, with prominent torsion present along the length of stipe, and several have one or more stipe crossings distally (at 45 mm and 80 mm in the largest specimen—Plate 9.2). Amongst the specimens showing distal stipe curvature, several observations can be made: 1) apparent stipe width, as well as apparent inclination of supragenicular walls, varies strongly along the stipe as a result of torsion and resulting angle of flattening; 2) basal webs and secondary thickening on spines only occur in specimens that are very mature; 3) although all are roughly ovoid, rhabdosome form varies considerably, with some specimens exhibiting a bullet-shaped form similar to specimens assigned by Mu et al. (1993) to *Dicellograptus complanatus arkansasensis,* and others possessing initially nearly vertical stipes, followed by dorsal curvature, similar to specimens illustrated as *Dicellograptus tumidus* by Mu et al. (1993, e.g., compare Plate 9.7 to Mu et al.'s plate 10.6, 12.4 and 12.7). The differences between the two morphs of *D. ornatus* in this collection in terms of DVW and rhabdosome form are most

likely due to variation in angle of compression, maturity, and intraspecific variation. A comparison of proximal and distal DVW for specimens of *D. ornatus* from China, Nevada, and the Yukon (Fig. 6.4) shows that dimensions are consistent within populations, but show considerable variation geographically and, in the case of the Blackstone River, stratigraphically. Consideration of any two of these populations in isolation from the rest could easily support division into separate species or sub-species. For example, the specimens from Nevada and the Yukon are non-overlapping in measurements of DVW (Fig. 6.4). However, in light of the many commonalities, e.g., rhabdosome form and spine length, they are considered conspecific.

Chen (1993, in Mu et al.) distinguished *Dicellograptus mirabilis* from *D. ornatus* based on very robust spines, the presence of a basal membrane, rapidly attained high DVW, and high axial width (2.0-2.5 mm). Robust specimens in this collection with basal membranes and thickened spines, such as those illustrated in Plate 19.1, 19.5, and 19.6, would likely be assigned to *D. mirabilis* under these criteria, e.g., the reassignment of William's (1982) specimens of *D. ornatus* to *D. mirabilis* by Chen et al. (2000). However, the present specimens, unlike those that occur higher in the section (see below) do not possess the wide axil or rapid widening of the type material of *D. mirabilis*. Several specimens from sample 8.8 m, e.g., Plates 5.6, 5.8, and 6.4, 19.7, 20.8-10 differ from the rest of the population in possessing smaller spines and a more rounded axial region. These specimens resemble those assigned to *Dicellograptus* cf. *complanatus* by Štorch et al. (2011). As the present specimens mostly occur in a sample that shows evidence of

deformation (8.8 m), and differ in characters that show considerable variation within *D. ornatus,* they are distinguished as *D*. cf. *ornatus* in plates and figures, but were retained within *D. ornatus* for the purpose of counts.

Dicellograptus minor **Toghill, 1970**

Plates: (Photos) 22.1a-b, 22.3, 22.7; (Line drawings) 8.4-6.

Material and stratigraphical level: Rare from the upper half of the *pacificus* Zone. Nine specimens measured in detail, some questionably included.

Description: Gracile rhabdosome with open axial region. Stipes up to 15 mm in length. Expands from 0.3-0.43 mm at th2, to ca. 0.33-0.48 at th3, 0.38-0.5 mm at th5, and up to 0.53 distally (n=1 at th15). 2TRD is 1.7-1.85 mm at th2, increasing to 2-2.4 mm distally (n=2). Axial width is 1.6-2.1 mm. Short and very thin subapertural spines are preserved on the first thecal pair of several specimens. The first thecal pair grows horizontally or is slightly deflexed, while the second and subsequent thecae flex slightly dorsally, often resulting in a conspicuous open 'w' form, with an axial angle of 80-125 degrees. Thecae are strongly geniculate, with straight supragenicular walls, and small, moderately introverted apertures, with slightly thickened rims. The sicula is rarely preserved, but is approximately 2.25 mm long in one specimen.

Remarks: The present collection of material is grouped based on its broad, open axial region, relatively low DVW, and slight or absent spines. It differs from material assigned to *Dicellograptus* aff*. mirabilis* in having a lesser DVW (see Plate 6.5), smaller spines, and more deflected first thecal pair (producing a w-shaped, rather than u-shaped, axial

region). *Pleurograptus lui* has a lower DVW, exceeding 0.3 mm only in extreme examples distally, and a more dish-shaped proximal region, without the dorsal bend present in *D. minor,* as well as metacladia in mature specimens. Specimens of *Dicellograptus tenuiculus* with a preservationally broadened axial angle can be distinguished by their lesser axial width and more rapidly attained DVW. The present specimens of *D. minor* widen somewhat more rapidly than those described by Štorch et al. (2011): 0.33-0.43 mm at th3 vs. 0.22-0.4 mm at th3, but agree with those described by Koren' et al. (1983). Most of the present material is immature, but the two most mature specimens reach 0.5 mm at th12 and 0.53 mm at th15, respectively. [Note: the left stipe on the latter specimen, Plate 8.5, reaches a maximum width of 0.63 mm, but this is likely a preservational artifact.] This compares well with maximum widths reported in other populations, e.g., Toghill (1970 = 0.5 mm (immature specimens); Koren' et al. (1980 = 0.55 mm; note: Williams, 1982, argued these specimens should be assigned to *D. complexus*, but they do not show any evidence of the rhabdosomal torsion seen in *D. complexus*); and Štorch et al. (2011 = ca. 0.5 mm "most distally"). *Dicellograptus graciliramosus* (Yin and Mu, 1945) is a similar species from China. Williams (1982) placed it into questionable synomymy with *D. minor*, and Mu et al. (1993) included Toghill's type material and later collections of *D. minor* within *D. graciliramosus*. Chen et al.'s (2000) revision of the material described by Mu et al. (1993) confirmed Mu et al.'s assignment of their material to *D. graciliramosus,* but did not tackle non-Chinese synonymies. Chen et al. (2005a), however, recorded *D. minor* as

a unique species, and Fan and Chen (2007) depicted *D. minor* and *D. graciliramosus* as co-occurring within the Yangtze region. The holotype of *D. graciliramosus* possesses stipes 25 mm in length, which slowly increase in DVW from 0.2 mm to 0.4 mm, dimensions consistent with *D. minor.* Mu et al. (1993), however, reported a maximum DVW of 0.72 mm for their collection of specimens of *D. graciliramosus*. Examination of newly collected slabs from the Wufeng Formation, Jeiling section, during part of this study, recovered a specimen (Plate 26.8) with a DVW of 0.33 mm at th2 and 0.63 mm at th10, and a maximum DVW of 0.66 mm. This specimen closely resembles specimens depicted by Mu et al. (1993*,* e.g., plate 6, figs. 2 and 12) as *D. graciliramosus*. Chen et al. (2005a) illustrated a specimen assigned to *D. minor* that, if the scale on the illustration is correct, expands much more rapidly than coeval specimens of *D. ornatus*. Restudy of the Chinese collections will be necessary to determine whether *D. minor* and *D. graciliramosus* should be regarded as separate species. If so, then some of the more robust specimens in the present collection may be better included in *D. graciliramosus.* A specimen assigned to *D. minor* by Tang and Chen (2014: text-fig. 14.g) from the *pacificus* Zone of northern Guangxi, China, is likely *D. tenuiculus*.

***Dicellograptus tenuiculus* Mu et al. *in* Li, 1984**

Plates: (Photos) 18.1-7; (Line drawings) 5.4-5, 5.9-10, 9.12-13

Material and stratigraphical range. Abundant to rare from the mid to upper *pacificus* Zone. 43 specimens measured in detail.

Description: Distinctive, gracile dicellograptid, with a moderately open to vase-like, concavo-convex form. Stipes reach a maximum observed length of 22 mm, and undergo gentle torsion distally in some specimens. The first thecal pair is weakly rounded, with upturned apertures. The second thecal pair forms the base of erect stipes. Average DVW is 0.45 mm at th2 (0.4-0.48 mm), increasing slightly to 0.43-0.5 mm at th3, 0.55-0.6 at th5, and 0.45-0.65 mm at th7. Maximum width is often reached at th5, sometimes with a slight decrease in width thereafter. Axial width is 1.4-1.75 mm (mean=1.55 mm). Thecae are climacograptid, with straight supragenicular walls, and strongly introverted narrow apertures. Prothecal folds are well-defined in proximal thecae, becoming faint distally. Thecal apertures and infragenicular walls are prominently thickened, forming slight flanges on many specimens. Delicate subapertural spines (maximum 0.35 mm long) are present on the first thecal pair. The sicula is 1.8-2.3 mm long, but is present only as a 0.5 mm stump on specimens with more than a few thecae.

Remarks: The present collection, in particular samples 14.15 m and 16.03 m, contains many hundreds of well-preserved specimens of this species, which show remarkable consistency in dimensions. Average maximum width is slightly higher in sample 16.03 m than in sample 14.15 m, but within each sample the standard deviation in DVWs at all points along the rhabdosome is only 0.02-0.04 mm. The combination of moderate DVW, upright stipes, rounded and narrow axil, and a single pair of modest proximal spines, readily distinguish mature specimens of this species from other dicellograptids in the collection (e.g., Fig. 6.6). Mu et al. (1993) figured several examples of gracile

dicellograptids with rounded axial regions, and maximum stipe widths of 0.56 mm and 0.6 mm, that they assigned to *Dicellograptus tenuiculus* and *Dicellograptus excavatus* (see Mu et al., 1993: plate 6.3-6.11 and 7.1-3 and 7.8-9), which match very well with the present material (e.g., compare Mu et al.'s plate 6.6 with Plate 18.4 here). The relationship between these two species is unclear in the literature. The name *D. tenuiculus* was first used by Mu et al. (in Li, 1984) to replace *D. tenuis* Mu et al. (1974), an unavailable name (already designated by Lapworth: 1886). The specimen that accompanies the 1984 description of *D. tenuiculus* (Li, 1984: plate 3.5) looks very different than the specimen that accompanied the 1974 description of *D. tenuis* (Mu et al., 1974: plate 70.9; reillustrated in Mu et al., 1993: plate 6.3). The 1984 specimen has a nearly v-shaped axil, similar to *Dicellograptus anceps*. The many specimens that Mu et al. (1993) illustrated as *D. tenuiculus*, however, closely resemble both the holotype for *D. tenuis* and the Blackstone material. Mu et al., 1993, also included *Dicellograptus undulatus* Li within *D. tenuiculus.* The holotype of *D. undulatus* resembles the present material and Mu et al.'s (1993) illustrations of *D. tenuiculus*, but the original description of *D. undulatus* gives a DVW of 0.7-0.8 mm.

Mu et al. (1993) also illustrated a collection of specimens, assigned to *D. excavatus*, that look very similar to those that they assigned to *D. tenuiculus*. Measurements given within the text also show that the two species are very similar. The types of *D. excavatus* were not available for examination during this study, but Mu's original (1945) diagnosis describes the species as being very small, with straight, uniform stipes, less

than 5 mm in length, and less than 0.8 mm wide, with distinct, but short spines, climacograptid thecae with straight supragenicular walls, and a quadrate axil. Only the holotype is illustrated at a scale that allows details to be observed, but it closely resembles the present material. Mu et al. (2002), considered *D. excavatus* to be the senior synonym for *D. tenuiculus*, but other recent authors (Chen et al., 2000; Štorch et al., 2011) considered *D. excavatus* to be a junior synonym of *D. ornatus.* At the very least, the Mu et al. (1993) specimens of *D. excavatus* appear equivalent to the material assigned here to *D. tenuiculus*. Although the name *D. excavatus* would have priority over *D. tenuiculus*, the present specimens are assigned to *D*. *tenuiculus* in light of the tendency of recent Chinese authors, with greater access to original material and publications, to include some or all specimens of *D. excavatus* within *D. ornatus*. *Dicellograptus uniformis* Li (1984: plate 2.15-16) has a uniform width of 0.4-0.5 mm, a relatively narrow axil with small spines, and an ovoid rhabdosome form that agrees with the present material. Koren' et al. (1983) noted the similarity between *D. tenuis* and *D. excavatus* and material that they assigned to *Dicellograptus complanatus.* It is likely that their material is equivalent to the material of *D*. *tenuiculus* described here. Štorch et al. (2011) included Koren' et al.'s (1983) specimens of *D. complanatus*, along with the specimens assigned by Mu et al. (1993) to *Dicellograptus* cf. *complanatus,* in their *D.* cf. *complanatus.* Štorch et al.'s and Mu et al.'s material appears to be more robust than the present material, with a wider and more quadrate axil, and more closely resembles the collection of specimens with short spines and rounded axial region from 8.8 m at the

Blackstone River section, referred to as *D.* cf. *ornatus* in graphs and figures. As noted above, the specimen assigned to *Dicellograptus minor* by Tang and Chen (2014—fig.2g) from the *pacificus* Zone of northern Guangxi, China, is likely *D. tenuiculus*.

Dicellograptus aff. *turgidus* Mu, 1963

Plates: (Photos) 12.1-4, 12.13; (Line drawings) 8.7, 9.1.

Material and stratigraphical range: Rare from the lower *pacificus* Zone. Nine mature specimens measured in detail.

Description: Sigmoidal stipes attain a maximum recorded length of 110 mm. DVW is 0.38-0.54 mm at th2, 0.45-0.58 mm at th3, 0.55-0.65 mm at th5, 0.58-0.7 mm at th7, with a maximum width slowly reached distally of 0.65-0.8mm. 2TRD is 1.55-1.7 mm at th2 (1 specimen is 1.4 mm), 1.75-2.05 mm at th5, 1.95-2.5 mm at th7 (1 specimen is 1.83 mm), and 2.4-2.75 mm distally. The first pair of thecae grow nearly horizontally and possess a robust subapertural spine that is up to 1.75 mm long, with a basal width of 0.18-0.25mm. The axial angle is 15-45 degrees. Th2 through th5-th7 are straight and erect, after which the stipes become strongly ventrally flexed, growing nearly perpendicular to the rhabdosomal axis in some specimens, until approximately th13, at which point they flex dorsally once again. Stipes exhibit very gentle torsion, with only one specimen becoming fully scalariform, and only at >110 mm. Thecae are sharply geniculate, with strongly introverted, narrow apertures. Supragenicular walls are long, straight, and gently to moderately inclined. Interthcal septa are straight and, distally, nearly perpendicular to the stipe axis. Thecae overlap approximately two-fifths of their

length. Most specimens possess a thick axial membrane reaching up to the aperture of th5-th9. However, one specimen has only an incipient membrane and another no membrane at all, despite each being >25 mm.

Remarks: These specimens closely resemble *Dicellograptus turgidus* in possessing a "square" axil with upright initial stipes, stout basal spines on the first thecal pair, sigmoidal stipes with a prominent ventral bend around th7, and a thick axial membrane. However, examination of the material housed at the Nanjing Institute of Palaeontology and Geology, including the holotype (reillustrated in Plate 12.6 and 8.1), along with new material recently collected from the Wufeng Formation, Jeiling section (see Plate 12.7 and 12.9), show considerable differences in rate of widening, axial width, and axial angle. The Chinese material widens consistently faster than the present material, reaching a DVW of 0.75-0.83 mm (1 specimen is 0.65 mm) at th3 and 0.73-0.93 at th5 versus 0.5-0.54 mm (1 specimen is 0.40 mm) at th3 and 0.5-0.65 mm at th5. Initial axial width (measured between the apertures of the first thecal pair) is somewhat broader in the Chinese material: 1.75-2.05 mm vs. 1.5-1.7 mm; however, the angle of divergence of the stipes in the Yukon material is higher, producing a broader, more open axial region (Fig. 6.7). Plots of the proximal measurements of the Yukon and Chinese collections show no overlap in dimensions. Maximum 2TRD is also higher in the Blackstone material, but this may simply be a function of the larger specimens in the collection. None of the Yukon material possesses spines on th2 or higher, a feature which is present in some of the Chinese material, but which is also variable between and within

populations in dicellograptids. The overall appearance of the Chinese material is robust and compact, with some specimens closely resembling *Diceratograptus mirus.* Williams (1982) illustrated a single specimen of *D. turgidus* [plate 1.8: assigned by Williams to *D. ornatus*]. The scale appears to be incorrect, but in general form this specimen agrees with the type material. Štorch et al. (2011) recently assigned four specimens from the *pacificus* Zone of Vinini Creek, Nevada, to *Dicellograptus turgidus,* two of which they illustrated. The illustrated specimens both possess the tight axial region characteristic of the Chinese specimens of *D. turgidus*, but vary in initial DVW (Fig. 6.7). During my examination of the new Jeiling collections, I found one specimen from the *pacificus* Zone that agrees reasonably well with my present material (Plate 8.3), suggesting that *D.* aff. *turgidus* has a broad distribution. *Dicellograptus sinicus* Mu and Zhang is very similar to the present material in dimensions and rhabdosomal form (see Plate 12.5), but possesses conspicuous apertural spines until at least th4.

***Dicellograptus turgidus* Mu, 1963**

Plates: (Photos) 12.10, 12.11?, 12.12; (Line drawings) 5.1-2.

Material and stratigraphical distribution: 2 specimens from just below the *D. mirus* Subzone, and another 3 specimens questionably assigned from the lower *pacificus* Zone.

Description: Compact rhabdosome with square axial region and prominent early ventral stipe curvature. Maximum observed stipe length 8.5 mm. DVW is 0.6 mm at th3, ca. 0.65-0.75 mm at th5, and 0.68 mm at the 7 (n=1). 2TRD appears to be ca. 1.25-1.5 mm at th2 and ca. 1.85 mm at th5 (n=1). The first thecal pair grows horizontally. A robust

subapertural spine is present on one specimen. Subsequent thecae grow nearly vertically, before flexing strongly ventrally at th5 and th3, respectively, in the two specimens. Axial width is ca. 1.7 mm. Thecae are strongly geniculate, with straight or slightly inclined supragenicular walls. The thecal apertures are introverted.

Remarks: These specimens contrast with the specimens assigned to *D.* aff. *turgidus* in possessing more robust and more rapidly expanding stipes, with a lesser axial angle. The difference between these two species is apparent upon visual inspection (e.g., compare Plate 12.6, the holotype of *D. turgidus*, with Plate 12.10, a Blackstone specimen assigned to *D. turgidus*, and Plate 12.4, a specimen of *D.* aff*. turgidus*), as well as through comparison of measurements (Fig. 6.7). Two additional specimens are intermediate in characters between specimens assigned to *D.* aff. *turgidus* and those of *D. turgidus*. Both of these have damaged proximal ends, resulting in an artificially decreased axial angle, so axial measurements cannot be accurately taken. One of these specimens is missing stratigraphical information, but the other occurs at 8.8 m, halfway between the confirmed occurrence of these two species at the Blackstone River, and may represent an evolutionarily intermediate form. Based on examination of the original illustration, *Dicellograptus turgidus membranaceus* Chen (in Ye, 1978) appears to be synonymous with *Dicellograptus turgidus* rather than *D.* aff. *turgidus.* An additional specimen (Plate 12.11) occurs along with specimens confidently assigned to *D. turgidus* at 12.67 m. This specimen possesses strongly upright stipes, similar to specimens assigned to

Dicellograptus tumidus (Chen, 1978[25]), and was assigned to this species earlier in the production of this thesis. Over the course of this study, however, all of the *D. tumidus* material illustrated in Mu et al. (1993) was examined, including Chen's holotype (reillustrated: Plate 26.9). While all specimens within that collection possess do possess the diagnostic features of the species (initially vertical stipes with subsequent ventral curvature) to some degree, many, including the holotype, are not markedly different in overall form from other dicellograptid species, e.g., specimens of *D. ornatus* with short spines. Some of the *D. tumidus* specimens illustrated by Mu et al., 1993 (e.g., plates 11.7, 11.10, and 11.11), as well as one specimen illustrated by Štorch et al. (2011: fig. 10s), exhibit a form that resembles *Diceratograptus mirus,* with a stout, downwards-directed spine (a feature absent from the *D. tumidus* holotype), and strongly concave stipe curvature, which results in the stipes' ventral walls very nearly contacting one another. Given the small number of specimens represented, this suite of morphologies may represent examples of the type of compaction artefact shown in the present collection of *D. ornatus* (e.g., Plate 9.7), rather than species-specific characters. The specimens illustrated as *D. tumidus* in Mu et al. (2002: plate 126.8-10) may be examples of the species assigned here to *D.* aff. *tenuiculus* or of the material assigned by Štorch et al. (2011) to *D.* cf. *complanatus*. Given the uncertainities about the status of *D. tumidus,* and given that the single plausible specimen in this collection co-occurs with specimens of *D. turgidus*, it is assigned to the latter species.

[25] In Stratigraphy Research Group of the Yangze Gorges, Hubei Bureau of Geology (1978).

Dicellograptus aff. *mirabilis* Mu and Chen*in* Mu et al., 1993

Plates: (Photos) 20.2, 20.7; (Line drawings) 5.3, 5.7, 5.11, 6.14, 9.9-11.

Material and stratigraphical level: Rare from the lower *mirus* Subzone; 16 poorly to very well-preserved specimens measured in detail.

Description: Broad open rhabdosome, with steadily expanding stipes up to 28 mm in length (most specimens are <5 mm). DVW is 0.25-0.35 mm at th1 (mostly 0.28 mm), 0.4-0.5 mm at th2, 0.48-0.55 mm at th3, 0.63-0.68 mm at th5, 0.75-0.83 (n=3) at th7, 0.88-0.95 at th10 (n=3). 2TRD is ca. 1.65-1.85 mm at th2 and 1.75-2 at th7. The first thecal pair is deflexed or horizontal, the second turns very gently upwards, and subsequent thecae grow near vertically, producing a rounded, open, u-shaped axial region. Thecae possess straight to moderately convex supragenicular walls. The first thecal pair bears subapertural spines that are nearly 4 mm in length in two specimens, and negligible in others. Interstipe angle is 45-75 degrees. Axial width is 1.9-2.05 mm. The sicula is 2-2.25 mm long, and furnished with a short virgella (ca. 0.25 mm).

Remarks: Mu and Chen (1993) distinguished *Dicellograptus mirabilis* from the similar *Dicellograptus ornatus* based on a greater DVW, greater axial width, the presence of an interstipe basal web, and particularly long and well-developed spines. They also included a specimen assigned to *Dicellograptus complanatus* var. *ornatus* by Berry (1960). Berry's specimen is illustrated only in a rough drawing of the proximal end, but it possesses very large and possibly secondarily strengthened basal spines, as well as strongly upright stipes. Chen et al. (2000) reassigned three specimens from Dob's Linn,

Scotland, which were originally assigned by Williams (1982) to *D. ornatus*. The illustrations show only the proximal regions of these specimens, but all show long thickened basal spines, and one shows the presence of a basal web (although it also shows strong rhabdosomal torsion; as such, its relationship to the other specimens is questionable). Štorch et al. (2011) assigned two specimens from Nevada to *D. mirabilis*, one of which they illustrated (fig. 10.s): a specimen with thick basal spines, a partial basal web, and long upright spines (ca. 32 degree interstipe angle). Despite its emphasis in the description, none of the illustrated specimens in Chen and Mu's type collection (reexamined in this study) possess a basal web. The presence of a basal membranous structure often only occurs in very mature specimens of *Dicellograptus ornatus* in the present collections, and shows regional variability in many graptolite species (e.g., Loxton et al., 2011), undermining this feature as diagnostic. The maximum DVW of 1 mm given by Chen and Mu is within or slightly above the upper range of *D. ornatus* (see *D. ornatus* description above), but the rapid expansion and wide axial are notably different. The present collection contains a number of specimens that are distinguishable from the specimens assigned to *D. ornatus* by their rapid widening and/or high axial width (see Figs. 6.8 and 6.9). These specimens are divisible into two populations based on axial width, axial rounding, and proximal DVW (Fig. 6.10), and are referred to *D.* cf. *mirabilis* and *D.* aff. *mirabilis*. *D.* cf. *mirabilis* resembles the holotype of *D. mirabilis*, as well as Štorch et al.'s (2011) illustrated specimen, in possessing upright stipes, rapid proximal DVW increase, and generally *ornatus*-like appearance, but differs

in possessing a narrower axial region, no inter-stipe membrane or secondary spine thickening, and shorter spines. *D.* aff. *mirabilis* resembles *D. mirabilis* in possessing long "saber-like" spines (in some specimens) and a broad axial, but differs in a relatively slow rate of widening, and in a more open and rounded, u-shaped, rather than square, proximal region (e.g., Plate 20.2 and 20.7). The degree of rounding in the type collection of *D. mirabilis* is somewhat variable. One of the paratypes has a significantly more rounded proximal region than the holotype (Mu et al., 1993: plate 10.3). Two unassigned specimens from the new Jeiling section collections are illustrated in Plate 26.6 and 26.7, and compared in Fig. 6.11. Both possess somewhat rounded and open axial regions, similar to the range of variation in the type collections, with one, Plate 26.7, showing a degree of axial rounding similar to specimens assigned here to *D.* aff. *mirabilis*. Within the Blackstone collection, most of the specimens assigned to *D.* aff. *mirabilis* come from slightly higher than those assigned to *D.* cf. *mirabilis* (16.03 m vs. 17.20-18.05 m), although one good specimen of *D.* aff. *mirabilis* occurs at 15.65 m (the base of the *D. mirus* Subzone). *D. mirabilis* sensu stricto is restricted to the *D. mirus* Subzone in China (Fan and Chen, 2007), but the specimens assigned to *D. mirabilis* in Nevada occur considerably lower: in the bottom quarter of the *pacificus* Zone.

Other authors have illustrated dicellograptids very similar to the material described here. Specimens from Dob's Linn (Anceps Bands D and E), with an open, rounded axial region as in *D.* aff. *mirabilis*, but lacking large spines, are illustrated by Williams as *D. ornatus* (1982: text-fig. 6b, 6c, and 6.d(?)). Chen et al. (2005a) illustrated two specimens

from the *extraordinarius-ojsuensis* Zone, 5 and 6 thecal pairs in length, which they assign to *D. ornatus,* despite possessing a rounded axial and very small spines (text-fig. 3a and b). Mu et al. (1993) illustrated as *D. ornatus* specimens with a broad, rounded, and open axil that closely resemble those assigned to *D.* aff. *mirabilis* here (plates 8.7-8, 8.10, and 9.10).

D. aff. *mirabilis*, with its broad and open, u-shaped axial region, resembles *D. minor*, but differs in possessing longer spines and a much higher DVW. It also resembles the larger *D. graciliramous,* and should be compared with that species during revision. One specimen (15.65 m, slab #45), with a distal maximum width of only 0.75 mm and an axial width of 1.75 mm is questionable. *Dicellograptus complanatus* resembles *D.* aff. *mirabilis* in rate of widening, maximum DVW, and roundedness of the axial region, but differs in possessing only minute spines, and in having a generally more v-shaped than open u-shaped axial region (compare Lapworth's (1880) plate 5.17c to Plate 5.3 and 5.7).

***Dicellograptus* cf. *mirabilis* Mu and Chen, 1993, in Mu et al.**

Plates: (Photos) 20.1, 20.3-4, 20.6, 22.8-12; (Line drawings) 6.5, 6.12, 8.13, 8.8, 9.8.

Material and stratigraphical level: Uncommon from the lower to middle *mirus* Subzone and rare from the upper *mirus* Subzone (1 specimen). 28 specimens measured in detail.

Description: Robust rhabodosome with upright stipes reaching a maximum recorded length of 31 mm (most <10 mm). Expands rapidly from 0.33-0.43 mm at th1, and 0.5-0.58 mm at th2, to 0.55-0.68 mm (most 0.6 mm) at th3, 0.63-0.85 mm (mean=0.75 mm)

at th5, 0.8-1 mm at th7, and 0.88-1.05 mm at th10. Maximum distal width observed 1.07, but variable depending on stipe torsion. 2TRD is 1.4-1.8 at th2[1], 1.65-2.05 mm at th5[1], and 1.75-1.85 at th7[1]. The axial width is 1.55-1.95 mm (mean 1.7 mm; varies by 0.2 mm if measured from thecae apertures rather than base of spines). Axial angle is 13-38 degrees. The first thecal pair is slightly deflexed, while the second thecal pair bends sharply upwards. Thecae are introverted, with moderately inclined and convex supragenicular walls. Interthecal septa are straight and at ca. 45 degrees to the axis of each stipe. Stipes show torsion distally, as well as gentle ventral flexure. Most specimens possess thin subapetural spines on the first thecal pair, 0.6-1 mm long, but one specimen questionably assigned to this species possesses a 2 mm spine, and another mature specimen possesses thin spines 1.5 mm long. The sicula is not preserved.

Remarks: These specimens primarily differ from the type material of *D. mirabilis* in having a lesser axial width and no proximal web. They differ from the specimens assigned here to *D. ornatus* in a more rapid increase in proximal DVW (Fig. 6.8) and a less rounded and open axil. There is some overlap between the stratigraphically higher specimens of *D. ornatus* and the present specimens, however, the largest specimens of *D. ornatus* are heavily mineralized, which likely exaggerates their dimensions, increasing apparent overlap in measurements. *Dicellograptus* aff. *mirabilis* can be distinguished from *Dicellograptus* cf. *mirabilis* even in proximal specimens, based on the former's wider axil, gentler upward bend of the second thecal pair, and the horizontal or

reclined, rather than inclined ventral side of first thecal pair (interior of the axil). Some of the specimens in Mu et al. (1993) assigned to *D. ornatus* (e.g., plate 8.14) resemble those assigned to *D.* cf. *mirabilis* here.

Genus *Diceratograptus* Mu, 1963

Type species *Diceratograptus mirus* Mu, 1963; by original designation.

***Diceratograptus mirus* Mu, 1963**

Plates: (Photos) 12.14-18, 22.13; (Line drawings) 6.6-11.

Material and stratigraphical range: Rare from the *mirus* Subzone. 23 specimens examined in detail.

Description: Biform rhabdosome with mesial biserial portion. Maximum stipe length is 21 mm, but almost all specimens are less than 5 mm. The first thecal pair grows horizontally. The second and third thecae grow nearly vertically, with a width of 0.53-0.75 mm at th2 and 0.7-0.8 mm at th3 (n=7). Subsequent proximal thecae become increasing inclined and elongate, with thecae about 2 mm long at th7-8, overlapping 2/3rds of their length. Proximal thecae expand dorsally, and merge to form a short biserial portion, beginning at the level of the aperture of th3-th4 and extending to the level of the aperture of th7-th8. Stipes curve sharply ventrally after the biserial portion ends, and thecal length and thecal overlap markedly decrease, with far distal stipes essentially indistinguishable from those of species of *Dicellograptus*. Stipe width is 1.05-1.25 mm at th7 (n=3), 0.7-0.9 mm at th10 (n=2), and 0.75-0.9 mm distally (n=1). 2TRD is 1.25-1.45 mm at th1^1, 1.3-1.5 mm at th2^1, ca. 1.6 mm at th5 (n=3), ca. 1.65-1.85 mm at

th7 (n=2), 1.7-ca. 2.1 mm at th10 (n=3), and 2.4-2.5 mm distally (n=1). Axial width is 1.53-1.75 mm. The sicula is 2.1-2.45 mm long, but is often broken, and only exposed as a stump within the open lumen formed by the dorsal merger of the stipes. The lumen is 1.5-2 mm high, and is sometimes partially filled with a membrane. The first thecal pair bears thin spines up to 0.75 mm long; additional apertural spines are sometimes present on th2 and th3. The virgella is rarely preserved, but is 0.2-0.5 mm long. The thecal apertures are introverted, and supragenicular walls are strongly inclined mesially, and slightly inclined proximally and distally.

Remarks: *Diceratograptus mirus* is an important index fossil in China, defining the base of the *Diceratograptus mirus* Subzone (upper *pacificus* Zone). *D. mirus* has previously been reported from the Peel River, Yukon (Chen and Lenz, 1984—referred to as *D.* cf. *mirus*). It also occurs in Nevada (Štorch et al., 2011) and in Idaho (Goldman et al., 2007). In China, *D. mirus* is restricted to a very thin interval in the uppermost *pacficus* Zone: it reaches a maximum thickness of 0.40 m at the Ludiping section, where it represents <4% of the total *pacificus* Zone thickness (Chen et al., 2000), and occupies approximately the top 20% of the *pacificus* Zone in the South China composite sequence of Fan and Chen (2007). [Relative thickness measurements taken from stratigraphic columns within Chen et al. (2000) and Fan and Chen (2007).] At the Blackstone River, the range of *D. mirus* occupies the top 27% of the *pacificus* Zone, with a total thickness of 5 m vs. a maximum of 0.4 m in China. [Note: If the specimen questionably assigned to *D. turgidus* is taken to be a poor specimen of *D. mirus*, the thickness of the *mirus*

Subzone at Blackstone increases to 6.48 m, making up 35% of the *pacificus* Zone.] Detailed occurrence information is not available for Idaho, nor for the Peel River (Yukon), but in Nevada the *D. mirus* Zone is 3.2 m thick (Vinini section), and includes 31% of the total *pacificus* Zone, suggesting either that the species appears earlier in Laurentia than in China or that the *mirus* Subzone is condensed in China. No major turnover in taxa occurs near the base of the *mirus* Subzone at any of the sections, making confirmation of correlation difficult.

Genus *Pleurograptus* Nicholson, 1867

Type species *Cladograptus linearis* Carruthers, 1858; by original designation.

***Pleurograptus lui* Mu, 1950**

Plates: (Photos) 10.2-4, 22.2, 22.4a-b; (Line drawings) 8.2, 8.9.

Material and stratigraphical range: Uncommon from the *ornatus* to the upper *pacificus* Zone (bottom third of *mirus* Subzone). 13 specimens with intact proximal ends and 32 stipe fragments of various sizes measured in detail.

Description: Gracile species with two reclined stipes reaching to at least 20.5 mm in length. Stipes widen very slowly from 0.2-0.24 mm at th2 (n=11; 1 specimen is 0.29 mm), 0.2-0.24 mm (1 specimen is 0.33 mm) at th3, 0.2-0.25 mm at th5 (n=6; 1 specimen is 0.35 mm), 0.23-0.26 mm at th7 (n=4), 0.25-0.3 mm at th10 (n=4; 1 specimen is 0.38 mm), and 0.25-0.35 mm at th15-20 (n=5). Distal fragments have a maximum width of 0.18-0.35 mm. 2TRD is 1.3-2.67 mm at th2 (n=9), 2-2.4 mm at th5 (n=2), and a distal 2TRD is 2.1-2.6 mm (n=5). Thecae are elongated simple tubes, with inclined ventral

walls, somewhat introverted apertures, and moderate geniculation. Many stipes show some torsion distally, but none is rotated more than ninety degrees from the dorsal-ventral plane. Axial width is 1.5-1.65 mm (n=9). The first thecal pair is horizontal to reclined. The second thecal pair is straight and projects upwards at ca. 20-45 degrees from the rhabdosomal axis, creating a characteristic open dish-like proximal region. A small pair of subapertural spines (ca. 0.2 mm) is preserved on the first thecal pair of several specimens. A complete sicula (ca. 1.65-2 mm long) is also present on several specimens, including one with a maximum stipe length of 17 mm. Distal stipe fragments are nearly straight.

Remarks: The present specimens agree well with the large collection described by Štorch et al. (2011), as well as descriptions of Chinese (Chen et al., 2005a) and Scottish material (Williams, 1982). Only a single specimen in the present collections possesses metacladia, and this is somewhat questionable: a small stub of a possible metacladium on a distal fragment from 16.03 m. A note from very early in this project also notes metacladia on a specimen from the sample Bulk ~5.5 m, but this slab has been misplaced, and so cannot be confirmed. Specimens with metacladia are also rare within the Nevada collections, however (Mitchell, pers. comm.), so this absence is likely not meaningful. Twenty-four distal fragments occur in the lowest *pacificus* Zone and highest *ornatus* Zone samples (1.32 m and 0.1 m) that are consistently at or slightly below 0.18-0.2 mm wide, which matches or is slightly below the proximal DVW of specimens that occur higher in the section. Most of these are relatively small fragments, however, and

likely represent proximal fragments or metacladia, which are often somewhat narrower than the main stipe (e.g., Williams, 1982). *P. lui* can be distinguished from the co-occurring *Dicellograptus minor* by the latter's greater distal width, more prominent spines, and dorsally upturned second thecal pair. Numerous other gracile species assigned to either *Dicellograptus* and *Leptograptus* have been described that, except for the absence of metacladia, are very similar to *P. lui.* In light of the near absence of metacladia in this large collection, as well as that of Štorch et al. (2011), some of these specimens may be reassignable to *P. lui*, such as some specimens assigned to *Leptograptus extremus* and *Leptograptus macer* in Mu et al., 1993 (see plates 4 and 5).

***Pleurograptus*? *grandis* (Mu and Chen, 1993)**

Plates: (Photos) 10.1, 10.5, 10.6; (Line drawings) 9.15

Material and stratigraphical range: Three specimens from just below the base of the *D. mirus* Subzone, one specimen from the uppermost *mirus* Subzone, plus additional distal fragments tentatively assigned.

Description: Measured material consists of two distal stipe fragments with attached metacladia (Specimen 1); one either cluster of overlapping stipes with metacladia or one stipe with multiple orders of metacladia (Specimen 2); and a cluster of at least several stipe fragments with attached metacladia, as well as numerous other large stipe fragments without metacladia (Specimen 3). The main stipe of Specimen 1 is 15 mm long, with a maximum DVW of 0.48 mm and 2TRD of ca. 2.05 mm, and three metacladia, 4 mm, 8.5 mm, and 8.5 mm long, at a spacing of ca. 6 mm. Metacladia appear to emerge

from the dorsal side of the stipe, at or very near thecal apertures. DVW of the metacladia is 0.28-0.3 mm basally, and up to 0.5 mm (at 7 mm). One metacladium possesses a possible secondary cladium at 4.8 mm (see Plate 10.5 and 9.15). The relationship between the components of one of the specimens (Plate 10.1) is unclear. If they all belong to a single specimen, then second order branching of the metacladia occurs at several places, and spacing of the metacladia is denser than described above, ranging from 2-6 mm. The main stipes of Specimen 2 also have a basal DVW of ca. 0.25-0.3 mm, a maximum width of ca. 0.5 mm, and 2TRD of ca. 2-2.25 mm. Most stipes are also preserved in scalariform or subscalariform view, with a prominent dorsal "rod' present. Specimen 3 (Plate 10.6) consists of a complex jumble of stipe fragments, many bearing metacladia. Basally, the metacladia are ca. 0.35 mm, but they widen relatively rapidly, e.g., 0.5 mm at 2 mm and 0.65 mm at 7 mm in the cladium to the right of the '6' in Plate 10.6. Maximum width of the metacladia is ca. 1 mm, depending on stipe orientation, but they are mostly 0.7-0.8 mm wide, with only a few sections less than 0.5 mm, and those are mostly scalariform. 2TRD is ca. 2 mm to ca. 2.6 mm. Individual fragments on the slab reach lengths of at least 47 mm, and metacladia that are clearly attached to stipes reach at least 24 mm long. In addition to metacladia, all three specimens described here possess a rigid dorsal tube or rod structure, ca. 0.18-0.25 mm wide, which runs the length of both stipes and metacladia. The widest stipe fragments, which do not show branching, are included in this species based on the presence of this tube/rod-like structure, as well as their co-occurrence with fragments that do possess

branching. The tube/rod structure is preserved with relief, either as a raised solid element positioned ventrally (or mesially in scalariform specimens) or, more commonly, as a deep linear depression. Where the "rods" are broken and the interior structure is visible, they appear to be made of carbonized material similar to the rest of the rhabdosome, and similar to broken spines in species such as *Appendispinograptus supernus*, rather than secondary mineralized material or sediment infilling a previously hollow tube. In several instances where the outside wall of the "rod" is removed, a mesial thread-like element is visible. This may be a preservational artifact, however. Thecal walls are straight and inclined, with narrow and strongly introverted apertures. Remarks: Štorch et al. (2011) noted that although metacladia in *Pleurograptus* appear to emerge from the dorsal side of the stipe, they actually arise from the lateral side of the thecal aperture. This is not clear in the present specimens, but is consistent with the position of the metacladia. These specimens resemble *Pleurograptus linearis* (Carruthers) in the curvature of their rhabdosome and apparent tertiary cladia; however, *P. linearis* is stratigraphically restricted to below the *complanatus* Zone (e.g., Zalasiewicz et al., 2009). The dorsal "rod" is an odd feature. It is not related to the nema, which in species of the Dicranograptoidea is very small and projects from the apical end of the normally resorbed sicula, and is unrelated to the stipes or metacladia. Although species of *Monograptus* possess a similar dorsal strengthening structure (Mitchell, pers. comm, 2013), no other species of dicranograptoid encountered during this study possesses anything similar. Mu and Chen (in Mu et al., 1993) described a new species,

Tangyagraptus? *grandis,* based on six distal fragments. Their material possesses a maximum distal width of 1-1.5 mm, along with multiple orders of cladia. The illustrated types (two specimens) were reexamined as part of this study, along with new material (two specimens, from 138 m and 143 m, respectively) from the Jeiling section, Wufeng Formation. The type material is of relatively poor quality. The holotype has a DVW of 0.9-1 mm, and the paratype a maximum DVW of 1-1.25 mm. Metacladia rapidly widen, reaching 1 mm by about th3 in the paratype. 2TRD is somewhat unclear, but appears to be ca. 2.35 mm in the holotype and is 2.25-3 mm in the paratype. Digital measurements from photographs of the Jeiling material (Plate 10.7) give a maximum DVW of 0.88 on the main stipe, and ca. 0.35 mm basally and ca. 1.1 mm distally on the metacladium. A second photographed, but unillustrated, specimen has a maximum metacladial width of ca. 1.30 mm. Both of the Jeiling specimens possess a thick dorsal "rod", as in the Blackstone material, which is up to 0.5 mm wide, but not preserved with strong relief as in the Blackstone material. Mu and Chen (in Mu et al., 1993) noted the similarity of their material with *Pleurograptus*, in terms of branching, but differentiated it based on thecal form. The larger of the present specimens (Plate 10.6) agrees well with the Chinese specimens. The smaller Blackstone specimens are included and assumed to be juvenile specimens of the same species. The Blackstone material is slightly younger than the Chinese material. The species ranges throughout the *mirus* Subzone at the Blackstone River section, and is restricted to the upper *typicus* Subzone in China (Fan and Chen, 2007). Mu et al. (1993) also illustrated additional material assigned to *Tanygraptus* that

resembles the present material. The types of *Tangyagraptus remotus* were reexamined during this study. The holotype and one of the paratypes (#56872) possess proximal ends. They widen from 0.46 mm at th2 to ca. 0.6 mm at th8-12, with a maximum DVW of 0.66 mm at th20 in the holotype and at least 0.75 mm in paratype. The paratype clearly possesses a dorsal "rod" distally. Both specimens possess metacladia that occur much later (th10 in the holotype and th8 in the paratype) than is normal in *Tangyagraptus*, where the first set of cladia originates from the second or third thecal pair, and most likely do not belong to *Tangyagraptus*. Mu et al. (2002) illustrated two additional specimens assigned to *T. remotus* (plates 125.6 and 125.11), with a maximum DVW of 0.5-0.7 mm, both of which also show late emergence of metacladia (more so in plate 125.6). *Tangyagraptus flexilis* Mu and Chen, also in Mu et al. (1993), resembles the present material. The proximal end is not obvious in the illustration of the holotype (Mu et al.'s (1993) plate 17.3), and from Mu and Chen's English description it appears that they may be referring to the paratype when they describe initial cladia at th3. These specimens should be reexamined with reference to the material described above. On a final note, many of the species assigned to *Tangyagraptus* by Mu et al. (1993), including the questionable assignments noted above, possess broad, open axial regions. Although it seems unlikely, given the length of some of the material and lack of cladia, the specimens assigned to *D.* aff. *mirabilis* above should be considered as possible, immature specimens of this species. The present collection is assigned questionably to *Pleurograptus,* rather than *Tangyagraptus*, based on 1) the fact that no species of

Tangyagraptus has ever been described outside of China, and 2) the presence of a dorsal "rod" in "*Tangyagraptus" remotus*, a species with *Pleurograptus*-like late appearing metacladia. All three specimens are assigned to *Pleurograptus grandis*, although it is possible that they belong to separate small and large species, as in Mu et al. (1993).

Superfamily Diplograptoidea Lapworth, 1880, emend. Mitchell et al., 2007b

Genus *Diplograptus* McCoy, 1850, emended Mitchell et al., 2009.

Type species: *Prionotus prisitis* Hisinger, 1837, designated by Gurley, 1896.

***Diplograptus rarithecatus* (Ross and Berry, 1963)**

Plates: (Photos) 11.16-17, 11.19-20, 16.1-2, 16.11-15; (Line drawings) 2.17, 7.4-8.

Material and stratigraphical range: Rare to common from the middle to upper *pacificus* Zone. 42 complete specimens measured in detail, along with 6 large distal fragments.

Description: Robust rhabdosome up to 78 mm long. Steadily widens from 1.15-1.6 mm at th1, to 1.25-1.8 mm at th3, 1.45-2 mm at th5, 1.55-2.1 mm at th7, 1.7-2.25 mm at th10, 2-2.55 mm at th15 (1 is 2.75 mm at th16), 2.1-2.8 mm at th20, and 2.45-3.3 mm distally, with maximum width not reached until after th15. 2TRD is 1-1.5 mm at th1^1, 1.33-1.75 mm at th3, 1.5-2 mm at th5, 1.75-2.4 mm at th7, 2-2.25 mm at th10, and up to 3.3 mm in the longest specimens distally. The sicula is ca. 1.6-1.8 mm long. It is exposed for 0.13-0.23 mm below th2^1, and its aperture is 0.3-0.45 mm wide. Th1^1 turns up 0.15-0.25 mm below the sicular aperture. The proximal end is broad, with an asymmetrical, inclined first thecal pair, with each theca possessing a 0.6-1 mm long, basally robust

spine, that emerges from or just below the thecal aperture. A thick virgella (0.4-1.05 mm long) is present, but no antivirgellar spines. Thecal appearance is strongly affected by preservation. Proximal thecae often show pseudogeniculae, whereas distal thecal are normally straight, simple tubes. The lower rim of the thecal aperture is strongly thickened, and is connected to the pseudogeniculum by a lateral process, which is often pressed through the rhabdosome wall in the proximal end of flattened specimens (e.g., see Plate 11.16).

Remarks: Mitchell et al. (2009) redescribed the genus *Diplograptus* and synonymized many of the previously described species. Although they did not provide a detailed description of any species other than *Diplograptus prisitis*, they divided known material into five species: *Diplograptus maximus* (a very large form)*, Diplograptus posterus* (a moderate-sized form, with protracted, and lesser inclined thecae)*, Diplograptus nicholsoni* (a minute form), *D. rigidus* (a form with wide proximal end and steeply inclined proximal thecae), and *Diplograptus rarithecatus*. Štorch et al. (2011), divided their material into two species: *Diplograptus rigidus* and *Diplograptus rarithecatus*, with the former distinguished by its “particularly wide proximal end” and “relatively dense thecal spacing and high angle of [thecal] inclination.” The present collection shows a very wide range of both proximal and distal dimensions, and individual specimens of *Diplograptus* from the Blackstone River look strikingly different from each other. Visual inspection would support assigning them to three species: a small species similar to *D. nicholsoni* (e.g., Plate 16.15 and Plate 11.20); a proximally narrow species,

corresponding with *D. rarithecatus* (e.g., Plate 16.11 and Plate 11.16); and a proximally wide species, corresponding to *D. rigidus* (e.g., Plate 16.14). However, when measurements of width and thecal spacing are plotted, the specimens cluster into a loose, but generally cohesive group (Figs 6.12-6.13). This group is centered between the Vinini *D. rarithecatus* and *D. rigidus* clusters, and overlaps both. Taken by themselves, Štorch et al.'s two species are distinct in comparisons of proximal and mesial width, proximal vs. distal width, and proximal width vs. 2TRD; the addition of the Blackstone material largely erases this distinction, although the Blackstone distribution resembles the Vinini distribution for distal widths (Fig. 6.13). Nearly all of the Blackstone specimens have higher th1 DVWs than the Vinini material (although still within the range given by Mu et al., 1993, for the species: 1.3-1.6 mm). Since the position of the thecal apertures on the first thecal pair is often obscured by the subapertural spines, making choice of where to take the DVW measurement more subjective than on subsequent thecae, part of this variation might be due to differing measurement strategy. If the entire set of Blackstone proximal data (Figs. 6.12-14) is shifted slightly to the left to account for this possibility, the species clusters in Vinini Creek and the Blackstone River correspond well for this measurement. Beyond th1, the Blackstone data falls between or includes both the Vinini *D. rarithecatus* and *D. rigidus* specimens by most measures. Several of the plots support division of the current collection into two species, but this is nowhere near as clear as it is in Nevada; further collections may support Štorch et al.'s division (2011). The present collections are conservatively considered to represent only *D. rarithecatus.*

For comparative purposes with Nevada, however, the population was split in Sheets et al. (2016). Further, both split and unsplit alternatives were considered in producing biodiversity curves in this thesis.

Genus *Rectograptus* Přibyl, 1949

Type species*: Diplograptus pristis* var. *truncatus* Lapworth, 1877, designated by Přibyl 1949.

***Rectograptus abbreviatus* (Elles and Wood, 1907)**

Plates: (Photos) 16.3, 16.5-10, 16.16; (Line drawings) 2.12-14.

Material and stratigraphical range: Common from the upper *ornatus* through *pacificus* Zones; possible occurrence in the basal *extraordinarius* Zone. 49 specimens measured in detail, and an additional 46 specimens measured for distal width, distal 2TRD, and rhabdosome length.

Description: Robust, aseptate rhabdosome reaches at least 48 mm long. Thecal spacing and DVW are highly variable. DVW is 0.75-1.05 mm at th1, 0.95-1.5 mm at th3 (mostly <1.3 mm), 1.03-1.95 mm at th5, 1.2-2.15 mm at th7, with a maximum of 1.7-ca. 4.0 mm slowly attained distally (maximum width normally reached by th17). Many specimens taper distally. 2TRD is 1.0-1.45 mm at th1^1, 1.35-1.7 mm at th5^1, and 1.5-2 mm distally. The proximal end is furnished with a short virgella, two antivirgellar spines, and a short mesial spine on th1^1 (all ca. 0.5 mm long). The first few thecae have sharp to rounded geniculae, and subsequent thecae are orthograptid, with a straight and long interthecal septa and everted thecal apertures. The external projection of the nema is rarely preserved, but when it is, it is short and thread-like.

Remarks: With its simple, orthograptid thecae, lack of a median septum, and relatively low distal 2TRD (relative to DVW), this species is easily identifiable from others in the collection. Individual specimens of *R. abbreviatus* are highly variable, resulting in a large number of redundant species in the literature. Chen et al. (2000) and Štorch et al. (2011) synonymized many of these species, but retained a large (*Rectograptus uniformis*) and thin form (*Rectograptus socialis*). Specimens within this collection approach the size of *R. uniformis* (numerous specimens over 3.5 mm, and several at or slightly more than 4 mm). A number of specimens in collection 17.20 m (*mirus* Subzone) fall within the range *of R. socialis*, with maximum widths of <2 mm (e.g., Plate 16.3 and 16.10). As the wide specimens appear to fall within a continuum of variation, however, and the narrow specimens are largely short and/or incomplete (and mostly within the low end of variation of *R. abbreviatus*, e.g., ca. 2 mm), all of these are retained within within *R. abbreviatus*.

Genus *Paraorthograptus* Mu et al., 1974 (in Nanjing Institute of Geology and Palaeontology, eds.)

Type species *Climacograptus innotatus* var. *pacificus*, Ruedemannn, p. 429, pl. 73, fig.20; designated by Williams (1982).

Remarks: Species of *Paraorthograptus* are distinguished from all contemporary species by the presence of paired genicular spines on all thecae except the first pair. Common preservational artifacts (e.g., apparent length and number of spines, and thecal inclination, etc.), high levels of intraspecific variation, as well as misattribution to

Paraorthogrpatus of unrelated Rhuddanian species with thecal spines (e.g., *Hirsutograptus*), and other species lacking spines but possessing flanges or hoods (e.g., *Paraclimacograptus*) has led to a confusing array of species being erected and subsequently synonomized or rejected from the genus (see Mu et al., 2002, for an example of misattributed species). Williams (1982) tentatively synonymized all species of *Paraorthograptus* with *Paraorthograptus pacificus*, arguing that tectonic artifacts made width, the most common character for distinction, suspect. Melchin (1987a) followed this approach. Chen et al.'s 2000 global biostratigraphic paper recognized three species of *Paraorthograptus* in the Wufeng material described by Mu et al. (1993): *P. pacificus, P. longispinus,* and *P. brevispinus*. Chen et al.'s (2005a) survey of Chinese Hirnantian material also recognized three species of Paraorthograptus: *P. pacificus* (= *P. longispinus*), *P. brevispinus,* and *P. uniformis* (restricted to the *extraordinarius* Zone). Fan and Chen (2007) gave ranges for the species in Chen et al. (2005a), but also include *P. p. affinis* (uppermost *typicus* Subzone)*, P.* sp. (*complexus* Zone), *P. tenuis* (uppermost *mirus* Subzone and *extraordinarius* Zone), and *P. longispinus* (mid-*typicus* to uppermost *mirus* subzones). Štorch et al. (2011) only recognized two species in their Nevada collections (*P. pacificus* and *P. uniformis*), both of which range from the base of the *pacificus* Zone through the *persculptus* Zone. Although abundant in most sections throughout the *pacificus* Zone, *Paraorthograptus* material tends to be fragmentary and/or only moderately to poorly preserved, a result of its thin rhabodosome walls and aseptate internal structure, making it difficult to gather large datasets of reliable rhabdosome

measurements. The present samples suffer from similar preservational issues, but the large number of specimens available (over 7,000 specimens, including fragments, counted) provides a unique opportunity for analysis. One hundred very well-preserved specimens spanning the whole *pacificus* Zone, plus an additional 113 less well-preserved specimens, were measured and plotted by width, thecal spacing, and widening ratio, resulting in three distinct populations, distinguished most clearly by distal thecal spacing and DVW (Fig. 6.15). Unfortunately, well-preserved material is rare in the middle of the section. As a result, it is difficult to determine whether the two main morphological clusters, largely confined to the upper and lower parts of the section, represent unique species or a single evolving lineage. Measured specimens were chosen to test the scheme shown in Chen et al. (2005a, text-fig, 4), i.e., specimens that had th3, th5, and th10 intact. Abundant proximal and distal fragmentary material remains unmeasured in this collection that could be exploited in future research. Other characters, such as spine length and apertural/supragenicular height, were considered too prone to preservational effects to be considered useful.

***Paraorthograptus kimi* Koren' (1979)**

Plates: (Photos) 17.6-8, 17.18; (Line drawings) 2.10-11.

Material and stratigraphical range: Abundant in the lower *pacificus* Zone, and questionably present throughout the entire *pacificus* Zone. 34 specimens measured in detail.

Description: Rhabdosome up to 25 mm long, but usually less than 10 mm. Expands rapidly until th5-7, and then slowly thereafter, sometimes tapering slightly distally. DVW at th1 is 0.75-1.0 mm, 0.85-1.2 mm at th3, 1-1.4 mm at th5, 1.15-1.55 mm at th7, 1.23-1.65 mm at th10, to a maximum of 1.2-1.7 mm distally. 2TRD is 0.9-1.2 mm at $th1^1$, 1.0-1.28 mm at $th3^1$, 1.05-1.45 mm at $th5^1$, 1.13-1.35 mm at $th7^1$, and 1.2-1.5 mm (mean 1.31 mm) at $th10^1$. Thecae are inclined and geniculate, with paired genicular spines up to 1.1 mm long present on the second and subsequent thecae. The proximal end is furnished with paired antivirgellar spines, a short virgella, and a mesial spine on $th1^1$.

Remarks: [Note: Dimensions in the Description section above include all measured *Paraorthograptus* material from 1.3 m and 8.8 m; dimensions for *P. pacificus* below, include all measured material from 14.15 m and above, less noted exceptions.] Koren' (1979) distinguished *Paraorthograptus kimi* as a subspecies of *Paraothrograptus pacificus* (*Pacificograptus pacificus kimi*), based on its relatively narrow and short rhabdosome, but subsequent authors have not recognized it as distinct from *Paraorthograptus pacificus*. *P. kimi* occurs in a monospecific assemblage slightly below the first appearance of the more common wider form of *P. pacificus* at its type location in the Southern Tien Shan (Koren et al., 1979), as well as in the Kolyma region (Siberia), where it occurs below *P. pacificus* where the two co-occur in the same section (Drevnyaya River: fig. 63, Koren' et al., 1983). At Blackstone River, *pacificus* Zone specimens of *Paraorthograptus* are divisible into two populations, with the stratigraphically lower population possessing a lesser width and closer thecal spacing.

This lower population plots with the types of *P. kimi,* in comparisons of both proximal and distal measurements (Figs. 6.15 and 6.16). Štorch et al. (2011) identified the same basic distinction between specimens of *Paraorthograptus* in their Nevada material: one form (assigned to *P. uniformis*) that rapidly reaches maximum distal width (1.2-1.7 mm), and possesses more closely spaced thecae (1.2-1.45 mm distally); and another form (assigned to *P. pacificus*) that widens until at least th10 (maximum 1.35-2.0 mm), with more widely spaced thecae (1.25-1.9 mm). In Nevada, both species co-occur from the base of the *pacificus* Zone until well into the *persculptus* Zone. Chen et al. (2005a) recognized three species of *Paraorthograptus* in the Hirnantian in the Yangtze region, *P. pacificus, P. uniformis,* and *P. brevispinus*, which formed overlapping clusters in plots of distal 2TRD and proximal and mesial DVW. The clearest division occurred between their *P. pacificus* and *P. uniformis/P. brevispinus* clusters, along distal thecal spacing (2TRD of greater or less than 1.5 mm at th10). This is also the clearest division in bulk plots (without prior species binning) of all of the Blackstone material (Fig. 6.14). Given the strong preservational impact on apparent spine length, Štorch et al. (2011) considered the diagnostic trait of *P. brevispinus*, short spines, to be unreliable, and considered *P. brevispinus* to be synonymous with *P. pacificus.* In both the original Chen et al. (2005a) plots, and in the graphs below, however, *P. brevispinus* tends to plot separately from specimens assigned to *P. pacificus* (Figs. 6.17 and 6.18), at least with regard to distal measurements. Based upon the limited metrical data available, it appears that the lower Blackstone collections, Koren's (1979) *P. pacificus kimi,* at least the Vinini *P. uniformis*

material from the lower *pacificus* Zone collections (as well as, possibly, their lower specimens of *P. pacificus*), and some of Chen et al.'s (2005a) *P. brevispinus* material, all form a single species. (This pattern is less clear when the Blackstone data is removed: Fig. 6.19.) As the oldest available name, *P. kimi* would have priority for this group of species.

At the Drevnyaya River and Southern Tien Shan sections, *P. kimi* and *P. pacificus* occur in discrete horizons, separated by non-graptolitic rocks. At the Blackstone River, there is no stratigraphic overlap between populations assigned to *P. kimi* and *P. pacificus*, but a 5.25 m interval separates high-quality collections of either species[26], so it is possible that they do overlap. That same stratigraphic gap also raises the possibility that the two populations are actually end members of a single evolving lineage, rather than unique species. The apparent co-occurrence of both species in the Hirnantian of China (Chen et al. 2005a) and the Katian and Hirnantian of Nevada supports separate species status, but larger populations, plotted by stratigraphic height, are required to clarify the relationships inferred here.

Paraorthograptus pacificus **(Ruedemannn, 1947)**

Plates: (Photos) 11.18, 15.4, 17.1-2, 17.5, 17.11-17, 17.19; (Line drawings) 2.9, 2.16.

[26] Several poor-quality specimens, assigned to *P. kimi,* occur at 12.67 m, but large well-preserved, measurable specimens of *P. kimi* last appear in the 8.80 m sample, and clear *P. pacificus* first appear at 14.15 m.

Material and stratigraphical range: Abundant throughout the mid and upper *pacificus* Zone, and questionably present throughout the entire *pacificus* Zone. 63 specimens measured in detail.

Description: Rhabdosome up to 31 mm long, but usually less than 12 mm. Expands from 0.7-1.05 mm at th1, to 0.85-1.2 mm at th3, 1.05-1.55 mm at th5, 1.25-1.78 mm at th7, 1.35-2.0 mm at th10, 1.5-2.15 mm at th15. Maximum DVW is reached around th12-16, after which it often markedly decreases. 2TRD is 0.9-1.3 mm at $th1^1$, 1-1.45 mm (1 specimen is 1.6 mm) at $th3^1$, 1.2-1.6 mm at $th5^1$, 1.25-1.55 mm at $th7^1$, 1.3-1.7 mm at $th10^1$, and 1.35-1.6 mm distally (mean=1.5 mm). Thecae are inclined and geniculate, with paired genicular spines up to 1.25 mm long present on the second and subsequent thecae. The proximal end is furnished with paired antivirgellar spines, a short virgella, and a mesial spine on $th1^1$. The rhabdosome is often strongly fusiform.

Remarks: The type material of *Paraorthograptus pacificus*, from the Phi Kapa Formation, Idaho, was reillustrated by Riva (1974), along with additional material from the same slab. It is clearly very strongly deformed, and mostly juvenile or damaged, but all specimens rapidly reach a maximum DVW and remain nearly parallel-sided (the holotype tapers slightly). This uniform width is more suggestive of the material assigned to *P. uniformis* by Štorch et al. (2011) or *P. p. kimi* by Koren' (1979), both assigned to *P. kimi* in this study, than it does to the wider, often strongly fusiform, material referred to *P. pacificus* by most authors. This raises the possibility that *P. pacificus* is actually the senior synonym for the material assigned to *P. kimi* above, and the material traditionally

assigned to *P. pacificus* should correctly be referred to another taxon, likely one of the species or subspecies other authors have considered equivalent to the type material of *P. pacificus.* For example, *P. pacificus pilosus* Riva (1974), possesses a fusiform profile. To circumvent the effects of deformation, ratios of distal/proximal 2TRD and proximal/distal DVW for the *P. pacificus* types were plotted, along with other type material, and material from the present and other illustrated collections (Fig. 6.20). One of each of the two plotted paratypes of *P. pacificus* falls into the morphospace occupied by the upper and lower Blackstone collections, respectively, but the holotype plots with the upper collection, while the holotype of *P. kimi* falls in with the lower Blackstone collection. This supports the traditional usage of *P. pacificus* to refer to material such as the present upper collections. Other collections of *P. pacificus* plot in both clusters. The material assigned here to *P. pacificus* can be distinguished from the material assigned to *P. kimi* by its greater distal 2TRD, greater mean width, and generally fusiform shape. It can be distinguished from *Paraorthograptus affinis* (below) by a lesser width overall, especially proximally.

***Paraorthograptus affinis* (Koren' and Tzaj) *in* Apollonov et al., 1980**

Plates: (Photos) 17.9a-b, 17.10, 17.3?, 17.4?, 26.4?; (Line drawings) 2.18.

Material and stratigraphical range: One well-preserved specimen and one fragmentary specimen from the basal *extraordinarius* Zone, plus several possible specimens from the upper *mirus* Subzone. Only the well-preserved specimens were measured in detail.

Description: A single complete fusiform rhabdosome 14 mm long. Widens rapidly from a width of 1.13 mm at th1, to 1.58 mm at th2, 1.75 mm at th4, ca. 1.9 mm at th5, ca. 2.05 mm at th7, and 2.6 mm at th10, and then decreases after th11. 2TRD is ca. 1.35 mm at th1[1], 1.45 mm at th3[1], 1.65 mm at th5[2], and ca. 1.7 mm at th7[2]. Apertural spines are ca. 0.8 mm long, and present on the second pair and all subsequent thecae. An additional specimen from the same collection (Plate 17.9a and 17.9b) reaches a maximum width of 2.55 mm, with a distal 2TRD of ca. 1.5 mm. Thecal form is as in other species of *Paraorthograptus*.

Remarks: The single well-preserved specimen is well outside the range of maximum proximal, mesial, and distal width of other specimens of *Paraorthograptus* in the present collections (several wide distal fragments from the upper-*mirus* Subzone attain a DVW of 2.4-2.5 mm, e.g., Plate 17.3 and 17.4, but the sample may be slightly deformed; see Figs. 6.14 and 6.17). The high DVW is unlikely to be the result of tectonic deformation, as 2TRD is also high, and both high distal 2TRD and DVW are shared with a second broken specimen. Several authors have noted a large species of *Paraorthograptus* occurring near the basal *extraordinarius* Zone boundary. *Paraorthograptus affinis* (Koren' and Tzaj) co-occurs with *M. ojsuensis* at the Ojsu section in Kazakhstan (Koren' and Sobolevskaya, 2008). *Paraorthograptus uniformis* also first occurs in the *extraordinarius-ojsuensis* Zone in China (Chen et al., 2000; Chen et al., 2005a), and is described by early authors (Mu and Li, in Mu and Lin, 1984; Mu et al., 1993) as rapidly reaching a high DVW (e.g., 2-2.4 mm at 5 mm in the type collection).

The holotype of *P. uniformis* is 1.23 mm at th1, 1.5 mm at th3, and 2.24 mm at th10 (Mitchell, pers. comm.). The type specimens of *P. affinis* are 1.1-1.25 mm wide at th1 and 1.6-2 mm wide at th5, with a maximum width of 2.1-2.4 mm (Koren' et al., 1980). Theca 1 and th3 measurements for the types of both these species well exceed those for all measured paraorthograptids in this collection, spanning the *pacificus* Zone, with the exception of those specimens described above (see Fig. 6.21). Although Štorch et al. (2011) considered *P. affinis* to be a junior synonym for *P. pacificus*, assuming that the Russian type material is not deformed, it appears that *P. affinis* is a distinct species, and also the senior synonym for *P. uniformis* (including the type material of that species, but not the stratigraphically lower specimens assigned to *P. uniformis* by Štorch et al. (2011), which are assigned here to *P. kimi*).

Genus *Anticostia* Stewart and Mitchell, 1997, emended in Štorch et al., 2011.

Type species: *Anticostia macgregorae* Stewart and Mitchell, 1997; by original designation.

Anticostia lata **(Elles and Wood, 1906)**

Plates: (Photos) 11.15, 26.5; (Line drawings) 2.15.

Material and stratigraphical range: Abundant throughout the upper *ornatus* to upper *pacificus* Zone. Many hundreds of specimens examined; 6 specimens measured in detail.

Description: Robust rhabdosome with prominently thickened and geniculate apertures, to at least 50 mm in length. Steadily widens from 0.88-0.95 mm at th1, to 1-1.1 mm at th3, 1.15-1.35 mm to th5, 1.35-1.53 at th7, 1.55-1.83 at th10, 1.8-2.1 mm at th15, to a

maximum of ca. 2.3 mm distally (up to at least 2.5 mm in large distal fragments). 2TRD is 1.15-1.3 mm at th2, 1.5-1.6 at th5, and 1.7-ca. 2 mm distally. Stout and robust virgella and paired antivirgellar spines (frequently only one visible), each about 0.4 mm long. $Th1^1$ grows ca. 0.1-0.15 mm below the sicular aperture, which is ca. 0.3 mm wide. Thecae are straight to slightly inclined distally. The thecal apertures are strongly geniculate and thickened, sometimes presenting as small flanges, with prominent lappets. The periderm is thick, and obscures the sicula and other internal features, but a gently wandering nema is often visible, suggesting that it is aseptate

Remarks: This species is extremely abundant in large parts of the section, sometimes nearly covering slabs with current-aligned specimens. Because it has been well described elsewhere, only a small number of specimens were measured or illustrated, although abundant material exists for future morphometric work. With its relatively broad proximal end, mesial and paired antivirgellar spines, broad distal width, thickened and geniculate apertures, and often well-preserved lappets, this species is readily distinguished from others in this collection. *Anticostia tenuissima* differs principally in having more rounded geniculae. At Vinini Creek, *Anticostia tenuissima* is restricted to the *ornatus* Zone (Štorch et al., 2011). In distal fragments or scalariform view, *Anticostia lata* can be distinguished from other species of *Anticostia,* and species of *Climacograptus* or *Styracograptus*, even in fully scalariform specimens, by the combination of geniculate thecae and lappets.

Anticostia macgregorae **Stewart and Mitchell, 1997**

Plate: (Photo) 11.6

Material and stratigraphical range: A single measured specimen from the lower *mirus* Subzone, plus an additional specimen from slightly higher in the subzone.

Description: Immature specimen is 5.5 mm long. DVW is 0.9 mm at th1, 0.88 mm at th2, 0.95 mm at th3, and 1.15 mm at th5. 2TRD is 1.55 mm at th1[1] and 1.8 mm at th3[1]. Thecae long, inclined, and nearly straight, with slight or no geniculae, and sharp lappets. The first theca is u-shaped, with an upwardgrown portion ca. 0.55 mm long. It bears a 0.63 mm subapertural spine. The sicula appears to be ca. 1.65 mm long. A thread-like nema projects 1 mm distally.

Remarks: This specimen agrees well with the single specimen assigned to *Anticostia macgregorae* species by Štorch et al. (2011: their fig. 19a. It is assigned to this species based upon the straighter and more upright thecae, its th2 constriction, and relatively high 2TRD. The specimen is preserved with torsion in an off-profile view, however, and some of the differences between it and those assigned to *A. uniformis* may be preservational artifacts.

***Anticostia uniformis* (Mu and Lin) *in* Mu et al., 1993**

Plates: (Photos) 11.4-5, 11.7-9, 11.11; (Line drawings) 2.1-8.

Material and stratigraphical range: Rare from the lower *mirus* Subzone and abundant in the uppermost *mirus* Subzone. 30 specimens measured in detail.

Description: Nearly parallel-sided Rhabdosome up to at least 17 mm long, but most commonly less than 10 mm. Expands from 0.95-1.2 mm at th1, to 1.08-1.4 mm at th3,

1.2-1.55 mm at th5, 1.25-1.65 mm at th7 (1 specimen is 1.8 mm), 1.4-1.75 mm at th10, and up to 1.75 mm distally. 2TRD is 1.3-1.65 mm at $th1^1$, 1.4-1.95 mm at $th3^1$, 1.55-2.0 mm at $th5^1$, 1.65-1.95 mm at $th10^1$. The proximal end is broad and possesses four spines: a mesial spine on $th1^1$, paired antivirgellar spines, and a virgella. $Th1^1$ is broadly u-shaped. It grows below the sicular aperture for 0.15-0.3 mm, and its upward-grown portion is 0.58-0.80 mm long. The sicula is ca. 2.8 mm long, and its aperture is ca. 0.3-0.4 mm wide. Thecae are glyptograptid to nearly orthograptid, with straight sides distally. Thecal apertures are introverted and lappeted, although the lappets are often indistinct. A short thread-like nema is present on some specimens. The rhabdosome is aseptate.

Remarks: The large present collection shows considerable variation in distal width and rate of widening, but most specimens reach an apparent maximum width of 1.4-1.5 mm, which is maintained throughout the preserved rhabdosome. Material from 19.05 m (the highest occurrence) seems to be more variable in rhabdosomal dimensions, with greater maximum widths, than lower collections; however, the population in this collection is also larger, with many times more specimens than occur in the lower collections combined. The collection is also relatively poorly preserved, and is possibly subject to minor deformation. In addition to possible differences in dimensions, the uppermost population (19.05 m), which immediately precedes the first appearance of *Metabolograptus ojsuensis*, is odd in that it is the only sample in the present collections where a species of *Anticostia* other than *A. lata* occurs as more than minor member of

the assemblage. In lower collections, *A. uniformis* always occurs as <1% of the population, but at 19.05 m it makes up 81% of the sample. No equivalent interval occurs in Nevada (Belscher, 2007), where *A. uniformis* is always a minor component of the assemblages. Sample 19.05 m also contains abundant small brachiopods, and is lacking in many species that were common throughout the lower parts of the section. Given that it just underlies the first appearance of neograptine graptolites, considered indicative of the onset of environmental changes associated with the Hirnantian glaciation in low latitude collections, this sample may capture the initial stages of these changes.

Although most authors have described *A. uniformis* as attaining a maximum width of less than the present collection (1.3 mm in Štorch et al., 2011; 1.5 mm in Koren' et al., 1983 (assigned to *Glyptograptus tenuissimus*--reassigned by Štorch et al., 2011), and 1.4 mm in Chen et al., 2005a), Mu and Lin observed a maximum distal width slowly attained of 1.8-2.0 mm in the type description. Specimens with widths greater than 1.5 mm are relatively rare in the present collection, and are mostly very mature. Therefore, the differences in reported maximum widths are likely due to the relatively small collections available to previous authors. Comparison of proximal vs. mesial DVW (the only measurement for which sufficient interregional data exists) in Nevada and Yukon specimens shows only slight overlap between the two clusters (Figs. 6.22 and 6.23). This is taken to represent regional variation, given the consistency in other characters, such as sicular length and thecal form. Štorch et al. (2011) highlighted a slightly lower 2TRD

(1.3-1.8 mm vs. 1.85 mm) as one of a suite of characters distinguishing the single specimen that they assigned to *A. macgregorae* from those that they assigned to *A. uniformis*. However, the present collection contains specimens with distal 2TRD greater than 2.0 mm, as does the type collection (including the holotype).

Genus *Parareteograptus* Mu, 1974; emended Štorch et al., 2011

Type species: *Parareteograptus sinensis* Mu, 1974; by original designation.

***Parareteograptus sinensis* Mu *in* Nanjing Institute of Geology and Palaeontology (eds.), 1974**

Plates: (Photos) 11.1-3, 11.14

Material and stratigraphical range: Rare from the upper *ornatus* to lowest *pacificus* Zone. 10 specimens measured in detail.

Description: Robust rhabdosome up to 11 mm long (but in all but one case 6 mm or less). Widens gradually from 1.03-1.1 mm at th1, to 1.1-1.35 mm at th2 (n=4), 1.5-1.66 mm at th3, 1.85-2 mm at th5 (n=3), 1.95-2.3 mm at th7 (n=4), and 2.5 mm at 10 (n=1). In the single mature specimen, a maximum width of 2.6 mm is reached at th11, after which the colony tapers to ca. 2 mm by th15. 2TRD is 0.95-ca. 1.15 mm at th1^1, 1-1.25 mm at th3^1, ca. 1.2-1.4 mm at th5^1, 1.4 mm at th7^1 (n=1), and 1.5 mm at th10^1 (n=1). Th1^1 turns upward approximately 0.2-0.35 mm below the sicular aperture. Its upward-grown portion is short (0.3-0.525 mm long) and u-shaped. Th1^2 turns up at or just above the level of the sicular aperture. The length of the sicula is unclear, but its aperture is ca. 0.28-0.35 mm wide. Paired antivirgellar spines are present, although rarely preserved.

When they are preserved, they are often at right angles to one another, with one spine projecting ventrally and the other down (e.g., see Plate 11.1), as a result of dorsal curvature of the sicular aperture upon compaction. A short, but robust virgella and subapertural spine on th1[1] are also present. Thecae are straight and moderately inclined. The apertures are horizontal, and made up of prominent apertural lists, which connect to a series of list-supported panels that make up the remainder of the rhabdosome (see Štorch et al., 2011, pp. 341-343, for detailed discussion of parareteograptid colony architecture). Thecal walls are present on mature specimens, but are often thin or absent in the distal end of immature specimens (e.g., Plate 11.14). The only mature specimen in the collection tapers after ca. th11.

Remarks: Štorch et al. (2011) provided a detailed discussion of *Parareteograptus* compared with other Late Ordovician retiolite-type graptolites, e.g., *Sinoreteograptus*. Many of these appear to be independently derived, but several are junior synonyms of *Parareteograptus*, e.g., *Orthoreteograptus* and *Pseudoreteograptus.* Within those species assignable to *Parareteograptus,* three species occur in Nevada: a rare, rapidly widening form (*Pr. turgidus*); a rare minute form (*Pr. parvus*); and common, more slowly widening, but robust form (*Pr. sinensis*). The present collections do not contain the minute form, but do contain two specimens that show much more rapid widening than other specimens in the collection (see discussion below); both are juvenile. Plots of proximal widths show clear and tight morphological clusters supporting these two forms in both Nevada and the Yukon (Fig. 6.24), with the slowly widening form relatively wider

in the Yukon than in Nevada. The stratigraphic distribution of these two forms is also the same. In Nevada, the slowly widening form is common in the upper *ornatus* and lower *pacificus* zones, and only questionably present higher in the *pacificus* Zone, whereas the rapidly widening form does not make its first appearance until the middle of the *pacificus* Zone. The same pattern of appearance occurs in the Yukon, with nearly 13 m separating the last occurrence of the first form and first occurrence of the second form. In addition to rate of widening, Štorch et al. (2011) distinguished these two forms by distal 2TRD (higher in the slow-widening form) and a particularly blunt, "dish-like", proximal end in the rapidly widening form. Although Chen et al. (2000) considered *Pr. turgidus* to be a junior synonym of *Pr. sinensis,* Štorch et al. (2011) retained the name *Pr. turgidus* for their rapidly widening specimens, in accordance with the original distinction made by Mu (in Mu et al., 1993). Along with their slowly widening forms, Štorch et al. (2011) placed a number of other species in synonymy with *Pr. sinensis,* including *Orthoreteograptus denticulatus* and, questionably, *Pr. magnus.* In addition to their rapidly widening specimens, they considered *Pseudorthograptus nanus* to be a junior synonym of *Pr. turgidus.* Whereas the present study did not examine the original type material (housed in China), Štorch et al. (2011) included a table of measurements from holo-, para-, or hypotypes of the various species they discussed. Figures 6.25-6.28 compare the Blackstone and Nevada *Parareteograptus* material to those type specimens, focusing on relative widening and proximal width versus distal thecal spacing (the characters highlighted by Štorch et al. (2011).

The results show convincing species groups within the North American material, with the Nevada specimens assigned to *Pr. sinensis* plotting separately from the Nevada material assigned to *Pr. turgidus* in all graphs (note: data are limited for distal DVW), and agreeing relatively well with the two species from the Blackstone River section, which also plot separately from each other. The Nevada specimens assigned by Štorch et al. (2011) to *Pr. sinensis* plot consistently with the *O. denticulatus* types; however, in all comparisons, the hypotypes of *Pr. sinensis* plot separately from the material assigned by Štorch et al. to *Pr. sinensis*. In terms of proximal width (th1), distal width (th10), and distal 2TRD, but not mesial (th5) DVW, the types of *Pr. turgidus* cluster with the Nevada specimens assigned to *Pr. sinensis* and the types of *O. denticulatus*, rather than with either the Nevada material assigned to *Pr. turgidus* material or *Pr. nanus*. On the basis of proximal widening rate (shown here as th1 vs. th5: Fig. 6.25), the primary basis for Mu's distinction of this species, the types of *Pr. turgidus* are ofdistinct and plot with the Nevada specimens of *Pr. turgidus* and equivalent Blackstone River material, however, they also plot with the type specimens of *Pr. sinensis* by this measure (Fig. 6.24-25). Based on the comparative data available, the most consistent and recognizable group includes the Nevada *Pr. Sinensis,* the types *O. denticulatus*, and the lower Blackstone River material, but excludes the hypotypes of *Pr. sinensis*. This group may be best assigned to *Pr*. *denticulatus.* A second group, distinguishable by a much more rapid widening rate, is also apparent.This group includes the upper Blackstone River material,

the Vinini Creek *Pr. turgidus* specimens, and the types of both *Pr. turgidus* and *Pr. sinensis* (Fig. 6.25). Among these species, *Pr. sinensis* would have priority.

In addition to widening rate and a resulting blunt proximal end, Štorch et al. (2011) distinguished their specimens of *Pr. turgidus* as possessing laterally growing, rather than upright, first thecal pair, and a dish-like apertural opening. These features are also present in the stratigraphically equivalent specimens from the Blackstone. It is unclear from available illustrations how consistent these features are within the various species noted above, but at least some of the specimens assigned to *Pr. sinensis* by Mu et al. (1993), e.g., plate 51.5, also seem to possess them. It is also worth noting that the type collection of *Pr. turgidus* is from the *D. szechuanensis* Zone (Mu et al.'s usage is equal to the upper *ornatus/*lower *pacificus* Zone: Chen et al., 2000), stratigraphically lower than the North American material.

Study of larger collections is required to determine the precise relationship between the various species of *Parareteograptus*, and in particular to control for intraspecific temporal and geographic variation. This study uses the species names of Štorch et al. (2011) to facilitate comparison between sections, despite the concerns raised above. Material illustrated by Lenz and McCracken (1982, fig. 3 i and j) from the Road River, Yukon, as *Reteograptus pulcherrimus* is likely *Pr. sinensis* (*sensu* Štorch et al., 2011), given its slow, steady distal widening. The magnification in the figure appears to be incorrect, however, based on the apparent dimensions of other well-known species (e.g., *Climacograptus hastatus*) illustrated on the same figure.

***Parareteograptus turgidus* Mu *in* Mu et al., 1993**

Plates: (Photos) 11.12-13

Material and stratigraphical range: Two flattened flattened specimens from just below the base of the *mirus* Subzone.

Description: Two small, partially sclerotized specimens, 2.75 mm and 3.5 mm long. The rhabdosome rapidly widens from 1.28-1.3 mm at th1, to 1.7-1.78 mm at th2, 2.05 mm at th3 (n=1), and ca. 2.2 mm at th5 (taken at $th5^2$). 2TRD is ca. 1.05 mm at th1 and ca. 1 mm at th3. $Th1^1$ and $th1^2$ are short (0.6 and 0.8 mm, respectively), grow nearly horizontally, with the base of $th1^1$ aperture only ca. 0.1 mm above the base of the virgella, and bearing a short subapertural spine. The rhabdosome consists of a well-defined framework of lists, and is completely sclerotized, except for the distal-most thecal pair, which consist only of lists. The sicular aperture is 0.45 mm wide, and bears a short virgella and a single antivirgellar spine.

Remarks: This extremely rare species was recovered only from a single sample. Despite a dedicated search of this and adjacent horizons after discovery of the first specimen, combined with additional slab splitting, only a second juvenile specimen was recovered. This specimen was, however, unfortunately destroyed during preparation, after only DVW measurements were taken. As a result, all measurements above, except DVW, come from one specimen. This species is distinguished from the more common, lower *Pr. sinensis* by its much more rapid rate of widening and a more inclined first thecal pair. As the present specimens are immature, distal width is unclear; however, it is wider at

all points preserved than all of the other specimens in this collection, and agrees very closely with specimens assigned to *Pr. turgidus* by Štorch et al. (2011) (Fig. 6.24). See discussion of *Pr. sinensis* above for comparison with types and other species of *Parareteograptus*.

Family: Lasiograptidae Lapworth, 1879; emended Mitchell, 1987

Remarks: The "naked" Late Ordovician lasiograptids are easily identifiable from other contemporary graptolites by their lack of rhabdosomal walls with fuselli. Instead, they possess a framework of lists, accompanied by mesh (reticulum) between the lists, which is variable in degree of development between species and specimens. Recognizing genera is complicated by the presence of lacinia, a three-dimensional mesh structure developed from the apertural spines, which in some species completely encloses the rhabdosome. This combination of non-sclerotized thecae and obscuring lacinial network results in a wide variety of apparent forms, depending on mode of preservation and angle of flattening. Fragmentary lasiograptid material is present in nearly all samples, but well-preserved mature specimens are rare. All of the best-preserved specimens appear to fall into two well-known species: *Phormograptus connectus* and *Yinograptus disjunctus.* Identifiable specimens of the genus *Paraplegmatograptus*, which occurs in coeval sections in Nevada and China (Štorch et al., 2011; Mu et al., 1993), were not recovered in the present collection. However, given the large percentage of unidentifiable lasiograptid specimens, as well as the difficulty in distinguishing species and genera of lasiograptids from one another (e.g., *Paraplegmatograptus* from the

broadly similar *Yinograptus*) it is likely that the present work underestimates the number of species of lasiograptids present. This material would benefit from thorough reexamination by a worker with specialization in the Lasiograptidae.

Genus *Phormograptus* Whittington, 1955

Type species: *Phormograptus sooneri* Whittington, 1955; by original designation.

***Phormograptus connectus*, Mu, in Wang et al., 1978**

Plates: (Photos) 13.2-4, 13.6-7, 16.4

Material and stratigraphical range: Uncommon from the *ornatus* to upper *pacificus* zones, and likely from the basal *extraordinarius* Zone. 6 specimens measured.

Description: Ovoid rhabdosome up to at least 12 mm long. Rapidly expands from approximately 1.3 mm proximally, to 3 mm wide at 2mm, and ca. 4-4.5 mm wide within 5 mm. Maximum width including lacinia is up to 5 mm. The rhabdosome is completely covered a dense lacinial network that makes thecae difficult to discern, but proximal 2TRD appears to be 1.25 mm in one specimen and distal 2TRD 2 mm in another. A prominent nema runs the length of the rhabdosome and projects up to 4 mm beyond. The sicula is ca. 0.15 mm wide and 0.75 mm long (n=2; 1 specimen is 0.6 mm, but likely broken: see lower specimen in Plate 13.4). A thin virgella extends for 6 mm in one specimen (Plate 13.6). Regular lateral spines, ca. 0.75 mm long, project beyond the lacinia along the entire margin of the rhabdosome.

Remarks: This species is characterized by a highly reduced thecal framework and well-developed and extensive lacinial network, which covers the entire rhabdosome. These

features, combined with the fact that it is frequently preserved in subscalariform view, produce a wide variety of appearances. The presence of a lacinia extending beyond the thecal apertures makes it readily distinguishable from *Yinograptus*. Within the present samples, *Phormograptus* usually occurs as either as isolated fragmentary material or within gregarious clusters of overlapping mature individuals (e.g., Plate 13.2 and 13.4).

Genus *Yinograptus* Mu, in Mu and Chen, 1962

Type species: *Gothograptus disjunctus* Yin and Mu, 1945; designated by Mu and Chen, 1962.

***Yinograptus disjunctus* (Yin and Mu, 1945)**

Plates: (Photos) 13.1, 13.5

Material and stratigraphical range: Four complete measured specimens from the lower to upper *pacificus* Zone; additional possible fragmentary material from within this range.

Description: Rhabdosome up to 22 mm in length. Proximal end preserved in three specimens. The sicula is short, ca. 0.53-0.65 mm long and 0.15-0.2 mm wide (n=2). The rhabdosome expands from ca. 1-1.25 mm proximally (n=2) to ca. 2.5 mm wide at 5 mm (n=3), ca. 3 mm wide at 10 mm, with a maximum distal width of ca. 3-4.2 mm (or up to 5 mm if mesial apertural spines and lacinia are included, e.g., Plate 13.5) (n=2). 2TRD is difficult to measure, but is 2.5 mm mesially and distally in one specimen. Multiple long septal spines (scapulae), up to 10 mm long, arise from or near the nema. They are oriented nearly horizontally proximally and at ca. 45° distally, and are spaced at 2.7-3.25

mm intervals (n=2). The proximal region is covered with a reticular framework, which is reduced or absent distally. Two vertically oriented spines, 0.75 and 1.75 mm in length, project from the proximal end in one specimen, apparently from the aperture of the sicula (Plate 13.5). All specimens are preserved in subscalariform or scalariform view.

Remarks: These specimens agree well in all ways with material described in detail by Štorch et al. (2011). A more detailed discussion of the construction of the colony in relation to other lasiograptid species can be found there. *Yingograptus* can be distinguished from *Phormograptus* by the presence of scapulae and a much more defined thecal framework, with lacinia restricted to the apertural margins.

Superfamily Climacograptoidea Frech, 1897, emended Mitchell et al. 2007[27]

Genus *Climacograptus* Hall, 1865, emended Štorch et al., 2011

Type species: *Graptolithus bicornis* Hall, 1847, by original designation.

***Climacograptus hastatus* T.S. Hall, 1902**

Plates: (Photos) 15.1, 15.3, 15.8, 15.10, 15.13, 21.3-4, 21.13-16;

(Line drawings) 3.10, 3.12

Material and stratigraphical range: Rare to uncommon from the uppermost *ornatus* Zone to the upper *mirus* Subzone. 24 specimens measured in detail.

Description: Robust rhabdosome reaching up to at least 34 mm long. Widens rapidly from 0.6-ca. 0.8 mm at th1, to 0.83-1.18 mm at th3, 1.2-1.6 mm at th5, 1.6-2.0 mm at

[27] Phylogeny of the Ordovician Diplograptoidea

th10, and 1.75-2.2 mm distally. 2TRD is 1.1-1.3 mm at $th1^1$, 1.45-1.68 at $th3^1$, 1.65-1.9 mm at $th5^1$ (one specimen is 1.5 mm), and 1.95-2.5 mm distally. Thecae are straight to slightly to moderately inclined, with sharp geniculae, but sometimes appear rounded when in off-profile view. Thecal apertures are large (ca. 0.55 mm high distally) and deep, with slightly thickened rims, and are almost the same height as the supragenicular walls. The proximal end is furnished with multiple spines. All specimens possess a virgella and two ventrally projected spines emerging from the upward-grown portion of the first thecal pair. Several specimens possess additional lateral spines (up to four in total). The length and width of both the virgella and lateral spines are highly variable and increase with rhabdosome maturity. Virgellae range from 0.5 mm to 12 mm long, and the lateral spines from 1.3 to 3.5 mm long. In mature specimens, parasicular growths cover the proximal end of the rhabdosome, and extend from the base of the spines along the virgella as a 0.3-0.4 mm wide tube, which is up to 4 mm long. The lateral spines also show progressive thickening, and may be up to ca. 0.3 mm wide basally. Gerontic thickening of the proximal end often obscures the first few thecae, making precise measurements of DVW difficult. The nema is also highly variable, ranging from thin and thread-like to very robust: up to 0.4 mm wide and 16 mm long.

Remarks: The present specimens agree with previous descriptions of this morphologically variable species. Variation seems to follow astogeny, rather than showing any meaningful evolutionary or environmental signal, with one possible exception: a large number of specimens occur in the *mirus* Subzone (especially samples

14.15 m and 16.03 m—see Plate 21.14-15) that possess well-developed lateral spines, but only very short and/or very thin virgellae. This combination of features is absent from all of Berry's (1966) eight "varieties" of *C. hastatus.* These specimens closely resemble *Climacograptus trifidus spectabilis* Koren' and Sobolevskaya (in Koren' et al., 1983). However, since these specimens are mostly immature, co-occur with more typical specimens of *C. hastatus*, and agree in all other ways (DVW, etc.) with specimens of *C. hastatus* in the present collection, they are considered to be within the range of variation of *C. hastatus.* It is possible that Koren' and Sobolevskaya's specimens are variants of *C. hastatus* as well. When the proximal end is intact, specimens of *C. hastatus* are easily identifiable, but they resemble specimens of *Styracograptus mississippiensis* when their lateral spines are missing or buried; even then, they can usually be distinguished based on their very large thecal apertures. Immature specimens of *C. hastatus* with short or missing virgellae can also be confused with species of *Appendispinograptus,* but in the latter the lateral spines are truly basal, rather than occurring mesially on the first thecal pair. *C. hastatus* is often preserved in subscalariform or scalariform view, due to the proximal spines forcing the rhabdosome into an oblique orientation during flattening.

Genus *Styracograptus* Štorch et al., 2011.

Type species: *Climacograpus tubuliferus* Lapworth, 1876, by original designation.

***Styracograptus mississippiensis* (Ruedemannn, 1908)**

Plates: (Photos) 15.2, 15.5-7, 15.9, 15.11, 21.1, 21.9-10, 21.12;

(Line drawings) 3.1-5, 3.13-14, 3.16

Material and stratigraphical range: Common from the upper *ornatus* Zone and rare to uncommon throughout the *pacificus* Zone, and probably present in the basal *extraordinarius* Zone. 67 specimens measured in detail.

Description: Straight-sided to fusiform rhabdosome up to 17 mm long. Variable rate of widening and maximum size. Widens from 0.68-0.95 mm at th1, to 0.88-1.25 mm at th2, 1.08-1.5mm at th3, 1.18-1.75 mm at th5, 1.125-1.9 mm at th7, 1.3-1.9 mm at th10, with a distal maximum of 1.35-2.1 mm. Some specimens taper distally. 2TRD is 1.25-1.55 mm at $th1^1$, 1.25-1.65 mm (1 specimen is 1.75 mm) at $th3^1$, 1.45-1.85 mm at $th5^1$ (1 specimen is 1.25 mm), 1.45-1.85 mm at $th7^1$, and 1.65-1.85 mm at $th10^1$. The sicula is rarely visible, but appears to be ca. 1.35 mm long. The virgella is 0.3-1.35 mm long. The nema is highly variable: up to 9 mm long, and thread-like to 0.8 mm wide, with some specimens showing distal expansion. Thecae are climacograptid, with straight to somewhat inclined supragenicular walls, and sharp to gently rounded geniculae. Thecal apertures and supragenicular walls are ca. 0.25-0.3 mm and ca. 0.55-0.65 mm high distally, respectively. Prominent cross-bars are visible on some specimens.

Remarks: This species closely resembles the coeval *Styracograptus tatianae*. It differs principally in its greater width (Figs. 6.29 and 6.30), and this feature alone can reliably distinguish the two species by at least th5. In a detailed study of populations of *S. tatianae* and *S. mississippiensis* from sections in China and Nevada, as well as specimens from the present collection, Robinson (2012) was also able to reliably distinguish the

two species based on differences in proximal development, including a relatively longer virgella in *S. tatianae* and a relatively more deflected virgella in *S. mississippiensis*. *Styracograptus mississippiensis* differs from *Climacograptus hastatus* in lacking any proximal spines other than the virgella, as well as generally possessing smaller, less semi-circular apertural openings, but it may be confused in specimens with an incomplete or absent proximal end. *Styracograptus tubuliferus* attains a much higher distal width. *Styracograptus putillus* overlaps in dimensions, but is septate distally (Štorch et al., 2011). The present population shows considerable morphological variability, which is partly the result of preservation (e.g., degree of apparent geniculation and/or thecal inclination) and maturity (e.g., width of nema). This species also appears to vary stratigraphically, with specimens from the *pacificus* Zone generally widening more rapidly than specimens from the *ornatus* Zone (Fig. 6.31). This observation is consistent with the results of Robinson's (2012) detailed morphometric study of *S. mississippiensis*. Due to limited high-quality mature material, Robinson only examined details of the proximal end and the third thecal pair, but statistical tests showed that younger populations were generally wider than older ones (see Figs. 9 and 10 in Robinson, 2012); his data did not support a consistent directional evolutionary trend, however. Comparison of the present populations with those recently described from Nevada by Štorch et al. (2011), as well as the type collections from Oklahoma, show very close agreement (Fig. 6.32). Robinson's study similarly found no statistically robust differences in morphology between his three study populations.

***Styracograptus tatianae* (Keller, 1956)**

Plates: (Photos) 15.12, 21.6-8, 21.17, 22.6; (Line drawings) 3.6-9

Material and stratigraphical range: Uncommon to rare from the *ornatus* to upper *pacificus* zones. 13 specimens measured in detail.

Description: Small and nearly parallel-sided Rhabdosome up to 11 mm long. Expands from 0.53-0.75 mm at th1, to 0.66-0.98mm at th2, 0.73-1.03 mm at th3, 0.8-1.0 mm at th5, and 0.92-1.05 mm at th7, which is maintained or slightly increases distally (several poorly preserved specimens from the upper *mirus* Subzone possess a maximum width of ca. 1.25 mm). 2TRD is 1.05-1.38 mm at $th1^1$, 1.35-1.6 mm at $th3^1$, 1.5-1.85 mm at $th5^1$, and 1.66-1.9 mm distally. Thecae are straight to slightly inclined, and sharply geniculate, with semi-circular apertures, and thickened apertural rims. The virgella is thin and up to 1.15 mm long, with a 0.5 mm wide parasicula present in one specimen. The nema is up to 8 mm long and 0.8-0.14 mm wide. The rhabdosome is aseptate, and the nema often wanders internally. Cross-bars are visible on some specimens.

Remarks: The narrowest biserial species in the Katian-lower Hirnantian collections, this species is readily distinguished from the otherwise very similar *Styracograptus mississippiensis* by its lesser DVW after the initial thecal pair (see Fig. 6.32). Species of *Appendispinograptus* lacking preserved lateral spines can be mistaken for *S. tatianae*. Several slender species of *Normalograptus* superficially resemble *S. tatianae,* but differ in possessing Pattern H astogeny. Chen et al. (2005a), Štorch et al. (2011), and Apollonov et al. (1980), all reported higher maximum distal DVW than in the present

material (1-1.3 mm, 0.95-1.4 mm, and 1.15-1.25mm, respectively, vs. a maximum of 0.92-1.05 mm). Material included here within *S. mississippiensis* falls within that range (e.g., maximum 1.38 mm); however, it is excluded because it falls outside of the clear morphometric clusters shown in Figs. 6.29, 6.30, and 6.32. *Styracograptus miserabilis* is superficially similar, but possesses a median septum (Goldman et al., 2011).

***Styracograptus* sp.**

Plates: (Photo) 21.5; (Line drawing) 3.11

Material and stratigraphical range: A single specimen from the *mirus* Subzone.

Description: Rhabdosome 8.3 mm long. Widens from 0.725 mm at th1, to 0.875 mm at th2, 1.125 mm at th3, 1.125 mm th5, ca. 1.225 mm at th7, and ca. 1.325 mm at th8. 2TRD is 1.7 mm at $th1^1$, 1.75 mm at $th3^1$, and 1.9 mm at $th5^1$. Specimen is slightly off profile, so details of the proximal end and sicula are unclear, but the upward-grown portion of $th1^1$ is ca. 0.7 mm long, and the proximal end is sharply tapered. Thecae are straight and inclined, with semi-circular apertures with thickened rims. The thin virgella is broken, but over 3.5 mm long. A parasicular tube 0.2 mm wide and 2.5 mm long extends along the length of the virgella for ca. 2.25 mm. Cross-bars connected to the nema are visible throughout the rhabdosome.

Remarks: Beyond the proximal end, this specimen closely resembles *Appendispinograptus leptothecalis* (inclined thecae, high 2TRD, etc.). The long virgella and parasicula, are characters of *Styracograptus tatianae,* however, it has a higher 2TRD than that species, and it widens at a rate that is intermediate between *Styracograptus*

mississippiensis and *S. tatianae*. It also differs from both of those species in having more strongly inclined thecae.

Genus *Appendispinograptus* Li Zhi-ming and Li Da-qing, 1985; emended Chen et al., 2005a.

Type species: *Climacograptus venustus* Hsü, 1959; by original designation.

***Appendispinograptus leptothecalis* (Mu and Ge) *in* Fu, 1982**

Plates: (Photos) 14.1-4, 14.8-9, 21.2, 26.1-3;

(Line drawings) 1.13-18, 7.1-3, 7.9

Material and stratigraphical range: Uncommon from the *mirus* Subzone and basal *extraordinarius* Zone. 32 specimens measured in detail.

Description: Slowly widening rhabdosome up to 46 mm in length. Width is 0.55-0.75 mm at th1, 0.53-0.75 mm at th2, 0.6-0.78 mm at th3, 0.75-0.97 mm at th5, 0.83-1.25 mm at th7, 1.05-1.4 mm at th10 (1 specimen is 1.55 mm), 1.38-1.77 mm at th15, 1.68-1.88 mm at th20 (n=4), with a distal maximum of 1.75-2.2 mm in large specimens. 2TRD is 1.3-1.7 mm at $th1^1$, 1.55-1.9 mm at $th2^1$ (most above 1.7 mm), 1.75-2.15 mm at $th5^1$, 1.75-2.15 mm at $th7^1$, 1.8-2.15 mm at $th10^1$, and 1.8-2.3 mm distally. Thecae are sharply geniculate, with straight, moderately inclined supragenicular walls. The apertural excavations are semi-circular, and can appear slightly introverted. Thin, curved basal spines are present on the first thecae pair; they are up to 8.3 mm long, but vary considerably depending on the maturity of the rhabdosome. The virgella is usually very short and deflected towards the sicular aperture. The zig-zag nema is often very

prominent internally, and it projects well beyond the end of the rhabdosome (to 9 mm in one specimen, but usually short). Six specimens possess a large, inverted, heart-shaped, web-like structure, 5.2-8.1 mm long and 4.3-5.5 mm wide, which completely covers the area between the basal spines. This structure extends above the spines, to the level of th2 or th3, immediately adjacent to the thecae, but is otherwise restricted to the area below the basal spines. Three specimens show slight thickening to the underside of the spines. Specimens possessing a basal membrane also show some rhabdosomal torsion, possibly an artifact of compression.

Remarks: *Appendispinograptus leptothecalis* was until recently known only from the Chinese literature, and descriptions of most of the material are still only available in Chinese. It is readily distinguishable from the more common *Appendispinograptus supernus* by its more inclined thecae and greater 2TRD (especially proximally), as well as generally slower rate of widening, generally greater distal width, and a tendency to narrow at the second thecal pair. In China, it first appears just below the base of the *typicus* Subzone and extends into the upper *extraordinarius* Zone (Fan and Chen, 2007). In Nevada, it occurs in the upper *pacificus* Zone, and possibly in the *ornatus* and *extraordinarius* zones (Štorch et al., 2011). Some of the specimens from Siberia assigned by Koren' et al. (1983, text-fig. 44 *И* and 3 and text-fig. 45 3) to *A. supernus*, as well as specimens identified as *A. longispinus,* but possessing a basal 'web' (Koren' et al., 1983, text-fig. 42 а, б, and В), are here considered to be specimens of *A. leptothecalis,* based on their high 2TRD and thecal inclination (Fig. 6.33). The precise stratigraphic position of

the Siberian specimens of *A. leptothecalis* is unavailable in English, but the range (fig. 63 and 64) given for the total collection of specimens of *Appendispinograptus* is *ornatus* Zone to two thirds of the way through the *pacificus* Zone. At the Blackstone River, six specimens, all from a narrow stratigraphic interval in the middle of the *mirus* Subzone (18.06 m), also possess the heart-shaped, web-like structure illustrated by Koren' et al. (1983). These specimens differ from *A. venustus* and *A. longispinus* in the apparent absence of discrete parathecal or parasicular tubes, and the fact that the structure entirely encloses the area between spines. The structure and method of growth of the basal structure is not clear from the present material, but one specimen, assigned by Koren' et al. (1983, plate XXXIVI, fig. 3; see also, fig. 5) to *A. supernus* shows individual sheets growing downwards from each spine, with maximum thickness reached in the middle of each sheet. A very similar specimen is illustrated from Alaska by Churkin et al. (1970: plate 24.f). These sheets presumably continue to descend until they contact and are joined into a single structure. Notably, there does not appear to be any growth above the spines in either the Koren' et al. (1983) or Churkin et al. (1970) specimens, suggesting that this occurs late in the production of the basal process, in contrast with both *A. venustus* and *A. longispinus,* which produce more or less simultaneous extrathecal and extrasicular material. More thorough discussion of the growth and possible function of this structure is presented in Chapter 7, but it presumably played a hydrodynamic role, perhaps controlling orientation in currents. An analogous structure

is seen in some specimens of *Climacograptis bicornis* var. *peltifer*: plate 26, 10a-c, in Elles and Wood (1906).

Three specimens in the present collection, from the same horizon as those possessing complete membranes, show incipient growth along the underside of the spines (e.g., Plate 14.4). Other very large specimens of *A. leptothecalis* throughout the section (e.g., Plate 7.9, 26.2 and 26.3), however, including one possessing spines greater than 8 mm long, do not possess any thickening. Complete membranes have not been reported outside of Russia and the Yukon, but in addition to the Churkin et al. (1970) specimen described above, Chen et al. (2005a) and Štorch et al. (2011) both reported *lepthothecalis*-like specimens, from the middle of the *extraordinarius* Zone and the upper *mirus* Subzone in Nevada, respectively, with thickened spines. These specimens should likely be assigned to *A. leptothecalis*. Why spine elaboration, and in particular the complete membranes seen in Russia and the Yukon, manifests so rarely is unclear, but given the close correspondence of rhabdosome dimensions (Figs. 6.33 and 6.35) and other characters (inclined thecae, constricted first thecal pair, etc.) they are considered an anomalous variant of *A. leptothecalis*, rather than a unique species.

Appendispinograptus supernus **(Elles and Wood, 1906)**

Plates: (Photos) 11.10, 14.5, 14.10-12; (Line drawings) 1.1, 1.9, 1.11-12, 3.15

Material and stratigraphical range: Common in the *ornatus* and *pacificus* zones; 56 specimens measured in detail.

Description: Rhabdosome up to 22 mm long. Widens steadily from 0.55-0.73 mm (1 = 0.88 mm) at th1, 0.53-0.8 mm at th2, 0.65-1.1 mm (only 3 of 56 are >0.85 mm) at th3, 0.8-1.25 mm at th5 (1 specimen is 0.7 mm), 0.9-1.35 mm at th7, 1-1.55 mm at th10 (n=12), and 1.1-1.6 mm at th15 and beyond (n=5). 2TRD 1.1-1.55 mm at $th1^1$, 1.13-1.5 mm at $th2^1$, 1.2-1.65 mm at $th3^1$, 1.25-1.75 mm at $th5^1$ (only 2 >1.65 mm), 1.25-1.6 mm at $th7^1$ (n=17), 1.35-1.65 mm at $th10^1$ (n=10), and 1.4-1.75 mm at th15 and beyond (n=8). Thecae are climacograptid, with sharp geniculae and straight supragenicular walls throughout. Semi-circular apertures are horizontal and symmetrical, with slightly thickened rims; they are ca. 0.175-0.25 mm high distally, occupying ca. 1/3 of rhabdomsal width. Rhabdosomal torsion is rarely present. Prominent basal spines emerge from the first thecal pair; they are variable in form, mostly forming an open parabola, but sometimes projecting horizontally or hanging pendently. Spine length is variable, but is usually less than 2 mm. A small amount of parasicular material, confined to near the sicular aperture, is present on a few specimens. The virgella is normally short, and deflected, but is elongated in several specimens (up to 1.4 mm), and secondarily thickened in one specimen.

Remarks: *A. supernus* is a well-known and easily recognizable species, which can be distinguished from other appendispinograptids by its box-like thecae (from *Appendispinograptus leptothecalis*), relatively small size (from *Appendispinograptus longispinus*), close thecal spacing (from *A. leptothecalis* and *A. longispinus*), lack of elaborate spine ornamentation (from *A. longispinus* and *A. venustus*), and general lack

of rhabdosomal torsion (from *A. longispinus* and *A. hvalross*)--see Figs. 6.33-6.35 for morphometric comparisons between these species. Štorch et al. (2011) followed Koren' et al.'s (1983) suggestion that *Appendispinograptus hvalross* is a junior synonym of *A. longispinus* (applied to immature specimens of the species), to which robust specimens of *A. supernus* have sometimes been assigned. The present collections contain some robust specimens with modest parasiculae, e.g., Plate 14.12, which resemble *A. hvalross,* but as none of the mature specimens exhibit the parathecal growths of *A. longispinus,* they are retained in *A. supernus.*

Parasiculae are nearly absent from the present collection, occurring on just a few of the thousands of specimens examined, and only in the lowest samples of the section. Parasiculae are common, however, in a collection from the neighboring Peel River (described by Lenz and McCracken (1982) and reexamined in this study). The stratigraphic position of these specimens is not precise, but they appear to be lower than the present collections, suggesting that the regional trends observed by other authors in parasicular growth may have a stratigraphic component (see Chapter 7 for further discussion).

***Appendispinograptus pogrebovi* (Koren' and Sobolevskaya, 1983)**

Plates: (Photos) 14.6-7, 14.13-14; (Line drawings) 1.2-8, 1.10

Material and stratigraphical range: Uncommon from the upper *mirus* Subzone; 24 specimens measured in detail.

Description: Narrow, protracted rhabdosome up 25 mm long. Widens from 0.55-0.65 mm at th1, 0.6-0.7 mm at th2, 0.66-0.83 mm at th3 (1 specimen is 0.9 mm), 0.8-1.03 mm at th5 (1 specimen is 1.2 mm), 0.95-1.25 mm at the7 (1 specimen is 1.35 mm), and ca. 1-1.5 mm by th10 (n=8). 2TRD is 1.45-1.73 mm at $th1^1$, 1.45-1.85 mm at $th2^1$, 1.63-1.9 mm at $th3^1$ (1 specimen is 1.53 mm), 1.65-1.9 mm at $th5^1$ (1 specimen is 1.5 mm), 1.6-1.9 mm at $th7^1$, ca. 1.65-1.9 at $th10^1$ and beyond (n=8). First thecal pair bears short basal spines up to 1.5 mm long. Thecae are geniculate and straight-sided, with long supragenicular walls relative to apertural height. Thecal apertures are narrow (0.05-0.13 mm high), and shallow and semi-circular to slit-like and introverted. The upper portion of the aperture often projects further than lower, producing an overhanging appearance, which may be enhanced by the presence of thickening or small flanges. The virgella is 0.33-1.4 mm long and deflected. The rhabdosome is sometimes constricted proximally, before noticeably widening around th5. Cross-bars attach to the nema throughout the rhabdosome.

Remarks: The specimens assigned to *Appendispinograptus pogrebovi* possess 2TRDs intermediate between those of *A. leptothecalis* and *A. supernus* (with very few exceptions, *A. supernus* specimens have 2TRDs of 1.5 mm or less at th2, whereas *A. leptothecalis* has values at or greater than 1.7 mm). In the uppermost *mirus* Subzone collections, a small number of specimens fell intermediate these two values. Following resplitting of slabs, additional material was uncovered, predominantly from level 19.0 m. Closer examination identified a number of characters that distinguish this material

from *A. supernus*: higher 2TRD (Fig. 6.36); generally slower rates of widening, especially proximally, producing a very constricted appearance; often very shallow apertures, sometimes with small flanges and/or introversion; and a tendency towards longer virgellae. Although there is some evidence of minor deformation in the samples where *A. pogrebovi* occurs, it could not produce both higher 2TRD and narrower apertures. It is possible that the present specimens are simply extreme examples of variation in *A. supernus*, perhaps in response to environmental stressors associated with the onset of Hirnantian environmental change, however, "normal" examples of *A. supernus* co-occur with the present material.

Koren' and Sobolevskaya (in Koren' et al., 1983) described *Appendispinograptus pogrebovi* as occurring in a narrow stratigraphic interval in the uppermost *pacificus* Zone, where it co-occurs with M. *ojsuensis* (see also Koren' and Sobolevskaya, 2008). *A. pogrebovi* possesses short infragenicular walls, relative to the supragenicular walls, narrow and shallow semi-circular apertures, a relatively long virgella, and short apertural spines. The present material agrees well on these characters. Koren' and Sobolevskaya also noted strongly asymmetrical orientation of the apertural spines, with the $th1^1$ spine always forming a lesser angle with the virgella than the $th1^2$ spine. However, it is clear from the illustrations (plate 39.1-2) that this strong asymmetry is the result of deformation. Melchin et al. (1991) identified *A. pogrebovi* in uppermost *pacificus* Zone strata on Cornwallis Island.

Appendispinograptus hubeiensis Ge, occurs from the *complexus* Zone to *extraordinarius* Zone in China (Chen et al., 2000), and has been considered synonymous with *A. supernus* by recent authors (Chen et al., 2005a; Štorch et al., 2011); it has narrow, slit-like apertures, which are sometimes introverted. Two specimens of *A. supernus* were highlighted as *hubeiensis*-like by Štorch et al. (2011), with the one from the uppermost *mirus* Subzone greatly resembling the present material (plate 24.e). In their review of Ordovician biostratigraphy, Chen et al. (2003), noted that *Appendispinograptus supernus sinicus* (*Climacograptus sinicus* Ge, in Mu et al., 1993) makes its first appearance at the base of the *ojsuensis-extraordinarius* Zone, slightly above the present material. The original description, however, gives a different range: *szechuanensis* to *typicus* zones (= approximately the lower two thirds of the *pacificus* Zone), and Chen et al. (2000) give its range as the lower *pacificus* to *extraordinarius-ojsuensis* Zone. The significance of the restricted range in Chen et al., 2003, is unclear, i.e., whether it represents a revision of what material is legitimately contained in *A. supernus sinicus* or is an error. Ge differentiated *A. supernus sinicus* from *A. supernus* in possessing wider thecal spacing, a thinner rhabodosome, especially proximally, and thin pendant basal spines. Additionally, *A. supernus sinicus* has relatively narrow and shallow apertures. Together, these features suggest that *A. supernus sinicus* may be a junior synonym of *A. pogrebovi.* Details of rhabdosome are difficult to determine from the illustrations in Mu et al. (1993). Examination of the type material is necessary to confirm this suggestion.

Superfamily RETIOLITOIDEA Lapworth, 1873, emended Melchin et al., 2011

Paraphyletic Family NEODIPLOGRAPTIDAE Melchin et al., 2011

Genus *Metabolograptus* Obut and Sennikov, 1985; emend. Melchin et al., 2011.

Type species: *Diplograptus modestus sibiricus* Obut 1955; by original designation.

***Metabolograptus extraordinarius* (Sobolevskaya, 1974)**

Plates: (Photos) 23.1, 24.1, 24.2a-b, 24.3-4, 25.1-2, 25.4-7, 25.11;

(Line drawings) 4.3, 4.7-8, 7.10

Material and stratigraphical range: Base of the *extraordinarius* Zone. Abundant poorly to well-preserved material; 18 specimens measured in detail.

Description: Robust rhabdosome up to at least 49 mm in length. Widens steadily from 1.05-1.4 mm at th1, to 1.5-1.85 mm (1 specimen is 1.3 mm) at th3, 1.65-2.3 mm (1 specimen is 1.53 mm) at th5, 1.85-2.6 mm at th7, 2.0-2.8 mm at th10, 2.2-3.15 mm at th15, and 2.35-3.25 mm at th20, after which width may be maintained, continue very slowly widening, or decrease mesially. Maximum recorded distal width is 3.4 mm (at th36 in one measured complete specimen, and common in distal fragments). 2TRD is 1.25-1.55 mm at $th1^1$, 1.5-1.75 mm at th^2, 1.45-1.8 mm at $th3^1$, 1.65-2.05 mm at $th5^1$, 1.65-2.15 mm at $th7^1$, 1.65-2.1 mm at $th10^1$, and 1.8-2.3 mm (mostly ca. 2 mm) distally. Thecae are geniculate throughout and straight or only slightly inclined; however, distally the geniculae may be difficult to discern, and pressed-through, the opposite side infragenicular walls can make them appear nearly orthograptid (e.g., Plate 24.1). Thecae are closely spaced, with very short, straight supragenicular walls (ca. 0.5-0.7 mm high distally), and semi-circular apertures. Sicular length is unclear, but its aperture is ca. 0.3

mm wide, and it is exposed a similar distance below th1[2]. Th1[1] turns upwards just below the sicular aperture, and its upward grown portion is 0.73-1 mm long. The virgella is usually short or absent, but is up to 1.5 mm long. A complete median septum is present.

Remarks: The present material agrees very well with previously described specimens of this species. The large size, close thecal spacing, high degree of thecal overlap (difficult to see, due to preservation, in most of the present specimens), and geniculate thecae allow well-preserved specimens of *M. extraordinarius* to be confidently distinguished from contemporary taxa. Species of *Neodiplograptus* reach similar maximum widths, but possess strongly biform thecae. *Metabolograptus ojsuensis* can appear similar, especially in specimens that have not reached maximum size, but *M. ojsuensis* normally has a narrower proximal end, with higher initial 2TRD, as well as a lesser width, and more inclined and less geniculate thecae, distally. Kraft et al. (2015) illustrated several specimens assigned to *M. ojsuensis* with maximum widths similar normally associated with *M. extraordinarius*; these specimens may actually be *M. extraordinarius* or *Neo. charis.* Brussa et al. (1999) illustrated two specimens from Argentina with long virgellae and expanded nemas, features that are more commonly seen in *Neodiplograptus charis*; these specimens may be *Neo. charis.*

***Metabolograptus ojsuensis* (Koren' and Mikhaylova) *in* Apollonov et al., 1980**

Plates: (Photos) 21.11?, 23.6, 24.8, 25.9; (Line drawings) 4.5?, 4.6

Material and stratigraphical range: Common from uppermost *pacificus* Zone and basal *extraordinarus* Zone. 13 specimens measured in detail.

Description: Rhabdosome up to 36 mm long. Expands from 0.95-1.2 mm at th1, to 1.35-1.55 mm at th3, 1.7-1.9 mm at th5 (n=5), 1.7-2.05 mm at th7, 1.75-2.25 mm at th10 (mostly ca. 2 mm), which is maintained or slightly increases (maximum recorded width 2.3 mm). 2TRD is 1.65-2 mm at th1 (1 specimen is 1.35 mm), 1.6-1.8 mm at th2 (n=5), 1.7-2.0 mm at th3, 1.95-2.2 mm at th5, 1.95-2.25 at th7, and 2.0-2.4 mm distally. Thecae are straight and strongly geniculate proximally, but become rounded and moderately inclined distally. Th1[1] grows 0.1-0.25 mm below the sicular aperture, and its upward grown portion is 0.95-1.03 long. The sicular aperture is 0.3 mm wide. A prominent virgella and nema are common: up to 1.4 mm long, and up to 0.4 mm wide and 21 mm long, respectively.

Remarks: The first appearance of *Metabolograptus ojsusensis* occurs slightly below that of *Metabolograptus extraordinarius* in the present and some other paleotropical sections (e.g., South China: Chen et al., 2006; Siberia: Koren' et al., 1983; and Kazakhstan: Apollonov et al., 1980). Finney et al. (1999) recorded *N. ojsuensis* from the uppermost *pacificus* Zone in Nevada, but restudy of those collections and new material from the Vinini Creek section (Belscher, 2007; Štorch et al., 2011), shows the species to be restricted to the *extraordinarius* Zone. At the Blackstone River section, where the *pacificus* Zone is >18 m thick, *M. ojsuensis* first occurs just 5 cm below the base of *extraordinarius* Zone, an interval which could easily be missed with coarser sampling, and which might be impossible to capture in a condensed section. *M. ojsuensis* closely resembles the later appearing *Metabolograptus persculptus* (="*G.*" *bohemicus*: Štorch

and Loydell, 1996), and confusion between the two species has caused considerable problems in the literature (Delabroye and Vecoli, 2010). Fan (1998) conducted a detailed morphometric study of these species as part of his graduate work (available only in Chinese, but utilized in Chen et al. 2005a), demonstrating that the two species are distinguishable; similarly, Melchin (unpublished observations) has shown that comparison of ratios of supragenicular height to apertural height can reliably distinguish the two species, even in deformed populations. In general, *M. ojsuensis* differs from *M. persculptus* in widening more slowly, attaining a lesser maximum DVW, possessing more geniculate thecae (especially proximally), and possessing longer and less overlapping thecae. Based on external morphology, *M. ojsuensis* can easily be confused with *Styracograptus mississippiensis*, with which it co-occurs. It can be distinguished by its generally larger rhabdosome, the presence of a median septum, and the lack of cross-bars and zig-zag nema. *Neodiplograptus charis* attains a greater distal DVW and possesses more rounded thecae. *Metabolograptus extraordinarius* is generally much wider, has more densely spaced (especially proximally) and geniculate thecae, with more narrow and semi-circular apertural openings. One specimen (Plate 4.5; Plate 21.11), which widens very slowly, but possesses very closely spaced and sharply geniculate thecae, is assigned questionably to *M. ojsuensis.*

Genus *Neodiplograptus* Legrand, 1987; emend. Melchin et al., 2011.

Type species *Diplograptus magnus* Lapworth, 1900

***Neodiplograptus charis* (Mu and Ni, 1983)**

Plates: (Photos) 23.2-5, 23.8-10, 24.5-7, 25.3, 25.8, 25.10;

(Line drawings) 4.1-2, 4.4, 7.11

Material and Stratigraphical range: Uppermost *pacificus* and basal *extraordinarius* Zone. Numerous specimens, 16 measured in detail.

Description: Robust and rapidly widening rhabdosome up to greater than 37 mm in length. Expands from 1.2-1.35 mm at th1 (1 specimen is 1.5 mm and 1 specimen is 1.15 mm), to 1.5-1.9 mm at th3, 1.83-2.25 mm at th5 (1 specimen is 1.75 mm), 2.05-2.55 mm at th7, 2.35-2.8 mm at th10, ca. 2.35-2.9 mm at th15, and up to 3.2 mm distally. Some specimens decrease slightly in width distally. 2TRD is 1.65-2 mm at $th1^1$ (1 specimen is 1.35 mm), 1.6-1.95 mm at $th2^1$, 1.7-2.25 mm at $th3^1$, 1.95-2.25 mm at $th5^1$, and 2.05-2.5 mm distally, with most specimens 2.25 mm or greater. The sicula is of unknown length. The sicular aperture is 0.25-0.35 m wide and slightly introverted, rarely projecting beyond the upwards-grown portion of $th1^2$, lending the proximal end a distinctly tapered look. The upward grown portion of $th1^1$ is 0.9-1.2 mm long. The virgella is prominent and at least 1.35 mm long. The initial thecae are climacograptid, but become strongly inclined and rounded by ca. th5, and are nearly orthograptid distally (a weak geniculum is always retained). Thecae overlap for about half their length. Interthecal septa are straight to gently sigmoid. A complete median septum is present, and a prominent nema, up to 0.63 mm wide (although usually <0.3 mm) and 21 mm long, is present on nearly all specimens.

Remarks: *Neodiplograptus charis* occurs with *Metabolograptus ojsuensis* in the uppermost *pacificus* Zone and *extraordinarius* Zone in China (Chen et. al., 2003; Chen et al., 2005b). It has also recently been described from Spain, where it occurs in strata that are most likely latest Katian-earliest Hirnanatian (Mitchell et al., 2011). Individual specimens of *Metabolograptus extraordinarius, M. ojsuensis,* and *Neo. charis* can be difficult to distinguish from each other, especially when poorly preserved, which often obscures geniculae in *M. extraordinarius*. As a population, however, *Neo. charis* has a consistently higher DVW and 2TRD than *M. ojsuensis*, as well as more gently rounded thecae distally. Compared to *M. extraordinarius*, *Neo. charis* has a more protracted and asymmetrical proximal end; higher initial DVW; higher 2TRD throughout; a more developed virgella and nema, the latter sometimes distally expanding; and more widely spaced and less geniculate thecae, with much longer supragenicular walls and more open apertures. From *Metabolograptus persculptus,* it differs in a greater maximum width and more inclined distal thecae.

6.3. Supporting graphs for chapter 6.2

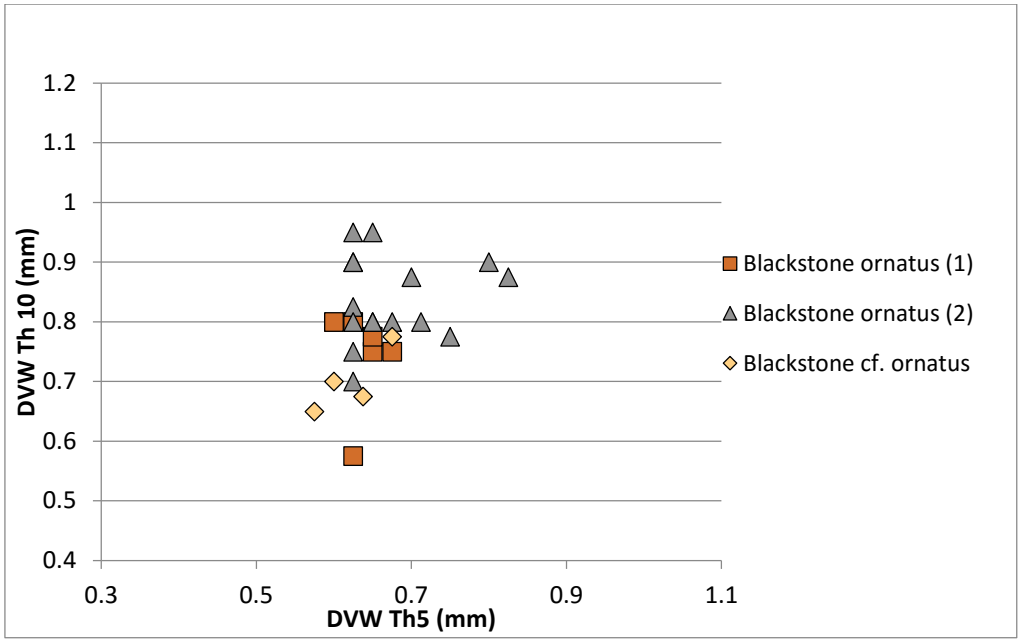

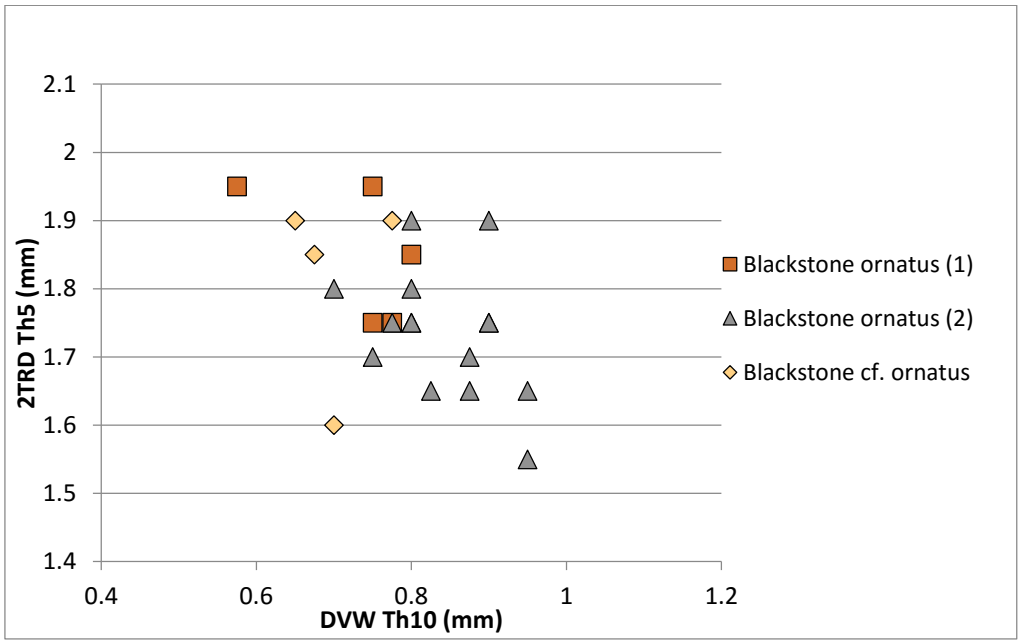

Figure 6.2 & 6.3. Blackstone River D. ornatus. Blackstone *ornatus* 2 includes data from 5.5-5.6 m and 5.5 m Bulk; Blackstone *ornatus* 1 includes data from 0.10-0.20 m, 1.3-1.42 m, and 12.67-12.77 m; Blackstone cf. *ornatus* includes data from 8.8-8.9 m.

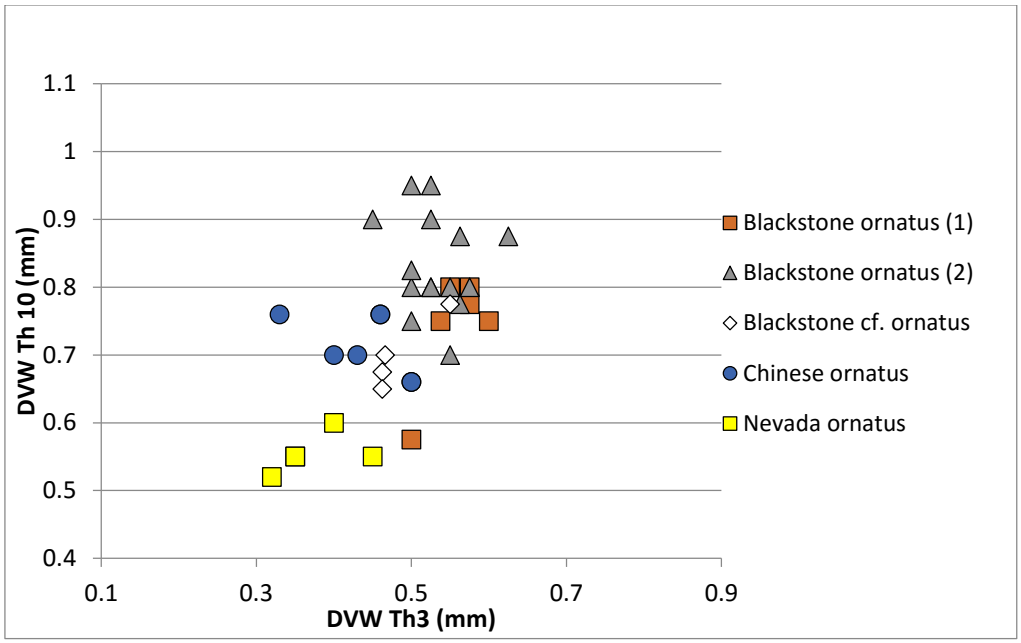

Figure 6.4. Proximal vs. distal DVW in D. ornatus. Chinese *ornatus* specimens illustrated in Mu et al., 1993; measurements made by Loxton on original material (specimens 21408-1, 56728-65, 56707-12, 56701-8, 56719-465, 56726-7, 56705-11, 56700-10). Nevada *ornatus* data provided by Petr Štorch. Blackstone *ornatus* as described above.

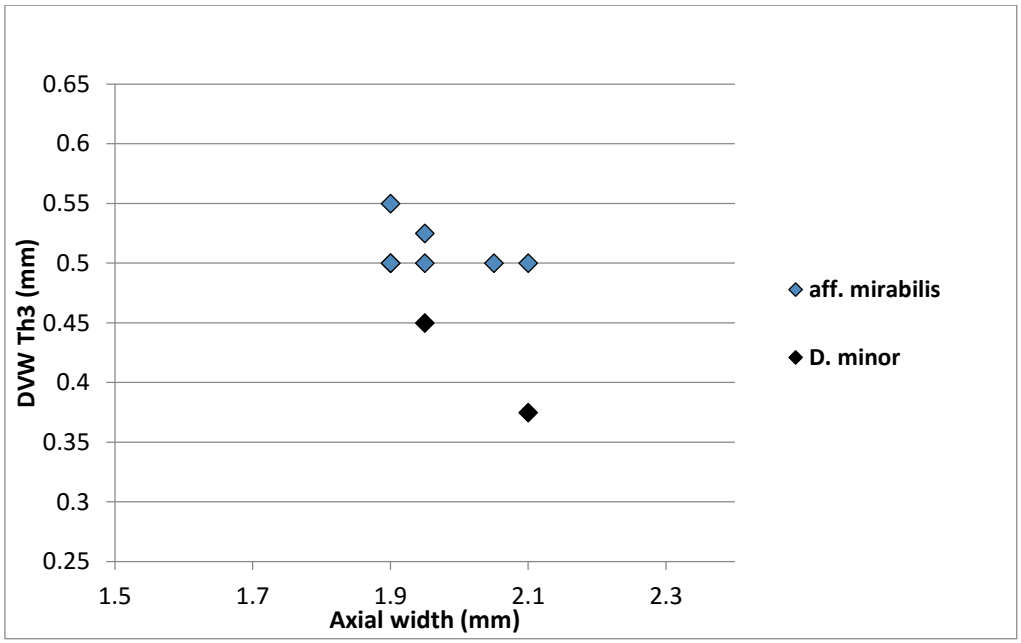

Figure 6.5. Blackstone River D. aff. mirabilis vs. D. minor. Species show little overlap even in juvenile specimens. All specimens from the current collections.

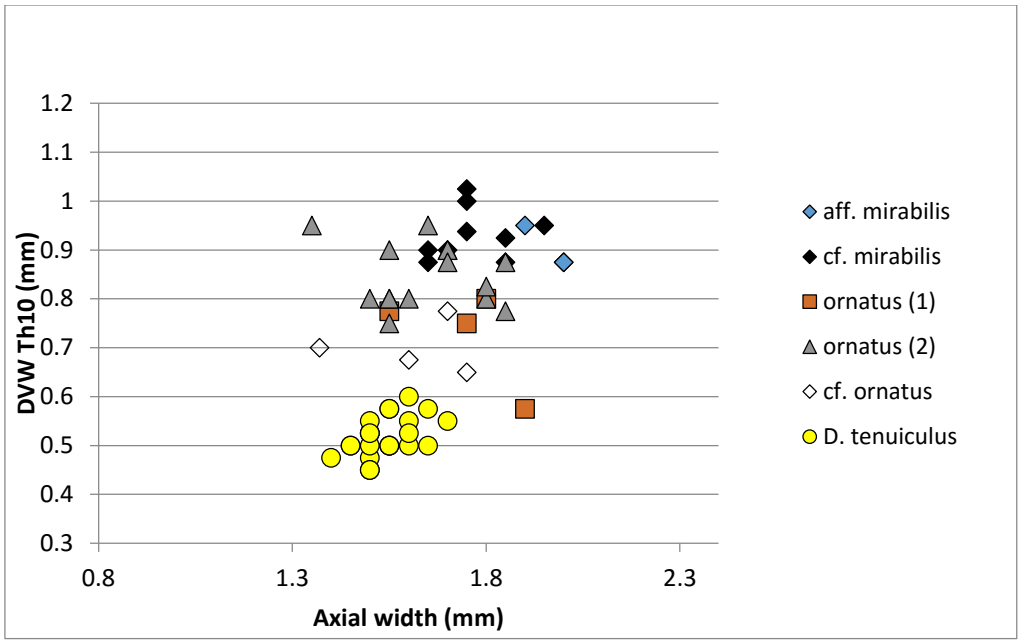

Figure 6.6. Blackstone River Dicellograptus species. All measured specimens of species noted are plotted above. Horizons as listed in descriptions.

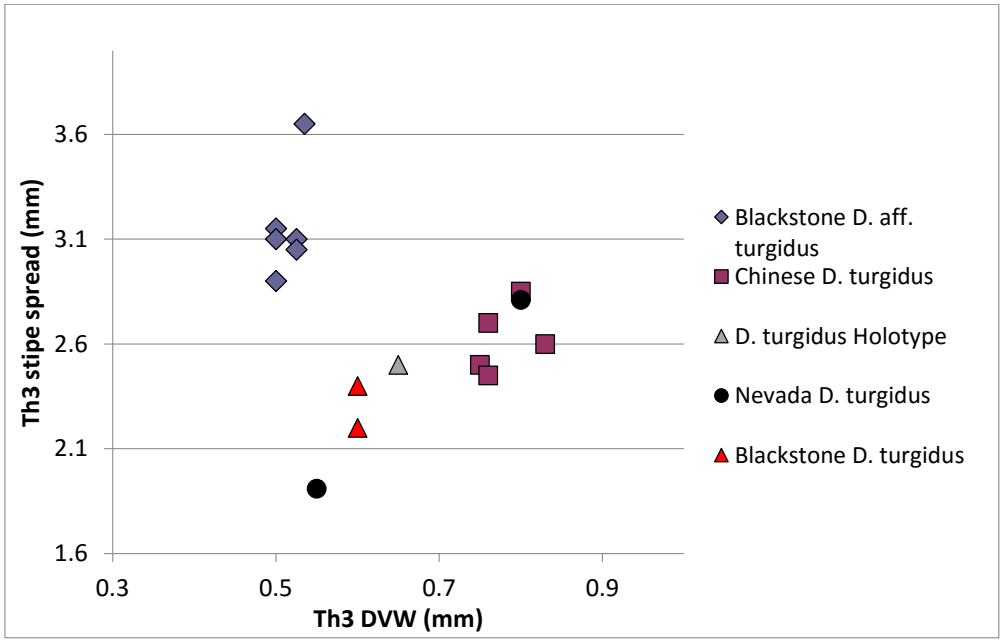

Figure 6.7. 'D. turgidus' specimens. All measurements by Loxton on original material, except Nevada *D. turgidus*, which is based upon measurements made from illustrations in Štorch et al. (2011). 'Th3 stipe spread' measured from the aperture of th3[1] to the aperture of th3[2].

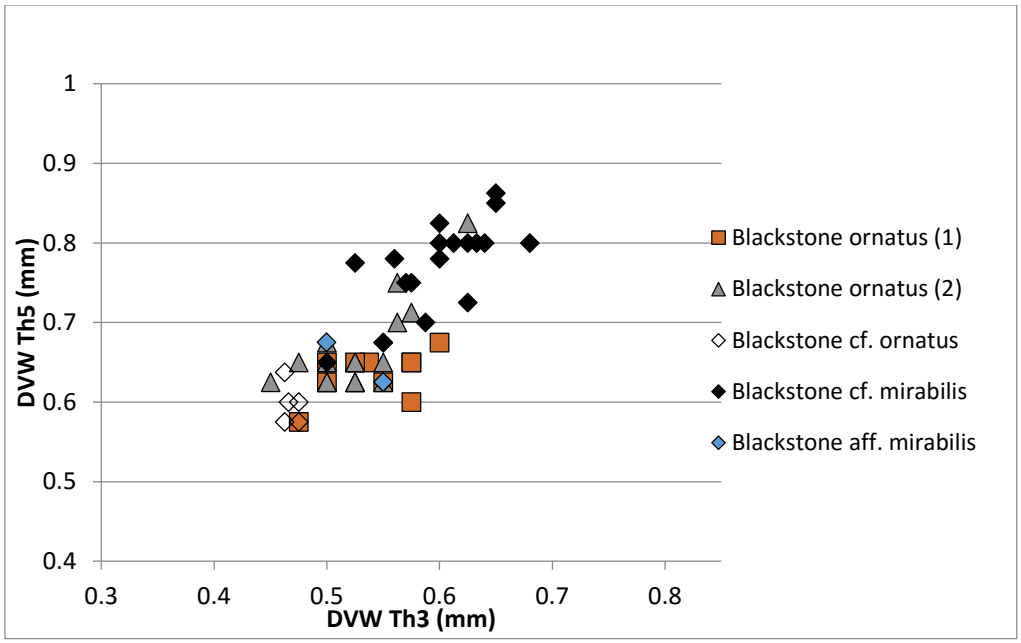

Figure 6.8. Large-spined dicellograptids (A). Horizons as listed in descriptions.

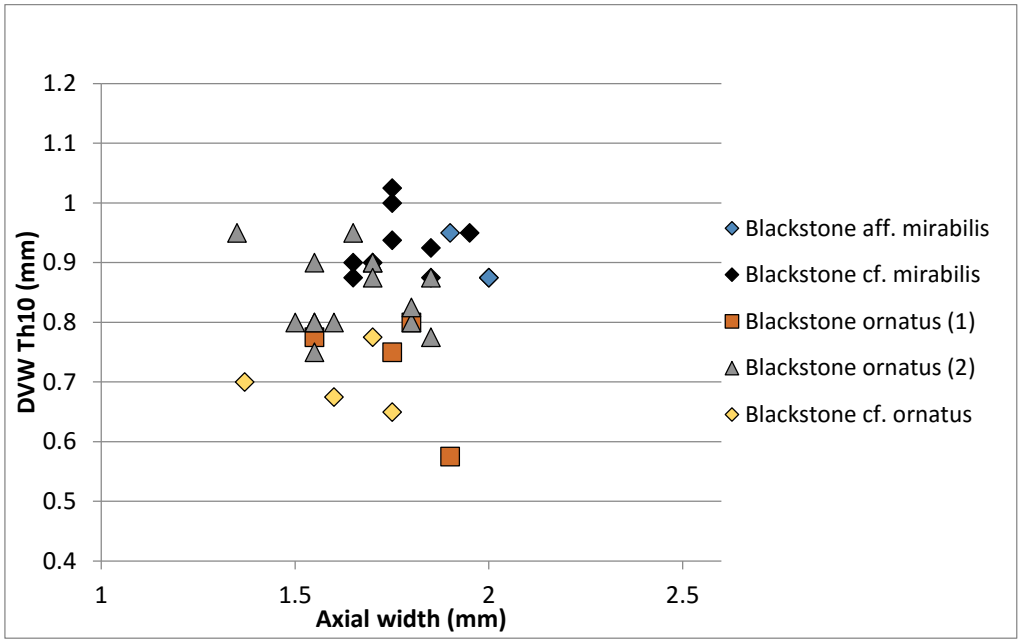

Figure 6.9. Large-spined dicellograptids (B). Horizons as listed in descriptions.

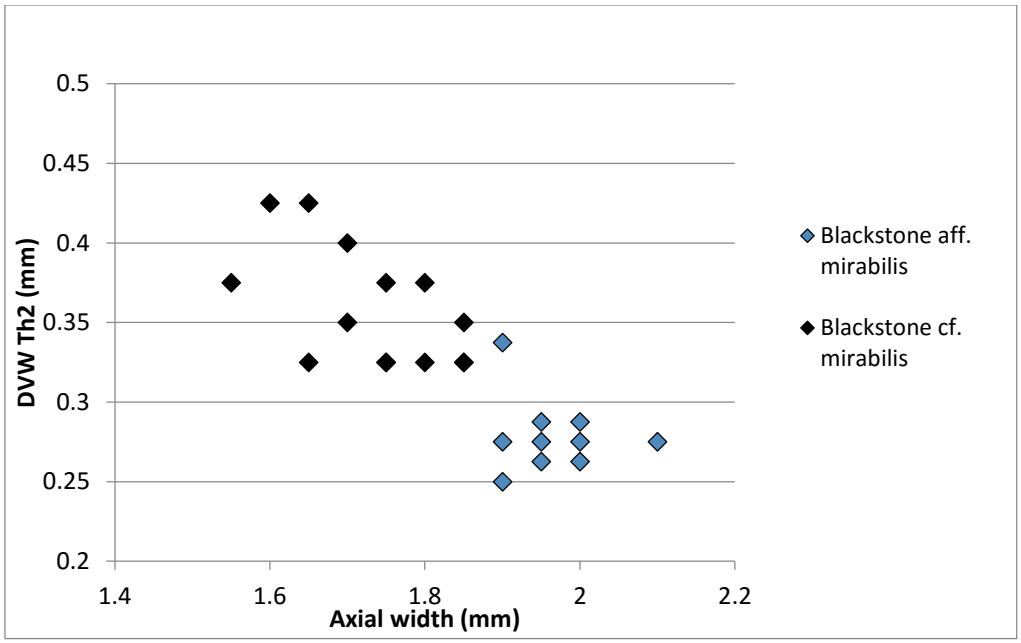

Figure 6.10. Blackstone 'D. mirabilis' material. Specimens assigned to group based on axil form: rounded vs. 'square'. Horizons as listed in descriptions.

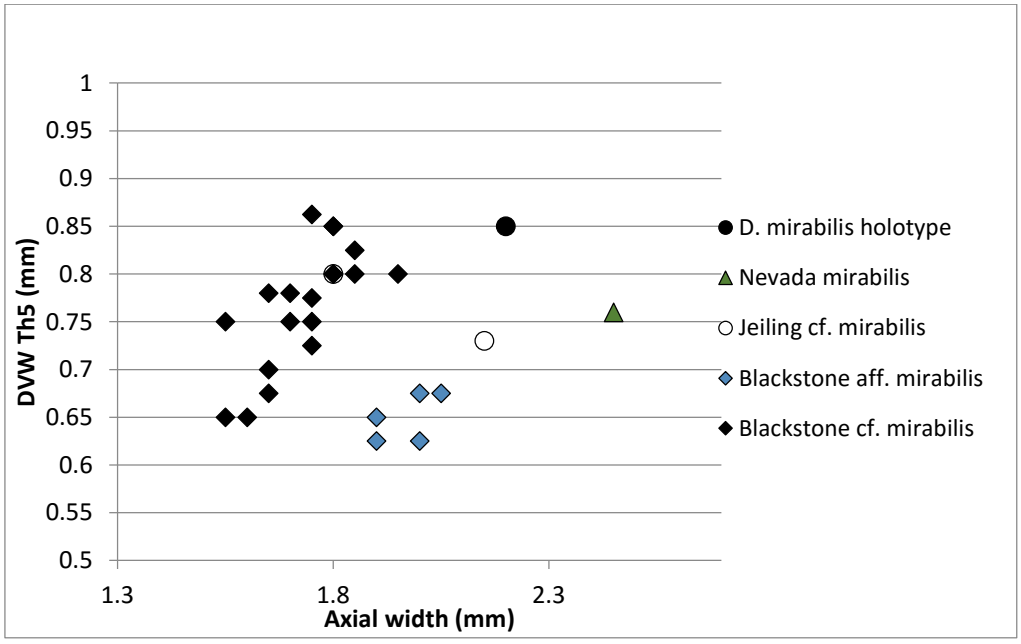

Figure 6.11. International specimens of 'D. mirabilis'. All measurements made on original material by Loxton, except 'Nevada *mirabilis*', which isbased upon measurements made on Štorch et al.'s (2011) illustration. Jeiling specimens from slabs 150-2, 150-5, and 150-7. *D. mirabilis* paratype material examined, but preservation made measurements unreliable, and so it is not included.

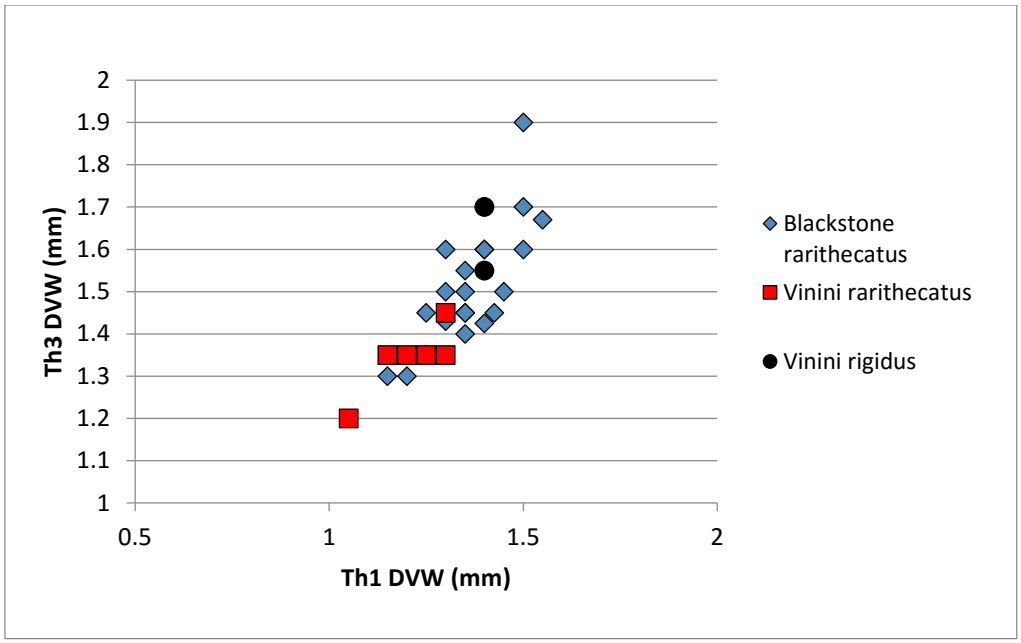

Figure 6.12. Diplograptus (A). Measurements of Vinini Creek specimens provided by Petr Štorch.

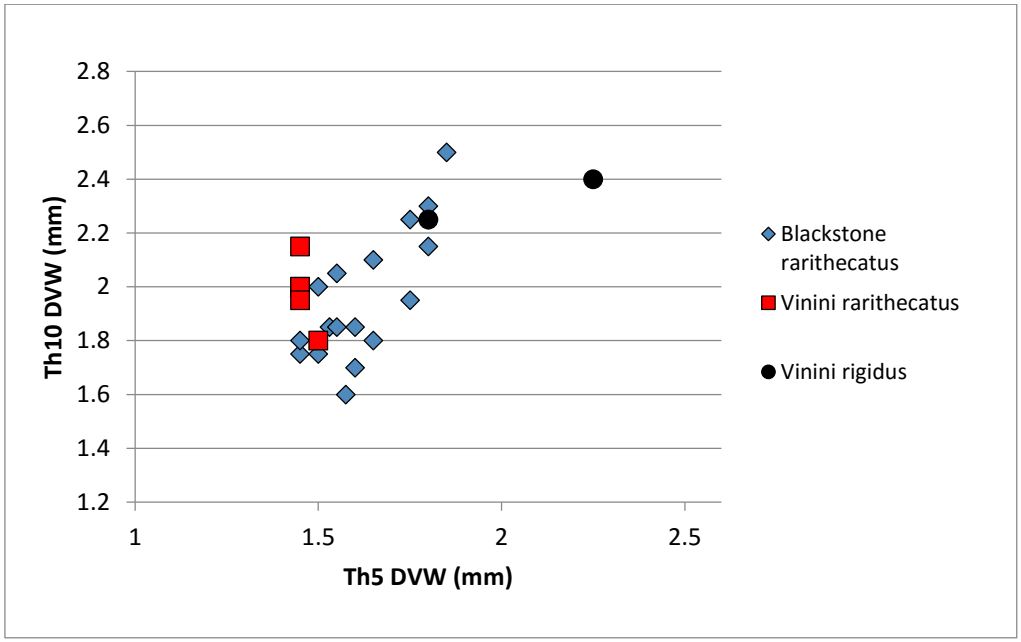

Figure 6.13. Diplograptus (B). Measurements of Vinini Creek specimens provided by Petr Štorch.

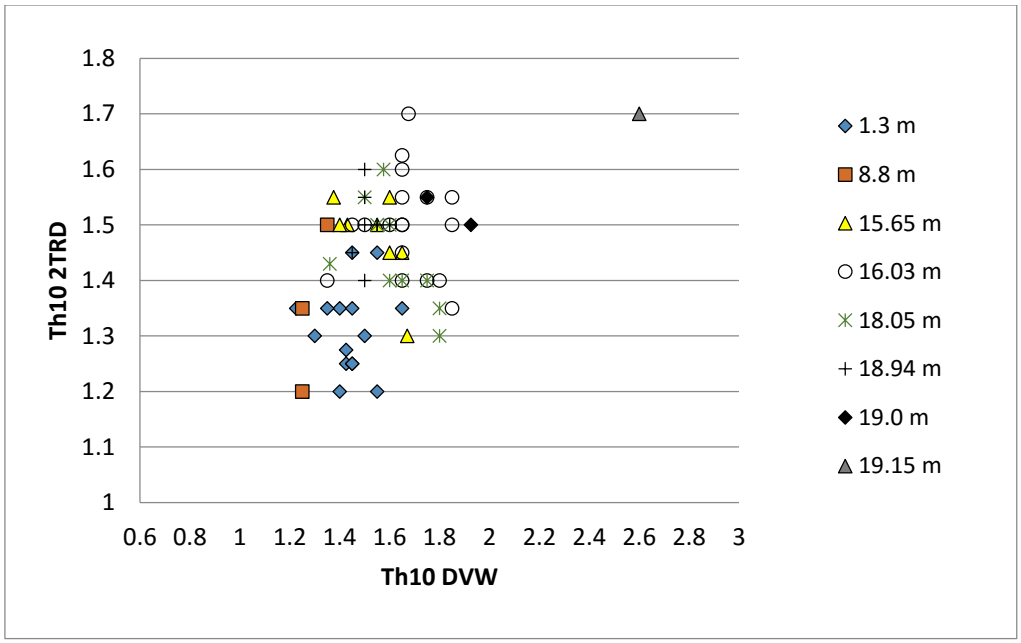

Figure 6.14: Blackstone River specimens of Paraorthograptus. Base of *pacificus* and *extraordinarius* zones, and *mirus* Subzone = 0.83 m, 19.15 m, and 14.15 m, respectively.

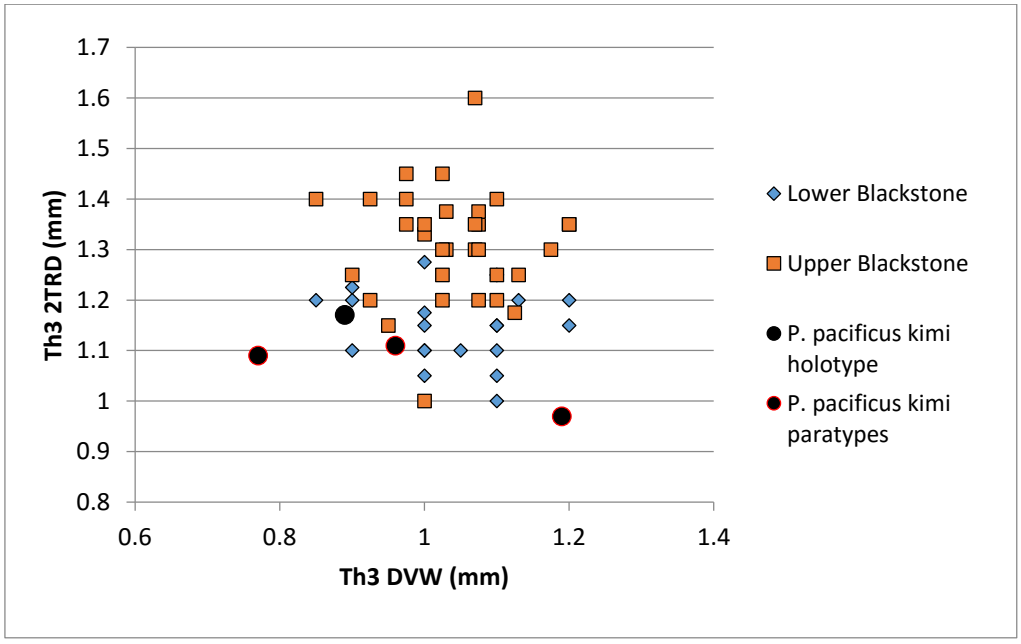

Figure 6.15. Blackstone River Paraorthograptus vs. types of P. p. kimi (A). Comparison of proximal measurements. Measurements for *P. p. kimi* types, taken from illustrations in Koren' (1979): holotype and paratypes 'F', 'C', and 'B'.

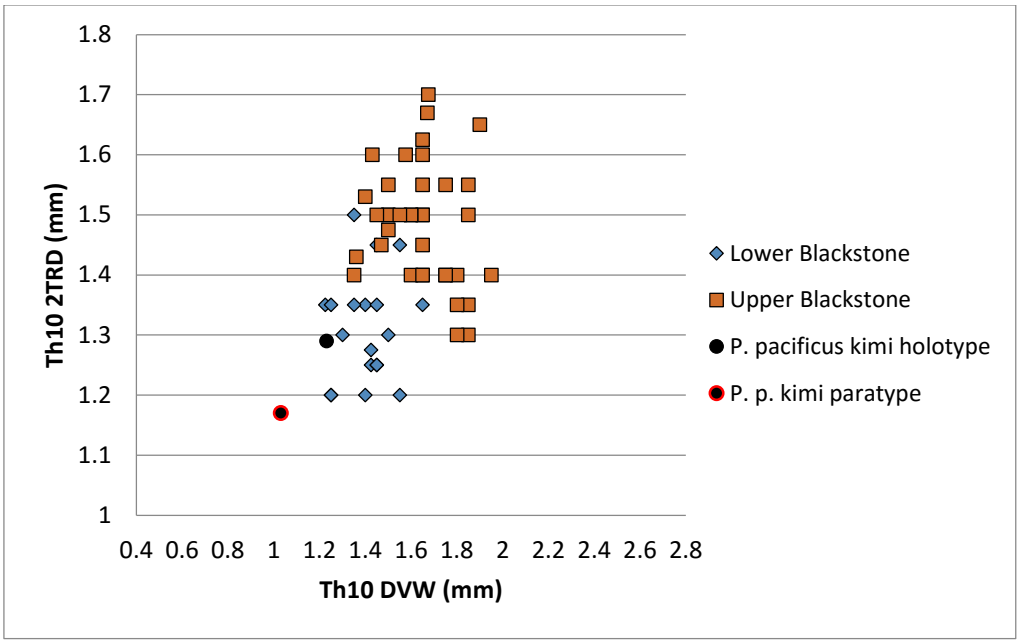

Figure 6.16. Blackstone River Paraorthograptus vs. types of P. p. kimi (B). Comparison of distal measurements. Measurements for *P. p. kimi* types are taken from illustrations in Koren' (1979): Holotype and paratype 'F'. Note: th9 2TRD substituted for th10 in specimen 'F'.

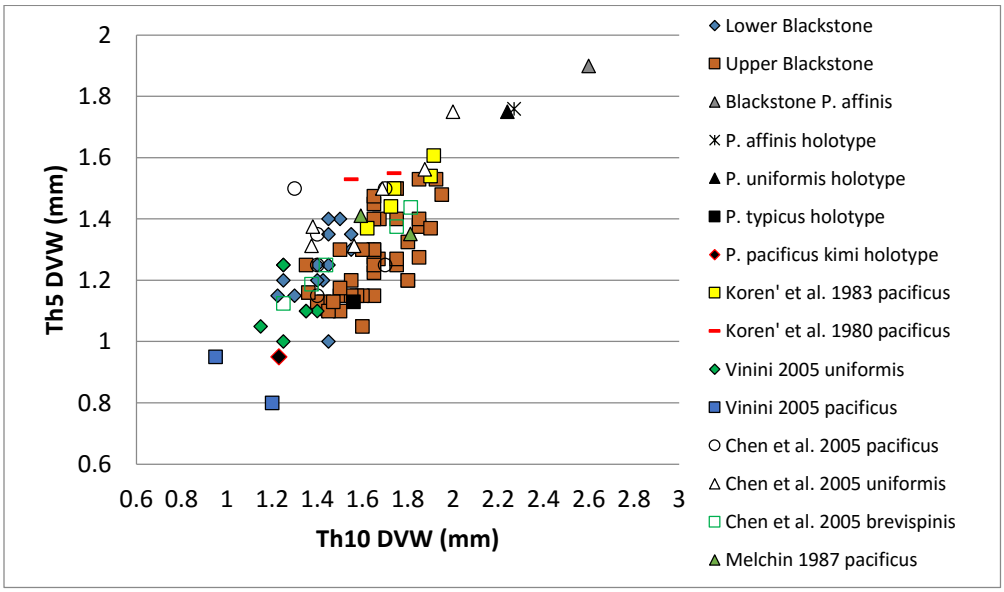

Figure 6.17. Widening in Paraorthograptus. P. uniformis and *P. typicus* holotypes: data provided by Mitchell; Koren' et al. 1980 and 1983, Melchin 1987, and *affinis* holotype (in Koren' et al., 1980): measurements made from illustrations by Loxton; Chen et al. 2005 = specimens referred to in Chen et al., 2005a: data provided by Mitchell; Vinini 2005 collections data provided by Mitchell (lower *pacificus* Zone collections); other collections as described in graphs above.

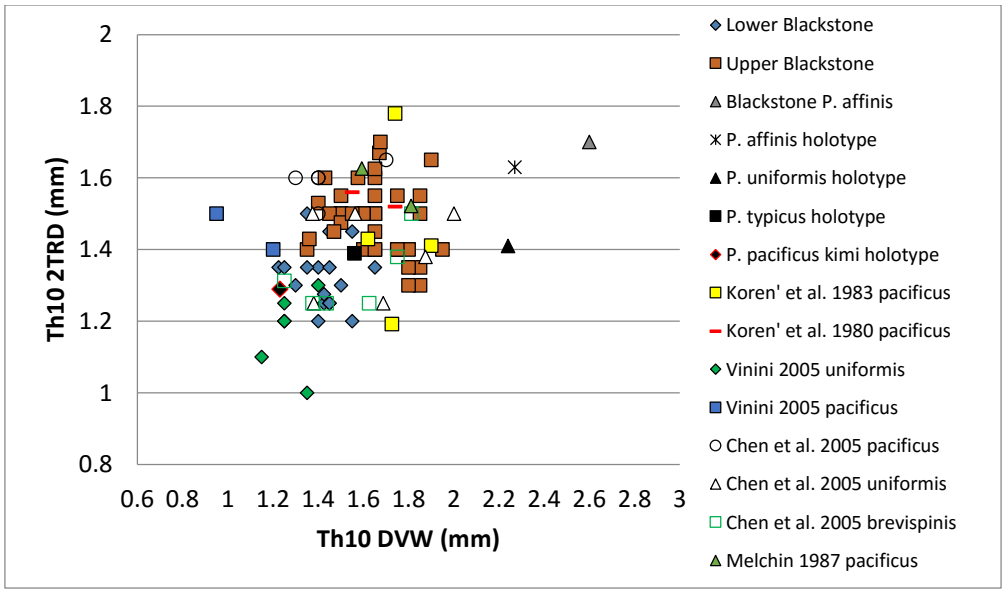

Figure 6.18. Distal DVW and 2TRD in Paraorthograptus. Data sources as described in Fig. 6.17. Vinini 2TRD = Howe.

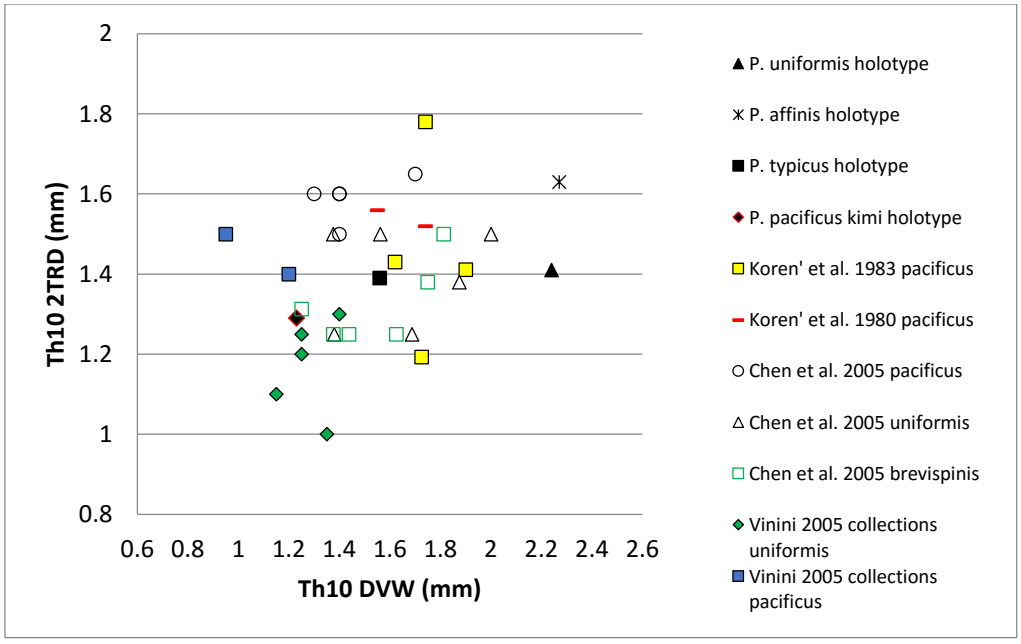

Figure 6.19. Distal DVW and 2TRD in non-Blackstone Paraorthograptus. Data sources as described Fig. 6.17. Vinini 2TRD = Howe.

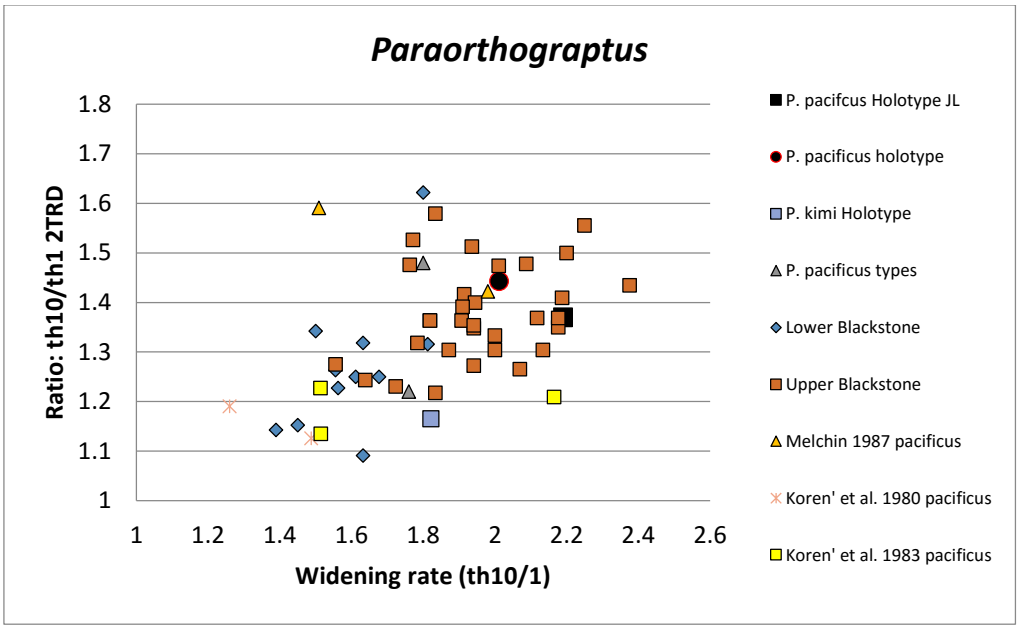

Figure 6.20. Widening and thecal spacing ratios in Paraorthograptus. P. pacificus and *P. kimi* holotype data from Mitchell. *P. pacificus* types (paratypes 'E' and 'G') and *P. pacificus* Holotype JL measured off Riva (1974) illustrations by Loxton. The following substitutions were made due to poor preservation: th6 and 9 measurements for th5 and 10 in paratype 'E' and th8 for th10 in paratype 'G'. $Th1^1$ is damaged in the holotype, so DVW ratios were made by comparing the distance from 1^2 and $th10^2$ to the rhabdosome axis.

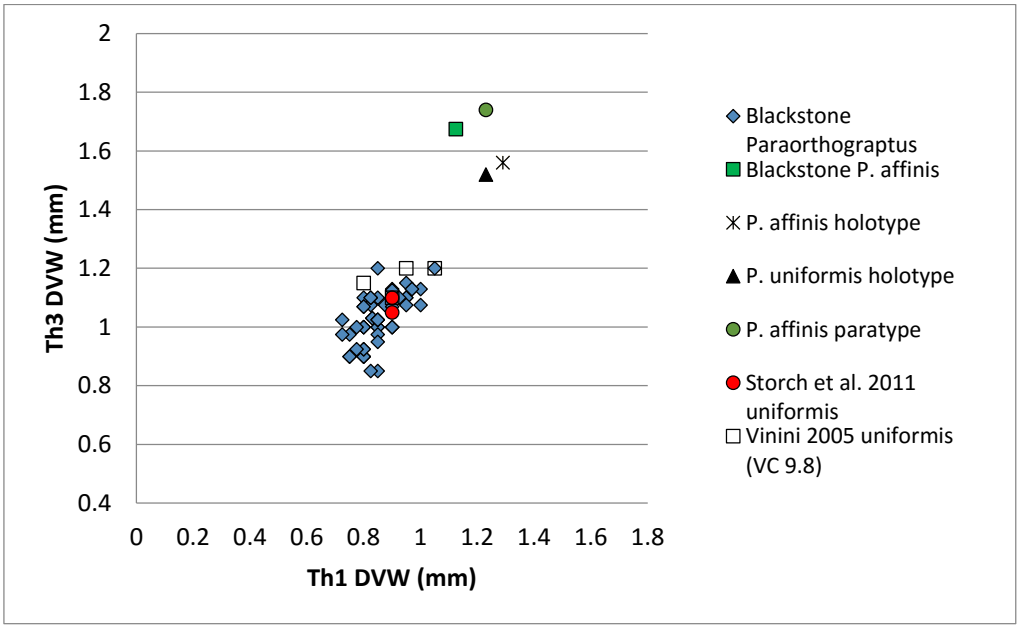

Figure 6.21. Blackstone Paraorthograptus vs. P. affinis and P. uniformis. Data sources as in previous graphs. Štorch et al., 2011, data from table in publication. Vinini and Štorch et al. 2TRD = Howe.

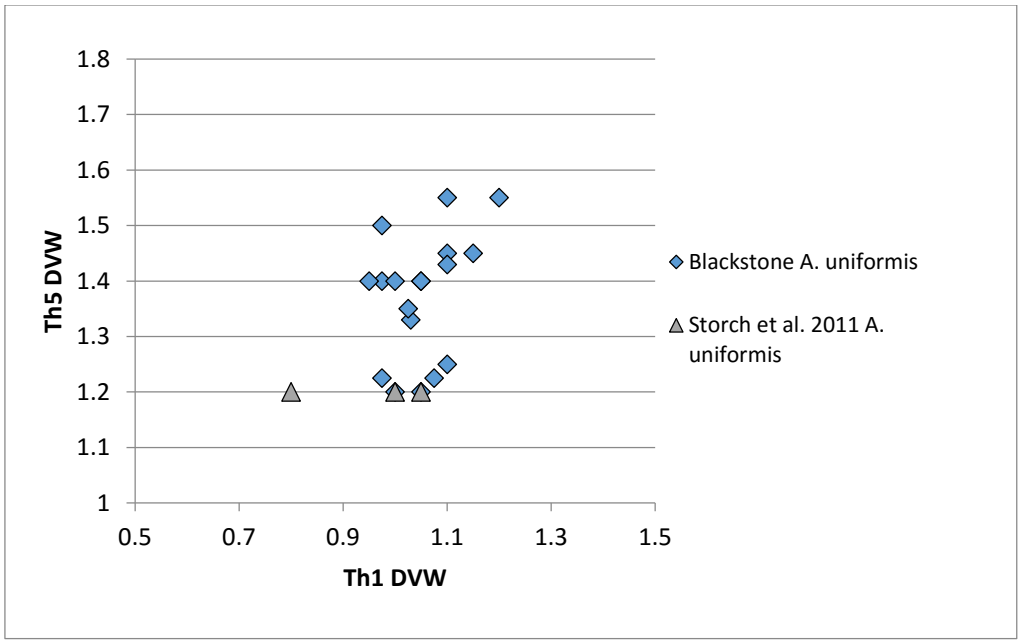

Figure 6.22. Proximal vs. mesial width in Anticostia uniformis. Štorch et al. (2011) data taken from table in publication.

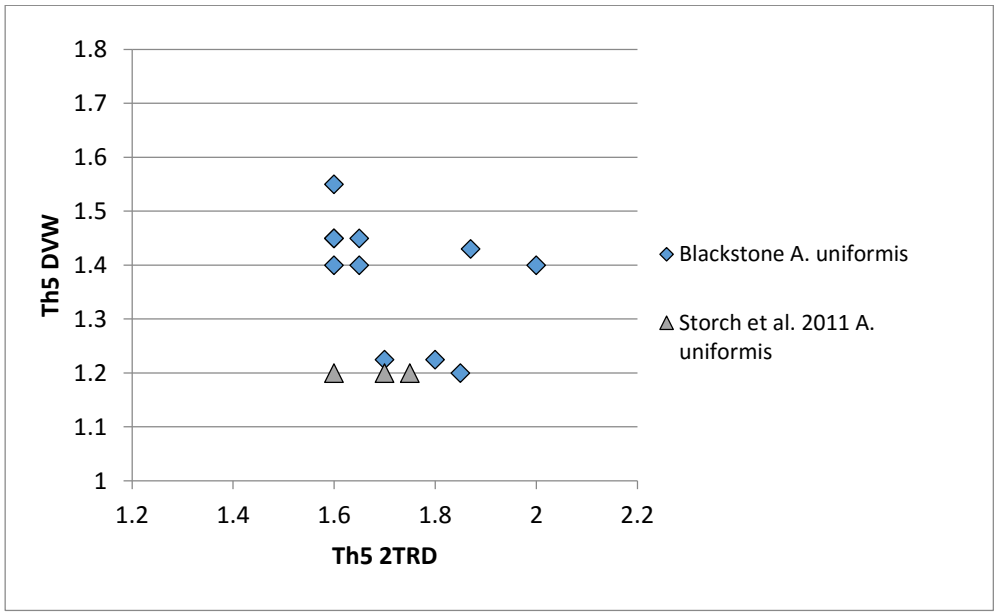

Figure 6.23. Mesial width vs. 2TRD in Anticostia uniformis. Štorch et al. (2011) data taken from table in publication. Štorch et al. 2TRD = Howe.

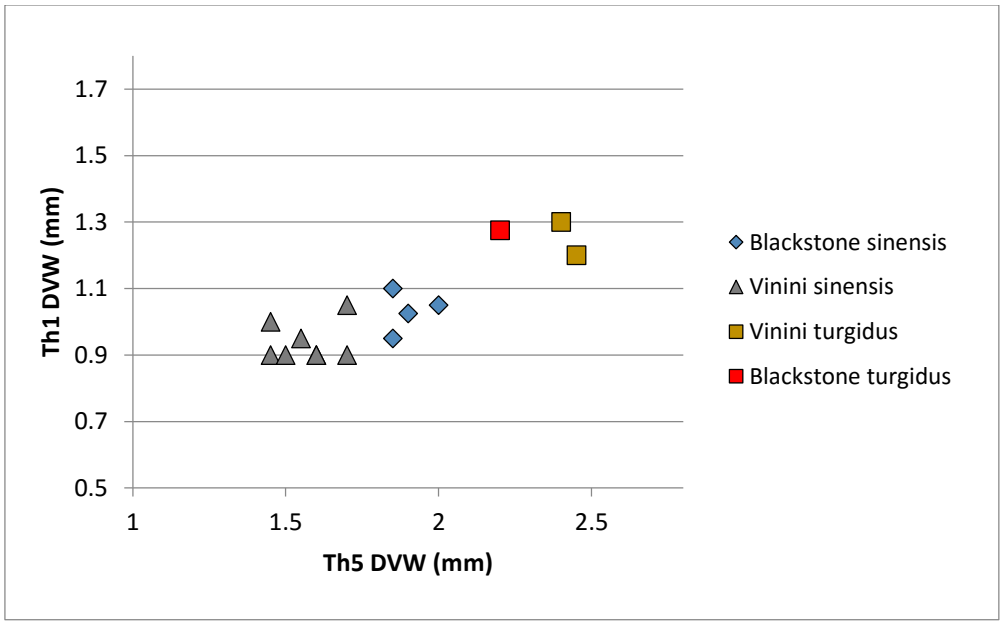

*Figure 6.24. Proximal vs. mesial width in Parareteograptus.*Vinini data taken from tables in Štorch et al. (2011).

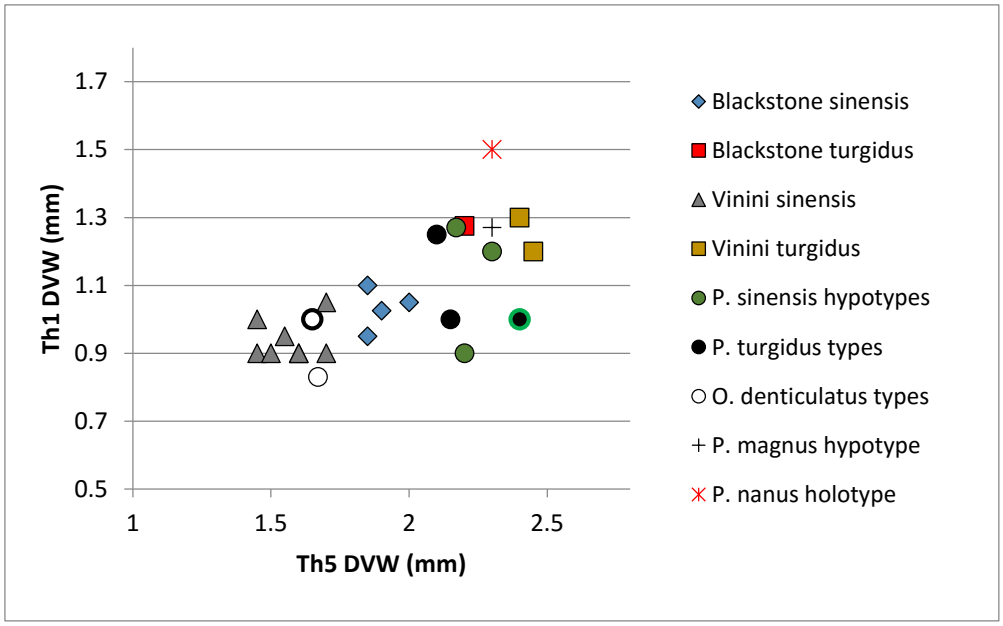

Figure 6.25. Proximal vs. mesial width in global collections of Parareteograptus. Vinini and type data taken from tables in Štorch et al. (2011). Holotypes of *O. denticulatus* and *Pr. turgidus* indicated by thick black circle and green outline, respectively. Vinini 2TRD = Howe.

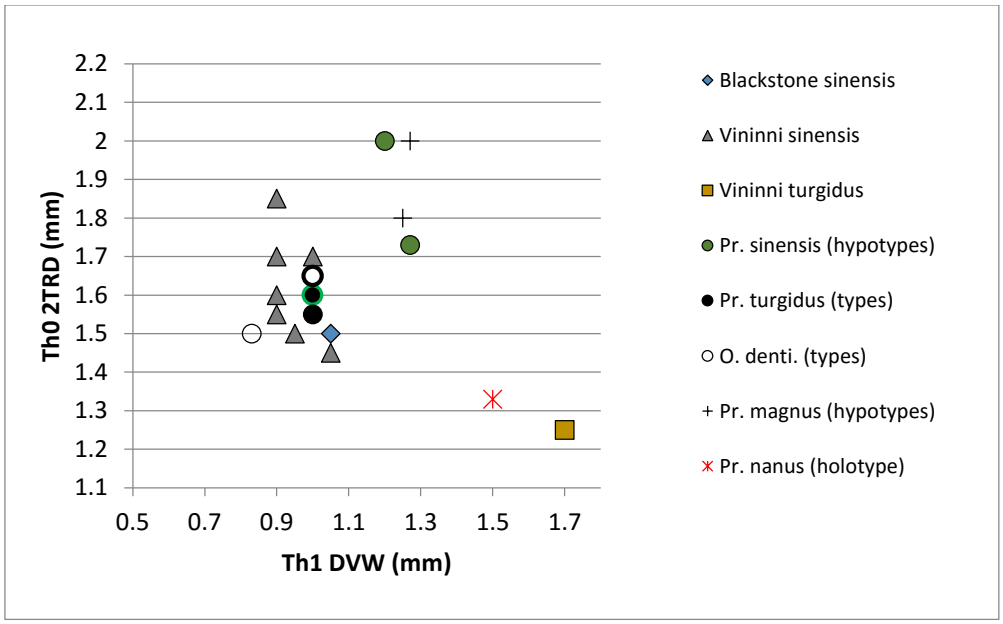

Figure 6.26. Proximal DVW vs. distal 2TRD in global collections of Parareteograptus. Data sources as in Fig. 6.24 & 6.25. Vinini 2TRD = Howe.

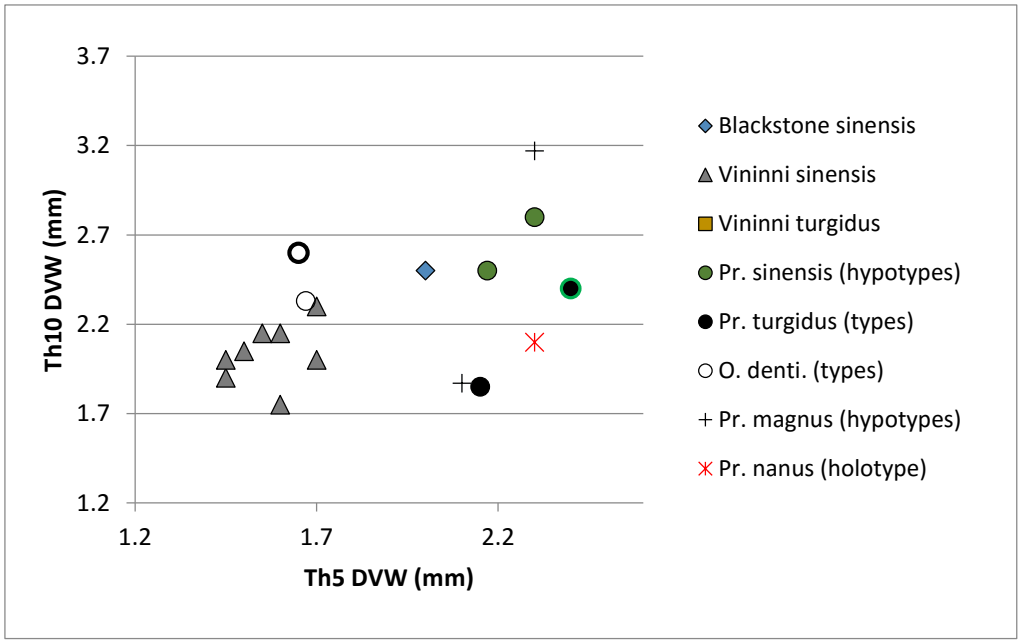

Figure 6.27. Distal vs. mesial width in global collections of Parareteograptus. Data sources as in Fig. 6.24 & 6.25.

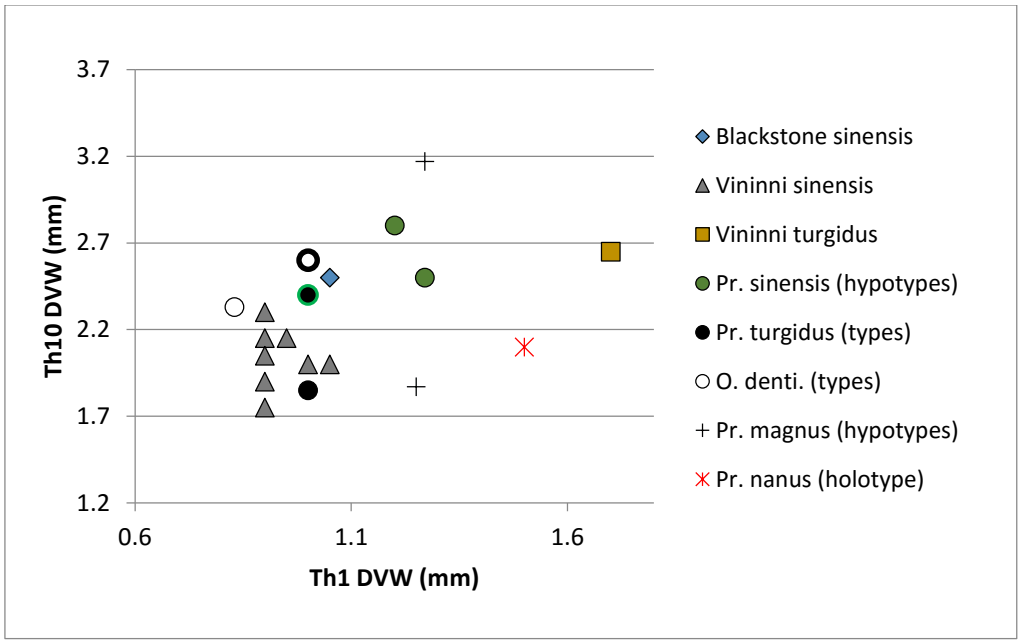

Figure 6.28. Distal vs. proximal width in global collections of Parareteograptus. Data sources as in Fig. 6.24 & 6.25.

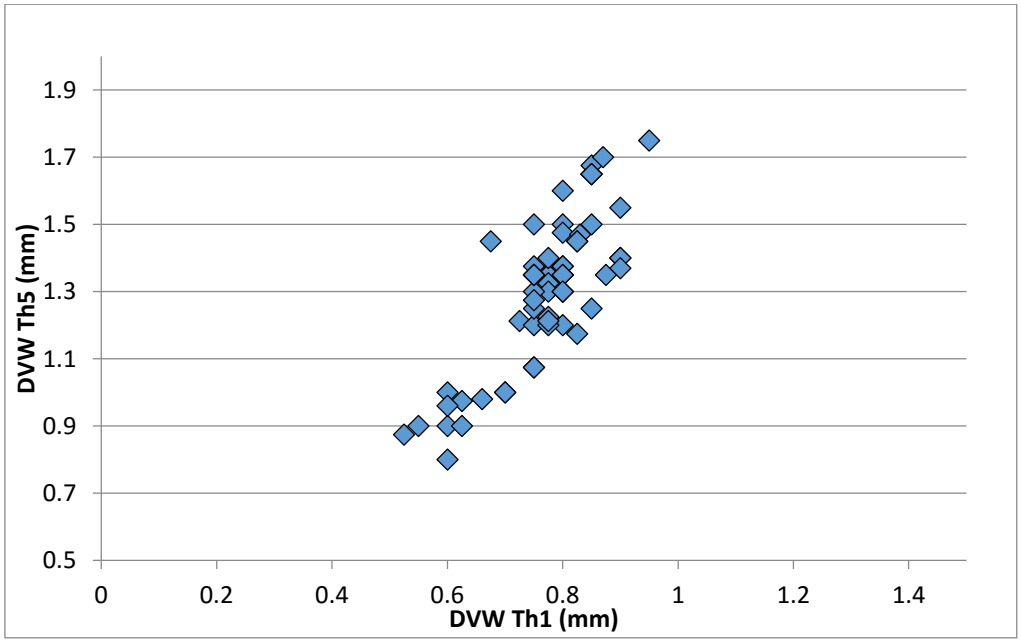

Figure 6.29. Bulk plot of mesial vs. proximal width in Blackstone Styracograptus. Plot of all specimens (unbinned).

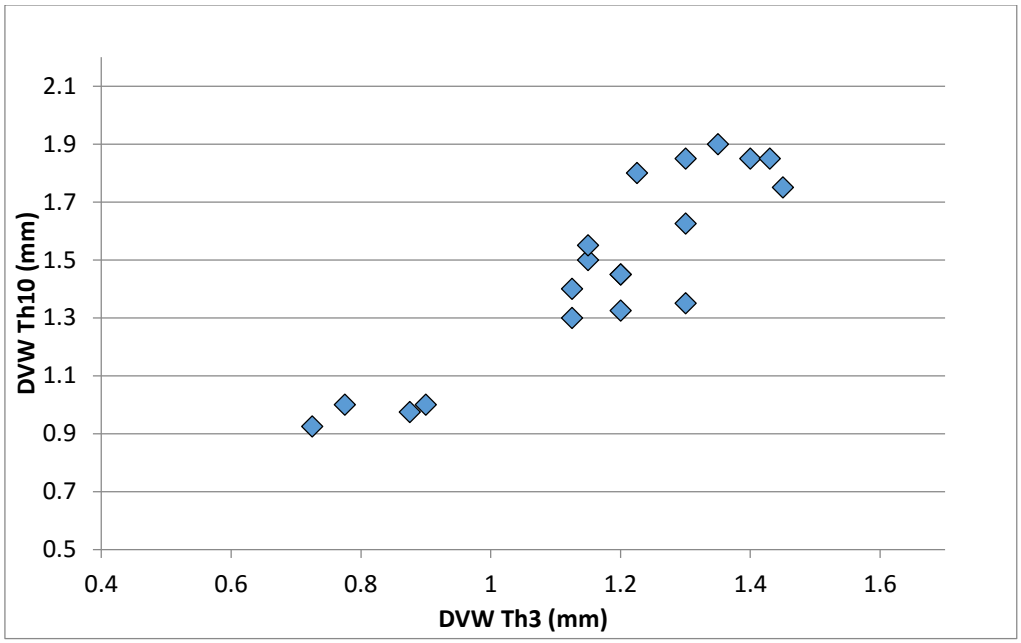

Figure 6.30. Bulk plot of distal vs. proximal width in Blackstone Styracograptus. Plot of all specimens (unbinned).

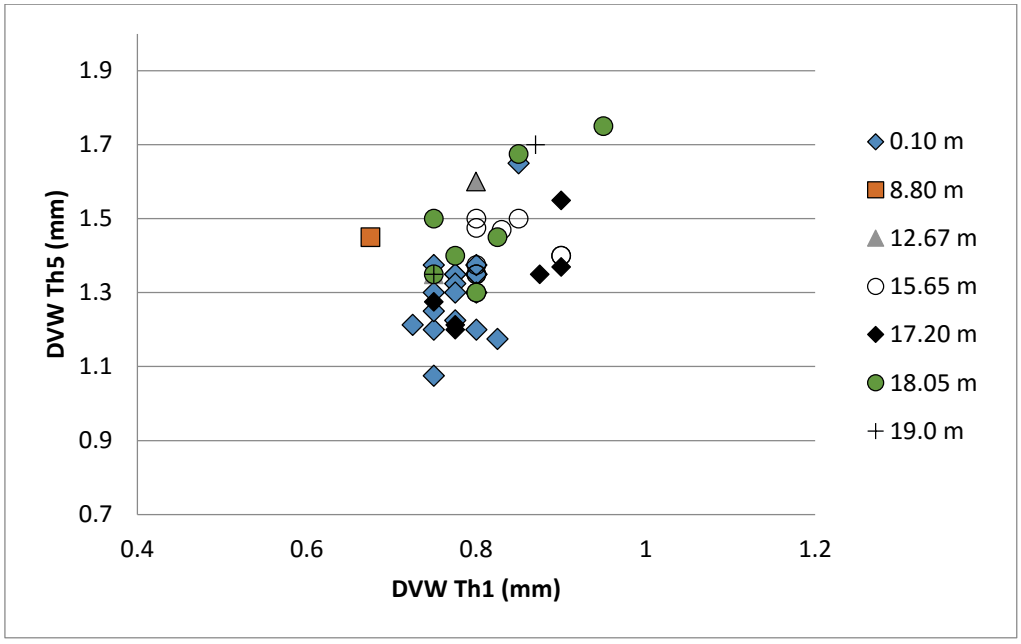

Figure 6.31. Blackstone Styracograptus mississippiensis by stratigraphic level.

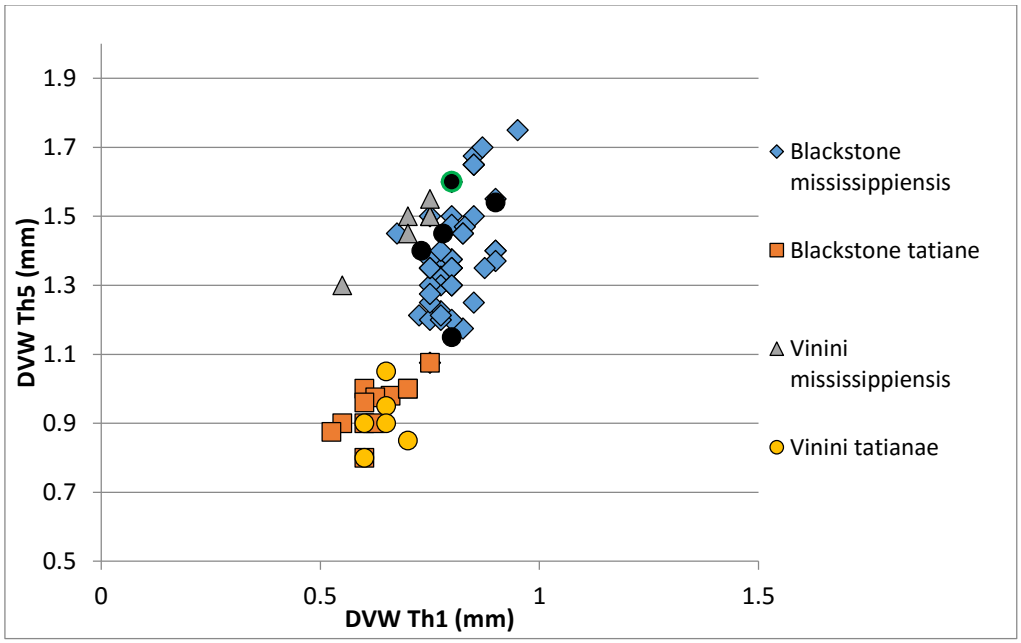

Figure 6.32. Mesial vs. proximal width in global Styracograptus specimens. Vinini and Ruedemann data from Štorch et al. (2011). Holotype indicated with Green outline.

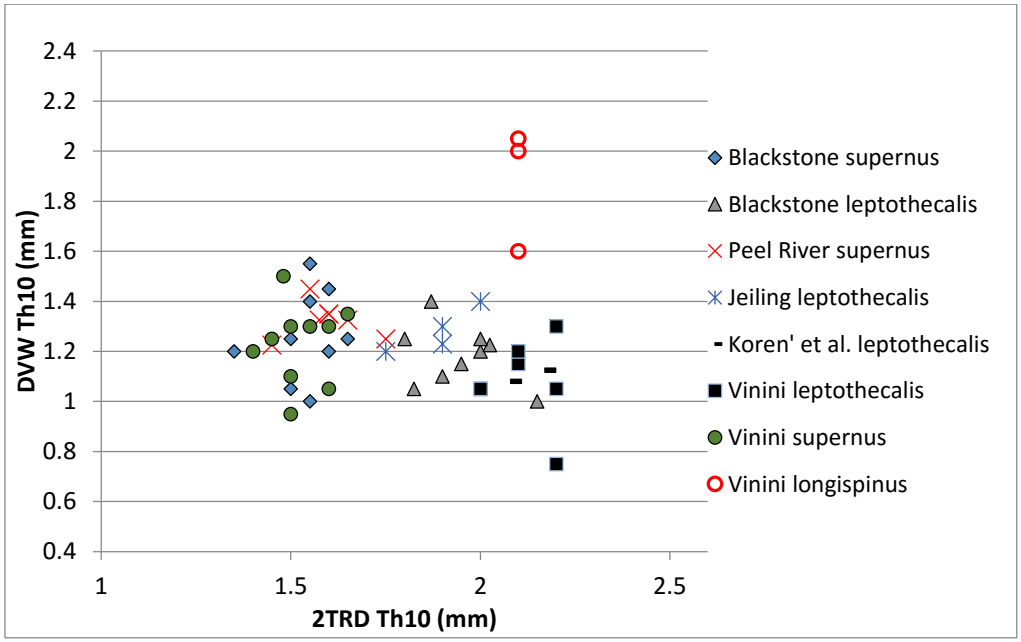

Figure 6.33. Distal width vs. distal 2TRD in species of Appendispinograptus. Vinini data provided by Mitchell; Koren' et al. data taken from illustrations in Koren' et al., 1983; all other data original measurements: Peel River specimens = material collected by Lenz and McCracken and housed in the GSC type collections, Jeiling material = bulk collections examined at the NIGP. Vinini 2TRD = Howe.

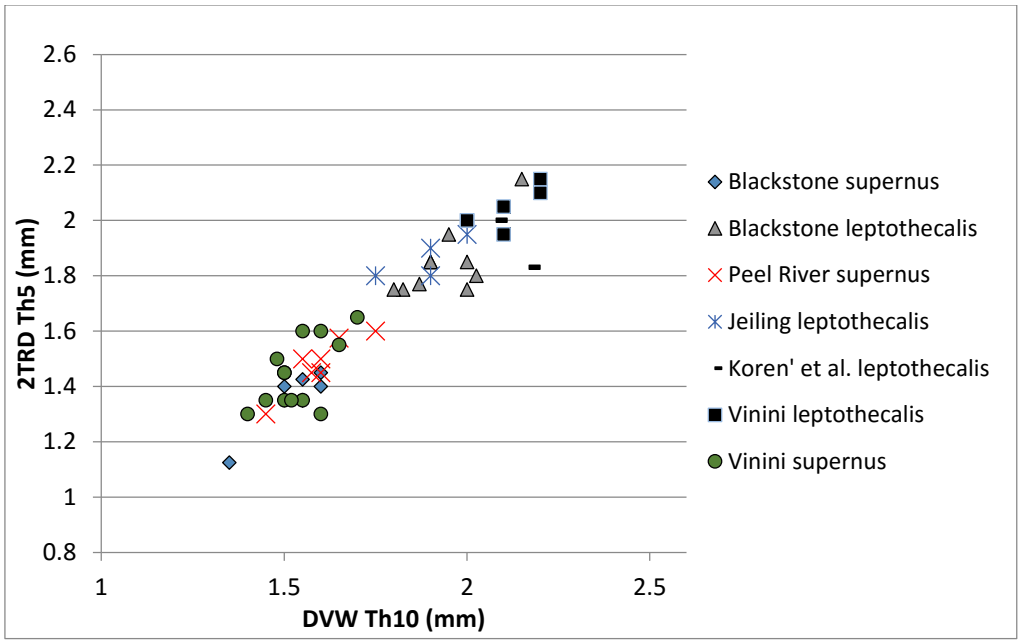

Figure 6.34. Mesial 2TRD vs. distal DVW in Appendispinograptus. Data sources as described in Fig 6.33. Vinini 2TRD = Howe.

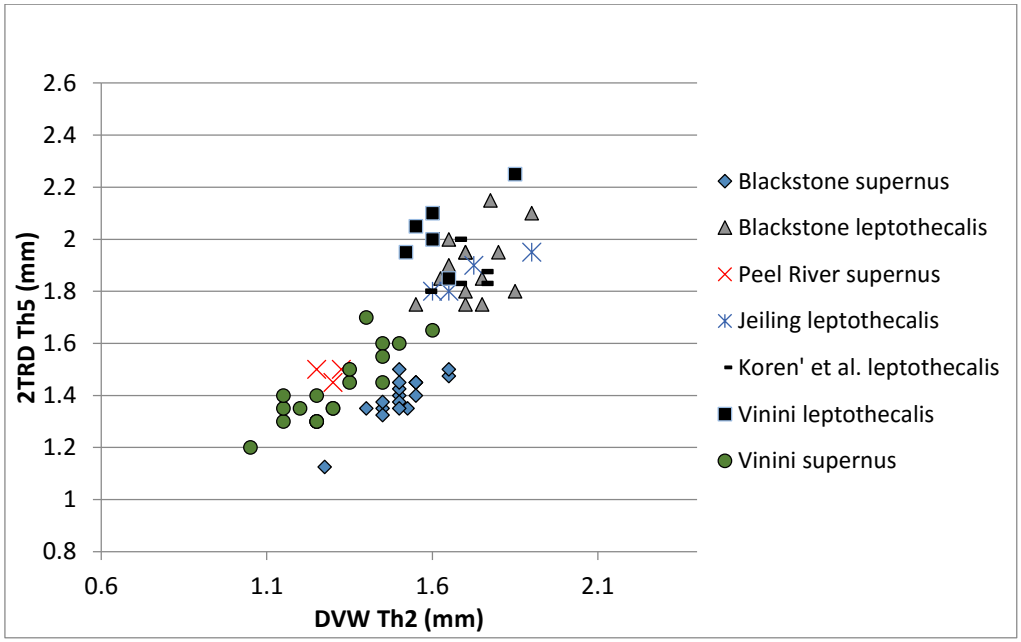

Figure 6.35. Mesial DVW vs. proximal DVW in Appendispingraptus. Data sources as described in Fig 6.33. Vinini 2TRD = Howe.

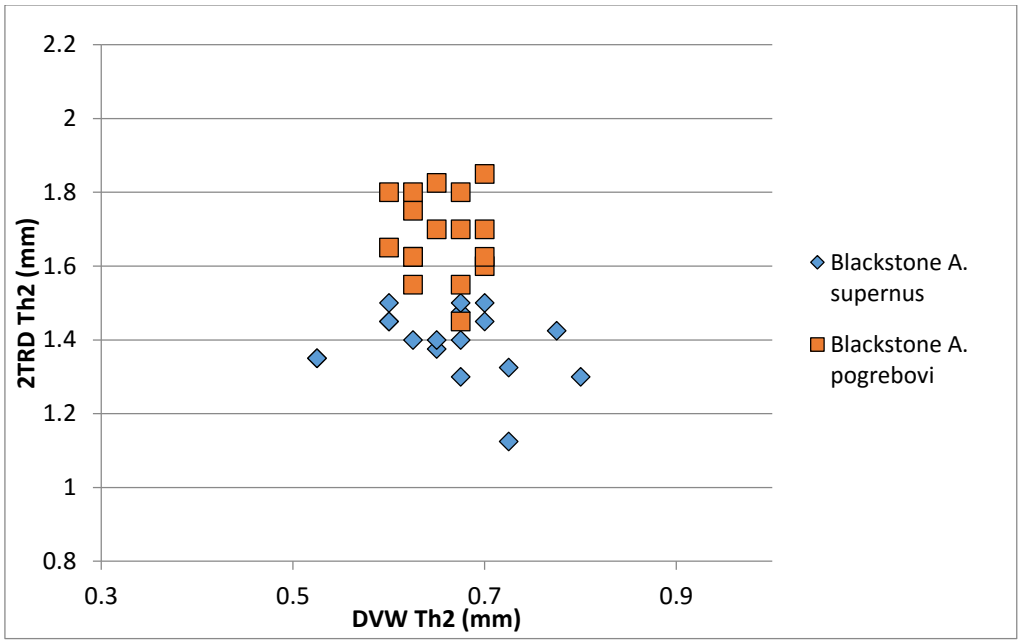

Figure 6.36. A. supernus vs. A. pogrebovi. All data original measurements on material from the present Blackstone River collections.

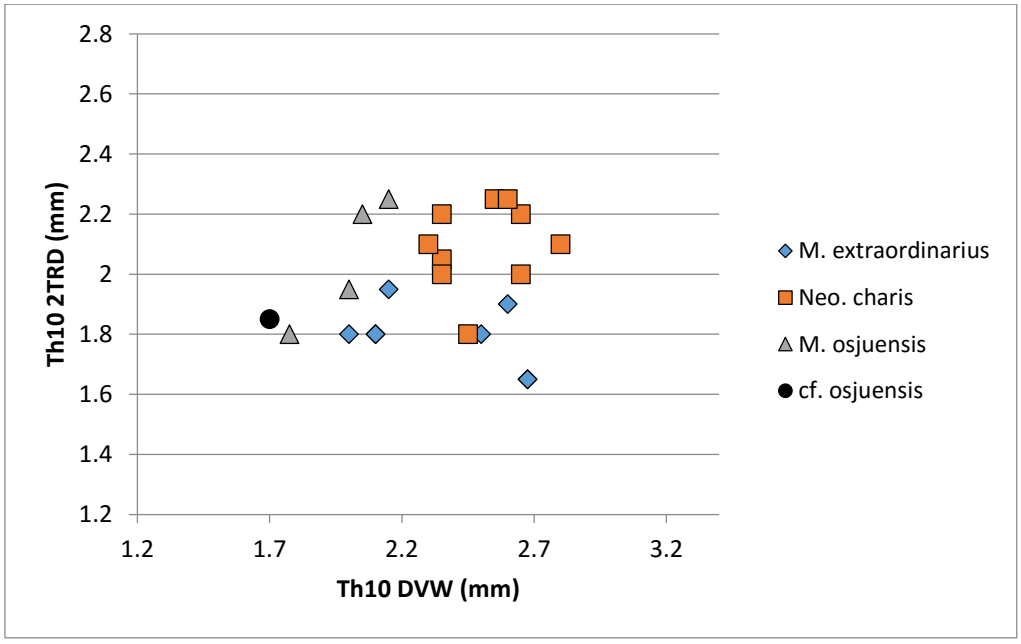

Figure 6.37. Neograptine species: distal 2TRD vs. Distal DVW. All data original measurements on material from the present Blackstone River collections.

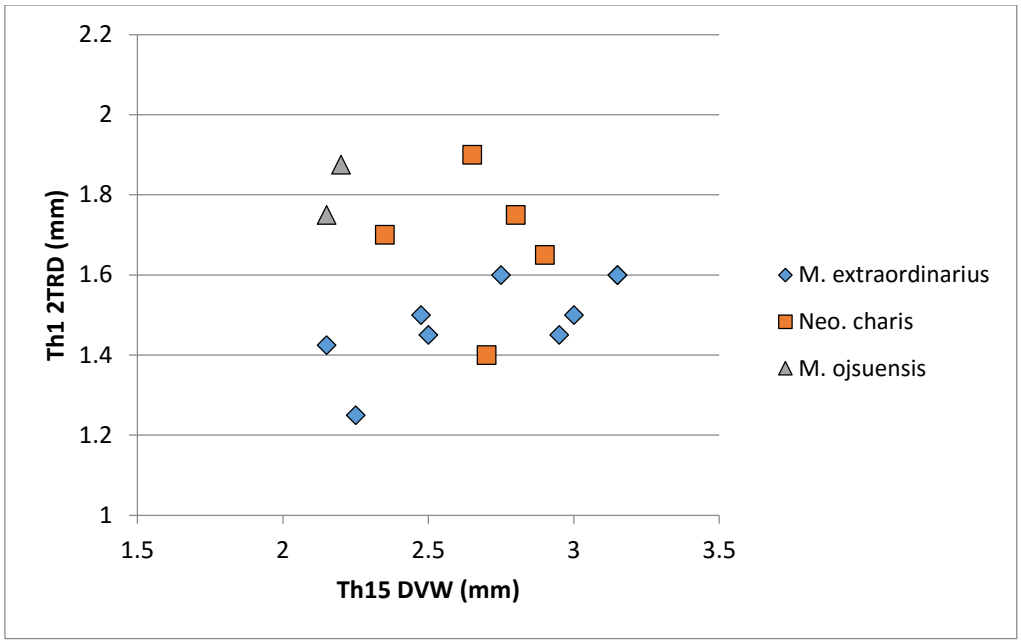

Figure 6.38. Neograptine species proximal 2TRD vs. distal DVW. All data original measurements on material from the present Blackstone River collections.

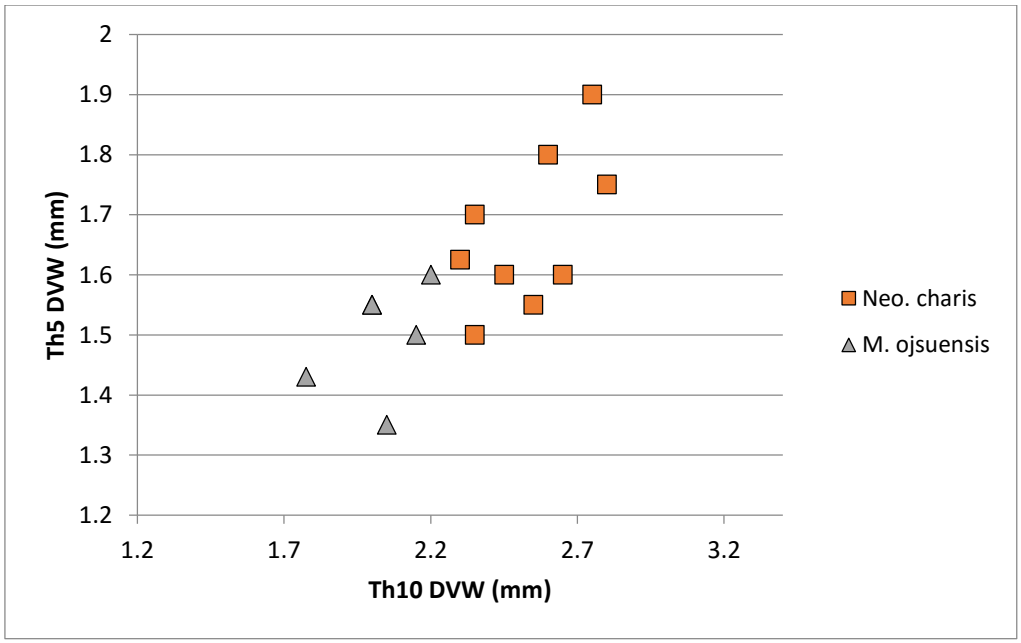

Figure 6.39. Neo. charis vs. M. ojsuensis. All data original measurements on material from the present Blackstone River collections.

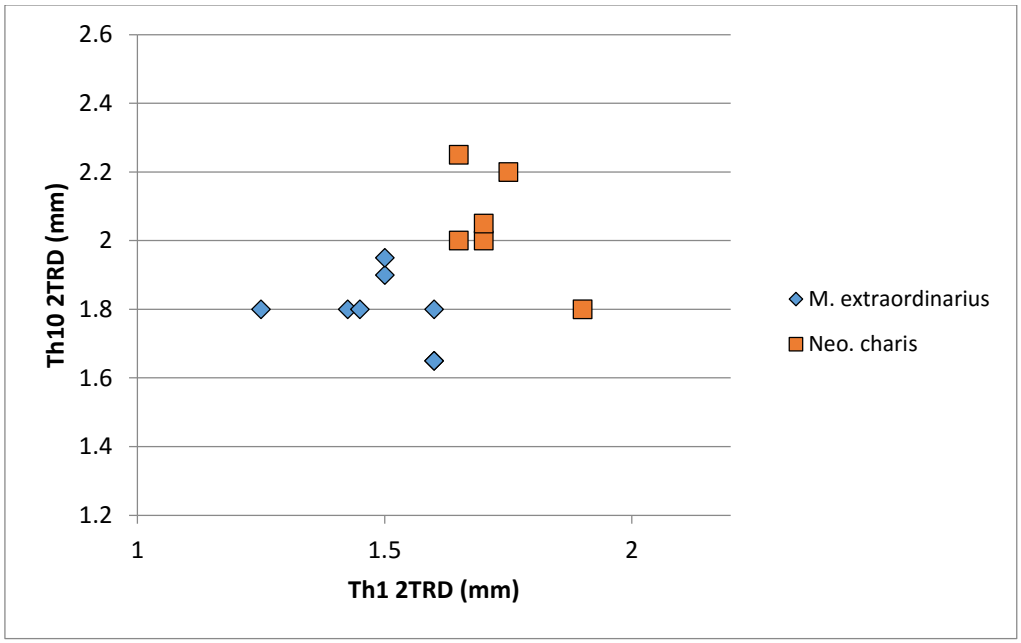

Figure 6.40. M. extraordinarius vs. Neo charis. All data original measurements on material from the present Blackstone River collections.

6.4 *Metabolograptus persculptus, Akidograptus ascensus* and *Parakidograptus acuminatus* zones

Suborder AXONOPHORA Frech, 1897

Infraorder NEOGRAPTINA Štorch, Mitchell, Finney and Melchin, 2011

Paraphyletic Family NORMALOGRAPTIDAE Štorch and Serpagli, 1993, emend Melchin et al., 2011

Genus *NORMALOGRAPTUS* Legrand, 1987, emend. Melchin and Mitchell, 1991

Type species: *Climacograptus scalaris normalis Lapworth,* 1877, by original designation.

***Normalograptus ajjeri* (Legrand, 1977) Form A**

Plates: (Photos) 47.9, 50.4, 55.1-6, 55.9; (Line drawings) 39.8, 39.10-13, 39.15, 39.25

Material and stratigraphical range: Common to abundant from the mid *acuminatus* Zone. 17 specimens measured in detail.

Description: Distinctly tapered rhabdosome up to at least 26 mm in length. Expands from 0.68-0.75 mm (rarely to 0.83 mm) at th1, to 1.05-1.23 mm at th3 (1=1.4 mm), to 1.23-1.45 mm at th5 (most </=1.35 mm), to 1.3-1.6 mm at th10, which is maintained. 2TRD is variable: 1.4-2 mm at $th1^1$, 1.63-2 mm at $th5^1$, 1.75-2 mm distally (1=1.65 mm). Thecae are straight and sharply geniculate, with thickened apertural rims. The apertures are horizontal, ca. 0.25 mm high, and occupy about 1/3 of the width of the rhabdosome. $Th1^1$ turns upwards 0.1 mm below the sicular aperture and its upward-grown portion is 0.9 mm long. All specimens possess a thin, rigid, and tapered virgella, up to 8.6 mm long, as well as a long, thin distally projecting nema; both a long nema and virgella are present even on juvenile specimens, e.g., one specimen that is 6.5 mm in length

possesses a 5.3 mm long virgella and a nema that projects 15 mm beyond the rhabdosome. A complete median septum is present.

Remarks: These specimens differ from the material assigned to *Normalograptus ajjeri* Form B in possessing a long virgella, a more tapered proximal end, and generally higher thecal spacing. Loydell (2007) noted that virgellar length is highly variable within the species, and the measurements of both forms recorded in the present collections fall within the range for the species, but they are clearly distinguishable, even without reference to the virgella, from the material here assigned to from *N. ajjeri* Form B (Figs. 6.42-43). They resemble *N. premedius,* but differ in possessing more closely spaced thecae and a conspicuous virgella. *Normalograptus larini* is also tapered and possesses a very long virgella, but reaches a lesser distal width and possesses very narrow apertures. The present form is common in samples 42.83 m, 44.02 m, and above, and is extremely abundant in 44.02 m; Form B is common in the *ascensus* Zone. This material closely matches specimens referred to *Climacograptus* cf. *C. medius* by Churkin and Carter (1970), which occurs throughout the Rhuddanian. Note: The lettered notation for the material described as forms of *N. ajjeri* here does not correspond to the forms of Legrand (1999).

***Normalograptus ajjeri* (Legrand, 1977) Form B**

Plates: (Photos) 55.7-10, 55.12; (Line drawings) 39.3, 39.6, 40.11, 40.17-18

Material and stratigraphical range: Common in the *ascensus* Zone, rare in the lower *acuminatus* Zone. 24 specimens measured in detail.

Description: Rhabdosome up to at least 20 mm in length. Expands from 0.75-1.08 mm (mean = 0.88 mm), to 0.88-1.2 mm at th3, 1.05-1.45 mm at th5, and a maximum of 1.25-1.63 mm between th10 and th15. 2TRD is variable: 1.15-1.55 mm at th1[1], 1.45-1.9 mm at th5[1], and 1.75-2 mm at th10[1] (1=1.5 mm). Thecae are climacograptid, with horizontal apertures, and slightly thickened apertural rims. The proximal end is blunt. The virgella is 0.7 mm long or less and robust. A full median septum is present. In some cases, the thickened geniculae appear to form small flanges upon compression.

Remarks: This form is distinguished from *N. ajjeri* Form A in possessing a wider, more rounded proximal end, short virgella, and closer proximal thecal spacing. Some of the more robust specimens possess possible small flanges. This appears to be a preservational artifact from specimens being pressed slightly into the substrate, accentuating their thickened apertural rims, but it is possible that they are actually specimens of *Normalograptus jideliensis* Koren' and Melchin (e.g., Plate 40.11, 40.17-18).

Normalograptus anjiensis **(Yang, 1964)**

Plates: (Photos) 54.25-26; (Line drawing) 39.22

Material and stratigraphical range: Numerous specimens from the lower *ascensus* Zone. 20 specimens measured in detail, many more observed.

Description. Rhabdosome is up to 23 mm long. DVW is 0.68-0.8 mm at th1, 0.83-0.93mm at th3, and 0.95-1.1 mm at th5, 0.93-1.13 at th7, and 0.95-1.3 mm at th10. Maximum width of 0.95-1.4 is usually reached between th5 and th10, and is maintained.

2TRD is 1.45-1.7 mm at th11 and ca. 1.8 mm distally. Details of the proximal end are difficult to ascertain, as most specimens are preserved in sub-scalariform view. A trifurcating virgella is present on all specimens (one measured specimen possesses four basal spines), although frequently only two spines are visible due to the orientation of the specimen. All three spines are approximately the same length (0.65-2 mm) and thin. Thecae are climacograptid, with straight suprageniculare walls and well-defined geniculae. The thecal apertures are modest with slightly thickened apertural margins. Interthecal septae are straight, and there is a complete median septum. The nema is up to 11.5 mm long, and varies from 0.08-0.18 mm wide.

Remarks: *N. anjiensis* is common in the lowest *ascensus* Zone samples. This is consistent with first occurrence data reported from Uzbekistan (Koren' and Melchin, 2000), Arctic Canada (Melchin et al. 1991), where the specimens were identified as *N. lubricus,* and South China (Fan et al., in prep.), and close to that in Dob's Linn, Scotland (Williams, 1983, identified as *C*. sp. cf. *C. miserabilis*), where it occurs just above the base of the *ascensus* Zone. This supports its role as an index taxon for the base of the Silurian. Rare members of this collection possess four, rather than three, basal spines, a character that also appears to occur rarely in China (see Chen and Lin, 1978, text fig. 6 b and c). The present material shows the same range of morphology recorded in China and elsewhere, but also appears to show stratigraphic variation in maximum width, with the majority of specimens ca. 1 mm in the 38.19 m sample and ca. 1.2 mm in the 37.43? m sample. This difference does not appear to be preservational (although the lithology

does vary between the two samples): specimens in both samples are flattened and preserved in a variety of orientations. When its spines are not preserved, *N. anjiensis* can be easily confused with a number of co-occurring species, such as *N. mirnyensis. N. anjiensis* can be distinguished from *N. trifilis* by its much lower distal width and from *N. gnaurus,* which is otherwise very similar, by its less developed spines and lack of an elongated, spatulate virgella. The specimen from Clearwater Creek illustrated as *Climacograptus trifilis* by Lenz and McCracken (1982) is actually *N. anjiensis.* It is next to a specimen of *Paramplexograptus wuningensis,* making it probable that that sample represents the *ascensus* Zone at Clearwater Creek.

***Normalograptus gnaurus* (Chen and Lin, 1978)**

Plates: (Photos) 45.9, 45.14-16, 45.18, 48.1-3, 56.21-22; (Line drawings) 41.5, 41.9

Material and stratigraphical range: Moderately common from the upper *ascensus* Zone. 23 specimens measured in detail.

Description. Rhabdosome is up to 28 mm long, but usually less than 15 mm. DVW is 0.65-0.78 mm at th1, 0.8-1.03 mm at th3, 0.9-1.15 mm at th5, 1-1.1.2 m at th7, and ca. 1-1.35 at th10, with a maximum distal width of 1.2-1.45 mm distally. 2TRD is 1.5-1.8 at th1^1 (but mostly <1.6 mm) and 1.75-2 mm distally. Three spines project from the proximal end: a virgella and two laterally projecting spines that originate from the base of the virgella. In many cases, specimens are preserved in scalariform or subscalariform orientation, with only a single lateral spine visible (always projecting towards th1^1). The virgella is 2.5-8.5 mm long, and expands distally to a maximum width of 0.5 mm. The

two lateral spines are normally shorter than the virgella (0.85 mm to a maximum of 2.5 mm), and may be either thin and tapered or spatulate, with widening appearing to progress with maturity. Thecae are climacograptid, with straight suprageniculare walls and well-defined geniculae. The median septum is complete. The nema is robust and distally projects up to 15 mm beyond the rhabdosome, with a width of up to 0.35 mm. Remarks: Degree of spine expansion is variable between specimens, but even immature specimens possess a lengthy virgella, secondary spines, and a long nema. For example, one 6 mm long specimen has a uniformly thin 4.5 mm virgella and a thin 1.3 mm long visible secondary basal spine, as well as a >5 mm long distally projecting nema. The spatulate structure is produced by modifying initially thin proximal spines (see Plate 45.18), and only very mature specimens possess fully developed spatulate basal spines. *Normalograptus trifilis* also sometimes possesses a distally-expanding virgella and/or unequally sized lateral spines (e.g., see an example of the latter in Štorch and Feist, 2008, text-fig. 9.14). However, *N. trifilis* reaches a considerably greater maximum distal width. Koren' and Rickards (1996) reported several immature specimens, which they assign to *Normalograptus trifilis trifilis* Manck, with a maximum DVW of only 1.2-1.4 mm. These specimens may be equivalent to the present material or may represent specimens of *Normalograptus anjiensis*. Chen and Lin (1978) illustrated only a single specimen of *Normalograptus gnaurus* (their text-fig. 6f). This specimen appears to have an incorrect scale. The text description gives a proximal DVW of 0.8 mm and a distal DVW of 1.2 mm, which closely agrees with the present material. Chen and Lin's

specimen possesses a long virgella and a second, shorter downwards-directed spine that appears to emerge from the base of the virgella. As in the present specimens, the second spine is directed to th1[1]. Both spines are distally expanding, as is the case with mature specimens in our current collection. Chen and Lin also included a specimen assigned by Schauer (1971) to *Climacograptus longifilis* (tafel 3.6) that appears to show two spatulate proximal spines; that specimen is poorly illustrated and deformed, and so is not synonymized with confidence here. The present material is nearly identical to *Normalograptus* aff. *rhizinus* and *N. anjiensis* in all aspects, except for the number and/or development of proximal spines, and can easily be confused when these are not preserved or are poorly developed. For example, the specimen illustrated on Plate 56.20-21 shows only a single, barely visible secondary spine, which could easily be missed. When only the virgella is present, it is also similar to *Normalograptus*? *radicatus,* but the latter has considerably higher thecal spacing. It differs from *N.*? *rhizinus* in possessing straight, rather than inclined thecae and having a generally lower 2TRD.

***Normalograptus imperfectus*? (Legrand, 1986)**

Plates: (Photos) 49.15-19, 49.39; (Line drawings) 39.1, 39.7

Material and stratigraphical range: Basal *acuminatus* Zone. 9 specimens measured in detail, many more examined.

Description. Fusiform rhabdosome up to at least 18 mm in length. Expands from 0.83-1 mm wide at th1, to 1.15-1.2 mm at th3 (1=1.4 mm), 1.45-.1.6 at th5, 1.65-1.75 at th5, and maximum of 1.7-2.05 mm reached at or just after th10; in many cases, width

decreases substantially around th15, which is maintained distally (some examined specimens reach distal widths of only 1.5 mm). 2TRD is 1.25-1.4 mm at th1[1], 1.35-1.55 mm at th3[1], 1.55-1.6 mm at th5[1], and 1.7-1.8 mm at th10[1]. Thecae are geniculate, with large and thickened apertures. The subapertural walls are moderately inclined proximally and distally, and more strongly inclined mesially, with inclination highest at maximum width. Mesial and distal thecal apertures are slightly everted. Supragenicular walls are straight. The virgella is short.

Remarks: Legrand (1986) illustrated only a single specimen of *N. imperfectus,* but described a larger collection, some of which he subsequently reassigned to a series of "aff. *imperfectus*" categories or new species (Legrand, 1999). Melchin (2008) and Fan et al. (in prep.) assigned material from Anticosti Island and China, respectively, to *N. imperfectus.* The present specimens agree with Legrand's description and/or illustrated material in bearing enlarged apertural excavations and inclined thecae, a tendency to decrease in width distally, as well as in overall dimensions. They differ in lacking genicular flanges (which are present on the holotype and Melchin's illustrated specimen), although they do possess thickening around the aperture. They also taper earlier and more consistently than the material illustrated by Legrand (1999). They agree well with the material assigned by Fan et al. (in prep.) to *N. imperfectus* and occur at a similar level. Material assigned by Li (1995) to *Climacograptus pseudonormalis*, and reassigned by Štorch et al. (2011) and Wang et al. (2015) to *Normalograptus ajjeri*, resembles this material, especially Li's plate 8.1, and disagrees with *N. ajjeri* in having

distally inclined thecae. Li did not give measurements for his 1995 material, but measurements from a photocopy of the plates give distal widths for specimens on plate 8.1-2 (from the *persculptus* and *acuminatus* zones, respectively) of ca. 1.65-1.7 mm, consistent with the present material. In contrast, Li's type description gives a maximum width of "1.3-1.4 mm (rarely 1.7 mm)" and the illustrations, especially plate 14.13 and 14.17, show a distinctly tapered rhabdosome similar to material assigned by Chen and Lin (1978) to *N. nanjingensis,* including the specimen that Fan et al. (in prep.) will propose as a neotype for that species. *N. imperfectus*? can be distinguished from other species in this collection by its relatively high maximum width, gently fusiform shape, and slight thecal inclination.

***Normalograptus medius* (Törnquist, 1897)**

Plates: (Photos) 56.28-32

Material and stratigraphical range: Rare in the upper *acuminatus* Zone. 9 specimens measured in detail.

Description: Robust rhabdosome, with deep and tall apertural excavations, up to 21 mm in length. Expands from 0.83-1.1 mm at th1, 1.05-1.35 mm at th3, 1.25-1.55 mm at th5, 1.45-1.7 mm at th7 (1=1.3 mm), and 1.55-1.8 mm at th10; some specimens taper very slightly distally. 2TRD is 1.35-1.55 at $th1^1$ (1=1.7 mm), 1.55-1.75 mm at $th3^1$ (1=1.9 mm), 1.7-2 mm at $th5^1$, and 1.8-2.1 mm beyond. $Th1^1$ turns up just below the sicular aperture, and grows upwards for 0.73-0.83 mm. The sicular aperture is 0.2-0.3 mm wide. In one instance, it is constricted and oddly centrally located (Plate 56.29). The proximal end is

rounded. The thecae are climacograptid, although they are often preserved at low inclination, with slightly everted apertures, in off-profile specimens. The thecal apertures are thickened, deep, and tall: 0.35-0.4 mm distally. In comparison, the supragenicular walls are 0.63-0.75 mm high. A short and fine virgella is present on several specimens, as well as a thin distally projecting nema. The median septum is complete.

Remarks: Loydell (2007) provided a detailed restudy of this species, excluding many previously assigned specimens from synonymy. The characteristic features of *N. medius* are its rounded proximal end and wide and deep thecal excavations. All of the present specimens possess deep and tall apertural excavations, and many possess rounded proximal ends; those preserved off profile appear less rounded than others, but that is the case with the lectotype as well. These specimens agree well with material illustrated by Loydell (2007), Štorch (1996), and Bjerreskov (1975). The robust rhabdosome and large thecal excavations in *N. medius* distinguish it from all other species in this collection; however, when flattened, especially when off-profile, which is common in this species, the infragenicular wall and opposite apertural rim often fills the apertural excavation, masking its true height, and obscuring this diagnostic feature.

***Normalograptus*? *minor* (Huang, 1982)**

Plates: (Photos) 31.13-14, 31.19, 31.20(?), 37.13; (Line drawings) 27.12, 29.12?, 29.13

Material and stratigraphical range: Rare from the upper *persculptus* Zone and questionably from the lower *ascensus* Zone. 6 specimens, 4 measured in detail, plus additional questionable material.

Description: Rhabdosome up to 13 mm in length. Expands from 0.7-0.85 mm at th1, to 0.9-1.05 mm at th3, 1-1.25 mm at th5, 1.15-1.28 mm at th7, with a distal maximum of up to 1.4 mm. 2TRD is 1.45-1.55 mm at $th1^1$, 1.55-1.75 mm at $th3^1$, increasing to ca. 2 mm distally. Thecae are straight and slightly inclined, with sharp geniculae. Thecal apertures are slightly everted and the infragenicular walls slightly inclined. A thin distally projecting nema is present, along with a long virgella that branches distally. In addition, the portion of the virgella preceding branching is secondarily thickened in specimens with well-developed branching. In specimens with branching, it begins between 1 and 3.8 mm below the sicular aperture; the resulting structure is up to 4 mm wide.

Remarks: The most characteristic feature of *N.*? *minor* is its distally branching virgella. Without this feature, identifying *N.*? minor is difficult. Initiation of branching appears to be variable within the species. Chen et al. (2005a) illustrated two specimens with branching that are only five and six thecal pairs long, respectively, as well as a specimen that is >14 thecal pairs in length that possesses only incipient branching (see their text-fig. 8). The description above applies only to the four specimens that possess clearly branching virgellae. These specimens are restricted to two samples from the middle of the graptolitic portion of the *persculptus* Zone at the Blackstone River section (=upper *persculptus* Zone). Additional specimens with possible distal thickening or without fully

preserved virgellae, but which possess close thecal spacing, slightly inclined thecae, and a maximum width of ca. 1.25 mm are tentatively assigned to the species, but are not included in the written description. The specimen shown in Plate 29.12 possesses a thin, non-expanding virgella 6 mm in length; it is questionably included. Including these questionable specimens extends the species' range to all of the preserved *persculptus* Zone. In addition, isolated branching virgellae are present from the *ascensus* Zone, although these may belong to *N.*? *radicatus*. In the present specimens, branching first occurs at 1 mm, 2.5 mm, 3.5mm, and 3.8 mm. This is somewhat higher than the 1-2 mm given in Chen et al. (2005a), but is consistent with the starting point for the specimen illustrated by Fang et al., 1990 (assigned to *Climacograptus radicatus minor*), which branches at about 2.5-3 mm. The Chen et al. (2005) and Fang et al. (1990) specimens tend to have a wide u- or v-shaped primary virgellar bifurcation, with lesser, thin, additional branches; whereas the branches of the present specimens are somewhat more evenly dendritic. *N.*? *minor* differs from *N.*? *radicatus* primarily in possessing considerably more closely spaced proximal thecae (see Fig. 6.44). The virgella of *N.*? *radicatus* also appears to possess fewer and thicker branches than *N.*? *minor*, although the small number of specimens of *N*.? *minor* makes this uncertain. *N.*? *radicatus* also seems to have somewhat more inclined thecae. *N*.? *minor* differs from specimens assigned to *N.* aff. *mirnyensis* in possessing a branching virgella, a slightly greater distal width, less rounded geniculae, and more inclined thecae. *N*.? *rhizinus* is very similar in thecal form and dimensions, but possesses a spatulate virgella, and sometimes

additional long spines that branch off the base of the virgella. A single specimen from the mid *ascensus* Zone, consisting only of a detached branching structure, may belong to *N.*? *minor* (Plate 47.13) or may represent a more dendritic version of *N.*? *radicatus.*

***Normalograptus mirnyensis* (Obut and Sobolevskaya, 1967)**

Plates: (Photos) 51.16-18, 51.25, 54.28; (Line drawings) 39.16

Material and stratigraphical range: Present throughout the *ascensus* and *acuminatus* zones, and likely in the *persculptus* Zone.

Remarks: Specimens at or close to a maximum width of 1 mm, with moderate thecal spacing, i.e., 1.4-1.8 mm, and climacograptid thecae, which did not fit into one of the other categories of thin normalograptids were assigned to *N. mirnyensis.* This collection includes specimens showing large variation in virgellar length, which is consistent with previous descriptions of this long-ranging species (see comments in Loydell, 2007). No detailed attempt was made to examine the collection for subtle differences in dimensions that might allow subdivision, but the material exists for future investigation.

***Normalograptus*? *radicatus* (Chen and Lin, 1978)**

Plates: (Photos) 47.13?, 50.6-8, 55.11?; (Line drawings) 41.1-4

Material and stratigraphical range: Uncommon from the upper *ascensus* Zone. Twenty-five specimens measured, including 12 specimens with well-developed branching structures at the distal end of their virgellae.

Description: Strongly tapered rhabdosome up to 27 mm in length. Slowly widens from 0.7-0.9 mm at th1 (most specimens 0.7-0.75 mm), 0.8-0.98 mm at th3, 1.03-1.13 mm at

th5, 1.18-1.35 at th7 (1.10 mm, n = 1), and a maximum width of 1.4-1.55 mm is attained at or after th10 (1.2-1.55 mm at th10), with some specimens continuing to expand to th20. 2TRD is 1.7-2.15 mm at 11, but is most commonly 1.95 mm, and is consistently close to 2 mm throughout the rhabdosome (1.85-2.3 mm at extremes). The sicula is difficult to discern, but appears to be ca. 1.9 mm long. The sicular aperture is 0.23-0.3 mm wide, and the sicula is exposed for ca. 0.4 mm below th1[2]. Theca 1[1] turns upward just below the sicular aperture (0.1-0.15 mm), and its upward-grown portion is 0.85-0.95 mm long (n = 5). The virgella is long, up to 9 mm, even in comparatively small specimens. It is very thin for the first several mm (<0.1 mm), becoming spatulate at about 3.5-5.0 mm, and then expanding into a wide (up to 2.4 mm) branching structure at a distance of 4.0-6.5 mm. The nema is long and prominent in all specimens (up to 22 mm long), with a highly variable width (0.1-0.38 mm), which is maintained throughout its length. Thecae possess sharp geniculae and straight, but slightly to moderately inclined supragenicular walls, and often slightly everted apertures. The median septum appears to be complete.

Remarks: This species is common in sample 39.30 m (upper *ascensus* Zone), questionably present in samples 38.62 m and 38.18 m, and apparently absent from the lowest *ascensus* Zone. The lowest occurring probable specimen is represented only by a detached branching virgella from sample 38.18 m (Plate 47.13); it may actually be a specimen of *N.*? *minor,* which seems to have a more dendritic virgellar structure. Chen and Lin (1978) erected two new species with a long, branching virgellae from the *A.*

ascensus-N. bicaudatus Biozone in northern Guizhou, China: *Climacograptus radicatus* and *Diplograptus coremus*, the latter distinguished by a higher distal width (1.8 mm in text description) and more inclined to orthograptid thecae distally. Chen et al. (2005a), however, in their discussion of *Normalograptus minor* (formerly a subspecies of *C. radicatus*), argued that these apparent differences were preservational artifacts and regarded *C. radicatus* and *D. coremus* to be synonymous. M.J. Melchin provided access to camera lucida drawings that he prepared of the holotype of *D. radicatus* and two syntypes of *C. coremus.* The present specimens match the dimensions and thecal character of the holotype of *C. radicatus* (which is in near profile view), but differ greatly from the illustrations of two syntypes of *D. coremus*, which have distal widths of 2 mm or greater. Tectonic deformation, which appears to be present in some of the Chinese specimens (Melchin, pers. comm.) is unlikely to account for these differences, as both 2TRD and width in the *D. coremus* syntypes exceed those in the present specimens. As such, the present specimens are assigned to *N.*? *radicatus.* Further collections may support assigning all of these specimens to *D. coremus*, following Chen et al. (2005a). *N.*? *radicatus* resembles *N.*? *minor*, but differs in a greater distal width and especially higher 2TRD (see Fig. 6.44). The younger *Glyptograptus bulbus* (Koren' and Rickards, 1996), is similar in rhabdosomal form and dimensions, but possesses a distal bulb on its virgella, rather than a branching structure. *Normalograptus premedius* is very similar, but possesses a simple virgella. In the early stages of work for this thesis, a measurement category was created for tapered specimens with very high thecal spacing

encountered during slab scans. Reexamination of many of these specimens has shown that many of them are *N.*? *radicatus* with broken virgellae. Time did not allow all specimens to be reexamined, however, and it is possible that *Normalograptus premedius* may be present in the *ascensus* Zone at the Blackstone River section. In addition to the distally branching structure, *N.*? *radicatus* can be distinguished from specimens assigned here to *Normalograptus ajjeri* Form A by its higher 2TRD and inclined thecae, and from *Normalograptus*? r*hizinus* by its higher proximal 2TRD (Fig. 6.45). These specimens are only questionably assigned to *Normalograptus* due to their thecal inclination.

***Normalograptus rectangularis* (McCoy, 1850)**

Plates: (Photos) 45.1?-3?, 45.5-7, 47.6, 57.1?-2?; (Line drawings) 42.2

Material and stratigraphical range: Common from the uppermost *acuminatus* Zone and present throughout the zone. 22 specimens measured in detail.

Description: Robust and strongly tapered rhabdosome up to 23 mm long. Expands slowly from 0.68-0.83 mm at th1, to 0.9-1.1 at th3, 1.15-1.63 mm at th5 (most often <1.4 mm), 1.4-1.6 mm at the 7 (1=1.7 mm), 1.65-1.95 mm at th10, and a distal maximum of up to 2.2 mm reached at th15 or beyond. One specimen tapers slightly distally. 2TRD is 1.35-1.75 mm at th1^{1}, 1.5-1.8 mm at th3^{1}, 1.6-1.85 mm at th5^{1}, 1.85-2.05 at th10^{1}, and 1.75-2.2 mm distally. The sicular length is unclear, but its aperture is 0.25 mm wide. Th1^{1} grows below the sicular aperture for 0.1 mm, and its upward-grown portion is 0.75-0.88 mm long. Thecae are straight and sharply geniculate, very slightly

inclined proximally and parallel distally. The distal length of the supragenicular wall is ca. 0.7 mm. The apertures are horizontal and relatively narrow (ca. 0.3-0.38 mm high distally). The infragenicular walls are slightly inclined. The virgella is long, robust, and tapered, up to 9 mm long. The nema is rarely preserved, but is ca. 0.15 mm wide and at least 9 mm long. There is a complete median septum.

Remarks: In possessing a robust and strongly tapered rhabdosome, these agree well with the types of *Normalograptus rectangularis,* as redescribed by Elles and Wood (1906), but differ in possessing consistently very long virgellae (up to >9 mm vs. "about 1 mm"), a somewhat lower proximal width (0.8 mm vs. 1 mm), and less rapid widening. Many other collections referred to *N. rectangularis*, e.g., Koren' and Rickards, 1996 (plate 5, figs 4-5 and 7-8); Underwood et al., 1998 (text-fig. 5k); Melchin, 1989 (text-fig 7g); Cuerda et al., 1998 (text-fig. 6h), etc., also show short and robust virgellae, but this is variable. For example, some of Loydell's (2007), Jordanian specimens possess long virgellae (up to 5.5 mm), specifically specimens that show the same very strong tapering as in the present collection. Lenz and McCracken (1982) illustrated a specimen of *N. rectangularis* from the Peel River, Yukon, which was examined as part of this thesis: it possesses a 3 mm long virgella, and is only slightly less tapered than the present specimens. Similarly, Fang et al. (1990) illustrated specimens assigned to *Climacograptus medius* (assigned by Loydell, 2007, to *N. rectangularis*) with a 2 mm virgella. In both virgellar length and their high degree of tapering, the present specimens most closely resemble *Normalograptus* (*Normalograptus*) *normalis ajjeri* Forme 'C' Legrand (1999),

differing only in that two of the three illustrated specimens show thickening along the virgella. Legrand contrasted the very pronounced tapering in his specimens with lesser tapering in *N. rectangularis,* and compared his material with specimens he collected (Legrand, 1977) from the *vesiculosus* Zone in Dob's Linn; that collection also closely matches the present specimens. The present specimens also resemble *Climacograptus* cf. *rectangularis* Churkin and Carter (1970), but widen somewhat more rapidly (see Fig. 6.46) and possess a long virgella. At the Blackstone River section, *N. rectangularis* is common in the collection just underlying the *atavus* Zone and is rare throughout the entire *acuminatus* Zone. Several specimens that taper less dramatically than those confidently assigned to *N. rectangularis,* have deeper excavations, and/or lack a long virgella are only questionably assigned (indicated with question marks above). These specimens match many past descriptions of the species, but are noticeably different from the most common material in the present collection; their measurements are not included in the description above. Distally, *N. rectangularis* is similar to the material here assigned to *N.* aff. *medius,* but it is easily distinguished by its strong tapering when the proximal end is intact (Fig. 6.52)

***Normalograptus*? *rhizinus* (Li and Yang) *in* Nanjing Institute of Geology and Mineral Resources ed., 1983**

Plates: (Photos) 32.1-3, 32.6-7; (Line drawings) 28.1-2, 28.10, 29.14

Material and stratigraphical range: Rare from the upper *persculptus* Zone. 16 specimens measured in detail.

Description: Rhabdosome up to at least 24 mm long. Septate distally and likely proximally. DVW is 0.65-0.85 mm at th1 (1=1.05 mm), 0.8-1.05 mm at th3 (1=1.2 mm), 0.95-1.25 mm at th5, 1.25-1.5 mm at th10 (1=1.65 mm), and 1.3-1.6 mm distally. 2TRD is 1.5-1.85 mm at $th1^1$ and 1.8-2.1 at $th3^1$, which is maintained after. Thecae are sharply geniculate and moderately inclined throughout. Thecal apertures are everted. The sicula is exposed below th1.2 for 0.50-0.65 mm. The proximal end is pointed, and moderately elongate. The upward-grown portion of $th1^1$ is 0.8-1 mm. The virgella is long and straight, up to 0.30 mm wide, and may bifurcate one or more times basally and/or (rarely) distally. One or more anti-virgellar spines project at ca. 45 degrees to the rhabdosomal axis on most specimens. Including the virgella, up to seven spines may be present, although the majority of specimens possess two to three. The prominent nema is 0.15-.20 mm wide, non-expanding, and extends up to 20 mm distally.

Remarks: In thecal form and dimensions, these specimens closely resemble previous descriptions of *N.*? *rhizinus*, which occurs at a similar horizon and in association with a similar fauna in China (Chen et al., 2005). Unlike most of the present specimens, however, illustrated Chinese specimens of *N.? rhizinus* possesses no proximal spines except the virgella, which sometimes expands into a spatulate or vane-like structure. (Note: The holotype of *N.? rhizinus* differs from other illustrated material in possessing a dramatic bulb-like expansion at the distal end of the virgella—see reillustration in Li, 1999.) All of the specimens that possess multiple spines in this collection occur in a gregarious cluster on a single slab, are mostly very mature, and are intermixed with

specimens that appear to possess only an expanding virgella. Several other specimens, from a slightly higher collection also possess only a spatulate virgella. These specimens are slightly, but consistently, wider proximally than the multispined specimens (e.g., 0.85-1.05 mm vs. 0.65-0.75 at th1—see 'MS' in Fig. 6.47), but are otherwise identical. Since these younger specimens would be readily included in *N.? rhizinus,* all specimens are conservatively assigned to the species; larger collections may support splitting the collection into two species. Although several specimens have distally expanding, club-like virgellae, none of them possesses the paddle-like expansion seen in Chen et al. (2005a) plate 9.v-w or—in a more extreme form—the holotype. The present collection resembles the Jordanian species *Normalograptus bifurcatus* Loydell in rhabdosomal dimensions, and also in commonly possessing one or more bifurcating antivirgellar spines and a long, sometimes bifurcating virgella; however, they differ in having inclined thecae, with everted apertures.

***Normalograptus skeliphrus* Koren' and Melchin, 2000**

Plates: (Photos) 48.21-22, 51.4-6; (Line drawings) 39.14, 39.17-18, 39.23?

Material and stratigraphical range: Uncommon to rare from the lowest *ascensus* Zone. 16 specimens measured in detail.

Description: Narrow, parallel-sided rhabdosome up to 9.5 mm in length. Expands slightly from 0.6-0.78 mm at th1, to 0.74-0.84 mm at th3, which is maintained distally. 2TRD is 1.4-1.6 mm (n=4) at $th1^1$ and 1.36-1.75 mm at $th5^1$. Thecae are climacograptid, with shallow semi-circular excavations, and straight to slightly concave supragenicular walls.

A prominent thin virgella, up to 1.9 mm in length, is present on most specimens. A complete median septum appears to be present.

Remarks: In width and the presence of a long virgella, this species resembles *Paramplexograptus* aff. *madernii*, which is common in the sample immediately underlying the one where this species is most common. *P.* aff. *madernii* has a generally higher thecal spacing (see Fig. 6.48) and is aseptate. The internal structure of most of these specimens is difficult to see, but the nema is consistently straight and centrally positioned in both profile and sclariform flattening, whereas it is commonly zigzag in *P.* aff. *madernii*. This material matches the type material well, except that it is slightly wider throughout with somewhat higher thecal spacing. The type material is from with Koren' and Melchin's (2000) *cuneatus* Subzone, i.e., it precedes the appearance of *Hirsutograptus sinitizini* (as it does in the Blackstone River), but lies above the first appearance of *Paramplexograptus wuningensis* (referred to as "*Paraclimacograptus" kiliani kuramaensis*), and coincides with the first appearance of *Akidograptus ascensus* (both latter species first appear together at the Blackstone section, coincident with *N. skeliphrus*). In Sweden (Koren' et al., 2003), *N. skeliphrus* is reported to precede the *ascensus* Zone fauna, and occurs with species such as *N.*? *minor* and *A. avitus*, which in the present samples co-occur with *P.* aff. *madernii.* Given their external similarities, it is possible that the Swedish material is actually *P.* aff. *madernii,* not *N. skeliphrus.* The younger material here assigned to *Normalograptus*? aff. *melchini* differs from *N. skeliphrus* in possessing narrower and shallower apertures and generally lower 2TRD.

Normalograptus? *transgrediens* (Waern, 1948)

Plates: (Photos) 34.7, 34.14?, 34.16, 34.17, 35.17, 37.19?, 37.25, 38.3; (Line drawings) 27.4, 27.14, 29.15

Material: Rare throughout the upper *persculptus* Zone. 8 specimens measured.

Description: Strongly tapered rhabdosome up to at least 25 mm long. Widens slowly from 0.7-0.83 mm at th1, 0.9-1.1 mm at th3, 1.05-1.25 mm at th5, 1.2-1.45 mm at th7, 1.38-1.55 mm at th10, and 1.5-1.8 mm at th15. 2TRD is 1.3-1.6 mm at $th1^1$, 1.65-1.7 mm at $th3^1$, 1.7-1.95 mm at $th5^1$, 1.65-1.9 mm at $th7^1$, and ca. 1.9 distally. Thecae are straight and slightly inclined, with sharp geniculae, and horizontal apertures. The apertural rims are thickened, and sometimes form very slight flanges. Interthecal septa are straight and parallel to the rhabdosomal axis. A complete median septum is present. The virgella is short, when preserved.

Remarks: These specimens agree well with the types, except that they have a slightly higher DVW at th1 (0.7-0.85 mm vs. 0.7 mm) and reach a greater distal width (up to 1.8 mm vs. 1.5 mm); but note that maximum width is very slowly attained (at or after th15) and the types are both short and appear to be in partial relief. The two illustrated specimens are only ca. 5.5 mm and 7.5 mm long, and they very closely match the present material in terms of rates of widening, thecal spacing, and thecal form, i.e., thecae are slightly inclined with very small flanges on some thecae (compare Plate 34.17 with the types). They also agree in widening rate with Loydell (2007) and Howe (1982). An additional population of common tapered normalograptidsin this section occurs in

the *ascensus* Zone that is very similar to the present specimens and the other examples of *N.*? *transgrediens* described previously, except that they are slightly narrower throughout, and reach considerably lower distal width (see Fig. 6.49, as well as Fig. 6.56 for comparison with the holotype). These specimens are assigned to *N.*? cf. *transgrediens* and are described separately. Given the small amount of comparative material available, both populations might actually belong to *N.*? *transgrediens,* but they are separated here, as they are both stratigraphically and morphologically distinct.

The present specimens are similar to those assigned by Chen et al. (2005a) to *Avitograptus avitus,* with the exception that the latter appear to have more rounded geniculae distally; both collections differ from specimens of *A. avitus sensu stricto* in lacking the protracted first thecal pair and having consistently lower thecal spacing (compare, for example, Plate 27.14 and 27.17), as well as lacking a long and thickened virgella. They differ from specimens assigned here to *Glyptograptus*? sp. 1 in possessing a lower 2TRD and proximal and mesial DVW (Figs. 6.70 and 6.72), less inclined thecae, lacking a prominent externally projecting nema, and lacking an internally wandering nema. They differ from *Metabolograptus parvulus* in possessing straight interthecal septae and sharper geniculae, although these differences are not always obvious, and some specimens are only questionable assigned. For example, compare the somewhat ambiguous cluster of specimens in Plate 35.15-17 to the clearly distinct examples in Plates 35.21 and 34.17. It differs from the younger *Normalograptus premedius* in lacking a long virgella and possessing more closely spaced thecae. *N.*? *radicatus* possesses a

distally branching virgella and higher thecal spacing. Specimens of *Korenograptus laciniosus* reach a lesser average distal width and possess more inclined thecae, which usually appear strongly glyptograptid. The damaged specimen shown in Plate 34.14 in partial relief may be *K. laciniosus* or *M. parvulus,* and is illustrated to show ambiguity that arises with differences in style of preservation. Owing to its inclined thecae, the species is only questionably assigned to *Normalograptus.*

***Normalograptus*? *nanjingensis* (Chen and Lin, 1978)**

Plates: (Photo) 49.8; (Line drawing) 39.9

Material and stratigraphical range: Rare from the basal to mid *ascensus* Zone. 6 specimens measured in detail.

Description: Tapered rhabdosome up to at least 14 mm in length. Progressively expands from 0.6-0.9 mm at th1, to 0.78-1.1 mm at th3, 0.9-1.18 mm at th5, 1.2-1.35 mm at th7, and 1.3-1.45 mm at th10; maximum width is not known. 2TRD is consistently high: 1.7-1.9 mm at $th1^1$, 1.9-1.95 mm at $th3^1$, and up to 2.05 mm distally. Thecae are sharply geniculate and gently inclined throughout, with semi-circular, non-thickened apertures, but can appear rounded when compressed. A long, thin, and straight virgella is present on all specimens, up to 6.5 mm in length. A long, thin, distally projecting nema is also present. There is a complete median septum.

Remarks: These specimens agree well with the lengthy redescription in Fan et al. (in prep.), as well as with their proposed neotype: the specimen illustrated in plate 14 fig. 17 in Chen and Lin (1978). In possessing a tapered rhabdosome with moderate distal width they are similar to material assigned here to *N.*? *transgrediens*, *Normalograptus*?

cf. *transgrediens,* and *Normalograptus*? *radicatus.* They differ from the first two in possessing a long virgella and much higher thecal spacing, especially proximally (see Fig. 6.50), and from the latter species in lacking a distally expanding virgella, as well as somewhat lower thecal spacing. *N.*? aff. *mirnyensis* reaches a lower distal width and has more closely spaced thecae. *Normalograptus ajjeri* Form A possesses non-inclined thecae, and also tends to have slightly lower thecal spacing and is slightly wider mesially and distally.

***Normalograptus* cf. *ajjeri* Legrand 1977**

Plates: (Photos) 48.6-7, 50.1-3; (Line drawing) 41.6

Material and stratigraphical range: Very rare from the basal to mid *acuminatus* Zone. 3 specimens, all measured.

Description: Rhabdosome up to at least 34 mm in length. Expands from 0.73-0.78 mm at th1, to 1.03-1.18 mm at th5, 1.23-1.55 mm at th10, and 1.35-1.58 at th15. 2TRD is 1.53-1.78 mm at $th1^1$, 1.65-2 mm at $th10^1$, and up to 2.25 mm in the one very long specimen. Thecae are climacograptid. A median septum is present. The proximal end possesses a stout virgella (0.75-1.5 mm), as well as a secondary, laterally-directed spine that extends from the exposed wall of the sicula. This spine is the same length as the virgella. All three specimens are preserved in subscalariform orientation.

Remarks: These specimens agree closely with *N. ajjeri* Form A in rhabdosomal dimensions (Figs. 6.42 and 6.43), but differ in possessing both a short virgella and a secondary antivirgellar spine. They also resemble two specimens assigned to *Normalograptus* sp. A (aff. *trifilis*) by Štorch and Serpagli (1993), but the latter are

considerably wider throughout. Legrand (1999) illustrated a single specimen (text-fig. 3-2-6B), assigned to *N. normalis ajjeri*, that shows a second spine emerging from the sicular aperture, but both it and the virgella are much longer than in the present specimens. When preserved off profile, so that only one spine is visible, *N. gnaurus* resembles the present specimens, but its spines emerge from the base of the virgella, not the rim of the sicula.

Normalograptus aff. *angustus* (Perner, 1895)

Plates: (Photos) 51.7-14, 51.20, 54.23, 54.31; (Line drawings) 39.19-21

Material and stratigraphical range: Uncommon to rare from the mid to upper *ascensus* Zone. 14 specimens measured in detail.

Description: Thin rhabdosome with sharp to bluntly rounded weak geniculae, up to at least 21 mm in length. Nearly parallel-sided. Rapidly expands from 0.65-0.75 mm at th1, to 0.8-1 mm at th3 to th5, which is maintained throughout. 2TRD is consistently moderate: 1.13-1.6 mm at $th1^1$ (1=1.9 mm), 1.5-1.6 mm at $th2^1$, 1.38-1.75 mm at th3, and 1.4-1.65 mm at $th5^1$ (1=1.9 mm). Thecae are geniculate, but unthickened and with inclined infragenicular walls, which leads them to appear glyptograptid when flattened, especially off-profile. A median septum is present. A short thin virgella and thin distally projecting nema is present on some specimens.

Remarks: *Normaloraptus angustus* is distinguished from other thin normalograptids by its consistently high thecal spacing and thecae that tend to appear strongly rounded when compressed. This material matches previous descriptions of *N. angustus* in all regards except high thecal spacing. Figure 6.41 compares the present specimens with

early Silurian material from China (Melchin, unpub. data) and Katian and early Hirnantian material from the Czech Republic, including some of the type material (data from Kraft et al., 2015); limited data is available for graphical comparison, but the present specimens plot separately from those populations. Loydell (2007), Koren' and Melchin (2000), Chen et al. (2005a), also report thecal spacing greater than in the present material, as do previous authors who give thecal spacing in thecae per cm. As such, these specimens are left in open nomenclature. Due to their narrow DVW and tendency to preserve apparently glyptograptid thecae, this species is easily confused *Paramplexograptus* aff*. madernii,* however, the latter has consistently wider thecae spacing and lacks a median septum; the median septum in the present species can be seen clearly on Plate 54.31 and ambiguously on some of the other plates. The specimen shown on 54.23 and another on the slab with it have somewhat higher 2TRD than the other specimens and may be *Normalograptus angustus. N.* aff. *mirnyensis* has a similar tendency to preserved with rounded geniculae, but reaches a higher maximum width and is more tapered (see Fig. 6.53; data for thecae to thecae comparison is limited, but pattern is clear from observation).

***Normalograptus*? aff. *medius* (Törnquist, 1877)**

Plates: (Photos) 31.8-11, 31.24; (Line drawings) 27.2, 27.5, 28.4, 28.6, 29.11

Material: Rare from the upper *persculptus* Zone. 10 complete specimens measured.

Description: Robust rhabdosome up to at least 17 mm in length. Expands from 0.73-0.9 mm at th1, to 1.1-1.3 mm at th3, 1.3-1.55 m at th5, 1.45-1.6 mm at th7, 1.55-1.8 mm at

th10, and 1.8-2.05 at th15 (n=1). 2TRD is 1.3-1.55 mm at th1[1], 1.5-1.8 mm at th5[1], 1.6-1.8 mm distally. Thecae are straight and slightly inclined, with sharp geniculae. Thecal apertures are horizontal, semi-circular, and occupy approximately 1/3 of the rhabodomal width. Sicular length is unclear. It is apparently fully septate. A prominent, but non-widening nema extends beyond the rhabdosome in several specimens. The virgella is stout.

Remarks: This material is similar to that assigned *N.*? *medius* by Chen et al. (2005a), but different from true specimens of *N.*? *medius* (see Loydell, 2007), in possessing slightly inclined thecae and a blunt, rather than rounded proximal end. It differs from the Chen et al. (2005a) material in lacking narrow and shallow apertures, and in possessing a narrower, more tapered proximal end; however, only two specimens were illustrated by Chen et al. (2005a). *N.* aff. *medius* differs from younger material assigned to *Normalograptus rectangularis* in this study in widening more rapidly and lacking a conspicuous virgella (see Fig. 6.51). *Normalograptus*? *transgrediens* is more tapered (see Fig. 6.52), with a less rounded proximal end, and narrower, less thickened apertures, although the populations overlap, and some specimens are difficult to assign, e.g., Plate 31.8 and 31.11. Due to its inclined thecae, the species is only questionably assigned to *Normalograptus.*

Normalograptus? aff. _melchini_ Koren' and Rickards, 2004

Plates: (Photos) 48.8, 51.15, 52.2, 52.20, 56.10, 56.13, 56.15

Material and stratigraphical range: Rare from the upper *acuminatus* Zone. 7 specimens measured.

Description: Minute and nearly parallel-sided rhabdosome up to 6.6 mm long. 0.6-0.7 mm wide at th1 and 0.7-0.9 mm distally. 2TRD is consistently 1.4-1.5 mm. The thecae are sharply geniculate, with straight supragenicular walls, and distinctive, shallow, semi-circular excavations, some bearing thickening or very slight flanges. The proximal end is tapered in several specimens and more rounded in others. A full median septum is present; it appears to be straight.

Remarks: These specimens co-occur with *Metaclimacograptus hughesi,* and are close in width and thecal spacing to the material assigned to that species from 48.10 m. Some of the apertures also appear slightly introverted, and as such many of these specimens were originally assumed to belong to the narrower forms assigned questionably to *M. hughesi.* However, the latter has much deeper and more consistently introverted apertural excavations (e.g., Plate 56.11 and 56.14) and is slightly wider. In addition, the proximal end in *N.*? aff. *melchini* tends to be more tapered and the virgella longer. The internal structure is unclear. The specimen in Plate 52.2 clearly has a straight median septum, but the specimen shown in Plate 52.20 appears to possess an undulose median septum. Some specimens also appear to have minute flanges (e.g., Plate 51.15). This material is similar to *Normalograptus melchini* in possessing a tapered proximal end and very shallow, semi-circular excavations, but the latter is considerably narrower than the present material. *Normalograptus skeliphrus* is a similar width, but lacks the very small thecal excavations in the present material, e.g., see Plate 56.10 and 56.13. *Metaclimacograptus* sp. (Štorch and Feist, 2008) is also similar to this material in width,

possesses shallow, rounded thecal excavations, and an undulose median septum, but has somewhat higher 2TRD. As the internal structure is uncertain, this material is only questionably assigned to *Normalograptus.* It is also possible that the collection is an artificial one, which contains a mixture of a species of *Metaclimacograptus* and a species of *Normalograptus.*

***Normalograptus* aff. *mirnyensis* (Obut and Sobolevskaya) *in* Obut et al., 1967**

Plates: (Photos) 31.3, 31.5?, 31.6-7, 31.16, 33.9, 34.1-2, 37.5-8, 37.14, 38.8, 51.19; (Line drawings) 27.9, 28.13

Material and stratigraphical range: Rare to common from the upper *persculptus* Zone and rare from the lower *ascensus* Zone. 27 specimens measured in detail, many more examined.

Description: Rhabdosome up to at least 21 mm. Expands from 0.65-0.83 mm at th1, to 0.8-1.05 mm at th3, 0.95-1.2 mm at th5, 1-1.3 mm at th7, and a distal maximum of up to 1.35 mm (but mostly 1.25 or less). 2TRD is variable: 1.4-1.75 mm at $th1^1$, 1.55-1.75 mm at $th3^1$, and 1.6-2 mm distally. Thecae parallel-sided to gently inclined, with straight supragenicular walls. Thecal apertures are horizontal. Geniculation varies with compression and preservation, with some specimens apparently possessing only weak geniculae distally, and others being consistently climacograptid. The infragencular wall is arched, which exaggerates thecal rounding upon compression. A full median septum is present. A conspicuous, but thin virgella is present on some specimens, up to at least 1.75 mm long.

Remarks: These specimens differ from *N. mirnyensis* in possessing infragenicular walls that are slightly inclined, and which appear rounded when compressed. In both of these features, they resemble *Normalograptus angustus*; they differ from most descriptions of *N. angustus* in possessing a more tapered rhabdosome, with a greater distal width—although Kraft et al. (2015) described two specimens at 1.2 mm and 1.25 mm, respectively, and Štorch et al. (2011) described specimens with a DVW of >1.15 mm. *N. angustus* also has higher average 2TRD, especially distally. Some specimens included here were assigned to *N.*? *minor* and *N. mirnyensis* at earlier points in the study, due to the possession of long, but broken, virgellae or simple climacograptid thecae. Given the variability of virgellar length and apparent geniculation, however, and the relative abundance of specimens that are clearly *N.* aff. *mirnyensis* in the upper *persculptus* Zone, questionable specimens are assigned to this species. This conservative approach has almost certainly resulted in some specimens being misassigned. *Normalograptus*? *nanjingensis* Chen and Lin possesses similar dimensions and gently inclined thecae, but the type material has consistently sharp geniculae and appears to be more tapered than the present specimens, as do the specimens assigned to that species in this thesis, which also have considerably higher thecal spacing. Specimens assigned to *M.*? sp. 1 tend to reach a higher distal width and have more inclined thecae. A small number of specimens of *N.* aff. *mirnyensis* occur in the *ascensus* Zone (see 37.43? m specimen data in Fig. 6.54).

***Normalograptus*? aff. *nanjingensis* (Chen and Lin, 1978)**

Plates: (Photos) 47.7, 47.8?, 49.4-7, 49.14?; (Line drawings) 39.2, 39.45, 43.14?

Material and stratigraphical range: Rare from the mid *ascensus* and lowest *acuminatus* zones, and questionably from the middle *acuminatus* Zone. 9 specimens measured in detail.

Description: Rhabdosome up to at least 12.5 mm long. Widens from 0.75-0.9 mm at th1 (1=0.6 mm), to 1.05-1.25 mm at th3, 1.2-1.38 mm at th5, and to a distal maximum of 1.3-1.5 mm, reached mesially, after which most specimens taper slightly. 2TRD is 1.13-1.35 mm at $th1^1$, 1.25-1.5 mm at $th3^1$, and 1.4-1.55 mm beyond. Thecae have large, thickened apertural excavations, semi-circular proximally, and slightly arched distally; they are geniculate throughout and often slightly everted. Thecae are moderately inclined. All specimens possess a prominent virgella, up to at least 3 mm maximum length, and a distally projecting nema, which is greater than the length of the rhabdosome in several specimens. A median septum is present.

Remarks: This material is distinguished from other species in the collection by its combination of long virgella, large and generally thickened thecal excavations, inclined thecae, and moderate width. It resembles *Normalograptus*? *nanjingensis* in possessing inclined, geniculate thecae, and a moderate width, but differs from the material considered by Fan et al. (in prep.) to be most representative of the species in possessing more open apertures and being less tapered; and from the material here assigned here to *N.*? *nanjingensis* in both in more rapid widening and much lower 2TRD (Fig. 6.55). It is also similar to *Glyptograptus xiushuiensis* Fang et al., 1990, especially their plate 6.5.

However, the latter seems to have a more asymmetrical proximal end, with a very prominently exposed sicula; additionally, Fang et al. (1990) described the thecae as glyptograptid throughout (although the illustrated specimens appear to have quite sharp geniculation). Material illustrated as *Neodiplograptus* sp. 3 by Loydell (2007) matches the present material, but appears to lack a long virgella (although the virgella is only preserved in one specimen). A specimen from the middle *acuminatus* Zone (45.38 m) is questionably assigned (Plate 49.14). Its thecae are more weakly geniculate, but in other respects it is very similar. An additional specimen from 41.66 m is very questionably assigned. It bears sharp geniculae proximally, but apparently glyptograptid thecae distally. In addition, it tapers very strongly distally and possesses an expanding nema. This suite of features is not seen in any other specimen in the collection (although the probable specimen from 45.38 m does possess thickening mesially along the projecting portion of the nema), but on whole, it is most similar to the present species.

***Normalograptus* aff. *rhizinus* (Li and Yang), in Nanjing Institute of Geology and Palaeontology, ed., 1983**

Plates: (Photos) 50.15, 52.1, 55.14-15; (Line drawings) 41.7-8, 41.10-12

Material and stratigraphical range: Abundant well-preserved specimens from the lower *acuminatus* Zone and rare from the mid and upper *ascensus* Zone. 20 specimens measured in detail and many more observed.

Description: Rhabdosome up to 25 mm long, expanding from 0.68-0.73 mm at th1 to 0.83-1.0 mm at th3, 1-1.1.15 mm at th5, 1.05-1.25 mm at th7. Maximum width is

attained at th10 and is nearly always 1.15 mm (1.10-1.23 mm); this is maintained distally even in specimens with greater than 25 thecal pairs. 2TRD is fairly consistent throughout the rhabdosome, ranging from 1.6-1.8 mm at th1^1 to 1.65-1.90 mm at th10^1, and maintained distally. Theca 1^1 turns upward slightly below the sicular aperture (ca. 0.10 mm). The upward grown portion is 0.78-0.95 mm long. The sicular aperture is ca. 0.2 mm wide and it is exposed for 0.25-0.33 mm below th1^2. The sicula is not clear, but appears to be 2.25-2.4 mm long. The virgella is up to 1.7-5.2 mm long and spatulate, with rates of widening variable: some specimens possess a short, club-like virgella that begins expanding near its base, whereas others begin to expand only after a distance of several millimeters. In rare cases, the virgella bears additional growths on one or both sides, most commonly a square, "flag-like" projection from one side (see Plates 41.10, 50.15, and 52.1). The nema projects distally from the rhabdosome for up to 14.5 mm, is 0.13-0.18 mm wide, and bears a single medial vein that runs along its length. In one case, the nema bears secondary growths above the last thecal pair that raises its width to 0.4 mm. Thecae are climacograptid with straight and parallel supragenicular walls. Thecal excavations are ca. 0.15 mm high and occupy about one-fifth of the rhabdosome width. The median septum appears to be complete.

Remarks. *N.? rhizinus* occurs both in the Hirnantian (Chen et al., 2005a) and in the lower Rhuddanian (Fan et al., in prep.) in China. Chen et al.'s Hirnantian specimens of *N.*? rhizinus higher thecal spacing than the present specimens, and both the Hirnantian and Rhuddanian Chinese specimens of *N.*? rhizinus possess distinctly inclined thecae, as do

the specimens of *N.? rhizinus* from the Blackstone River (current collections). The present specimens, which show remarkable constancy in rhabdosomal dimensions (max. ca. 1.15 mm), are also consistently smaller than many reported specimens of *N.? rhizinus*, although they overlap in range. The specimen illustrated by Fang et al. (1990) as *Climacograptus acus*, and assigned by Chen et al. (2005a) to *Normalograptus rhizinus*, resembles the present material in lacking inclined thecae. It also occurs in a similar horizon, but has a greater maximum width. The present specimens can be distinguished from others in the collection by the combination of expanding virgellae, straight, non-inclined supragenicular walls, and low DVW. They are very abundant in sample 41.66 m, and rare or questionably present elsewhere in their illustrated range. In general form and dimensions they are almost identical to *N. gnaurus*, and can easily be mistaken if the additional proximal spines in the later are not preserved or visible.

***Normalograptus* cf. *transgrediens* (Waern, 1948)**

Plates: (Photos) 56.17-20; (Line drawings) 39.24?

Material and stratigraphical range: Common to rare throughout the *ascensus* and *acuminatus* zones. 12 specimens measured in detail.

Description: Tapered rhabdosome up to 26 mm in length. Gradually expands from 0.63-0.7 mm at th1, to 0.75-0.8 mm at th3, 0.98-1.1 mm at th5, 1.08-1.18 mm at th7, with a distal maximum of 1.15-1.4 mm reached at th10 or beyond. 2TRD is 1.5-1.58 mm at th1[1], 1.55-1.7 mm at th3[1], 1.6-1.75 mm at th5[1], and 1.7-1.9 mm distally. Virgella length is variable: often 1 mm or less, but sometimes longer and threadlike. Thecae are sharply

geniculate, and straight to very slightly inclined. Apertures are horizontal to slightly everted. A complete median septum is present, but it is unclear at what level it begins.

Remarks: These specimens match the types of *N*.? *transgrediens* well in terms of general rhabdosomal form, but reach a lesser distal width than the maximum that Waern reported. Waern does not provide a range of distal measurements, but from the plates the holotype is ca. 1.4 mm at th7, which plots in the morphospace of the *persculptus* Zone specimens assigned to *N*.? *transgrediens* (Fig. 6.56). This collection of specimens falls within the lower range of distal widths for *Normalograptus ajjeri* (Loydell, 2007; unpublished Chinese data provided by M.J. Melchin), but are more tapered. They resemble *Normalograptus mirnyensis,* but possess a greater distal width and slightly inclined thecae. *Normalograptus larini* is similar, but possesses a conspicuous virgella and has constricted apertures. They differ from the specimens assigned here to *N. ajjeri* Forms A and B in widening less rapidly mesially, and also in having a very low initial width—see Fig. 6.42. They resemble *Normalograptus*? *radicatus* in width and thecal form, but differ in having much lower thecal spacing, both proximally and distally (Fig. 6.45), as well as lacking an expanding virgella. *Paramplexograptus madernii* is similar in thecal form and dimensions, but is aseptate.

The present specimens are most similar to the material assigned to *N.*? *transgrediens* from the *persculptus* Zone of this section, but these have a lower width throughout, especially distally (Fig. 6.49), and possess less strongly thickened apertures. Štorch and Schönlaub (2012) described a collection from the *acuminatus* Zone (and possibly

persculptus Zone) of Austria that they also assigned to *N.* cf. *transgrediens;* this material reaches a similar maximum width to the present material (Štorch and Schönlaub (2012): 1-1.3 mm—up to 1.5 mm with strain).

***Normalograptus* sp.**

Plates: (Photos) 50.9-10, 54.29

Material and stratigraphical range: Four mature specimens and one probable juvenile specimen from the uppermost *acuminatus* Zone.

Description: Strongly tapered rhabodome to at least 20 mm in length. Slowly expands from 0.6-0.7 mm at th1, to 0.8 mm at th3, 0.9-0.95 mm at th5, ca. 1.25-1.3 mm at th10, and ca. 1.4 mm distally. 2TRD is consistently high: 2.15-2.3 mm at th1^1, 2.25 at th3^1, with a maximum of 2.15-2.38 mm distally in the two specimens where thecal position can be measured accurately; 1.9 mm at th1^1 in the probable juvenile specimen; and consistently 2 mm or greater at all points on the other two mature specimens. Th1^1 turns up at or just slightly below the sicular aperture, and grows straight upwards for ca. 1. mm. Th1^2 is slightly convex, resulting in the proximal end displaying a distinctive blunt, protracted, and constricted look. The apertures are shallow, narrow, and thickened proximally, and slightly everted, deep and ca. 0.3 mm tall distally, with less or no thickening. The supragenicular walls are straight proximally and slightly inclined distally. A long and thin virgella is present on all specimens with the proximal end intact, up to >8.5 mm in length. A thin nema projects up to 11 mm beyond the rhabdosome. A complete median septum is present, at least distally.

Remarks: This species is superficially very similar to proximal specimens of *Normalograptus magnus* and *Normalograptus*? cf. *transgrediens* (see Plate 50.14, for example), but has much higher thecal spacing and widens even more slowly (Fig. 6.57). It is similar in overall dimensions to *Normalograptus*? *radicatus*, but the latter species possesses a distally expanding virgella, inclined thecae along the entire rhabdosome, and lacks the proximal constriction present in *N.* sp.

Genus METACLIMACOGRAPTUS Bulman and Rickards, 1968, emended Melchin et al., 2011.

Type species. *Diplograptus hughesi* Nicholson, 1869.

***Metaclimacograptus hughesi* (Nicholson, 1869)**

Plates: (Photos) 49.20, 49.27, 51.21-22, 51.24, 56.11-12, 56.14, 56.33;
(Line drawings) 42.16

Material: Rare from the uppermost *acuminatus* Zone. Eighteen specimens measured in detail.

Description: Rhabdosome up to at least 7.3 mm in length. The rhabdosome is 0.6-0.83 mm wide at th1, 0.7-0.9 mm at th3, and reaches a maximum width of 0.8-1 mm at or just after th5, which is maintained or slightly decreases distally. [Measurements are taken from the thecal aperture, and are slightly higher if measured from the midpoint of the slightly convex supragenicular walls.] 2TRD is 1.15-1.4 mm at $th1^1$, 1.38-1.53 at $th3^1$ and beyond. The sicula is 1.3 mm long (n=1), is exposed ca. 0.1 mm below $th1^2$, and its aperture is ca. 0.15-0.23 mm wide. The upward-grown portion of $th1^1$ is 0.63-0.75 mm long. The proximal end is bluntly rounded and slightly asymmetrical. Thecae are strongly

geniculate. The apertural excavations are slit-like (<0.1 mm tall) and inclined, and occupy ca. 1/4-1/3 of the width of the rhabdosome. The supragenicular walls are straight to moderately convex, ca. 0.6 mm long, and sometimes slightly inward sloping. The virgella is short and thin. The nema is extremely thin (ca. 0.03 mm) and up to 3.6 mm long. There is a complete median septum with angled undulation.

Remarks: The present specimens come from two consecutive samples, separated by a meter, both from the upper *acuminatus* Zone. The lower collection is consistently slightly narrower, with a slightly higher thecal spacing (see Fig. 6.58). Given that the populations are stratigraphically close, do not overlap temporally, and are similar in all other ways, they are assumed to be a single evolving lineage, rather than two species. *Metaclimacograptus pictus*, which is recorded at from the *acuminatus* Zone of Uzbekistan (Koren' and Melchin, 2000), Wangjiawan, China (Fan et al., in prep.), and Kazakhstan (Koren' et al., 1980), differs from the present material in possessing a more tapered proximal end and a lower proximal 2TRD (ca. 1 mm). Bulman and Rickards (1968) provided a detailed description of a large population of minute metaclimacograptids that they wrongly identified as *Metaclimacograptus hughesi.* This error was corrected by Zalasiewicz (1996), who erected *Metaclimacograptus slalom* to accommodate them; the present upper population and some of the lower population reach a higher maximum width than *M. slalom*. Loydell (2007) provided a detailed discussion of *M. hughesi,* noting that in addition to being larger than species like *M. slalom, M. hughesi* has an angled, rather than wavy median septum. Comparison of

species of *Metaclimacograptus* is somewhat complicated by the fact that much of the European reference material is in partial or complete relief. As well, the diagnostic median septum is often not clearly preserved, especially in compressed specimens. The present specimens, even though compressed, are less robust than some previous descriptions, e.g., 1-1.25 mm maximum width in Štorch and Massa (2006) and 1-1.2 mm in Loydell (2007), but the upper population (max=0.9-1 mm) is consistent with those of Churkin and Carter (1970), ca. 1 mm, and Koren' and Rickards (1996), 0.8-1.0 mm (in low relief). The median septum is unclear on most of the present specimens, but is clearly angular on several specimens. *M. hughesi* has a long stratigraphical range: from the *vesiculosus* Zone (Koren and Rickards, 1996) to the *sedgwickii* Zone (Štorch and Massa, 2006). The present collections slightly extend its range to include the uppermost *acuminatus* Zone.

***Metaclimacograptus*? sp.**

Plates: (Photos) 51.1-3, 51.23, 57.16

Material and stratigraphical range: Lower *ascensus* Zone. 8 specimens measured, mostly juvenile, plus several more poorly preserved specimens.

Description. Parallel-sided rhabdosome up to 7.5 mm in length. The proximal end is blunt and asymmetrical. $Th1^1$ turns up sharply 0.1-0.25 mm below the sicular aperture, and grows nearly parallel to the rhabdosomal axis; its upward-grown portion is 0.8-1.05 mm long. DVW at th1 is 0.7-0.85 mm, expanding only 0.05-0.8 mm in the two specimens with multiple thecae. 2TRD is 1.75-1.95 mm at $th1^1$ and 1.85-2 mm at $th3^1$. Thecae are sharply geniculate, with straight suprageniculare walls. The thecal apertures are narrow

(ca. 0.1 mm) and moderately to strongly introverted. A short virgella is present, which bifurcates basally on three specimens. Only two specimens possess more than two thecal pairs. Both possess a robust, distally projecting nema, 0.2 mm wide and >3 mm and >10 mm in length, in specimens 4.3 mm and 7.5 mm in length, respectively. Four well-preserved juvenile specimens, all less than two full thecal pairs in length, possess what appears to be a sicula 3.5-4.4 mm in length (3=4.4 m, 1=3.5 mm). It is possible that the apparent length of the sicula is enhanced by a nematularium or other structure growing along the sicula, but in one specimen that possesses only $th1^1$ completely formed it is 4.4 mm long, suggesting that it is unenhanced.

Remarks: These specimens resemble *Metaclimacograptus* in possessing a bluntly rounded proximal end, narrow, inverted apertures (see Plate 51.23), and a nearly parallel-sided rhabdosome. They do not possess convex supragenicular walls as is characteristic of many species in the genus, and their internal structure is not clear, however. Because of this, and the odd combination of an apparently extremely long sicula and bifurcating virgella, they are only questionably assigned to the genus. They resemble *Normalograptus angustus* in width and thecal spacing, but differ in possessing a prominent distal lying projecting nema, a more rounded proximal end, and narrower, inverted thecae. They differ from the younger *Metaclimacograptus hughesi* in possessing more widely spaced thecae, a robust distally projecting nema in mature specimens, and a long sicula or combined sicula/nematularium structure in juvenile specimens.

Family *incertae sedis*

Genus HIRSUTOGRAPTUS Koren' and Rickards, 1996, emended Melchin et al., 2011.

Type species: *Hirsutograptus longispinosus* Koren' and Rickards, 1996

***Hirsutograptus comantis* (Chaletzkaya, 1960)**

Plates: (Photos) 52.9-12; 52.14?, 52.16, 53.12

Material and stratigraphical range: Abundant from the lower *acuminatus* Zone, and questionably from the upper-mid *acuminatus* Zone, 10 specimens measured in detail; additional isolated material from Arctic Canada examined but not illustrated, including 57 measured proximal and distal fragments.

Description: Fusiform rhabdosome up to at least 17 mm long. The Yukon specimens expand from 0.8-0.9 mm at th1 to a maximum width of 1.4-1.8 mm mesially (most commonly ca. 1.5 mm), usually at th5-th7, after which width decreases distally. 2TRD is 1.15-1.3 (n=3) at $th1^1$ and 1.55-1.7 mm by $th5^1$. DVW of the Arctic material is 0.6-0.8 mm at th1, 0.6-1 mm at th2, 0.8-1 mm at th3, with a distal maximum width of 1.05-1.35 mm. 2TRD is 1.30-1.60 mm proximally 1.55-2.00 mm distally. In the Arctic material, the length of the sicula is ca. 1.60 mm, and the aperture is 0.19 mm wide. Thecae are climacograptid, with sharp geniculae furnished with paired laterally and ventrally projecting spines, plus additional genicular or—rarely—apertural spines; the spines may bifurcate. The sicula is exposed below $th1^2$ for 0.2-0.35 mm. Semi-circular apertural excavations occupy ¼ of dorsal-ventral width. The virgella is up to at least 1.15 mm, and commonly bi- or trifurcates basally or distally. Antivirgellar spines are also present,

bringing the total number of basal spines from 3 to at least 7 (6 are commonly preserved in the Yukon material). In the Arctic material, genicular spines are mostly ca. 0.50 mm long, but rarely to 1.5 mm, and decrease in both number and size distally. In the Yukon material, spines are of near uniform length along the rhabdosome, and are up to 2 mm in length, but always at least 1 mm. Supragenicular walls are straight and interthecal septa straight and parallel to the rhabdosome axis. A full median septum is present.

Remarks: The Yukon material is preserved in a manner that makes illustration and measurement difficult. Details are visible only for a few seconds after a slab is wetted, but before it has completely dried. As a result, despite many hundreds of specimens existing in the sample, minimal detailed metrical data were collected. The isolated Arctic material allowed details of the structure and growth of the spines to be examined closely. Both light and infrared microscopy were used. Spines grow as an extension of the genicular hoods, which expand first laterally to produce two incipient spines, and then ventrally to a point that differentiates into one or more additional spines. In the isolated material, average spinosity increased with astogeny, but was also highly variable, both along an individual rhabdosome and between individuals, with some specimens possessing multiple spines on one theca, and no spines at all on neighboring thecae. Rare and perhaps immature specimens with normal sicular spinosity possessed no genicular spines and most distal thecae showed only incipient spine growth. In the Yukon material, spinosity is more uniformly developed, with all thecae possessing

robust spines at all stages of development, but in most cases all but the lateral spines are buried, so comparison of the order and rate of development is difficult. However, the common number and position of the spines (two lateral and two ventral spines per theca, sometimes with additional spines), is clear in specimens preserved in cross-section (see Plate 52.10 and 52.16). The material from Arctic Canada and the Yukon agrees well with material from China described by Fan et al. (in prep.), except for greater maximum widths and thecal spacing in the Yukon material. In these features, the Yukon material matches *Hirsutograptus villosus* Koren' and Rickards. Given the similarity in all other features, and the large degree of overlap in measurements, all of the Canadian material is assigned to *H. comantis,* with *H. villosus* considered a likely synonym.

***Hirsutograptus jinyangensis* (Ye) *in* Geological Institute of Southwest China, 1978**

Plates: (Photos) 47.11, 52.3, 53.17-19, 53.23

Material and stratigraphical range: Numerous poorly to moderately preserved specimens from the upper *ascensus* Zone in the Blackstone River, plus additional isolated and flattened material from the *acuminatus* Zone, Cornwallis Island, Canadian Arctic Islands; measurements are from from the Arctic Canada specimens: >150 isolated proximal and distal fragments, plus 11 flattened specimens.

Description: Rhabdosome septate (complete median septum after th3^2) and more than 12 mm long. Thecae are climacograptid, with semi-circular excavations occupying ca. 1/3 of dorsal-ventral width. Supragenicular walls are straight to concave. Apertures are moderately everted proximally. Thecae have sharp geniculae with pronounced

genicular hoods on all but the first thecal pair. Hoods extend 0.08-0.15 mm ventrally and wrap laterally around the rhabdosome up to 1/2-2/3 of dorsal-ventral width. A small flange, 0.05 mm wide, is present on the geniculum of theca 1^2. Dorso-ventral width at first thecal pair 0.65 -0.95 mm, 0.68- 1.08 at the second, 0.85-1.10 mm at third, and 1.05-1.15 mm at fifth. Maximum width is 1.05-1.40 mm (rarely 0.95-1.0 mm). Proximal 2TRD is 1.2-1.45 mm (rarely <1.2 mm) and distal 2TRD 1.25-1.8 mm, but most commonly ca. 1.5 mm. The length of the sicula is 1.60-1.87 mm. The width of the sicular aperture is 0.19-0.24 mm. The sicula is exposed below $th1^2$ for 0.28-0.45 mm. The virgella is 0.30-0.65 mm long (rarely to 0.9 mm.)

Remarks: The numerous Blackstone River specimens match the Arctic Canada material closely, with a maximum and average distal width of ca. 1.4 mm and 1.25 mm respectively, and distinctive "wrap-around" hoods and a $th1^2$ flange (see Plates 53.23, 47.11, and 52.3), but are difficult to measure in detail and illustrate, due to preservation, so detailed measurements are provided from the Arctic material. The type material has a maximum width of 1.4 mm, excluding hoods, which is in keeping with the upper end of variation in the Blackstone and Arctic material. The types have not been examined in person, but Ye's illustrations clearly show the wrap-around hoods and plate 174, fig. 18b appears to show a flange on $th1^2$. Fan et al. (in prep.) describe a new species that is similar to *H. jinyangensis*, but has a lesser maximum width (1.1 mm, excluding flanges), as well as possessing a secondary basal spine. From the illustration, the structure of the hoods in this species seems to be similar to those in *Hirsutograptus*?

sp., i.e., an expanded and flared aperture, rather than a hood that extends beyond the aperture. The material assigned here to *H. jinyangensis* differs from *Hirsutograptus*? sp. in having lesser distal width, the possession of a flange on th1[2], a more uniform, rather than tapered appearance, a shorter virgella, and most importantly, in possessing hoods that leave the aperture and proceed laterally around the rhabdosome (see Plate 47.10 vs. 47.11). Species of *Talacastograptus* (Cuerda et al., 1988) are readily distinguished from *H. jinyangensis* by their possession of zig-zag lists connected to an undulating median septum and more hook-like hoods.

***Hirsutograptus longispinosus* Koren' and Rickards, 1996**

Plates: (Photos) 52.6-7; (Line drawings) 40.16

Material and stratigraphical range: A single specimen from the mid-*acuminatus* Zone.

Description: The rhabdosome expands from 0.8 mm at th1, to 1.05 mm at th3, and 1.2 mm at th5, with a distal maximum reached beyond th10 of ca. 1.4 mm. 2TRD is 1.9 mm at th1, increasing to ca. 2.1 mm distally. Thecae are climacograptid, with thickened apertures, which expand into a single, robust, downward-curving genicular spine, 0.5 mm in length, which is present on all thecae, except the first pair. The virgella bifurcates at its base, and there is a single anti-virgellar spine present, 1 mm in length.

Remarks: The single robust spine on each thecae on this specimen emerges ventrally from the geniculum (the middle), whereas other spinose species of *Hirsutograptus* have either exclusively lateral genicular spines or lateral spines that develop in concert with ventral spines. The present specimen, agrees very well with the previous descriptions in terms of the number of spines, as well as in the robustness and curvature of the spines

(see Plate 52.7). It has a lesser maximum distal width than the type collection, but most of those specimens were preserved off-profile, which can exaggerate apparent width. Thecal spacing is similar to the types of *H. longispinosus*.

Hirsutograptus sinitzini **(Chaletzkaya, 1960)**

Plates: (Photos) 52.8, 52.13?, 52.15, 52.17-18, 53.11, 53.13?

Material and stratigraphical range: Rare or common(?) from the lower *acuminatus* Zone.

Remarks: Rare examples of specimens in scalariform view appear to have only a single pair of laterally projecting spines on each thecae (see Plate 53.11 and a higher magnification image of that same specimen in 52.8). Additional, more common, specimens in profile appear to have only two spines per thecae, and these specimens also show lower sicular spinosity, a lower maximum width (0.9-ca. 1.25 mm) and a more uniform width, rather than fusiform, rhabdosome. In possessing a low DVW, they match material described by Koren' and Melchin (2000) and Fan et al. (in prep.). Given both the high degree of variability seen within the Arctic collections in spinosity, as well as the strong influence of preservation on apparent spinosity, it is possible that the present specimens of *H. sinitzini* are actually *H. comantis.* For example, in the scalariform specimens possessing two spines, it is possible that ventral spines were actually present, but projected into the overlying or underlying sediment, and are thus not preserved along the bedding surface. No cross sections of specimens exist in the present collection that possess less than four spines per thecae.

Hirsutograptus tuberculatus **(Nicholson, 1869)**

Plates: (Photos) 48.23-25; (Line drawings) 43.1-2, 43.4-5

Material: Uncommon poorly to moderately preserved material from the upper *ascensus* Zone. Twelve specimens measured.

Description: Rhabdosome up to 15 mm long. Expands from 0.75-0.88 mm at th1, to 0.95-0.1 mm at th3, 1.03-1.18 mm at th5, 1.23-1.33 at th7, and 1.35-1.5 mm at th10, which is maintained or slightly exceeded distally. (Maximum recorded width is 1.55 mm, excluding hoods.) Thecal spacing is relatively consistent throughout the rhabdosome: 1.35-1.5 mm at th1^{1}, 1.45-1.5 mm at th3^{1} (n=3), and ca. 1.5-1.6 mm in the few distal measurements available. The sicula is ca. 2.1-2.3 mm long. The upward-grown portion of 1^{1} is 0.6-0.9 mm (n=5). The virgella trifurcates basally (two specimens appear to have four or five basal spines), and the resulting spines are 1-1.6 mm long. Thecae are climacograptid, with relatively straight suprageniculars walls, and thickened apertural rims and a prominent flange or hood that expands from the geniculum, but is confined to the apertural margin. There is a complete median septum. A thin nema 0.08-0.13 mm wide extends up to 6 mm distally (n=4).

Remarks: The type specimens of this species are deformed, but the present specimens agree in overall characters. These specimens also agree with material assigned to *Climacograptus spinosus* by Fang et al. (1990), and placed in synonymy with *H. tuberculatus* in Fan et al. (in prep.), except that the latter report somewhat higher maximum widths, and may have less robust hoods (although this is difficult to tell from the illustrations). Due to hoods obscuring the apertures, the measurements above in

most cases only involve six or fewer data points, despite being based on twelve specimens, and therefore likely to do not capture the full range of variation. This species occurs only in two samples, and only on a small number of slabs. In one sample, however, it is numerous on the slabs on which it occurs, with a considerable amount of fragmentary material present, but no evidence of current alignment. The presence of multiple proximal spines and prominent genicular hoods distinguishes this species from other contemporaries. When its proximal end is missing, this species resembles *Hirsutograptus* sp. and *Hirsutograptus jinyangensis.* Isolated proximal ends could be confused with other species of *Hirsutograptus* or *Normalograptus anjiensis*.

***Hirsutograptus* sp.**

Plates: (Photos) 44.17, 47.10, 52.4-5, 53.1-10, 53.14, 54.20?, 54.30; (Line drawings) 43.3, 43.7

Material and stratigraphical range: Rare from the uppermost *ascensus* through to upper-mid *acuminatus* zones. Eight specimens measured in detail, plus additional comparative material from the *acuminatus* Zone of Cornwallis Island, Canadian Arctic, and Dob's Linn, Scotland.

Description: Robust, tapered rhabdosome, up to 20 mm in length. Expands from 0.8-0.9 mm at th1, to 1.03-1.2 at th3, 1.3-1.55 mm at th5, 1.45-1.6 mm at th7, 1.45-1.7 mm at th10, with distal maximum of 1.45-1.8 mm. 2TRD is 1.55-1.7 mm at th1^1 and ca. 1.6-1.85 mm distally. Th1^1 turns up just below the sicular aperture and its upward-grown portion is 0.75-0.9 mm. The thecae are geniculate, with straight supragenicular walls. The thecal apertures are strongly thickened throughout, and develop into ventrally and laterally

projecting genicular hoods, especially distally, which pinch mesially towards the aperture. The lower portion of the aperture is also thickened, and flared, resulting in the aperture becoming constricted distally in some specimens (see Plate 47.10, 53.4, and 53.6), although this varies along the rhabdosome and between specimens. A complete median septum is present from at least the 3rd thecal pair. A robust virgella, up to 2 mm long, is present. The nema projects distally in many specimens, up to 5 mm.

Remarks: This species is superficially similar to the specimens assigned here to *Hirsutograptus jinyangensis,* in that the apertures are adorned with prominent genicular flanges, however in the former the hood extends laterally beyond the aperture, whereas in the latter the rim of the aperture itself is flared laterally. The difference is clear in Plate 47.10-47.11—see also Plate 54.30. *Hirsutograptus* sp. also lacks a flange on th1^2, a feature that is present on *H. jinyangensis,* has a greater distal width, a more tapered rhabdosome, and often a robust virgella. The specimens illustrated by Melchin (1987b) as *Paraclimacograptus jinyangensis* (text-fig. 7, N, O, Q, and R) seem to have a thecal form like *Hirsutograptus* sp., but one specimen (7Q) has a flange on th1^2 (this specimen is also illustrated in Melchin, 1989), and all specimens seem less tapered than the present material. Some of the material assigned by Fan et al. (in prep.) to *H. jinyangensis* appear as if they may belong to the present species. The illustrations are unclear, but the material assigned by Fang et al. (1990) to *Orthograptus insectiformis* may also be the present species (see flared apertures in plate 18.5 and 21.14). Regardless of the attribution of the material from Melchin's thesis, *Hirsutograptus* sp. occurs in Arctic

Canada in the *acuminatus* Zone (pers. observation; see material illustrated in Plate 53.9-10, 47.10, and 52.4-5). A single specimen was also recovered from the upper *acuminatus* Zone of the Linn Branch trench, Dobs Linn, Scotland during fieldwork conducted as part of this thesis (Plate 53.5). *Hirsutograptus tuberculatus* is similar to the *Hirsutograptus* sp., but possesses multiple proximal spines.

Genus *SONGXIGRAPTUS* Fang et al., 1990

Type species *Songxigraptus elongatus* Fang et al., 1990

"Songxigraptus elongatus" Fang et al., 1990

Plates: (Photos) 48.5, 53.15-16

Material and stratigraphical range: Rare from the lowest *ascensus* Zone and questionably from the lowest *accuminatus* Zone. 10 specimens examined.

Description: Rapidly expands from ca. 1 mm proximally to a maximum of up to ca. 3 mm mesially and then tapers distally. Most aspects of the rhabdosome, including thecal form and internal structure are unclear.

Remarks: This material perfectly matches the type material, and occurs at an equivalent stratigraphic level. All of the present material is poorly preserved, as is the type material, and details of thecal form and internal structure are difficult to determine. The specimens do appear to possess flared, "hooked-shaped" thecae, as described by Fang et al. (1990). However, the specimens co-occur with abundant specimens of *Paramplexograptus kiliani,* which are similar in dimensions and possess highly variable genicular hoods. It is possible that these specimens are actually examples of *P. kiliani*

with highly enlarged hoods, which have been flattened so that the hoods partially cover the aperture, creating the illusion of a novel thecal form (the relatively thin material with thickened rims is more consistent with hoods than thecae). Based on the present material, this genus and species are considered questionable, but better-preserved material is necessary to determine definitively. Given the uncertainty on proximal development and internal structure, assigning this genus confidently to a family is impossible. Its placement here with *Hirsutograptus* is based on their shared apertural elaboration. An ambiguous specimen occurs the basal *acuminatus* Zone that may belong either to this species or to *Hirtsutograptus* sp. (Plate 53.20).

Superfamily RETIOLITOIDEA Lapworth, 1873, emended Melchin et al., 2011

Paraphyletic Family NEODIPLOGRAPTIDAE Melchin et al., 2011

Genus *METABOLOGRAPTUS* Obut and Sennikov, 1985, emended Melchin et al., 2011

Type species. *Diplograptus modestus sibericus* Obut 1955.

***Metabolograptus parvulus* (Lapworth, 1900)**

Plates: (Photos) 35.8-11, 35.13, 35.14?, 35.15-16, 35.18-22, 37.12?, 37.21;

(Line drawing) 28.17

Material: Uncommon from the lowest *persculptus* Zone collections (=lowest part of the upper *persculptus* Zone), flattened or with partial relief, mostly fragmentary. 9 specimens measured.

Description: Rhabdosome up to at least 19.5 mm long. Progressively expands from 0.75-0.9 mm at th1, 0.93-1.15 mm at th3, 1.15-1.28 mm at th5, 1.25-1.5 mm at th7, 1.45-1.6

mm at th10, and reaching a maximum width distally in very mature specimens of ca. 1.7-1.8 mm. 2TRD is 1.3-1.53 at th1[1], 1.65-1.75 mm at th5[1], and 1.75-1.9 mm distally. The thecae are gently inclined, with slightly rounded geniculae. The median septum is complete, prominent, and sinuous, and interthecal septa are doubly sigmoidal. A short virgella is preserved on a few specimens.

Remarks: These specimens agree well with Chinese (Chen et al., 2005a) and Scottish specimens (Williams, 1983: as *Glyptograptus* cf. *persculptus*). In both China and in the present samples, they co-occur with material that Chen et al. (2005a) assigned incorrectly to *Avitograptus avitus*, and which is assigned to *Normalograptus*? sp. 1 here. At the Blackstone River, *M. parvulus* is very often preserved in partial relief, with very clear internal structure, which makes it easy to distinguish from most other species in this collection. Some specimens not preserved in this manner, but which co-occur with specimens that are, are only tentatively assigned to *M. parvulus*, e.g., Plate 35.14. *M. parvulus* can be distinguished from *N.*? *transgrediens* by its more rounded proximal end, more inclined, and less sharply geniculate thecae, and sigmoidal, rather than straight, interthecal septae. Some specimens are ambiguous, however. For example, compare Plate 35.17 (assigned to *N.*? *transgrediens*) with the overlapping specimens illustrated as 35.15 and 35.16; in contrast see Plate 34.17 and Plate 35.21 for clear examples of the two species. *M. parvulus* can be distinguished from *Metabolograptus persculptus* by its lesser distal width. *Korenograptus laciniosus* is nearly parallel-sided, and its thecae have shorter supragenicular walls, and often appear strongly rounded to nearly orthograptid,

when compressed. *K. lungmaensis* possesses a greater distal width and more strongly rounded thecae. A well-preserved, but somewhat anomalous specimen, with a parallel-sided rhabdosome and low 2TRD, which does not match perfectly with any species in the collection, is included questionably in *M. parvulus* (Plate 37.12).

***Metabolograptus persculptus* (Elles and Wood, 1907)**

Plates: (Line drawing) 28.15

Material and stratigraphical range: Very rare material from the lowest *persculptus* Zone collections (=upper *persculptus* Zone), flattened or with partial relief, mostly fragmentary. 6 specimens measured (some only questionably assigned to *M. persculptus*).

Description: Width increases from ca. 0.85 mm proximally to ca. 2 mm distally. 2TRD is ca. 2 mm distally. Thecae possess bluntly rounded geniculae, with sigmoidal interthecal septa. The median septum is prominent and undulose. The virgella is short and blunt.

Remarks: The few specimens present are mostly fragmentary and are difficult to see and illustrate. They possess the characteristic thecal form of *M. persculptus,* which is shared with *M. parvulus,* but fall outside of the maximum range for *M. parvulus.* In the present collections, both *M. parvulus* and *M. persculptus* are notable in that they are often preserved with partial relief and with the median septum and interthecal septa clearly visible.

***Metabolograptus*? sp.**

Plates: (Photos) 33.14-17, 34.10-12, 35.23-26, 37.15-17; (Line drawings) 27.10-11

Material and stratigraphical range: Abundant from the uppermost *persculptus* Zone and questionably from adjacent strata. 26 specimens measured in detail, hundreds more examined.

Description: Rhabdosome up to at least 20 mm in length. Expands from 0.7-0.9 mm at th1, to 0.8-1.13 mm at th3 (mostly >1 mm), 1.13-1.45 mm at th5, 1.15-1.45 mm at th7, 1.28-1.53 mm at th10 (1=1.18 mm), and 1.23-1.45 mm at th15 (n=3). Distal maximum is up 1.55 mm. 2TRD is 1.3-1.5 mm at $th1^1$, 1.45-1.7 mm at $th3^1$, 1.5-1.8 mm at $th5^1$, 1.6-1.9 mm at $th7^1$ and beyond. The upward-grown portion of $th1^1$ is 0.75-1 mm in length. Thecae are climacograptid proximally, with sharp geniculae, and semicircular, sometimes slightly thickened apertures, and straight to slightly inclined supragenicular walls. Distally, the thecae become more strongly inclined, the apertures larger and more open, and the infragenicular walls more angled, with the effect that upon compression distal thecae can appear nearly orthograptid; geniculation is present throughout, however. A long, but non-expanding distally projecting nema, up to 6 mm in length, and stout virgella, are present on many specimens. A full median septum is present at least distally.

Remarks: These specimens resemble the types of *Glyptograptus xiushuiensis* Fang et al. (1990), which co-occur with similar taxa, especially the specimen they illustrated in plate 6.5. *G. xiushuiensis*, is reported to have glyptograptid thecae throughout, but the geniculae appear to remain sharp distally in the illustrations. They also resemble the much younger *Glyptograptus tangshanensis*. *Normalograptus*? *nanjinginensis* has

inclined thecae and similar dimensions. The holotype is lost, but examination of drawings (Melchin, unpublished) of paratype material illustrated by Chen and Lin (1978), as well as specimens illustrated by Fang et al. (1990) and a specimen illustrated by Li (1995), show that the species differs from the present material generally in being more tapered and possessing consistently semi-circular, rather than wedge-shaped apertural openings, and in lacking the tendency to towards a biform appearance distally. Otherwise very similar specimens from the basal *acuminatus* Zone (here *N.*? aff. *nanjingensis*—see Plate 49.4-7) differ from the present material in possessing thickened apertures throughout and closer thecal spacing (Fig. 6.60). In several instances, multiple individuals of *M.*? sp. are aggregated into "synrhabdosome" clusters, a characteristic not seen in other species in this collection. Specimens assigned to *N.*? aff. *mirnyensis* have a generally lower distal width (Fig. 6.54) and more inclined thecae, with more open apertures, and tend to take on a biform appearance when flattened. The species is only questionably assigned to *Metabolograptus*, as the internal structure, in particular the presence of characteristic undulose median septum and sigmoidal interthecal septa cannot be determined.

Genus *NEODIPLOGRAPTUS* Legrand, 1987, emended Melchin et al., 2011

Type species. *Diplograptus magnus* (Lapworth 1900).

***Neodiplograptus clavatus* (Yu et al., 1988)**

Plates: (Photos) 30.1-5, 30.32, 33.1-2, 33.18, 34.13, 36.3?, 36.14-15, 38.7;

(Line drawings) 27.3?, 27.15, 27.20-21

Material and stratigraphical range: Numerous specimens from the upper *persculptus* Zone (lower three collections). 23 specimens measured in detail.

Description: Nearly parallel-sided rhabdosome, up to at least 13 mm long. Expands from 0.85-1.13 mm at th1, to 1.25-1.6 mm at th3, 1.5-2 mm at th5, with a maximum width of 1.6-2.05 mm reached between th5 and th10 (1=2.25 mm). Many specimens decrease slightly in width distally. 2TRD is consistent along the rhabdosome: 1.25-1.45 mm at $th1^1$ (1=1.55 mm), 1.4-1.65 mm at $th3^1$ (1=1.95 mm) and between 1.4-1.7 mm distally (1=2.2 mm). Proximal and mesial thecae are strongly geniculate, and slightly inclined, with short supragenicular walls and slightly everted apertures. Thecae become more inclined, with weaker geniculae in some specimens at about th10. The proximal end is wedge-shaped and somewhat asymmetrical ($th1^2$ more inclined), but both initial thecae are at low angles relative to the rhabdosomal axis. The upward-grown portion of $th1^1$ is 0.7-0.88 mm long. A short virgella is present, as is a thin distally extending nema. A complete median septum appears to be present.

Remarks: This material resembles larger species of *Paramplexograptus* in general rhabdosomal and thecal form*,* and proximally its dimensions are close to those of *Paramplexograptus wuningensis* (although it has a higher overall 2TRD than the latter). It differs from species *Paramplexograptus,* however, in lacking apertural flanges. Despite a large number of specimens, the internal structure is very difficult to see because of the thick rhabdosomal walls of this species, but it also appears to possess a median septum, which is lacking in *Paramplexograptus*: the nema is consistently straight and centrally

located internally, and hints of a median septum can also be seen in several specimens, e.g., see Plate 36.14. The present collection matches the type description of *Neodiplograptus clavatus* very closely in both dimensions and morphology. In particular, Yu et al. (1988) highlight everted apertures, "climacograptid" thecae for the first 7 to 10 pairs, and a nearly parallel-sided rhabdosome, all features present in this collection. Chen et al. (2005) suggested that *Neo. clavatus* might be a junior synonym for *Neo. shanchongensis,* but in addition to having a greater width and lower thecal spacing (see Figs. 6.61-6.64), *Neo. shanchongensis* differs in possessing a consistently fusiform rhabdosome and more inclined thecae. Specimens of *Neo. clavatus* described by Fang *et al.* (1990) also closely agree with the present material, including the exact same range of distal widths (1.6-2.0 mm), but possess a lower minimum proximal width (0.6-0.9 mm). One specimen that matches *Neo. clavatus* in thecal form, but expands slightly more rapidly, reaches a greater distal width, and has slightly higher thecal spacing is questionably included (see Plate 36.3). In addition to the material described above, a collection of material is questionably referred to *Neo. clavatus* (see *Neo.* cf. *clavatus* on Plates 30.10-11, 33.19, 33.21, 37.18, 38.13-15, 38.17-20, 38.22-25, 38.29, 38.31, 27.6-7). These specimens differ from the majority of specimens of *Neo. clavatus* in widening less rapidly and in possessing a lesser average distal width. They resemble proximal specimens of *K. jiangxiensis ,* but have a more parallel-sided outline and less inclined and more closer spaced thecae. They differ from *M.*? sp.1 in widening more rapidly. This

material was originally assigned to *Korenograptus jerini* Koren and Melchin and may in fact represent that species..

***Neodiplograptus shanchongensis* (Li, 1984)**

Plates: (Photos) 30.12, 30.20-21, 30.29-31, 30.33, 33.5-7, 36.7-11, 36.13;

(Line drawings) 27.16, 27.19

Material and stratigraphical range: Numerous specimens from the upper *persculptus* Zone. 25 measured in detail.

Description: Robust, distally tapering rhabdosome up to 13 mm long, but usually less than 10 mm. The rhabdosome rapidly expands from 1.05-1.15 mm at th1, to 1.63-2.25 at th3, 2.1-2.6 mm at th5, and a maximum width of 2.4-2.95 mm, which is usually reached by th5-th7, after which width decreases. 2TRD is low throughout: 1.1-1.45 mm at th1 (mostly <1.2 mm), 1.05-1.5 mm at th3, 1.25-1.6 mm at th5, with a distal maximum of 1.5-1.7 mm. The upward-grown portion of $th1^1$ is 0.7-1 mm. The initial thecae are sharply geniculate, with very short, inclined supragenicular walls. Thecal inclination increases markedly mesially, with later thecae appearing nearly orthograptid, although at least a rounded geniculum in present on all thecae. A very short nema extends distally in a few specimens, but in most cases the virgella and distally extending nema are missing or minute.

Remarks: These specimens agree very well with the type description and with additional Chinese material described by Chen et al. (2005a), as well as specimens described from Jordan by Loydell (2007), differing only in a somewhat higher maximum width (2.2-26 mm, 2.3-2.5 mm, and 2.25-2.3 mm in the three papers, respectively), a fact likely

explained by the much larger collection in the present study, which more completely captures greater natural variation. Chen et al. (2005a) suggested that the smaller *Diplograptus clavatus* Yu et al. might represent an end member variant of *Neo. shanchongensis*, but in the relatively large present collection also has a consistently greater maximum width than *Neo. clavatus* (Figs. 6.61-6.64). *Dipograptus ovatus* Fang et al. (1990) appears to fall into the range of variation for the present material in terms of width and ovoid rhabdosome form, and may be a junior synonym of *Neo. shanchongensis*. *Neo. shanchongensis* can be distinguished from all other species of *Neodiplograptus* in this collection by its rapid rate of widening, low 2TRD, and tendency to taper distally (Figs. 6.61-6.64). The type and other confidently constrained material (see discussion in Chen et al., 2005) is from the Hirnantian. Loydell (2007) described one Jordanian specimen from the *persculptus* Zone and another that co-occurs with *A. ascensus,* and assigned material from the *acuminatus* Zone of Belgium questionably to the species. At the Blackstone River, *Neo. shanchongensis* is restricted to the *persculptus* Zone, and is absent from the uppermost *persculptus* samples. Additional material is common in a sample from the Blackstone River section that lost its label in transport from the field. Given the abundance of *P.* aff. *madernii* present in this collection, it is likely from very close to the 34.11 m sample. Some specimens in this sample (see Plate 36.8-11 and 36.13) are in excess of 3 mm in width and in excess of 22 mm in length. They also widen slightly less rapidly than is average for *Neo. shangchongensis* specimens from samples with known meterage. Given their length, width, and generally fusiform

shape, these specimens resemble *Neo. lanceolatus,* which is common from the lowest Rhuddanian in Europe; however, the distal 2TRD is consistently higher in the large described type collection of *Neo. lanceolatus* (only rarely as low as 12 thecae in 10 mm, and normally 10-11 thecae in 10 mm), and maximum width is somewhat higher, than the present material. As such, all of the present material is assigned to *Neo. shanchongensis*. Only measurements from specimens from the samples with known meterage are included in the description section above.

***Neodiplograptus xixiangensis* (Yu et al., 1988)**

Plates: (Photos) 30.22-23, 33.3-4, 33.8, 33.10-13, 38.6

Material: Common from the upper *persculptus* Zone. 26 specimens measured in detail.

Description: Robust rhabdosome up to at least 20 mm in length. Expands steadily from 0.9-1.25 mm at th1, to 1.3-1.7 mm at th3 (mostly 1.4-1.6 mm), 1.6-1.95 mm at th5, 1.9-2.1 mm at th7, and 1.95-2.25 at th10. A maximum distal width (2-2.4 mm) is reached by th7 to th10 in most specimens, often only maintained for a few thecal pairs, before tapering distally, although a few specimens continue to expand slowly. Thecal spacing is 1.1-1.6 mm (mostly in the middle of that range) at th1[1] and increases marginally to a maximum of 1.4-1.75 at th10. Thecal are strongly geniculate and moderately inclined proximally, with thecal inclination increasing and geniculation decreasing progressively. Distal thecae are strongly inclined, with everted apertures, and appear distinctly triangular when compressed, creating a strong contrast with the proximal thecae. A

geniculum is retained throughout the rhabdosome, however. The virgella is minute and a distally extending nema is rarely preserved. A full median septum is present.

Remarks: These specimens closely resemble the type material in thecal form and overall rhabdosomal outline. For example, compare the specimens in Plate 33.8, P33.11, and especially 33.13 with the holotype (Yu et al., 1988, plate IV, fig. 4). *Neodiplograptus elacatus* (Yu et al., 1988), erected at the same time as *Neo. xixiangensis*, is also similar to the present material. Yu et al. distinguished *Neo. elacatus* from *Neo. xixiangensis* by the latter's tendency to reach its widest point distally, rather than more mesially, and its higher thecal spacing. Both these features agree with the present specimens; however, they are both also variable. The present specimens of *Neo. xixiangensis* can be easily distinguished from the co-occurring *Neo. shanchongensis* by their much more gradual rate of widening (see Figs. 6.61-6.62), lesser average distal width (Fig. 6.63), and longer and more inclined, wedge-shaped distal thecae. Most other contemporary species of *Neodiplograptus* reach a greater distal width (the present specimens are often only a little over 2 mm, and never greater than 2.6 mm) and/or possess a higher thecal spacing. *Neodiplograptus clavatus* reaches a maximum width of 1.6-2 mm, the upper range of which is consistent with the majority of the present material, and possesses a similar proximal width and tightly spaced thecae as the present specimens, but the average distal width of the two species is very different (Fig. 6.63). Additionally, *Neo. clavatus* possesses climacograptid thecae up to at least the th7, in both the type and present collections.

***Neodiplograptus* sp. 1**

Plates: (Photos) 45.4?, 45.19, 46.1-3, 46.10?, 54.20?-22?

Material and stratigraphical range: Upper *ascensus* and basal *acuminatus* Zone, and questionably throughout the *ascensus* Zone. 13 specimens measured in detail. Many more examined.

Description. Tapered rhabdosome up to at least 47 mm in length. Expands slowly and progressively from 0.8-1 mm at th1, to 1.35-1.5 mm at th3 (1=1 mm), 1.65-1.9 mm at th5, 1.75-2.2 mm at th7, 2.1-2.4 mm at th10, 2.5-3 mm at th15, to a maximum of 2.5-3.3 mm, which sometimes decreases slightly distally. 2TRD is 1.2-1.5 mm at th1^1, 1.35-1.5 mm at th3^1, 1.5-1.7 mm at th5^1, and 2-2.4 mm distally. The upward-grown portion of th1^1 is ca. 0.75 mm. The first five to ten thecae are strongly geniculate and slightly inclined, and then rapidly transition to orthograptid to near orthograptid mesially and distally. Distal thecae are simple tubes, with straight interthecal septa, which overlap about half their length. Distal apertures are everted. A thick nema is visible internally and distally projects in some specimens. When preserved, the virgella is short and robust. A full median septum is present, and is very clearly visible through the periderm in most specimens.

Remarks: This distinctive species dominates the basal *acuminatus* Zone collection. It can be differentiated from other species of *Neodiplograptus* in the collection by its tapered width and combination of low proximal and high distal 2TRD (Figs. 6.64-6.65). A single specimen occurs from the uppermost *ascensus* Zone (40.5 m); only the proximal end is intact, but it widens at a similar rate and has the same thecal form as the *acuminatus*

Zone collections (Plate 45.19). Additional material occurs from the basal (one specimen) and mid *ascensus* Zone that agrees well with the *acuminatus* specimens in possessing a tapered proximal end, relatively late transition in thecal form (ca. th7), long and apparently orthograptid thecae distally, a thin periderm with clearly visible median septum and thick nema, and proximal dimensions. However, the *ascensus* Zone material reaches a lower distal maximum width (consistently ca. 2 mm vs. >2.5 mm). Given the similarity in other characters, the upper and lower collections are grouped, but greater collections may show them to represent different species. The lower *ascensus* Zone material is indicated with question marks in the illustrations.

***Neodiplograptus* sp. 2**

Plates: (Photos) 50.5, 50.11-13, 50.16, 50.18?; (Line drawings) 42.11-12

Material and stratigraphical range: Uncommon from the upper *acuminatus* Zone. Nine specimens measured in detail, several more examined.

Description: Rhabdosome up to at least 25 mm in length (but mostly much shorter). Expands from 0.68-0.78 mm at th1, to 0.95-1.13 mm at th3, 1.23-1.4 mm at th5 (1-1.15 mm), a distal maximum of 1.4-1.5 mm is attained between th7-th10 and is maintained distally. Thecae are relatively closely spaced throughout: 2TRD is 1.2-1.35 mm at $th1^1$ (1=1.55 m), 1.4-1.5 mm at $th3^1$ (1=1.3 mm), 1.5-1.55 mm at $th5^1$ (1=1.7 mm), 1.53-1.7 mm at $th7^1$, and ca, 1.75 mm distally. $Th1^1$ turns upwards just below the sicular aperture (0.1-0.18 mm) and has a short upward-grown portion: 0.55-0.63 mm. The proximal thecae are amplexograptid; after ca. th5-7 the thecae become more inclined, and the geniculae more rounded. This sometimes results in an abrupt apparent shift in thecal

form, e.g., Plate 50.12, but in most modes of preservation the change is less dramatic. Thecal inclination and form is variable with preservation, and they can be gently inclined distally to nearly triangular, sometimes on the same specimen, e.g., Plate 50.16. The lower rim of the thecal aperture is often thickened. A complete median septum is present, and a robust nema runs the length of the rhabdosome, sometimes slightly off-center. The virgella is short, where preserved.

Remarks: These specimens are very similar to *Korenograptus laciniosus,* which occurs in the *persculptus* Zone in this section. The present specimens differ from *K. laciniosus* in possessing a slightly lower width in the first thecal pair (average of 0.85 mm vs. 0.75 mm), possessing thickening along their lower apertural rim, and having a more pronounced change in thecal form mesially. Given the poor preservation in both species, detailed comparison of thecal from is impossible. They resemble *Glyptograptus* aff. *tamariscus* Štorch and Schönlaub (2012) in general form and dimensions, but possess a median septum.

Genus *KORENOGRAPTUS* gen. nov.

Type species. *Glyptograptus gnomus* Churkin and Carter 1970.

***Korenograptus bifurcus* (Ye, 1978)**

Plates: (Photo) 45.13; (Line drawings) 42.1, 42.8

Material and stratigraphical range: Rare from the upper *ascensus* Zone and lowest *acuminatus* Zone. 4 specimens showing bifurcation or incipient virgellar bifurcation measured, several other probable specimens examined.

Description: Rhabdosome up to at least 14 mm long. Widens progressively from a width of 1-1.15 mm at th1 to 1.25-1.45 mm at th3, 1.5-1.8 mm at th5, 1.6-1.9 mm at th7 (n=2) and up to 2.1 mm distally (n=1). 2TRD is 1.33- 1.55 mm at $th1^1$ and increases to ca. 1.8 mm distally (n=1). The thecae are straight and sharply geniculate proximally, and slightly inclined and rounded distally, especially in subscalariform preservation. The proximal end is acuminate. The sicula is ca. 1.8 mm long, and its aperture is ca. 0.25 mm wide. The upward-grown portion of $th1^1$ is 1.08-1.15 mm long. In the largest specimen, the virgella is robust and becomes thickened at 1.25 mm and then bifurcates at 1.75 mm, producing two thin branches at least 5 mm long. In the remaining specimens, the virgella is less robust and bifurcates, producing a short fork, just before terminating (at 4.65 mm, 5.9 mm, and 6.6 mm, respectively). A fifth, immature, specimen does not show evidence of bifurcation, but possesses a thin virgella 7 mm long, which is deflected laterally at ca. 4.5mm, perhaps representing a single preserved portion of a branch. The nema is preserved in only three specimens. In the specimen with a robust bifurcating virgella, it is broken, but 0.5 mm wide proximally. In the other specimens it is only ca. 0.08 mm wide, but up to at least 9 mm long. The median septum appears to be complete.

Remarks: These specimens resemble each other closely in terms of thecal form and the presence of a distally bifurcating virgella, however, the specimen with the clearest bifurcation widens more rapidly and seems to reach a greater maximum width. With so few specimens available, mostly juvenile, it is unclear whether this difference is

significant. The two specimens assigned to *Glyptograptus bifurcus* by Fang et al. (1990), especially their plate 5, fig. 5, seem to show amplexograptid thecae with short, inclined supragenicular walls and sharp geniculae, as is the case with the present specimens. The types have a maximum width of 2-2.1 mm, which also agrees with these specimens. Fang et al. (1990) reported a slightly wider maximum DVW: 2.4-2.5 mm. Measurements taken from Fang et al.'s illustrations are consistent with the largest specimen in this collection, but show a more rapid rate of widening than in the smaller specimens. Specimens assigned to the species by Štorch and Schönlaub (2012) give a considerably higher upper DVW: 2.9-3.5 mm distally. *Korenograptus bifurcus* resembles *Korenograptus bicaudatus,* with the exception that in the latter the virgellar branching begins very close to its base (e.g., see Chen and Lin, 1978; Koren' and Melchin, 2000); note that some of the material described by Fan et al. (in prep.) bifurcates 1.3 mm from the base of the virgella, intermediate between the present material and most illustrated specimens of *K. bicaudatus. Korenograptus bicaudatus* occurs at a similar stratigraphic position in China to the present material, and is considered (Fan et al., in prep.) as a proxy taxon for identification of the *ascensus* Zone. As Štorch and Schönlaub noted (2012), *Koreograptus bifurcus* and *Koreograptus bicaudatus* are two of a large number of species described from China with generally triangular outline and a bifurcating virgella; this group of taxa needs revision. As they lack tapered proximal end and a dramatic shift in thecal form mesially, these specimens are assigned to *Korenograptus,* rather than *Rickardsograptus,* as in Štorch and Schönlaub (2012). The present specimens

resemble those assigned here to to *Koreograptus lanpherei*, but the latter does not possess a bifurcating virgella, and has, on average, higher proximal 2TRD.

***Korenograptus*? *diminutus* (Elles and Wood, 1907)**

Plates: (Photos) 49.9, 49.13?, 49.40, 56.5?, 56.24,

Material and stratigraphical range: Common in the lower to mid? *acuminatus* Zone.

Remarks: With a maximum distal width and 2TRD of ca. 1.5 mm, specimens from 42.83 m match previous descriptions of this species well, including the specimens described from the nearby Peel River section by Lenz and McCracken (1982—reexamined during this thesis) and from Alaska (Churkin and Carter, 1970). The specimens assigned to *Paraclimacograptus obesus* from 44.02 m are similar, but clearly have small flanges, and tend to have shorter supragenicular walls. Some of the specimens assigned here to *Korenograptus*? *diminutus* from 42.83 m, and even more so from 43.5 m, have hints of incipient flanges; it is possible that this collection and the material from 44.02 m represent an evolutionary sequence towards the typical *Paraclimacograptus* material from 46 m and above. A specimen from the basal *acuminatus* Zone collection (41.66 m: Plate 49.13) is similar in general thecal form, but rapidly expands, before strongly tapering, and is only uestionably assigned. The present material is questionably assigned to *Korenograptus* since some of it seems to show genicular thickening or incipient flanges associated with *Paraclimacograptus.* See further discussion in the remarks on *Paraclimacograptus obesus.*

***Korenograptus jiangxiensis* (Fang, Liang, Zhang, and Yu) *in* Fang et al., 1990**

Plates: (Photos) 30.25-26, 33.22-24, 35.27, 36.1, 36.4, 36.6, 36.12, 36.16, 38.16;

(Line drawings) 29.1-3

Material and stratigraphical range: Uncommon from the upper *persculptus* Zone. 14 specimens measured in detail.

Description: Strongly tapered rhabdosome up to at least 20 mm in length. Expands from 0.88-1.08 mm at th1, to 1.1-1.45 mm at th3, 1.35-1.7 mm at th5, 1.55-1.8 mm at th7, 1.6-2.05 mm at th10, and 1.7-2.15 mm at th15 (n=4). Some specimens taper distally. 2TRD is 1.4-1.7 mm at $th1^1$, 1.6-1.85 mm at $th3^1$, 1.65-2 mm at $th5^1$, and 1.75-2.05 mm at $th10^1$. Thecae are consistently gently inclined, with narrow, everted apertures. They are at least weakly geniculate throughout, but appear orthograptid upon compression, especially distally (e.g., see Plate 33.22 and Plate 35.27). Interthecal septa are straight and inclined. A complete median septum is present. The virgella and nema are short where preserved.

Remarks: These specimens resemble *Normalaograptus guizhouensis* (Chen and Lin 1978; see also good illustrations in Chen et al., 2005a and Fang et al., 1990), in being strongly tapered, possessing geniculate thecae with a low inclination, and in maximum distal width, but they have a greater proximal width and more inclined thecae with more open apertures. They match Fang et al.'s (1990) original description in proximal dimensions and thecal spacing, although the type specimens have a somewhat lower maximum distal width. Fang et al. described the species as transitioning from glyptograptid to orthograptid thecae distally, but from their illustrations they appear to retain geniculae throughout, as do the present specimens. The large collection of

specimens illustrated by Fang et al. in their plate 3.7, in particular, match the present material well. These specimens differ from those assigned here to *Glyptograptus*? sp. 1 in expanding more rapidly and possessing more closely spaced thecae (Figs. 6.70-6.73). They differ from *Neo. clavatus* in possessing more inclined thecae distally, widening less rapidly, and a generally higherdistal 2TRD.

***Korenograptus laciniosus* (Churkin and Carter, 1970)**

Plates: (Photos) 30.13, 31.12, 31.26, 33.29, 37.1-4, 37.20, 38.4, 38.10-12;

(Line drawings) 29.6-8

Material and stratigraphical range: Abundant in the lowest *persculptus* Zone collections, and rare throughout the entire upper *persculptus* Zone (all *persculptus* Zone samples). 29 measured in detail.

Description: Long, nearly parallel-sided species reaching a maximum length of at least 37 mm. A complete median septum is present. DVW is 0.75-0.9 mm at th1, 0.93-1.05 mm at th3, 1.05-1.28 mm at th5, 1.25-1.4 mm at th7, 1.25-1.25-1.48 mm at th10, 1.25-1.6 mm at th15, and 1.3-1.65 mm distally, with some variation along the rhabdosome, but most commonly at or very close to 1.5 mm. 2TRD is 1.3-1.65 mm at th1, 1.5-1.95 mm at th5, and 1.7-2 mm distally. Thecae are inclined with sharp geniculae, straight to gently curved supragenicular walls, and horizontal apertures. The sicula is prominently exposed below $th1^2$. Its aperture is ca. 0.25 mm wide. $Th1^1$ turns upwards 0.1-0.2 mm below the sicular aperture. Specimens are often preserved in subscalariform view. A full median septum and short virgella are present. The portion of the nema extending from the rhabdosome is also short.

Remarks: Chen et al. (2005a) recorded this species from the *mirus* Subzone to the *vesiculosus* Zone in South China, and include a lengthy list of synonyms. Their descriptions and accompanying illustrations differ from the type material, however. Chen et al. (2005a) described the species as attaining a maximum width of 1.6-1.85 mm, with glyptograptid thecae with gentle sigmoidal curvature; the glyptograptid nature of the thecae is clearly illustrated in the accompanying text figures. In their original description, Churkin and Carter emphasized that the supragenicular wall is "nearly straight" and although variable, never exhibits more than "slight sigmoidal curvature". Additionally, all of their measured specimens (13), with two exceptions (1.7 mm and 1.4 mm) reach a consistent distal width of 1.5 mm. Finally, they noted that specimens were very frequently preserved in scalariform or subscalariform view. In all of these features, the abundant collection of specimens described here agree with the types. In particular, amongst the 33 measured specimens, and several hundred examined specimens, the distal width is consistently very close to 1.5 mm for most of the length, and never exceeds 1.7 mm. Clear and sharp geniculae are present on all thecae on most specimens, but are often obscured by preservation. Additional wider material, with more rounded thecae, co-occurs at the Blackstone River section with the material assigned to *K. laciniosus,* which matches material assigned to the species by Chen et al. (2005a); this material is here assigned to *K. lungmaensis* (Fig. 6.74). In light of the present restriction of *K. laciniosus* to include only specimens of ca. 1.5 mm in width, many of the Chinese assignments will need to be revisited, and the stratigraphic range

of the species given in Chen et al. (2005a) may be too broad. Churkin and Carter (1970) reported *K. laciniosus* from the *P. acuminatus* to the *C. gregarius* Zone in Alaska. In contrast, at the Blackstone River, *K. laciniosus* occurs in older strata: it is highly abundant in the lowest *persculptus* Zone collection (=upper *persculptus* Zone), the first graptolitic horizon following post-glacial flooding, and rare in subsequent upper *persculptus* Zone samples. Similarly, it occurs in the upper *persculptus* Zone at Dob's Linn (pers. observation) and in the uppermost *persculptus* and lowest *ascensus* zones in Scania, Sweden (Koren' et al., 2003). Specimens assigned to *Glyptograptus*? sp. 2 were originally assigned questionably to *K. laciniosus,* but the latter has higher thecal spacing and DVW, especially proximally (Fig. 6.67), and also appears to lack a complete median septum. *K. laciniosus* can be distinguished in mature specimens from other species in this collection by its rapidly attained, moderate width, parallel-sided rhabdosome, strongly inclined thecae, which appear strongly rounded to nearly orthograptid in preservation, and clear median septum (Figs. 6.71, 6.73, and 6.74). *Neodiplograptus* sp. 2 from the upper *acuminatus* Zone has more strongly biform thecae and thickened lower apertural rims.

Korenograptus lanpherei **(Churkin and Carter, 1970)**

Plates: (Photos) 45.8, 45.10-11, 45.17, 54.19; (Line drawings) 42.6, 42.9-10

Material and stratigraphical level: Uncommon through the mid and upper *acuminatus* Zone, and questionably from the lower *acuminatus* Zone. 18 specimens measured in detail.

Description: Rhabdosome up to at least 23 mm long. Expands rapidly from 1.05-1.35 mm (most <1.2 mm; 1=0.88 mm) at th1, to 1.48-1.7 mm at th3 (1=1.23 mm), 1.8-2.15 mm at th5, 2.05-2.25 mm at th7, and 2.05-2.45 mm (1=2.6 mm) at th10, with a maximum of 2.1-2.6 mm distally (n=3). 2TRD is 1.5-1.9 mm at $th1^1$, 1.55-1.95 mm at $th3^1$, 1.7-2 mm at $th5^1$, 1.85-2.15 mm at $th7^1$, and 2-2.15 mm thereafter. The sicula is ca. 2-2.1 mm long (n=3). The sicular aperture is 0.25-0.38 mm wide. Th 1^1 turns upwards 0.2-0.33 mm below the sicular aperture and its upward-grown portion is 1.18-1.35 mm long. Thecae are inclined and moderately to strongly geniculate proximally, becoming increasingly glyptograptid distally, but retaining weak geniculae throughout. Thecal apertures are horizontal or slightly everted and thickened, especially the lower rim. A prominent nema runs the length of the rhabdosome and extends a great distance distally (up to 20 mm), even in immature specimens, where it is often twice the length of the rhabdosome. The nema is 0.05-0.3 mm wide proximally, and in one specimen expands distally into a three-veined structure 0.5 mm wide (see Plate 45.8). The virgella is similarly robust (up to ca. 0.15-0.2 mm wide proximally in mature specimens), extending up to 18 mm long, often exceeding the length of the rhabdosome, and tapering distally. The presence of a median septum is unclear, but there are hints of one distally. The nema is often off-center, especially in specimens preserved off-profile, but it is not undulose.

Remarks: Churkin and Carter (1970) illustrated three specimens, and provide a table of measurements. The holotype and the specimen illustrated in plate 2.9 closely match the

present material (Fig. 6.68), with the exception of possessing lower proximal widths (up to 1.05-1.35 mm vs. 0.9-1.1 mm) and possibly a greater distal width (this is unclear, since only one of Churkin and Carter's specimens extends beyond 11 mm). The specimen illustrated in 2.10, however, widens less rapidly than the holotype, reaches a lesser maximum width, possesses shorter, more geniculate thecae, and a more protracted proximal end. In these features, it more closely resembles the material assigned here to *Korenograptus* sp. 1. Within Churkin and Carter's data table (1970: p. 27), there seem to be two populations: one that matches the holotype in rate of widening and maximum width and another that matches the pattern of the specimen shown on plate 2.10 (Fig. 6.69). It is possible that the type collection is a mixture of the material assigned here to *Korenograptus* sp. 1 and *Korenograptus lanpherei,* or the type collection may genuinely show a wide range of intraspecific variation. Ghavidel-Syooki et al. (2011) illustrated a specimen that they assigned to *Glyptograptus lanpherei* that co-occurs with a typical Hirnantian assemblage in the Sarchahan Formation of Kuh-e Faraghan, Iran. It closely resembles the present material; however, the scale appears to be incorrect, yielding a distal width of over 4 mm, and precluding confident comparison with the present specimens. The material illustrated as *Hedrograptus* cf. *H. lanpherei* in Melchin (1987b: text-fig. 20 a and d) matches the present material. Fang et al. (1990) illustrated a specimen from the *acuminatus* Zone (plate 9, fig. 14) with a proximal width of ca. 1 mm and a distal width of 1.6 mm, consistent with the low end of variation in Churkin and Carter's (1970) material. Several contemporary Chinese species possess the

combination of wide rhabdosome, long virgella, and weakly geniculate thecae seen in the present material. *Glyptograptus triangulatus* (Fang et al., 1990) widens more quickly, and has a greater distal width than the present specimens. Two of the paratypes of *Glyptograptus complanatus* (Fang et al., 1990) resemble the present material (plate 9, fig. 10 and 11); however, the holotype lacks a robust virgella and has smoothly rounded thecae (text-fig. 25). Specimens assigned by Fang et al. (1990) to *G. kaochiapienensis* (plate 6, figs. 6 and 12) are very similar to the present material. Churkin and Carter considered *G. kaochiapienensis* as a possible synonym for their new species, but rejected it based on the former's narrower proximal end, shorter virgella, and other features. Some of the specimens assigned by Fang et al. (1990) to *Glyptograptus lungmaensis* closely resemble the present material, e.g., plate 15.10. The types of *K. lanpherei* occur in a mixed collection that spans the *acuminatus* and *vesiculosus* zones, similar to its position at the Blackstone River. With its rounded and inclined thecae and long and robust virgella and nema, this species is easily identifiable from most other species in this collection. *Korenograptus bifurcus* is distinguished by a distally bifurcating virgella, but is otherwise very similar, and with larger collections may be shown to be a variant of *K. lanpherei.* The present specimens are easily distinguished from *Korenograptus* sp. 1 by their greater rate of widening and greater maximum width (Fig. 6.68).

***Korenograptus lungmaensis* (Sun, 1933)**

Plates: (Photos) 30.18-19, 30.27-28, 31.1,34.3-6, 34.8-9, 34.15;

(Line drawings) 28.11, 29.16-17

Material and stratigraphical range: Common from the upper *persculptus* Zone (lowermost collection). 11 specimens measured in detail, plus 12 distal fragments.

Description: Robust rhabdosome up to at least 27 mm in length. Expands from 0.8-0.95 mm at th1, to 1-1.15 mm at th3 (n=6), 1.25-1.35 mm at th5, 1.38-1.6 mm at th7, 1.58-1.83 mm at th10, 1.75-2.05 mm distally. 2TRD is 1.25-1.4 mm at $th1^1$, 1.45-1.7 mm at $th3^1$, 1.5-1.85 mm at $th5^1$, 1.5-1.75 mm at $th10^1$ (1=2.15 mm), and 1.6-2.1 mm distally. The first few thecal pairs are inclined and sharply geniculate. Later thecae remain inclined, but become increasingly rounded, appearing nearly orthograptid distally in many specimens when flattened, with presentation strongly influenced by preservation. Thecal apertures are horizontal or very slightly everted, and excavations are relatively deep and open, especially distally, with inclined infragenicular walls. The proximal end is wedge-shaped and asymmetrical. $Th1^1$ turns upwards 0.2 mm below the sicular aperture, which is prominently exposed. The upward grown portion of $th1^1$ is ca. 0.75 mm long. A short, but robust virgella is present in many specimens. The rhabdosome is fully septate. A thick nema is visible internally in many specimens.

Remarks: These specimens are within the range of descriptions given in the Chinese literature. Chen et al. (2005a) noted slightly higher widths (1-1.1 mm at th1 and 2.1-2.4 mm distally), but the type description gives a proximal width of 0.8 mm and distal width of 2 mm, Li (1984) gives a range proximally (0.7-0.8 mm, or rarely 1-1.1 mm, at th1), with a maximum width of 1.9-2 mm distally), and other authors (e.g., Lin and Chen, 1984, Fang et al. (1990) fall within this spectrum. While the precise character of the

thecae is difficult to determine in the published illustrations available, especially the type illustrations, the Chinese material appears to agree well with the present specimens. One exception is the specimen illustrated in Fang et al. (1990) in plate 15.10. With its long virgella and distally projecting nema, as well as its more rapidly expanding rhabdosome (and greater distal width, if the scale on the plate is correct), this specimen strongly resembles material from the *acuminatus* Zone at the Blackstone River assigned here to *Korenograptus lanpherei*. Especially proximally, these specimens of *K. lungmaensis* resemble *Korenograptus laciniosus*, but the former attains a greater distal width (after ca. th7), and has more rounded, rather than straight and inclined, thecae. As noted in the description for *K. laciniosus*, specimens assigned to that species by Chen et al. (2005a) and other Chinese authors with DVWs greater than 1.5 mm are likely better assigned to *K. lungmaensis* or other species. Earlier in this project, a subset was excluded due to possessing apparently more geniculate, longer thecae, mesially and distally, e.g., Plate 30.18 and 30.28, and especially 34.3-4; given the strong preservational effect on apparent thecal form, all of these specimens are now included in *K. lungmaensis*, but the possible difference is noted for comparison with future collections.

***Korenograptus ugurensis* (Koren' and Melchin, 2000)**

Plates: (Photos) 48.14-16, 48.20?, 49.1-2, 49.3?, 49.31-32, 54.15;

(Line drawings) 42.13?, 42.14-15

Material and stratigraphical range: Uncommon from the lower *ascensus* Zone and the upper *acuminatus* Zone. 7 specimens from the *ascensus* Zone measured in detail,

several dozen more examined, plus an additional 7 specimens measured from the mid and upper *acuminatus* Zone.

Description: Robust rhabdosome up to at least 12 mm in length. Expands from 1-1.1 mm at th1 to a maximum of 1.55-1.85 mm reached by th5, and then decreasing distally in many specimens. 2TRD is 1.45-1.65 mm at th1^{1}, increasing up to at least 1.9 mm distally. The proximal end is broad and strongly asymmetrical, and the sicula is well exposed below th1^{2}; its aperture is 0.3 mm wide. Thecae are glyptograptid throughout, with sharper geniculation proximally. The thecal apertures are open and slightly everted. A median septum is present, as is a stout virgella and thin, distally projecting nema.

Remarks: Specimens of *Korenograptus ugurensis* in the present collection, while well-preserved, are very difficult to see and illustrate, except under ideal levels of wetting, and so only a small number were measured. They match the types closely in all features, except maximum width, which is larger in the present collection, but similar to material described by Chen et al. (2005a) from China. The specimen illustrated in Plate 49.3 and Plate 42.13 may be *Korenograptus jerini.* It differs from the other described material in being narrower and possessing a more upright initial thecal pair. Given the limited numbers of comparative specimens, it is tentatively retained within *K. ugurensis.* Additional material occurs in the upper *acuminatus* Zone that agrees well with *K. ugurensis* in general features. These specimens have also thin periderm and are also very hard to see and measure, but are similarly well-preserved. Limited metrical data on both populations makes comparing them difficult, but the measured specimens from

the upper collection have slightly wider proximal ends. Given the large stratigraphic break between occurrences, it is possible that these two collections belong to different species, but they are grouped at present until a large measurement data set is produced. Measurement data above includes only specimens from the *ascensus* Zone.

***Korenograptus* sp. 1**

Plates: (Photos) 31.2, 37.9-11, 45.12, 46.9, 48.11, 48.18;

(Line drawings) 28.3, 28.5, 29.5, 42.3-5

Material and stratigraphical range: Uncommon from the upper *persculptus* Zone and throughout the *ascensus* Zone. 22 specimens measured in detail.

Description: Rhabdosome up to at least 22 mm in length. Expands from 0.88-1.13 mm at th1, 1.25-1.5 mm at th3 (1=1.15 mm), 1.45-1.6 mm at th5 (1=1.85 mm), 1.55-1.7 mm at th7 (1=1.9 mm), 1.65-2.1 mm at th10, and 1.5-1.95 mm at th15 (n=6; several specimens decrease slightly in width after th10). With rare exceptions, 2TRD is consistently high after the first thecal pair: 2TRD is 1.55-1.95 mm at $th1^1$ (mostly 1.75 mm or greater), 1.6-2 mm at $th3^1$ (mostly 1.85 mm or greater), and 1.8-2.2 mm at $th5^1$ and beyond. Thecae are inclined to the rhabdosome at ca. 20 degrees, with horizontal to slightly introverted apertures. Thecal geniculation is variable, but weak, rounded geniculae are present on all thecae, although this is often difficult to see, with thecae frequently appearing nearly orthograptid (see Plate 37.10). The supragenicular walls are slightly convex. The proximal end is acuminate: the first thecal pair is inclined at a similar angle to subsequent thecae, and are somewhat elongate: the upward grown portion of $th1^1$ is 0.9-1.13 mm and it is 1.2-1.5 mm from the sicular aperture to the aperture of $th1^2$. The

upward grown portion of $th1^1$ is gently convex and $th1^2$ is straight. The sicula is ca. 2 mm long and is exposed for 0.23-0.5 mm below $th1^2$; the sicular aperture is often slightly introverted and is 0.18-0.35 mm wide (n=7). $Th1^1$ turns up just below the sicular aperture (0.1-0.18 mm; n=4). A robust, but non-expanding virgella is present on all specimens, and is up to 11 mm long. The nema is prominently visible inside many specimens, and distally projects up to 12.5 mm, but does not expand. A full median septum is present at least mesially and beyond.

Remarks: With its orthograptid-looking thecae, moderate width, and robust virgella this species is distinct from all others in the collection. *Korenograptus lanpherei* also possesses a robust, tapering virgella, but widens much more rapidly and possesses wider and more horizontal apertures (Figs. 6.68 and 6.75). This species resembles *Normalograptus wangjiawanensis* Mu and Lin in dimensions and in possessing a robust virgella and distal nema, as well as in possessing inclined thecae. In the present material, the virgella tapers distally, rather than expanding, however. Additionally, the thecae on the present material are more strongly inclined, with more rounded geniculae. This material is also similar to *Korenograptus* sp. 3, but has a higher initial width and thecal spacing and a more elongate first thecal pair (Fig. 6.76). The specimen illustrated by Lenz and McCracken (1982) as *Glyptograptus lanpherei* (fig. 4a) was reexamined during this thesis; it is equivalent to the present material.

***Korenograptus* sp. 2**

Plates: (Photos) 54.14, 54.16-18; (Line drawing) 42.17

Material and stratigraphical range: Rare from the mid and uppermost *acuminatus* Zone. Eight specimens measured in detail, more examined.

Description: Small, nearly parallel-sided rhabdosome, up to 6.4 mm in length. Expands from 0.73-0.95 mm at th1, to 0.83-1.05 mm at th2, 0.8-1.1 mm at th3, which appears to be the maximum width. 2TRD is 1.65-1.8 mm at $th1^1$ and the same at $th3^1$; only one measurement exists for $th5^1$: it is 1.66 mm. The proximal end is asymmetrical. Theca 1^1 is gently convex and $th1^1$ nearly straight; both grow upwards at a low angle to the rhabdosomal axis. The thecae are inclined throughout, with straight or gently curved supragenicular walls, and sharp to rounded geniculae, although compression makes them appear orthograptid. The virgella is minute. A short thin nema projects distally in some specimens. It is also visible throughout the rhabdosome and is straight. A median septum appears to be present on at least one specimen, but this isn't clear. Most specimens are preserved off-profile.

Remarks: Material that matches very well with the present specimens is currently being described as a new species by Fan et al. (in prep.). It occurs in several sections in China, always as a rare component of the fauna. The proposed holotype is from the *ascensus* Zone, but it occurs in the mid *acuminatus* Zone at another section in China (Fan et al., in prep.). *Korenograptus* sp. 2 resembles *Sudburigraptus*? *cortoghianensis* (Štorch and Serpagli) in general dimensions and thecal form, but differs in possessing a median septum. *Sudburigraptus eberleini* (Churkin and Carter) is very similar in overall form, but is slightly larger throughout, has orthograptid thecae, and is also aseptate (Melchin et

al., 2011). The present specimens resemble those assigned to *N.* aff. *angustus* when the latter is preserved off profile, but have a generally higher proximal 2TRD.

***Korenograptus* sp. 3**

Plates: (Photos) 46.5-8, 47.12, 50.17?; (Line drawings) 42.7

Material and stratigraphical range: Uncommon from the mid to upper *acuminatus* Zone. 11 specimens measured in detail, many more examined.

Description: Often thin-walled rhabdosome, to at least 38 mm in length. Expands from 0.75-0.88 mm at th1, to 1.08-1.2 mm at th3, 1.3-1.5 mm at th5, 1.5-1.75 mm at th7, 1.6-2 mm at th10, with a distal maximum of 1.9 to 2.35 mm, the latter in a very mature specimen (th30). 2TRD is 1.35-1.5 mm at th1[1], 1.5-1.7 mm at th3[1], 1.65-1.85 mm at th5[1], 1.95-2.05 mm at th10[1], and ca. 2.25 mm distally. Thecae are geniculate throughout, but become more rounded distally. Distally, the infragenicular wall is inclined, and the geniculum is located far along the thecae, with only a short supragenicular wall, creating a shallow, but open aperture, and thecae that appear orthograptid on compression. Thecae are inclined throughout, increasing mesially and distally to ca. 30 degrees. A long and robust virgella is visible throughout the rhabdosome, extending distally, with a width in some specimens of up to 0.65 mm. A complete median septum is present, and commonly visible, as the thin rhabdosomal walls frequently lead specimens to be preserved in a translucent manner.

Remarks: These specimens superficially resemble the much younger British material of *Glypograptus enodis* Packham, 1962 (*triangulatus* to *magnus* zones: Zalasiewicz et al.,

2009) in possessing characteristically open and inclined thecae, with an elongated infragenicular wall. They differ in reaching a greater maximum width and possessing a complete median septum. The specimens described as *Glyptograptus* cf. *G. enodis* var. *enodis* by Churkin and Carter (1970) from Alaska match the present specimens perfectly externally, but their internal structure is not described or visible in the illustrations. Churkin and Carter (1970) correlated the collections of their specimens to the *vesiculosus* to *cyphus* zones, closer stratigraphically to the present collections than the British types. In possessing a long virgella and glyptograptid thecae, these specimens are superficially similar to *Korenograptus* sp. 1 and *Korenograptus lanpherei,* but are more tapered and have considerably lower proximal thecal spacing (Figs. 6.76-6.77).

Genus *RICKARDSOGRAPTUS* Melchin et al., 2011

Type species. *Diplograptus*(?) *tcherskyi* Obut and Sobolevskaya in Obut et al. 1967.

***Rickardsograptus lautus* (Štorch and Feist, 2008)**

Plates: (Photos) 44.3-7, 44.8?, 44.12, 57.3-7, 57.13-15; (Line drawings) 40.1-2, 40.5-6, 40.8, 40.10?

Material and stratigraphical range: Common from the mid to upper *acuminatus* Zone. 28 specimens measured in detail.

Description: Tapered rhabdosome up to at least 36 mm in length. Slowly widens from 0.85-1.1 mm at th1, to 1.1-1.45 mm at th3, 1.25-1.8 mm at th5, 1.48-2.05 mm at th7, 1.7-2.45 mm at th10, and 1.95-2.45 mm at th15. Maximum width of 2.1-2.45 mm is reached at th15 or beyond, sometimes decreasing slightly distally. 2TRD is 1.55-1.9 mm at th1^1 (but mostly 1.65 mm or less), 1.6-2.05 mm at th3^1, 1.65-2.25 mm at th5^1, and

1.9-2.25 mm distally (rarely to 2.5 mm). $Th1^1$ turns upward 0.1-0.18 mm below the sicular aperture and its upward-grown portion is 0.85-1 mm long. The sicular aperture is 0.2-0.28 mm wide, and is exposed below $th1^2$ for 0.3-0.45 mm. Proximal thecae are sharply geniculate, with thickened apertures and slightly inclined supragenicular walls. Mesially and distally apparent geniculation is variable, with some specimens retaining clear geniculae and others appearing almost orthograptid; distal thecae are straight or slightly inclined. The thecal excavations are shallow and semi-circular in the first few thecae, and become deeper and more open distally, and are horizontal to moderately everted. The virgella is up to 3.9 mm long and usually >1 mm. The distally projecting portion of the nema is up to 23 mm long, and varies from very thin (0.05 mm) to robust (0.23 mm wide). A complete median septum is present.

Remarks: These specimens match the types well (e.g., compare Plate 57.7 to the holotype), as well as with material described by Štorch (1983) and Hutt (1974), and synonymized in the original description, in possessing a tapered rhabdosome, with a shift mesially to inclined, weakly geniculate thecae. They are slightly wider proximally and reach a lower maximum width than the type material, but are close the Bohemian specimens described by Štorch (1983) in maximum DVW (2.2-2.4 mm), and match specimens from the Alps in proximal width (Štorch and Schönlaub, 2012: 0.9-1.1 mm); additionally, they lack the robust virgella that is common in European specimens. *Rickardsograptus tortithecatus* (Hsü) is a similar species that first appears in the *vesiculosus* Zone in China, stratigraphically just above the level of the present

collections. Li (1995) illustrated several specimens of the species, some of which look very similar to the present material (e.g., plate 5.6) and some of which appear to have much more strongly inclined thecae (e.g., plate 5 fig. 3 and 4); additionally, the specimens appear to be more gently tapered than the present material. Li (1995) suggested that the material assigned by Chen and Lin (1978) to *Diplograptus tcherskyi* should have been included in *R. tortithecatus,* along with the material they assign to the species; from the figures, the former material resembles the present collections, while the latter does not. Li (1995) also listed a number of other species in probable synonymy. Some of this material, as well as other illustrated specimens, such as Fang et al.'s specimens of *Diplograptus tcheriskyi latus* (plate 6.13) look very similar to the present material. High-quality illustrations and detailed measurements were not available for comparative purposes during the drafting of this thesis, but it is possible that some of the Chinese material is equivalent to either this species or the material assigned to *Rickardsograptus* aff. *lautus.* The specimens assigned to this species were split into a smaller and larger form earlier in the production of this thesis (e.g., Plate 44.4 vs. 44.7), with the smaller form appearing to have less inclined and more obviously geniculate thecae. All specimens are lumped, given no clear pattern in scatterplots (Figs. 6.79-6.80) and variation in appearance with flattening, but larger collections may support this distinction. The specimen identified on Plate 44.7 and 40.10 has more clearly geniculate and less inclined thecae than many others, and was also initially split from the other specimens, but this too appears to be intraspecific and preservational

variation. *Rickardsograptus* aff. *lautus* differs from the present material in having greater distal width and thecal spacing, as well as more abrupt transition in thecal form.

***Rickardsograptus magnus* (Churkin and Carter, 1970)**

Plates: (Photos) 47.1-5, 50.14? (Line drawings) 43.6

Material and stratigraphical range: Several dozen well-preserved to fragmentary specimens from the upper *acuminatus* Zone, 11 specimens measured in detail.

Description: Robust, thick-walled, conspicuously tapered rhabdosome up to at least 43 mm in length. Widens slowly from an initial width of 0.68-0.7 mm (1=0.78) at th1, to 0.8-0.9 mm at th3, 0.95-1.13 mm (1=1.2 mm) at th5, 1.15-1.35 mm at th7, 1.45-1.8 mm at 10, 1.7-1.95 at th15, and 1.85-2.13 mm at th20. Distal thecal widths are 1.85-2.2 mm, but most commonly ca. 2.0 mm. 2TRD is 1.23-1.73 mm at th1^{1}, 1.5-1.8 mm at th3^{1}, 1.5-1.95 at th5^{1}, 1.7-1.95 at th7^{1}, 1.75-2.05 mm at th10^{1}, 1.8-2.1 at th15^{1}, and ca. 1.85-2.3 mm distally. The sicula is unclear, but may be ca. 1.4 mm long. The sicular aperture is ca. 0.15 mm wide and slightly introverted. It is exposed for 0.23-0.4 mm below th1^{2}. Th1^{1} turns upwards just below the sicular aperture, and its upward-grown portion is 0.78-0.88 mm long. The proximal end is noticeably pointed and strongly tapered, with initial thecae displaying parallel-sided and sharply geniculate thecae, with shallow and thickened apertures. Geniculae gradually soften after about th7, and are noticeably rounded distally, with slightly inclined supragenicular walls, open apertures and inclined infragenicular walls. A prominent median septum is visible. The virgella is short and stout. The distally projecting portion of the nema is not preserved in most specimens,

but is 0.1-0.15 mm wide. Most specimens are preserved in profile, and some have partial relief.

Remarks: The present specimens agree nearly exactly with description and detailed measurements given by Churkin and Carter (1970) and are very similar to specimens identified as *Glyptograptus rigidus* by Fan et al. (1990), e.g., see plate 9, fig. 12. Both specimens illustrated as *Hedrograptus magnus* and *Hedrograptus elongatus* in Melchin (1987b—text-fig. 20 b, 20 e-g, and 20 k and m) resemble the current specimens, with the strongly glyptograptid thecae in the latter more closely matching the way that much present material is preserved than the former. Isolated specimens assigned to Melchin et al. (2011) to *Korenograptus magnus* differ from the type and present material in having glyptograptid thecae proximally.

Churkin and Carter (1970) reported *Rickardsograptus magnus* from two reconnaissance collections, one of which covers the *acuminatus* through *vesiculosus* zones and other the *cyphus* Zone (M1139-SD and M1138-SD, respectively). Fang et al. (1990) reported *Glytograptus rigidus* from the *cyphus* Zone, as well as the underlying *vesiculosus* Zone. The present collections occur in the uppermost *acuminatus* Zone and continue into the only *vesiculosus* Zone sample collected. With its combination of highly tapered rhabdosome, medium width, and biform thecae, this species is easily distinguished from others in our collections. It resembles the types of *Diplograptus elongatus* (Churkin and Carter, 1970), differing principally in that it widens less rapidly (ca. 1 mm at th5 vs. 1.3

mm) and has somewhat wider thecal spacing. The specimen shown in Plate 50.14 has a lower width mesially than other specimens, and is only questionably assigned.

***Rickardsograptus* aff. *lautus* (Štorch and Feist, 2008)**

Plates: (Photos) 44.1-2, 44.9-10, 44.13, 47.15, 54.1-2, 56.16, 57.8-12;

(Line drawings) 40.3-4, 40.7, 40.9

Material and stratigraphical range: Common from the mid *acuminatus* Zone. 19 specimens measured in detail.

Description: Strongly tapered rhabdosome up to 35 mm in length. Initial thecae are strongly geniculate, with thickened apertures and nearly parallel supragenicular walls. They transition rapidly beginning around th5-7, becoming strongly inclined (ca. 25 degrees), with geniculae weakened or absent: the thecal apertures are introverted distally, with the lower rim of the aperture remaining thickened, and often cover and obscure the aperture upon compression, making it difficult to discern thecal form (but see weak geniculae present distally in Plate 57.10—white arrows). In some specimens the thickened lower rim appears lappet-like when flattened. DVW is 0.85-1.03 mm at th3, 1.23-1.5 mm at th3 (1=1.15), 1.73-2.15 mm at th5 (1=1.48 mm), 2.15-2.55 mm at th7, 2.65-2.8 mm at th10, with a distal maximum of up to 3 mm reached distally. 2TRD is 1.85-2.25 mm at $th1^1$, 1.8-2.5 mm at $th3^1$, 1.9-2.5 mm at $th5^1$, 2.2-2.7 mm at $th10^1$, and 2.25-2.9 mm distally. The upward-grown portion of th^1 is 1-1.15 mm long. The sicular aperture is 0.25 mm wide, and it is exposed for 0.25-0.5 mm below $th1^2$. A robust virgella, to 1.5 mm, is present on most specimens. The nema projects beyond the

rhabdosome 6.5 mm or more, and is thin. Internal structure is unclear, but a consistently straight nema can be seen pressed through the rhabdosome. The pathological specimen illustrated in Plate 57.8 also suggests that the rhabdosome is septate.

Remarks: These specimens are similar to those assigned to *Rickardsograptus lautus* above. They differ in reaching a greater maximum width, possessing longer and more strongly inclined thecae, and tapering more dramatically. They possess both a greater maximum width and higher thecal spacing than the type collection of *R. lautus.* It is possible that these specimens represent an extreme form of *R. lautus,* but they plot distinctly from other specimens in this collection (Figs. 6.78-6.79), and differ both in terms of metrics and thecal form. These specimens resemble *Diplograptus* sp. (Churkin and Carter, 1970: see their fig. 9f); Churkin and Carter describe the distal thecae as orthograptid, but both illustrated specimens appear to show at least weak geniculae throughout the rhabdosome. Since only one specimen with a proximal end was described, a detailed comparison is not possible, but the intact specimen is close to the present material in dimensions. They resemble the younger *Rickardsograptus thuringiacus* (Kirste, 1919), but taper less dramatically; *Rickardsograptus elongatus* (Churkin and Carter) is more gradually tapered.

Genus *PARACLIMACOGRAPTUS* Přibyl, 1947, emended Melchin et al., 2011

Type species: *Climacograptus innotatus* Nicholson 1869.

***Paraclimacograptus obesus* (Churkin and Carter, 1970)**

Plates: (Photos) 44.14-16, 46.11-14, 49.10-12, 49.21-22, 49.24-26, 49.37-38, 55.16-23, 56.1, 56.3-4, 56.6-7; (Line drawings) 40.15, 43.15-17

Material and stratigraphical range: Very abundant from the upper *acuminatus* Zone to at least the basal *vesiculosus* Zone. 36 specimens measured in detail, many hundreds more examined.

Description: Fusiform rhabdosome up to at least 13 mm long. Specimens expand from 0.65-1 mm at th1, to 1.03-1.68 mm at th3, 1.23-2.25 mm at th5, with a maximum width of 1.5-2.25 mm reached between th5 and th10, followed by moderate to strong distal tapering. 2TRD is 1-1.4 mm at $th1^1$ and 1.3-1.5 mm distally. $Th1^1$ turns upwards 0.1-0.15 mm below the sicular aperture, which is 0.18-0.22 mm wide, and exposed below $th1^2$ for 0.22-0.5 mm. The upward-grown portion of $th1^1$ is 0.65-0.95 mm. The thecae are geniculate, with straight to concave, and gently inclined supragenicular walls, and everted apertures. The geniculum is furnished with a short flange. The virgella is normally stout, but in rare cases is up to 3 mm long. A thin nema projects beyond the rhabdosome up to 2 mm. A complete median septum is present. The sicula is difficult to see in most specimens, but is consistently 1.4-1.7 mm where it is visible.

Remarks: All measured specimens are from 46.0 m and above. An additional large population occurs from 44.02 m, and is commented on below. In both 46 m and above and 44.02 m, *Paraclimacograptus* dominates the collections, but is very rare in the 45 m collections. Churkin and Carter (1970) distinguished *P. obesus* from *P. innotatus* by its more tapered rhabdosome and greater width. Russell et al. (2000), in their detailed

examination of species of *Paraclimacograptus,* regarded specimens with a maximum DVW of 1.5 mm or greater to be *P. obesus,* and added greater sicular length as a distinguishing feature of *P. obesus.* The upper *acuminatus* Zone specimens match well the type description, but also show considerable variation in rate of widening and degree and point of distal tapering. In particular, some specimens have a distinctive ovate form, while others maintain their maximum width for many thecae before gently tapering (e.g., compare Plate 49.26, 55.17, and55.19 with 49.22 and 49.251); some of the ovate form also rapidly reach high DVWs, e.g., Plate 55.19. These specimens are similar to Fang et al.'s (1990) *Paraorthograptus ovatus* (here assigned to *Paraclimacograptus*). Plots of the 36 measured specimens do not show any clear division into morphological clusters, however, so they are all assigned to *P. obesus.* Considerable additional material exists for future work. A small number of specimens also fall within the upper range of widths for *Paraclimacograptus innotatus* (e.g., see Plate 56.1: maximum DVW of ca. 1.3 mm); given that these specimens occur amongst hundreds of unambiguous specimens of *P. obesus,* and given the large variation in DVWs present in the collection, these are considered outliers of *P. obesus*.

Abundant additional material occurs from 44.02 m that matches the less ovoid form, but reaches a consistent maximum width of ca. 1.5 mm, with less developed flanges, and generally less concave thecae. The apparent differences in thecal form may be at least partially preservational, as the material is preserved on a coarser grained substrate, but they also plot as a separate, but overlapping population (Figs. 6.80-6.81).

The 44.02 m specimens have sicular lengths in the range of *P. obesus,* i.e., ca. 1.6 mm consistently. The specimens assigned by Lenz and McCracken (1982) to *Climacograptus innotatus* from the nearby Peel River section were examined. Both of the specimens, plus additional material on the two slabs, have maximum widths of 1.75-2 mm, and are therefore reassigned to *Paraclimacograptus obesus.* Additional material occurs from 43.5 m and 42.83 m that generally matches the rhabdosomal characteristics of *P. obesus,* but either lacks flanges or has only traces of incipient flanges. This material is assigned to *K.*? *diminutus.*

Genus *CYSTOGRAPTUS* Hundt, 1942, emended Rickards, 1970

Type species: *Diplograptus vesiculosus* Nicholson, 1868, p. 57, pl. 3, fig. 11

Cystograptus cf. ancestralis Štorch, 1985

Plates: (Photos) 48.4, 48.9-10, 56.2

Material: Very rare, moderately preserved, material from the mid *acuminatus* Zone. Two juvenile and two mature specimens examined (one well-preserved and one poorly preserved, in both cases).

Description: The rhabdosome is at least 5 mm long, expanding rapidly from a width of 1.9(?)-2.3 mm at the first thecal pair to a maximum of ca. 3.5 mm by the third to fifth thecal pair. 2TRD is dependent on the orientation of the thecal apertures, and is 2 mm and 1.5 mm at $th1^1$ and $th1^2$, respectively, in the one specimen where it can be reliably measured. The sicula is 2.85-ca. 3 mm long. The sicular aperture is 0.43 mm wide. $Th1^1$ turns upwards 0.18-0.43 mm below the sicular aperture, and its upward-grown portion

is 1.55 mm long. Thecal form is difficult to determine, but they appear to be relatively simple and straight-sided. Thecal apertures are everted proximally and horizontal distally. The virgella is slight or absent. A prominent nema is present on one of the mature specimens. It is >8.5 mm long and 0.65 mm wide proximally, expanding into a three-vaned structure distally.

Remarks: The present material differs from *Cystograptus ancestralis* in several respects. It is somewhat wider than the type material (2.3 mm vs. 1.7-2.1 mm at th1[1] and a maximum of ca. 3.5 mm vs. a maximum of 2.2-3 mm (Štorch, 1985)), although it is consistent with unpublished Chinese specimens (Fan et al., in prep.). Štorch (1985) and Štorch and Serpagli (1993) described their specimens as having glyptograptid thecae, rapidly attained maximum width, and a distinctly rounded proximal end. Štorch (1985) also noted that *C. ancestralis* lacked a nematularium, but this feature was observed in specimens from Sardinia (Štorch and Serpagli, 1993), and also in one mature Bohemian specimen (Štorch, pers. comm.). In contrast with the above, the best-preserved specimen in the present collection seems to have straight, nearly orthograptid thecae, and, most notably, a triangular proximal end, resulting from the fact that the initial thecal pair lack the convex ventral walls normally associated with the species. There are two additional specimens, a juvenile specimen with only a single thecal pair, which, if completely developed, has a DVW at th1[1] of 1.9 mm, and a second mature specimen, which seems to have more rounded geniculae, but which also appears to possess more closely spaced thecae than the best specimen in the collection. All of the present

specimens agree with *C. ancestralis* in possessing a relatively short sicula (ca. 3 mm) for the genus and rapid DVW widening, features which are absent in *Cystograptus vesiculosus* and other known species of *Cystograptus*. Because of the striking difference in the shape of the proximal end, however, these specimens are left in open nomenclature. A specimen from the nearby Peel River, which occurs on the same slab as a specimen of *Parakidograptus acuminatus* illustrated by Lenz and McCracken (1982), is illustrated on Plate 47.14; it matches very well the types of *C. ancestralis*, demonstrating that the species does occur regionally.

Family RETIOLITIDAE Lapworth, 1873, emended Melchin et al., 2011

Paraphyletic Subfamily PETALOLITHINAE Bulman, 1955, emended Melchin et al., 2011

Genus *PARAMPLEXOGRAPTUS* Melchin et al., 2011

Type species. *Paraorthograptus paucispinus* Li, in Anhui Geological Survey Team 1982.

***Paramplexograptus kiliani* (Legrand, 1977)**

Plates: (Photos) 49.33-34, 54.27, (Line drawings) 43.19

Material. Numerous poorly preserved specimens from the basal *ascensus* Zone. 6 specimens measured in detail.

Description. Rhabdosome is at least 22 mm long and fusiform, widening from 1-1.3 mm at th1, to 1.8-2.2 at th5, reaching a maximum width of ca. 2.9 mm by th10-12, and decreasing distally. The 2TRD is about 1.15 at th1, increasing to 1.5-1.85 mm distally. Sicular length is unclear, but its aperture is 0.35-0.40 mm wide, and it is exposed about 0.275-0.375 mm below $th1^2$. Theca 1^1 turns up just below the sicular aperture (0.1 mm).

Thecae have moderately inclined short supragenicular walls and everted apertures. The geniculae are sharp and bear broad, thin, semi-circular flanges, with thickened rims, up to 0.3 mm wide proximally, which become less prominent or absent distally. The rhabdosome is aseptate. A consistently thin (0.05 mm) nema runs the length of rhabdosome and extends just beyond it. In some cases, the nema is slightly undulose. It is connected by small bars to the interthecal septa (although these are only visible in rare specimens).

Remarks. This species occurs in a single sample, 37.43 m, a tan-weathering siltstone, where it dominates the collection. Most specimens are large and complete, but details of both internal and external morphology are difficult to distinguish due to poor preservation. The periderm appears to be much thinner than many co-occurring species, which are preserved with considerably more detail or even relief. Flange size is highly variable, and in some cases large flanges combined with poor preservation make this species difficult to distinguish from hooded species such as *Paraclimacograptus jingyanensi*s. *P. kiliani* co-occurs with specimens identified as *Songxigraptus elongatus*. The latter species appears to possess highly inclined and flared apertures, however, rather than flanges or hoods (but see remarks for *Songxigraptus elongatus* above). The high distal width of *P. kiliani* easily distinguishes it from other species of *Paramplexograptus* in the collection (Fig. 6.84). This species was originally described from North Africa, where is was considered an index taxon correlatable to the base of

the *ascensus* Zone. It is restricted to the basal-most *ascensus* Zone in the present collection, supporting its biostratigraphic utility.

***Paramplexograptus madernii* (Koren' and Mikhailova) in Apollonov et al., 1980**

Plates: (Photos) 30.15, 31.17-18, 33.25-27, 36.5; (Line drawings) 27.8, 27.24

Material and stratigraphical range: Rare from the *persculptus* Zone and lower *ascensus* Zone, questionably throughout the *ascensus* Zone. 11 specimens measured (all from the *persculptus* Zone).

Description: Rhabdosome up to at least 15 mm long. Nearly parallel sided. Expands from 0.73-0.8 mm at th1, to 0.9-1.25 mm at th5, with a maximum of 0.98-1.4 mm, reached by th10. 2TRD is 1.1-1.4 mm at th1, 1.4-1.6 mm at th5 (1-1.75 mm), and ca. 1.65-1.75 mm distally. Thecae possess sharp geniculae, slightly inclined and concave suprageniculum walls, and slightly everted apertures, that appear to possess small flanges in some cases. Sicular length is unclear. The sicular aperture is angled and ca. 0.2 mm wide. $Th1^1$ turns upwards at the same level as the lowest part of the sicular aperture, and its upward-grown portion is ca. 0.65-.73 mm. The rhabdosome is aseptate and the nema prominently zig-zags where it is attached to the interthecal septa. The virgella is thin and up to 0.6 mm long.

Remarks: These specimens agree very well with the type material, as well as those described as *Normalograptus* sp. aff. *N. indivisus* by Chen et al. (2005a) and reassigned to *P. madernii* in Fan et al., (in prep.). The Chinese material described by Chen et al. (2005a) also occurs in the *persculptus* Zone. When the internal structure is not visible, this species can be confused with narrow species of *Normalograptus*, but differs in the

inclined and slightly concave thecae. Specimens assigned to *P.* aff. *madernii* have a lesser maximum width and higher 2TRD, and possess a prominent virgella. Both species occur on the same slabs in this collection. *Paramplexograptus paucispinus* is wider proximally and has generally lower 2TRD throughout.

***Paramplexograptus paucispinus* (Li, 1982) in Anhui Geological Survey Team ed.**

Plates: (Photos) 48.12-13, 49.28-30, 52.19; (Line drawings) 40.14, 43.18, 43.21-23, 43.25

Material. Numerous poorly to well-preserved specimens from the *A. ascensus* Zone. Nine measured in detail.

Description. Small rhabdosome up to 8 mm long (most ca. 5 mm long). Widens from 0.83-1.0 mm at th1, to 1.0-1.23 mm at th3, with a maximum width of 1.1-1.4 mm reached by th5, which is maintained or decreases slightly distally. The 2TRD is 1.0-1.2 mm at th1, 1.2-1.43 mm at th3, with a maximum 2TRD of 1.3-1.5 mm reached around th5, decreasing slightly distally. The sicula is ca. 1.25 mm long; its aperture is 0.2-0.25 mm wide and inclined toward the virgella at an angle of about 45 degrees (length measurements taken from proximal-most point of sicula). It is exposed below $th1^2$ for 0.25-0.3 mm. The virgella is short (up to 0.6 mm) and thin. The proximal end is v-shaped. Thecae are inclined, with sharp geniculae furnished with stout (0.125 mm) flanges proximally, which are reduced or absent distally. Thecal excavations are small, shallow, and everted. The rhabdosome is aseptate. The nema is gently undulose to zigzag, and small lists connecting it to the interthecal septa can be seen on some specimens (see Plate 52.19).

Remarks. This species closely resembles *Paraclimacograptus innotatus* in overall morphology; however, *P. innotatus* can be easily distinguished, when internal structure is preserved, by the presence of a complete median septum distally. Koren' and Melchin (2000) recorded *P. innotatus* from their *N. lubricus* Subzone (=basal *A. ascensus* Zone); however, all of their illustrated specimens showing a clear median septum occur in collections assigned to the *P. acuminatus* Zone (*A. cuneatus* Subzone). In the present collections, species of *Paramplexograptus*, including *P. paucispinus*, occur in abundance in the basal *ascensus* Zone, whereas *Paraclimacograptus innotatus* first occurs in the middle *acuminatus* Zone. This is in keeping with a recent examination of Chinese collections (Fan et al., in prep.). A combination of low 2TRD, moderate proximal, and low maximum DVW distinguish *P. paucispinus* from other species of *Paramplexograptus* in the collection (Fig. 6.82).

***Paramplexograptus wuningensis* (Fang, Liang, Zhang and Yu, 1990)**

Plates: (Photos) 48.17, 49.35-36, 53.21-22, (Line drawings) 40.12-13, 43.20, 43.24

Material: Common from the basal and lower *ascensus* Zone. 13 specimens measured in detail.

Description: Rhabdosome parallel-sided and up to at least 19 mm in length. Widens rapidly from a width of 1-1.2 mm at th1, to 1.35-1.6 mm at th3, and 1.45-1.7 mm at th5. Maximum width of 1.45-1.8 is reached between th5 and th10. Some specimens taper distally. 2TRD is 0.95-1.15 mm at th1[1] and 1.4-1.65 mm distally. Thecae are amplexograptid, with short, straight or slightly concave supragencicular walls, and small

genicular flanges. Thecal apertures are everted. The proximal end is wedge-shaped and asymmetrical, with th1[2] inclined at a much higher angle relative to the rhabdosomal axis than th1[1]. The interthecal septa are connected to the nema. A small, thin virgella is present.

Remarks: This species closely resembles *Paramplexograptus paucispinus*, and to a lesser extent other species of *Paramplexograptus* in this collection, but is consistently distinguishable by its greater width at all points (Fig. 6.82). The present collection agrees very closely with the type description, as well as detailed unpublished measurements of additional Chinese material made by Fan et al. (in prep.). "*Paraclimacograptus" kiliani kuramaensis* (Koren' and Melchin, 2000) is almost certainly a junior synonym of *P. wuningensis.* The well-illustrated types and measurements provided by M.J. Melchin agree perfectly with the present material (Fig. 6.83).

***Paramplexograptus* aff. *madernii* (Koren' and Mikhailova) *in* Apollonov et al., 1980**

Plates: (Photos) 31.4, 31.15, 31.21-23, 33.28, 38.5, 38.9;
(Line drawings) 27.22-23, 27.25, 28.8, 28.12, 28.14, 28.16

Material and stratigraphical range: Rare to abundant throughout the upper *persculptus* Zone and questionably present in the basal *ascensus* Zone. 21 specimens measured in detail, hundreds more examined.

Description: Narrow, parallel-sided rhabdosome, up to 8 mm in length. Expands from 0.6-0.75 mm at th1, to 0.68-0.9 mm at th3, 0.8-0.93 mm at th5 (1=0.68 mm), with a distal maximum not exceeding 0.95 mm, or even narrower when preserved in subscalariform view, e.g., two specimens at right angles to each other at 35.15 m have

maximum widths of only 0.6 mm. 2TRD is 1.45-1.9 mm at th1, 1.5-2.1 mm at th3, and 1.55-1.9 mm at th5, tending towards the higher end of those ranges. A thread-like, but prominent virgella (often >2 mm long, when preserved) and nema (up to 5 mm long) are present even on immature specimens, where both may be equal to the rhabdosome length. The virgella bifurcates in five specimens, with one specimen showing additional levels of branching similar to the pattern seen in *N. minor*. This specimen is only six thecal pairs long. Where present, bifurcation takes place between 1 mm and 2 mm from the base. Thecae are long, with narrow and shallow apertures, sharp geniculae, and straight and parallel to moderately inclined supragenicular walls, although they may appear nearly glyptograptid when preserved off profile, which is common. $Th1^1$ turns upwards just below the sicular aperture. Its upward-grown portion is 0.8-1 mm long. The rhabdosome is aseptate, and interthecal septa are attached to the nema, which undulates throughout.

Remarks: The present specimens differ from *Paramplexograptus madernii* in possessing longer and more widely spaced thecae throughout the rhabdosome, with straighter supragenicular walls, a lesser proximal and distal width, a more protracted proximal end, and a longer virgella and nema. The younger *Normalograptus skeliphrus* differs in possessing a complete median septum (and a slightly less distal width), as does *Normalograptus angustus.* A small number of specimens of *P.* aff. *madernii* possess a branching virgella similar to that of *N.*? *minor.* Many hundreds of specimens of *P.* aff. *madernii* were examined in this collection, with only five (one specimen was lost early in

the study) showing evidence of branching. However, the virgella is very thin and easily broken, and in two of the specimens showing branching it does not begin until 2 mm from its base, so this may represent either uncommon variation or a common but rarely preserved feature. *Metaclimacograptus* sp. 1 of Štorch and Feist (2008), from the lowest Silurian of Montagne Noire, France, agrees with the present species in general respects, but its 2TRD is slightly lower and it lacks a long virgella; additionally, it possesses an undulose median septum, whereas *P.* aff. *madernii* is aseptate (but note that the nema often undulates due to its connection to the interthecal septae). *P.* aff. *madernii* is abundant through the upper half of the preserved *persculptus* Zone at the Blackstone. A single specimen also occurs in the basal *ascensus* Zone collection that plots in the zone of overlap with *P. madernii* in proximal thecal spacing and width measurements, but in an area of morphospace most commonly occupied by *P.* aff. *madernii.* This specimen also possesses a 1 mm long virgella, and so is most probably *P.* aff. *madernii,* but confirmed specimens of *P. madernii* occur in the same sample, so it is not clear whether this species persists into the Silurian.

Genus *GLYPTOGRAPTUS* Lapworth, 1873, emended Melchin et al., 2011

Type species: *Diplograpsus tamariscus* Nicholson 1868.

***Glyptograptus* sp.**

Plates: (Photos) 30.14, 30.16-17, 33.20, 38.26

Material and stratigraphical range: Rare from the upper *persculptus* Zone. 6 specimens measured in detail.

Description: Rhabdosome up to 7 mm in length. Expands from 0.73-0.88 mm at th1, to 0.98-1.13 mm at th3, and 1.15 mm at 5 (n=4). Distal maximum is unclear. 2TRD is 1.25-1.6 mm at $th1^1$, 1.5-1.85 mm at $th3^1$ (n=3), and 1.5-1.55 mm at $th5^1$ (n=2). Supragenicular walls are straight and parallel to the rhabdosomal axis or very slightly inclined. Sharp geniculae are present throughout. The sicula is ca. 1.6.-1.7 mm long, its aperture is 0.2 mm wide. The upward grown portion of $th1^1$ is 0.8 mm long, and it turns upwards ca. 0.2 mm below the sicular aperture. The proximal end is wedge-shaped, with the first thecal pair inclined only at a low angle to the rhabdosomal axis. The distally projecting portion of the nema and the virgella are both thin and short. In several specimens, preserved off-profile, the nema is off-center. In the longest specimen, the nema undulates proximally (Plate 33.20), but a thin, likely partial, median septum is possibly present after th8.

Remarks: Most of this material was figured in Melchin et al., 2011, with the exception of the specimens illustrated as Plate 30.14, 33.20, and one other specimen on the same slab. This material resembles immature specimens of *Glyptograptus*? sp. 1, which may also possess a partial median septum, but it differs in possessing a lower thecal spacing, and less inclined thecae.

***Glyptograptus*? sp. 1**

Plates: (Photos) 30.24, 34.18-21, 35.1-7, 36.2, 38.2; (Line drawings) 27.1, 29.4

Material and stratigraphical range: Common from one sample in the upper *persculptus* Zone (all measured specimens are from 32.97 m) and questionably present in adjacent samples. 24 specimens measured in detail.

Description: Strongly tapered rhabdosome up to at least 26 mm in length. Expands from 0.75-0.93 mm at th1, to 0.88-1.2 mm at th3, 1.08-1.45 mm at th5, 1.25-1.6 mm at th7, 1.35-1.7 mm at th10, and 1.35-1.75 mm at th15 (1=1.95 mm). 2TRD is 1.4-1.6 mm at th1^1, 1.6-2 mm at th3^1 (mostly >1.7 mm), and 1.75-2.05 mm at th7 and beyond. Thecae are inclined, with everted, narrow, and straight supragenicular walls. Proximal thecae are strongly geniculate. Geniculae become more rounded distally, but are retained throughout. The interthecal septa are straight (see Plate 38.2). Other aspects of the internal structure are unclear, but the nema notably wanders throughout the rhabdosome, both proximally and distally, and is frequently preserved off centre in subscalariform specimens. (For example, see white arrows in Plate 35.2, 35.5, and 35.7) The upward-grown portion of th1^1 is 0.73-0.83 mm (n=5). Sicular length is unclear. A short virgella is preserved occasionally. Most specimens possess a prominent distally projecting nema, up to a maximum of 11 mm long, which is often nearly as long as the rhabdosome itself, and is up to 0.23 mm wide.

Remarks: Specimens are variable in terms of degree of apparent thecal inclination (mostly the result of the common subscalariform mode of preservation). They are united by their moderate distal width, relatively high 2TRD, strongly tapering rhabdosome, everted apertures, and distinctly wide and long nema projecting beyond the rhabdosome, a feature that is present even in immature specimens. In overall morphology, these specimens resemble the type illustrations of *Normalograptus guizhouensis,* especially text-fig. 9a (Chen and Lin, 1978), but differ in possessing a

somewhat lower DVW. Other higher quality illustrations and photographs of material assigned to *N. guizhouensis* by Chinese authors (e.g., Chen et al., 2005a; Fang et al., 1990; Li, 1995) show less angled thecae, with obvious, horizontal or only slightly everted apertures; additionally, some illustrated specimens possess a distally expanding nema (e.g., Fang et al., 1990, plate 21.15), although this is variable. Most importantly, however, *N. guizhouensis* possesses a complete median septum (Chen et al., 2005a), while the present specimens are likely either aseptate or possess only a partial median septum, based on the behaviour of the nema. For this reason they are assigned questionably to *Glyptograptus,* despite their external similarities with *Korenograptus*. *Korenograptus jiangxiensis* Fang, Liang, Zhang and Yu (in Fang et al., 1990) resembles this material in general form and the possession of a distinctly robust external nema, but possesses a greater proximal and distal width, and generally closer thecal spacing proximally (Figs. 6.70-6.73). *Glyptograptus*? sp.1 is distinguished from those assigned here to *K. laciniosus* by their higher mesial and distal widths (Figs. 6.71 and 6.73); more tapered, less parallel-sided rhabdosome; prominent distally projecting nema; less inclined and less rounded thecae; and a wandering internal nema. They are distinguished from those assigned to *Normalograptus* sp. 1 by their more inclined thecae; slightly higher rate of widening and proximal 2TRD (Fig. 6.72); robust distally projecting nema; and the absence of a prominent median septum proximally. These specimens resemble *N.? rhizinus* Li and Yang in thecal form and in possessing a prominent nema, but are wider mesially and beyond, and do not possess a long virgella

or other proximal spines. The stratigraphically higher *Normalograptus radicatus* Chen and Lin is narrower, has a much higher proximal 2TRD (Fig. 6.85), and possesses an elaborate branching virgella.

***Glyptograptus*? sp. 2**

Plates: (Photos) 30.6-30.9; (Line drawing) 27.18

Material and stratigraphical range: Rare from the upper *persculptus* Zone, mid *ascensus* Zone, and upper *acuminatus* Zone. 7 specimens from the *persculptus* Zone and 7 specimens from the *ascensus* and *acuminatus* zones measured in detail.

Description: Rhabdosome up to 9 mm in length. Widens from 0.68-0.78 mm at th1, to 0.9-1.1 mm at th3, to 1-1.15 mm at th5, and 1.05-1.2 mm at th7-th10 (nearly parallel-sided after th3). One probable distal fragment has a maximum width of 1.35 mm. 2TRD is consistently low: 1.05-1.45 mm at $th1^1$ (average=1.2 mm), 1.25-1.45 mm at $th3^1$, 1.3-1.55 mm at th5, and 1.35-1.45 mm at $th7^1$ (n=4). Thecae are inclined and geniculate throughout, but can appear nearly orthograptid when compressed, especially distally. Thecal apertures are everted. Supragenicular walls are long relative to the thecal opening. The nema is very thin and wanders or is offset in many specimens, suggesting that the species is either aseptate or only partially septate, at least proximally. The virgella is rarely preserved. A threadlike nema projects distally in some specimens.

Remarks: *Glyptograptus*? sp. 2 is superficially very similar to *K. laciniosus,* especially in proximal specimens, but has closer thecal spacing, narrower DVW (Fig. 6.67), and often more rounded thecae, although this latter feature is strongly affected by preservation.

K. laciniosus also usually has an obvious complete median septum throughout, whereas in *G.*? sp. 2, the threadlike nema wanders proximally, suggesting that they are aseptate (a partial median septum is questionably present in several specimens; see Plate 30.7. *Glyptograptus*? sp. 2 differs *Glyptograptus* sp. in possessing more rounded and inclined thecae and closer thecal spacing (Fig. 6.86).

Superfamily MONOGRAPTOIDEA Lapworth, 1873, emended Melchin et al., 2011.

Paraphyletic Family DIMORPHOGRAPTIDAE Elles and Wood, 1908, emended Melchin et al., 2011.

Genus *AVITOGRAPTUS* Melchin et al., 2011.

Type species: *Glyptograptus*(?) *avitus* Davies 1929.

***Avitograptus avitus* (Davies, 1929)**

Plates: (Photos) 31.25, 32.4-5, 32.8-9, 37.24, 38.1;

(Line drawings) 27.13, 27.17, 28.7, 29.9-10

Material and stratigraphical range: Uncommon throughout the upper *persculptus* Zone and rare in the lowest *ascensus* Zone. More than 27 specimens measured in detail.

Description: Tapered rhabdosome up to at least 39 mm long. Gradually expands from 0.68-0.9 mm at th1, to 0.85-1.15 mm at th3, 1.05-1.33 mm (1=1.45 mm) at th5, 1.2-1.6 mm at th7, 1.4-1.55 at th 10 (1=1.7 mm), 1.4-1.65 mm (1-1.78 mm) at th15, 1.45-1.73 mm at th20. 2TRD is consistently high throughout: 1.95-2.5 mm at $th1^1$ and 2-2.4 mm distally. The first thecal pair is elongate. $Th1^1$ turns up at or slightly above the level of the sicular aperture. Its upward grown length is 0.88-1.3 mm. A prominent virgella is

present even on immature specimens. The virgella is up to 10 mm long, often deflected away from the sicular aperture, and sometimes bearing small nodular or long parasicular growths, the latter running the length of the virgella and reaching widths of up to 0.5 mm. A prominent nema extends from the rhabdosome up to 21 mm long. Thecae possess sharp geniculae and straight supragenicular walls, which are parallel to the rhabdosomal axis or slightly inclined, depending on angle of compression.

Remarks: These specimens match well with illustrations of the holotype and other material from the type locality (Williams, 1983; Melchin et al., 2011). None of the present specimens possesses the forked virgella that characterizes the specimens described by Williams (1983) that were reassigned to *Avitograptus* aff. *avitus* by Melchin et al. (2011). A distally expanded virgella, as sometimes occurs in the present specimens, was figured by Chen et al. (2007). The present material is restricted to the *persculptus* Zone, whereas the species extends to the *ascensus* Zone at Dob's Linn (Melchin et al., 2011). *Avitograptus avitus* can be distinguished from the co-occurring *Normalograptus*? *rhizinus* by its higher thecal spacing and elongate proximal end (Fig. 6.59), and from *Korenograptus* sp. 1 by its greater thecal spacing and less inclined, more strongly geniculate thecae.

Genus AKIDOGRAPTUS Davies, 1929, emended Melchin et al., 2011.

Type species. *Akidograptus ascensus* Davies 1929.

***Akidograptus ascensus* Davies, 1929**

Plates: (Photos) 54.6-8, 54.12; (Line drawings) 43.8-11

Material and stratigraphical range: Rare from the lowest *ascensus* to the upper-middle Zone. Seven specimens measured in detail.

Description: Rhabdosome up to at least 19 mm long. 0.5-0.58 mm at th1, 0.78-0.88 mm at th3, 0.83-1.03 mm at th5, 0.98-1.1 mm at th7, 1.08-1.2 mm at th10, and 1.08-1.28 at th15 (n=3). 2TRD is consistently high: from 2-2.35 mm at $th1^1$ and 1.75-2.25 along the rest of the rhabdosome. Thecae are straight and gently inclined, with thickened and slightly everted apertures. The rhabdosome is straight to slightly curved proximally. The first thecal pair are elongate. $Th1^1$ turns upwards 0.25-0.38 mm above the sicular aperture. Its upwards grown portion is 1.33-1.85 mm long. The sicular aperture is 0.18-0.23 mm wide. The distally projecting nema is variable in robustness: thin to up to 0.25 mm wide and 15 mm long, often nearly the same length as the rhabdosome. The virgella branches several times proximally, forming a bush-like structure 0.5-1.5 mm long.

Remarks: This species first appears in a collection dominated by species of *Paramplexograptus* (*Para. kiliani, Para. wuningensis,* and *Para. paucispinus*), along with abundant *Normalograptus anjiensis.* The basal specimens and specimens that occur higher in the *acuminatus* Zone (44.04 m and 45.38 m, in particular) match very well with traditional descriptions of this species: supragenicular walls nearly parallel to the rhabdosomal axis and a maximum width of ca. 1 mm. Other specimens reach greater distal widths and have noticeably more inclined thecae. Fan et al. (in prep.) found that in bulk plots of akidograptines, *A. ascensus* and *P. acuminatus* separated into non-

overlapping clusters divisible principally by distal thecal inclination (<10 degrees vs. >15 degrees), with *P. acuminatus* also showing a strong stratigraphic trend towards greater thecal inclination (older specimens inclined at ca. 15-20 degrees and younger at ca. 15-20 degrees). Under this scheme, specimens of *A. ascensus* such as the one illustrated by Koren' and Melchin (2000), in figure 13.2, would likely be assigned to *P. acuminatus.* In addition, Fan et al. (in prep.) record specimens of *A. ascensus* of up to 1.4 mm wide, and recognize an intermediate, co-occurring species, *Akidograptus giganteus* Yang, 1964. Collectively, these observations mirror independent observations at the Blackstone River section: specimens of *P. acuminatus* from higher in the section have very strongly inclined thecae (see Plate 54.3-4 and 54.9-11), whereas those from lower in the section have less inclined thecae (Plate 43.12-13, 54.5). Similarly, a number of specimens exist with distal widths greater than is traditionally recognized for *A. ascensus* (ca. 1.25 mm), along with gently inclined thecae (see Plate 43.10 and 54.6); many of these specimens also possess a robust distally projecting nema. Except for width (which is generally higher), these are features that are characteristic of *Akidograptus giganteus* Yang*,* but they also grade into those in the lower population of *P. acuminatus* at the Blackstone. These rare, difficult to assign specimens, with features intermediate between *A. ascensus* and *P. acuminatus,* exist as low as sample 38.62 m, with increasingly *acuminatus*-like specimens occurring in 39.59 m, a meter below those confidently assigned to *P. acuminatus*. Assigning some or all of these specimens to *P. acuminatus* would greatly reduce the thickness of the *ascensus* Zone (by up to half), and would also

result in *Hirsutograptus tuberculatus* and *Atavograptus primitivus* being entirely restricted to the *acuminatus* Zone, out of stratigraphic position relative to China and Scotland (Williams, 1983--based on Melchin and Williams' (2000) revision of the base of the *acuminatus* Zone; Fan et al., in prep.; personal observ.). It is possible that *P. acuminatus* does actually occur lower and/or that a fourth species of akidograptid is present in the lower Rhuddannian at the Blackstone River section (perhaps *A. giganteus*), but until further comparative metrical work can be conducted, specimens with robust specimens and clearly inclined supagenicular walls are assigned to *P. acuminatus,* and both those with parallel supragenicular walls and those with moderately inclined walls and widths up to 1.25 mm are included in *A. ascensus.* The base of the *acuminatus* Zone is placed at the sample (41.66 m) where common specimens confidently assignable to *P. acuminatus* first occur.

Akidograptus cuneatus

Plates: (Photos) 53.24, 54.13, 56.8-9, 56.25?, 56.27?

Material and stratigraphical range: Rare in the lower to upper *acuminatus* Zone, and possibly present from the *ascensus* to basal *atavus* zones.

Remarks: Rare examples of specimens of *Akidograptus* with very low distal width occur episodically throughout the *acuminatus* Zone. These match previous descriptions of *A. cuneatus* in having a low DVW (<0.7 mm) and low thecal inclination. Specimens from 42.65 m to 47 m are confidently identified as *Akidograptus cuneatus*. Specimens from the basal *acuminatus* Zone do not appear to have the high 2TRD that is normally characteristic of the species (e.g., Koren' and Melchin, 2000), and possibly represent

abnormally thin examples of *Akidograptus ascensus.* They are only questionably assigned to *A. cuneatus.*

Genus *PARAKIDOGRAPTUS* Li and Ge, 1981

Type species: *Diplograptus accuminatus* (sic) Nicholson, 1867.

***Parakidograptus acuminatus* (Nicholson, 1867)**

Plates: (Photos) 54.3-5, 54.9-11, 56.23; (Line drawings) 43.12-13

Material and stratigraphical range: Uncommon throughout the *acuminatus* Zone.

Remarks: The specimens at the Blackstone River section match well with previous descriptions of this species. As has been noted elsewhere (e.g., Štorch, 1983), there is a stratigraphic shift in the morphology of this species. At the Blackstone River section, this is most noticeable in a trend towards greater thecal inclination, especially proximally, and rhabdosomal curvature in the younger specimens (e.g., compare basal specimen Plate 54.5 with the younger specimen show on 54.4). As Fan et al. (in prep.) note, this species possesses geniculae, not truly orthograptid thecae; this is clear in the well-preserved specimens in the present collection (see arrows on Plate 56.23). Basal specimens of *P. acuminatus* resemble *A. ascensus,* especially when both are preserved off-profile. They are distinguishable, however, by their greater width even when thecal form is not clear. Further discussion of identification issues with this species occurs in the discussion of *Akidograptus ascensus* (above) and in Chapter 4.1.

Genus *DIMORPHOGRAPTUS* Lapworth, 1876, emended Melchin et al., 2011

Type species: *Dimorphograptus elongatus* Lapworth 1876

Dimorphograptus swanstoni Lapworth, 1876

Plates: (Photo) 44.11

Material and stratigraphical range: A single mature specimen from the *atavus* Zone.

Description: Rhabdosome greater than 40 mm long, preserved in subscalarifrom view. Proximal end is broken, but at least three thecae are uniserial. Uniserial thecae are acuminate and the uniserial portion of the rhabdosome is strongly dorsally curved. The biserial portion rapidly reaches a width of 2 mm, which is maintained or increases distally (up to 2.25 mm, depending on angle at which thecae are flattened). Distal 2TRD varies between 2.25 mm and 2.5 mm. Thecae are inclined throughout, and apparently less so distally, but precise thecal form is difficult to determine given scalariform preservation. Thecae are consistently geniculate. A slightly wider distal fragment of the species is preserved adjacent to the illustrated specimen. It has a maximum distal width of 2.5 mm.

Remarks: This specimen agrees with the types in its wide thecal spacing, thecal form, and rhabdosome size. It differs in having a more strongly curved uniserial portion, but this may be an artifact of the subscalariform mode of preservation. The total number of uniserial thecae is unclear, as the proximal end is broken, but given that the sicula is not preserved, it must be at least four, which is also consistent with the species. Churkin and Carter (1970) reported the species from Alaska in the *vesiculosus* through *cyphus* zones. In the Yukon, it has previously been reported by Lenz (1982) from the Blackstone River section in the *atavus*? and *acinaces* zones, and from the Peel River and Rock River sections in the *acinaces* Zone and the *gregarius* Zone.

Family MONOGRAPTIDAE Lapworth 1873, emended Melchin et al., 2011

Genus *ATAVOGRAPTUS* Rickards, 1974

Type species: *Monograptus atavus* Jones, 1909, by original designation

***Atavograptus primitivus* (Li, 1983)**

Plates: (Photo) 49.23

Material and stratigraphical range: Rare specimens from the upper *ascensus* Zone. One specimen with proximal end, and several distal fragments measured.

Description: $Th1^1$ grows upwards 0.7 mm above the sicular aperture. DVW is 0.25 at th1 and 0.3-0.35 mm distally. 2TRD is ca. 2.3 mm at $th1^1$ and ca. 1.95 mm distally. The thecae are geniculate throughout, with straight, inclined supragenicular walls, and slightly everted apertures. The rhabdosome is gently curved dorsally.

Remarks: These specimens closely match the detailed redescription by Lukasik and Melchin (1994), as well as Chinese material described by Fan et al. (in prep.). Specimens occur in only a single sample, in the upper *ascensus* Zone. *Atavograptus ceryx,* a species that differs principally in its closer thecal spacing (although the types are deformed), also occurs over a very brief stratigraphic interval in the middle *ascensus* Zone (Williams, 1983; Melchin, unpublished data). This is the only occurrence of a monograptid at the Blackstone River section below the base of the *atavus* Zone.

***Atavograptus atavus* (Jones, 1909)**

Plates: (Photos) 56.26

Material and stratigraphical range: Basal *atavus* Zone (likely higher-only a single sample collected from the zone). Mostly fragmentary material.

Remarks: Fragmentary distal material is assigned based on relatively simple apertures and high distal DVW (up to 1.10 m). The small amount of fragmentary material is insufficient to determine whether more than one species is present, but Lenz (1982) observed several species of *Atavograptus* from a similar stratigraphic height at the Blackstone River section and other regional sections.

Genus *HUTTAGRAPTUS* Koren' and Bjerreskov, 1997

Type species: *Atavograptus praestrachani* Hutt and Rickards

***Huttagraptus* sp.**

Plates: (Photos) 56.34

Material and stratigraphical range: Basal *atavus* Zone (likely higher). Mostly fragmentary material. One proximal fragment measured.

Description: Sicula is 1.7 mm long. DVW is ca. 0.4 mm at th1, 0.45 mm at th5, 0.5 mm at th10. 2TRD is ca. 2 mm at th1, 2.1 mm at th5. Thecae are simple and geniculate, with someapertural thixening. The rhabdosome is dorsally curved. Thecal apertures are slightly everted.

Remarks: This species id distinguished from *Atavograptus* by its strongly geniculate, slightly thickened apertures. Insufficient material was examined to provide a species-level identification. The relatively short sicula is atypical of many well-known species of *Huttagraptus* (Koren' and Bjerreskov, 1997).

6.5 Supporting Graphs for 6.4

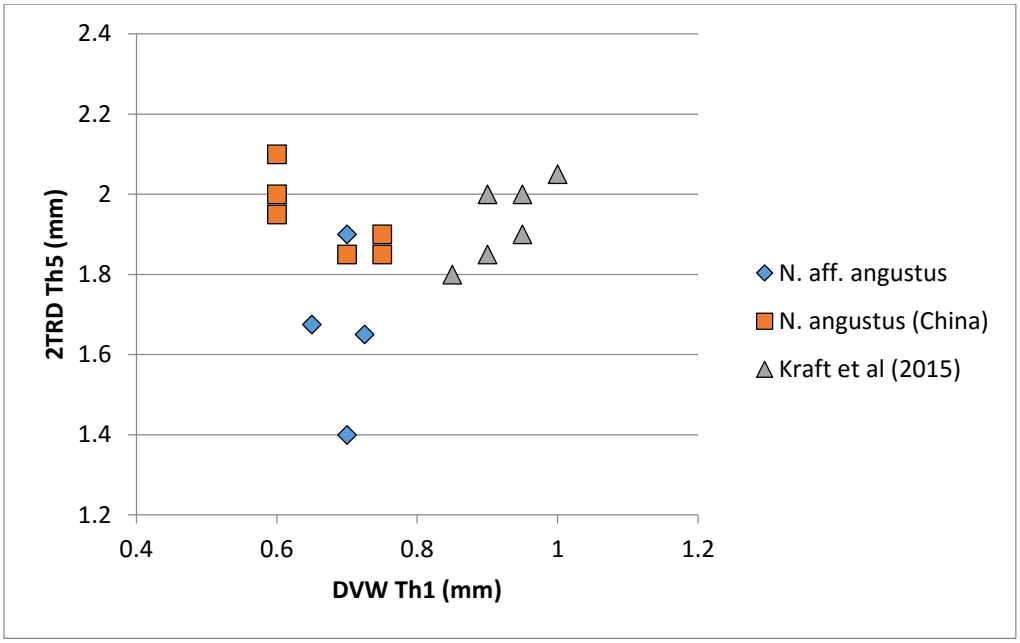

Figure 6.41. N. angustus vs. N. aff. angustus. N. angustus (China) = unpublished early Silurian data provided by M.J. Melchin. Kraft et al. (2015) = data in table 4 (specimens from the Czech Republic). Other data from the Blackstone River. Kraft et al. 2TRD = Howe.

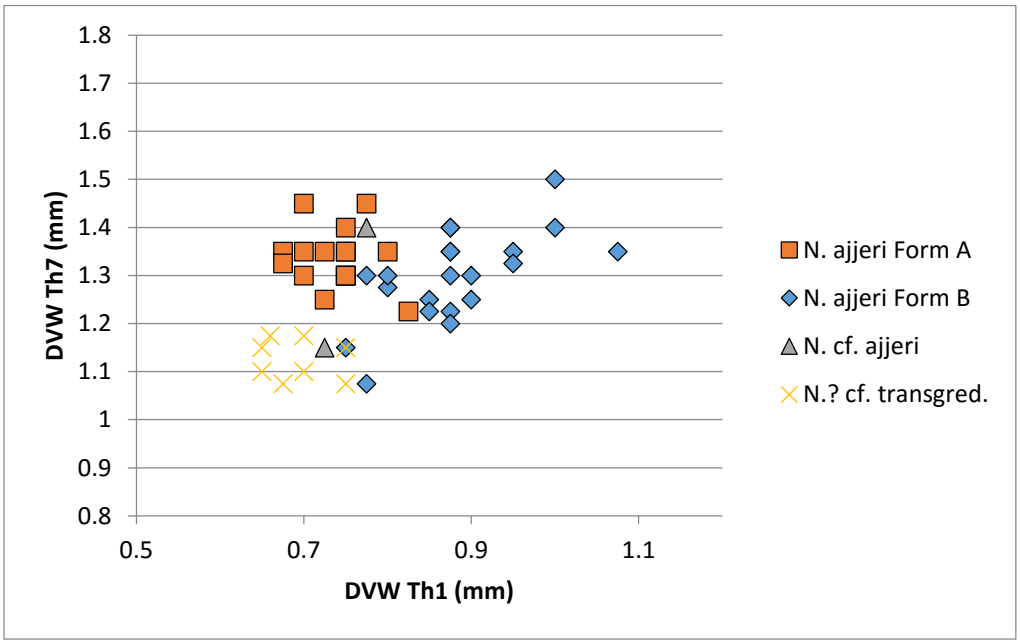

Figure 6.42. Normalograptus: Mesial 2TRD vs. proximal DVW. All specimens from the Blackstone River.

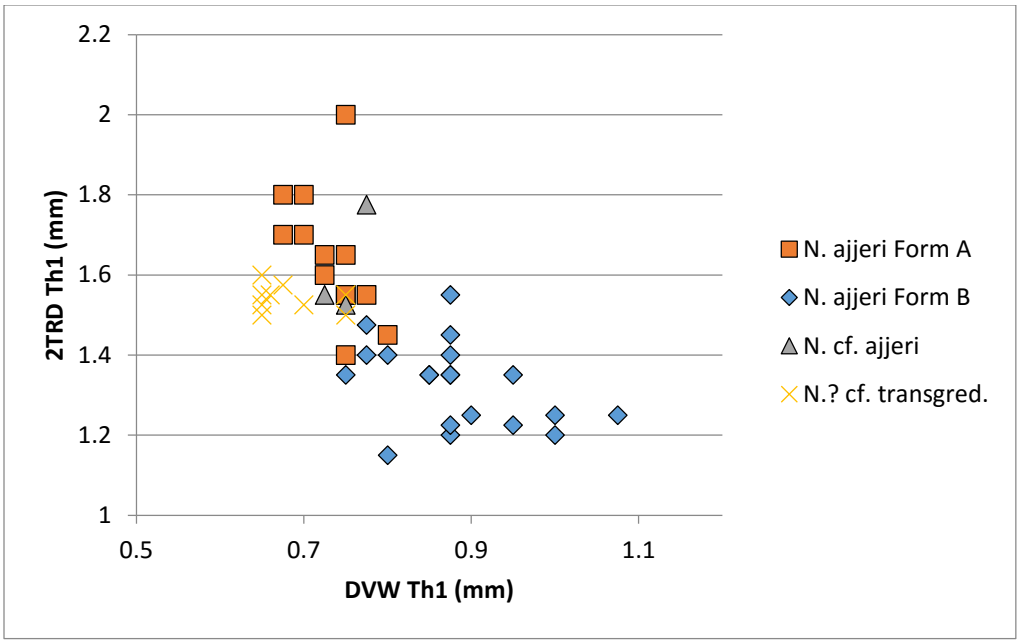

Figure 6.43. Normalograptus: Proximal 2TRD vs. proximal DVW. All specimens from the Blackstone River.

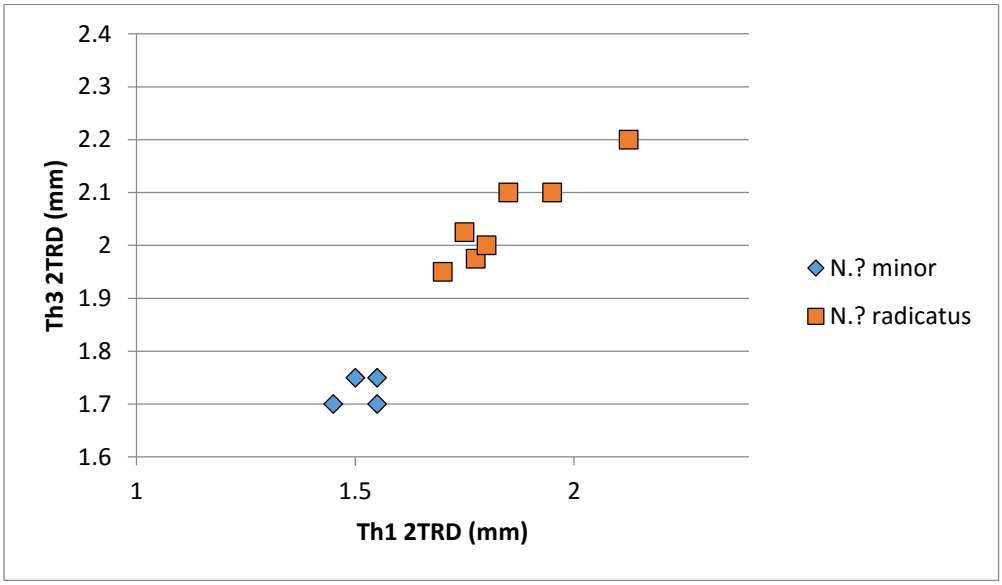

Figure 6.44. N.? minor vs. N.? radicatus: Proximal 2TRD. All specimens from Blackstone River.

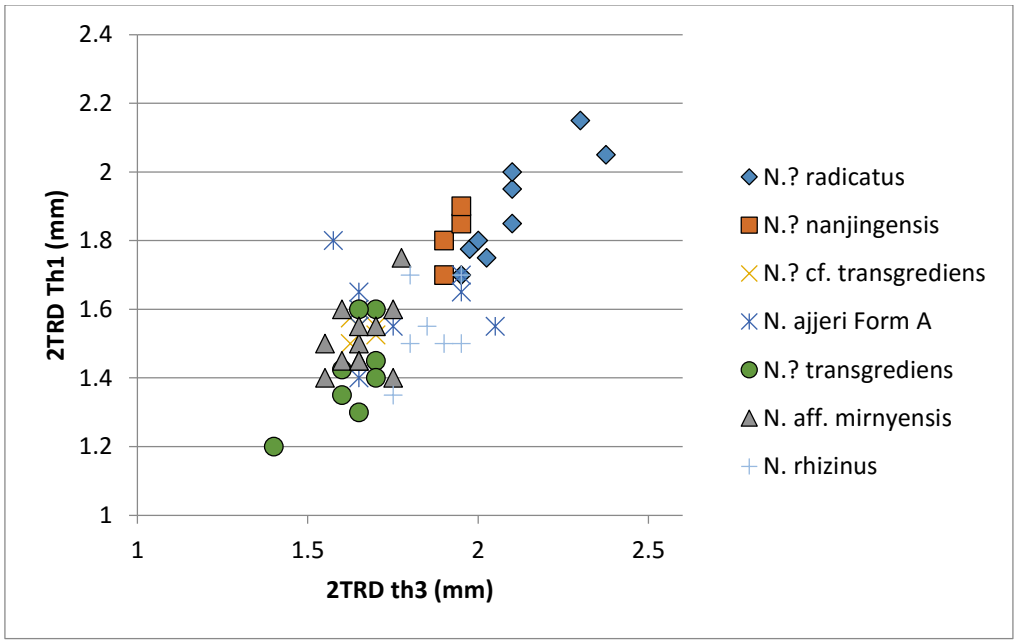

Figure 6.45. N.? radicatus vs. other Normalograptus species. All specimens from Blackstone River.

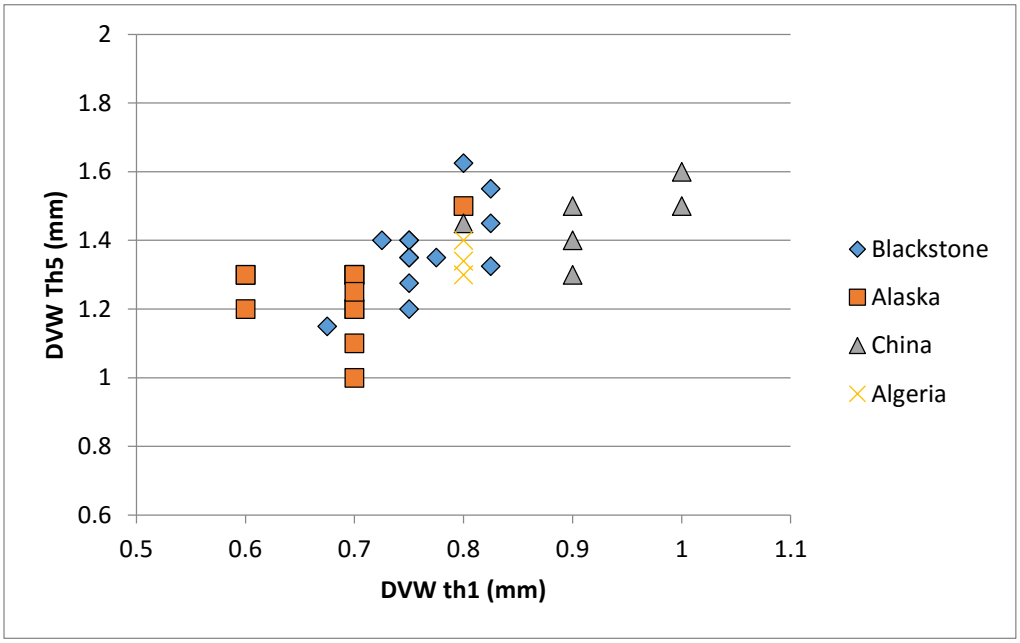

Figure 6.46. N. rectangularis: Global comparison. Blackstone=specimens measured from current section; Alaska specimens of *Climacograptus* cf. *rectangularis* in data table of Churkin and Carter (1970); Algeria=*N. N. normalis* aff. a*jjeri* Forme C, specimens 'A', 'B', and 'C', data table in Legrand (1999)*;* China=unpublished data provided by M.J. Melchin.

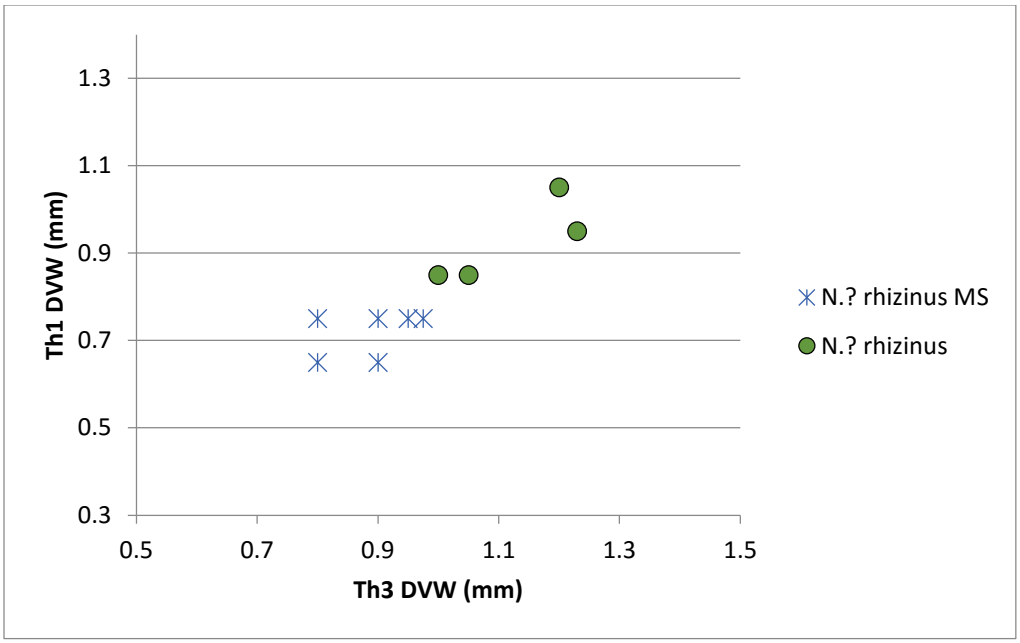

Figure 6.47. N.? rhizinus comparison. MS=specimens with proximal spines in addition to the virgella and/or a bifurcating virgella. All specimens from the Blackstone River.

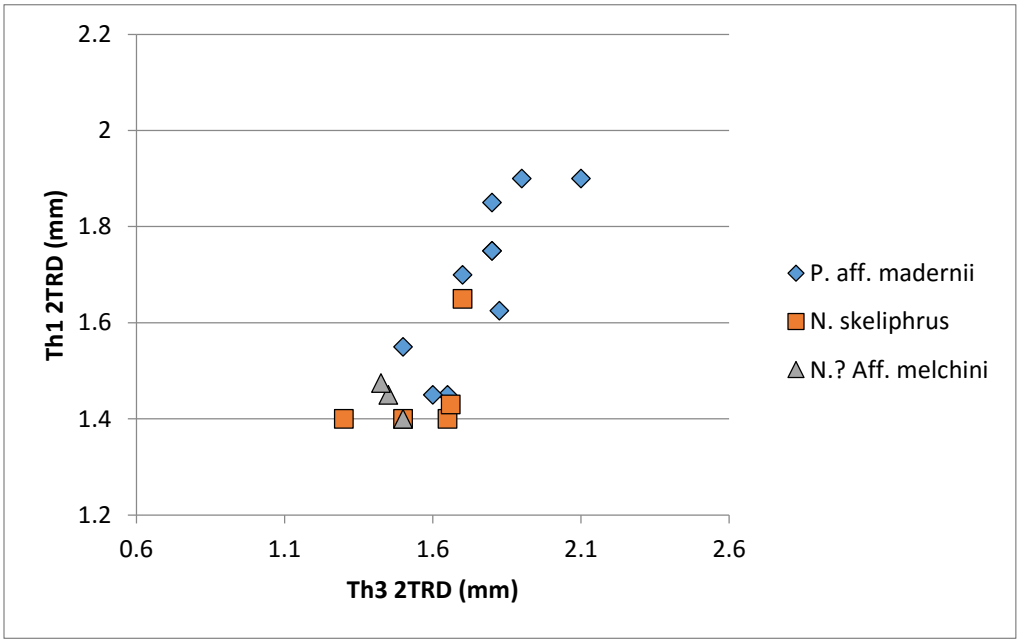

Figure 6.48. Thin "normalograptids". All specimens from the Blackstone River.

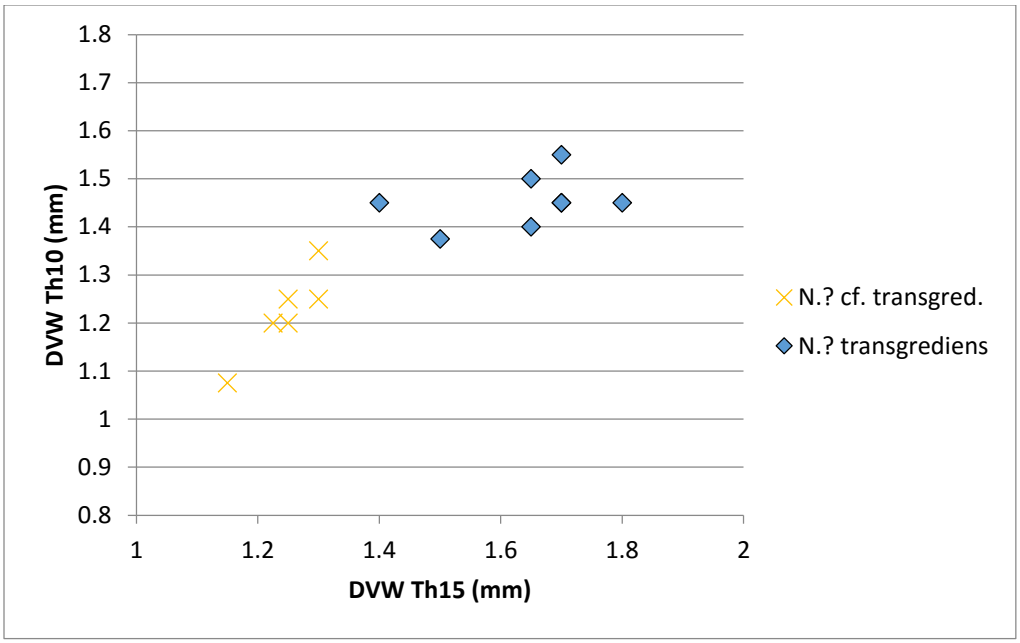

Figure 6.49. N.? transgrediens. Specimens of *N.*? cf. *transgrediens* all from the mid *ascensus* Zone. Specimens of *N.*? *transgrediens* specimens from the upper *persculptus* Zone. All specimens from the Blackstone River.

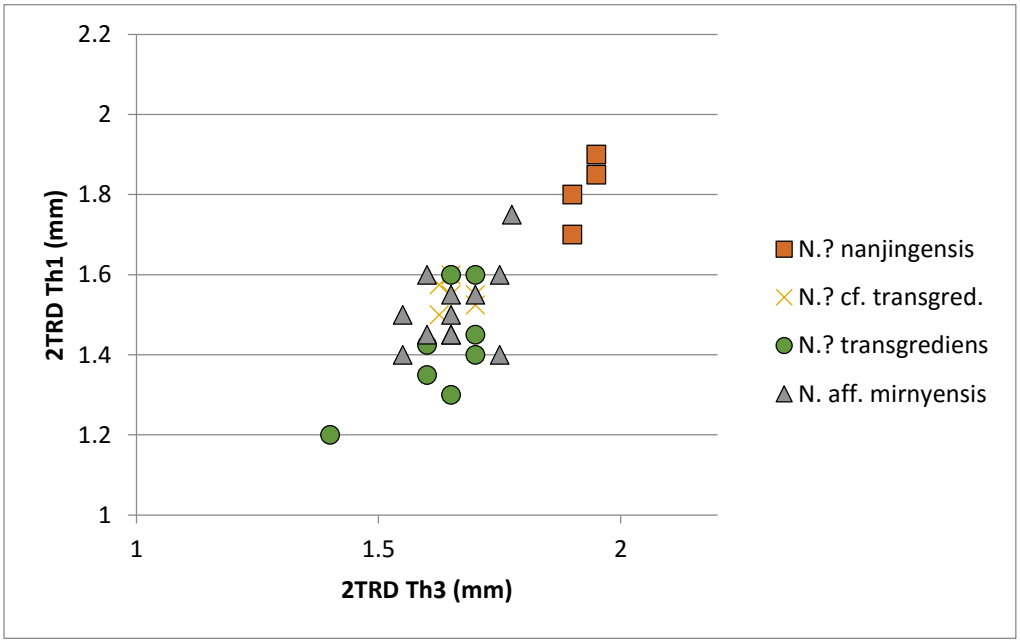

Figure 6.50. N. nanjingensis comparison. All specimens from the Blackstone River.

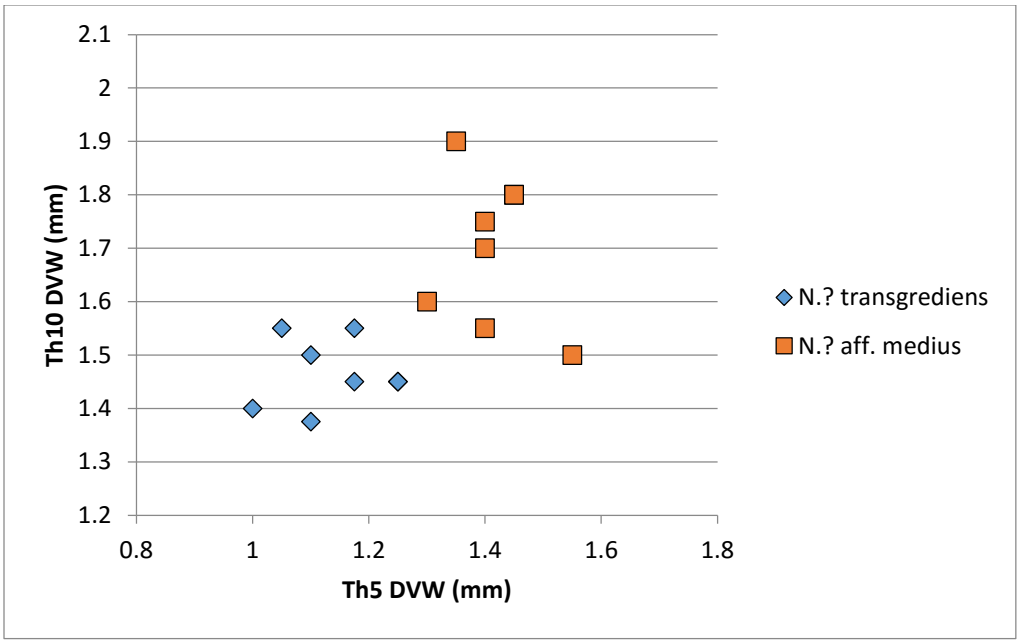

Figure 6.51. N.? aff. medius vs. N.? trangrediens. All specimens from the Blackstone River.

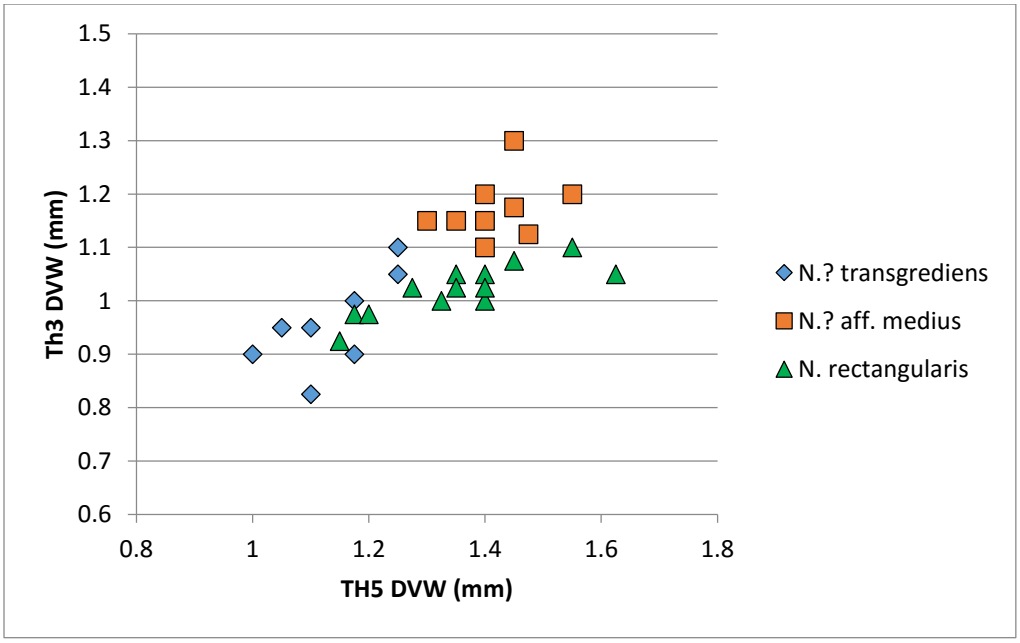

Figure 6.52. N.? aff. medius vs. N. rectangularis. All specimens from the Blackstone River.

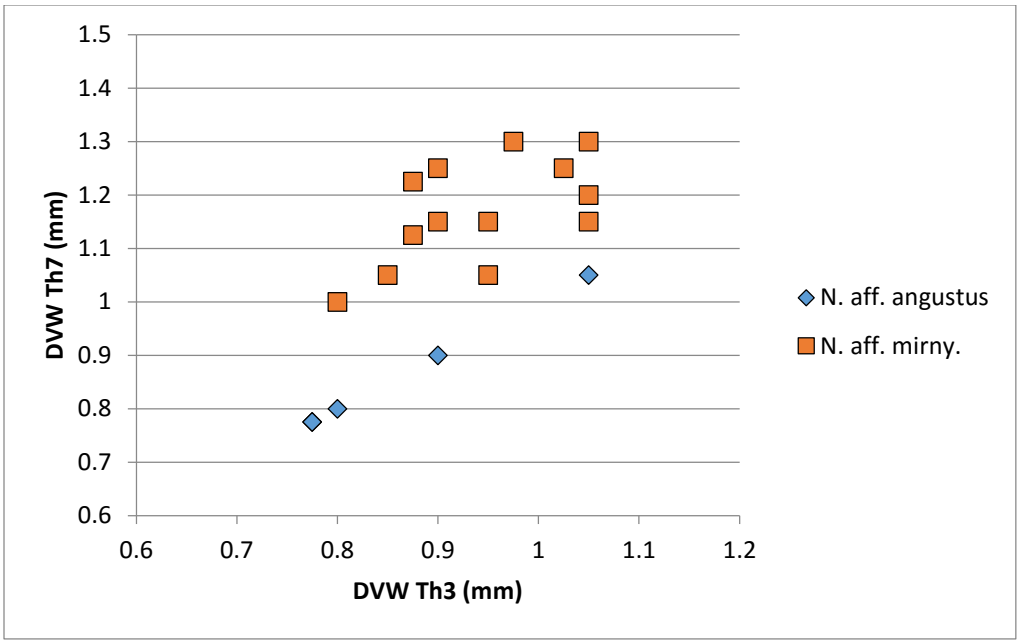

Figure 6.53. N. aff. mirnyensis vs. N. aff. angustus. All specimens from the Blackstone River.

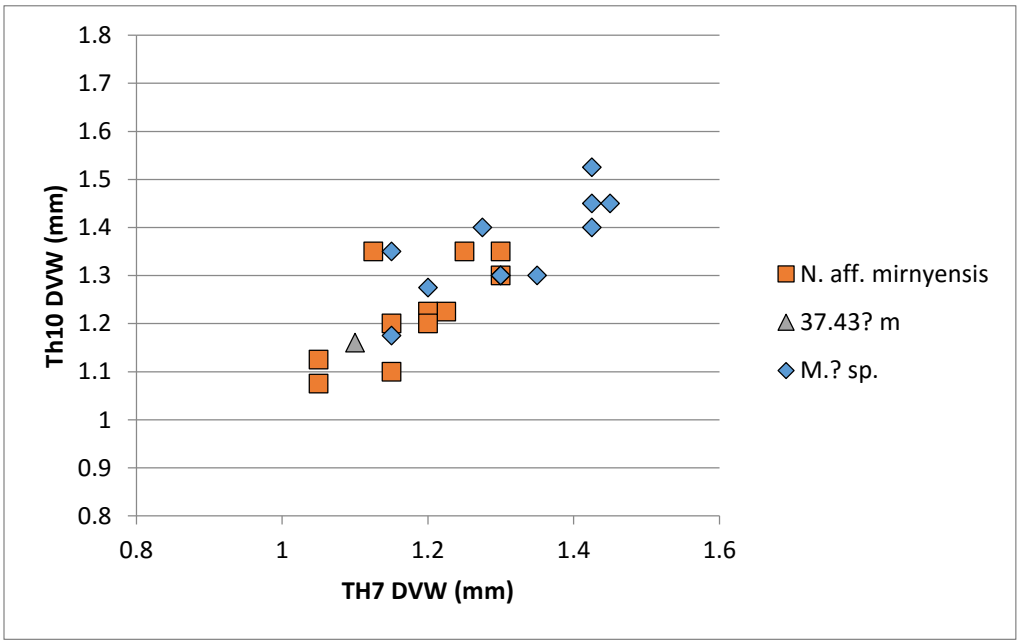

Figure. 6.54. *N*. aff. *mirnyensis* vs. *M.*? sp. 37.43? = *ascensus* Zone specimens assigned to *N.* aff. *mirnyensis* showing that they fall within *N.* aff. *mirnyensis*' morphospace. All specimens from the Blackstone River.

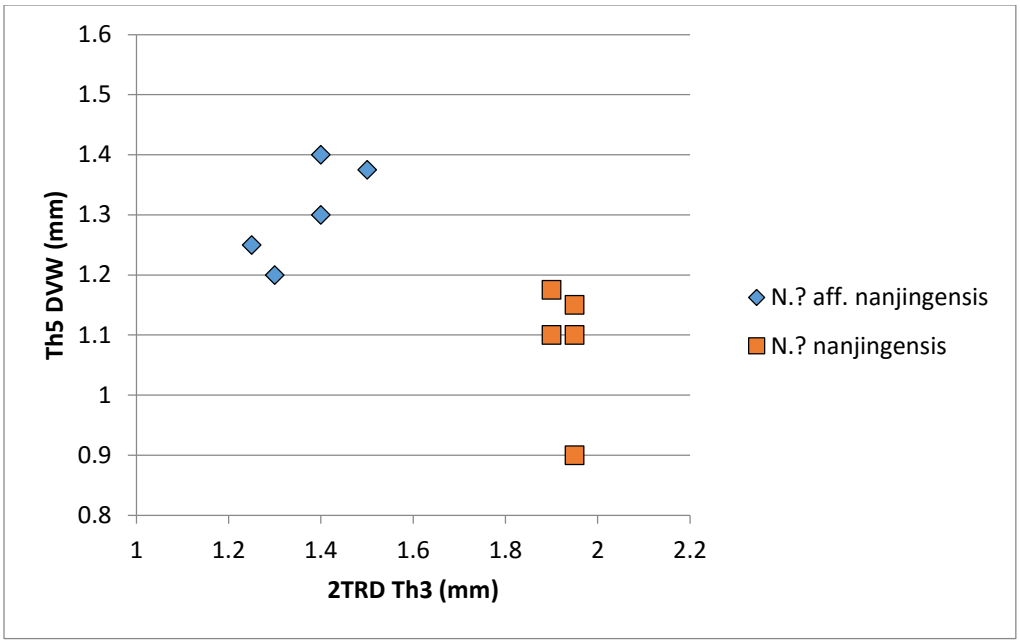

Figure 6.55. N. aff. nanjingensis vs. N. nanjingensis. Only confidently assigned specimens graphed. All specimens from the Blackstone River.

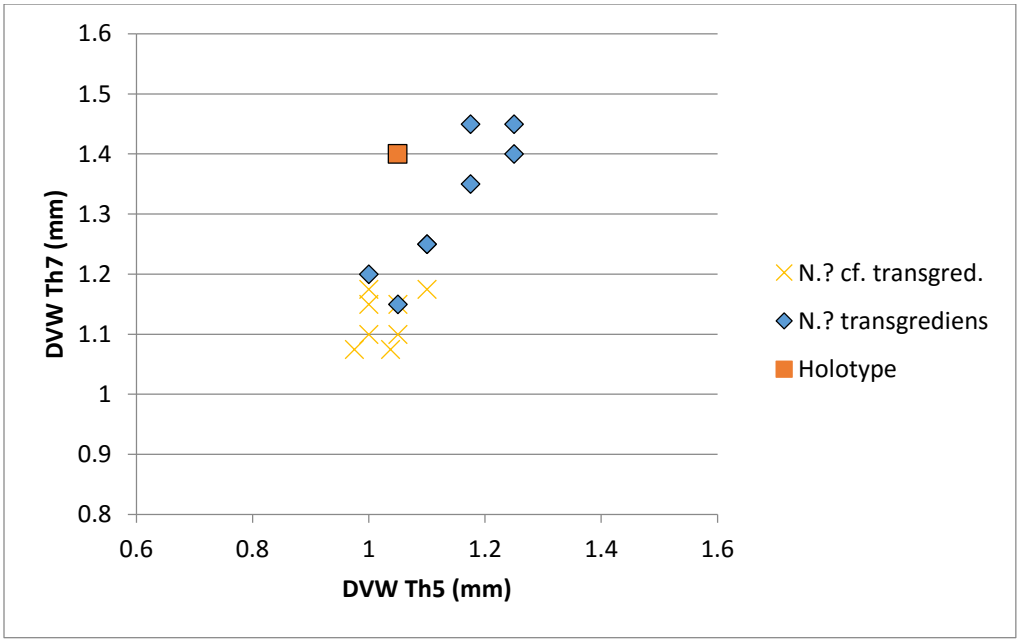

Figure 6.56. N.? transgrediens comparison. Holotype measured from plate in Waern (1948). Th7 is highest measurable pair on the illustrated types. All other data from the Blackstone River.

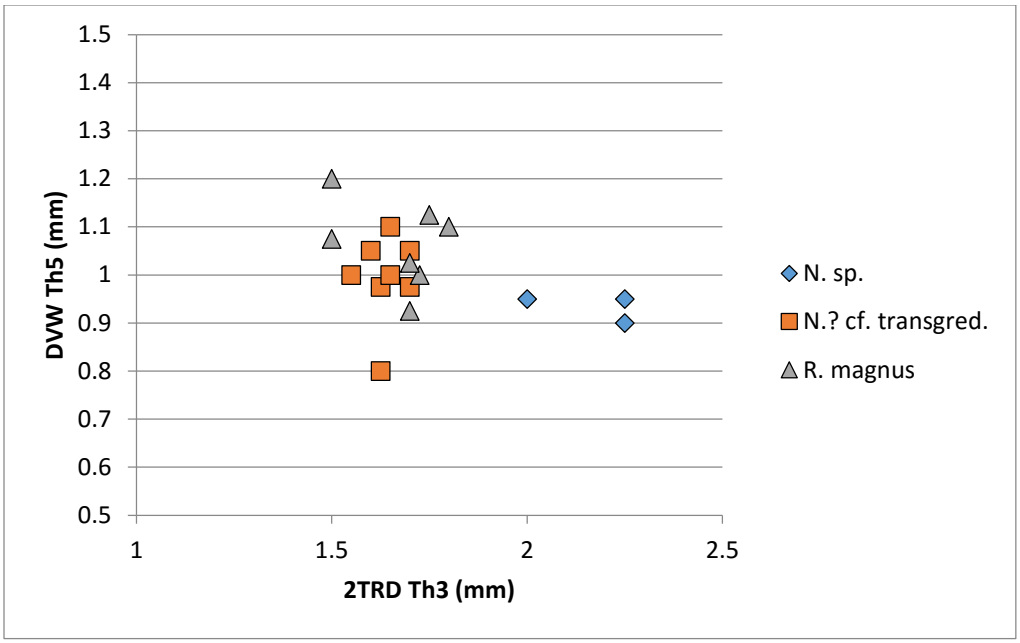

Figure 6.57: Normalograptus sp. Mesial DVW vs. proximal 2TRD. All specimens from the Blackstone River.

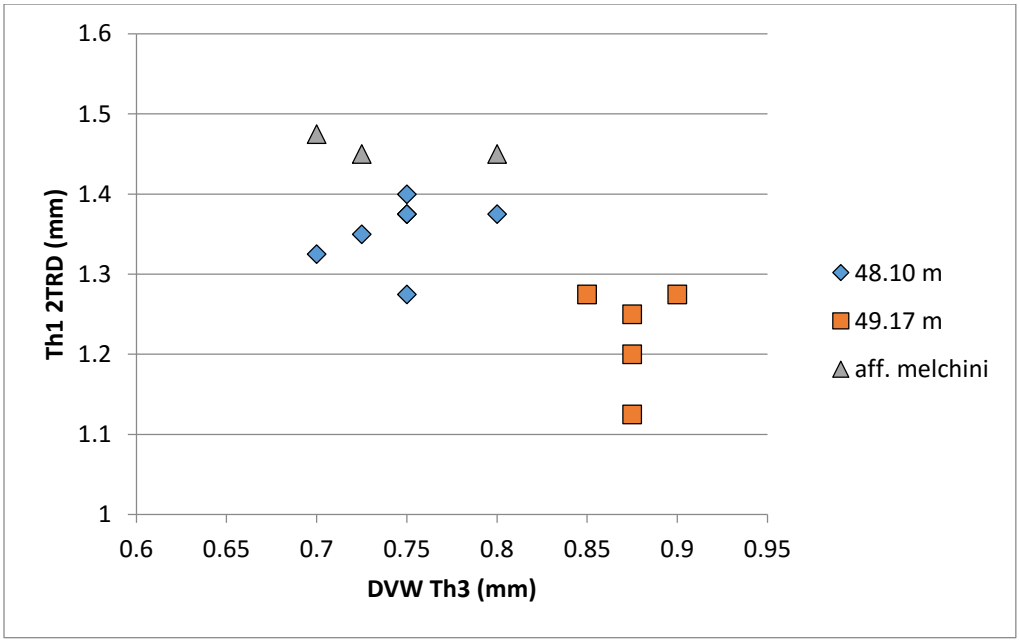

Figure 6.58. Metaclimacograptus hughesi by stratigraphic height. N.? aff. *melchini* specimens are from throughout the upper *acuminatus* Zone. DVW. All specimens from the Blackstone River.

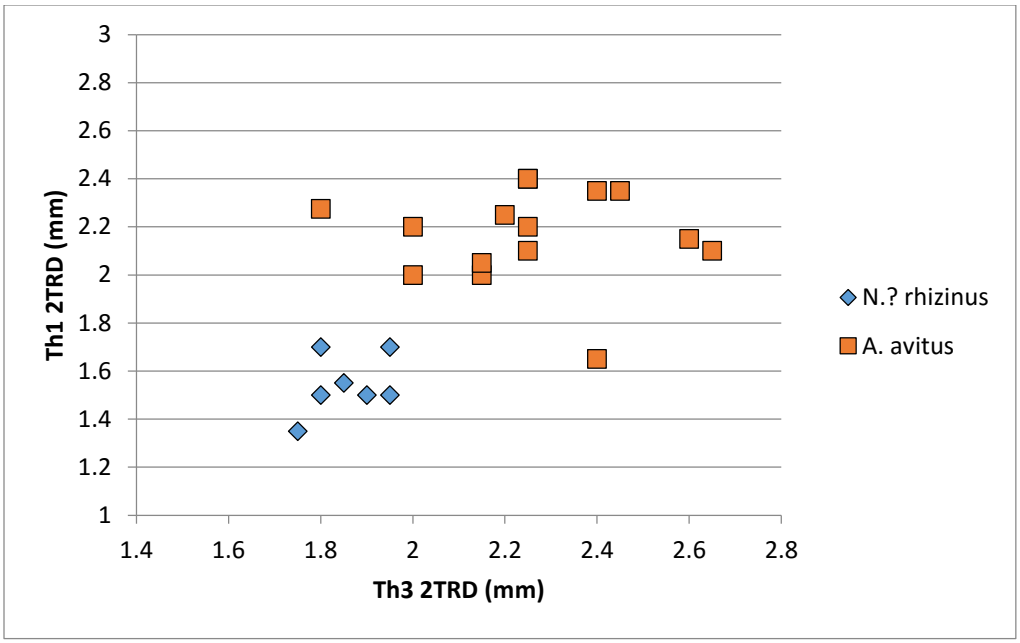

Figure 6.59. Avitograptus avitus vs. *N.*? *rhizinus*. All specimens from the Blackstone River.

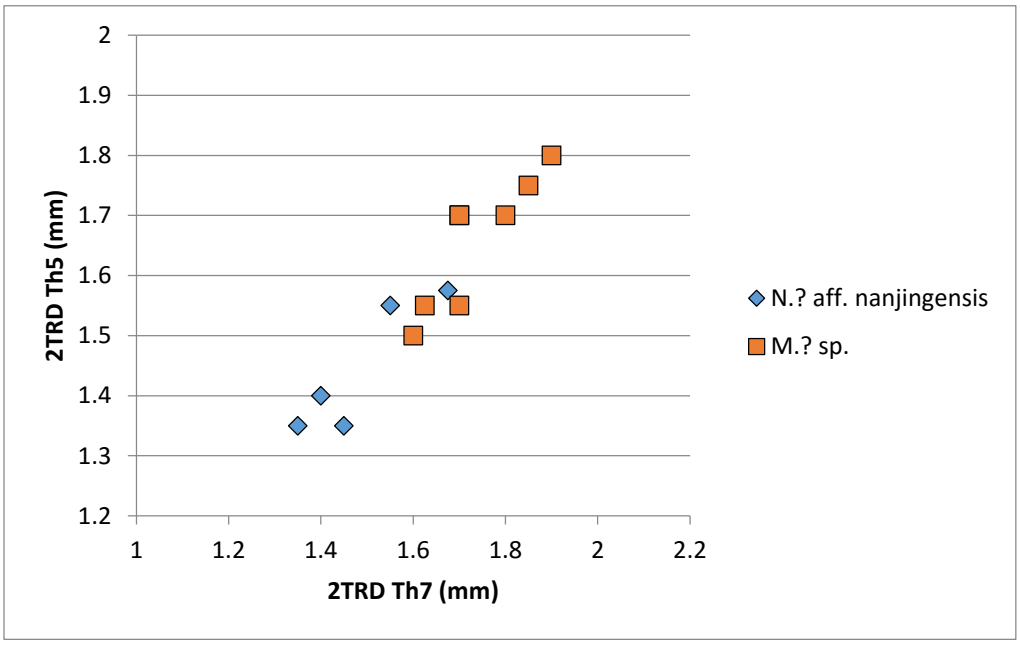

Figure 6.60. Metabolograptus? sp. vs. N.? aff. nanjingensis. All specimens from the Blackstone River.

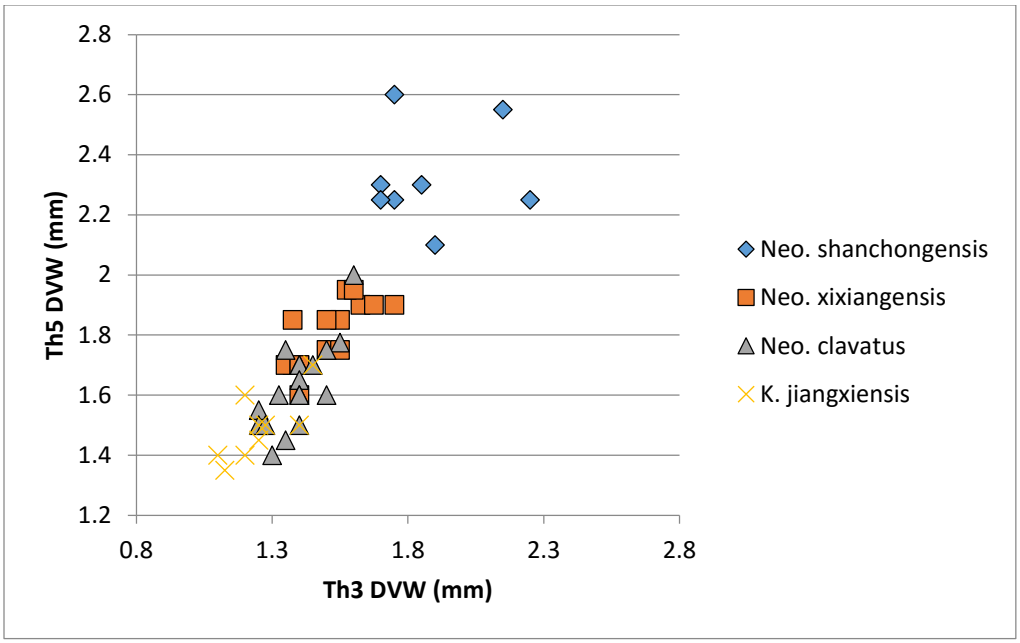

Figure 6.61. Neodiplograptus comparison (A). All specimens from the Blackstone River.

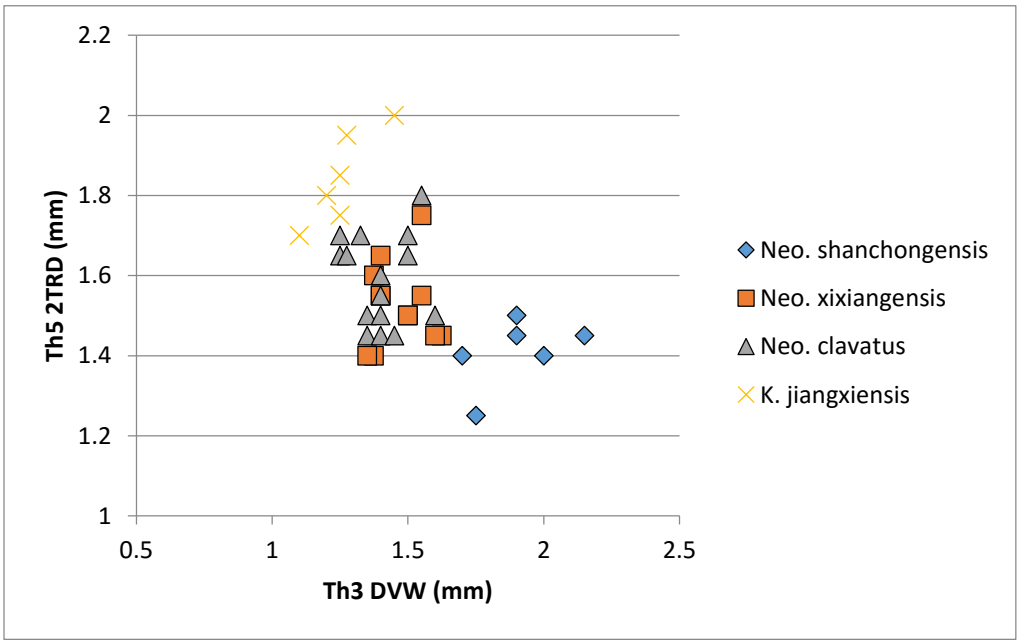

Figure 6.62. Neodiplograptus comparison (B). All specimens from the Blackstone River.

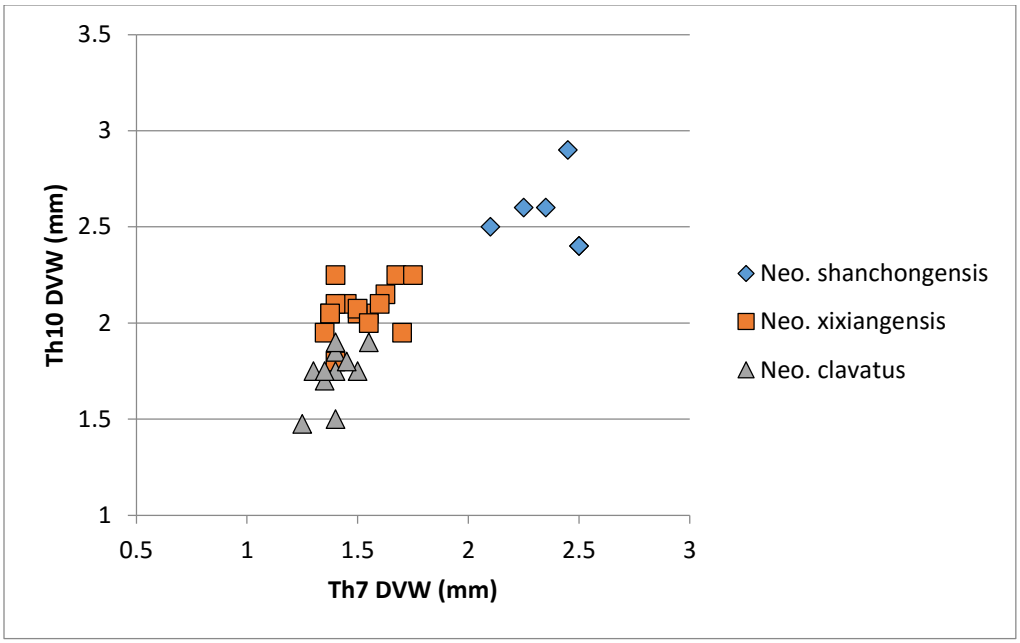

Figure 6.63. Neodiplograptus comparison (C). All specimens from the Blackstone River.

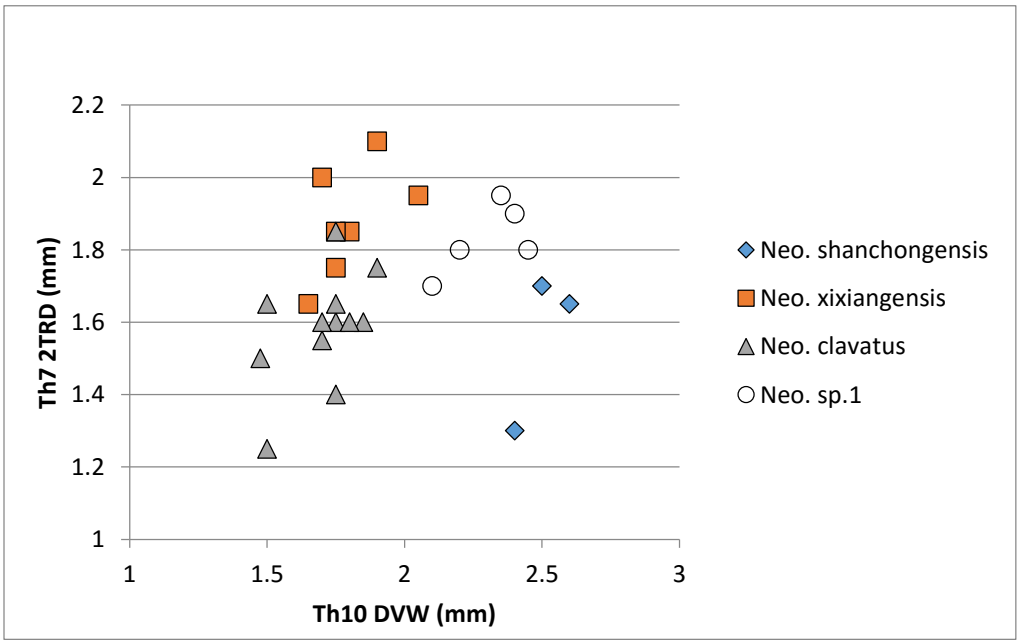

Figure 6.64. Neodiplograptus comparison (D). All specimens from the Blackstone River.

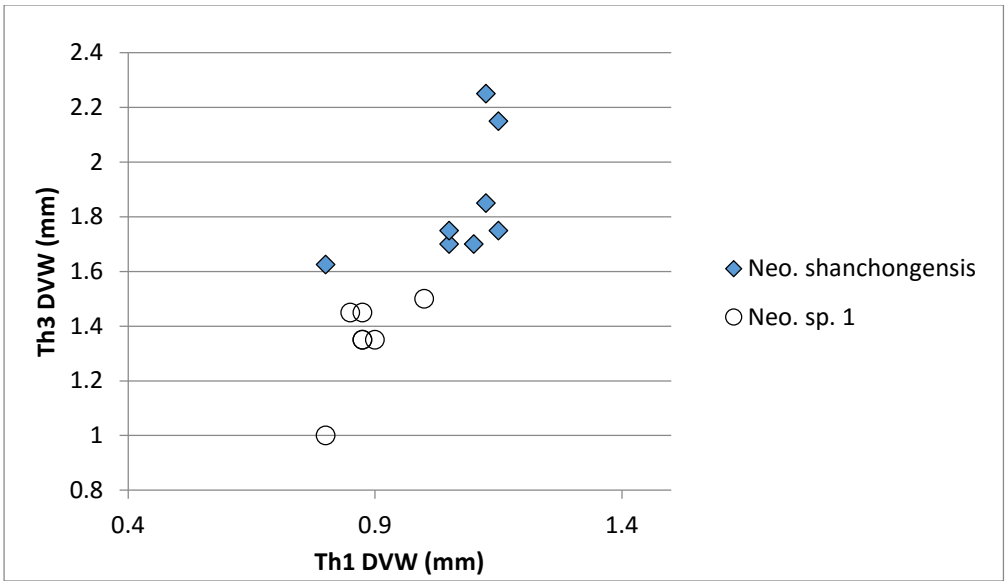

Figure 6.65. Neodiplograptus comparison (E). All specimens from the Blackstone River.

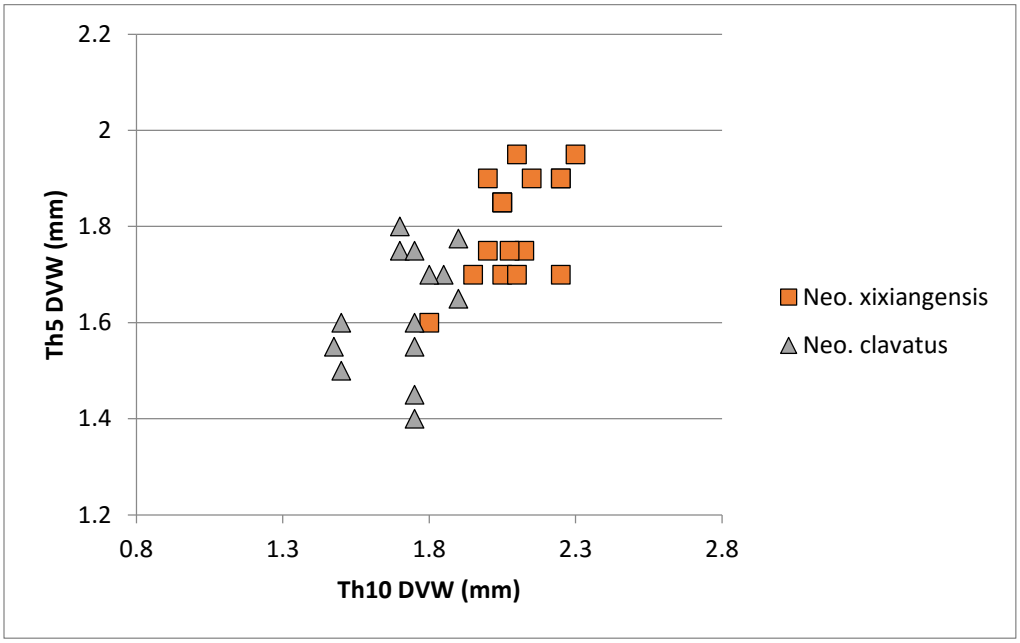

Figure 6.66. Neodiplograptus comparison (F). All specimens from the Blackstone River.

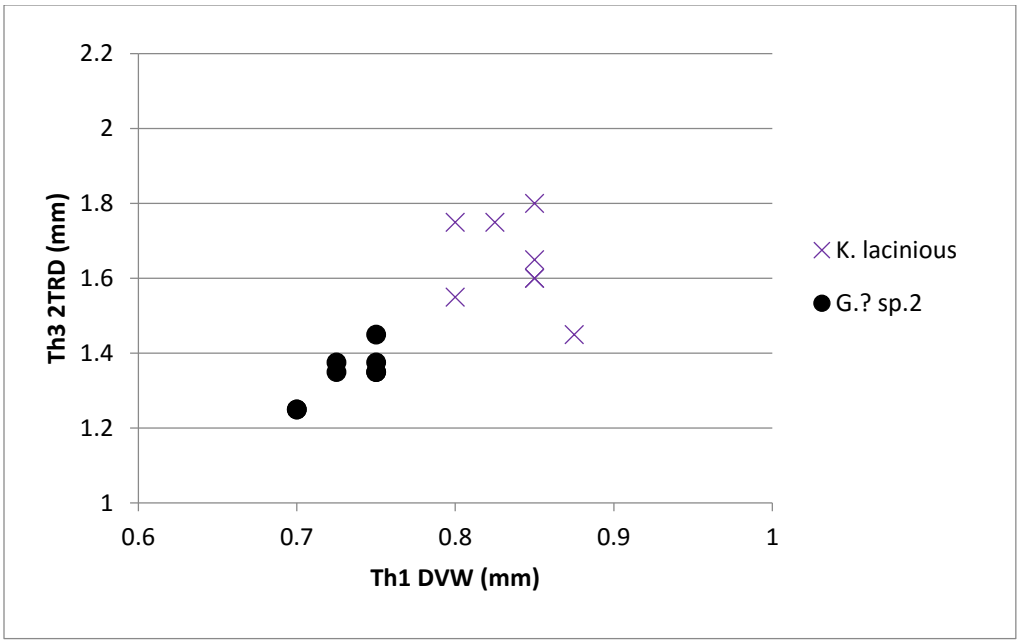

Figure 6.67. Glyptograptus? sp. 2 vs. K. laciniosus. All specimens from the Blackstone River.

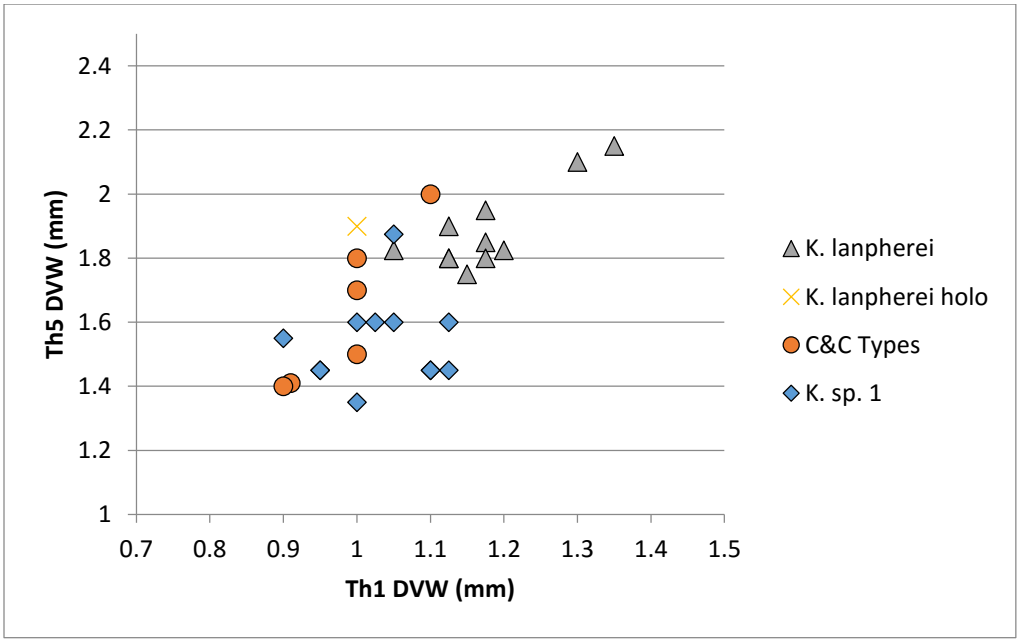

Figure 6.68. Korenograptus lanpherei. All specimens from Blackstone except types (shown as 'holo' and 'C&C types'). Measurements from types (*Glyptograptus lanpherei*) taken from data table in Churkin and Carter (1970). Distinction between species becomes more pronounced distally, but data not available for specific thecae distally in Churkin and Carter's table.

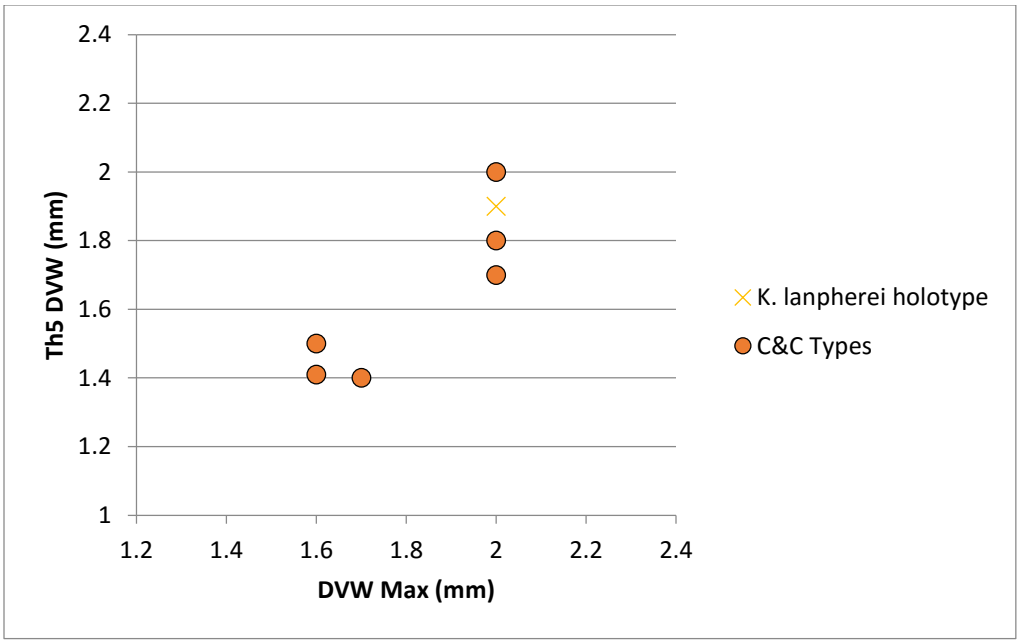

Figure 6.69. Korenograptus lanpherei (Churkin and Carter) types. Th5 DVW vs. maximum width in types. Measurements from data table in Churkin and Carter (1970).

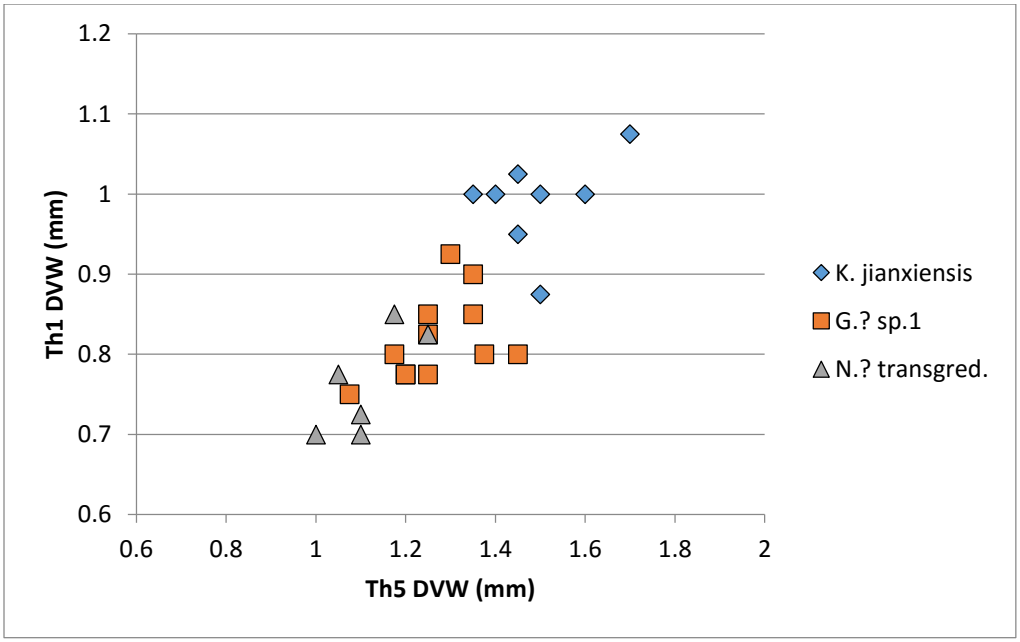

Figure 6.70. Korenograptus: Proximal vs. mesial DVW. All specimens from the Blackstone River.

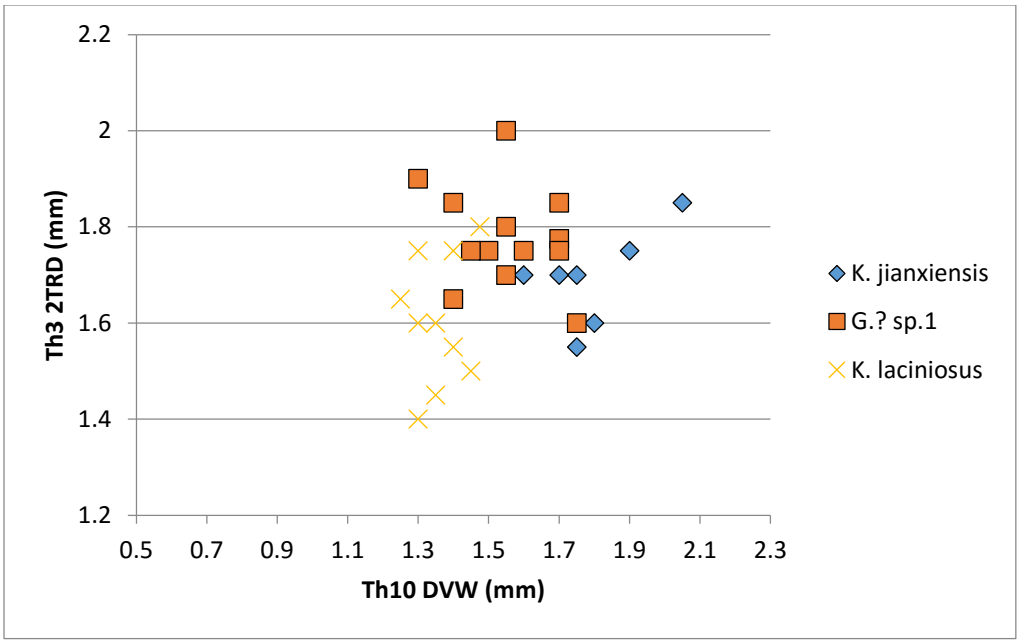

Figure 6.71. Korenograptus: Proximal 2TRD vs. distal DVW. All specimens from the Blackstone River.

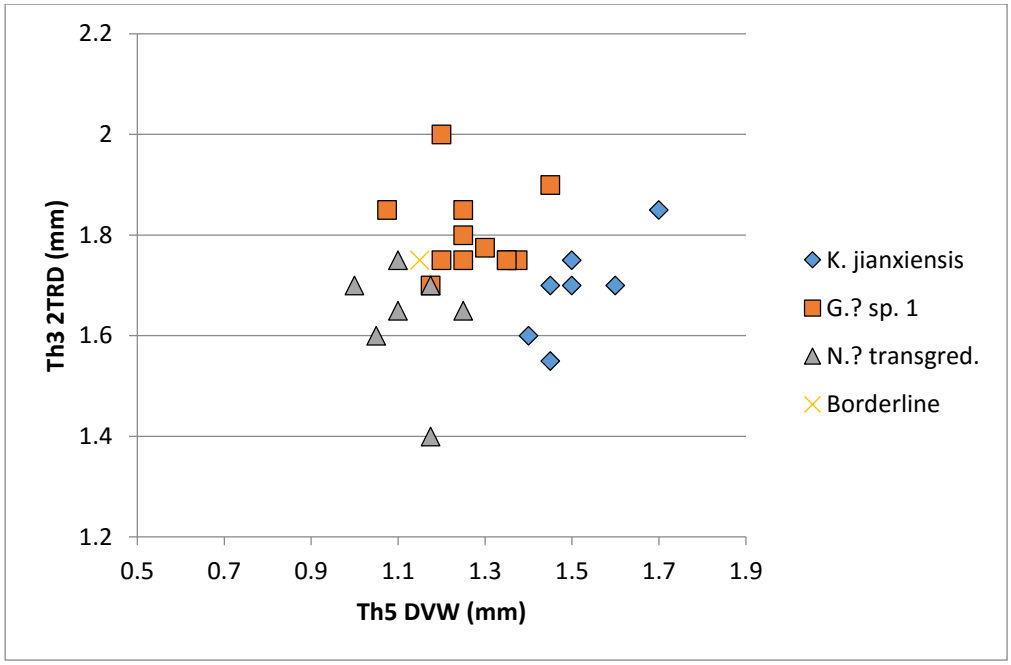

Figure 6.72. Korenograptus: Proximal 2TRD vs. mesial DVW. All specimens from the Blackstone River. Borderline are questionable specimens that were not referable confidently to either *Glyptograptus*? sp. 1 or *N.*? *transgrediens*.

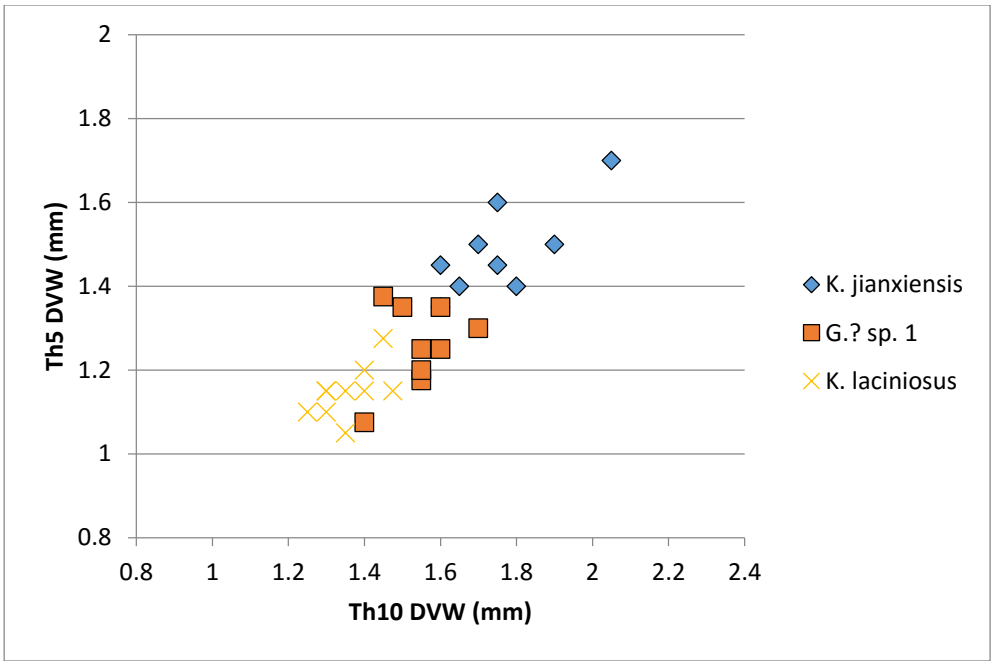

Figure 6.73. Korenograptus: Mesial DVW vs. distal DVW. All specimens from the Blackstone River.

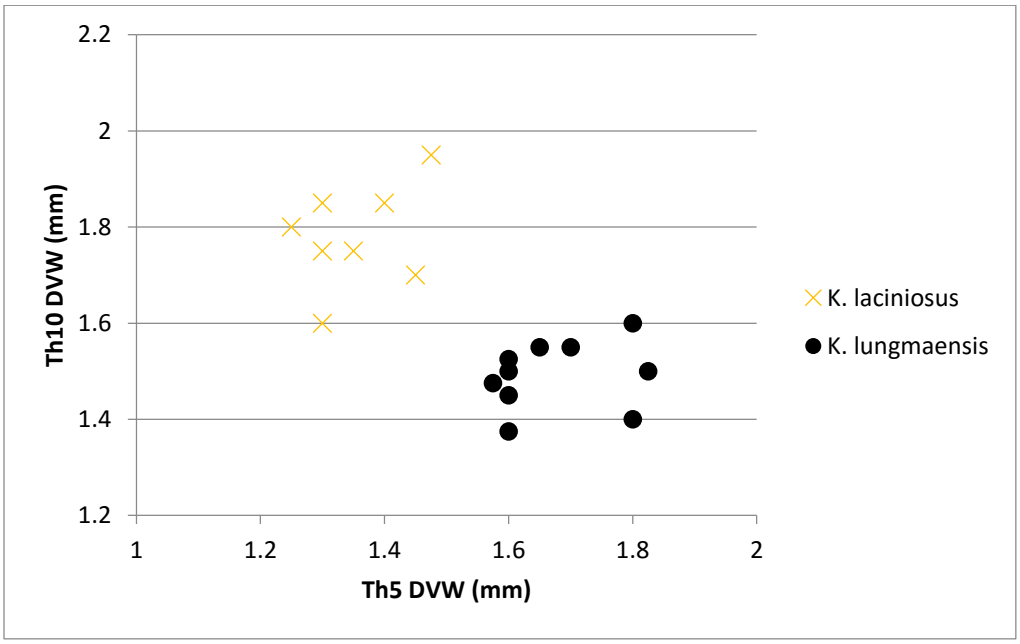

Figure 6.74. K. laciniosus vs. K. langmaensis. All specimens from the Blackstone River.

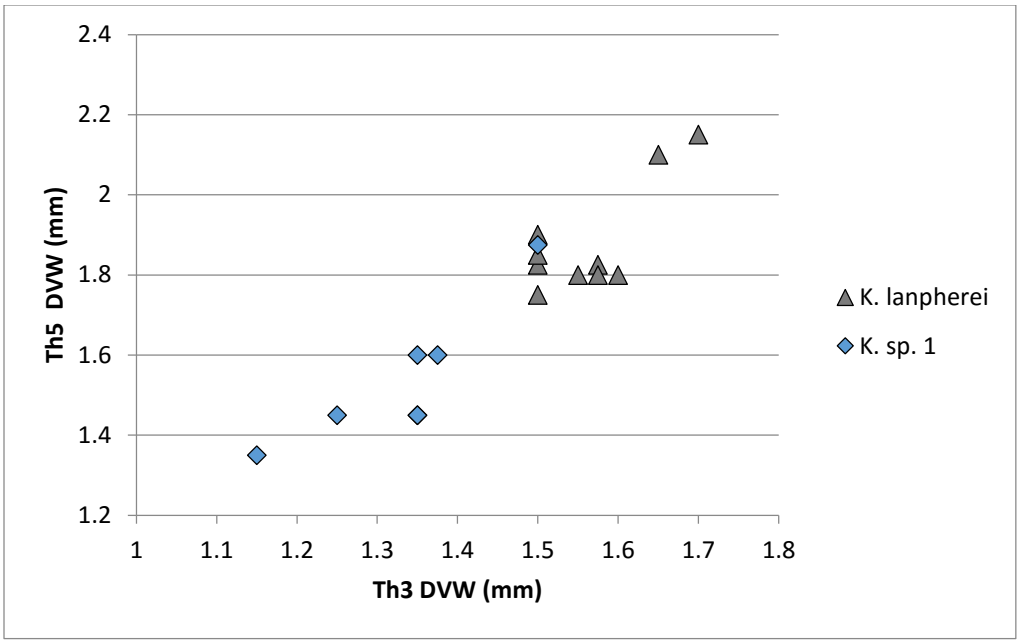

Figure 6.75. K. lanpherei vs. K. sp. 1. All specimens from the Blackstone River.

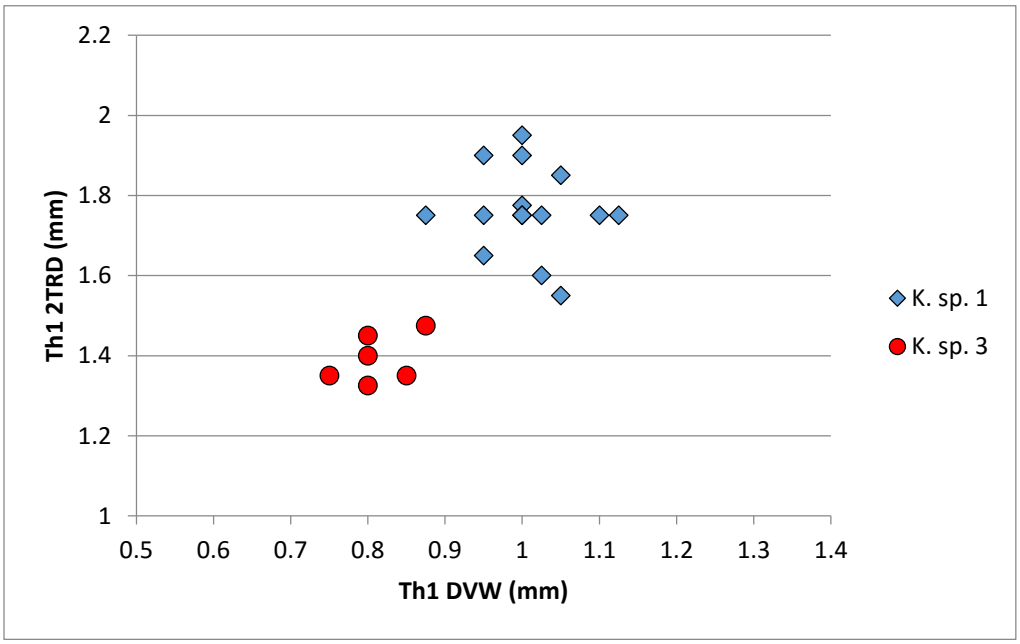

Figure 6.78. Korenograptus sp. 3 vs. K. sp. 1. All specimens from the Blackstone River.

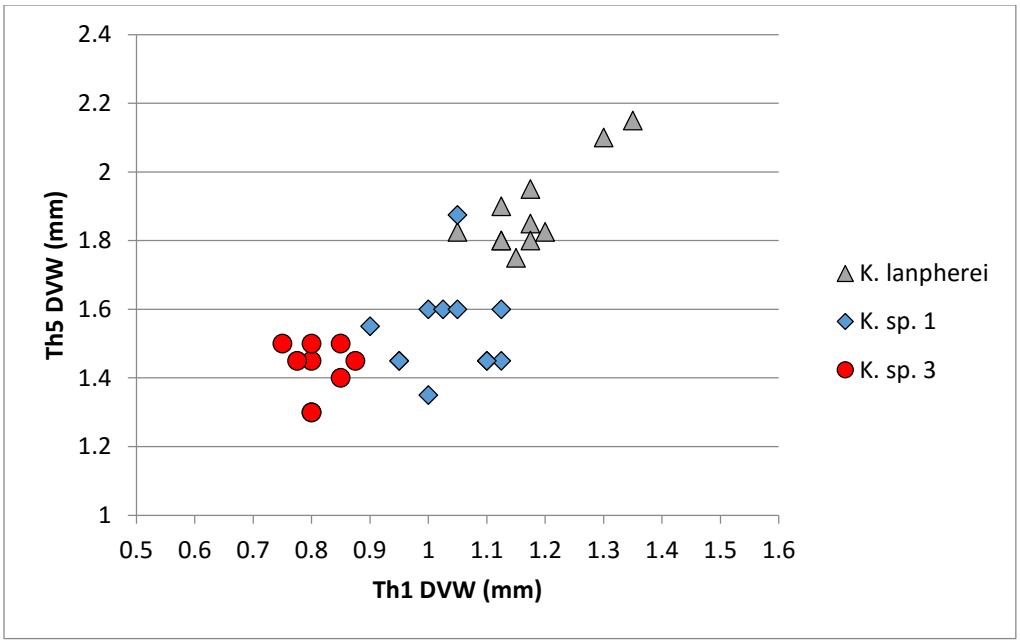

Figure 6.77. Korenograptus sp. 3. All specimens from the Blackstone River.

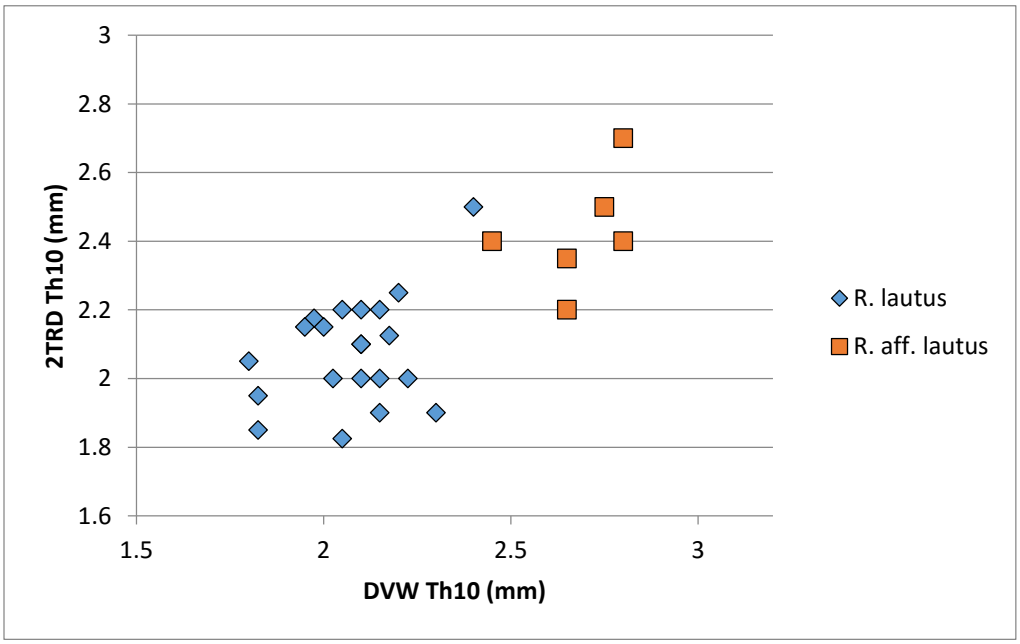

Figure 6.78. Rickardsograptus comparison (A). Specimens were chosen based on thecal morphology, and not preconceptions about size distinctions. Note that the one specimen of *R. lautus* that plots in *R*. aff. *lautus* morphospace has low distal thecae inclination. All specimens from the Blackstone River.

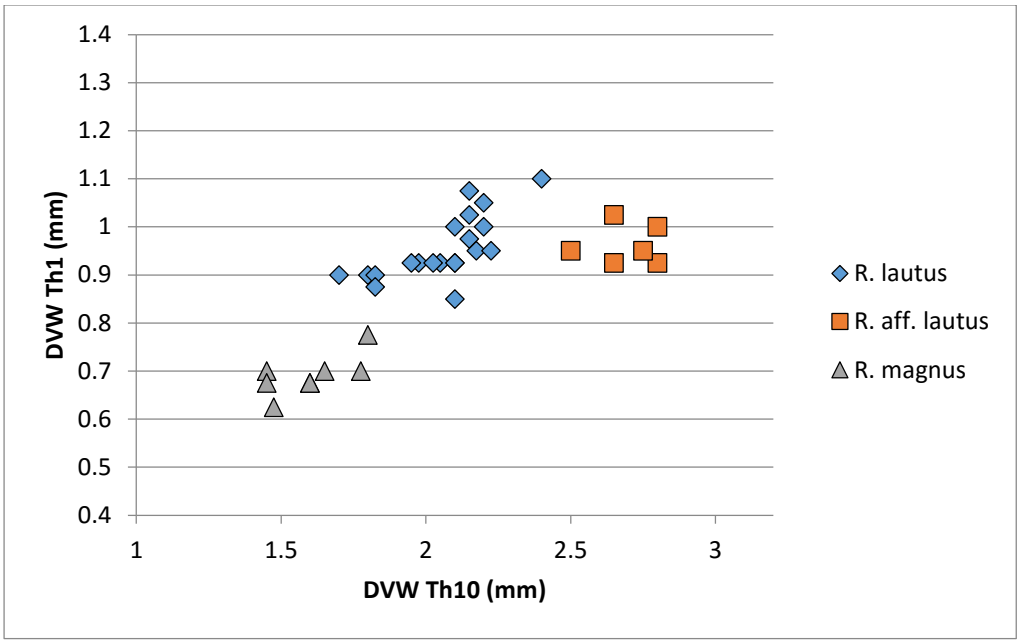

Figure 6.79. Rickardsograptus comparison (B). All specimens from the Blackstone River.

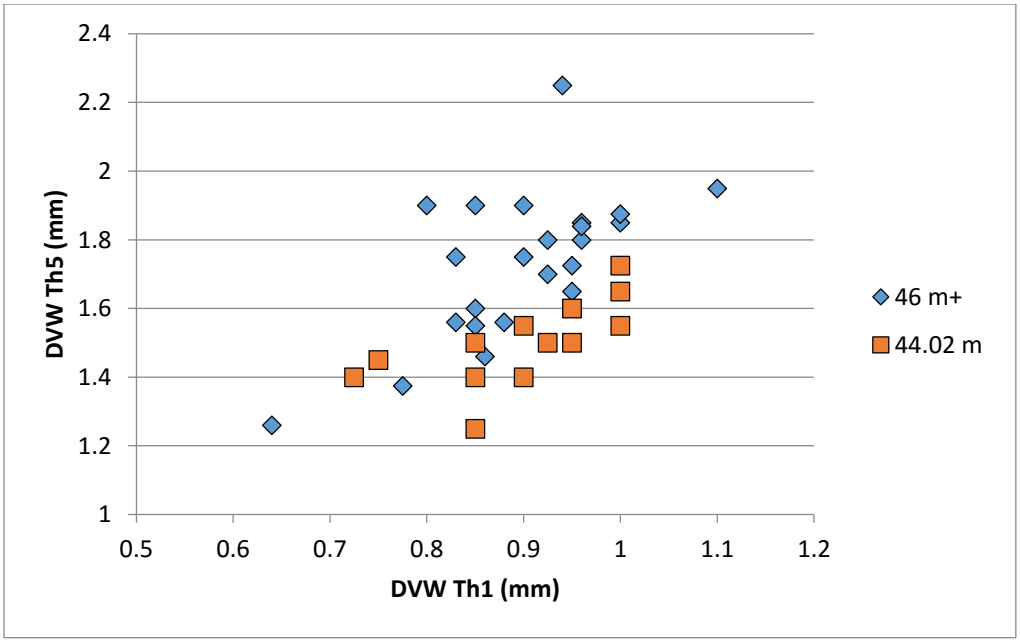

Figure 6.80. Paraclimacograptus: Th5 vs. Th1 DVW. All specimens from the Blackstone River.

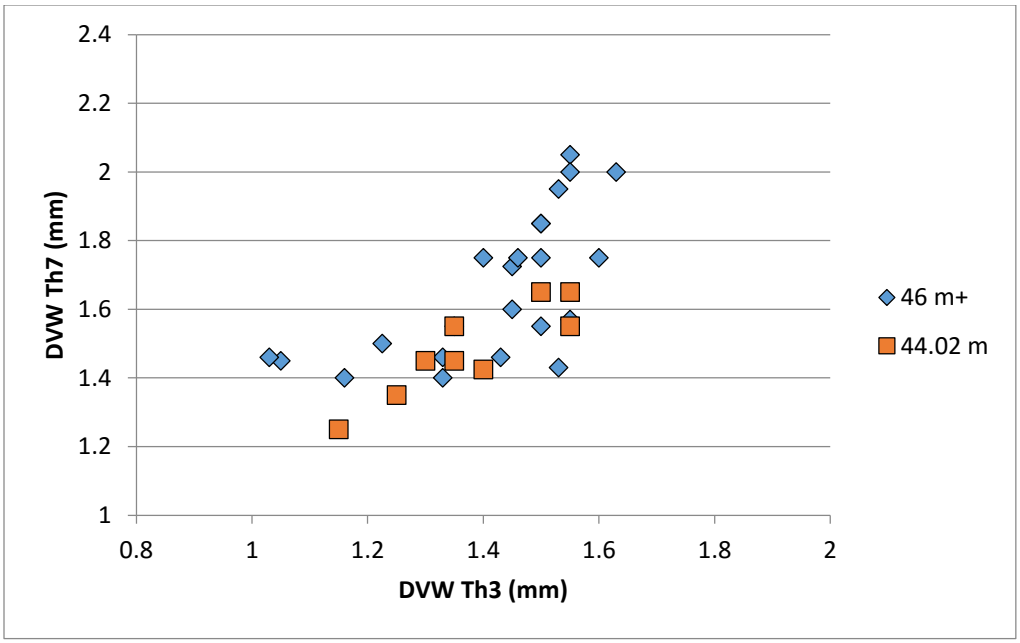

Figure 6.81. Paraclimacograptus: Th7 vs. th3 DVW. All specimens from the Blackstone River.

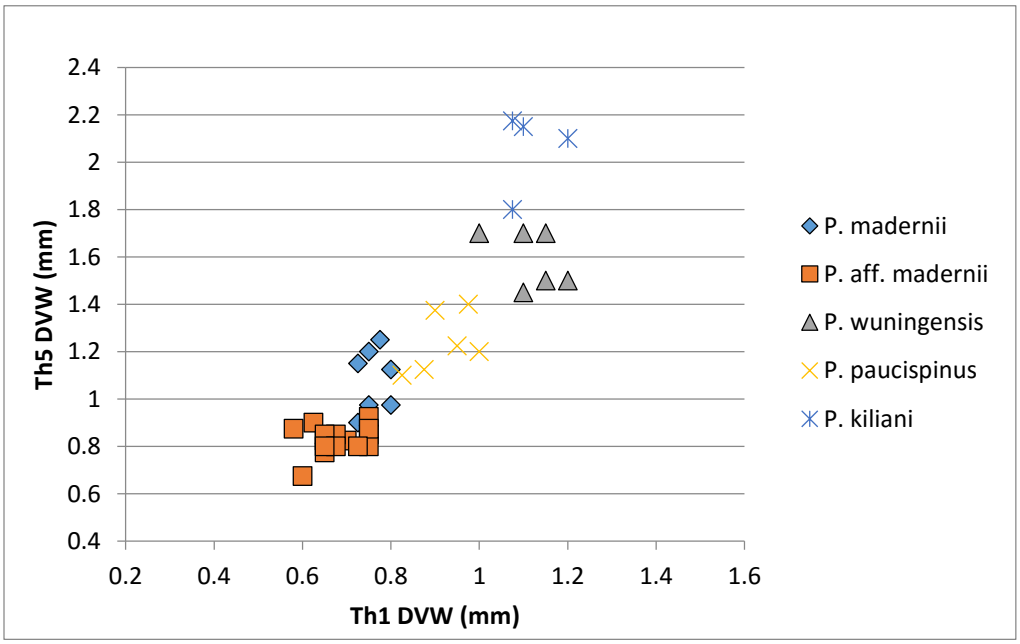

Figure 6.82. Paramplexograptus: Mesial DVW vs. proximal DVW. All specimens from the Blackstone River.

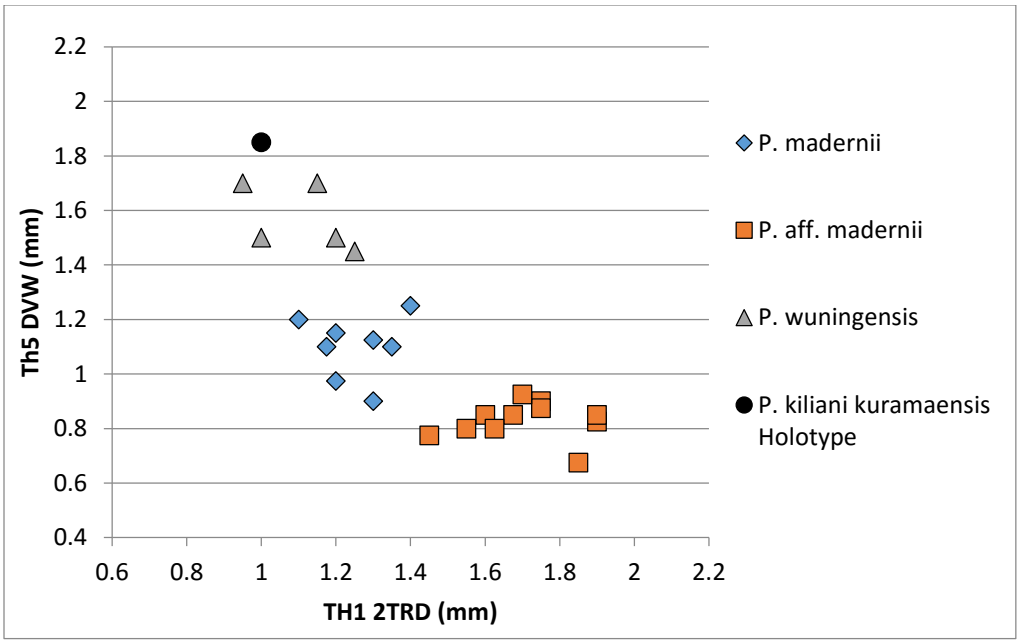

Figure 6.83. Paramplexograptus: Mesial DVW vs. proximal 2TRD. All specimens from the Blackstone River. *P. kiliani kuramaensis* holotype measurements from M.J. Melchin. All other specimens from the Blackstone River.

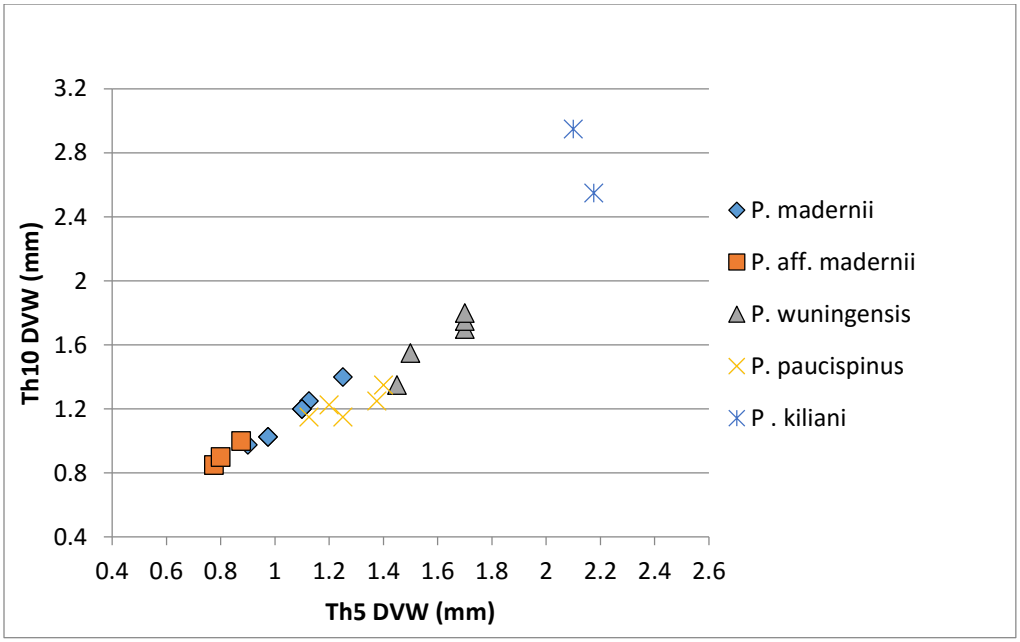

Figure 6.84. Paramplexograptus: Distal DVW vs. mesial DVW. Due to limited data, measurements for th8[1], th9, or th11 were substituted for th10 for several specimens of *P. paucispinus, P. madernii,* and *P.* aff. *madernii.* Note: these species reach maximum widths at or before th10. All specimens are from the Blackstone River.

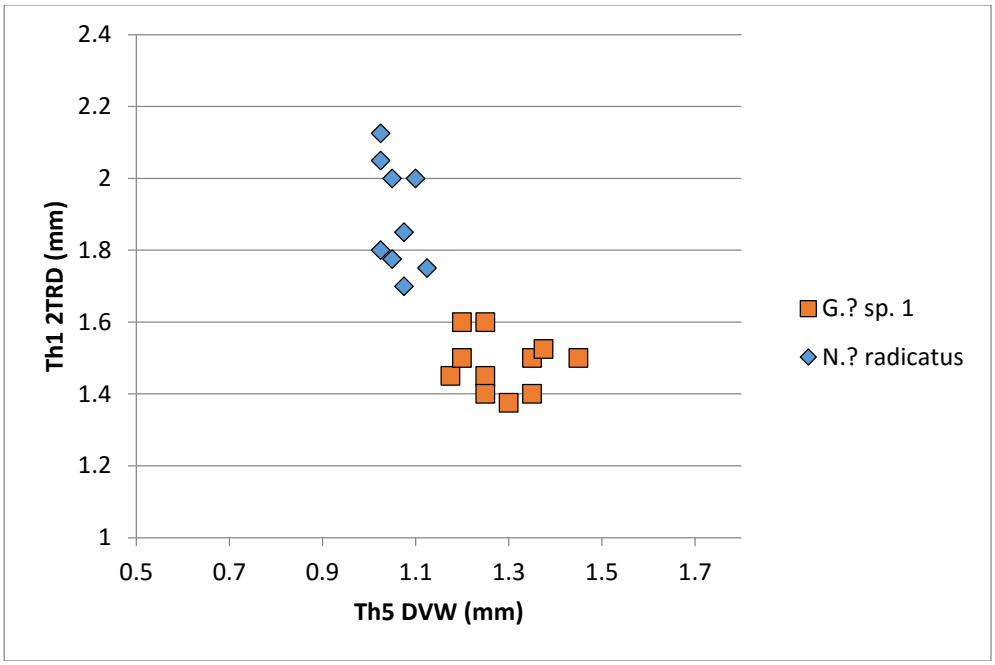

Figure 6.85. Glyptograptus? sp. 1 vs. Normalograptus? radicatus. All specimens are from the Blackstone River.

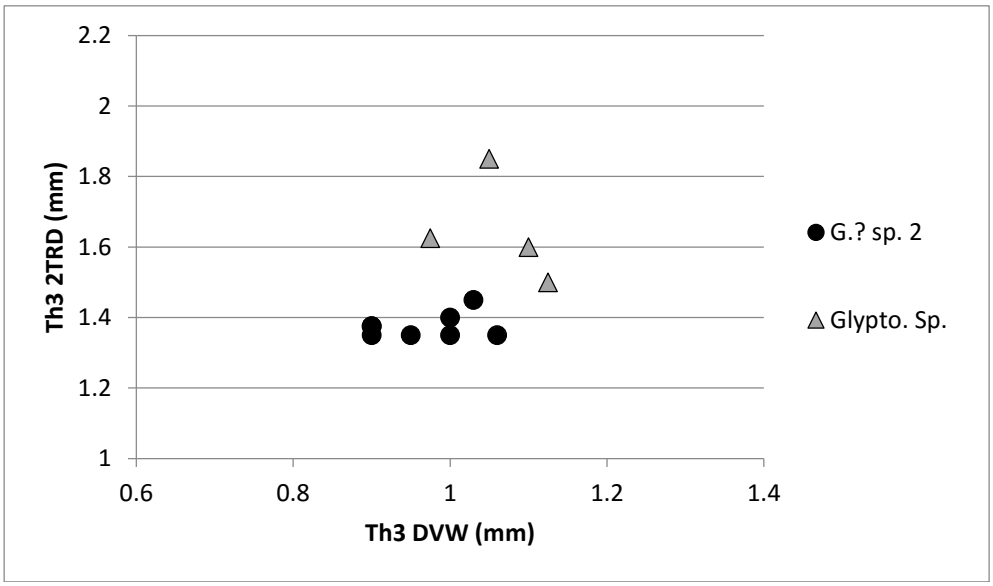

Figure 6.86. Glyptograptus comparison. Proximal 2TRD vs. DVW. All specimens are from the Blackstone River.

Chapter 7. Ontogeny and Astogeny of the Graptolite Genus *Appendispinograptus* (Li and Li, 1985)

Preamble

Chapter 7 is the reformatted manuscript by J. Loxton, M.J. Melchin, C.E., Mitchell, and S.J.H. Senior (2011), "Ontogeny and astogeny of the graptolite genus *Appendispinograptus* (Li and Li, 1985)", published in the *Proceedings of the Yorkshire Geological Society*, volume 58, p.253-260. J. Loxton wrote the principal text (other authors provided editorial comment and revision) and produced all analysis and illustrations, except those concerning early growth patterns in graptolites, which were modified from thesis work conducted by Senior (1993). Some additional specimen illustrations are also reproduced from previously published work for comparative purposes in Fig. 7.4. These are noted in figure captions.

7.1 Abstract

Graptolites of the genus *Appendispinograptus* feature prominently in Late Ordovician biostratigraphy and studies of biodiversity. Well-documented, but enigmatic, secondary structures extend along the basal spines in mature specimens of three of the four common late Katian species of the genus*: A. supernus, A. longispinus*, and *A. venustus*. Using SEM imaging of isolated, three-dimensional specimens of *A. supernus*, we provide a detailed description of its early growth, as well as confirm that its secondary structures are composed of hollow tubes extending from the sicular and

thecal apertures ('parasiculae' and 'parathecae', respectively). We also describe a collection of Canadian (northern Yukon) appendispinograptids that possess a large heart-shaped, sheet-like basal structure. Detailed comparison (width, thecal length, and inclination) with immature specimens from our collection, as well as collections from Russia, China, and Nevada, identifies these specimens as *A. leptothecalis*, a species not previously known to exhibit any secondary spine modification. The observation of spine modification in *A. leptothecalis* allow previously unclassified specimens from China, Siberia, and Nevada to be assigned to this species, clarifying our understanding of appendispinograptid biogeography and diversity. However, these structures are difficult to explain functionally. Unlike structures found in other *Appendispinograptus* species, those in *A. leptothecalis* decrease usable thecal space, shift drag proximally, and provide no obvious feeding advantage.

7.2 Introduction

Graptolites of the genus *Appendispinograptus* (Li and Li, 1985) were among the most abundant species in Late Ordovician, low latitude, basinal ecosystems, and feature prominently in biostratigraphy and studies of biodiversity. All appendispinograptids possess three basal spines (mesial spines on the first thecal pair and a virgella), but many also possess extravagant species-specific modifications to their proximal regions, modifications that make *Appendispinograptus* unique amongst late Katian and Hirnantian graptolite faunas. These structures pose three related problems: first, their construction is unclear, i.e., whether they are solid structures, thin membranes, or, as

recently proposed (Mitchell et al., 2007a), hollow tubes; second, their function is unclear, i.e., whether they housed zooids, performed a hydrodynamic or locomotor function, or served another unknown purpose; and third, their taxonomic significance is uncertain.

This third point is of greatest practical concern. Although these structures have long been recognized as variable in some species, e.g., *A. supernus* (Elles and Wood), in others they have been considered diagnostic, leading to differences of opinion in taxonomic assignments or open nomenclature identifications, i.e., 'sp.' assignment (e.g., Ross and Berry, 1963; Riva, 1974; Koren' et al., 1983; Li, 1984; Mu et al., 1993; Chen et al., 2005a). Distinguishing genuine species from pseudospecies (regional or ontogenetic species variants) is essential for ongoing efforts to standardize global biostratigraphy and quantify inter-regional patterns of species abundance and global biogeography, and is of particular importance during the Late Ordovician, a period of profound environmental change, culminating in the Hirnantian Mass Extinction. In light of this, we present comparative morphological data on populations of several cosmopolitan species of *Appendispinograptus* that vary greatly in degree of spine modification, as well as the first report of modified spines in *A. leptothecalis* (Mu and Ge, 1982).

As with many issues in palaeontology, the lack of clarity about the structure (and by extension possible function) of the secondary features associated with appendispinograptid spines results from a paucity of appropriately preserved material. Although observed for over one hundred years (Hall, 1902; Elles and Wood, 1906) all

that is possible to determine in flattened specimens is that spine modifications were either thinner or more compressible than the spines themselves, and were therefore either membranous or hollow. Comparison with other graptolite species is unhelpful as both types of structures occur frequently, even amongst the closely related climacograptines (Bulman, 1944-1947 and 1970). Hsü (1959) argued that the upright portions of the candelabra-like proximal structures of *A. venustus* were hollow tubes. Based on an exceptionally preserved, pyritized internal mould, Mitchell et al. (2007a) determined that the under-spine structures present on *A. supernus* were a direct extension of the sicula, presumably constructed in a similar manner, i.e., hollow. Based on this, close examination of above-spine "membranes" emerging from the thecal apertures in *A. longispinus*, comparison with similar structures identified as tubes in serial sections of *Climacograptus bicornis* (Hall) by Bulman (1944-1947), and the fact that many graptolites are known to produce a secondary tubular extension that grew down the virgella from the sicular aperture (named a 'parasicula' by VandenBerg, 1990), Mitchell et al. (2007a) argued that all of these structures were hollow extensions of existing rhabdosomal features, and labelled them 'parasiculae' and 'parathecae', respectively, depending on their point of origin (terminology that we adopt).

We report the first ever isolated, three-dimensional specimen of *Appendispinograptus* with intact parasiculae (clearly identifiable as hollow tubes) bringing resolution to the "membrane" debate. We also present additional, isolated appendispinograptid sicular and early growth stage material that illustrates the

structure and timing of the growth of the mesial spines and virgella, as well as the position of the primary porus on the metasicula. This latter feature is of particular interest; it is shared with specimens of *Climacograptus* sp. described by Senior (1993, possibly specimens of *Styracograptus tatianae* (Keller), recently redescribed by Štorch et al., 2011), but differs markedly from co-occurring Pattern K and G diplograptid graptolites, *Anticostia* (Stewart and Mitchell) and *Paraorthograptus* (Ruedemannn), and therefore may be a family or higher level character.

7.3 Materials and Methods

Flattened specimens examined in this study were collected from late Katian (Late Ordovician) sections in China (Yangtze Platform), Nevada (Roberts Mountains), and the Canadian Yukon (Peel and Blackstone Rivers)—see Mu et al., 1993; Štorch et al., 2011; and Lenz and McCracken, 1982, for detailed locality information. Additional three-dimensionally preserved specimens were obtained from calcareous nodules collected from the *P. pacificus* Zone, lower Cape Phillips Formation, Cornwallis and Dundas Islands, in the Canadian Arctic Archipelago. Concretions from this region, lithified during shallow burial (Coniglio and Melchin, 1995), yield exceptionally preserved partially flattened to uncompressed graptolites (Lukasik and Melchin, 1994; Melchin, 1998) that can be isolated by bulk dissolution in a dilute hydrochloric acid bath. Flattened specimens were examined under a light microscope, and measurements made with an eyepiece micrometer. Isolated specimens were studied under both a light and JEOL 5300 scanning electron microscope. Additionally, as the graptolite rhabdosomal wall is

translucent under infrared light, study of thecal, sicular, and parasicular structure was conducted with an infrared video camera attached to a transmitted-light microscope (see Melchin and Anderson, 1998, for a detailed description of methodology). Measurements on some specimens that could not be examined directly (e.g., Koren' et al., 1983) were taken from published illustrations. Area measurements were calculated in Adobe Photoshop from illustrations of flattened specimens (with total living surface area equal to twice the visible compressed area).

7.4 *A. supernus* Early Growth

Appendispinograptus supernus exhibits Pattern E proximal development. The prosicula is replaced by a single short dorsally located rod, which distally merges into the nema (Fig. 7.1A). As the metasicula approaches two thirds of its mature length, a reinforced rim of closely spaced fuselli appears along the leading edge. Fuselli added beyond the rim bend sharply downwards along the ventral edge of the metasicula to form the virgella, and the metasicula as a whole becomes angled towards its dorsal side, angling the sicular aperture oblique to, and causing the virgella to grow across, the sicular axis (Fig. 7.1B). The initial virgellar fuselli are widely spaced, and connected by thin, membranous tissue. This tissue and the supporting fuselli are subsequently resorbed to form the th1[1] foramen/primary porus synchronously with or just prior to the completion of the virgella (Fig. 7.1J). The foramen is located directly on the virgellar axis, and not adjacent to it, as is the case in diplograptid (Fig. 7.1K) and normalograptid

species. Th1[1] grows straight down the virgellar axis, before turning sharply upwards

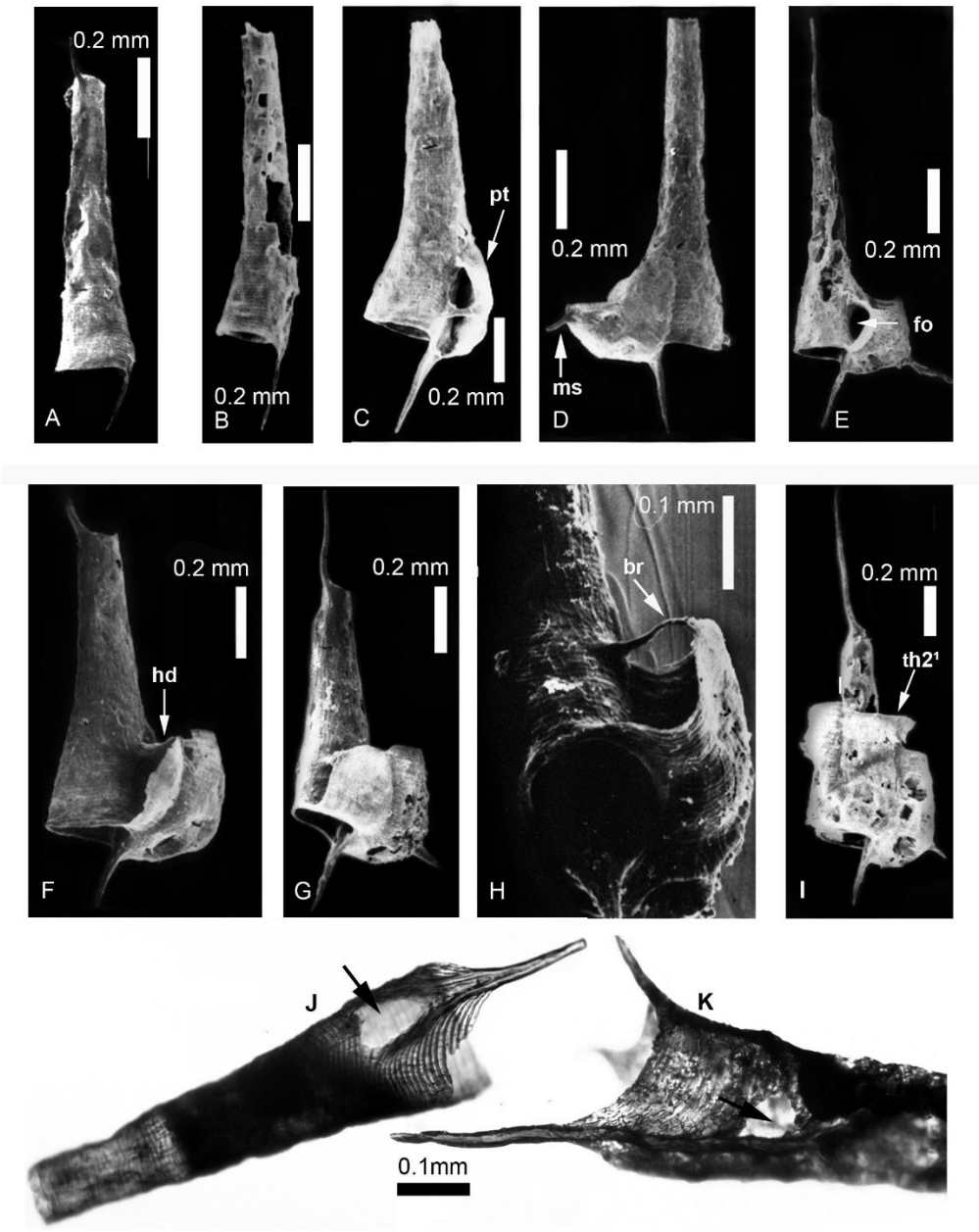

Figure 7.1. Electron micrographs of isolated growth stages of A. supernus and Anticostia sp. (A-I): Growth series of *A. supernus*. Labels: pt = th1[1] protheca; ms = mesial spine; fo = th1[2] resorption foramen; hd = theca 1[2] hood/protheca; br = th1[2] attachment bar ; th1[2] = protheca of th1[2]. (J): Metasicula of *A. supernus* showing th1[1] resorption foramen along virgellar axis (arrow). (K) Sicula of *Anticostia* sp. showing th1[1] resorption foramen on reverse side of sicula, adjacent to virgellar axis (arrow). All specimens from lower *P. pacificus* Zone (55 m), Eleanor Lake section, Cape Phillips Formation, Cornwallis Island (see Melchin and Holmden, 2006, for locality and section

approximately 0.1 mm below the sicular aperture, terminating just below above the resorption foramen (Fig. 7.1C and 7.1D). A laterally directed, slightly off-profile, mesial spine is produced as a fusellar extension as the metatheca nears the level of the sicular aperture (Fig. 7.1D and 7.1E). Th1² arises from a foramen in the reverse wall of the th1¹ protheca (Fig. 7.C and 7.1E), and expands horizontally across the sicula (Fig. 7.1F and 7.1G). As the leading edge approaches the dorsal side of the sicula, it is joined by a small bar that grows out from the sicula, approximately at the level of the th1¹ aperture, and divides the flange in two (Fig. 7.1H). The th1² metatheca grows from the lower side of the bar, turns sharply upwards and along the dorsal edge of the sicula, producing a mesial spine at the level of the sicular aperture. Th2¹ arises from the upper side of the bar (Fig. 1.I), growing upward along the dorsal wall of th1² and laterally over the th1¹ aperture. Subsequent thecae grow as described in Mitchell (1987) and Senior (1993).

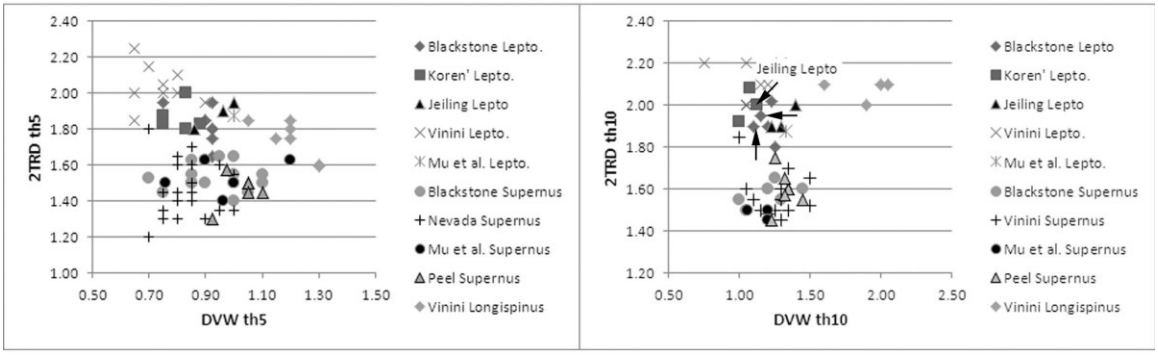

Figure 7.2. Comparison of proximal and distal dorsal ventral width (DVW) and thecal height (2TRD) in various populations of three species of Appendispinograptus. A. supernus: Peel River, GSC types – 69205, 69209, and 69215; Mu et al., 1993, Nanjing Institute of Geology and Palaeontology (NIGP) collections - 57514, 57517, 57521, 57523, 57541, 57543, *D. complexus* Zone to *T. typicus* Subzone; Nevada: various samples, lower to upper *P. pacificus* Zone, Vinini Creek –10.30-18.00 m and Martin Ridge – 105.20 and 112. 80 m; Blackstone river: various samples, lower to upper *P. pacificus* Zone – 1.3 m and 16.03 m. *A. leptothecalis*: Jeiling: various samples, 148-150 m, *P. pacificus* Zone, Wufeng Formation; Mu et al., 1993, NIGP collections – 57653 and 57667, *T. typicus* Subzone; Koren' et al., fig. 42.a and fig. 44.3, B, and И; Nevada: Vinini Creek: various samples, *D. mirus* Subzone – 17.80-18.80 m; Blackstone river: various samples, *D. mirus* Subzone – 15.65-19.00 m; *A. longispinus*: Nevada: various samples, lower *D. ornatus* Zone, Vinini Creek –7.50-9.20 m and Martin Ridge – 95.00 and 96.10 m. Arrows show *A. leptothecalis* specimens with complete basal webs.

7.5 *A. supernus* Parasiculae

Material isolated from a concretion from the lower part of the *P. pacificus* Zone of a previously undescribed section on northwestern Dundas Island, Arctic Canada (76º7.3'N, 95º6.7'W), produced 25 specimens of *Appendispinograptus supernus*, among which is one specimen that exhibits a small tubular parasicula attached to the underside of its mesial spines (Fig. 73A and 7.3B). The presence of a parasicula and well-developed (2 mm) mesial spines make this specimen unique amongst our Arctic Canada material, both flattened and compressed. Despite being a proximal fragment, it can be confidently assigned to *A. supernus* based on its form and dimensions (Fig. 7.2), particularly its low DVW (0.725 mm at th4²) and 2TRD (1.35 mm at th3) (Riva, 1974; Melchin, 1987; Chen et al., 2005a; Štorch et al., 2011). Other samples from the same region in Arctic Canada have yielded many hundreds of specimens of *A. supernus*, but no other specimens with clearly developed parasiculae have been found to date.

The parasicula is composed of extremely narrow fusellae, approximately two to four µm wide (Fig. 7.3C); cortical bandages appear to be absent. Initial fuselli produced below th1² are sub-parallel to the sicular aperture, and increase in angle as the parasicular tube grows outwards. Parasicular fuselli below th1¹ are consistently oblique to the sicular aperture, becoming nearly parallel to the rhabdosomal axis as they expand along the spine (Fig. 7.3C). From flattened material in our collection, construction of the parasicular tube below th1² appears to progress until it completely fills the area below the sicula before growth of the th1¹ parasicular tube is begins. The junction between the

two parasicular tubes is obscured in our infrared images by the virgella, but the respective fusellar angles suggest they meet in an unconformity, which may be visible as a raised line highlighted by an asterisk in Fig. 7.3B. The parasiculae expand along the spines, with the dorsal edge leading throughout growth (Fig. 7.3A). Fuselli attach to the base of the spine, forming semicircles. The virgella is embedded in the obverse wall of the th1² parasicula. It is unclear from the present material whether the th1¹ and th1² apertures connect and/or whether the sicular aperture remains open, however, the parasicular structure described by Mitchell et al. (2007a) suggests this is likely.

Parasicular growth is highly variable in our samples of flattened specimens, both between species and populations. In our Blackstone and Vinini collections, parasiculae are almost completely absent in *A. supernus* at all levels of development; when they do occur, however, they are restricted to mature specimens. This is consistent with Riva (1974) and Williams (1982), who noted that parasiculae occurred in their *A. supernus* specimens only after about 7-8 thecal pairs were completed. Amongst our limited material from the Peel River, parasiculae are ubiquitous in two small samples (probably latest *D. ornatus* Zone—Lenz, pers. comm.), and nearly absent in a slightly younger (*P. pacificus* Zone) sample. In the lower samples they are present on specimens at 8-9 thecae, and well-developed (up to 4 mm from aperture to aperture) on specimens 15 to 20 thecal pairs long; in the upper sample, however, they are absent on most even very mature (>15 thecal pairs) specimens.

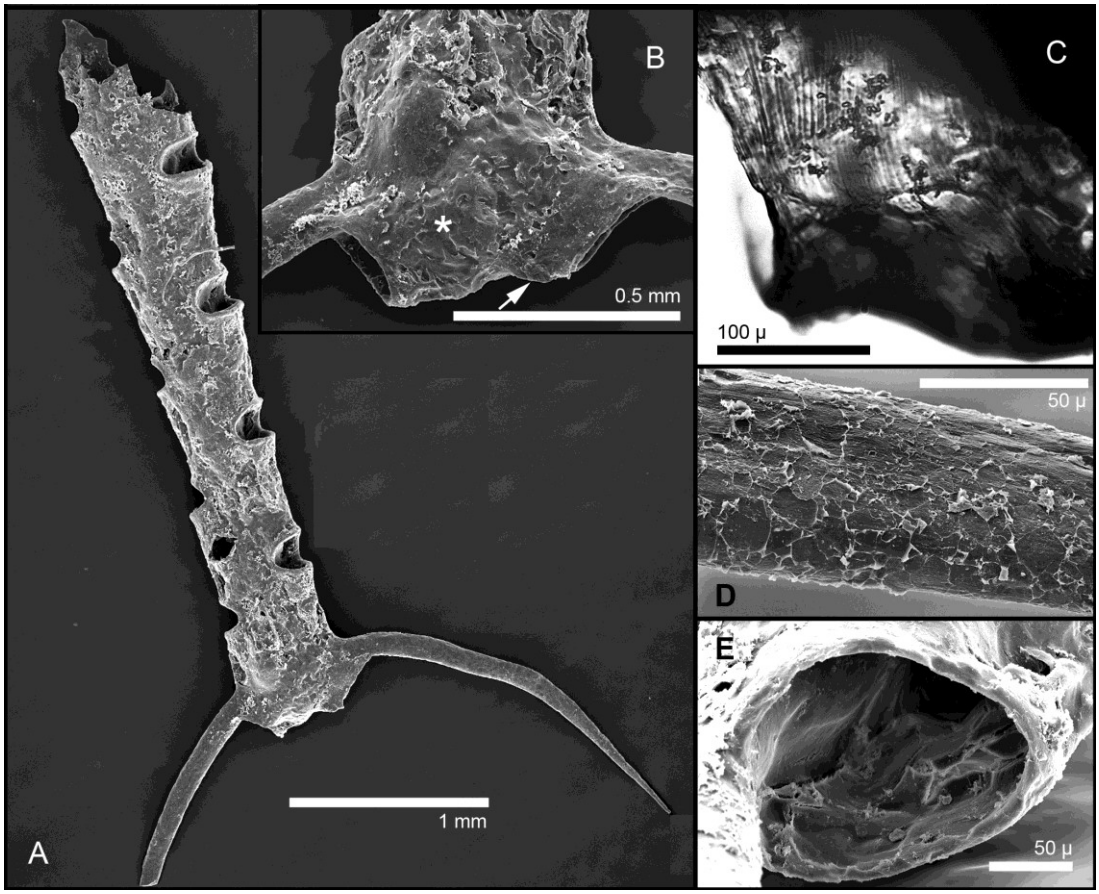

*Figure 7.3. Electron micrographs and infrared photographs of an isolated specimen of A. supernus. (*A-B) Electron micrographs. Embedded virgella is visible as a bulge on the side and underside of the th1² parathecal tube (white arrow). Asterisk marks position of possible line of unconformity, adjacent to virgella, between the th1¹ and th1² parathecal tubes (C) Infrared photograph of th1¹ paratheca: Note fine fuselli perpendicular to spine. (D) Electron micrograph of th2 spine: Possible linear cortical material visible in center of image, but structure ambiguous. Examination of the broken end of th1¹ spine showed no further structural information preserved. (E) Electron micrograph view into aperture of th1¹ parasicular tube. Specimen is from lower *P. pacificus* Zone, northwestern Dundas Island, Arctic Canada (76º7.3'N, 95º6.7'W), and co-occurs with specimens of *Anticostia lata, Anticostia fastigata*, and possibly *Styracograptus tatianae* and *Anticostia thorsteinssoni*. Scales are as indicated.

Most specimens with developed parasiculae show moderate to strong rhabdosomal torsion (also seen in our isolated specimen), a feature that is common in larger specimens of the parasiculae-possessing *A. longispinus,* but absent in many specimens of *A. supernus* in our samples lacking parasiculae. As the spines are oblique

to the dorsal-ventral plane in all appendispinograptids, it is possible that spines strengthened by parasiculae force the rhabdosome out of profile upon compaction, and that the torsion common in these *A. supernus* specimens is a taphonomic consequence of their parasiculae, rather than an independent, correlative character.

7.6 *A. leptothecalis* "Membranes"

Four mature specimens from our Blackstone River collections, which otherwise agree perfectly with descriptions of *A. leptothecalis* (Fig. 7.2), exhibit odd, inverted heart-shaped structures that completely enclose their proximal ends (e.g., Fig 4.C and F). With one possible exception with apparent thickening along the base of the spines (Fig. 7.4E), we have no intermediate stages, making interpretation of their structure and mode of growth difficult. The heart-shaped structure extends up to the aperture of th3-th4 (Fig.7. 4 and 7.5), and extends below the spines, completely filling the space between them. Although one specimen shows hints of what could be parasicular tubes incorporated into the web (see arrow—Fig. 7.5B), other specimens show no evidence of either parasiculae or parathecae. Although it is possible that the area closest to the spines was constructed of parasicular and/or parathecal tubes, the central portion of the structure appears to be featureless, and in absence of the folding one would expect in a compressed, three-dimensional structure, was most likely planar, i.e., a web. Three of the Blackstone River specimens have web length and width values of 8.10 x 5.63 mm, 5.90 x 4.16 mm, and 5.45 x 4.41 mm. They agree well in size, morphology, and apparent structure with specimens (6.50 x 5.54 mm and 5.25 x 4.65 mm) illustrated by Koren' et

al. (1983—fig. 42, and partially reproduced in Fig. 7.4, herein) and assigned to *Climacograptus longispinus longispinus.*

As with our Blackstone specimens, Koren' et al. (1983) noted that the thickness of the proximal web material obscured growth features. They speculated that the structure was a composite of two separately produced membranes, one descending from the underside of the spines, and another expanding along the upper sides of the spines, which bent around at the spine ends, and traced their underside, merging with the lowering initial membrane, and producing the characteristic concave base seen in both of our collections. Perplexingly, the specimens illustrated by Koren' et al. also lacked intermediate growth stages, but one specimen illustrated as *Climacograptus longispinus supernus* (text-fig. 45, 3—reproduced here in Fig. 7.4G) is suggestive. Its dimensions and thecal form match those of *A. leptothecalis*, and it exhibits a partially formed membrane underlying each spine, forming a lenticular, "rabbit ear" structure. Interestingly, the area directly below the first thecal pair and surrounding the sicular aperture appears to be free of any material. This contrasts with all other contemporary appendispinograptid species, which uniformly produce parasicular tubes at an early stage in their colonial development. Combined with the apparently novel membranous web structure, the apparent lack of parathecae and parasiculae, if confirmed, may be of systematic value.

7.7 Discussion

7.7.1 Systematics

Recent investigations (e.g., Chen et al., 2000, 2005a; Štorch et al., 2011—see also Chapter 6 of this thesis) have shown thecal spacing and inclination, mesial to distal DVW (e.g. Fig. 7.2), rhabdosomal torsion, and distal internal structure to be species-diagnostic traits for species of *Appendispinograptus*, but other potentially useful characters, such as virgellar and spine length, proximal DVW and 2TRD, and apertural inclination, show considerable intraspecific variation. All of these latter characters are useful in diagnosing species in other genera, and their variability in species of *Appendispinograptus* could only be identified through a population-based approach, utilizing large samples from multiple sections, with the direct cooperation of international workers familiar with the idiosyncrasies of both regional populations and modes of preservation. Those recent studies resulted in many previously split taxa being placed in synonymy. Our observation of membranes/webs and possible parasiculae on *A. leptothecalis* extends this process of taxonomic reconciliation by further documenting the range of morphologic variability within the genus, and by providing a likely home for enigmatic "*leptothecalis* like" *Appendispingraptus* sp. specimens with spine modifications described in China and Nevada (Chen et al., 2005a; Štorch et al., 2011). As a result, the biostratigraphic and palaeogeographic distribution of this taxon is more thoroughly documented.

Figure 7.4. Comparison of variation in spine length and web development in specimens of A. leptothecalis from four global populations. (A), (G), (I), and (J): Kolymna, northeastern Siberia - reproduced from Koren' et al., 1993, Figs. 42.a, 44.B & 3, and 45.3. (G), (I), and (J) originally identified *as Climacograptus longispinus supernus*; (A) originally *Climacograptus longispinus longispinus*. (B-F): Blackstone River, Yukon, *D. mirus* Subzone, 18.05 m-18.94 m. Arrow next to (E) indicates possible incipient web. H: Wangjiawan, South China - reproduced from Chen et al., 2005a, fig. 7.A, *N. extraordinarius-N. ojsuensis* Zone. (K) Vinini Creek, Nevada, USA - reproduced from Štorch et al., 2011, fig. 16.L, *D. mirus* Subzone. Scales as indicated.

7.7.2 Form and Function

Clarifying the structure of appendispinograptid parasiculae does not immediately solve the riddle of their function. Williams (1982) suggested these structures may have acted to increase spine strength, rhabdosome stability, or feeding efficiency. Mitchell et al. (2007a) expanded on these suggestions and noted that if these structures were in fact tube-like, they may have served to provide housing for additional zooids, increasing total colony size, as well as to provide a protected passageway to the spine tips to access preferred feeding areas and/or assist in locomotion. They also noted that since both parathecae and other modifications of spines occur exclusively in mature specimens, the function of these structures must have been related to factors arising in large rhabdosomes, e.g., stability and overlap in feeding space of sequential zooids. Although our confirmation that parasiculae are tubes is consistent with these hypotheses, other observations raise vexing questions.

In light of the functional hypotheses of Mitchell et al. (2007a), the variability in the size and frequency of occurrence of both spines and parasiculae in many appendispinograptid species is difficult to explain. Spine length in *A. supernus* apparently decreases up section in the Phi Kappa Formation, Idaho (Riva, 1974), as it does in Arctic Canada, despite being anomalously low for the species (often <1 mm), even in lower levels (Senior, 1993). Spine length is also highly variable in *A. leptothecalis.* In collections from the *N. extraordinarius* Zone of the Wufeng Formation (Wangjiawan and Fenxiang sections) described by Chen et al. (2005a), large, mature

specimens (>30 thecal pairs) possess spines only slightly longer than the virgella (<1.5 mm), whereas some similarly sized specimens we recently examined from the *P. pacificus* Zone from another Wufeng section (Jeiling) possess spines in excess of 8.5 mm. Mature specimens from the upper *P. pacificus* Zone in Nevada examined by Štorch et al. (2011) have spines between 1.0-2.6 mm, with three specimens between 20-33 mm long possessing spines <1.2 mm, whereas most specimens from the Blackstone River possess spines >4 mm in length.

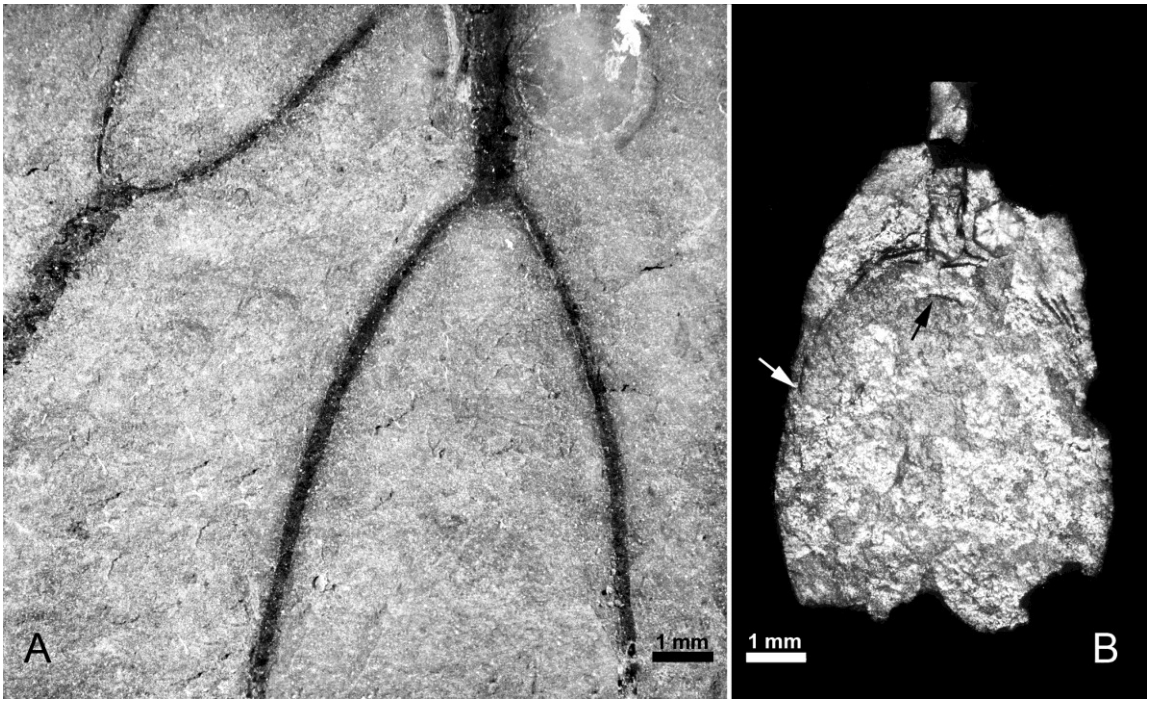

Figure 7.5. Examples of extremely mature A. leptothecalis with and without basal webs. (A) Unpublished section (Jeiling), Wufeng Formation, near Wangjiawan, South China, *P. pacificus* Zone. No web present. (B): Blackstone River, 18.05 m, D. mirus Subzone. Web encompasses entire illustrated area (background rock digitally removed for clarity). Black arrow indicates possible base of remnant parasicula. White arrow shows distal portion of imbedded spine. Hexagonal mineral in upper right corner unrelated to graptolite. Scales as indicated.

Secondary additions to spines are similarly variable. In some populations of *A. supernus,* parathecae are very common (e.g., Dob's Linn, Scotland, Williams, 1982; and

the Peel River, Yukon), whereas in other populations of equivalently sized specimens they are rare or entirely absent (e.g., Arctic Canada, Nevada, and the Blackstone River, Yukon), despite no other differences in morphology (Fig. 7.3), and no obvious changes in community composition, water depth, and so on. Similarly, the development of a basal web in *A. leptothecalis* is highly variable among regions, even in specimens of comparable rhabodosomal maturity (Fig. 7.5). So far, complete webbed specimens have been recovered only from Siberia and the Yukon; they are absent in both published and large unpublished collections from Nevada and Scotland (pers. observ.), as well as China (Fan Jun-Xuan, pers. comm.). If these elaborate structures served an important role in normal feeding or locomotion, the erratic nature of their appearance in apparently equivalent populations is difficult to explain. Thus, any functional role they played must have been facultative, contingent upon particular conditions that varied in time and space.

The basal web in *A. leptothecalis* also poses other questions. Although initial growth could involve parasicular (and possibly parathecal) tubes, the completed structure appears to lack any openings, making it unlikely to function as an aid to zooid feeding or colony locomotion. Further, in contrast to other appendispinograptid spine modifications, which increase total zooid habitat, modified *A. leptothecalis* specimens appear to obscure the apertures of up to eight thecae (a loss of at least seven percent of habitable space), as well as the sicula and any parasicular tubes.

Whatever their primary function, these structures would have had a large hydrodynamic effect. The spines of all appendispinograptids would have increased drag and produced rotation in current (Rigby and Rickards, 1989), as well as, in proximal end first models of locomotion, perhaps created turbulent flow behind the spines, pulling water from the spine tips towards the thecal apertures (Mitchell et al., 2007a). All of these latter functions would likely have been enhanced by the addition of parasiculae and/or parathecae.

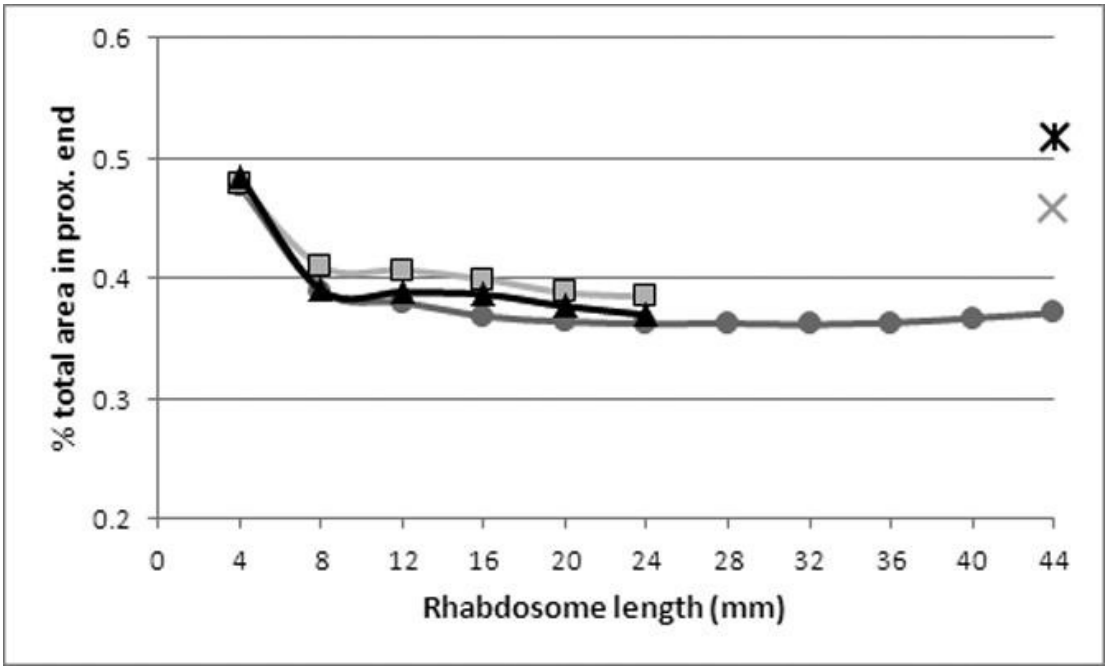

Figure 7.6. Distribution of surface area in three specimens of A. leptothecalis with basal webbing. Vertical axis is percent of total area located in proximal half of rhabdosome; horizontal axis is total rhabdosome length in millimetres. Specimens are illustrated in Fig. 7.4: triangle (7.4C), circle (7.4F), and square (7.4A). Spines are not included in area calculations. Star and 'X' show change in area distribution at 44 mm in the largest specimen (7.4C) that would occur with addition of the complete basal webs present on specimens 7.4F and 7.4A, respectively. Note: midpoint adjusted to account for increase in length with addition of web, i.e., total specimen lengths of 52 mm and 50 mm, and midpoints of 26 mm and 25 mm.

It is unclear what effects the basal web of *A. leptothecalis* would have had on water flow and rotation, but it would have affected the distribution of both mass and

surface area, the latter resulting in an increase in drag. Since the few specimens available are missing distal ends, it is unclear at what length web growth was complete (specimens with complete webs are 26-46 mm long). Using the largest specimen available (Fig. 4.C), the web would have conservatively increased total surface area by 25-50% (170-205 mm^2 vs. 137mm^2), with the addition of the smallest and largest webs in our collections, respectively. Since the web may have occurred earlier in astogeny, it is possible that the increase may have been even more profound. Since the proximal webs occur only sporadically and in very mature rhabdosomes, and do not show clear evidence of progressive, astogenetic increase is size, it seems unlikely that they served a simple function of balance as colony proportions changed.

The web would have redistributed both mass and surface area, and therefore drag, along the rhabdosome (Fig. 7.6). In particular, the balance of drag and mass resulting from the large proximal web that is found in these specimens would contrast markedly with most other specimens at all astogenetic stages, unless there was a corresponding structure developed at the distal end, which has not been found preserved in any of our material. Although not tested experimentally, the resulting weathervane-like form may actually have made it difficult to remain in a stable proximal-end-first orientation, as is predicted by some models of graptolite locomotion (see Mitchell, 2007, and citations therein), especially in currents even slightly oblique to the rhabdosomal axis.

7.8 Conclusion

1) We confirm that the material present along the base of some appendispinograptid spines (the 'parasicula') is a tube, similar in structure and size to regular thecae. As such, it can reasonably be assumed that it housed zooids. By extension, it is highly likely that equivalent structures present above the spines ('parathecae') were also zooid-housing tubes. However, the apparently structureless feature that encloses the proximal end of very mature specimens of *A. leptothecalis* appears to be a two-dimensional, web-like feature. 2) Although confirmation that parasiculae are tubes, supports the parasiculazooid-assisted locomotion model described by Mitchell et al. (2007a), the basal structure in mature *A. leptothecalis* is problematic: the enclosing web would not appear to offer easy, if any, access for zooids to assist in either feeding or locomotion. Further, although not tested experimentally, the weather vane-like shape of the mature *A. leptothecalis* rhabdosome suggests that a proximal end-first current orientation would be very difficult to maintain. 3) Spine and virgellar length, the presence and degree of development of parasiculae and parathecae, and the presence of proximal webbing is highly variable geographically, even at a local level. For example, spine length in very mature *A. leptothecalis* differs by an order of magnitude among collections from the South China sections. Any satisfying functional explanation for characters such as these must also be able to explain their absence or partial development in otherwise equivalent specimens or populations.

4) Comparison of global collections confirms that secondary proximal end features such as spine development and parasiculae, with the exception of some species-specific features in very mature specimens, are unreliable taxonomic characters in appendispinograptids. Reliance on these features has tended to overestimate endemicity and underestimate regional biodiversity. Identifying species specific features requires a population-based approach that utilizes large samples and accounts for intraspecific and regional variation in character presentation and preservation.

7.8 Acknowledgements

This work was supported by NSF grant EAR 0418790 to CEM and MJM, a NSERC (Canada) Discovery Grant to MJM, and a GSA Student Research Grant to JL. Petr Štorch is thanked for access to unpublished metrical data and illustrations; Fan Juan-Xuan, Chen Xu, and Qing Chen are thanked for financial and logistical support accessing collections at NIGP. Finally, we wish to acknowledge our debt to the late Tatjana Koren' for her pioneering insights, and meticulous care in observation and illustration—a legacy that will serve graptolite researchers for generations.

Chapter 8. Conclusion and Outstanding Issues

8.1 Project Overview

When conceived, this project was considerably more limited in scope than the final product. The result of the first field season in the Yukon[28] surpassed expectations, and the combined efforts of two field seasons yielded an unexpectedly rich graptolite record spanning the pre-extinction, extinction, and post-extinction intervals. The abundance of material allowed large quantities of metrical data to be gathered to aid in identification of fragmentary material during the count. This metrical data in turn raised a number of issues with species categories recognized in the literature, leading to a refocusing of efforts towards clarifying systematic issues before counting could be completed. This redirection added considerable extra time to the project, but ultimately produced a much more meaningful outcome. The emphasis on refining bins through independently gathered data, rather than relying on published descriptions, improved counts and resulted in detailed species descriptions that aided comparison with other sections during this thesis. These descriptions will continue to aid other researchers as the process of revising and refining the global graptolite record through the interval of extinction and biotic recovery proceeds.

[28] Collecting was also untaken at Dob's Linn, Scotland. That material was to have formed the main body of the thesis, but was downgraded to a supporting role after the success of fieldwork in the Yukon.

8.2 Status of Project Objectives

Objective 1: Evaluate the suitability of the Blackstone River section as a comparative section for studies of Late Ordovician graptolite biodiversity patterns in China and elsewhere.

Detailed field study and laboratory examination of 44 samples, collected over 50 m of strata exposed along the Blackstone River, Yukon, identified a continuous sequence of seven biozones, spanning the immediate pre-extinction to post-extinction interval of the Late Ordovician Mass Extinction (Fig. 2.3). All but one of these zones is globally recognized, with the one exception (the North American *ornatus* Zone), which is readily correlatable to sections in Europe and China (= *complexus* Zone). In addition, one of the Chinese pre-extinction subzones (the *mirus* Subzone) was recognized, along with a large number of post-extinction species useful for secondary correlation in China and Europe (e.g., *Paramplexograptus paucispinus, Normalograptus anjiensis, Hirsutograptus tuberculatus*). *Metabolograptus extraordinarius,* the index taxon for the base of the Hirnantian, was recognized for the first time from Canada. In all, 103 species were identified in the upper *ornatus* through *acuminatus* zones, belonging to 28 different genera, plus an additional three species/genera from the *atavus* Zone[29]. This represents a minimum estimate of diversity, as a number of specimens or collections of specimens

[29] This zone was only studied in sufficient depth to confirm its presence, i.e., to identify biostratigraphically useful taxa.

were assigned conservatively to species categories, but likely actually represent additional species.

The confirmed diversity at the Blackstone River section makes it the most biodiverse Ordovician-Silurian boundary section in the world. In addition to high diversity, the Blackstone River section has abundant and well-preserved taxa, making it ideal for systematic studies and other studies that require large amounts of occurrence data (in many cases hundreds of individual specimens were available in the current collections, and considerably more material could be recovered with targeted collection). Finally, the thickness of the Blackstone River section and its apparently unaltered isotopic record (see LaPorte et al., 2009) make it an ideal location for high-resolution geochemical studies. The Blackstone River section is shown to be a reference section of global quality for the study of the Ordovician-Silurian boundary interval.

Objective 2: Test the geographic exclusion hypothesis for neograptines during the latest Ordovician (pre-Hirnantian)

The failure of systematic searching to recover any neograptines in late Katian strata below the uppermost *pacificus* Zone, combined with rarefaction analysis supporting collection completeness, demonstrates that they were absent during most of the late Katian at the Blackstone River location. Combined with previous absence reports from lower resolution collecting at the nearby Peel River site (see Goldman et al., 2011), these results support the geographic exclusion hypothesis of Goldman et al. (2011), i.e., that environmental barriers and/or competitive interactions with

diplograptines excluded neograptines from the paleotropical realm for most of the Katian. This hypothesis is further supported by the correlation between the invasion of the first neograptines (*Neodiplograptus charis* and *Metabolograptus ojsuensis*) and evidence for environmental changes (increased in accessory fauna, community changes—see Chapter 5).

Objective 3: Test the impacts of sampling intensity on patterns of apparent species diversity (and establish a collecting standard for future sampling)

At the initiation of the project, a minimum sample size of 300 identified specimens per collection was chosen to give a 95% confidence that rare species (≤1% of sample) would be recovered. During research, analysis continued beyond 300 specimens through additional counts or scans, to capture taxa that fell below this 1% threshold. Slabs were also resplit after counting, to create more surface area for scans. This allowed taxa that comprised 0.06% of the sample or less to be identified in a number of instances. The counts revealed that most species occurred as minor components of the community even during the pre-extinction interval, often at or below the 1% threshold, and this unevenness trend was enhanced during the extinction interval. These results confirm that apparent patterns of diversity are likely to be strongly affected by low sampling intensity. At the same time, rarefaction analysis showed that, with the exception of the extinction interval, where communities became very strongly uneven, the level of sampling conducted in this study was sufficient to accurately capture diversity trends. While more intensive than many previous efforts,

the 0.25 m^2 samples[30] collected during this study are small enough that they could be collected in a realistic amount of time and transported out of the field in most cases. A 300 specimen sample is suggested as a minimum standard for future collecting efforts. In collections where graptolites are abundant, a 0.25 m^2 sample appears to be sufficient to reach this number.

Object 4: Test the refugium hypothesis, i.e., determine whether intensive sampling at the Blackstone River site could produce levels and patterns of diversity similar to those in China.

The intensive sampling during this thesis dramatically increased the known diversity in the Yukon during the Katian, including identifying a number of likely endemic species, identifying taxa previously thought to be endemic to China, and showing that diplograptine taxa extend into the lower Hirnantian (past the first main extinction interval). Diversity levels relative to the Yangtze platform were lower in the Katian and earliest Hirnantian at the Blackstone River, but were as high or higher during the late Hirnantian and early Rhuddanian. This partially supports the contention that the environment in South China manifested uniquely favourable conditions for graptolites prior to the extinction (although less profoundly than indicated by previous data). The diversity levels also indicate that South China was not unique in the recovery interval, as

[30] Assumes moderate to high specimen density; larger samples would be required to hit the 300 specimen minimum in areas with low density.

diversity at both sites was equivalent, with the apparent differences noted in the past the result of more intensive sampling in China.

Objective 5: Test whether two additional periods of diversity loss in the early Silurian suggested by Chinese data represented additional, global extinction events.

Diversity, extinction, and origination curves for the *persculptus-ascensus* and *ascensus-acuminatus* boundaries show drops in diversity and high species turnover rates that correspond to patterns seen in China. The diversity drop at the base of the Silurian is acute and well-correlated with that in China; the *ascensus-acuminatus* boundary changes are less well-resolved, due to questions about range lengths in this interval at the Blackstone River, but species turnover does seem to be elevated, as it is in China. The Blackstone River data support an additional global interval of extinction, related to sea level drop, at the Ordovician-Silurian boundary, and suggests global ecological instability among the plankton continued into the Silurian.

Objective 6: Examine the timing of the Late Ordovician Mass Extinction relative to community structural changes and test whether community changes preceded or followed from extinction.

The high-resolution collecting (5 cm intervals) just prior to and during the main pulse of extinction showed gross community compositional changes preceding maximum species loss, e.g., *Anticostia uniformis* dominates the last horizon before the invasion of neograptines; neograptines appear before the base of the Hirnantian and

immediately become dominant; and two morphologically "odd"[31] and short-lived diplograptine species arise during the first extinction pulse. Counts of specimen abundance throughout the Katian and early Hirnantian showed statistically significant changes in the composition and character of communities well before peak extinction, with communities becoming increasing uneven, simpler, and dominated by epipelagic species (see Sheets et al., 2016, for further discussion). Comparison of data with research recently conducted at a coeval section in Nevada showed that the patterns and timing of community changes seen at the Blackstone River section were generalizable trends, not the idiosyncratic response of local communities to local conditions. This analysis clearly shows that graptolite communities responded to environmental crises in ways that are not detectable through presence/absence data, and suggests that community structural changes are predictive of—and possibly causally related to—extinction.

Objective 7: Determine the relationship between extinction events seen at the Blackstone River site and environmental changes, specifically their relationship with sea level fall and oxygenation.

Comparison of diversity, extinction, and origination curves and lithological, paleontological, and geochemical data collected to indicate changes in water depth and

[31] The size and thecal spacing of *Paraorthograptus affinis* makes it an outlier relative to other known species of of the genus, with the exception of *P. uniformis*, which is a likely synonym (Fig. 6.17), and the constricted thecal apertures in *Appendispinograptus pogrebovi* are unlike those seen in any other Katian appendispinograptid (e.g., *A. supernus, A. venustus, A. leptothecalis,* or *A. longispinus*).

subsurface mixing, show a clear connection between diversity loss and sea level fall/oxygenation. The peaks of both extinction intervals (the *pacificus-extraordinarius* and *persculptus-ascensus* boundaries) correlate with neodymium excursions indicative of falling sea level, as well as evidence of increased oxygenation (the appearance of benthic fauna and a shift from black to pale lithology, respectively). This association of extinction and sea level/water mass changes is what is predicted by the biotope model for the extinction of graptolites during the LOME, and—along with the shifts in community structure (i.e., more mesopelagic species/specimens)—provides strong support for the model.

8.3 Issues Arising from this Thesis

The principal limitation of this research is that the data were gathered from a single section. While many of the patterns observed at the Blackstone River section were also seen elsewhere, lending support to the global relevance of the environmental and evolutionary trends interpreted, several other patterns were unique to the Blackstone River site. Evaluating the significance of these unique patterns, i.e., whether they represent sampling artifacts or local or regional conditions, is impossible from a single section. For example, diversity peaks later in the *pacificus* Zone at the Blackstone River site than elsewhere. However, the interval preceding the diversity peak has limited sampling, a result of the limited availability of black shales in that interval (itself intriguing), so it is difficult to know how to interpret the delayed diversity peak. The strong influence of local conditions on occurrence data is well-demonstrated in China,

where adjacent deeper and shallower water sections show different magnitudes and rates of response to the LOME (Chen et al., 2005b); similarly, the shallower Martin Ridge section responded differently than the deeper Vinini Creek section in Nevada in terms of the timing and degree of species turnover with the onset of glacial conditions (Štorch et al., 2011). Distinguishing local patterns at the Blackstone River section from regional patterns in the Yukon requires regional data, which at the present does not exist at sufficient resolution. Field collecting completed at the Peel River section (M.J. Melchin) in July, 2017 will hopefully produce additional comparative material to clarify regional patterns.

An additional sampling issue arises from gaps in the Blackstone River section collections themselves. Although extensive efforts were made to anticipate the needs of future researchers and collect accordingly, several interesting patterns (e.g., the *persculptus-ascensus* diversity drop) were recognized only after fieldwork was completed, resulting in lower than desirable sampling through these intervals. Similarly, the limited sampling in the *atavus* and *ornatus* zones is also regrettable, since the edge effect produced by the artificial range truncations at the end and beginning of sampling makes it impossible to determine true extinction and origination trends in the early *pacificus* and late *acuminatus* zones. Finally, a number of rare species occur in the collections that have uncertain identifications and/or ranges. These species could be targeted for recollection now that laboratory work has indicated where to look, but at present they inject uncertainty into analyses.

8.4 Future Research

Considerable opportunity exists for future work at the Blackstone River section. Large portions of the section remain unsampled, in particular younger material that is exposed beyond the end of the study interval and in additional outcrop just to the east of the section (Lenz, pers. comm.).

Within the study interval, a portion of the section also remains relatively unexplored. It was not until the late stages of the second field season that the upper portions of the two traverses at the Blackstone River (sections 'A' and 'B' in Fig. 3.2) were correlated. Collection of adequate material across the Ordovician-Silurian boundary was very difficult at Section B (where all the collections were made) owing to poor preservation and the steep and dangerous inclination of the section. Measurements down from correlated marker beds suggest that the boundary may be preserved at Section A, above an interval of cover (it was believed that the cover obscured the interval, so this part of the section was not well explored). Collecting there may allow high resolution sampling that could clarify extinction patterns at the base of the Silurian. Additionally, although sedimentological descriptions were made for the glacial interval (Melchin, pers. comm.), the detail of study was much lower at other points in the section, some of which show intriguing and counter-intuitive patterns. Within the lower *pacificus* Zone, for example, strata are mostly calcareous mudstones, with only intermittent black shales. This is superficially suggestive of generally lower, fluctuating local sea level, but this interpretation conflicts with the neodymium data for

the section, as well as global sea level trends for this interval. Illuminating the depositional conditions in the early *pacificus* Zone would clarify the significance of the pre-extinction diversity trends at the Blackstone River, as well as providing additional information to help unravel regional and global climate patterns.

Finally, unstudied or understudied material exists from the Blackstone River site that is available for future researchers. This consists of paleontological (trilobites, brachiopods, and large collections of graptolites), geochemical (surplus slabs from the graptolite samples are available for analysis), and lithological material (which could be thin-sectioned and examined).

Works Cited

ANHUI GEOLOGICAL SURVEY TEAM 1982. *Graptolites from Anhui*. Anhui Science and Technology Publishing House, Hefei, 166 pp. [in Chinese].

APOLLONOV, M. K., BANDALETOV, S. M., & NIKITIN, J. F. 1980. *The Ordovician-Silurian boundary in Kazakhstan.* Nauka, Kazakhstan SSR, Alma Ata, 232 pp.

ARMSTRONG, H. A. & COE, A. L. 1997. Deep-sea sediments record the geophysiology of the late Ordovician glaciation. *Jornal of the Geological Society, London* **154**, 929-934.

BAMBACH, R. K., KNOLL, A. H. & WANG, S. C. 2004. Origination, extinction, and mass depletions of marine diversity. *Paleobiology* **30**(4), 522–542.

BAPST, D. W., BULLOCK, P. C., MELCHIN, M. J., SHEETS, H. D. & MITCHELL, C. E. 2012. Graptoloid diversity and disparity became decoupled during the Ordovician mass extinction. *Proceedings of the National Academy of Sciences* **109**(9), 3428–3433.

BELSCHER, K. 2007. Species abundance changes during mass extinction and the inverse Signor-Lipps effect: apparent abrupt graptolite mass extinction as an artifact of sampling. MSc thesis, University at Buffalo, SUNY, USA, 84 pp. *Unpublished thesis*.

BERRY, W. B. N. 1960. *Graptolite faunas of the Marathon region, west Texas*. Bureau of Economic Geology, The University of Texas, Austin, 179 pp.

BERRY, W. B. N. 1966. *Climacograptus hastatus* T. S. Hall – its lectotype and some local populations. *Journal of Paleontology*, **40**, 162-176.

BJERRESKOV, M. 1975. Llandoverian and Wenlockian graptolites from Bornholm. *Fossils and Strata* **8**, 1-94.

BOND, D. P. G. & GRASBY, S. E. 2017. On the causes of mass extinctions. *Palaeogeography, Palaeoclimatology, Palaeoecology* **478**, 3–29.

BOYLE, J., SHEETS, H. D., WU, S.-Y., GOLDMAN, D., MELCHIN, M. J., COOPER, R. A., SADLER, P. M. & MITCHELL, C. E. 2017. The impact of geographic range, sampling, ecology, and time on extinction risk in the volatile clade Graptoloida. *Paleobiology* **43**(1), 85–113.

BRENCHLEY, P. J., MARSHALL, J. D., CARDEN, G. A. F., ROBERTSON, D. B. R., LONG, D. G. F., MEIDLA, T., HINTS, L. & ANDERSON, T. F. 1994. Bathymetric and isotopic evidence for a short-lived Late Ordovician glaciation in a greenhouse period. *Geology* **22**(4), 295–298.

BRUSSA, E. D., MITCHELL, C. E. & ASTINI, R. A. 1999. Ashgillian (HirnantiaN.?) graptolites from the western boundary of the Argentine Precordillera. In *Quo vadis* OrdoviciaN.? *Acta Universitatis Carolinae, Geologica* (eds P. Kraft and O. Fatka), pp. 199-202, no. 43 (1/2).

BULMAN, O .M. B. &RICKARDS, R. B. 1968. Some new diplograptids from the Llandovery of Britain and Scandinavia. *Palaeontology* **11**, 1–15.

BULMAN, O. M. B. 1945. A monograph of the Caradoc (Balclatchie) graptolites from limestones in Laggan Burn, Ayrshire, part 1. *Monograph of the Palaeontographical Society*, 1-42.

BULMAN, O. M. B. 1946. A monograph of the Caradoc (Balclatchie) graptolites from limestones in Laggan Burn, Ayrshire, part 2. *Monograph of the Palaeontographical Society*, 43-58.

BULMAN, O. M. B. 1947. A monograph of the Caradoc (Balclatchie) graptolites from limestones in Laggan Burn, Ayrshire, part 3. *Monograph of the Palaeontographical Society*, 59-78.

BULMAN, O. M. B. 1970. Graptolithina with sections on Enteropneusta and Pterobranchia. In *Treatise on Invertebrate Paleontology, Pt. V* (ed. C. Teichert). Geological Society of America and University of Kansas Press, 163 pp.

CARRUTHERS, W. 1858. Dumfriesshire graptolites, with descriptions of three new species. *Proceedings of the Royal Physical Society of Edinburgh* 1: 466-470.

CARRUTHERS, W. 1867. Graptolites: their structure and systematic position. *Intellectual Observer*, **11**, **10**, 64, 65.

CECILE, M. P., MORROW, D. W. & WILLIAMS, G. K. 1997. Early Paleozoic (Cambrian to Early Devonian) tectonic framework, Canadian Cordillera. *Bulletin of Canadian Petroleum Geology* **45**(1), 54–74.

CHALETSKAYA, O. N. 1960. New species of the Llandovery graptolites of Central Asia. *In New species of ancient plants and invertebrates in the USSR. II*. (ed B.P. Markovsky), pp. 373-375. Gosudarstvennoe Nauchno-Teknicheskoye Izdatel'stvo, Moscow. [In Russian].

CHEN, X., FAN, J.-X., MELCHIN, M. J. & MITCHELL, C. E. 2005a. Hirnantian (latest Ordovician) graptolites from the Upper Yangtze Region, China. *Palaeontology* **48**(2), 235–280.

CHEN, X. & LENZ, A. C. 1984. Correlation of Ashgill graptolite faunas of Central China and Arctic Canada, with a description of *Diceratograptus* cf. *mirus* Mu from Canada. In *Stratigraphy and palaeontology of systemic boundaries in China, Ordovician-Silurian boundary* (1) (ed. Nanjing Institute of Geology and Palaeontology, Academia Sinica), pp. 247-258. Hefei: Anhui Science and Technology Publishing House. [In English]

CHEN, X. & LIN, Y.-K., 1978. Lower Silurian graptolites from Tongzi, northern Guizhou. *Memoir of Nanjing Institute of Geology and Palaeontology, Academia Sinica* **12**, 1-106. [In Chinese, English summary].

CHEN, X., MELCHIN, M. J., SHEETS, H.D., MITCHELL, C. E. & FAN, J.-X. 2005b. Patterns and processes of latest Ordovician graptolite extinction and recovery based on data from South China. *Journal of Paleontology* **79**(5), 842–861.

CHEN, X., MELCHIN, M. J., FAN, J.-X., & MITCHELL, C.E. 2003. Ashgillian graptolite fauna of the Yangtze region and the biogeographical distribution of diversity in the latest Ordovician. *Bulletin de la Société Géologique de France* **174**(2), 141–148.

CHEN, X., RONG, J., MITCHELL, C. E., HARPER, D. A. T., FAN, J.-X, F., ZHAN, R., ZHANG, Y., LI, R. & WANG, Y. 2000. Late Ordovician to earliest Silurian graptolite and brachiopod biozonation from the Yangtze region, South China, with a global correlation. *Geological Magazine* **137**(6), 623–650.

CHEN, X., RONG, YU., J., FAN J.-X., ZHAN R.-B., MITCHELL, C. E., HARPER, D. A. T., MELCHIN, M. J., & WANG X.-F., 2006. The Global Boundary Stratotype Section and Point (GSSP) for the base of the Hirnantian Stage (the uppermost of the Ordovician System). *Episodes* **29**(3), 183-196.

CHEN, X., ZHANG, Y. D., YU, G. H. & LIU, X. 2007. Latest Ordovician and earliest Silurian graptolites from northwestern Zhejiang, China. *Acta Palaeontologica Sinica* **46**, 77–82.

CHEN, Z.-Y., KIM, M.-H., CHOH, S.-J., LEE, D.-J. & CHEN, X. 2016. Discovery of *Anticostia uniformis* from the Xiazhen Formation at Zhuzhai, South China and its stratigraphic implication. *Palaeoworld* **25**(3), 356–361.

CHURKIN, M. JR. & CARTER, C. 1970. Early Silurian graptolites from Southeastern Alaska and their correlation with graptolitic sequences in North America and the Arctic. *Geological Survey Professional Paper* **653**, 1-51.

CHURKIN, M., CARTER, C. & EBERLEIN, G. D. 1970. Graptolite succession across the Ordovician–Silurian boundary in south-eastern Alaska. *Quarterly Journal of the Geological Society* **126**(1–4), 319–330.

COCKS, L. R. M. & TORSVIK, T. H. 2011. The Palaeozoic geography of Laurentia and western Laurussia: A stable craton with mobile margins. *Earth-Science Reviews* **106**(1), 1–51.

CONIGLIO, M. & MELCHIN, M. J. 1995. Petrography and isotope geochemistry of diagenetic carbonates in the lower Cape Phillips Formation, Cornwallis Island, Arctic Archipelago, Canada. *Bulletin of Canadian Petroleum Geology*, **43**, 251-266.

COOPER R. A., RIGBY S., LOYDELL D. K., & BATES D. E. B. 2012. Palaeoecology of the Graptoloidea. *Earth-Science Reviews* **112**(1-2), 23-41.

COOPER, R. A. & SADLER, P. M. 2010. Facies preference predicts extinction risk in Ordovician graptolites. *Paleobiology* **36**(2), 167–187.

COOPER, R. A., SADLER, P.M., HAMMER, O. & GRADSTEIN, F. M. 2012. Chapter 20 - The Ordovician Period. In *The Geologic Time Scale*, pp. 489–523, Boston: Elsevier.

CRAMPTON, J. S., COOPER, R. A., SADLER, P. M. & FOOTE, M. 2016. Greenhouse−icehouse transition in the Late Ordovician marks a step change in extinction regime in the marine plankton. *Proceedings of the National Academy of Sciences* **113**(6), 1498–1503.

CUERDA, A. J., RICKARDS, R. B. & CINGOLANI, C. 1988. A new Ordovician–Silurian boundary section in San Juan Province, Argentina, and its definitive graptolite fauna. *Journal of the Geological Society* **145**(5), 749–757.

DAVIES, K. A. 1929. Notes on the graptolite faunas in the Upper Ordovician and Lower Silurian. *Geological Magazine* **66**, 1-27.

DELABROYE, A. & VECOLI, M. 2010. The end-Ordovician glaciation and the Hirnantian Stage: A global review and questions about Late Ordovician event stratigraphy. *Earth-Science Reviews* **98**(3), 269–282.

DELABROYE, A., MUNNECKE, A., VECOLI, M., COPPER, P., TRIBOVILLARD, N., JOACHIMSKI, M. M., DESROCHERS, A. & SERVAIS, T. 2011. Phytoplankton dynamics across the Ordovician/Silurian boundary at low palaeolatitudes: Correlations with carbon isotopic and glacial events. *Palaeogeography, Palaeoclimatology, Palaeoecology* **312**(1), 79–97.

ELLES, G. L. & WOOD, E. M. R. 1904. A monograph of British graptolites, part 4. *Monograph of the Palaeontographical Society* **58**(277), liii-lxii, 135-180.

ELLES, G. L. & WOOD, E. M. R. 1906. A monograph of British graptolites, part 5, (*Climacograptus*). *Monograph of the Palaeontographical Society* **60**, lxxiii-xcvi, 181-216.

ELLES, G. L. AND WOOD, E. M. R. 1907. A Monograph of British graptolites, part 6. *Monograph of the Palaeontographical Society* **61**, xcvii-cxx, 217-272.

ELLES, G. L. AND WOOD, E. M. R. 1908. A Monograph of British graptolites, part 7. *Monograph of the Palaeontographical Society* **62**(305), cxxi-cxlviii, 273-358.

FAN, J.-X. 1998. Studies on the Hirnantian graptolite fauna of Late Ordovician of Yichang with morphometric analysis of some normalograptids. MSc thesis, Nanjing Institute of Geology and Palaeontology, Academia Sinica, China, 81 pp. *Unpublished thesis* [In Chinese, English summary].

FAN, J.-X. & CHEN, X. 2007. Preliminary report on the Late Ordovician graptolite extinction in the Yangtze region. Palaeogeography, Palaeoclimatology, Palaeoecology **245**(1), 82-94.

FAN, J.-X., CHEN, X., MELCHIN, M. J. & FANG, Y.-T. Lower Rhuddanian (Llandovery, Silurian) graptolites from the Yangtze region, China. *In preparation*.

FANG, Y.-T., LIANG, S.-J., ZHANG, D.-L., & YU, J.-L., 1990. *Stratigraphy and graptolite fauna of Lishuwo Formation from Wuning, Jiangxi*, pp. 155. Nanjing University Publishing House, Nanjing, China [In Chinese with English Summary].

FANTON, K. C., HOLMDEN, C., NOWLAN, G. S., & HAIDL, F. M. 2002. 143Nd/144Nd and Sm/Nd stratigraphy of Upper Ordovician epeiric sea carbonates. *Geochimica et Cosmochimica Acta* **66**, 241–255.

FINNEGAN, S., BERGMANN, K., EILER, J.M., JONES, D. S., FIKE, D. A., EISENMAN, I., HUGHES, N. C., TRIPATI, A. K. & FISCHER, W. W. 2011. The magnitude and duration of Late Ordovician-Early Silurian glaciation. *Science (New York, N.Y.)* **331**(6019), 903–906.

FINNEGAN, S., HEIM, N. A., PETERS, S. E. & FISCHER, W. W. 2012. Climate change and the selective signature of the Late Ordovician mass extinction. *Proceedings of the National Academy of Sciences* **109**(18), 6829–6834.

FINNEY, S. C, & BERRY, W. B. N. 1997. New perspectives on graptolite distributions and their use as indicators of platform margin dynamics. *Geology*, **25**, 919-922.

FINNEY, S. C., BERRY, W. B. N. & COOPER, J. D. 2007. The influence of denitrifying seawater on graptolite extinction and diversification during the Hirnantian (latest Ordovician) mass extinction event. *Lethaia* **40**(3), 281–291.

FINNEY, S. C., BERRY, W. B. N., COOPER, J. D., RIPPERDAN, R. L., SWEET, W. C., JACOBSON, S.R., SOUFIANE, A., ACHAB, A. & NOBLE, P.J. 1999. Late Ordovician mass extinction: A new perspective from stratigraphic sections in central Nevada. *Geology* **27**(3), 215–218.

FOOTE, M. 2000. Origination and extinction components of taxonomic diversity: General problems. *Paleobiology* **26**(sp4), 74–102.

FORTEY, R. A. & COOPER, R. A. 1986. A phylogenetic classification of the graptoloids. *Palaeontology*, **29**, 631-654.

FRECH, F. 1897. *Lethaea geognostica oder Beschreibung und Abbildung fur die Gebirgs-Formationen bezeichnendsten Versteinerungen. Herausgegeben von einer Vereinigung von Palaeontologen, 1. Teil, Lethaea Palaeozoica*. E. Schweizerbart'sche Verlagshandlung, Stuttgart, pp. 544–684.

FRITZ, W. H., 1985. *The basal contact of the Road River Group—a proposal for its location in the type area and other selected areas in the northern Canadian Cordillara. In* Current Research, Part B. Geological Survey of Canada, Paper 85-1b, pp. 205-215.

FU, H.-Y. 1982. Graptolithina. 410-479, pls 269-299. In *GEOLOGICAL BUREAU OF HUNAN (ed.). The palaeontological atlas of Hunan*. Geological Memoirs of the Ministry of Geology and Mineral Resources, Geological Publishing House, Beijing, People's Republic of China, **2**(1), 997 pp. [In Chinese].

GHAVIDEL-SYOOKI, M., ÁLVARO, J.J., POPOV, L., POUR, M.G., EHSANI, M.H. & SUYARKOVA, A. 2011. Stratigraphic evidence for the Hirnantian (latest Ordovician) glaciation in the Zagros Mountains, Iran. *Palaeogeography, Palaeoclimatology, Palaeoecology* **307**(1), 1–16.

GOLDMAN, D., MITCHELL, C. E., MALETZ, J., RIVA, J. F. V., LESLIE, S. A. & MOTZ, G. J. 2007. Ordovician graptolites and conodonts of the Phi Kappa Formation in the Trail Creek egion of Central Idaho: A revised, integrated biostratigraphy. In *Proceedings of the 10th International Symposium on the Ordovician System, Nanjing China. June 2007* (eds J. Li, J.-X. FAN, & I. Percival) pp. 155-162. *Acta Palaeontologica Sinica 46 (Supplement)*.

GOLDMAN, D., MITCHELL, C. E., MELCHIN, M. J., FAN, J.-X., WU, S.-Y. & SHEETS, H. D. 2011. Biogeography and Mass Extinction: Extirpation and re-invasion of *Normalograptus* species (Graptolithina) in the Late Ordovician Palaeotropics. *Proceedings of the Yorkshire Geological Society* **58**(4), 227–246.

GOODFELLOW, W. D., NOWLAN, G. S., MCCRACKEN, A. D., LENZ, A.C . & GRÉGOIRE, D. C. 1992. Geochemical anomalies near the Ordovician-Silurian boundary, Northern Yukon Territory, Canada. *Historical Biology* **6**(1), 1–23.

GORDEY, S. P., 2013. Evolution of the Selwyn Basin region, Sheldon Lake and Tay River map areas, central Yukon. Geological Survey of Canada, Bulletin 599, 190 pp.

GURLEY, R. R. 1896. North American graptolites; new species and vertical range. *Journal of Geology* **4**, 63-102.

HALL, J. 1847. Descriptions of the organic remains of the lower division of the New York System. *Paleontology of New York* **1**, 265-274.

HALL, J. 1865. *Figures and descriptions of Canadian organic remains. Decade II, Graptolites of the Quebec Group*. Geological Survey of Canada, Montreal. Dawson Brothers, 151 pp.

HALL, T. S. 1902. The graptolites of New South Wales in the collections of the Geological Survey. Records of the Geological Survey of New South Wales **7**, 49-59.

HAWKINS, A. D. 2011. Quantifying change in community structure and extinction selectivity in late Katian graptolite communities. MS thesis, University at Buffalo, SUNY, 106 pp.

HISINGER, W. 1837. *Lethaea Suecica seu Petrifacta Sueciae, Supplementum 1*. Holmiae, Stockholm, 124 pp.

HOLMDEN, C., MITCHELL, C. E., LAPORTE, D. F., PATTERSON, W. P., MELCHIN, M. J. & FINNEY, S. C. 2013. Nd isotope records of late Ordovician sea level change—Implications for glaciation frequency and global stratigraphic correlation. *Palaeogeography, Palaeoclimatology, Palaeoecology* **386**, 131–144.

HOPKINSON, J., 1871. On *Dicellograptus*, a new species of *Graptolites*. *Geological Magazine* **8**, 20-26, pl. 1.

HOWE, M. P. A. 1982. The lower Silurian graptolites of the Oslo region, 21–23. In *IUGS, Subcommission on Silurian Stratigraphy, Field Meeting Oslo region 1982* (ed. D. Worsley), pp. 1-175. Palaeontological Contributions from the University of Oslo no. 278.

HOWE, M. P. A. 1983. Measurement of thecal spacing in graptolites. *Geological Magazine* **120**(6), 635–638.

HSÜ, S. C. 1959. A new graptolite fauna from the Lower Ordovician shale of Tsaidam, Chinghai Province. *Acta Palaeontologica Sinica* **7**, 161-192. [In Chinese with English Summary]

HUANG, Z.-G. 1982. Latest Ordovician and earliest Silurian graptolite assemblages of Xainza district, Xizang (Tibet) and Ordovician-Silurian boundary. In *Contribution to the geology of the Qinghai-Xizang (Tibet) Plateau* (7) (ed. Editorial Committee of Ministry of Geology and Mineral Resources), pp. 27–52. Beijing, People's Republic of China: Geological Publishing House. [In Chinese, English abstract].

HUNDT, R. 1942. Der Schwebeapparat der diprionitischen Graptolithen. *Beiträge zur Geologie von Thüringens* **7**, 71-74.

HUTT, J. E. 1974. The Llandovery graptolites of the English Lake District, part 1. *Monograph of the Palaeontographical Society* **128**, 1-56.

JACKSON, D. E. & LENZ, A. C. 1962. Zonation of Ordovician and Silurian graptolites of northern Yukon, Canada. *AAPG Bulletin* **46**(1), 30–45.

JONES, D. S., MARTINI, A. M., FIKE, D. A. & KAIHO, K. 2017. A volcanic trigger for the Late Ordovician mass extinctioN.? Mercury data from south China and Laurentia. *Geology* **45**(7), 631–634.

JONES, O. T. 1909. The Hartfell-Valentian succession around Plynlimon and Pont Erwyd. *Quarterly Journal of the Geological Society of London* **65**, 463-537.

KELLER, B. M. 1956. Ordovician graptolites of the Chi-Illi Mountains, Kazakhstan. *Trudy Geologicheskogo Instituta, Akademiya Nauk SSSR* **1**, 50-102. (In Russian).

KOREN, T. N. 1979. *Pacificograptus* a new late Ordovician diplograptid genus. *Paleontological Journal* **1979**, 65-70.

KOREN, T. N., AHLBERG, P. & NIELSEN, A. T. 2003. The post-*persculptus* and pre-*ascensus* graptolite fauna in Scania, south-western Sweden: Ordovician or SiluriaN.? In *Proceedings of the 7th International Graptolite Conference and Field meeting of the International Subcommission on Silurian Stratigraphy* (eds G. Ortega & G. F. Acenolaza). INSUGEO, serie Correlación Geologica **18**, 133-138.

KOREN, T. N. & BJERRESKOV, M. 1997. Early Llandovery monograptids from Bornholm and the southern Urals: taxonomy and evolution. *Bulletin of the Geological Society of Denmark* **44**, 1-43.

KOREN, T. N., ORADOVSKAYA, M. M. & SOBOLEVSKAYA, R.F. 1988. The Ordovician-Silurian boundary beds of the north-east U.S.S.R., In*A global analysis of the Ordovician-Silurian boundary* (eds L. R. M. Cocks & R. B. Rickards), pp. 133-138. Bulletin British Museum (Natural History), Geology, no. 43.

KOREN, T. N. & MELCHIN, M. J. 2000. Lowermost Silurian Graptolites from the Kurama Range, Eastern Uzbekistan. *Journal of Paleontology* **74**(6), 1093–1113.

KOREN, T. N., PYMA, L. J., SOBOLEVSKAYA, R. F., & CHUGEVA, M. N. 1983. *The Ordovician and Silurian boundary in the north-east of the USSR.* Trudy Mezhvedomstvennogo Stratigraficheskogo Komiteta SSSR, 11, 205 pp. [In Russian].

KOREN, T. N. & RICKARDS, R. B. 1996. Taxonomy and evolution of graptoloids from the Southern Urals, Western Kazakhstan. *Special Papers in Palaeontology* **54**, 1-103.

KOREN, T. N. & RICKARDS, R. B. 2004. An unusually diverse Llandovery (Silurian) diplograptid fauna from the southern Urals of Russia and its evolutionary significance. *Palaeontology* **47**, 859-918.

KOREN, T. N., SOBOLEVSKAYA, R. F., MIKHAILOVA, N. F., AND TASI, D. T. 1979. New evidence on graptolite succession across the Ordovician-Silurian Boundary in the Asian part of the USSR. *Acta Palaeontologica Polonica* **24**(1), 125-136.

KOREN, T. N. & SOBOLEVSKAYA, R. F. 2008. The regional stratotype section and point for the base of the Hirnantian Stage (the uppermost Ordovician) at Mirny Creek, Omulev Mountains, Northeast Russia. *Estonian Journal of Earth Sciences* **57**, 1–10.

KRAFT, P., ŠTORCH, P. & MITCHELL, C. E. 2015. Graptolites of the Kralův Dvůr Formation (mid Katian to earliest Hirnantian, Czech Republic). *Bulletin of Geosciences* **90**(1), 195–225.

KUMP, L. R., ARTHUR, M. A., PATZKOWSKY, M. E., GIBBS, M. T., PINKUS, D. S. & SHEEHAN, P. M. 1999. A weathering hypothesis for glaciation at high atmospheric pCO2 during the Late Ordovician. *Palaeogeography, Palaeoclimatology, Palaeoecology* **152**(1), 173–187.

LANE, S. L. 2007. Devonian–Carboniferous paleogeography and orogenesis, northern Yukon and adjacent arctic Alaska. *Canadian Journal of Earth Sciences* **44**, 679-694.

LAPORTE, D. F., HOLMDEN, C., PATTERSON, W. P., LOXTON, J. D., MELCHIN, M. J., MITCHELL, C. E., FINNEY, S. C. & SHEETS, H. D. 2009. Local and global perspectives on carbon and nitrogen cycling during the Hirnantian glaciation. *Palaeogeography, Palaeoclimatology, Palaeoecology* **276**(1), 182–195.

LAPWORTH, C. 1873. Notes on the British graptolites and their allies. 1. On an improved classification of the Rhabdophora. *Geological Magazine* **10**, 500-504, 555-560, table 1.

LAPWORTH, C. 1877. On the graptolites of County Down. *Proceedings of the Belfast Naturalists` Field Club* **1876-1877**, 125-148.

LAPWORTH, C. 1879. On the geological distribution of the Rhabdophora. *Annals and Magazine of Natural History, Series 5*, **3**, 245-257, 449-455; **4**, 333-341, 423-431.

LAPWORTH, C. 1880. On new British graptolites. *Annals and Magazine of natural History* **5**(5), 149-177.

LAPWORTH, C. 1886. Preliminary report on some graptolites from the Lower Paleozoic rocks on the south side of the St. Lawrence from Cape Rosier to Tartigo River, from the North Shore of the Island of Orleans, one mile above Cap Rouge, and from the Cove Fields, Quebec. *Royal Society of Canada Transactions* **4**, 167–184.

LAPWORTH, H. 1900. The Silurian sequence of Rhayader. *Quarterly Journal of the Geological Society of London* **56**, 67–137.

LEFEBVRE, V., SERVAIS, T., FRANÇOIS, L. & AVERBUCH, O. 2010. Did a Katian large igneous province trigger the Late Ordovician glaciatioN.? *Palaeogeography, Palaeoclimatology, Palaeoecology* **296**(3), 310–319.

LEGRAND, P. 1977. Contribution à l'etude des graptolites du Llandoverien inferieur de l'Oued In Djerane (Tassili N'ajjer oriental, Sahara algérien). *Bulletin de la Société d'Histoire Naturelle de l'Afrique du Nord* **67**, 141-196.

LEGRAND, P. 1986. The Lower Silurian graptolites of Oued In Djerane: a study of populations at the Ordovician-Silurian boundary. In *Palaeoecology and Biostratigraphy of Graptolites* (eds C. P. Hughes, R. B. Rickards, & A. J. Chapman), *Geological Society Special Publication* **20**, 145-153.

LEGRAND, P. 1987. Modo de desarrollo del suborden Diplograptina (Graptolithina) en el Ordovício superior y en el Silúrico. Implicaciones taxonómicas. *Revista Española de Paleontologia* **2**, 59-64.

LEGRAND, P. 1999. Approche stratigraphique de l'Ordovician terminal et du Silurien inferieur du Sahara algerien par l'etude des Diplograptides (Graptolites). PhD thesis, Université Michel de Montaigne-Bordeaux III, Institut *EGID* Bordeaux III. *Unpublished thesis.*

LEGRAND, P. 2003 Silurian Stratigraphy and Paleogeography of the Northern African Margin of Gondwana. In Silurian Land and Seas - Paleogeography outside of Laurentia (eds Landing E.D. and Johnson M.E.), pp. 59-104. New York State Museum, Albany.

LENTON, T. M., CROUCH, M., JOHNSON, M., PIRES, N. & DOLAN, L. 2012. First plants cooled the Ordovician. *Nature Geoscience* **5**(2), 86–89.

LENZ, A. 1979. Llandoverian graptolite zonation in the northern Canadian Cordillera. *Acta Palaeontologica Polonica* **24**(1), 137–153.

LENZ, A. C. 1982. Llandoverian graptolites of the northern Canadian Cordillera*: Petalograptus, Cephalograptus, Rhaphidograptus, Dimorphograptus, Retiolitidae,* and *Monograptidae.* Royal Ontario Museum, Life Sciences Contributions 130, 154 pp.

LENZ, A. C. 1988. Upper Silurian and Lower Devonian graptolites and graptolite biostratigraphy, northern Yukon, Canada. *Canadian Journal of Earth Sciences* **25**(3), 355–369.

LENZ, A. C. & CHEN, X. 1985. Graptolite distribution and lithofacies: Some case histories. *Journal of Paleontology* **59**(3), 636–642.

LENZ, A. C., & MACCRACKEN, A. D. 1982. The Ordovician–Silurian boundary, northern Canadian Cordillera: graptolite and conodont correlation. *Canadian Journal of Earth Sciences* **19**, 1308-1322.

LENZ, A. C. & MCCRACKEN, A. D. 1988. Ordovician-Silurian boundary, northern Yukon, Canada. *Bulletin of the British Museum of Natural History (Geology)* **43**, 265-271.

LI, J.-J. 1984. Graptolites from the Xinling Formation (Upper Ordovician) of South Anhui. *Memoirs of Nanjing Institute of Geology and Palaeontology, Academia Sinica* **20**, 145-194.

LI, J.-J. 1995. Lower Silurian graptolites from the Yangtze Gorge district. *Palaeontologica Cathayana* **6**, 215-344.

LI, J.-J. 1999. Lower Silurian graptolites from Southern Anhui. *Bulletin of the Nanjing Institute of Geology and Palaeontology, Academia Sinica* **14**, 70-157. [In Chinese, English summary].

LI, J.-J. & GE, M.-Y.. 1981. Development and systematic position of akidograptids. *Acta Palaeontologica Sinica* **2**, 225-235. [In Chinese, English abstract]

LI, Z.-M., & LI, D.-Q. 1985. *Appendispinograptus*, a new subgenus of *Climacograptus*. *Earth Science Journal of Wuhan College of Geology* **10**, 35-42. [In Chinese with English abstract].

LIN, Y.-K. & CHEN, X. 1984. *Glyptograptus persculptus* Zone - the Earliest Silurian graptolite zone from Yangtze Gorges, China. In *Stratigraphy and Palaeontology of Systemic Boundaries in China, Ordovician-Silurian Boundary* (1) (ed Nanjing Institute of Geology and Palaeontology), pp. 203-232. Hefei: Anhui Science and Technology Publishing House.

LINK, C. M. & BUSTIN, R. M., & GOODARZI, F. 1990. Petrology of graptolites and their utility as indices of thermal maturity in Lower Paleozoic strata in northern Yukon, Canada. *International Journal of Coal Geology,* **15**, 113-135.

LIU, Z., ALGEO, T. J., GUO, X., FAN, J.-X., DU, X., & LU, Y. 2017. Paleo-environmental cyclicity in the Early Silurian Yangtze Sea (South China): Tectonic or glacio-eustatic control? *Palaeogeography, Palaeoclimatology, Palaeoecology* 466, 59-76.

LOXTON, J., MELCHIN, M. J., MITCHELL, C. E. & SENIOR, S. J. H. 2011. Ontogeny and astogeny of the graptolite genus *Appendispinograptus* (Li and Li, 1985). *Proceedings of the Yorkshire Geological Society* **58**(4), 253–260.

LOYDELL, D. K. 2007. Graptolites from the Upper Ordovician and lower Silurian of Jordan. *Special Papers in Palaeontology* **78**, 1-78.

LUKASIK, J. J., & MELCHIN, M. J. 1994. *Atavograptus primitivus* (Li) from the earliest Silurian of Arctic Canada: implications for monograptid evolution. *Journal of Paleontology* **68**, 1159-1163.

McCOY, F. 1850. On some new genera and species of Silurian adiata in the collection of the University of Cambridge. *Annals and Magazine of Natural History* **6**, 270-290.

McCRACKEN, A. D. & LENZ, A. C. 1987. Middle and Late Ordovician conodont faunas and biostratigraphy of graptolitic strata of the Road River Group, northern Yukon Territory. *Canadian Journal of Earth Sciences* **24**(4), 643–653.

MELCHIN, M. J. 1987a. Upper Ordovician graptolites from the Cape Phillips Formation, Canadian Arctic Islands. *Bulletin of the Geological Society of Denmark* **35**, 191-202.

MELCHIN, M. J. 1987b. Late Ordovician and Early Silurian graptolites, Cape Phillips Formation, Canadian Arctic Archipelago. PhD thesis, University of Western Ontario, Canada. *Unpublished thesis.*

MELCHIN, M. J. 1989. Llandovery graptolite biostratigraphy and paleobiogeography, Cape Phillips Formation, Canadian Arctic Islands. *Canadian Journal of Earth Sciences* **26**(9), 1726–1746.

MELCHIN, M. J. 1998. Morphology and phylogeny of some Early Silurian 'diplograptid' genera from Cornwallis Island, Arctic Canada. *Palaeontology* **41**, 2, 263–315.

MELCHIN, M. J. 2008. Restudy of some Ordovician–Silurian boundary graptolites from Anticosti Island, Canada, and their biostratigraphic significance. *Lethaia* **41**(2), 155–162.

MELCHIN, M. J., & ANDERSON, A. J. 1998. Infrared video microscopy for the study of graptolites and other organic-walled fossils. *Journal of Paleontology* **72**, 397-400.

MELCHIN, M. J., HOLMDEN C., & WILLIAMS, S. H. 2003. Correlation of graptolite biozones, chitinozoan biozones, and carbon isotope curves through the Hirnantian. In *Ordovician from the Andes* (eds G. L. Albanesi, M. S. Beresi, & S.H. Peralta), pp. 101-104. Tucumán, Argentina: INSUEGO, Serie Correlación Geológica, Comunicarte Editorial.

MELCHIN, M. J. & HOLMDEN, C. 2006. Carbon isotope chemostratigraphy of the Llandovery in Arctic Canada: Implications for global correlation and sea level change. *GFF* **128**(2), 173–180.

MELCHIN, M. J., McCRACKEN, A. D. & OLIFF, F. J. 1991. The Ordovician-Silurian boundary on Cornwallis and Truro islands, Arctic Canada: preliminary data. *Canadian Journal of Earth Sciences* **28**, 1854-1862.

MELCHIN, M. J. & MITCHELL, C. E. 1991. Late Ordovician extinction in the Graptoloidea. In *Advances in Ordovician Geology* (eds C. R. Barnes & S. H. Williams), pp. 143-156. Geological Survey of Canada, Paper 90-9.

MELCHIN, M. J., MITCHELL, C. E., HOLMDEN, C. & ŠTORCH, P. 2013. Environmental changes in the Late Ordovician–early Silurian: Review and new insights from black shales and nitrogen isotopes. *GSA Bulletin* **125**(11–12), 1635–1670.

MELCHIN, M. J., MITCHELL, C. E., NACZK-CAMERON, A., FAN, J.-X. & LOXTON, J. 2011. Phylogeny and adaptive radiation of the Neograptina (Graptoloida) during the Hirnantian mass extinction and Silurian recovery. *Proceedings of the Yorkshire Geological Society* **58**(4), 281.

MELCHIN, M. J., SADLER, P. M., CRAMER, B. D., COOPER, R. A., GRADSTEIN, F. M. & HAMMER, O. 2012. Chapter 21 - The Silurian Period. In *The Geologic Time Scale*, pp. 525–558., Boston: Elsevier.

MELCHIN, M. J. & WILLIAMS, S. H. 2000. A restudy of the akidograptine graptolites from Dob's Linn and a proposed redefined zonation of the Silurian Stratotype. Palaeontology Down Under 2000, Geological Society of Australia, Abstracts 61, 63.

MELOTT, A. L., THOMAS, B. C., HOGAN, D. P., EJZAK, L. M. & JACKMAN, C. H. 2005. Climatic and biogeochemical effects of a galactic gamma ray burst. *Geophysical Research Letters* **32**(14), L14808.

MITCHELL, C. E. 1987. Evolution and phylogenetic classification of the Diplograptacea. *Palaeontology* **30**, 353-405.

MITCHELL, C. E., CHEN, X., & FINNEY, S. C. 2007a. The structure and possible function of 'basal membranes' in the spinose climacograptid graptolite *Appendispinograptus* Li and Li 1985. *Journal of Paleontology* **81**, 1122-1127.

MITCHELL, C. E., GOLDMAN, D., KLOSTERMAN, S. L., MALETZ, J., SHEETS, H. D. & MELCHIN, M.J. 2007b. Phylogeny of the Ordovician Diplograptoidea. In *Proceedings of the 10th International Symposium on the Ordovician System, Nanjing China, June 2007* (eds J. Li, J.-X. FAN, & I. PERCIVAL), pp. 332-339. *Acta Palaeontologica Sinica* **46** (Supplement).

MITCHELL, C. E., MALETZ, J. & GOLDMAN, D. 2009. What is *Diplograptus*? *Bulletin of Geosciences* **84**(1), 27–34.

MITCHELL, C. E., SHEETS, H. D., BELSCHER, K., FINNEY, S. C., HOLMDEN, C., LAPORTE, D. F., MELCHIN, M. J. & PATTERSON, W. P. 2007c. Species abundance changes during mass extinction and the inverse Signor-Lipps effect: Apparently abrupt graptolite mass extinction as an artifact of sampling. In *Proceedings of the 10th International Symposium on the Ordovician System, Nanjing China, June 2007* (eds. J. Li, J.-X., & I. Percival), pp. 340-346. *Acta Palaeontologica Sinica* **46** (Supplement).

MITCHELL, C. E., ŠTORCH, P., HOLMDEN, C., MELCHIN, M. J. & GUTIÉRREZ-MARCO, J. C. 2011. New stable isotope data and fossils from the Hirnantian Stage in Bohemia and Spain: implications for correlation and paleoclimate. In *Ordovician of the World* (eds J. C. Gutiérrez-Marco, I. Rábano & D. García-Bellido), pp. 371-378. Cuadernos del Museo Geominero 14, Instituto Geológico y Minero de España, Madrid.

MU, E.-Z. 1945. Graptolite faunas from the Wufeng Shale. *Bulletin of the Geological Society of China* **25**, 201-209.

MU, E.-Z. 1950. On the occurrence of *Pleurograptus* in China. *Novitates of the Palaeontological Society of China* ***7***, 1–4.

MU, E.-Z. 1963. On the complication of graptolite rhabdosome. *Acta Palaeontologica Sinica* **11**, 346-377. [in Chinese with English summary].

MU, E.-Z. & CHEN, X. 1962. *Graptolites of China.* Science Press, pp. 1-171. [in Chinese].

MU, E.-Z., LI, J.-J., GE, M.-Y., CHEN, X., LIN, Y.-K. & NI, Y.-N. 1993. Upper Ordovician graptolites of Central China Region. *Palaeontologia Sinica, New series B* **189**(29), 1-393. [In Chinese with English Summary]

MU, E.-Z., LI, J.-J., GE, M.-Y., LIN, Y.-K. & NI Y.-N. 2002. *Graptolites of China.* Science Press, Beijing, 1205 pp. [in Chinese]

MU, E.-Z. & LIN, Y.-K. 1984. Graptolites from the Ordovician-Silurian boundary sections of the Yichang area. In *Stratigraphy and paleontology of systemic boundaries in China, Ordovician-Silurian boundary* (1) (ed. W. Hubei, Nanjing Institute of Geology and Palaeontology, Academia Sinica) pp. 45-82. Hefei: Anhui Science and Technological Publishing House.

MU, E.-Z. & NI, Y.-N. 1983. Uppermost Ordovician and lowermost Silurian graptolites from Xainza area of Xizang (Tibet) with a discussion on the Ordovician – Silurian boundary. *Paleontologia Cathayana* **1**, 155-179.

NANJING INSTITUTE OF GEOLOGY AND MINERAL RESOURCES 1983. *Palaeontological Atlas of East China. 1. Early Paleozoic.* Geological Publishing House, Beijing, 657 pp. [In Chinese].

NANJING INSTITUTE OF GEOLOGY AND PALAEONTOLOGY 1974. *A handbook of stratigraphy and palaeontology of south-west China*. Science Press, Beijing, 454 pp. [In Chinese]

NICHOLSON, H. A. 1867. On a new genus of graptolites. *Geological Magazine* **4**, 256-263.

NICHOLSON, H. A. 1868. On the graptolites of the Coniston Flags, with notes on the British species of the genus Graptolites. *Quarterly Journal of the Geological Society of London* **24**, 521-545.

NICHOLSON, H. A. 1869. On some new species of graptolites. *Annals and Magazine of Natural History* **4**(4), 231-242.

NORFORD, B. S. 1997. Ordovician and Silurian. In *Geology and mineral and hydrocarbon potential of northern Yukon Territory and northwestern District of Mackenzie* (ed. D. K. Norris), pp. 21–61. Bulletin 422, Geological Survey of Canada.

NORRIS, D. K. 1997. Geological setting. In *Geology and mineral and hydrocarbon potential of northern Yukon Territory and northwestern District of Mackenzie* (ed. D. K. Norris), pp. 119–162. Bulletin 422, Geological Survey of Canada.

OBUT, A. M. 1955. *Klass Graptolithina - Graptolity.* Polevoy Atlas Ordovician and Silurian Fauna of the Siberian Platform. Gosgeoltechizdat, Moscow, 136-139.

OBUT, A. M. & SENNIKOV, N. V. 1985. Osobennosti llandoveriyskikh planktonovykh soobschestv Sibirskoy platformy, 51-60. In Sreda i zhizn' v geologicheskom proshlom (Paleobasseyny i ich obivateli) (eds O. A. Betekhtina & I. T. Zhuravleva). Trudy Instituta geologii i geofyziki **628**, 137 pp. [in Russian]

OBUT, A. M., SOBOLEVSKAYA, R. F. & NIKOLAEV, A. N. 1967. *Graptolites and stratigraphy of Lower Silurian parts of the uplifted Kolyma Massif.* Nauka Akademiya Nauk SSSR, Sibirskoe Otdelenie, Institut Geologii i Geofiziki, Nauka, Moskva, 162 pp. [In Russian].

OSADETZ, K. G., ZHUOHENG, C., & BIRD, T. D. 2005. *Petroleum Resource Assessment, Eagle Plain Basin and Environs, Yukon Territory, Canada, Yukon.* Geological Survey Open File 2005-2, Geological Survey of Canada, Open File 4922, 88 p.

PANNELL, C. L., CLARKSON, E. N. K. & ZALASIEWICZ, J. 2006. Fine-scale biostratigraphy within the *Stimulograptus sedgwickii* Zone (Silurian: Llandovery) at Dob's Linn, Southern Uplands. *Scottish Journal of Geology* **42**(1), 59.

PERNER, J. 1895. *Études sur les Graptolites de Bohême. Illième Partie. Monographie des Graptolites de l`Étage D*. Raimond Gerhard, Prague, 31 pp.

PHLEGER, F. B. 1960. *Ecology and Distribution of Recent Foraminifera*, Johns Hopkins Press, 320p.

PŘIBYL, A. 1947. Classification of the genus *Climacograptus* Hall 1865. *Bulletin Internationale de l'Académie tchèque des Sciences* **48**(2), 17-29.

PŘIBYL, A. 1949. Revision of the Diplograptidae and Glossograptidae of the Ordovician of Bohemia. *Bulletin Internationale de l`Acadėmie Tchèque des Sciences*, **50**, 1-51.

PYLE, L.J. & BARNES, C. R. 2001. Conodonts from the Kechika Formation and Road River Group (Lower to Upper Ordovician) of the Cassiar Terrane, northern British Columbia. *Canadian Journal of Earth Sciences* **38**(10), 1387–1401.

RICKARDS, R. B. 1970. The Llandovery (Silurian) graptolites of the Howgill Fells, Northern England. *Palaeontographical Society Monographs*, 1-108.

RICKARDS, R. B. 1974. A new monograptid genus and the origins of the main monograptid genera. *In*: R.B. Rickards, D.E. Jackson, and C.P. Hughes (eds.), Graptolite Studies in honour of O.M.B.Bulman. *Special Papers in Palaeontology* **13**, 141-147.

RICKARDS, R. B., RIGBY, S., SWALES, C., & RICKARDS, J. 1998. Fluid dynamics of the graptolite rhabdosome recorded by laser Doppler anemometry. *Palaeontology* **41**, 737–752.

RICKARDS, R. B. & WRIGHT, A. J. 2002. Lazarus taxa, refugia and relict faunas: Evidence from graptolites. *Journal of the Geological Society* **159**(1), 1–4.

RIGBY, S. & RICKARDS, R. B. 1989. New evidence for the life habitats of graptolites from physical modeling. *Paleobiology* **41**, 737-752.

RIVA, J. 1974. Late Ordovician spinose climacograptids from the Pacific and Atlantic faunal provinces. In *Graptolite Studies in honour of O.M.B.Bulman* (eds R. B. Rickards, D. E. Jackson, C. P. Hughes). *Special Papers in Palaeontology* **13**, 107-126.

RIVA, J. 1988. Graptolites at and below the Ordovician-Silurian boundary on Anticosti Island, Canada. *Bulletin of the British Museum (Natural History) Geology* **43**, 221–237.

ROHRSSEN, M., LOVE, G. D., FISCHER, W., FINNEGAN, S. FIKE. D. A. 2013. Lipid biomarkers record fundamental changes in the microbial community structure of tropical seas during the Late Ordovician Hirnantian glaciation. *Geology* **41**(2), 127-130.

ROBINSON, D. 2012. Application of geometric morphometrics to late Katian and early Hirnantian-aged climacograptid populations: An investigation of graptoloid shape evolution at the end-Ordovician mass extinction. MS thesis, University at Buffalo, SUNY, 90 pp.

RONG, J., MELCHIN, M., WILLIAMS, S. H., KOREN, T. N. & VERNIERS, J. 2008. Report of the restudy of the defined global stratotype of the base of the Silurian System. *Episodes* **31**(3), 315–318.

ROSS, R. B. & BERRY, W. B. N. 1963. Ordovician graptolites of the Basin Ranges in California, Nevada, Utah and Idaho. *United States Geological Survey, Bulletin* **1134**, 1-177.

RUEDEMANNN, R. 1908. Graptolites of New York, Part 2. Graptolites of higher beds. *Memoirs of the New York State Museum of Natural History, Albany* **11**, 457-583.

RUEDEMANNN, R. 1947. Graptolites of North America. *Geological Society of America Memoir* **19**, 1-652.

RUSSEL, J. C., MELCHIN, M. J. & KOREN, T. N. 2000. Development, taxonomy, and phylogenetic relationships of species of *Paraclimacograptus* (Graptoloidea) from the Canadian Arctic and the Southern Urals of Russia. *Journal of Paleontology* **74**(1), 84–91.

SCHAUER M., 1971. Biostratigraphie und taxionomie der Graptolithen des tieferen Silurs unter besonderer Berucksichtigung der tektonischen Deformation. *Freiberger Forschungshefte C273 Palaeontologie*, 1-94.

SENIOR, S. J. H. 1993. Uncompressed Late Ordovician graptolites from the Cape Phillips Formation of Cornwallis and Truro islands, arctic Canada. MSc Thesis, University of Waterloo. *Unpublished thesis.*

SHEEHAN, P.M. 1973. The relation of Late Ordovician glaciation to the Ordovician-Silurian changeover in North American brachiopod faunas. *Lethaia* **6**(2), 147–154.

SHEEHAN, P.M. 2001. The Late Ordovician Mass Extinction. *Annual Review of Earth and Planetary Sciences* **29**(1), 331–364.

SHEETS, H. D., BELSCHER, K., FINNEY, S. C., HOLMDEN. C., LaPORTE, D. F., MELCHIN, M. J. & PATTERSON, W. P. 2007. Species abundance changes during mass extinction and the inverse Signor-Lipps effect: Apparently abrupt graptolite mass extinction as an artifact of sampling. In *Proceedings of the 10th International Symposium on the Ordovician System, Nanjing China, June 2007* (eds. J. Li, J.-X. FAN, & I. PERCIVAL), pp. 340-346. *Acta Palaeontologica Sinica* **46** (Supplement).

SHEETS, H. D., MITCHELL, C. E., MELCHIN, M. J., LOXTON, J., ŠTORCH, P., CARLUCCI, K. L. & HAWKINS, A. D. 2016. Graptolite community responses to global climate change and the Late Ordovician mass extinction. *Proceedings of the National Academy of Sciences* ***113***(30), 8380–8385.

SOBOLEVSKAYA, R. F. 1974. New Ashgill graptolites in the middle flow basin of the Kolyma River. 63-71. *In Graptolites of the USSR* (ed. A. M. Obut). Nauka, Siberian Branch, Novosibirsk, 160 pp. [In Russian].

STEWART, S. & MITCHELL, C. E. 1997. *Anticostia*, a distinctive new Late Ordovician "glyptograptid" (Diplograptacea, Graptoloidea) based on three-dimensionally preserved specimens from Anticosti Island, Quebec. *Canadian Journal of Earth Sciences* **34**, 215-228.

ŠTORCH, P. 1983. The genus *Diplograptus* (Graptolithina) from the lower Silurian of Bohemia. Vestnik Ustredniho ustravu geologickeho **58**(3), 159-170.

ŠTORCH, P. 1985. *Orthograptus* s.l. and *Cystograptus* (Graptolithina) from the Bohemian lower Silurian. *Vestnik Ustredniho ustravu geologickeho* **60**(2), 87-100.

ŠTORCH, P. 1996. The basal Silurian *Akidograptus ascensus-Parakidograptus acuminatus* Biozone in peri-Gondwanan Europe: graptolite assemblages, stratigraphical ranges and palaeobiogeography. Vestnik Ceskeho geologickeho Ustavu **71**, 177-188.

ŠTORCH, P. 2015. Graptolites from the Rhuddanian-Aeronian boundary interval (Silurian), Prague Synform, Czech Republic. *Bulletin of Geosciences* **90**(4), 841–891.

ŠTORCH, P. & FEIST, R. 2008. Lowermost Silurian graptolites of Montagne Noire, France. *Journal of Paleontology* **82**(5), 938–956.

ŠTORCH, P., & LOYDELL, D. K. 1996. The Hirnantian graptolites *Normalograptus persculptus* and *'Glyptograptus' bohemicus*: stratigraphical consequences of their synonymy. *Palaeontology*, **39**(4), 869–881.

ŠTORCH, P. & MASSA, D. 2006. Middle Llandovery (Aeronian) graptolites of the Western Murzuq Basin and Al Qarqaf Arch region, South-West Libya. *Palaeontology* **49**(1), 83–112.

ŠTORCH, P., MITCHELL, C. E., FINNEY, S. C. & MELCHIN, M. J. 2011. Uppermost Ordovician (upper Katian-Hirnantian) graptolites of north-central Nevada, U.S.A. *Bulletin of Geosciences* **86**(2), 301–386.

ŠTORCH, P. & SCHÖNLAUB, H.-P. 2012. Ordovician-Silurian boundary graptolites of the Southern Alps, Austria. *Bulletin of Geosciences* **87**(4), 755–766.

ŠTORCH, P. & SERPAGLI, E. 1993. Lower Silurian Graptolites from Southwestern Sardinia. *Bollettino della Societa Paleontologica Italica* **32**(1), 3-57.

STRATIGRAPHY RESEARCH GROUP OF THE YANGZE GORGES, HUBEI BUREAU OF GEOLOGY 1978. *Sinian to Permian Stratigraphy and Paleontology of eastern Yangtze Gorges*. Geological Publishing House, Beijing, 381 pp. (In Chinese).

SUN, Y. C. 1933. Ordovician and Silurian graptolites from China. *Palaeontographica Sinica* B(14): 1-52. [in English].

TANG L., & CHEN X. 2014. Late Katian *Paraorthograptus pacificus* graptolite Biozone from Xing'an, northern Guangxi, China. *GFF,* **136**(1), 259-261.

TOGHILL, P. 1970. Highest Ordovician (Hartfell Shales) graptolite faunas from the Moffat area, south Scotland. *Bulletin of the British Museum (Natural History), Geology*, **19**(1), 1-26.

TÖRNQUIST, S. L. 1897. On the Diplograptidae and the Heteroprionidae of the Scanian Rastrites beds. *Acta Regiae Societatis Physiographicae Lundensis* **8**: 1-22.

UNDERWOOD, C. J., CROWLEY, S. F., MARSHALL, J. D. & BRENCHLEY, P. J. 1997. High-resolution carbon isotope stratigraphy of the basal Silurian Stratotype (Dob's Linn, Scotland) and its global correlation. *Journal of the Geological Society* **154**(4), 709–718.

UNDERWOOD, C. J., DEYNOUX, M. & GHIENNE, J.-F. 1998. HIGH palaeolatitude (Hodh, Mauritania) recovery of graptolite faunas after the Hirnantian (end Ordovician) extinction event. *Palaeogeography, Palaeoclimatology, Palaeoecology* **142**(3), 91–105.

VANDENBROUCKE, T. R. A., ARMSTRONG, H. A., WILLIAMS, M., ZALASIEWICZ, J. A. & SABBE, K. 2009. Ground-truthing Late Ordovician climate models using the paleobiogeography of graptolites. *Paleoceanography* **24**(4), PA4202.

WAERN, B. 1948. The Silurian strata of the Kullatorp Core. *Bulletin of Geological Institute of Upsala* **32**, 433-474.

WANG, W., MUIR, L. A., CHEN, X. & TANG, P. 2015. Earliest Silurian graptolites from Kalpin, western Tarim, Xinjiang, China. *Bulletin of Geosciences* **90**(3), 519–542.

WANG X.-F., JIN Y.-Q. & WU, Z.-T. 1978. Graptolites of central South China. *In Handbook of Palaeontological Atlas of central South China, Part 1: Early Palaeozoic.* (ed. Hubei Institute of Geological Sciences), pp. 266-371. Geological Publishing House, Beijing. [In Chinese] 266-371.

WHITTINGTON, H. B. 1955. Additional new Ordovician graptolites and a chitinozoan from Oklahoma. *Journal of Paleontology* **29**(5), 837–851.

WIGNALL, P. B. & BENTON, M. J. 1999. Lazarus taxa and fossil abundance at times of biotic crisis. *Journal of the Geological Society* **156**(3), 453–456.

WILLIAMS, S. H. 1981. Form and mode of life of *Dicellograptus* (Graptolithina). *Geological Magazine* **118**(4), 401–408.

WILLIAMS, S. H. 1982. The late Ordovician graptolite fauna of the Anceps Bands at Dob's Linn, southern Scotland. *Geologica et Palaeontologica*, **16**, 29-56.

WILLIAMS, S. 1983. The Ordovician-Silurian boundary graptolite fauna of Dob's Linn, southern Scotland. *Palaeontology*, **26**, 3, 605–639.

YANG D.-Q. 1964. Latest Ordovician graptolites from Northwestern Zhejiang. *Acta Palaeontologica Sinica*, **22**(6), 597-605. [In Chinese, English abstract].

YE S.-H. 1978. Graptolithina. In *Palaeontological Atlas of Southwest China, Sichuan Volume, Part* 1, *From Sinian to Devonian,* 431-486 pp. Geological Publishing House, Beijing. 431-486. [In Chinese].

YIN, T.H. and MU, A.T. 1945. Lower Silurian Graptolites from Tungtzu. *Bulletin of the Geological Society of China* **25**, 211-220. (in English).

YU J.-H., FANG Y.-T., & ZHANG D.-L. 1988. Lungmachi Formation graptolites from Sanlangpu of Xixiang, southern Shaanxi. *Acta Palaeontologica Sinica*, **27**(2), 150-163.

ZALASIEWICZ, J.A., TAYLOR, L., RUSHTON, A.W.A., LOYDELL, D.K., RICKARDS, R.B. & WILLIAMS, M. 2009. Graptolites in British stratigraphy. *Geological Magazine* **146**(6), 785–850

Plates

Note: Scale bar in all figures = 1 mm

Plate 1

All figures x6

Fig.	Species	Level (m)	Slab	#
1	*Appendispinograptus supernus* (Elles & Wood)	1.30	002a	3
2	*Appendi. pogrebovi* (Koren' & Sobolevskaya)	19.00		1
3	*Appendi. pogrebovi* (Koren' & Sobolevskaya)	19.00	23	3
4	*Appendi. pogrebovi* (Koren' & Sobolevskaya)	19.00	013a-1	1
5	*Appendi. pogrebovi* (Koren' & Sobolevskaya)	19.00	010a	4
6	*Appendi. pogrebovi* (Koren' & Sobolevskaya)	19.00	010a	3
7	*Appendi. pogrebovi* (Koren' & Sobolevskaya)	19.00	010a	1
8	*Appendi. pogrebovi* (Koren' & Sobolevskaya)	19.00	29	1
9	*Appendispinograptus supernus* (Elles & Wood)	1.30	001ax	1
10	*Appendi. pogrebovi* (Koren' & Sobolevskaya)	19.00		
11	*Appendispinograptus supernus* (Elles & Wood)	1.30	001ax	2
12	*Appendispinograptus supernus* (Elles & Wood)	1.30	103a	
13	*Appendispinograptus leptothecalis* (Mu & Ge)	19.05	021b	3
14	*Appendispinograptus leptothecalis* (Mu & Ge)	18.05	12b-1	
15	*Appendispinograptus leptothecalis* (Mu & Ge)	17.20	001bx	
16	*Appendispinograptus leptothecalis* (Mu & Ge)	18.94	12a	
17	*Appendispinograptus leptothecalis* (Mu & Ge)	17.20	26	
18	*Appendispinograptus leptothecalis* (Mu & Ge)	18.05 (06)		

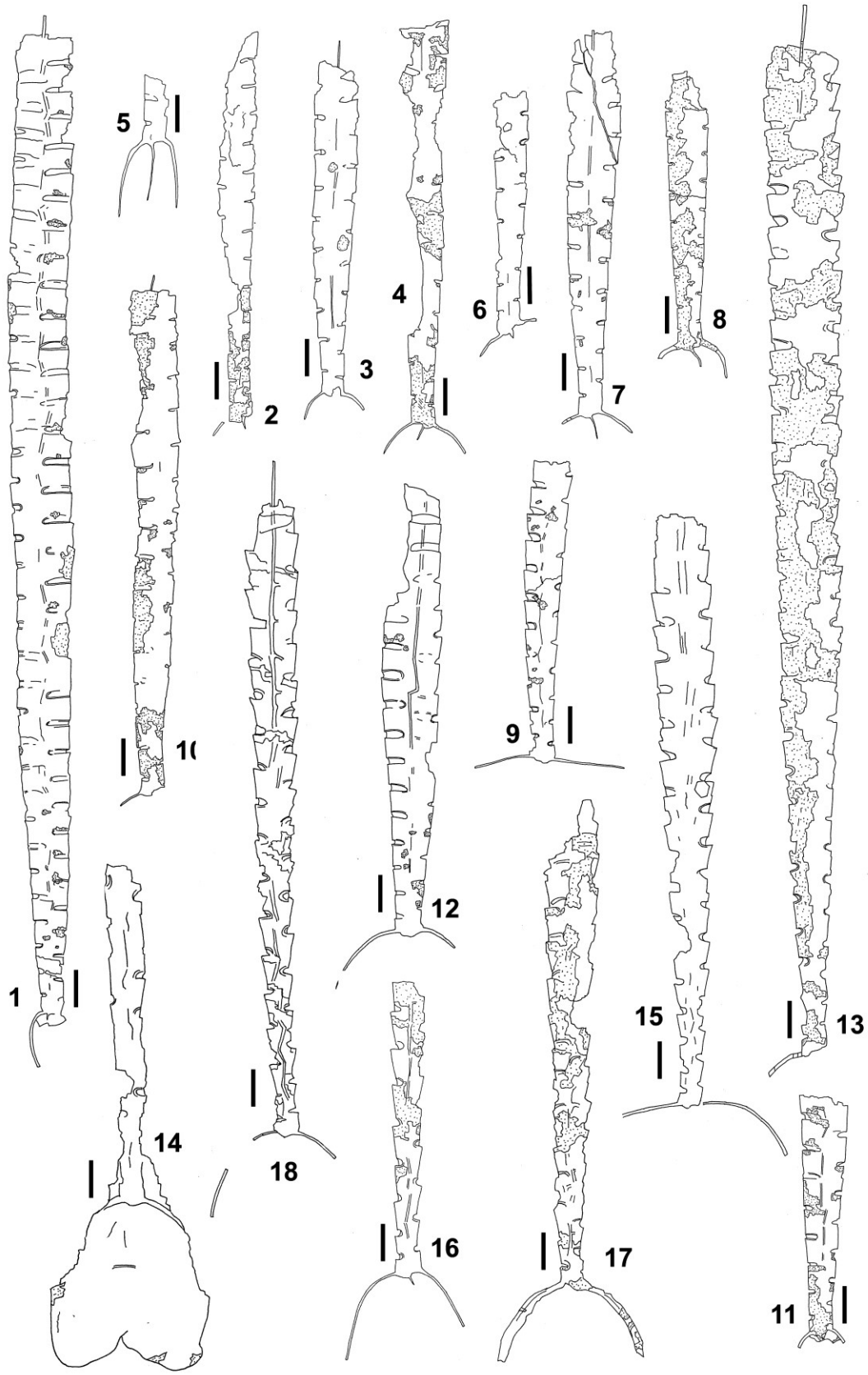
1
2
3
4
5
6
7
8
9
10
11
12
13
14
15
16
17
18

Plate 2

All figures x6

Fig.	Species	Level (m)	Slab	#
1	*Anticostia macgregorae* Stewart & Mitchell	15.65	31	A
2	*Anticostia uniformis* (Mu & Lin)	19.00	29	2
3	*Anticostia uniformis* (Mu & Lin)	16.03	002b-2	1
4	*Anticostia uniformis* (Mu & Lin)	19.00	010a	1
5	*Anticostia uniformis* (Mu & Lin)	16.03	016bx	1
6	*Anticostia uniformis* (Mu & Lin)	19.00	3	1
7	*Anticostia uniformis* (Mu & Lin)	19.00	028b	1
8	*Anticostia uniformis* (Mu & Lin)	19.00	8	1
9	*Paraorthograptus pacificus* (Ruedemannn)	19.00	12b	
10	*Paraorthograptus kimi* Koren’	1.30	28	
11	*Paraorthograptus kimi* Koren’	1.30	37	
12	*Rectograptus abbreviatus* (Elles & Wood)	12.67	33	
13	*Rectograptus abbreviatus* (Elles & Wood)	0.10	15ax	
14	*Rectograptus abbreviatus* (Elles & Wood)	17.20	007bx	1
15	*Anticostia lata* (Elles & Wood)	16.03	010b	
16	*Paraorthograptus pacificus* (Ruedemann)	1.30	001c	1
17	*Diplograptus rarithecatus* (Ross & Berry)	15.65	17	1
18	*Paraorthograptus affinis* Koren’ & Tzaj	19.15	014a	1
19	*Paraorthograptus affinis* Holotype[1]			

[1]Reproduced from Apollonov et al., 1980, text-fig. 32.

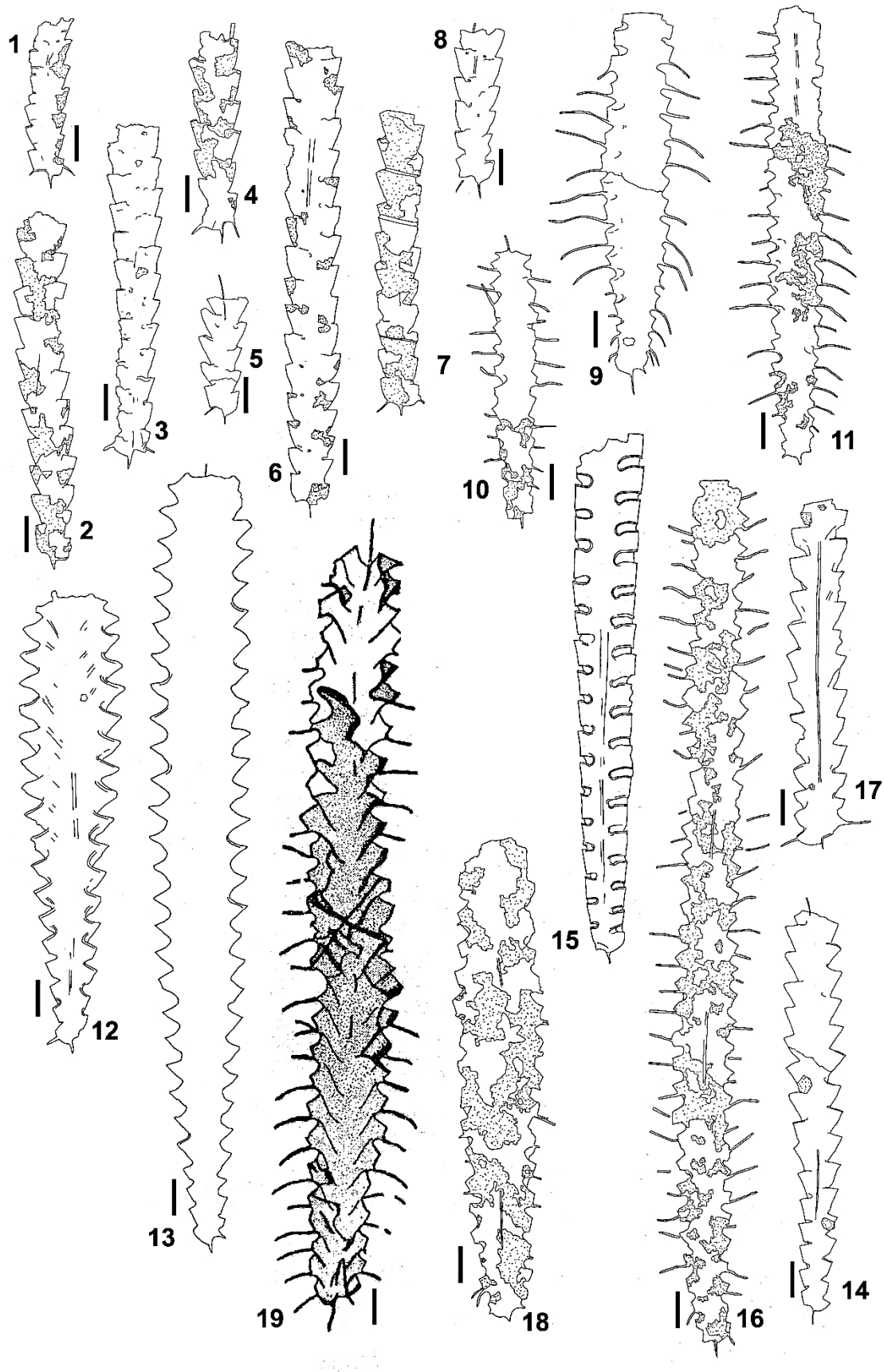
1
2
3
4
5
6
7
8
9
10
11
12
13
14
15
16
17
18
19

Plate 3

All figures x6

Fig.	Species	Level (m)	Slab	#
1	*Styracograptus mississippiensis* (Ruedemannn)	0.10	006bx (inside)	1
2	*Styracograptus mississippiensis* (Ruedemannn)	17.20	21-.1	
3	*Styracograptus mississippiensis* (Ruedemannn)	18.05	001a	
4	*Styracograptus mississippiensis* (Ruedemannn)	0.10	001b	1
5	*Styracograptus mississippiensis* (Ruedemannn)	12.67	33	
6	*Styracograptus tatianae* (Keller)	19.00	012a	
7	*Styracograptus tatianae* (Keller)	0.10	004ax	1
8	*Styracograptus tatianae* (Keller)	0.10	2	
9	*Styracograptus tatianae* (Keller)	0.10	020b	
10	*Climacograptus hastatus* Hall	18.05	008a	1
11	*Styracograptus* sp.	18.05	023-1	
12	*Climacograptus hastatus* Hall	0.10	17	
13	*Styracograptus mississippiensis* (Ruedemannn)	0.10	16x	2
14	*Styracograptus mississippiensis* (Ruedemannn)	17.20	004b_2	
15	*Appendispinograptus supernus* (Elles & Wood)	0.10	006a	
16	*Styracograptus mississippiensis* (Ruedemannn)	17.20	003a	

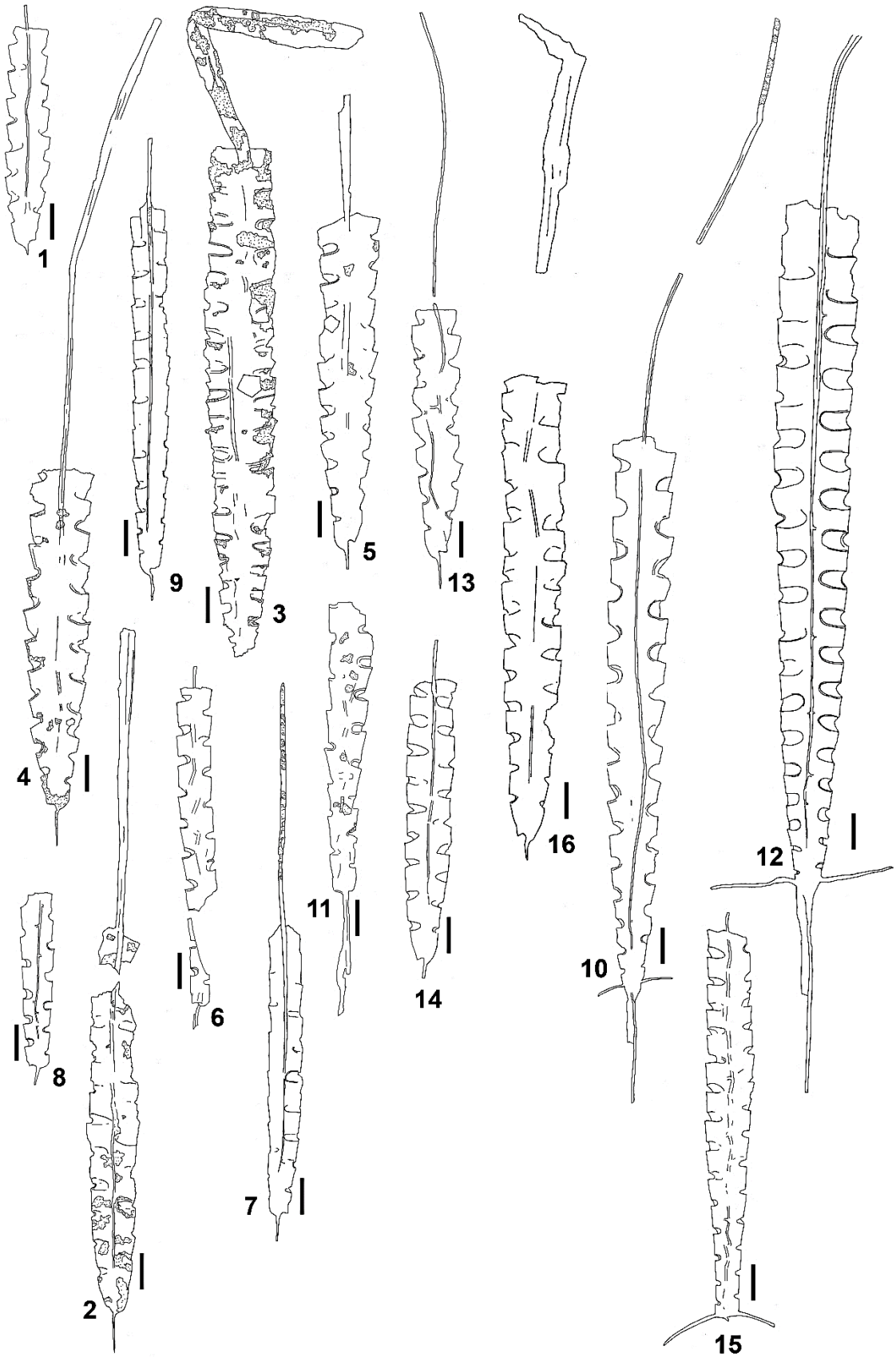
1
2
3
4
5
6
7
8
9
10
11
12
13
14
15
16

Plate 4

All figures x6

Fig.	Species	Level (m)	Slab	#
1	*Neodiplograptus charis* (Mu & Ni)	19.20	046b	1
2	*Neodiplograptus charis* (Mu & Ni)	19.20	020a	1
3	*Metabolograptus extraordinarius* (Sobolevskaya)	19.15	009b	1
4	*Neodiplograptus charis* (Mu & Ni)	19.20	020a	2
5	*Meta. ojsuensis*? (Koren' & Mikhaylova)	19.20 (06)	050a	
6	*Metabolograptus ojsuensis* (Koren' & Mikhaylova)	19.20	020b	
7	*Metabolograptus extraordinarius* (Sobolevskaya)	19.20	OWL	1
8	*Metabolograptus extraordinarius* (Sobolevskaya)	19.15	009b	1

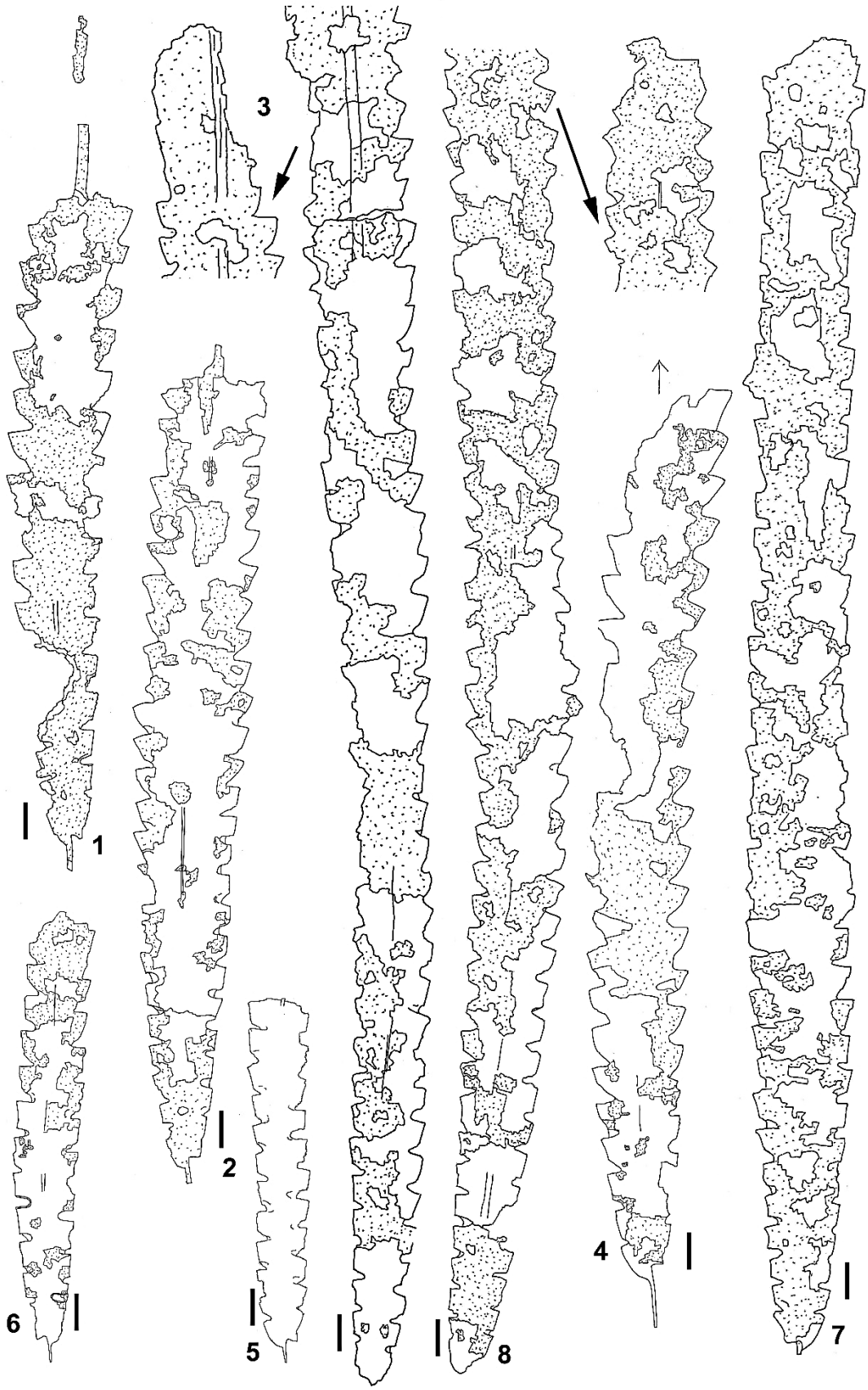
1
2
3
4
5
6
7
8

Plate 5

All figures x6

Fig.	Species	Level (m)	Slab	#
1	*Dicellograptus turgidus* Mu	8.80	004ax	
2	*Dicellograptus turgidus* Mu	12.67	unlabeled	
3	*Dicellograptus* aff. *mirabilis* Mu & Chen	17.20	15	
4	*Dicellograptus tenuiculus* Mu et al.	14.15	009c	pink/1
5	*Dicellograptus tenuiculus* Mu et al.	16.03	011a/white	
6	*Dicellograptus* cf. *ornatus* Elles & Wood	8.80	5000	
7	*Dicellograptus* aff. *mirabilis* Mu & Chen	18.05	22	
8	*Dicellograptus* cf. *ornatus* Elles & Wood	8.80	010b	
9	*Dicellograptus tenuiculus* Mu et al.	16.03	011a/green	
10	*Dicellograptus tenuiculus* Mu et al.	14.15	009c/blue	
11	*Dicellograptus* aff. *mirabilis* Mu & Chen	18.05 (06)	OWL9	

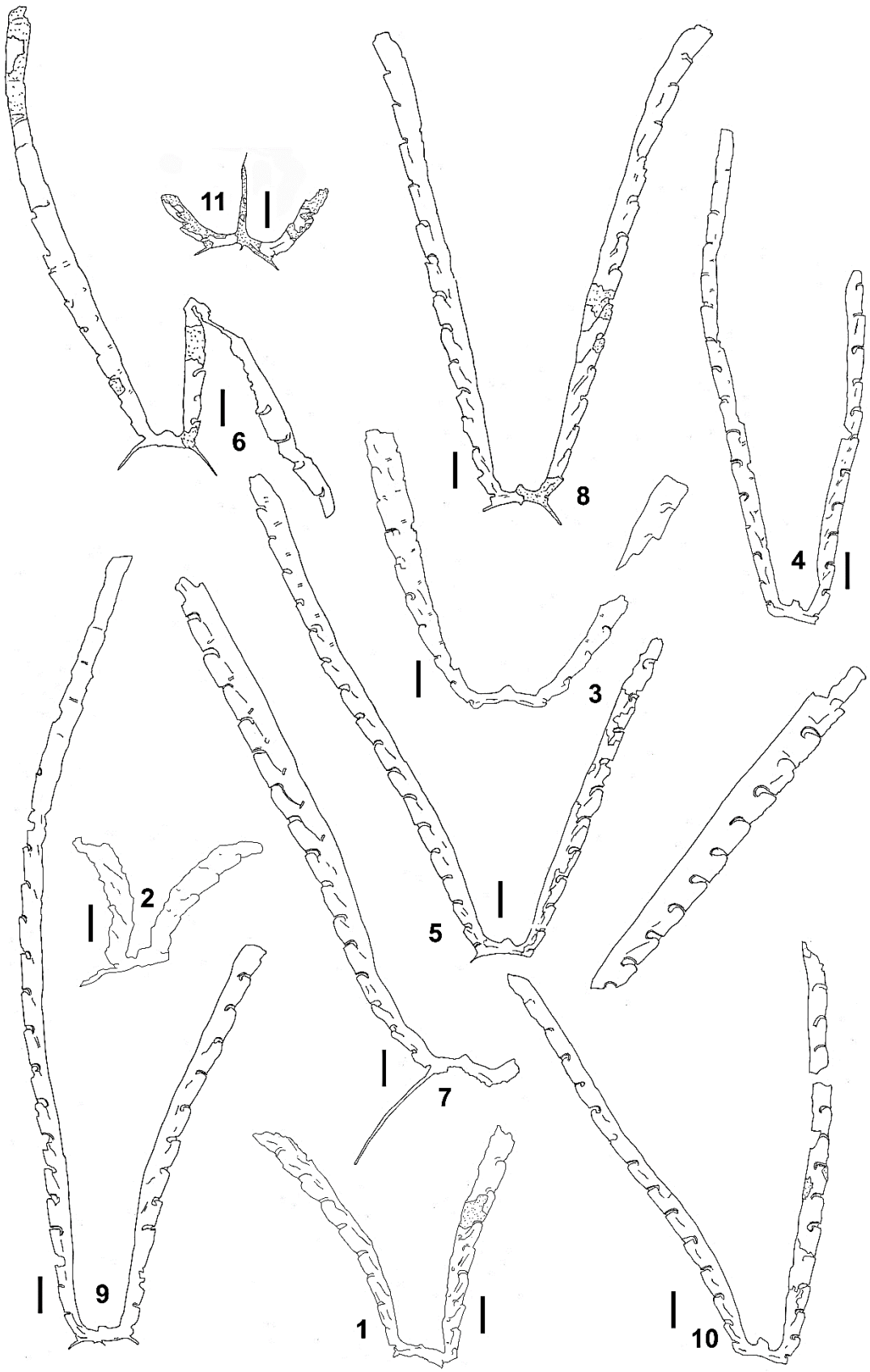
11
6
8
4
3
2
5
9
7
1
10

Plate 6

All figures x6

Fig.	Species	Level (m)	Slab	#
1	*Dicellograptus ornatus* Elles & Wood	ca. 5.50	"Big Euryp."	
2	*Dicellograptus ornatus* Elles & Wood	0.10	2	1
3	*Dicellograptus ornatus* Elles & Wood	12.67	001a	
4	*Dicellograptus* cf. *ornatus* Elles & Wood	8.80	1000	
5	*Dicellograptus* cf. *mirabilis* Mu & Chen	16.03	016a	id.
6	*Diceratograptus mirus* Mu	15.65		41
7	*Diceratograptus mirus* Mu	19.00	22a	
8	*Diceratograptus mirus* Mu	16.03	12	
9	*Diceratograptus mirus* Mu	18.94	019a	
10	*Diceratograptus mirus* Mu	16.03	11cx	1
11	*Diceratograptus mirus* Mu	18.05	001bx2	
12	*Dicellograptus* cf. *mirabilis* Mu & Chen	16.03	OWL7	1
13	*Dicellograptus* cf. *mirabilis* Mu & Chen	16.03	010a FRAG	6
14	*Dicellograptus* aff. *mirabilis* Mu & Chen	15.65	004b	

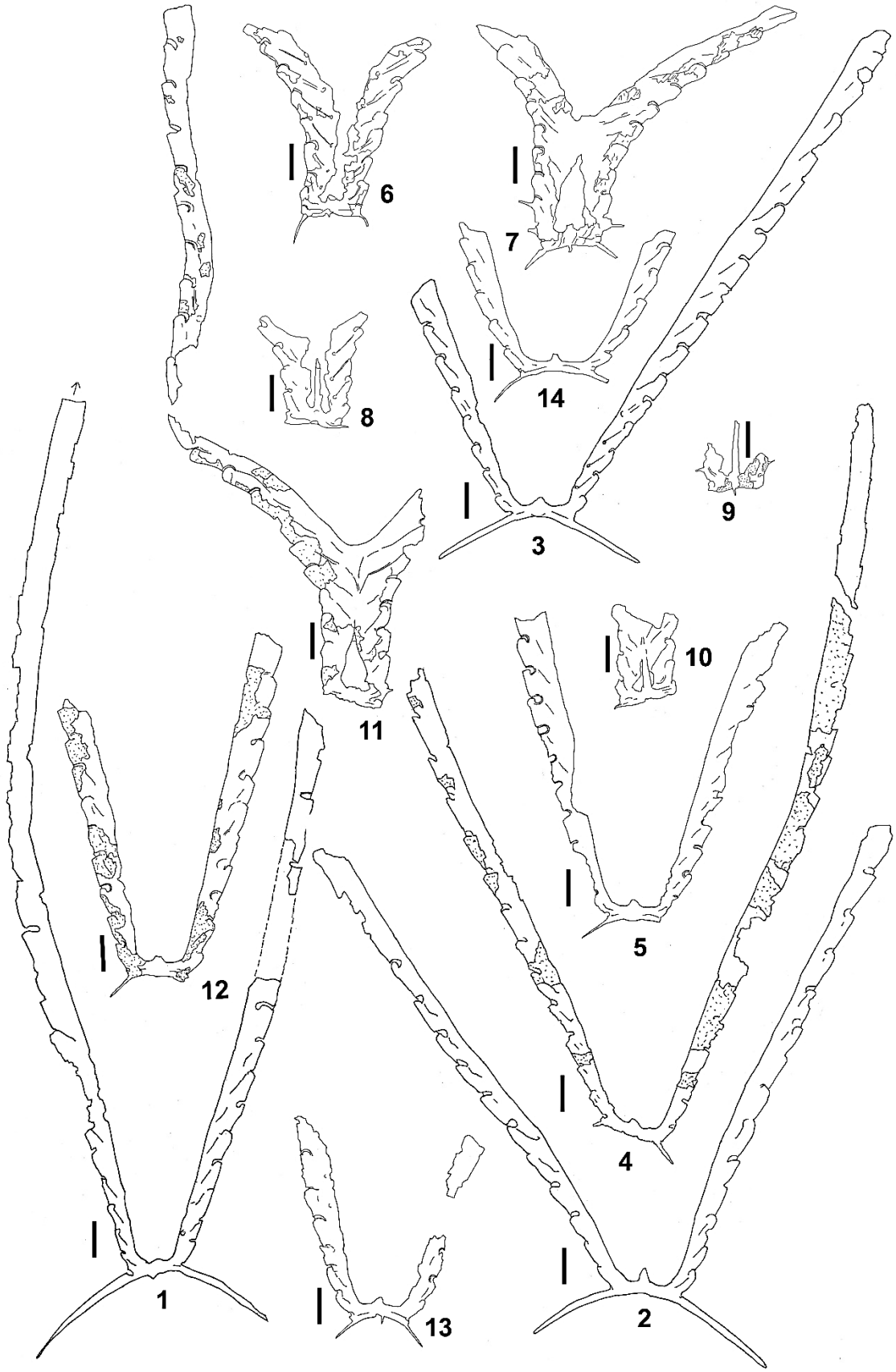
6
7
8
14
9
3
11
10
12
5
4
1
13
2

Plate 7

All figures x6

Fig.	Species	Level (m)	Slab	#
1	*Appendispinograptus leptothecalis* (Mu & Ge)	18.05	19	
2	*Appendispinograptus leptothecalis* (Mu & Ge)	18.05 (06)	1000	
3	*Appendispinograptus leptothecalis* (Mu & Ge)	18.05	26x	
4	*Diplograptus rarithecatus* (Ross & Berry)	16.03	012b	
5	*Diplograptus rarithecatus* (Ross & Berry)	16.03	011a	
6	*Diplograptus rarithecatus* (Ross & Berry)	15.65	007ax	
7	*Diplograptus rarithecatus* (Ross & Berry)	15.65	19	
8	*Diplograptus rarithecatus* (Ross & Berry)	15.65	011b	
9	*Appendispinograptus leptothecalis* (Mu & Ge)	17.20	010b_2	
10	*Metabolograptus extraordinarius* (Sobolevskaya)	19.25	112	1
11	*Neodiplograptus charis* (Mu & Ni)	19.20	36a	

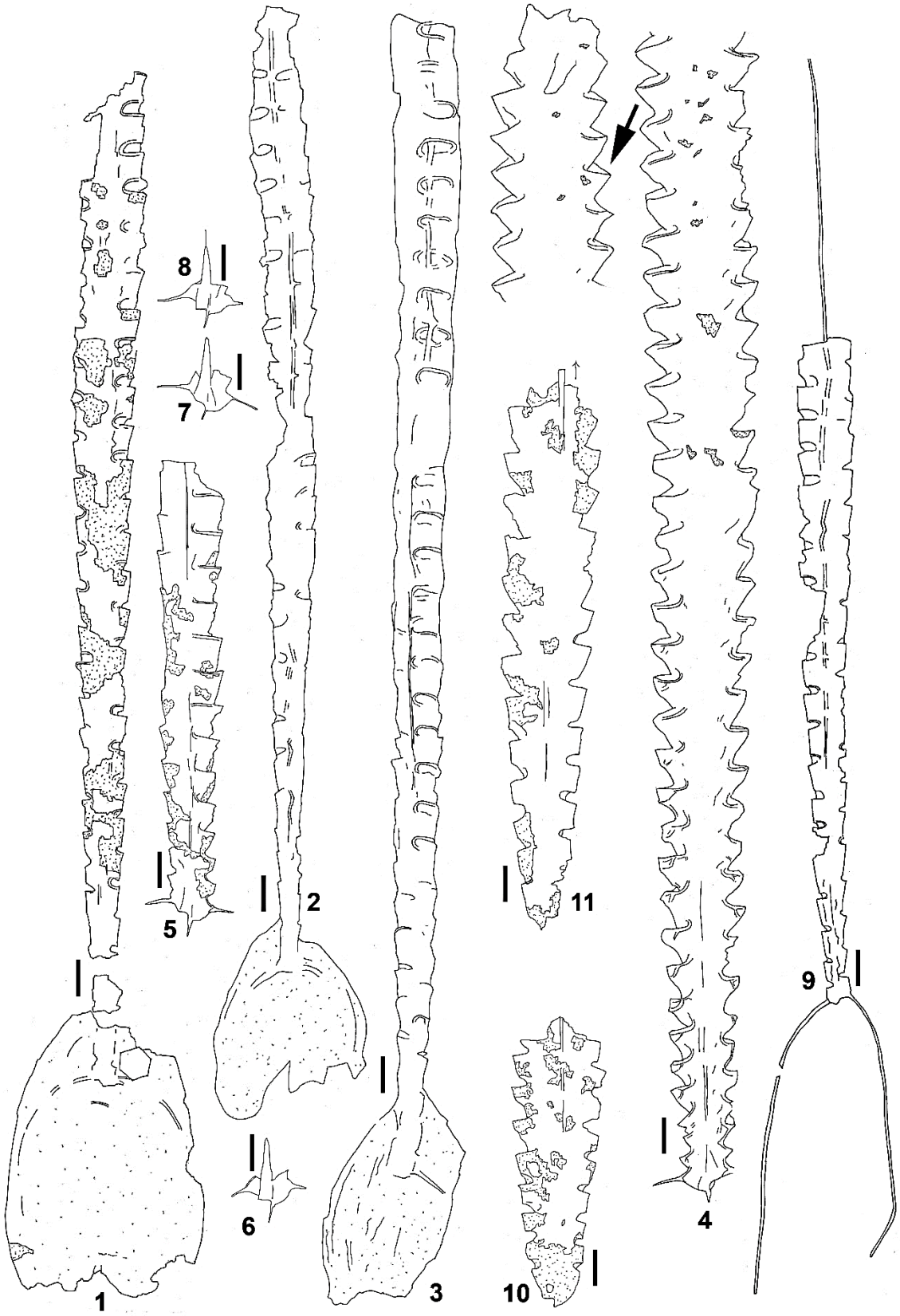
1
2
3
4
5
6
7
8
9
10
11

Plate 8

All figures x6

Fig.	Species	Level (m)	Slab	#
1	*Dicellograptus turgidus* Mu HOLOTYPE	NA	56764	
2	*Pleurograptus lui* Mu	16.03	002a	
3	*Dicellograptus* aff. *turgidus* Mu	Jeiling	138 CP	
4	*Dicellograptus minor* Toghill	16.03	16a	blue
5	*Dicellograptus minor* Toghill	12.67	12a	
6	*Dicellograptus minor* Toghill	17.20	23	
7	*Dicellograptus* aff. *turgidus* Mu	ca. 5.50	100	
8	*Dicellograptus* cf. *mirabilis* Mu & Chen	17.20	004b_2	1
9	*Pleurograptus lui* Mu	16.03	013b	
10	*Pleurograptus lui* Mu	16.03	015b	

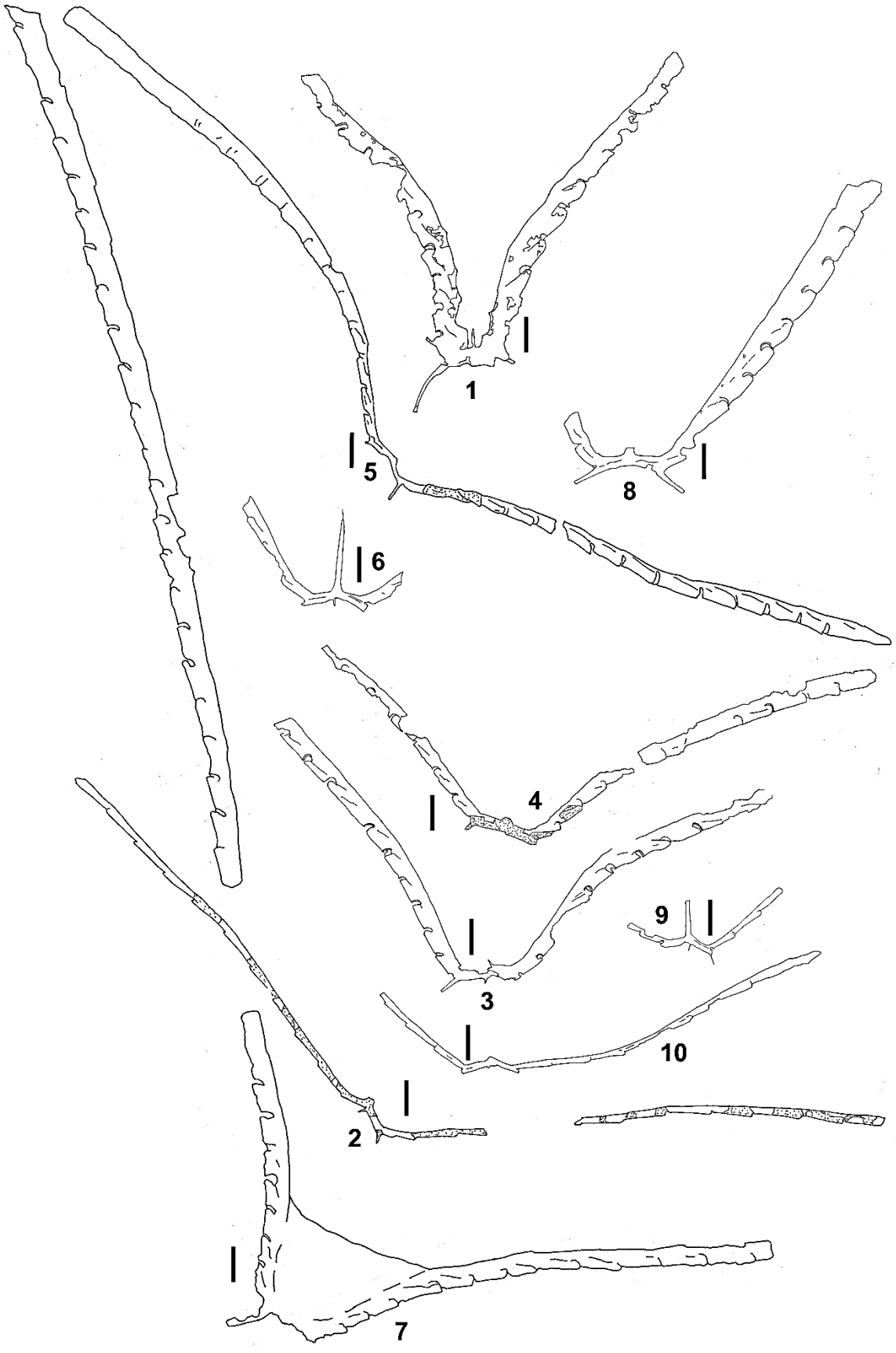
1
5
8
6
4
9
3
10
2
7

Plate 9

Figure 1-2x2; 3-7 x3; all other figures x6

Fig.	Species	Level (m)	Slab	#
1	*Dicellograptus* aff. *turgidus* Mu	ca. 5.50	200	
2	*Dicellograptus ornatus* Elles & Wood	ca. 5.50	200	
3	*Dicellograptus ornatus* Elles & Wood	5.50	001a	
4	*Dicellograptus ornatus* Elles & Wood	5.50	015a	
5	*Dicellograptus ornatus* Elles & Wood	5.50	015a	
6	*Dicellograptus ornatus* Elles & Wood	5.50	6	
7	*Dicellograptus ornatus* Elles & Wood	5.50	6	
8	*Dicellograptus* cf. *mirabilis* Mu & Chen	16.03	010a	1/blue
9	*Dicellograptus* aff. *mirabilis* Mu & Chen	18.05	003a	1
10	*Dicellograptus* aff. *mirabilis* Mu & Chen	16.03	006 (cp)	
11	*Dicellograptus* aff. *mirabilis* Mu & Chen	17.20	004b_3	3
12	*Dicellograptus tenuiculus* Mu et al.	16.03	013b-2	1
13	*Dicellograptus tenuiculus* Mu et al.	16.03	013b-2	2
14	*Dicellograptus tenuiculus* Mu et al.	16.03 m	013b-2	3
15	*Pleurograptus*? *grandis* (Mu & Chen)	14 bulk	1	

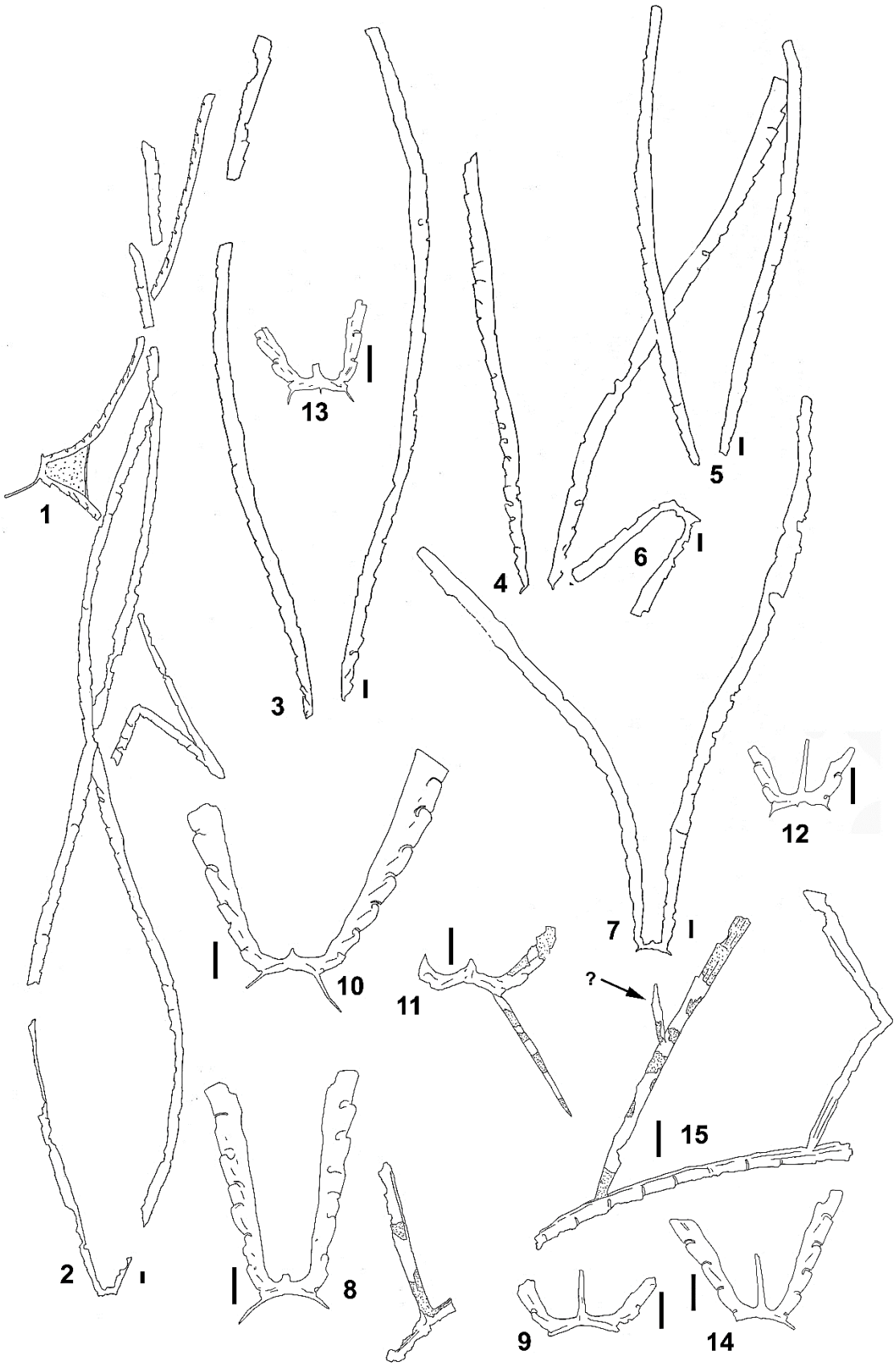
1
2
3
4
5
6
7
8
9
10
11
12
13
14
15
?

Plate 10

Figures 1, 5-6 x4, 4 x10; all other figures x6

Fig.	Species	Level	Slab	#
1	*Pleurograptus*? *grandis* (Mu & Chen)	14 bulk	1	
2	*Pleurograptus lui* Mu	16.03	012ax-1	1
3	*Pleurograptus lui* Mu	16.03	011d	2
4	*Pleurograptus lui* Mu	16.03	011d	1
5	*Pleurograptus*? *grandis* (Mu & Chen)	14 bulk	2	
6	*Pleurograptus*? *grandis* (Mu & Chen)	14 bulk	3	
7	*Pleurograptus*? *grandis* (Mu & Chen)	Jeiling	143_1	

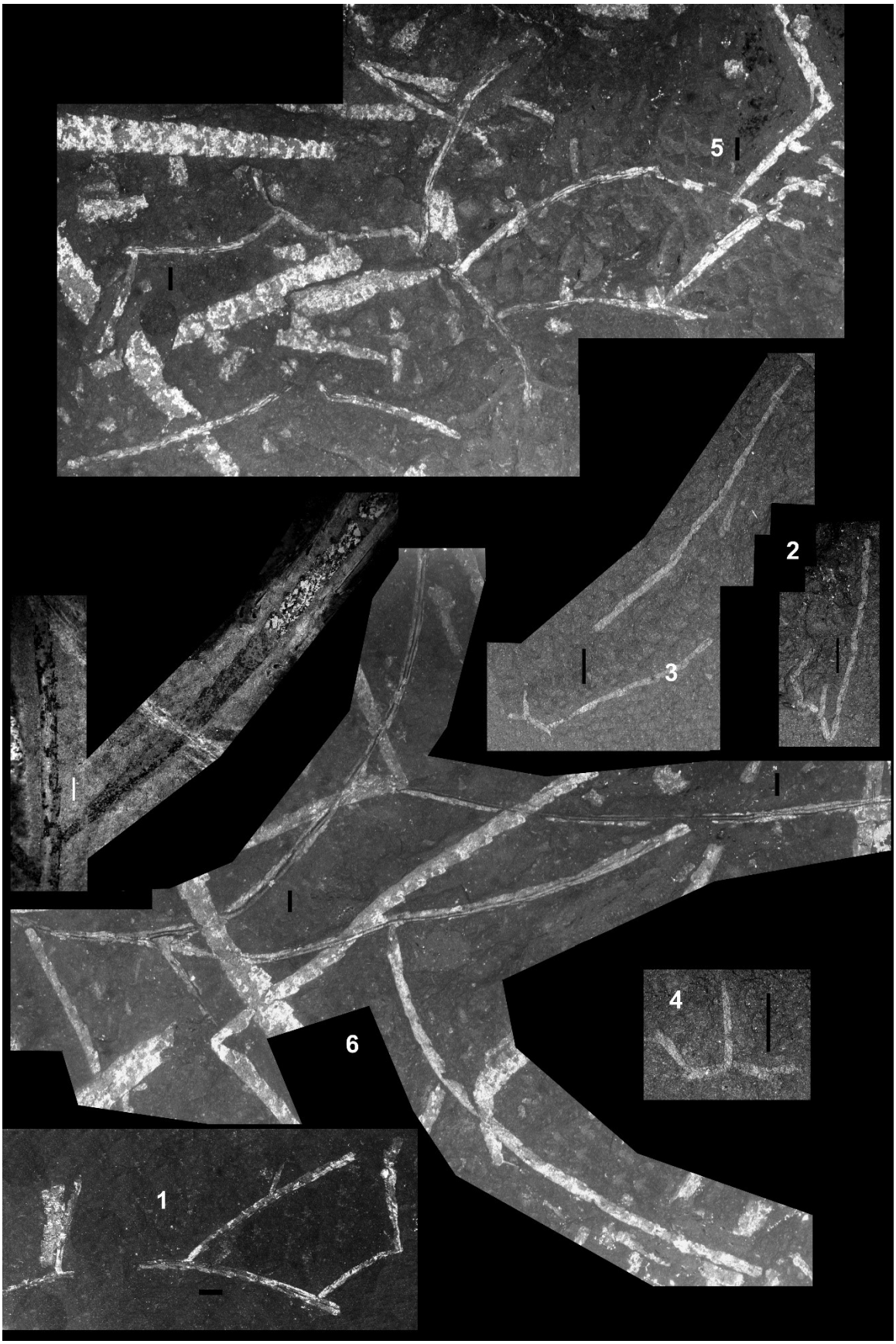
5
2
3
4
6
1

Plate 11

Figures 1, 13-14 x10; all other figures x6

Fig.	Species	Level	Slab	#
1	*Parareteograptus sinensis* Mu	1.30	17bx	
2	*Parareteograptus sinensis* Mu	0.10	14	
3	*Parareteograptus sinensis* Mu	0.10	11	
4	*Anticostia uniformis* (Mu & Lin)	19.00	027c	
5	*Anticostia uniformis* (Mu & Lin)	16.03	010a	
6	*Anticostia macgregorae* Stewart & Mitchell	15.65	004b	
7	*Anticostia uniformis* (Mu & Lin)	16.03	002b-2	
8	*Anticostia uniformis* (Mu & Lin)	15.65	031b	1
9	*Anticostia uniformis* (Mu & Lin)	16.03	011ax	2
10	*Appendispinograptus supernus* (Elles & Wood)	16.03	011ax	
11	*Anticostia uniformis* (Mu & Lin)	16.03	011ax	1
12	*Parareteograptus turgidus* Mu	14.15	005a[1]	
13	*Parareteograptus turgidus* Mu	14.15	005b[1]	
14	*Parareteograptus sinensis* Mu	1.30	31	
15	*Anticostia lata* (Elles & Wood)	14.15	018a	1
16	*Diplograptus rarithecatus* (Ross & Berry)	16.03	012bx	1
17	*Diplograptus rarithecatus* (Ross & Berry)	15.65	17	
18	*Paraorthograptus pacificus* (Ruedemann)	15.65	17	
19	*Diplograptus rarithecatus* (Ross & Berry)	15.65	17x	2
20	*Diplograptus rarithecatus* (Ross & Berry)	15.65	8	1
21	*Rectograptus abbreviatus (Elles & Wood)*	17.20 m	002a	1

[1]Part and counterpart

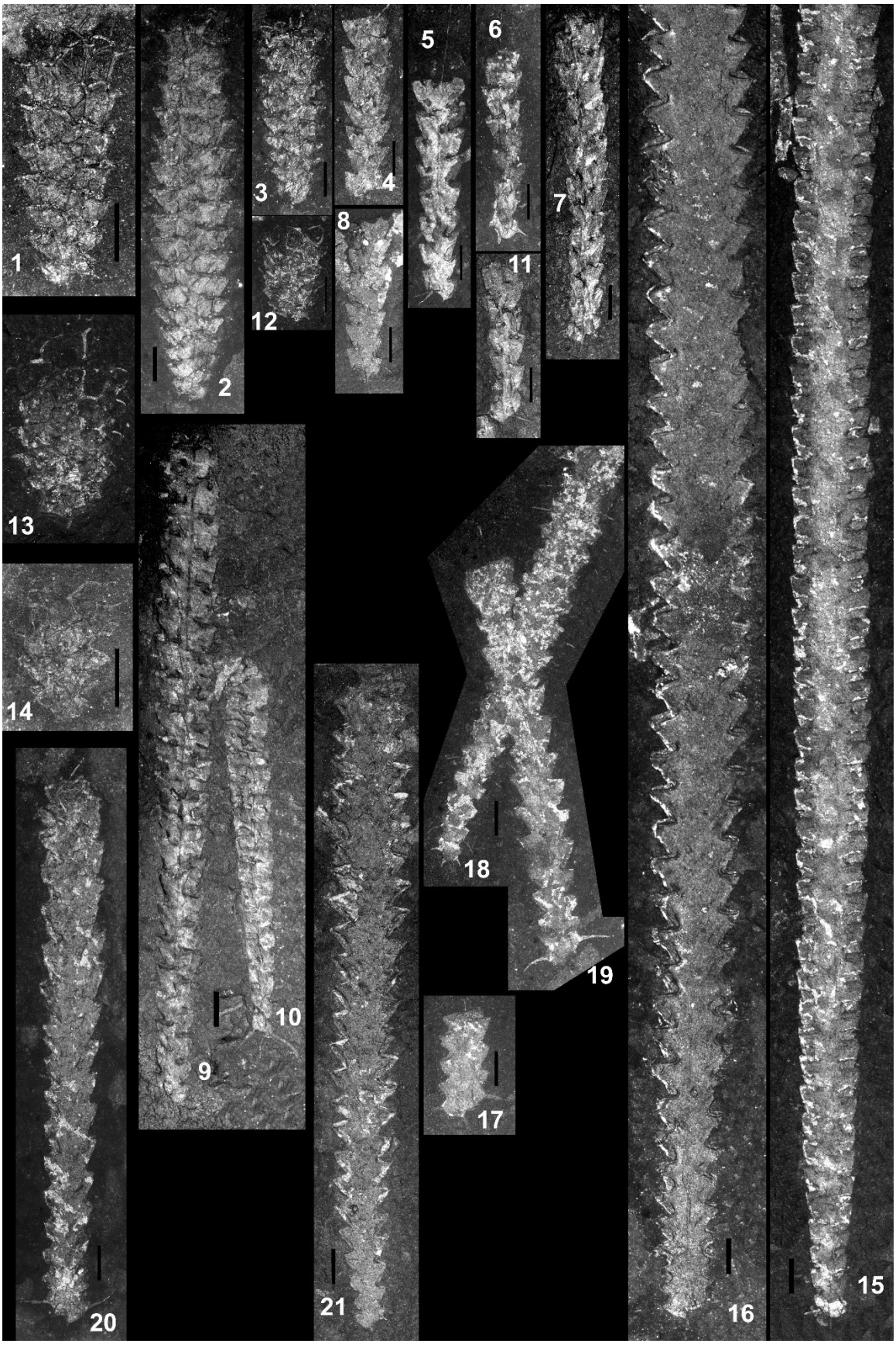
1
2
3
4
5
6
7
8
9
10
11
12
13
14
15
16
17
18
19
20
21

Plate 12

Figures 1-3, & 9 x3; 15-16 x10; all other figures x6

Fig.	Species	Level	Slab	#
1	*Dicellograptus* aff. *turgidus* Mu	ca. 5.5	10	5[1]
2	*Dicellograptus* aff. *turgidus* Mu	ca. 5.5	4	
3	*Dicellograptus* aff. *turgidus* Mu	ca. 5.5	1	1[1]
4	*Dicellograptus* aff. *turgidus* Mu	ca. 5.5	10	purp./2
5	*Dicellograptus sinicus* Mu & Zhang	NA	NIGP	11649a
6	*Dicellograptus turgidus* Mu HOLOTYPE	NA	NIGP	56764
7	*Dicellograptus turgidus* Mu	JL 148	16	2
8	*Dicellograptus turgidus* Mu	NA		56765
9	*Dicellograptus turgidus* Mu	JL 148	16	1
10	*Dicellograptus turgidus* Mu	12.67	unlabeled	
11	*Dicellograptus turgidus* Mu?	12.67	013b	
12	*Dicellograptus turgidus* Mu	12.67	003a	
13	*Dicellograptus* aff. *turgidus* Mu	ca. 5.5	100	
14	*Diceratograptus mirus* Mu	15.65	41	
15	*Diceratograptus mirus* Mu	16.03	012ax-1	1
16	*Diceratograptus mirus* Mu	16.03	012ax-1	2
17	*Diceratograptus mirus* Mu	16.03	012ax-1	3
18	*Diceratograptus mirus* Mu	16.03	13bx	

[1]Part and counterpart

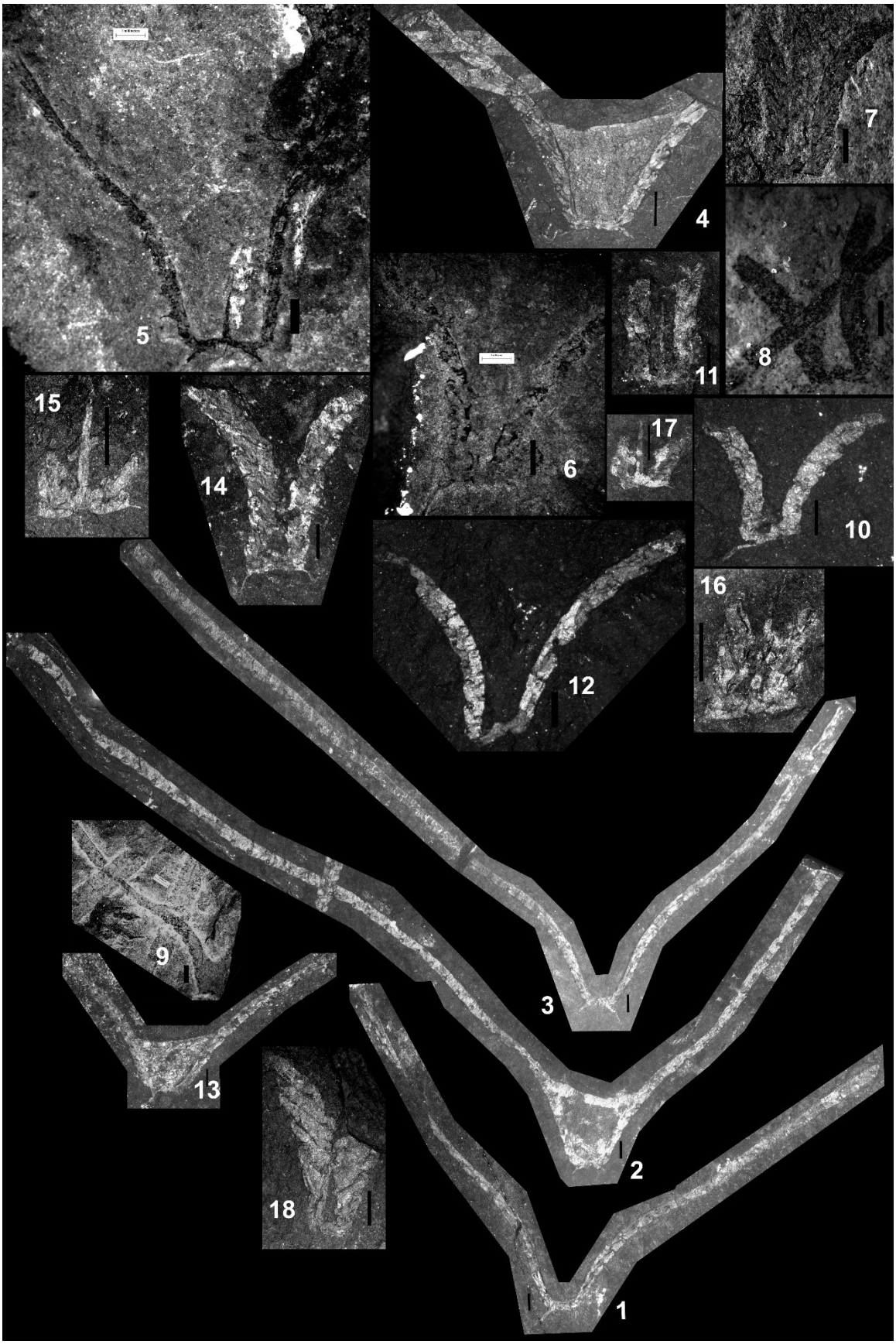
5
4
7
6
11
8
15
14
17
10
12
16
9
3
13
2
18
1

Plate 13

All figures x6

Fig.	Species	Level	Slab	#
1	*Yinograptus disjunctus* (Yin and Mu)	8.80	25a	
2	*Phoromograptus connectus* Mu	ca. 5.5	13	
3	*Phoromograptus connectus* Mu	8.80	15	
4	*Phoromograptus connectus* Mu	5.50	2	
5	*Yinograptus disjunctus* (Yin and Mu)	1.30	012bx	
6	*Phoromograptus connectus* Mu	16.03	8	1
7	*Phoromograptus connectus* Mu	5.50	024b	

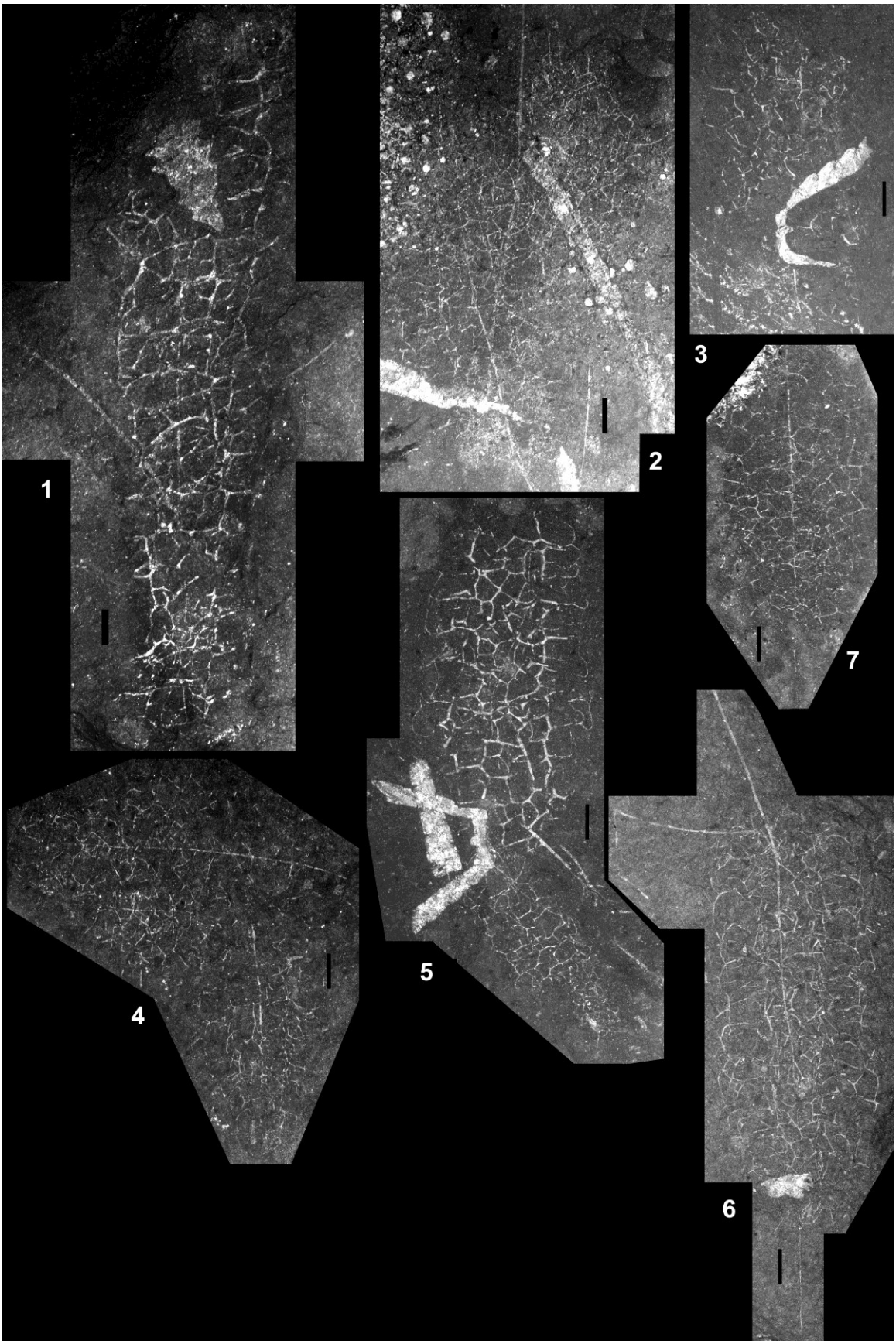
1
2
3
4
5
6
7

Plate 14

Figure #3a x4; #3b & #11 x10; all other figures x6

Fig.	Species	Level	Slab	#
1	*Appendispinograptus leptothecalis* (Mu & Ge)	17.20	26	
2	*Appendispinograptus leptothecalis* (Mu & Ge)	18.94	13	v2.
3a	*Appendispinograptus leptothecalis* (Mu & Ge)	18.05	001a	
3b	*Appendispinograptus leptothecalis* (Mu & Ge)	18.05	001a	
4	*Appendispinograptus leptothecalis* (Mu & Ge)	18.05	2000-2	
5	*Appendispinograptus supernus* (Elles & Wood)	16.03	011ax	1
6	*Appendi. pogrebovi* (Koren' & Sobolevskaya)	19.00	008b	1
7	*Appendi. pogrebovi* (Koren' & Sobolevskaya)	19.00	010a	
8	*Appendispinograptus leptothecalis* (Mu & Ge)	19.00	22A	
9	*Appendispinograptus leptothecalis* (Mu & Ge)	18.05	26	
10	*Appendispinograptus supernus* (Elles & Wood)	16.03	011c	1
11	*Appendispinograptus supernus* (Elles & Wood)	16.03	011c	2
12	*Appendispinograptus supernus* (Elles & Wood)	1.30	103a	
13	*Appendi. pogrebovi* (Koren' & Sobolevskaya)	19.00	023a	2
14	*Appendi. pogrebovi* (Koren' & Sobolevskaya)	19.00	023a	1

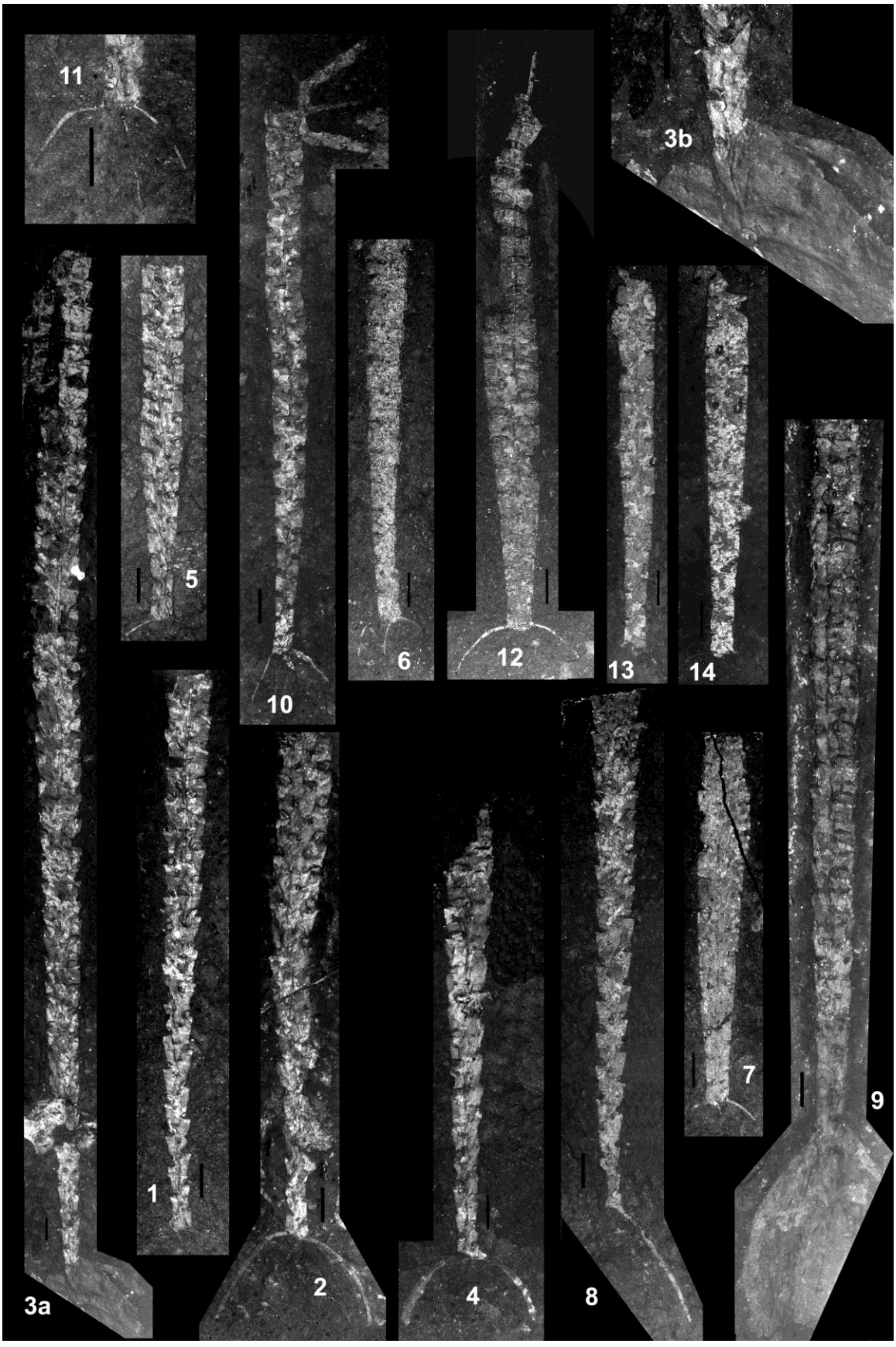
11
3b
5
10
6
12
13
14
1
2
4
8
7
9
3a

Plate 15

Figure #13 x10; all other figures x6

Fig.	Species	Level	Slab	#
1	*Climacograptus hastatus* Hall	16.03	011d	
2	*Styraco. mississippiensis* (Ruedemannn)	18.05	001ax	1
3	*Climacograptus hastatus* Hall	14.15	22a	
4	*Paraorthograptus pacificus* (Ruedemann)	14.15	22a	
5	*Styraco. mississippiensis* (Ruedemannn)	19.00	22A	
6	*Styraco. mississippiensis* (Ruedemannn)	18.05	010ax	1
7	*Styraco. mississippiensis* (Ruedemannn)	12.67	33x	
8	*Climacograptus hastatus* Hall	18.05 (06)	OWL	
9	*Styraco. mississippiensis* (Ruedemannn)	18.05	001a	1
10	*Climacograptus hastatus* Hall	0.10	003a	
11	*Styraco. mississippiensis* (Ruedemannn)	0.10	001bx	1
12	*Styraco. tatianae* (Keller)	0.10	003a	
13	*Climacograptus hastatus* Hall	16.03	012ax-1	

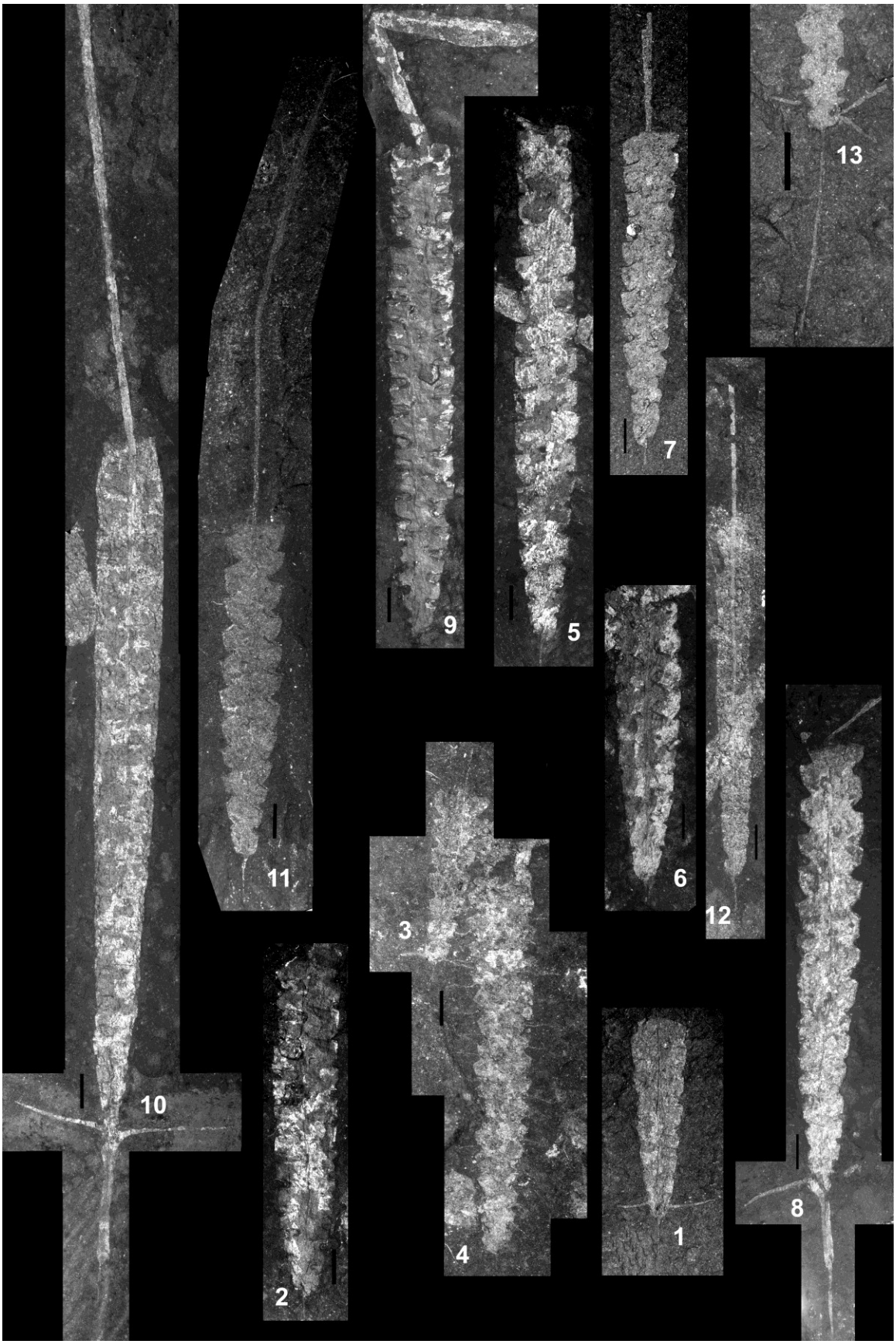
13
7
9
5
11
6
12
3
10
8
4
1
2

Plate 16

Figure #1 x3; all other figures x6

Fig.	Species	Level	Slab	#
1	*Diplo. rarithecatus (Ross & Berry)*	16.03	011d	
2	*Diplo. rarithecatus (Ross & Berry)*	15.65	047a	
3	*Recto. abbreviatus (Elles & Wood)*	17.20	007b	1
4	*Phoromograptus connectus* Mu	5.50	20	
5	*Recto. abbreviatus (Elles & Wood)*	5.50	12x	Yellow
6	*Recto. abbreviatus (Elles & Wood)*	5.50	12x	Brown
7	*Recto. abbreviatus (Elles & Wood)*	5.50	12x	2
8	*Recto. abbreviatus (Elles & Wood)*	5.50	23	1
9	*Recto. abbreviatus (Elles & Wood)*	16.03	002a	1
10	*Recto. abbreviatus (Elles & Wood)*	16.03	002a-2	1
11	*Diplo. rarithecatus (Ross & Berry)*	16.03	chuck	
12	*Diplo. rarithecatus (Ross & Berry)*	15.65	011bx	1
13	*Diplo. rarithecatus (Ross & Berry)*	15.65	011b	1
14	*Diplo. rarithecatus (Ross & Berry)*	16.03	012bx	2
15	*Diplo. rarithecatus (Ross & Berry)*	15.65	17x	1
16	*Recto. abbreviatus (Elles & Wood)*	17.20	16	1

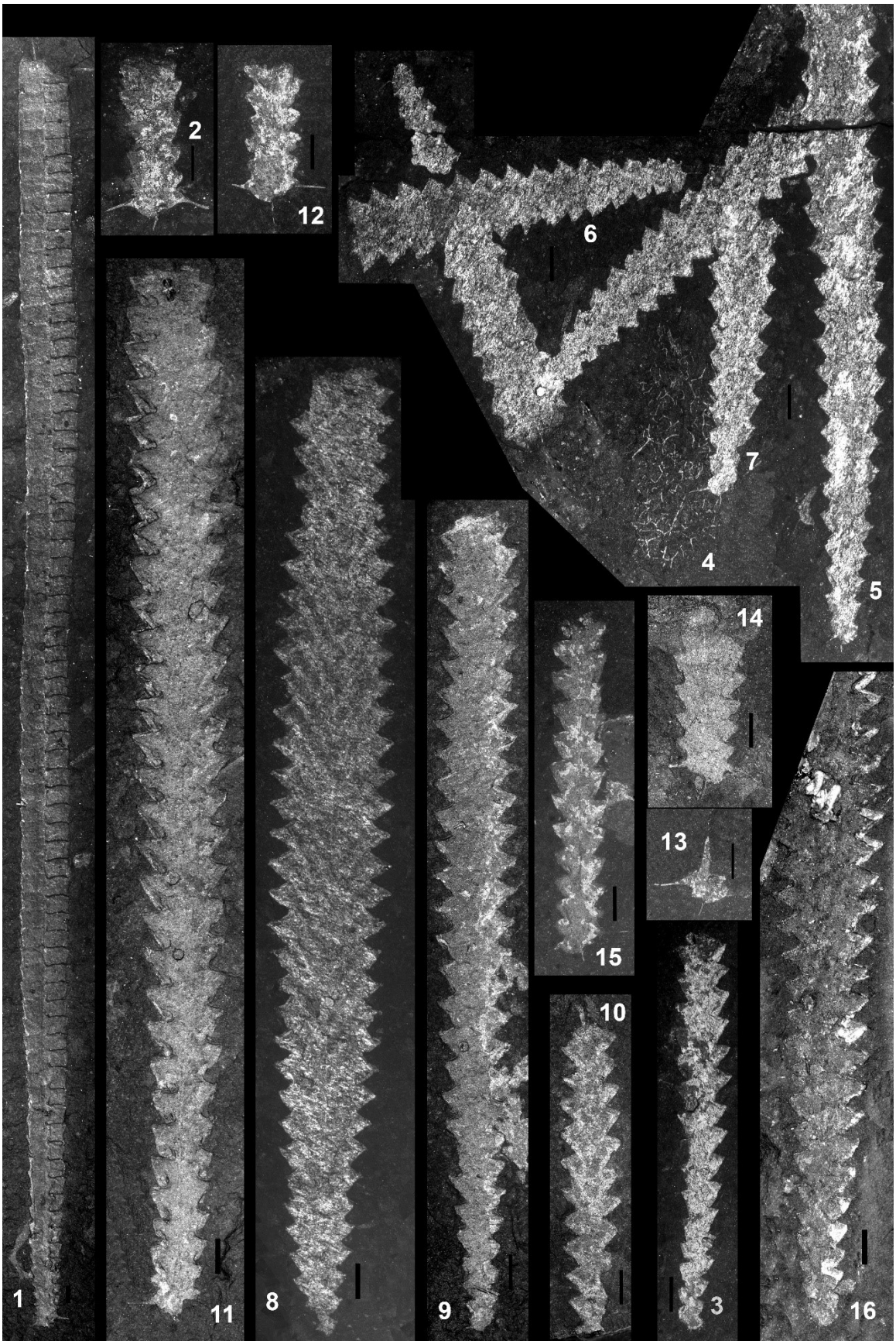
1
2
12
6
7
4
5
14
13
15
10
11
8
9
3
16

Plate 17

Figure 9b x3; all other figures x6

Fig.	Species	Level	Slab	#
1	*Para. pacificus* (Ruedemann)	19.00	8	
2	*Para. pacificus* (Ruedemann)	18.05	016ax	1
3	*Para. affinis* (Koren' & Tzaj)?	18.05	016a	1
4	*Para. affinis* (Koren' & Tzaj)?	18.05	012a	
5	*Para. pacificus* (Ruedemann)	19.00	024b	
6	*Para. kimi* (Koren')	1.30	37	
7	*Para. kimi* (Koren')	1.30	28	
8	*Para. kimi* (Koren')	1.30	017bx	1
9a	*Para. affinis* (Koren' & Tzaj)	19.15	15bx	
9b	*Para. affinis* (Koren' & Tzaj)	19.15	15bx	
10	*Para. affinis* (Koren' & Tzaj)	19.15	014a	1
11	*Para. pacificus* (Ruedemann)	16.03	002bx_1	1
12	*Para. pacificus* (Ruedemann)	15.65	777	
13	*Para. pacificus* (Ruedemann)	16.03	002bx_1	2
14	*Para. pacificus* (Ruedemann)	16.03	012a-1	1 CP
15	*Para. pacificus* (Ruedemann)	14.15		
16	*Para. pacificus* (Ruedemann)	15.65	003a	2
17	*Para. pacificus* (Ruedemann)	15.65	003a	1
18	*Para. kimi* (Koren')	0.10	001c	
19	*Para. pacificus* (Ruedemann)	19.00	025b	

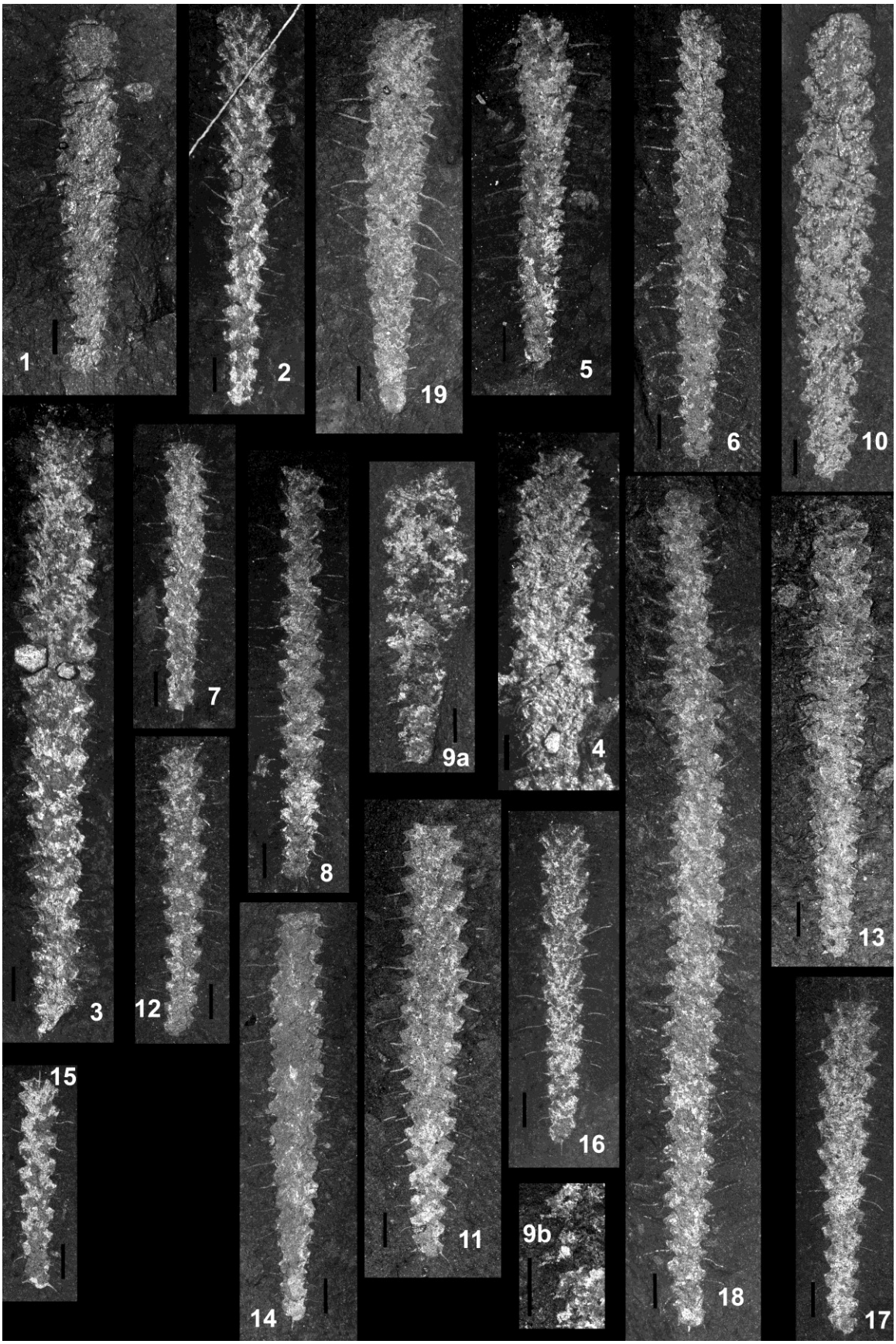
1
2
19
5
6
10
3
7
8
9a
4
12
13
15
14
11
16
9b
18
17

Plate 18

All figures x6

Fig.	Species	Level	Slab	#
1	*Dicellograptus tenuiculus* Mu et al.	16.03	011ax	1
2	*Dicellograptus tenuiculus* Mu et al.	14.15	99	1
3	*Dicellograptus tenuiculus* Mu et al.	14.15	99x	1
4	*Dicellograptus tenuiculus* Mu et al.	14.15	009a	1
5	*Dicellograptus tenuiculus* Mu et al.	14.15	009c	3
6	*Dicellograptus tenuiculus* Mu et al.	14.15	14bx	1
7	*Dicellograptus tenuiculus* Mu et al.	14.15	14bx	2
8	*Dicellograptus tenuiculus* Mu et al.	16.03	013bx	1

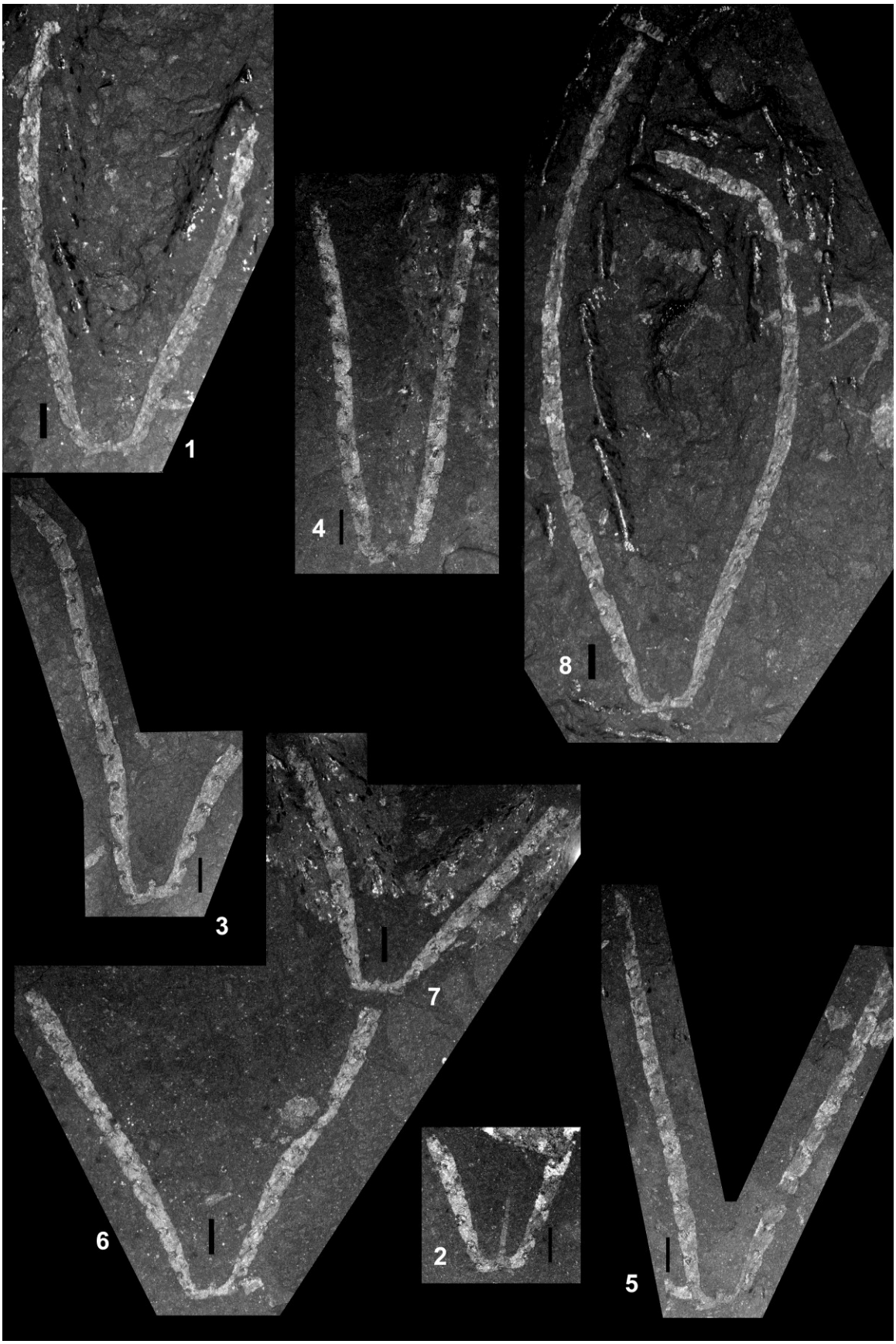
1
4
8
3
7
6
2
5

Plate 19

Figures 1a, 2, 5a, & 6a x2; all other figures x6

Fig.	Species	Level	Slab	#
1a	*Dicello. ornatus* Elles & Wood (2)	ca. 5.5	15	
1b	*Dicello. ornatus* Elles & Wood (2)	ca. 5.5	15	
2	*Dicello. ornatus* Elles & Wood (1)	12.67	001b	
3	*Dicello. ornatus* Elles & Wood (1)	12.67	001a	
4	*Dicello. ornatus* Elles & Wood (2)	ca. 5.5	"Big Eurypt."	
5a	*Dicello. ornatus* Elles & Wood (2)	ca. 5.5	7	1
5b	*Dicello. ornatus* Elles & Wood (2)	ca. 5.5	7	1
6a	*Dicello. ornatus* Elles & Wood (2)	ca. 5.5	7	2
6b	*Dicello. ornatus* Elles & Wood (2)	ca. 5.5	7	2
7	*Dicello.* cf. *ornatus* Elles & Wood	8.80	010b	

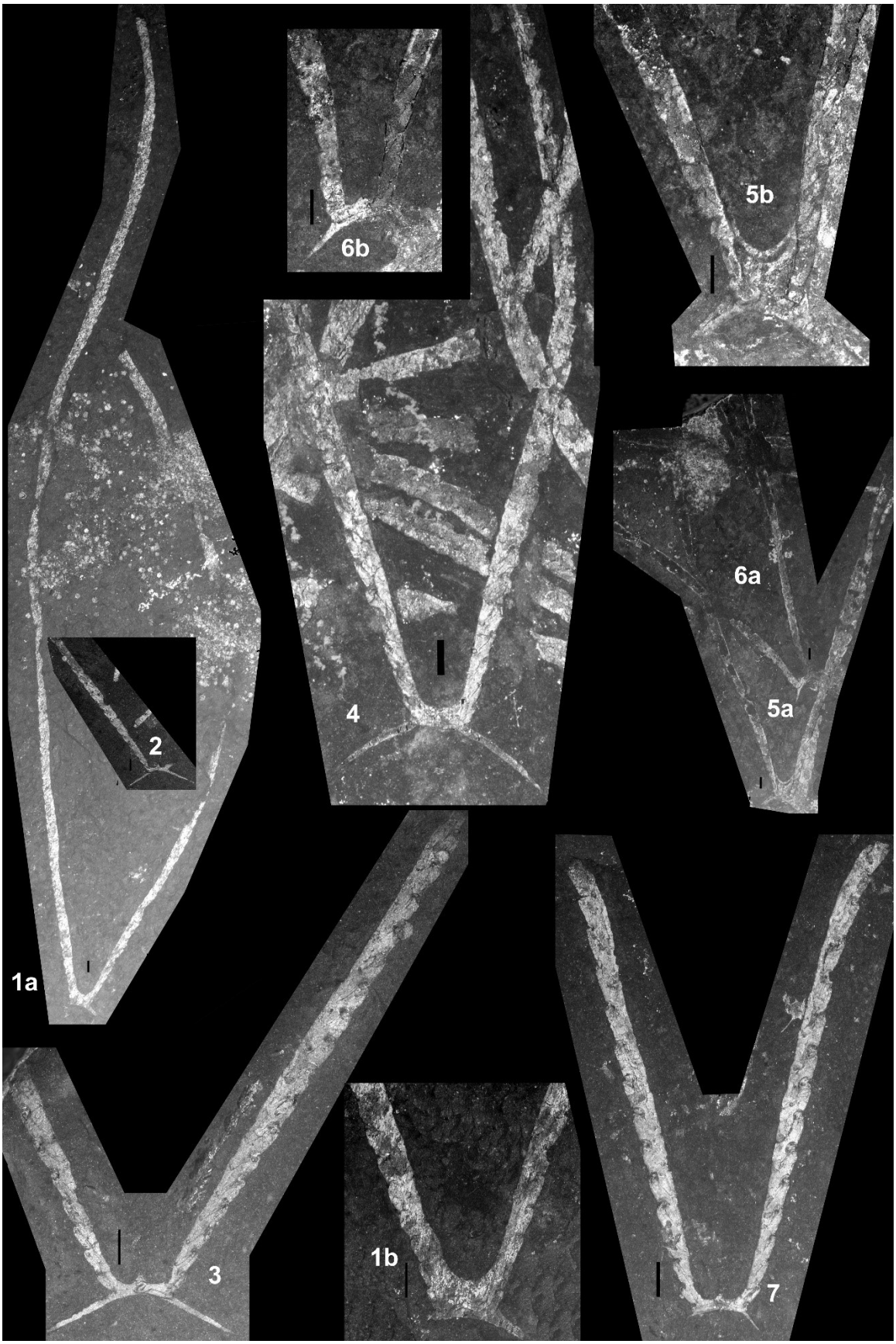
6b
5b
4
6a
2
5a
1a
3
1b
7

Plate 20

All figures x6

Fig.	Species	Level	Slab	#
1	*Dicello.* cf. *mirabilis* Mu & Chen	19.00	31b	
2	*Dicello.* aff. *mirabilis* Mu & Chen	18.05	22	
3	*Dicello.* cf. *mirabilis* Mu & Chen	16.03	012ax-1	1
4	*Dicello.* cf. *mirabilis* Mu & Chen	16.03	010a	5
5	*Dicello. ornatus* Elles & Wood (1)	0.10	007a	
6	*Dicello.* cf. *mirabilis* Mu & Chen	16.03	010a	4
7	*Dicello.* aff. *mirabilis* Mu & Chen	17.20	15	
8	*Dicello. ornatus* Elles & Wood (1)	8.80	1000/cp 009a	
9	*Dicello. ornatus* Elles & Wood (1)	8.80	14	1
10	*Dicello. ornatus* Elles & Wood (1)	8.80	5000	

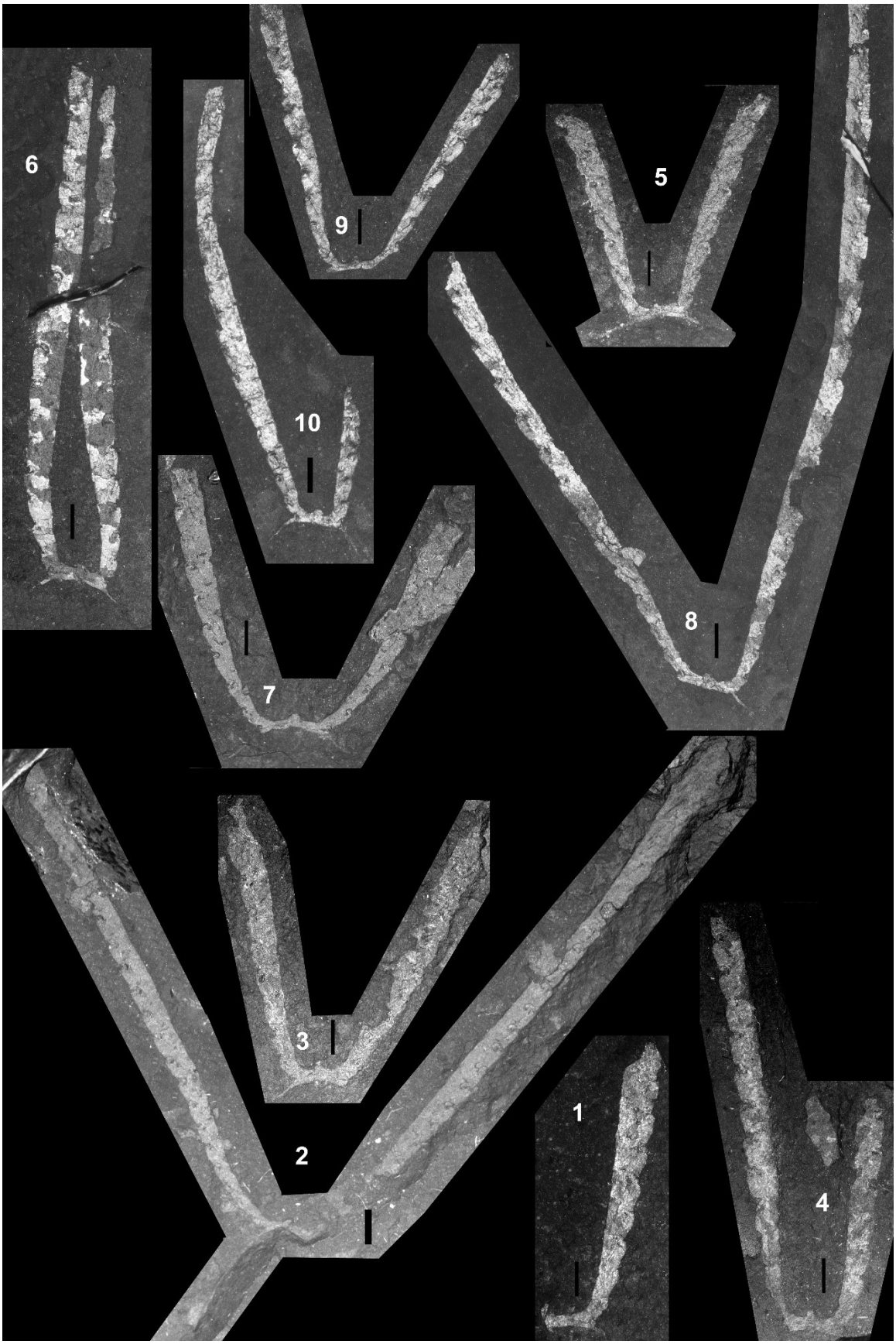
6
9
5
10
8
7
3
2
1
4

Plate 21

All figures x6

Fig.	Species	Level	Slab	#
1	*Styracograptus mississippiensis* (Ruedemannn)	5.50	13	
2	*Appendispinograptus leptothecalis* (Mu & Ge)	18.05	19a	
3	*Climacograptus hastatus* Hall	5.50	13	
4	*Climacograptus hastatus* Hall	5.50	13	
5	*Styracograptus* sp.	18.05	22	2
6	*Styracograptus tatianae* (Keller)	0.10	020bx	
7	*Styracograptus tatianae* (Keller)	19.00	012b	
8	*Styracograptus tatianae* (Keller)	0.10	016x	1
9	*Styracograptus mississippiensis* (Ruedemannn)	0.10	016x	2
10	*Styracograptus mississippiensis* (Ruedemannn)	17.20	021-1	
11	*Meta. ojsuensis* (Koren' & Mikhaylova)?	19.20	050a	
12	*Styracograptus mississippiensis* (Ruedemannn)	0.10	004a	
13	*Climacograptus hastatus* Hall	5.50	20	
14	*Climacograptus hastatus* Hall	14.15	013b	1
15	*Climacograptus hastatus* Hall	14.15	013b	2
16	*Climacograptus hastatus* Hall	14.15	015a	1
17	*Styracograptus tatianae* (Keller)	19.05	5	

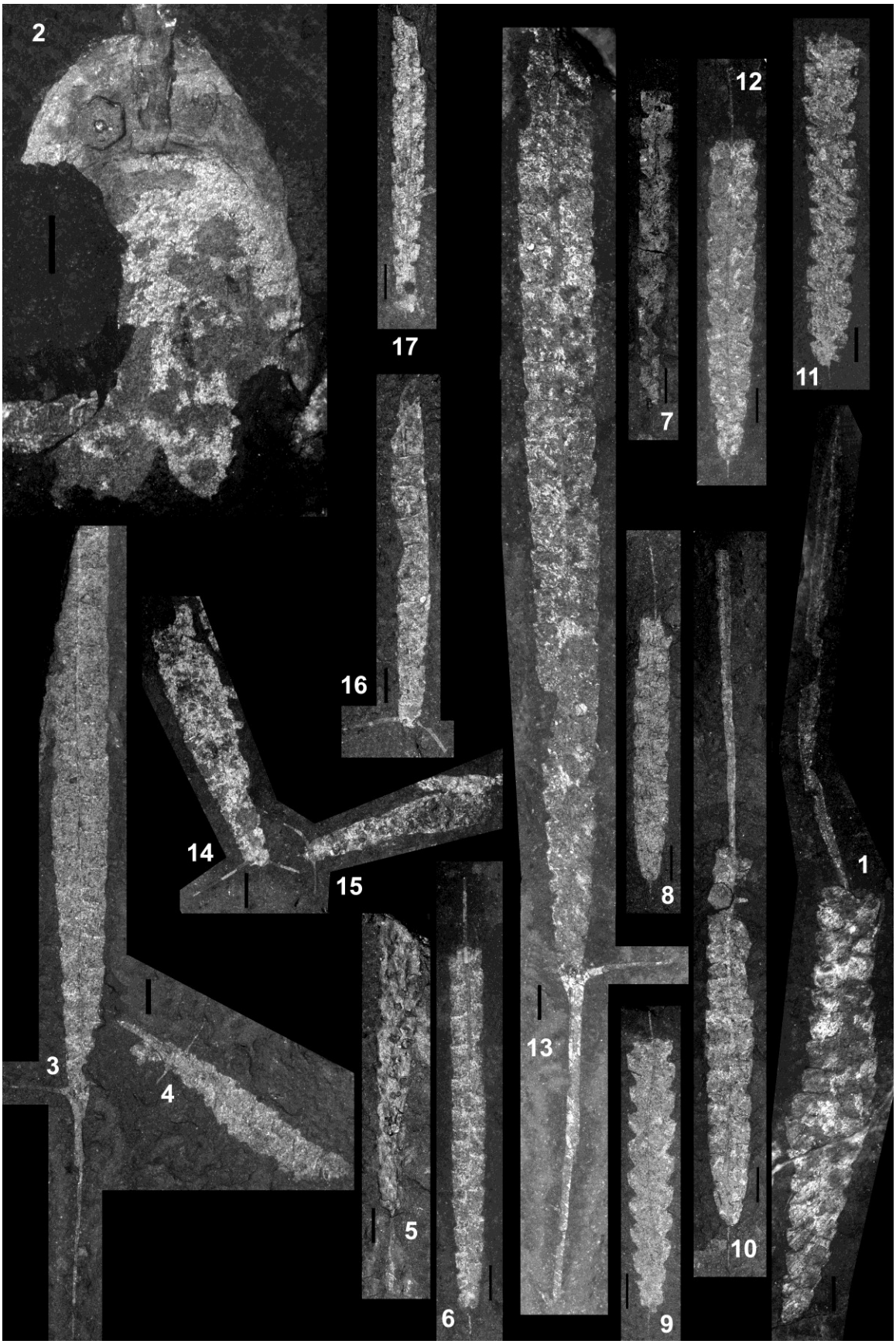
2
17
12
11
7
16
1
8
14
15
13
3
4
5
6
10
9

Plate 22

Figures #1b & #4b x10; all of the figures x6

Fig.	Species	Level	Slab	#
1a	*Dicellograptus minor* Toghill	12.67	12ax	
1b	*Dicellograptus minor* Toghill	12.67	12ax	
2	*Pleurograptus lui* Mu	16.03	004a	
3	*Dicellograptus minor* Toghill	17.20	012bx	
4a	*Pleurograptus lui* Mu	1.30	001a	
4b	*Pleurograptus lui* Mu	1.30	001a	
5	*Dicello. ornatus* Elles & Wood (1)	0.10		
6	*Styracograptus tatianae* (Keller)	0.10		
7	*Dicello. minor* Toghill	16.03	016a-2	1
8	*Dicello.* cf. *mirabilis* Mu & Chen	16.03	001a-2	3
9	*Dicello.* cf. *mirabilis* Mu & Chen	16.03	001a-2	4
10	*Dicello.* cf. *mirabilis* Mu & Chen	16.03	001a-2	2
11	*Dicello.* cf. *mirabilis* Mu & Chen	16.03	001a-2	1
12	*Dicello.* cf. *mirabilis* Mu & Chen	16.03	001a-3	1
13	*Diceratograptus mirus* Mu	18.94	019a	

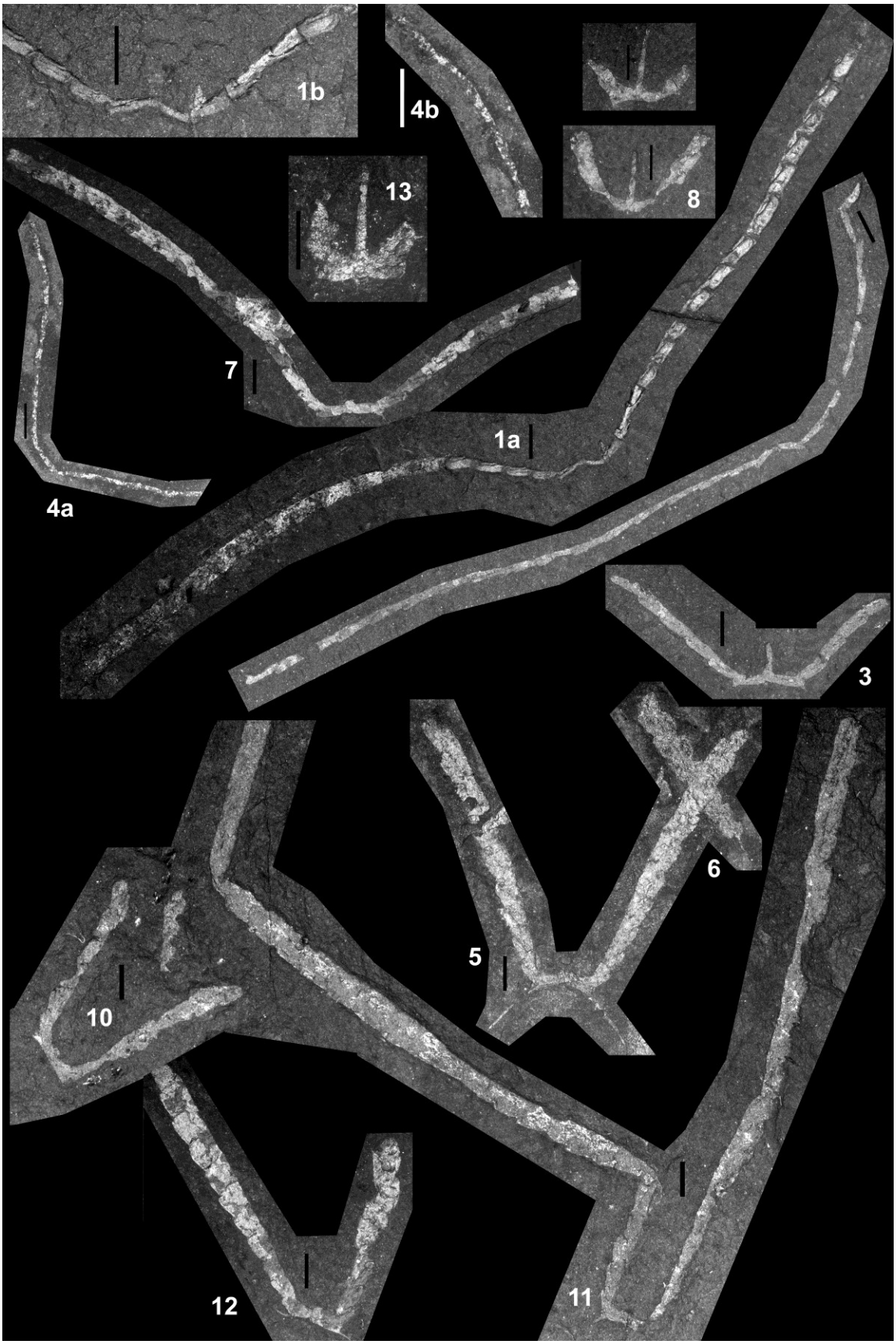
1b
4b
13
8
7
1a
4a
3
6
5
10
12
11

Plate 23

All figures x6

Fig.	Species	Level	Slab	#
1	*Meta. extraordinarius* (Sobolevskaya)	19.20	020a	1
2	*Neodiplograptus charis* (Mu & Ni)	19.20	020a	2
3	*Neodiplograptus charis* (Mu & Ni)	19.20	041b	1
4	*Neodiplograptus charis* (Mu & Ni)	19.20	024b	1
5	*Neodiplograptus charis* (Mu & Ni)	19.20	036bx	1
6	*Meta. ojsuensis* (Koren' & Mikhaylova)	19.20	036b	1
7	*Neodiplograptus charis* (Mu & Ni)	19.20?	012a	1
8	*Neodiplograptus charis* (Mu & Ni)	19.20	20a	3
9	*Neodiplograptus charis* (Mu & Ni)	19.20	34	
10	*Neodiplograptus charis* (Mu & Ni)	19.20	7	

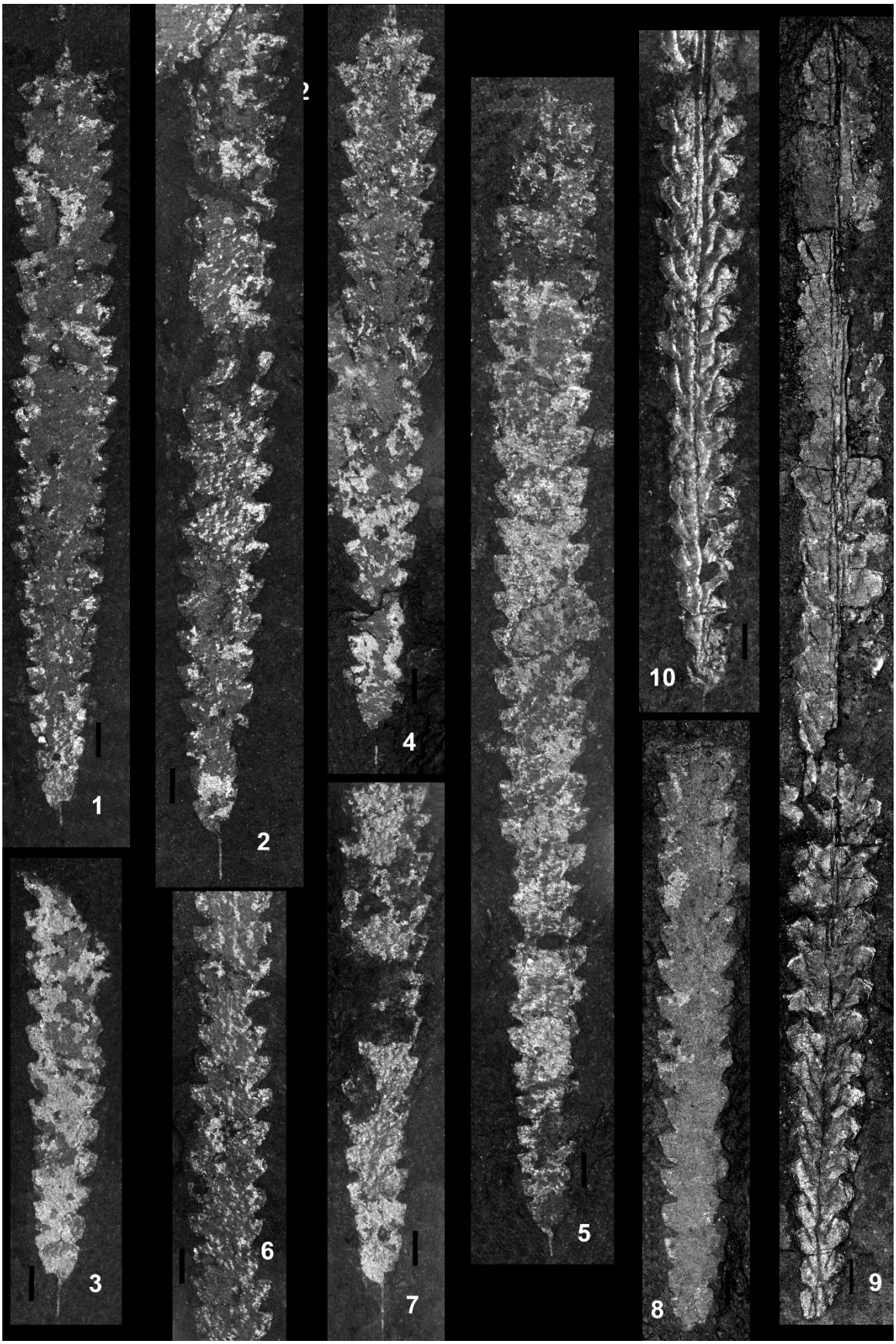
1
2
3
4
5
6
7
8
9
10

Plate 24

Figure #2a x5; all other figures x6

Fig.	Species	Level	Slab	#
1	*Meta. extraordinarius* (Sobolevskaya)	19.15	009b	2
2a	*Meta. extraordinarius* (Sobolevskaya)	19.15	009b	1
2b	*Meta. extraordinarius* (Sobolevskaya)	19.15	009b	1
3	*Meta. extraordinarius* (Sobolevskaya)	19.15	009b	3
4	*Meta. extraordinarius* (Sobolevskaya)	19.15	009b	4
5	*Neodiplograptus charis* (Mu & Ni)	19.15	021bx	1
6	*Neodiplograptus charis* (Mu & Ni)	19.15	015b	1
7	*Neodiplograptus charis* (Mu & Ni)	19.15	015b	2
8	*Meta. ojsuensis* (Koren' & Mikhaylova)	19.15	014b	1


1
2a
2b
3
4
5
6
7
8

Plate 25

All figures x6

Fig.	Species	Level	Slab	#
1	*Meta. extraordinarius* (Sobolevskaya)	19.20 (06)	OWL	1
2	*Meta. extraordinarius* (Sobolevskaya)	19.15	023c	3
3	*Neodiplograptus charis* (Mu & Ni)	19.20	46b	1
4	*Meta. extraordinarius* (Sobolevskaya)	19.15	23c-2	2
5	*Meta. extraordinarius* (Sobolevskaya)	19.15	23c-2	1
6	*Meta. extraordinarius* (Sobolevskaya)	19.15	23c	2
7	*Meta. extraordinarius* (Sobolevskaya)	19.15	23c	1
8	*Neodiplograptus charis* (Mu & Ni)	19.20	036a	
9	*Meta. ojsuensis* (Koren' & Mikhaylova)?	19.20	020b	2
10	*Neodiplograptus charis* (Mu & Ni)	19.15	36	1
11	*Meta. extraordinarius* (Sobolevskaya)	19.25	112	1


1
2
3
4
5
6
7
8
9
10
11

Plate 26

All figures x6

Fig.	Species	Level	Slab	#
1	*Appendi. leptothecalis* (Mu & Ge)	17.20	006bx (inside)	1
2	*Appendi. leptothecalis* (Mu & Ge)	19.00	6 CP	1
3	*Appendi. leptothecalis* (Mu & Ge)	19.00	6	1
4	*Paraorthograptus affinis* (Koren & Tzaj)?	18.05	012b	
5	*Anticostia lata* (Elles & Wood)	15.65	005b1 (inside)	1
6	*Dicellograptus mirabilis* Mu & Chen?	JL 150	5	5
7	*Dicellograptus mirabilis* Mu & Chen?	JL 150	2	2
8	*Dicellograptus graciliramosus* (Yin & Mu)	JL 131	1	1
9	*Dicellograptus tumidus* HOLOTYPE	NA		56750

Note: Figure 6 includes a digital scale bar (horizontal white rectangle) inserted by the digital camera used in China, as well as a standardized scale bar. The original scale bar was not removed to preserve the retiolitid in the background.

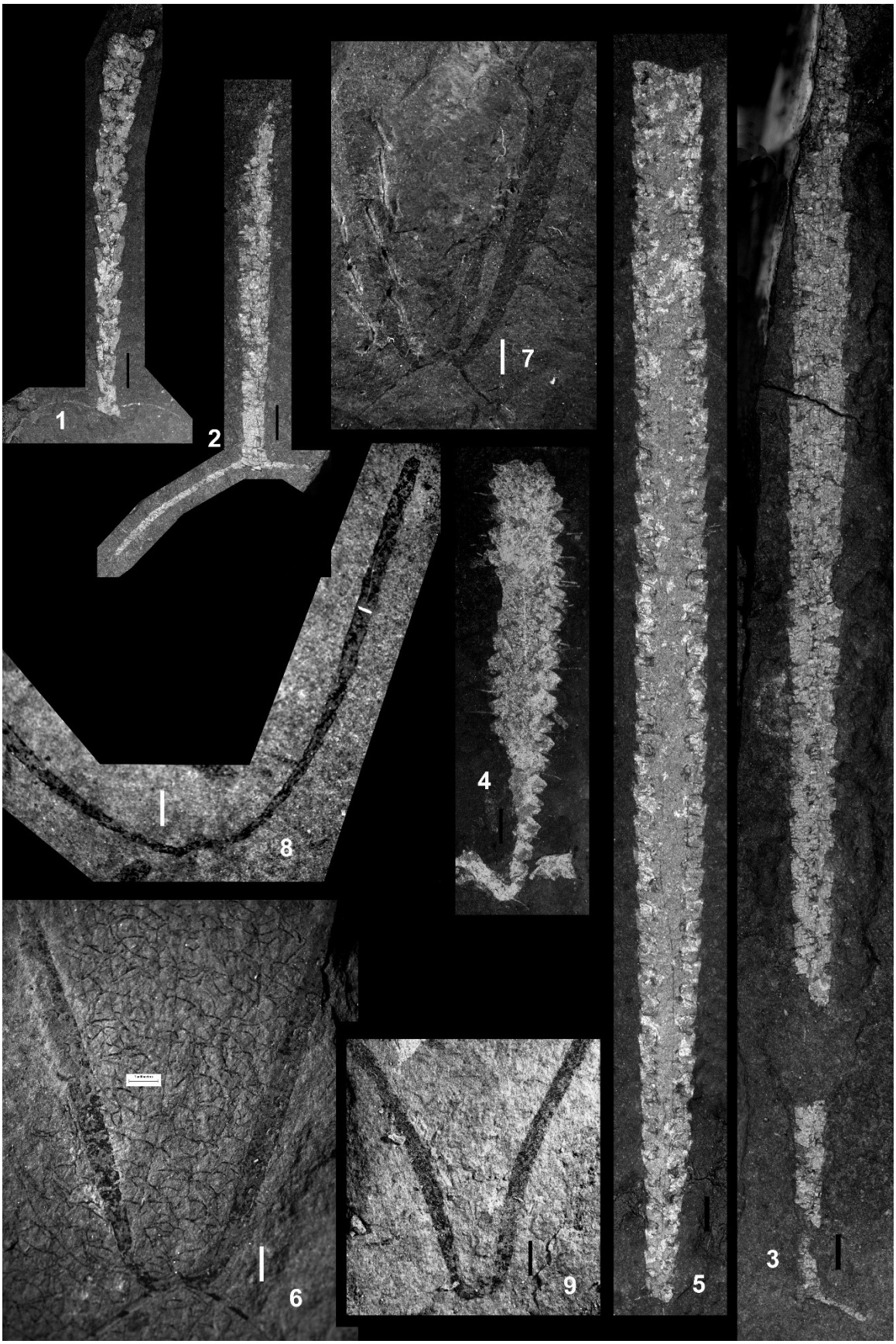
1
2
7
4
8
6
9
5
3

Plate 27

All figures x6

Fig.	Species	Level (m)	Slab	Spec. #
1	*Glyptograptus*? sp. 1	32.97	008ax	1
2	*Normalograptus*? aff. *medius* (Törnquist)	32.84	100a	
3	*Neodiplograptus clavatus*? (Yu et al.)	32.97	004a_2	
4	*Normalograptus*? *transgrediens* (Waern)	32.84	68	
5	*Normalograptus*? aff. *medius* (Törnquist)	32.84	67	
6	*Neodiplograptus* cf. *clavatus* (Yu et al.)	33.37	039b	2
7	*Neodiplograptus* cf. *clavatus* (Yu et al.)	33.37	039b	1
8	*Paramplex. madernii* (Koren' & Mikhailova)	33.37	7	2
9	*Normalo.* aff. *mirnyensis* (Obut & Sobolevskaya)	34.11	#	2
10	*Metabolograptus*? sp.	36.3	42a	
11	*Metabolograptus*? sp.	36.3	028a	1
12	*Normalograptus*? *minor* (Huang)	34.11	062a	
13	*Avitograptus avitus* (Davies)	34.11	80	
14	*Normalograptus*? *transgrediens* (Waern)	35.15	010b	
15	*Neodiplograptus clavatus* (Yu et al.)	33.37	61	
16	*Neodiplograptus shanchongensis* (Li)	33.37	59	
17	*Avitograptus avitus* (Davies)	33.37	052b	
18	*Glyptograptus*? sp. 2	33.37	002b	
19	*Neodiplograptus shanchongensis* (Li)	32.97	?	Purple
20	*Neodiplograptus clavatus* (Yu et al.)	32.97	045f	
21	*Neodiplograptus clavatus* (Yu et al.)	32.97	012a	
22	*Paramplex.* aff. *madernii* (Koren' & Mikhailova)	34.11	10	A
23	*Paramplex.* aff. *madernii* (Koren' & Mikhailova)	34.11	10	2
24	*Paramplex. madernii* (Koren' & Mikhailova)	32.97	045a	
25	*Paramplex.* aff. *madernii* (Koren' & Mikhailova)	~34.11	2	2

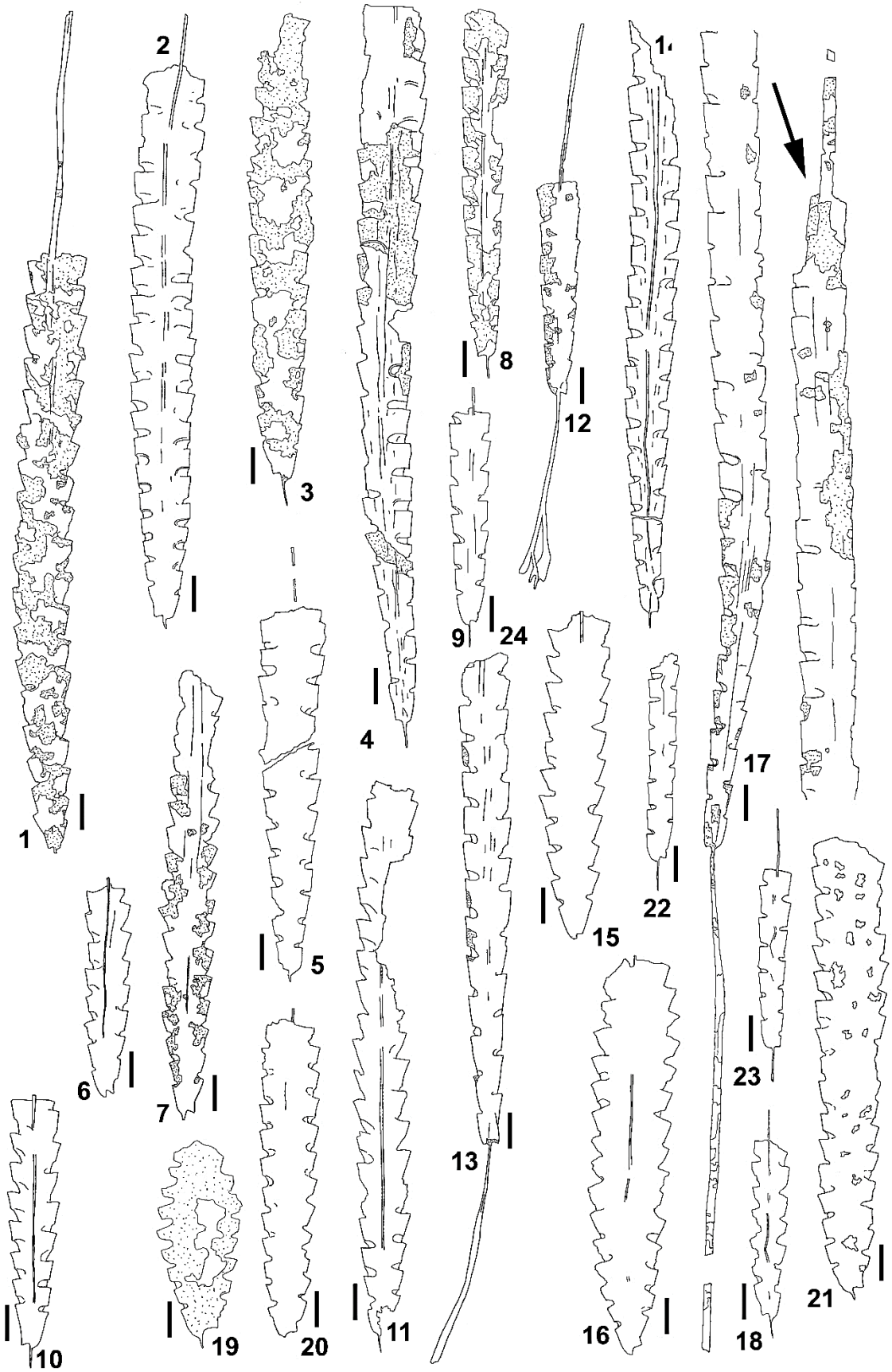
1
2
3
4
5
6
7
8
9
10
11
12
13
14
15
16
17
18
19
20
21
22
23
24

Plate 28

All figures x6

Fig.	Species	Level (m)	Slab	#
1	*Normalograptus*? *rhizinus* (Li & Yang)	33.37		#6
2	*Normalograptus*? *rhizinus* (Li & Yang)	33.37		#1
3	*Korenograptus* sp. 1	36.30	026b	
4	*Normalograptus*? aff. *medius* (Törnquist)	35.15	005b	
5	*Korenograptus* sp. 1	33.37	56	
6	*Normalograptus*? aff. *medius* (Törnquist)	32.84	100	
7	*Avitograptus avitus* (Davies)	35.15	32	
8	*Paramplexo.* aff. *madernii* (Koren' & Mikhailova)	34.11	#	
9	*Normalo.* aff. *mirnyensis* (Obut & Sobolevskaya)	34.11	042b	2
10	*Normalograptus*? *rhizinus* (Li & Yang)	33.37		II
11	*Korenograptus lungmaensis* (Sun)	32.84	011a	
12	*Paramplexo.* aff. *madernii* (Koren' & Mikhailova)	34.11	031a	Red
13	*Normalo.* aff. *mirnyensis* (Obut & Sobolevskaya)	33.37	30	
14	*Paramplexo.* aff. *madernii* (Koren' & Mikhailova)	~34.11	1	
15	*Metabolograptus persculptus* (Elles & Wood)	32.84	61	
16	*Paramplex.* aff. *madernii* (Koren' & Mikhailova)	~34.11	2	1
17	*Metabolograptus parvulus* (Lapworth)	32.84	10	1

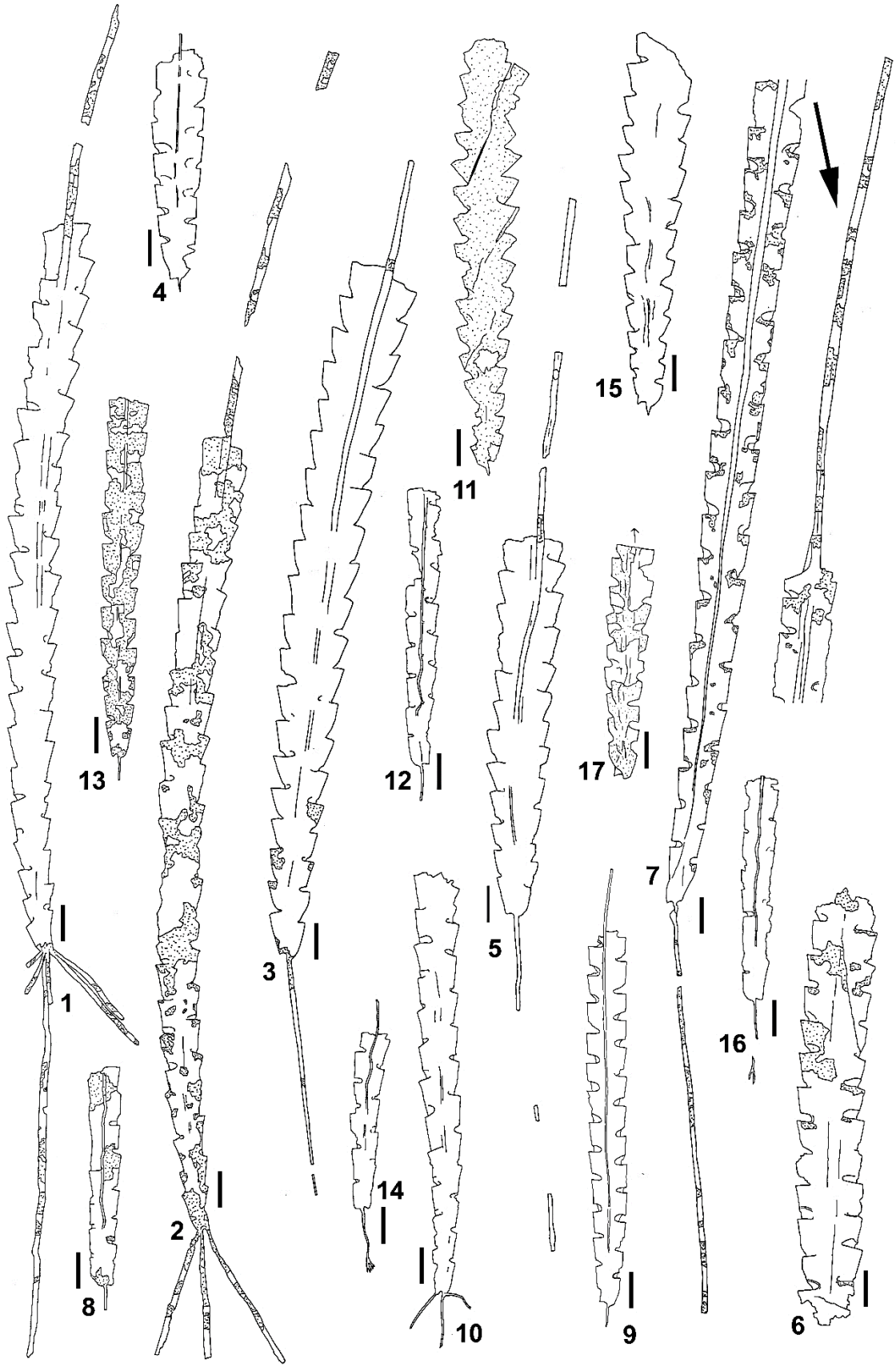
1
2
3
4
5
6
7
8
9
10
11
12
13
14
15
16
17

Plate 29

All figures x6

Fig.	Species	Level (m)	Slab	#
1	*Korenograptus jiangxiensis* (Fang et al.)	33.37	077x	
2	*Korenograptus jiangxiensis* (Fang et al.)	32.97	016g	
3	*Korenograptus jiangxiensis* (Fang et al.)	33.37	026a	2
4	*Glyptograptus*? sp. 1	32.97	020a[1]	
5	*Korenograptus* sp. 1	34.11	063a	
6	*Korenograptus laciniosus* (Churkin & Carter)	32.84	12	4
7	*Korenograptus laciniosus* (Churkin & Carter)	32.84	002a_2	2
8	*Korenograptus laciniosus* (Churkin & Carter)	32.84	006a	1
9	*Avitograptus avitus* (Davies)	32.97	40	
10	*Avitograptus avitus* (Davies)	32.97	16b	
11	*Normalograptus*? aff. *medius* (Törnquist)	32.84	005b	
12	*Normalograptus*? *minor* (Huang)?	32.97	14	
13	*Normalograptus*? *minor* (Huang)	34.11	23	
14	*Normalograptus*? *rhizinus* (Li & Yang)	33.37	40	
15	*Normalograptus*? *transgrediens* (Waern)	32.84	005a	
16	*Korenograptus lungmaensis* (Sun)	32.84	003b	2
17	*Korenograptus lungmaensis* (Sun)	32.84	99	

[1]Newly split ‘inside’ surface

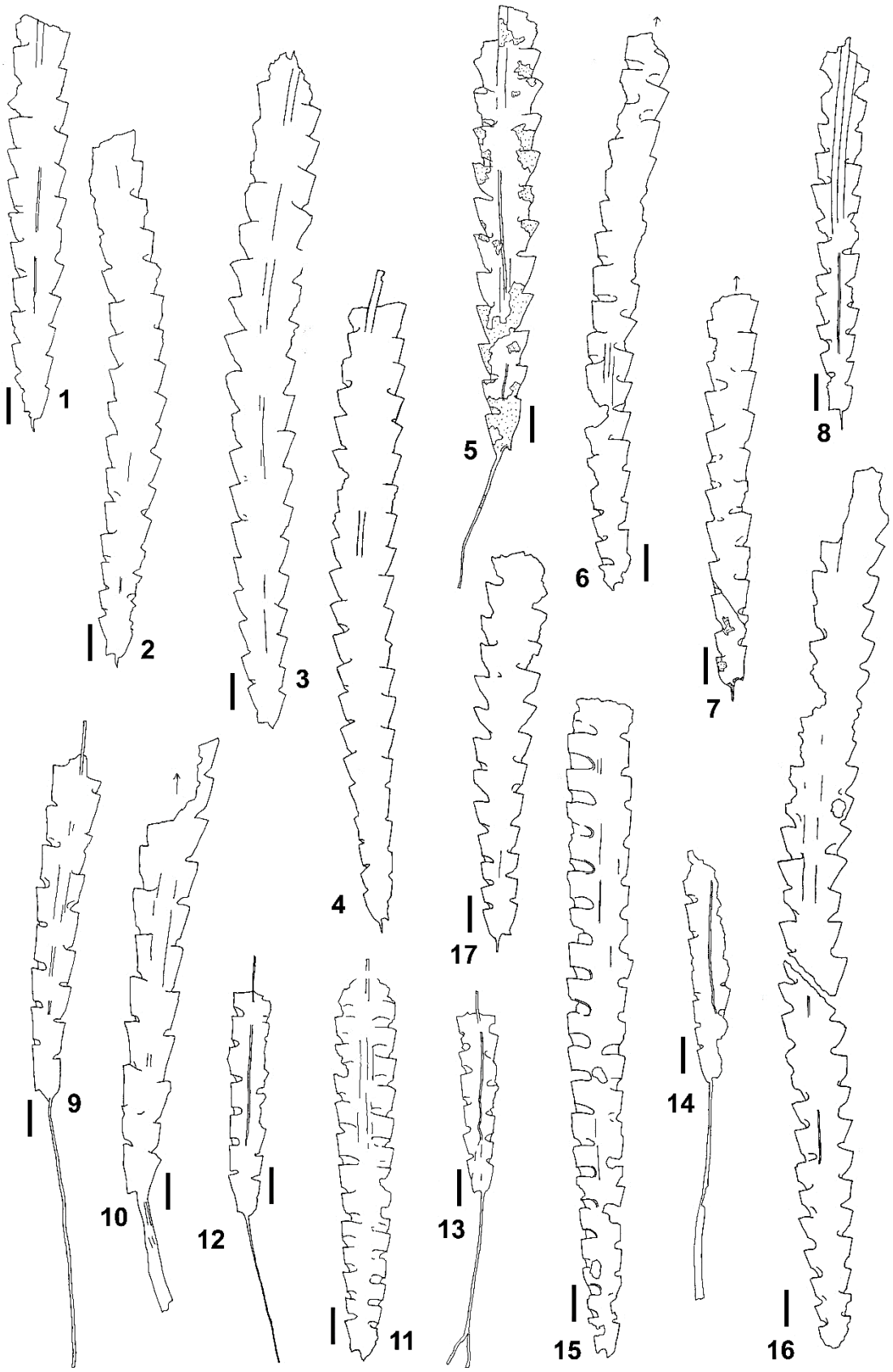
1
2
3
4
5
6
7
8
9
10
11
12
13
14
15
16
17

Plate 30

All figures x6

Fig.	Species	Level	Slab	#
1	*Neodiplograptus clavatus* (Yu et al.)	33.37	49	3
2	*Neodiplograptus clavatus* (Yu et al.)	33.37	49	5
3	*Neodiplograptus clavatus* (Yu et al.)	33.37	49	2
4	*Neodiplograptus clavatus* (Yu et al.)	33.37	029c	
5	*Neodiplograptus clavatus* (Yu et al.)	33.37	61	
6	*Glyptograptus*? sp. 2	33.37	4	
7	*Glyptograptus*? sp. 2	33.37	53	
8	*Glyptograptus*? sp. 2	33.37	36	
9	*Glyptograptus*? sp. 2	33.37	6	
10	*Neodiplograptus* cf. *clavatus* (Yu et al.)	33.37	OWL	
11	*Neodiplograptus* cf. *clavatus* (Yu et al.)	32.97	22	1
12	*Neodiplograptus shanchongensis* (Li)	32.97	009c	
13	*Korenograptus laciniosus* (Churkin & Carter)	32.84	66	
14	*Glyptograptus* sp.	33.37	72	
15	*Paramplexo. madernii* (Koren' & Mikhailova)	33.37	7	2
16	*Glyptograptus* sp.	33.37	7	GSC135134
17	*Glyptograptus* sp.	33.37	7	GSC135131
18	*Korenograptus lungmaensis* (Sun)	32.84	8	2
19	*Korenograptus lungmaensis* (Sun)	32.84	010a_2	
20	*Neodiplograptus shanchongensis* (Li)	33.37	?	Red
21	*Neodiplograptus shanchongensis* (Li)	32.84	Unlabelled	Red
22	*Neodiplograptus xixiangensis* (Yu et al.)	34.11	70	1
23	*Neodiplograptus xixiangensis* (Yu et al.)	34.11	70	5
24	*Glyptograptus*? sp. 1	32.97	001a	1
25	*Korenograptus jiangxiensis* (Fang et al.)	33.37	026a	1
26	*Korenograptus jiangxiensis* (Fang et al.)	33.37	47c	
27	*Korenograptus lungmaensis* (Sun)	32.84	010a	1
28	*Korenograptus lungmaensis* (Sun)	32.84	99	
29	*Neodiplograptus shanchongensis* (Li)	32.97	016h	
30	*Neodiplograptus shanchongensis* (Li)	32.97	007c	1
31	*Neodiplograptus shanchongensis* (Li)	32.97	007c	2
32	*Neodiplograptus clavatus* (Yu et al.)	32.97	045z	2
33	*Neodiplograptus shanchongensis* (Li)	32.97	045z	1

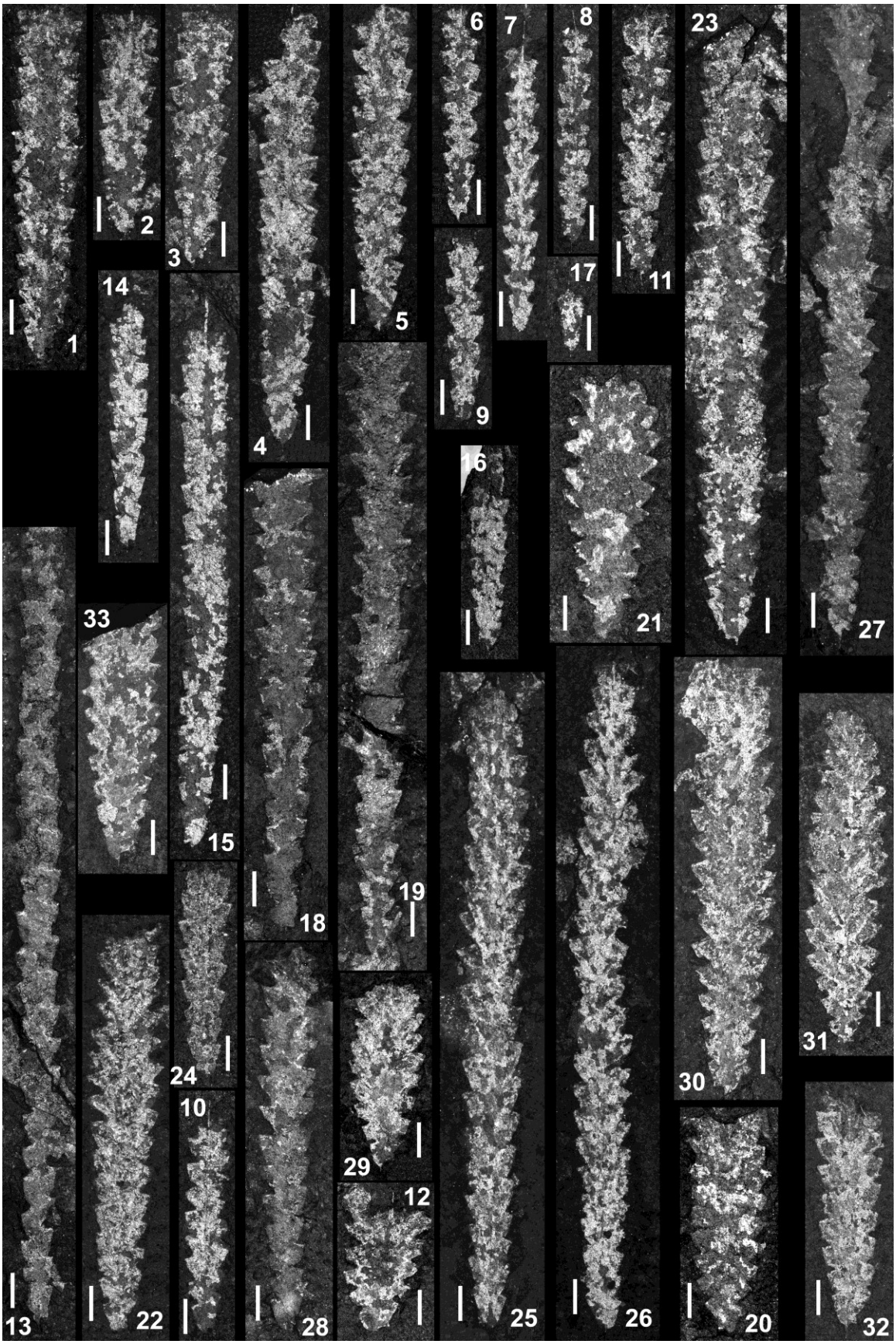
1
2
3
4
5
6
7
8
23
14
17
11
9
16
21
27
33
15
18
19
31
24
10
29
12
30
13
22
28
25
26
20
32

Plate 31

All figures x6

Fig.	Species	Level (m)	Slab	#
1	*Korenograptus lungmaensis* (Sun)	32.84	012b	
2	*Korenograptus* sp. 1	33.37	56	
3	*Normalo.* aff. *mirnyensis* (Obut & Sobolevskaya)	?		
4	*Paramplexo.* aff. *madernii* (Koren' & Mikhailova)	34.11	54b	2
5	*Normalo.* aff. *mirnyensis* (Obut & Sobolevskaya)?	34.11	54b	1
6	*Normalo.* aff. *mirnyensis* (Obut & Sobolevskaya)	34.11	13	1
7	*Normalo.* aff. *mirnyensis* (Obut & Sobolevskaya)	33.37	36	
8	*Normalograptus*? aff. *medius* (Törnquist)	35.15	37	
9	*Normalograptus*? aff. *medius* (Törnquist)	32.84	100a	
10	*Normalograptus*? aff. *medius* (Törnquist)	32.84	67	
11	*Normalograptus*? aff. *medius* (Törnquist)	32.84	36	
12	*Korenograptus laciniosus* (Churkin & Carter)	32.84	22	4
13	*Normalograptus*? *minor* (Huang)	34.11	1	
14	*Normalograptus*? *minor* (Huang)	34.11	70x	
15	*Paramplexo.* aff. *madernii* (Koren' & Mikhailova)	33.37	53	
16	*Normalo.* aff. *mirnyensis* (Obut & Sobolevskaya)	33.37	30	
17	*Paramplexo. madernii* (Koren' & Mikhailova)	32.97	045a	
18	*Paramplexo. madernii* (Koren' & Mikhailova)	34.11	NL	
19	*Normalograptus*? *minor* (Huang)	34.11	062a	
20	*Normalograptus*? *minor* (Huang)?	34.11	062a	
21	*Paramplexo.* aff. *madernii* (Koren' & Mikhailova)	34.11	056a	
22	*Paramplexo.* aff. *madernii* (Koren' & Mikhailova)	34.11	054a	
23	*Paramplexo.* aff. *madernii* (Koren' & Mikhailova)	34.11	22	1
24	*Normalograptus*? aff. *medius* (Törnquist)	32.84	66	
25	*Avitograptus avitus* (Davies)	34.11	66a	
26	*Korenograptus laciniosus* (Churkin & Carter)	32.84	006a	1
27	*Korenograptus laciniosus* (Churkin & Carter)	32.84	006a	2

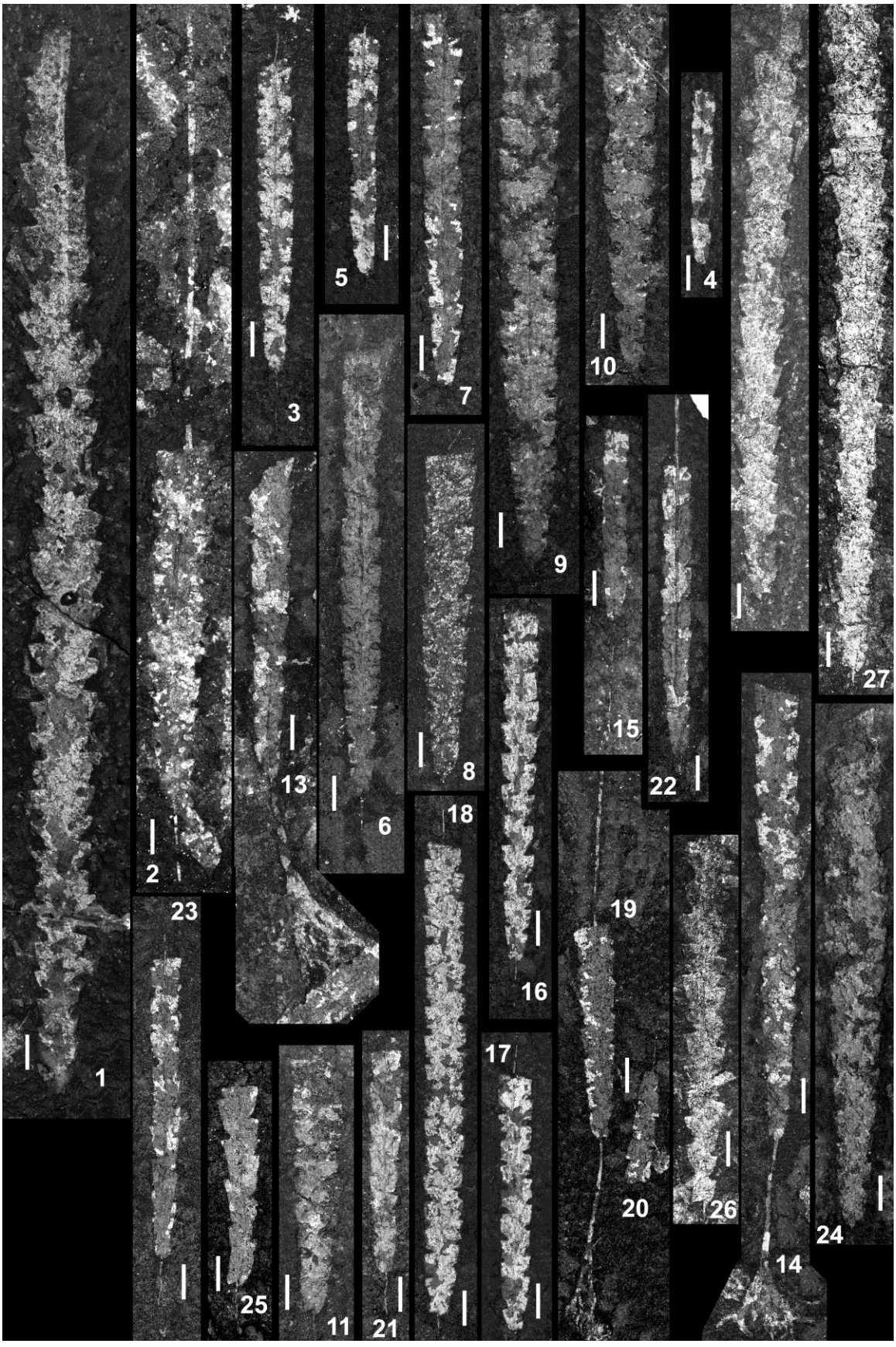
1
2
3
4
5
6
7
8
9
10
11
13
14
15
16
17
18
19
20
21
22
23
24
25
26
27

Plate 32

Figure 1b x10; all other figures x6

Fig.	Species	Level (m)	Slab	#
1a	*Normalograptus*? *rhizinus* (Li & Yang)	33.37	444	6
1b	*Normalograptus*? *rhizinus* (Li & Yang)	33.37	444	6
2	*Normalograptus*? *rhizinus* (Li & Yang)	33.37	444	9
3	*Normalograptus*? *rhizinus* (Li & Yang)	33.37	444	3
4	*Avitograptus avitus* (Davies)	33.37	052b	
5	*Avitograptus avitus* (Davies)	33.37	40	1
6	*Normalograptus*? *rhizinus* (Li & Yang)	34.11	74	
7	*Normalograptus*? *rhizinus* (Li & Yang)	34.11	74	
8	*Avitograptus avitus* (Davies)	34.11	062a	
9	*Avitograptus avitus* (Davies)	34.11	058b	

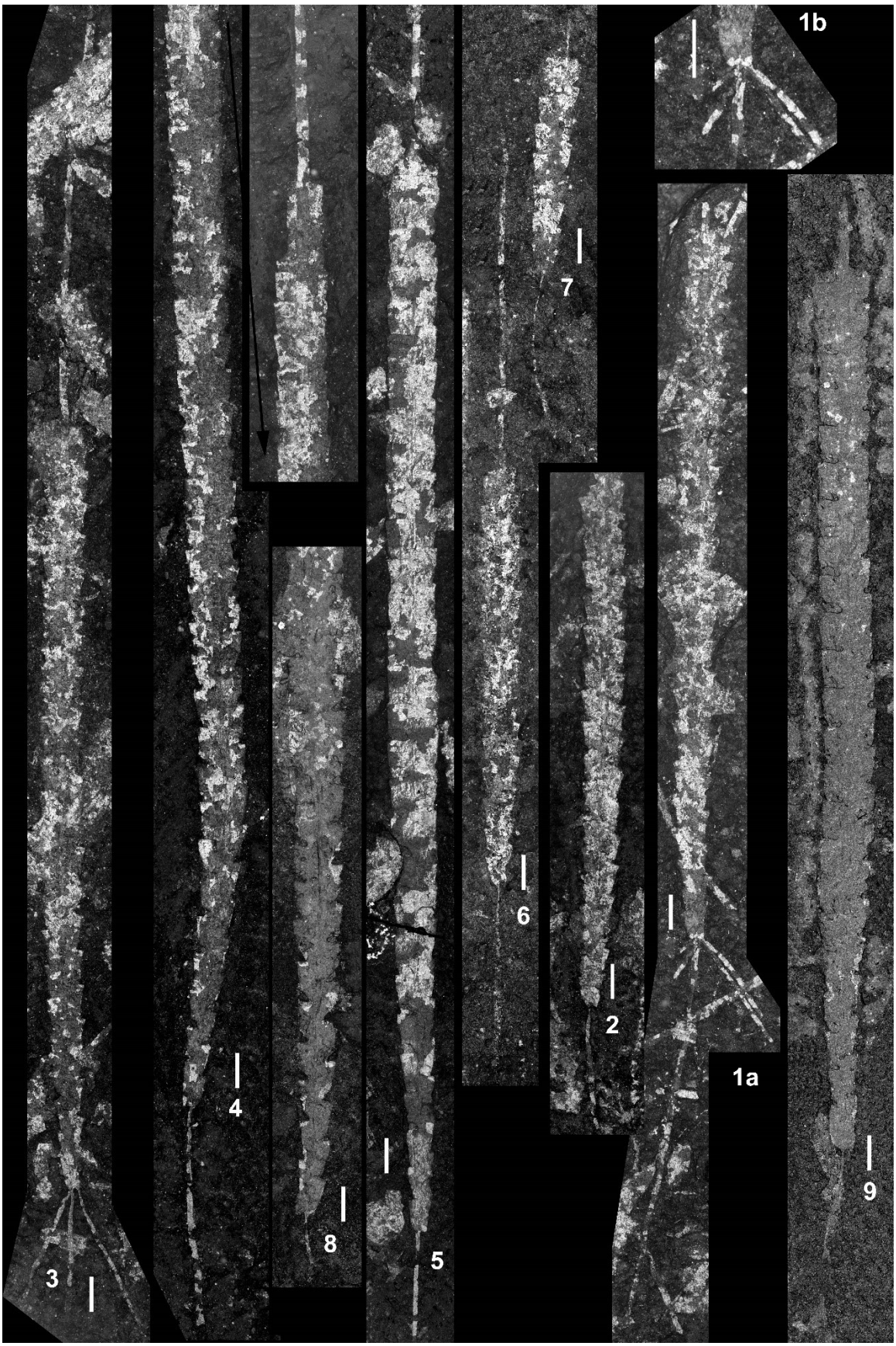
1b
7
6
2
1a
4
8
5
9
3

Plate 33

Figure 24 x10; all other figures x6

Fig	Species	Level (m)	Slab	#
1	*Neodiplograptus clavatus* (Yu et al.)	32.97	012a	
2	*Neodiplograptus clavatus* (Yu et al.)	32.97	020c	
3	*Neodiplograptus xixiangensis* (Yu et al.)	34.11	DL[1]	1
4	*Neodiplograptus xixiangensis* (Yu et al.)	34.11	DL[1]	Purple
5	*Neodiplograptus shanchongensis* (Li)	33.37	63	
6	*Neodiplograptus shanchongensis* (Li)	33.37	010a	
7	*Neodiplograptus shanchongensis* (Li)	33.37	44	
8	*Neodiplograptus xixiangensis* (Yu et al.)	33.37	64	
9	*Normalo*. aff. *mirnyensis* (Obut & Sobolevskaya)	33.37	64	
10	*Neodiplograptus xixiangensis* (Yu et al.)	34.11	26b	1
11	*Neodiplograptus xixiangensis* (Yu et al.)	34.11	048a	
12	*Neodiplograptus xixiangensis* (Yu et al.)	34.11	040a	Purple
13	*Neodiplograptus xixiangensis* (Yu et al.)	34.11	26b	2
14	*Metabolograptus*? sp.	36.30	007c	1
15	*Metabolograptus*? sp.	36.30	025b	2
16	*Metabolograptus*? sp.	36.30	025b	1
17	*Metabolograptus*? sp.	36.30	025c	3
18	*Neodiplograptus clavatus* (Yu et al.)	32.97	45f	
19	*Neodiplograptus* cf. *clavatus* (Yu et al.)	32.97	22	8
20	*Glyptograptus* sp.	32.97	013b	
21	*Neodiplograptus* cf. *clavatus* (Yu et al.)	32.97	22	3
22	*Korenograptus jiangxiensis* (Fang et al.)	32.97	016f	1
23	*Korenograptus jiangxiensis* (Fang et al.)	32.97	016g	
24	*Korenograptus jiangxiensis* (Fang et al.)	33.37	011a	2
25	*Paramplexo. madernii* (Koren' & Mikhailova)	34.11	74	1
26	*Paramplexo. madernii* (Koren' & Mikhailova)	35.15	008b	
27	*Paramplexo. madernii* (Koren' & Mikhailova)	34.11	031b	
28	*Paramplexo.* aff. *madernii* (Koren' & Mikhailova)	32.97	016e	
29	*Korenograptus laciniosus* (Churkin & Carter)	32.84	005a	

[1]DL = Damaged label

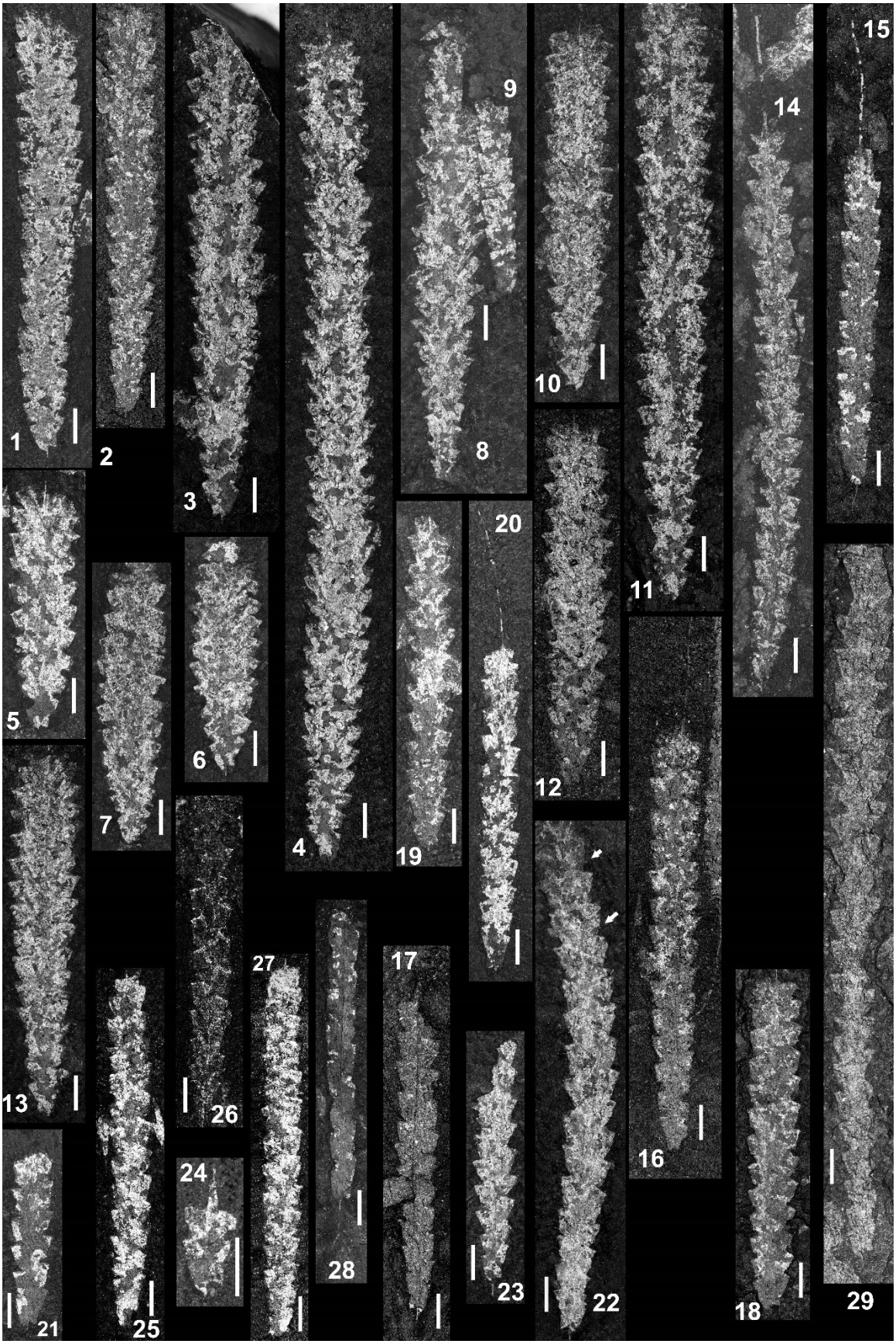
1
2
3
4
5
6
7
8
9
10
11
12
13
14
15
16
17
18
19
20
21
22
23
24
25
26
27
28
29

Plate 34

All figures x6

Fig.	Species	Level (m)	Slab	#
1	*Normalo.* aff. *mirnyensis* (Obut & Sobolevskaya)	33.37	44	
2	*Normalo.* aff. *mirnyensis* (Obut & Sobolevskaya)	32.97	OWL	
3	*Korenograptus lungmaensis* (Sun)	32.84	072a	2
4	*Korenograptus lungmaensis* (Sun)	32.84	072a	1
5	*Korenograptus lungmaensis* (Sun)	32.84	011a	1
6	*Korenograptus lungmaensis* (Sun)	32.84	91	
7	*Normalograptus*? *transgrediens* (Waern)	32.84	003a	
8	*Korenograptus lungmaensis* (Sun)	32.84	21	
9	*Korenograptus lungmaensis* (Sun)	32.84	003b	1
10	*Metabolograptus*? sp.	36.30	Scott	1
11	*Metabolograptus*? sp.	36.30	BBB	5
12	*Metabolograptus*? sp.	36.30	028a	
13	*Neodiplograptus clavatus* (Yu et al.)	32.97	13b (inside)	
14	*Normalograptus*? *transgrediens* (Waern)	32.84	17	
15	*Korenograptus lungmaensis* (Sun)	32.84	010a	1
16	*Normalograptus*? *transgrediens* (Waern)	32.84	052b	
17	*Normalograptus*? *transgrediens* (Waern)	32.84	68	
18	*Glyptograptus*? sp. 1	32.97	11	
19	*Glyptograptus*? sp. 1	?	Red	
20	*Glyptograptus*? sp. 1	?		
21	*Glyptograptus*? sp. 1	32.97	016A	

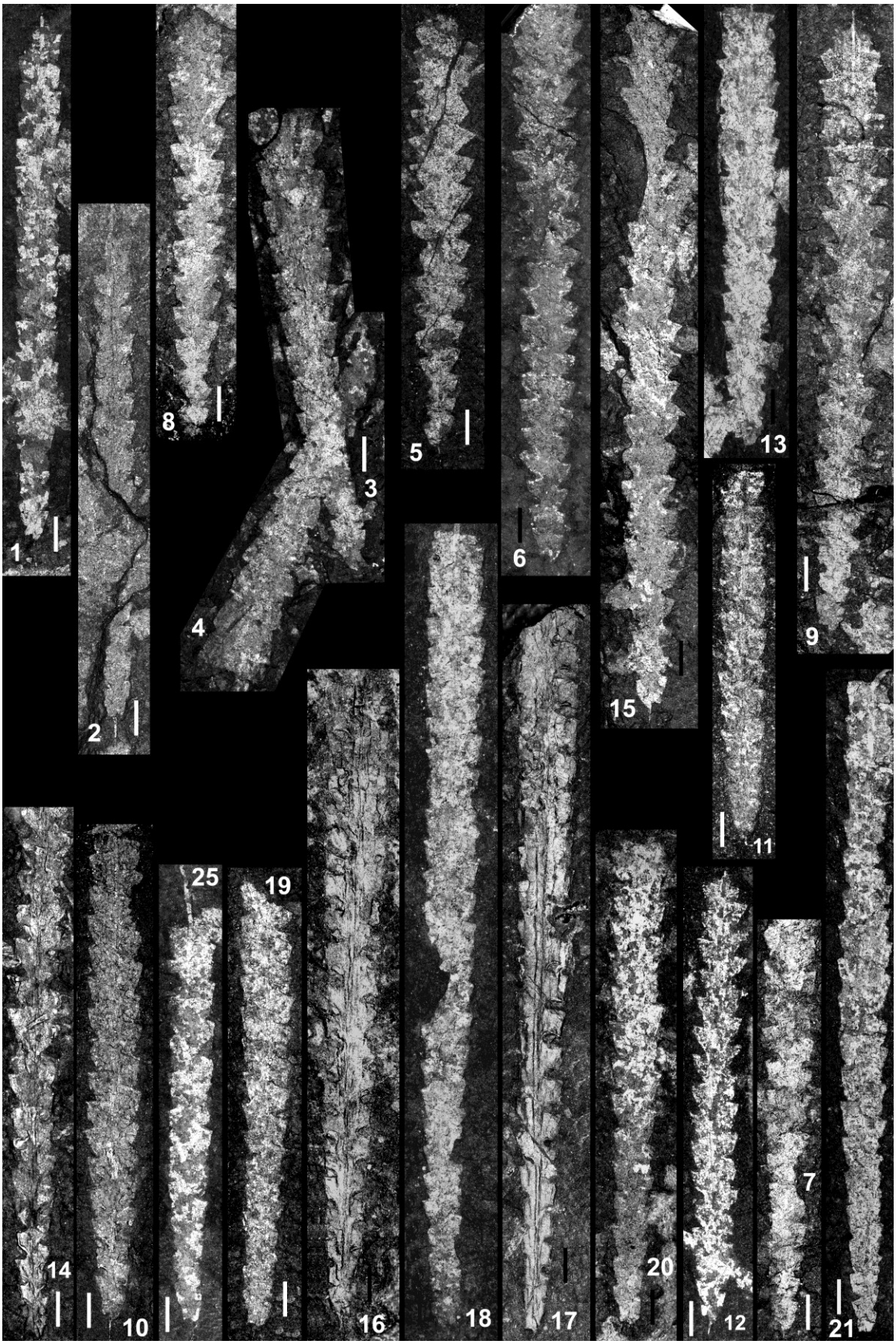
1
2
8
4
3
5
6
15
13
9
11
25
19
14
10
16
18
17
20
12
7
21

Plate 35

All figures x6

Fig.	Species	Level (m)	Slab	#
1	*Glyptograptus*? sp. 1	32.97	008a	1
2	*Glyptograptus*? sp. 1	32.97	003a	
3	*Glyptograptus*? sp. 1	32.97	045z	A
4	*Glyptograptus*? sp. 1	32.97	xxx	1
5	*Glyptograptus*? sp. 1	32.97	010a	
6	*Glyptograptus*? sp. 1	32.97	70	D
7	*Glyptograptus*? sp. 1	32.97	70	2
8	*Meta. parvulus* (Lapworth)	32.84	10	1
9	*Meta. parvulus* (Lapworth)	32.84	10	5
10	*Meta. parvulus* (Lapworth)	32.84	10	7
11	*Meta. parvulus* (Lapworth)	32.84	10	8
13	*Meta. parvulus* (Lapworth)	32.84	002c	
14	*Meta. parvulus* (Lapworth)?	32.84	10	6
15	*Meta. parvulus* (Lapworth)	32.84	33	1
16	*Meta. parvulus* (Lapworth)	32.84	33	2
17	*Normalo.*? *transgrediens* (Waern)	32.84	33	3
18	*Meta. parvulus* (Lapworth)	32.84	008a	
19	*Meta. parvulus* (Lapworth)	32.84	76	
20	*Meta. parvulus* (Lapworth)	32.84	76	
21	*Meta. parvulus* (Lapworth)	32.84	76 (inside)	
22	*Meta. parvulus* (Lapworth)	32.84	76 (inside)	
23	*Metabolograptus*? sp.	36.30	026a	2
24	*Metabolograptus*? sp.	36.30	28a	1
25	*Metabolograptus*? sp.	36.30	BBB	2a
26	*Metabolograptus*? sp.	36.30	BBB	2b
27	*Koreno. jiangxiensis* (Fang et al.)	33.37	025a1	

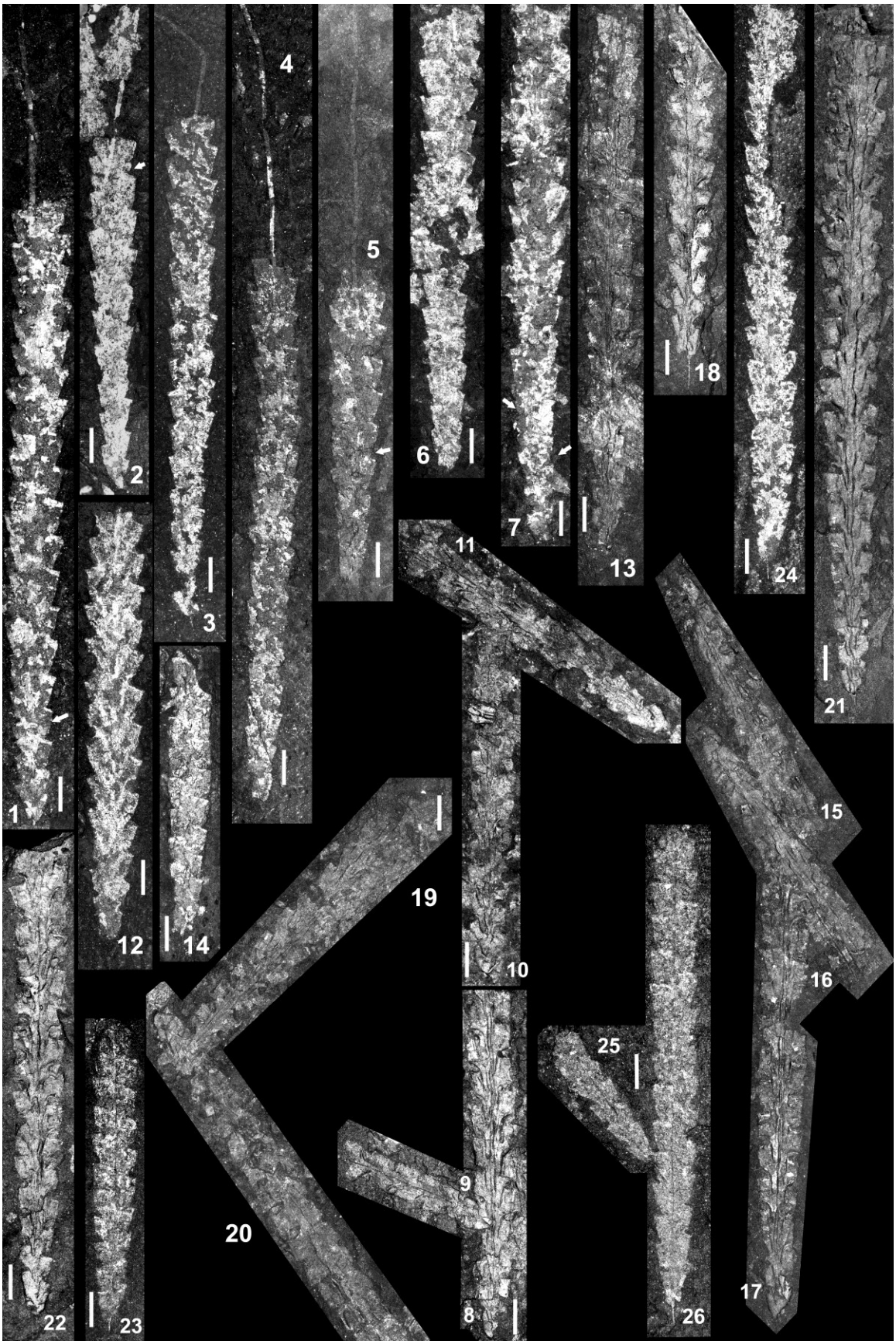
1
2
3
4
5
6
7
8
9
10
11
12
13
14
15
16
17
18
19
20
21
22
23
24
25
26

Plate 36

All figures x6

Fig.	Species	Level (m)	Slab	#
1	*Korenograptus jiangxiensis* (Fang et al.)	33.37	052bx	red
2	*Glyptograptus*? sp. 1	32.97	020a[1]	
3	*Neodiplograptus clavatus* (Yu et al.)?	32.84	FOX	
4	*Korenograptus jiangxiensis* (Fang et al.)	33.37	77	
5	*Paramplexo. madernii* (Koren' & Mikhailova)	33.37	42	
6	*Korenograptus jiangxiensis* (Fang et al.)	33.37	052bx	
7	*Neodiplograptus shanchongensis* (Li)	ca. 34.11	2	
8	*Neodiplograptus shanchongensis* (Li)	ca. 34.11	1	
9	*Neodiplograptus shanchongensis* (Li)	ca. 34.11	3	
10	*Neodiplograptus shanchongensis* (Li)	ca. 34.11	4	
11	*Neodiplograptus shanchongensis* (Li)	ca. 34.11	5	
12	*Korenograptus jiangxiensis* (Fang et al.)	34.11	23	
13	*Neodiplograptus shanchongensis* (Li)	ca. 34.11	6	
14	*Neodiplograptus clavatus* (Yu et al.)	ca. 34.11	8	
15	*Neodiplograptus clavatus* (Yu et al.)	ca. 34.11	9	
16	*Korenograptus jiangxiensis* (Fang et al.)	33.37	77x	

[1]Newly split 'inside' surface

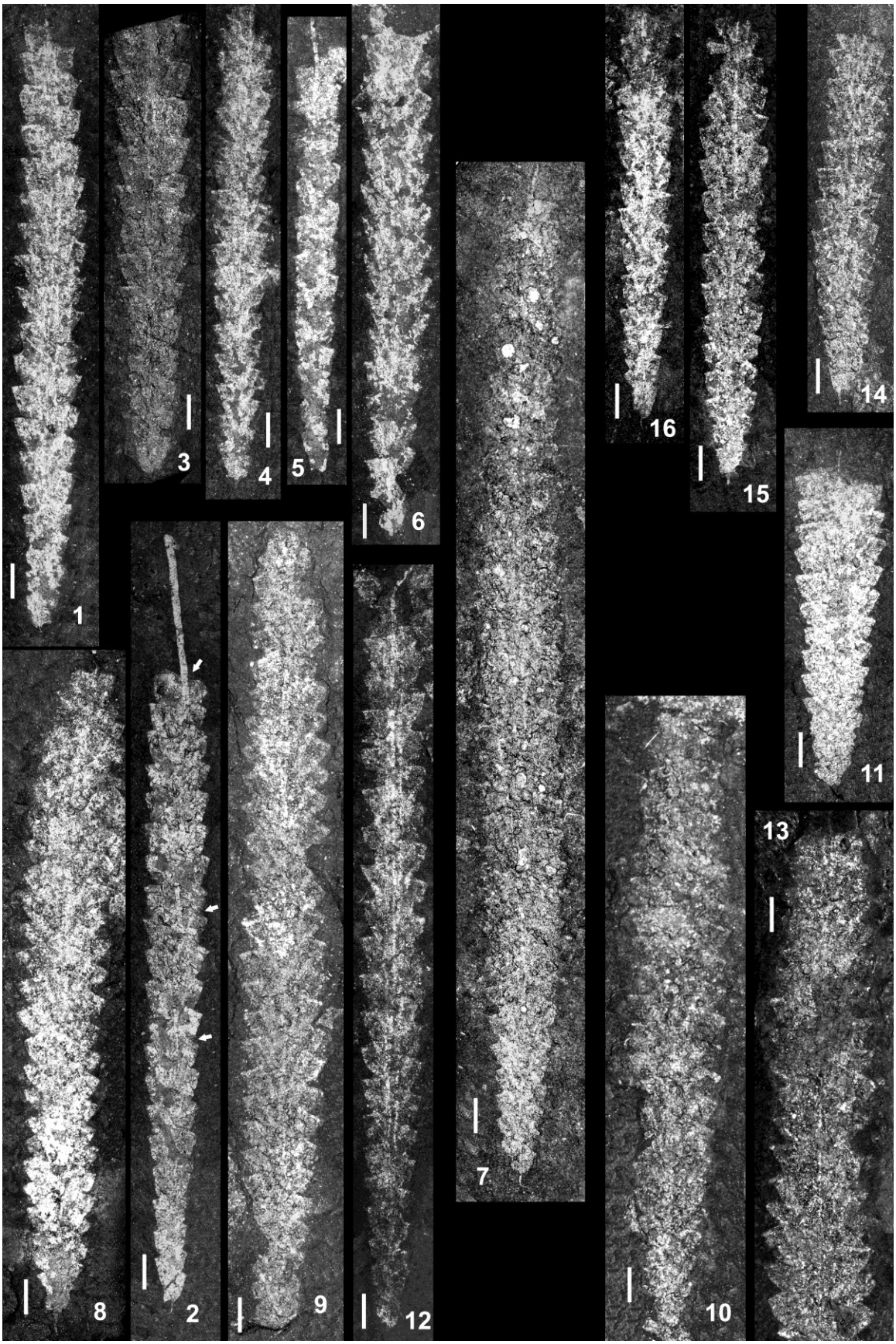
1
3
4
5
6
16
15
14
11
13
7
8
2
9
12
10

Plate 37

Figure 23b x12; all other figures x6

Fig.	Species	Level (m)	Slab	#
1	*Korenograptus laciniosus* (Churkin & Carter)	32.84	22	5
2	*Korenograptus laciniosus* (Churkin & Carter)	32.84	22	6
3	*Korenograptus laciniosus* (Churkin & Carter)	32.84	100b	2
4	*Korenograptus laciniosus* (Churkin & Carter)	32.84	100b	1
5	*Normalo.* aff. *mirnyensis* (Obut & Sobolevskaya)	ca. 34.11	A9	
6	*Normalo.* aff. *mirnyensis* (Obut & Sobolevskaya)	ca. 34.11	A8	
7	*Normalo.* aff. *mirnyensis* (Obut & Sobolevskaya)	ca. 34.11	A5	
8	*Normalo.* aff. *mirnyensis* (Obut & Sobolevskaya)	ca. 34.11	A4	
9	*Korenograptus* sp. 1	35.15	009a	
10	*Korenograptus* sp. 1	34.11	063A	
11	*Korenograptus* sp. 1	35.15	34	
12	*Metabolograptus parvulus* (Lapworth)?	32.84	20 or 30	
13	*Normalograptus*? *minor* (Huang)	33.37	016b	
14	*Normalo.* aff. *mirnyensis* (Obut & Sobolevskaya)	34.11	3	
15	*Metabolograptus*? sp.	36.30	25c	4
16	*Metabolograptus*? sp.	36.30	26a	4
17	*Metabolograptus*? sp.	36.30	26a	8
18	*Neodiplograptus* cf. *clavatus* (Yu et al.)	33.37	37	
19	*Normalograptus*? *transgrediens* (Waern)?	32.84	090x	
20	*Korenograptus laciniosus* (Churkin & Carter)	32.84	33	
21	*Metabolograptus parvulus* (Lapworth)	32.84	96	
22	*Neodiplograptus clavatus* (Yu et al.)	33.37	34	
23a	*Paramplexo.* aff. *madernii* (Koren' & Mikhailova)	33.37	72CP	
23b	*Paramplexo.* aff. *madernii* (Koren' & Mikhailova)	33.37	72CP	
24	*Avitograptus avitus* (Davies)	32.97	046a	
25	*Normalograptus*? *transgrediens* (Waern)	32.84	005a	


9
4
8
10
11
15
19
2
3
23a
7
5
14
24
18
12
17
13
6
16
21
20
23b
25
22

Plate 38

Figure 23b x12; all other figures x6

Fig.	Species	Level (m)	Slab	#
1	*Avitograptus avitus* (Davies)	32.97	TTT	
2	*Glyptograptus*? sp. 1	32.97	4	
3	*Normalograptus*? *transgrediens* (Waern)	32.84	CCC	
4	*Korenograptus laciniosus* (Churkin & Carter)	32.84	LLL	
5	*Paramplexo.* aff. *madernii* (Koren' & Mikhailova)	34.11	6	
6	*Neodiplograptus xixiangensis* (Yu et al.)	34.11	ABC	
7	*Neodiplograptus clavatus* (Yu et al.)	33.37	73	
8	*Normal.* aff. *mirnyensis* (Obut & Sobolevskaya)	32.97	030a	
9	*Paramplexo.* aff. *madernii* (Koren' & Mikhailova)	ca. 34.11	ABC	
10	*Korenograptus laciniosus* (Churkin & Carter)	32.84	7	1
11	*Korenograptus laciniosus* (Churkin & Carter)	32.84	7	3
12	*Korenograptus laciniosus* (Churkin & Carter)	32.84	7	4
13	*Neodiplograptus* cf. *clavatus* (Yu et al.)	32.97	19	1
14	*Neodiplograptus* cf. *clavatus* (Yu et al.)	32.97	37	
15	*Neodiplograptus* cf. *clavatus* (Yu et al.)	32.97	43	1
16	*Korenograptus jiangxiensis* (Fang et al.)	32.97	43	2
17	*Neodiplograptus* cf. *clavatus* (Yu et al.)	32.97	007b	3
18	*Neodiplograptus* cf. *clavatus* (Yu et al.)	32.97	007b	2
19	*Neodiplograptus* cf. *clavatus* (Yu et al.)	32.97	007b	1
20	*Neodiplograptus* cf. *clavatus* (Yu et al.)	32.97	007b	4
21	*Glyptograptus*? sp. 2	33.37	5	
22	*Neodiplograptus* cf. *clavatus* (Yu et al.)	33.37	5	1
23	*Neodiplograptus* cf. *clavatus* (Yu et al.)	33.37	39a	1
24	*Neodiplograptus* cf. *clavatus* (Yu et al.)	33.37	39a	2
25	*Neodiplograptus* cf. *clavatus* (Yu et al.)	33.37	48	1
26	*Glyptograptus* sp.	33.37	8	
27	*Korenograptus laciniosus* (Churkin & Carter)	34.11	030a	
28	*Korenograptus laciniosus* (Churkin & Carter)	32.97	TA	
29	*Neodiplograptus* cf. *clavatus* (Yu et al.)	32.97	001b	1
30	*Korenograptus laciniosus* (Churkin & Carter)	32.97	001b	
31	*Neodiplograptus* cf. *clavatus* (Yu et al.)	33.37	48	1

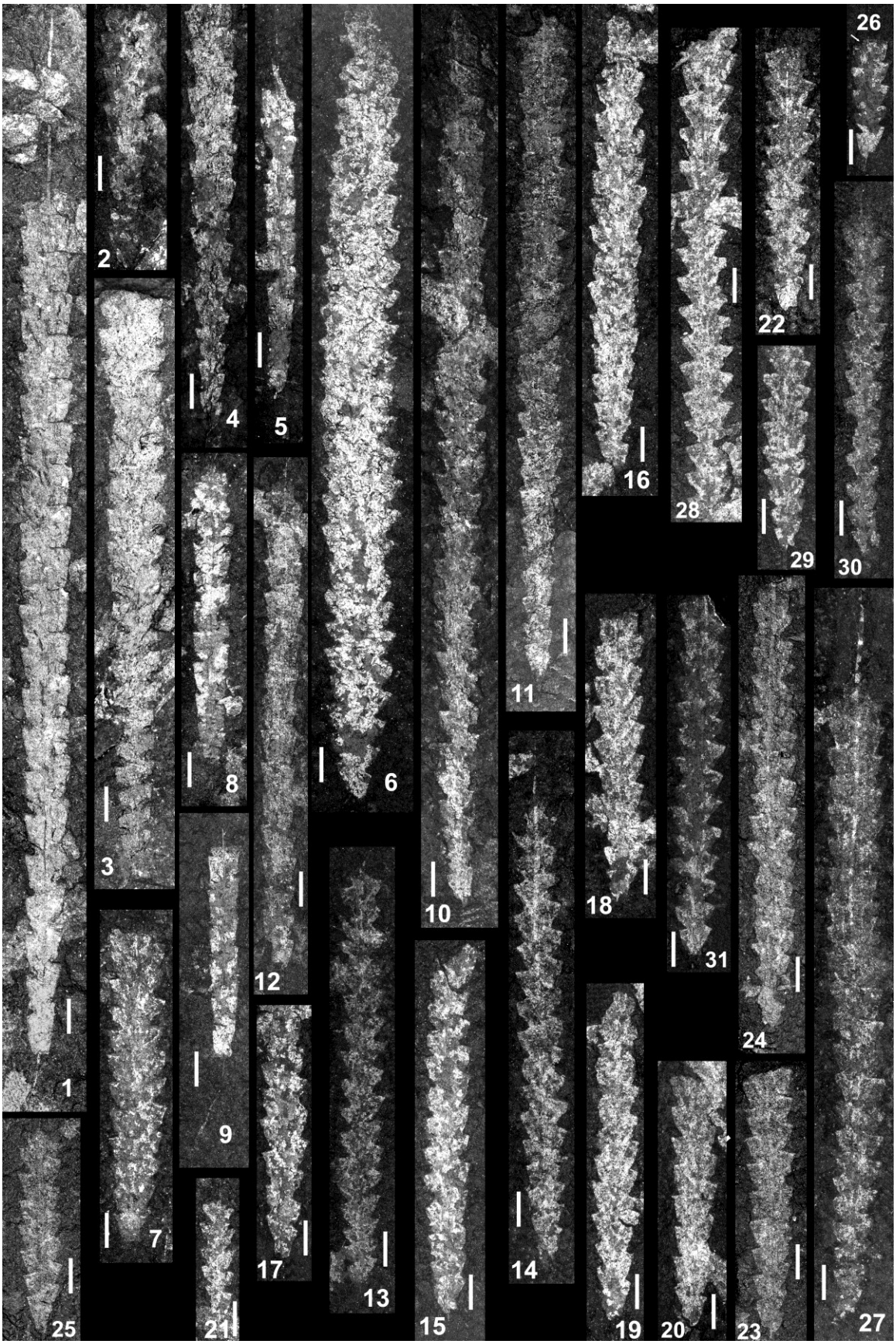
1
2
3
4
5
6
7
8
9
10
11
12
13
14
15
16
17
18
19
20
21
22
23
24
25
26
27
28
29
30
31

Plate 39

All figures x6

Fig.	Species	Level (m)	Slab	#
1	*Normalo. imperfectus* (Legrand)?	41.66	027x	1
2	*Normalo.*? aff. *nanjingensis* (Chen & Lin)	41.66	018d	
3	*Normalo. ajjeri* (Legrand) Form B	38.62	27a	3
4	*Normalo.*? aff. *nanjingensis* (Chen & Lin)	41.66	5	1
5	*Normalo.*? aff. *nanjingensis* (Chen & Lin)	39.59	42	
6	*Normalo. ajjeri* (Legrand) Form B	38.62	27a	1
7	*Normalo. imperfectus* (Legrand)?	41.66	27	3
8	*Normalo. ajjeri* (Legrand) Form A	45.30 (06)	106	
9	*Normalo.*? *nanjingensis* (Chen & Lin)	37.43	12	
10	*Normalo. ajjeri* (Legrand) Form A	45.00	105	
11	*Normalo. ajjeri* (Legrand) Form A	45.38	19	
12	*Normalo. ajjeri* (Legrand) Form A	45.38	002b	
13	Normalo. ajjeri (Legrand) Form A	45.00	105	
14	*Normalo. skeliphrus* (Koren' & Melchin)	39.30	027c	
15	*Normalo. ajjeri* (Legrand) Form A	44.02	034a	7
16	*Normalo. mirnyensis* (Obut & Sobolevskaya)	38.19	064a	
17	*Normalo. skeliphrus* (Koren' & Melchin)	37.43	EEE	2
18	*Normalo. skeliphrus* (Koren' & Melchin)	37.43	EEE	1
19	*Normalo.* aff. *angustus* (Perner)	38.62	27a	
20	*Normalo.* aff. *angustus* (Perner)	39.30	049b	2
21	*Normalo.* aff. *angustus* (Perner)	39.30	049b	1
22	*Normalo. anjiensis* (Yang)	38.19	087a	
23	*Normalo. skeliphrus* (Koren' & Melchin)?	38.19	086b	
24	*Normalo.* cf. *transgrediens* (Waern)?	49.17	17	
25	*Normalo. ajjeri* (Legrand) Form A	45.00	105	

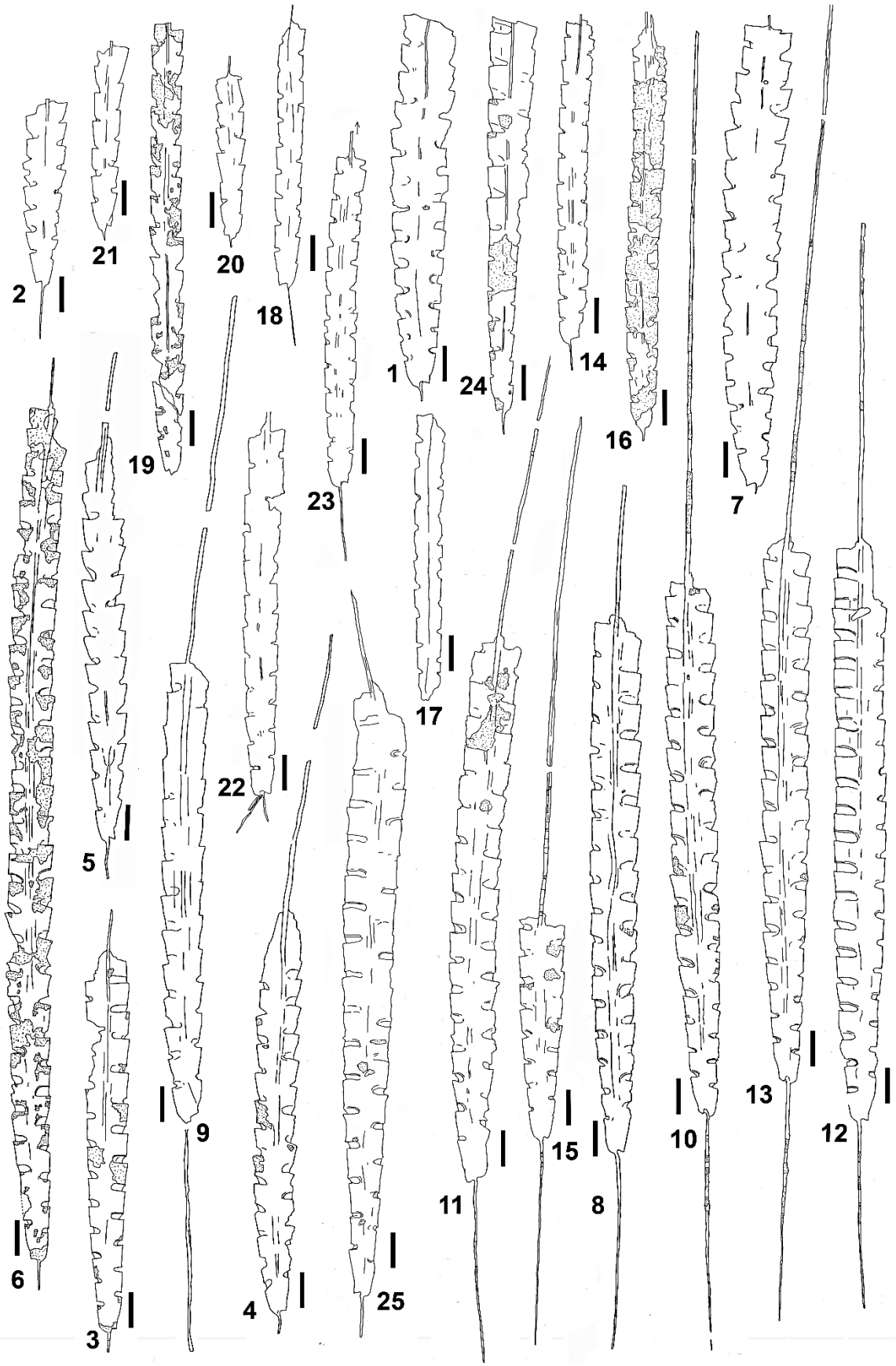
2
21
20
18
1
24
14
16
7
19
23
17
22
5
9
11
15
8
10
13
6
3
4
25
12

Plate 40

All figures x6

Fig.	Species	Level (m)	Slab	#
1	*Rickardsograptus lautus* (Štorch and Feist)	49.17	025b	1
2	*Rickardsograptus lautus* (Štorch and Feist)	46.00	0038b	1
3	*Rickardsograptus* aff. *lautus* (Štorch & Feist)	45.38	"b"	1
4	*Rickardsograptus* aff. *lautus* (Štorch & Feist)	45.38	050b	1
5	*Rickardsograptus lautus* (Štorch and Feist)	46.00	001c	1
6	*Rickardsograptus lautus* (Štorch and Feist)	46.00	25	2
7	*Rickardsograptus* aff. *lautus* (Štorch & Feist)	45.38	12/"E"	1
8	*Rickardsograptus lautus* (Štorch and Feist)	49.17	036a	1
9	*Rickardsograptus* aff. *lautus* (Štorch & Feist)	45.38	?	
10	*Rickardsograptus lautus* (Štorch and Feist)?	49.17	040c	1
11	*Normalograptus ajjeri* (Legrand) Form B	39.59	53	1
12	*Paramplexo. wuningensis* (Fang et al.)	38.19	077B	1
13	*Paramplexo. wuningensis* (Fang et al.)	37.43	036-2	2
14	*Paramplexo. paucispinus* (Li)	37.43	11	1
15	*Paraclimac. obesus* (Churkin & Carter)	46.00	036b	
16	*Hirsuto. longispinosus* Koren' & Rickards	42.65	1	
17	*Normalograptus ajjeri* (Legrand) Form B	39.59	10_2	
18	*Normalograptus ajjeri* (Legrand) Form B	39.59	50x	

Note: Arrow on plate indicates that specimen continues beyond illustrated portion.

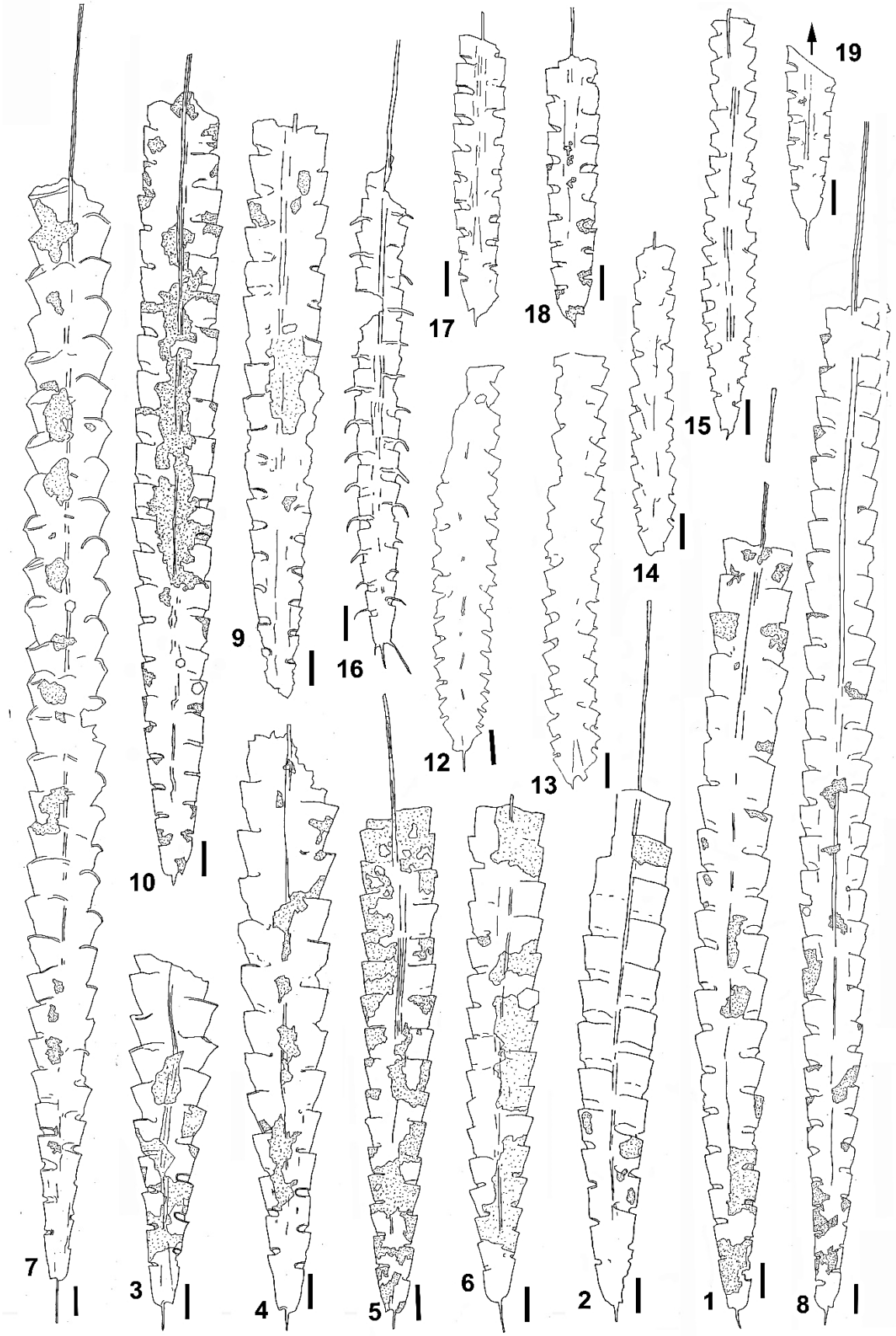
7
10
9
16
17
18
19
15
14
12
13
3
4
5
6
2
1
8

Plate 41

All figures x6

Fig.	Species	Level (m)	Slab	#
1	*Normalograptus*? *radicatus* (Chen & Lin)	39.30	57	2
2	*Normalograptus*? *radicatus* (Chen & Lin)	39.30	46b3	
3	*Normalograptus*? *radicatus* (Chen & Lin)	?		
4	*Normalograptus*? *radicatus* (Chen & Lin)	?		
5	*Normalograptus gnaurus* (Chen & Lin)	39.59	022b	1
6	*Normalograptus* cf. *ajjeri* (Legrand)	45.38	"b"	
7	*Normalo.* aff. *rhizinus* (Lee & Yang)	41.66	049c	
8	*Normalo.* aff. *rhizinus* (Lee & Yang)	41.66	021a	
9	*Normalo. gnaurus* (Chen & Lin)	39.59	025b2 (2?)	
10	*Normalo.* aff. *rhizinus* (Lee & Yang)	41.66	34	
11	*Normalo.* aff. *rhizinus* (Lee & Yang)	41.66	054a	1
12	*Normalo.* aff. *rhizinus* (Lee & Yang)	41.66	63	1

Note: Arrow on plate indicates that specimen continues beyond illustrated portion.


3
2
4
1
5
9
8
10
11
12
6
7

Plate 42

All figures x6

Fig.	Species	Level (m)	Slab	#
1	*Korenograptus bifurcus* (Ye)	39.30	62.2	
2	*Normalograptus rectangularis* (McCoy)	49.19	005b	
3	*Korenograptus* sp. 1	38.19	1100	
4	*Korenograptus* sp. 1	38.19?	ABC	
5	*Korenograptus* sp. 1	39.59	1000	
6	*Korenograptus lanpherei* (Churkin & Carter)	46.00	AAA	
7	*Korenograptus* sp. 3	44.02	44	
8	*Korenograptus bifurcus* (Ye)	40.5 (ISO)		
9	*Korenograptus lanpherei* (Churkin & Carter)	46.00	001c	2
10	*Korenograptus lanpherei* (Churkin & Carter)	47.00?	1000	
11	*Neodiplograptus* sp. 2	48.10	030a	
12	*Neodiplograptus* sp. 2	48.10	22	
13	*Koreno. ugurensis* (Koren' and Melchin)?	38.19	3	
14	*Koreno. ugurensis* (Koren' and Melchin)	48.10	009b	
15	*Koreno. ugurensis* (Koren' and Melchin)	46.00	AAA	
16	*Metaclimacograptus hughesi* (Nicholson)	49.17	004b	
17	*Korenograptus* sp. 2	45.30 (06)	101	

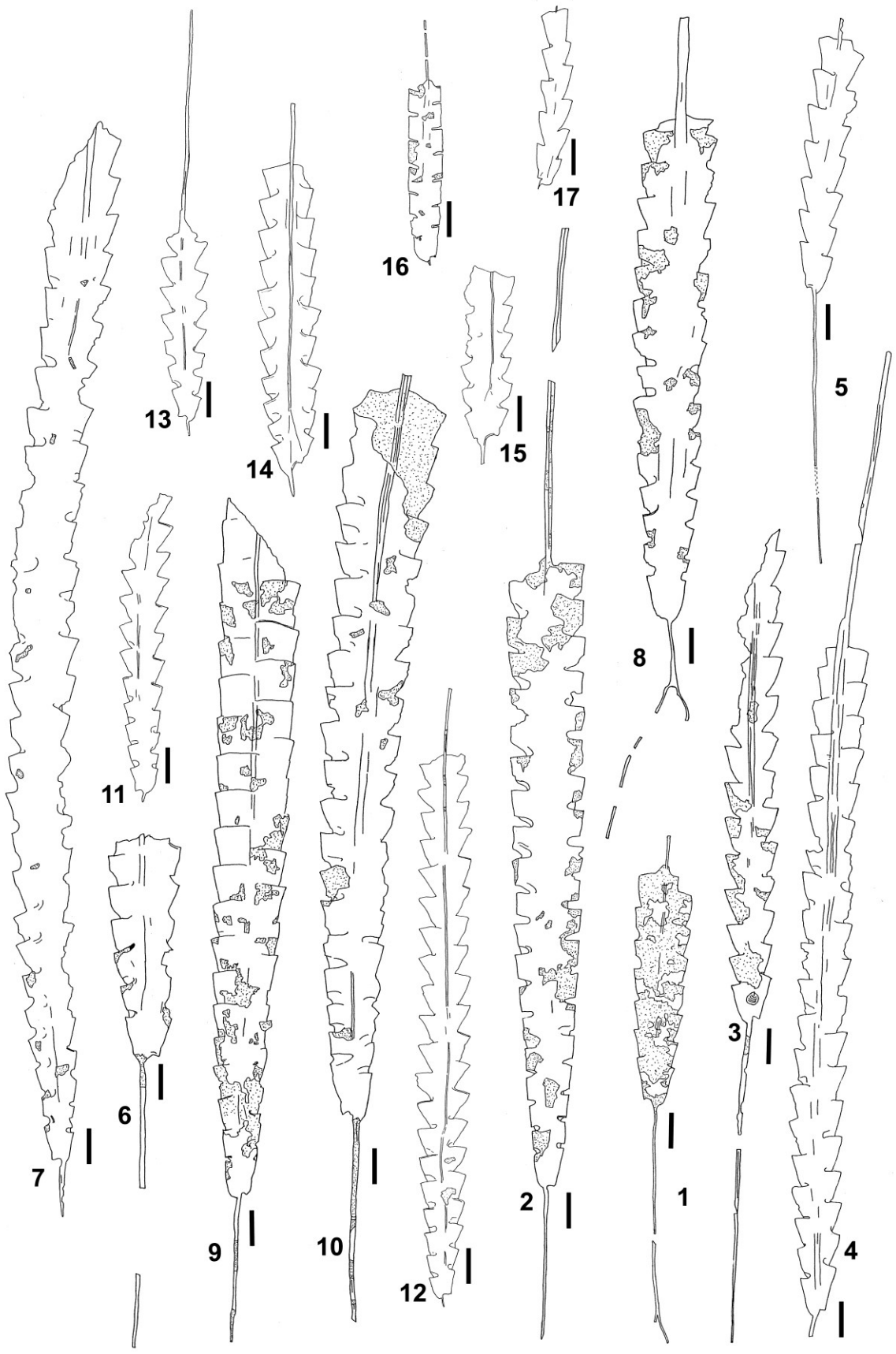
1
2
3
4
5
6
7
8
9
10
11
12
13
14
15
16
17

Plate 43

All figures x6

Fig.	Species	Level (m)	Slab	#
1	*Hirsutograptus tuberculatus* (Nicholson)	39.59	2000	
2	*Hirsutograptus tuberculatus* (Nicholson)	39.59	021c	
3	*Hirsutograptus* sp.	40.5 or 39.59	3000	
4	*Hirsutograptus tuberculatus* (Nicholson)	39.59	3	
5	*Hirsutograptus tuberculatus* (Nicholson)	39.59	30	
6	*Rickardsograptus magnus* (Churkin & Carter)	49.17	046b	
7	*Hirsutograptus* sp.	41.66	44a	
8	*Akidograptus ascensus* Davies	45.38	46	
9	*Akidograptus ascensus* Davies	37.43	UL	
10	*Akidograptus ascensus* Davies	38.62	15b	
11	*Akidograptus ascensus* Davies	44.02	11b	1
12	*Parakidograptus acuminatus* (Nicholson)	41.66	059a	2
13	*Parakidograptus acuminatus* (Nicholson)	41.66	059a	1
14	*Normalo.*? aff. *nanjingensis* (Chen & Lin)?	41.66	28b	
15	*Paraclimaco. obesus* (Churkin & Carter)	46.00	035a	1
16	*Paraclimaco. obesus* (Churkin & Carter)	46.00	020/AAA	10
17	*Paraclimaco. obesus* (Churkin & Carter)	46.00?	“FIND CP”	1
18	*Paramplexograptus paucispinus* (Li)	38.62	009b	
19	*Paramplexograptus kiliani* (Legrand)	37.43	34	1
20	*Paramplexograptus wuningensis* (Fang et al.)	37.43	016/1000	1
21	*Paramplexograptus paucispinus* (Li)	38.62	013a	1
22	*Paramplexograptus paucispinus* (Li)	38.19	087a	1
23	*Paramplexograptus paucispinus* (Li)	38.19	087a	2
24	*Paramplexograptus wuningensis* (Fang et al.)	37.43	34	1
25	*Paramplexograptus paucispinus* (Li)	38.62	031a	1

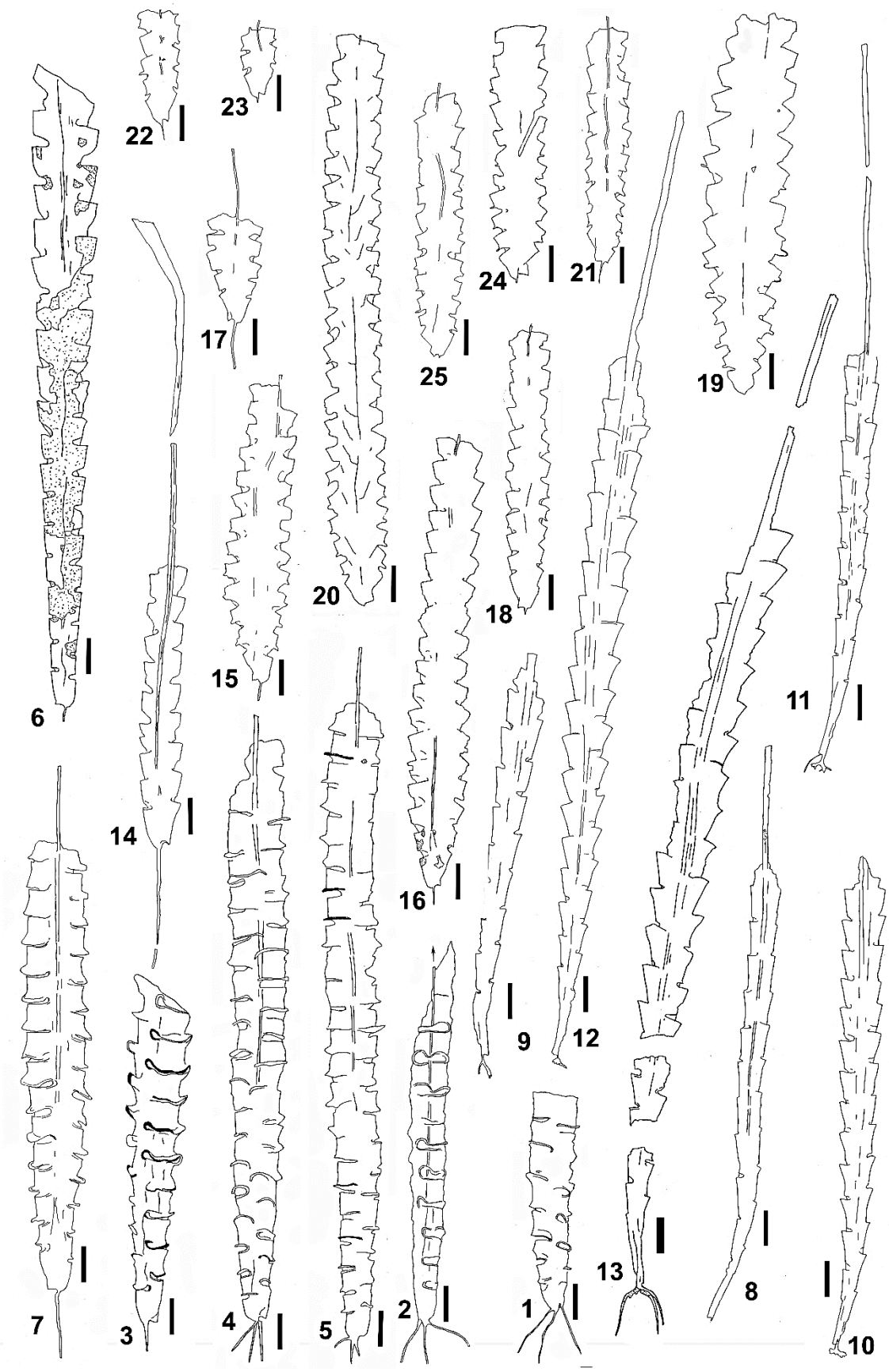
1
2
3
4
5
6
7
8
9
10
11
12
13
14
15
16
17
18
19
20
21
22
23
24
25

Plate 44

Figures 14-16 x10; all other figures x6

Fig.	Species	Level	Slab	#
1	*Rickardsograptus* aff. *lautus* (Štorch & Feist)	45.38	12	1
2	*Rickardsograptus* aff. *lautus* (Štorch & Feist)	45.38	32a	1
3	*Rickardsograptus lautus* (Štorch and Feist)	45.30 (06)	700	1
4	*Rickardsograptus lautus* (Štorch and Feist)	46.00	40	1
5	*Rickardsograptus lautus* (Štorch and Feist)	46.00	25	3
6	*Rickardsograptus lautus* (Štorch and Feist)	46.00	25	2
7	*Rickardsograptus lautus* (Štorch and Feist)	49.17	39	1
8	*Rickardsograptus lautus* (Štorch and Feist)?	49.17	040c	1
9	*Rickardsograptus* aff. *lautus* (Štorch & Feist)	45.38	70	
10	*Rickardsograptus* aff. *lautus* (Štorch & Feist)	45.38	050b	
11	*Dimorphograptus swanstoni* Lapworth	49.50	3	
12	*Rickardsograptus lautus* (Štorch and Feist)	46.00	04b	
13	*Rickardsograptus* aff. *lautus* (Štorch & Feist)	45.38	6	
14	*Paraclimaco. obesus* (Churkin & Carter)	47.00	001b	3 & 2
15	*Paraclimaco. obesus* (Churkin & Carter)	47.00	001b	3 & 2
16	*Paraclimaco. obesus* (Churkin & Carter)	47.00	001b	6
17	*Hirsutograptus* sp.	41.66	23b	

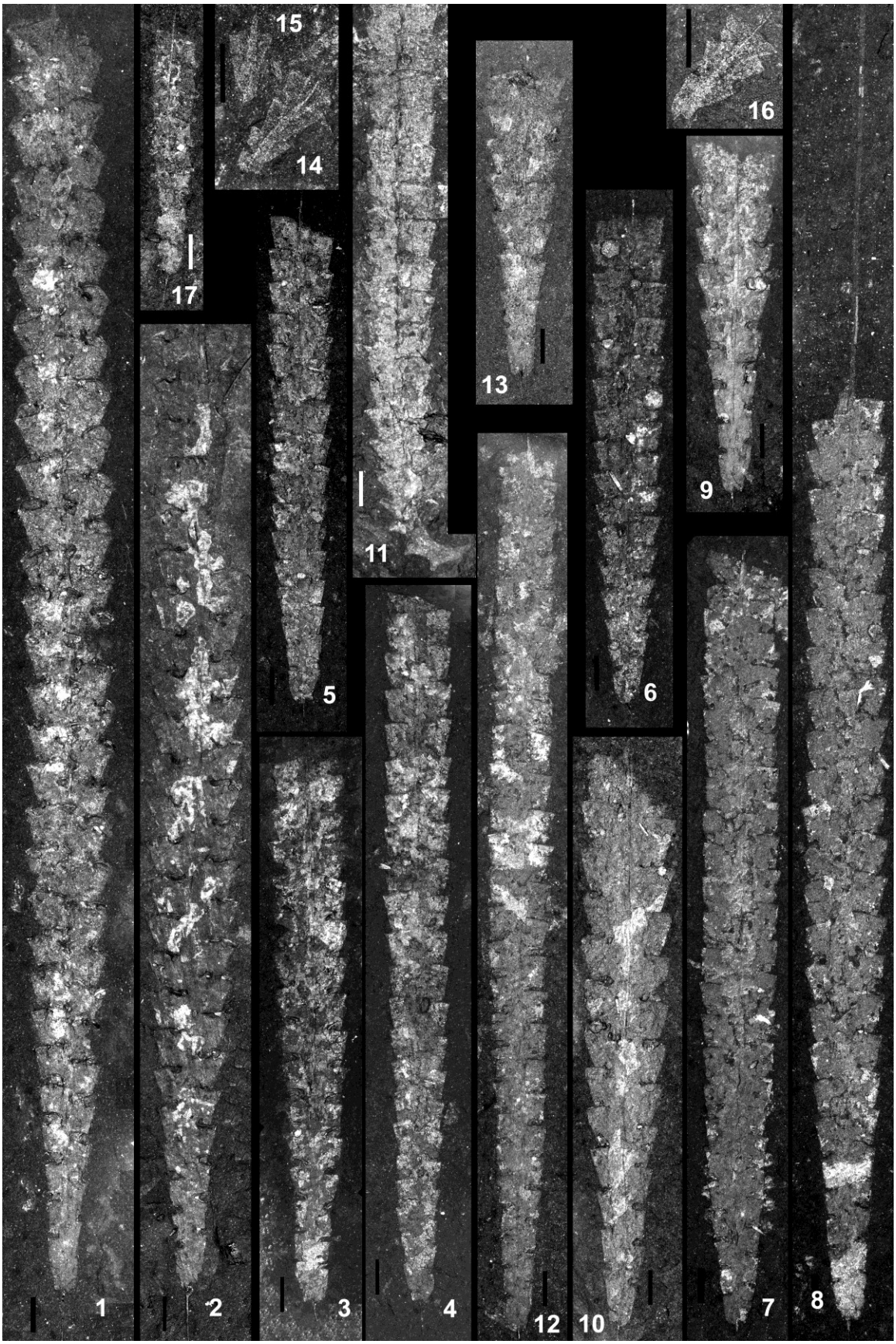
15
14
16
17
13
9
11
5
6
1
2
3
4
12
10
7
8

Plate 45

Figures 18 x15; all other figures x6

Fig.	Species	Level (m)	Slab	#
1	*Normalograptus rectangularis* (McCoy)?	46.00	004b	1
2	*Normalograptus rectangularis* (McCoy)?	45.38	37	1
3	*Normalograptus rectangularis* (McCoy)?	45.38	46	1
4	*Neodiplograptus* sp. 1?	38.90	013b	
5	*Normalograptus rectangularis* (McCoy)	49.17	17	1
6	*Normalograptus rectangularis* (McCoy)	49.17	034c	1
7	*Normalograptus rectangularis* (McCoy)	49.17	005c	1
8	*Korenograptus lanpherei* (Churkin & Carter)	46.00	?	1
9	*Normalograptus gnaurus* (Chen & Lin)	39.59	31	
10	*Korenograptus lanpherei* (Churkin & Carter)	46.00	47	1
11	*Korenograptus lanpherei* (Churkin & Carter)	48.10	005a	
12	*Korenograptus* sp. 1	38.19	1000	
13	*Korenograptus bifurcus* (Ye)	39.30	62.2	1
14	*Normalograptus gnaurus* (Chen & Lin)	39.59	007a	
15	*Normalograptus gnaurus* (Chen & Lin)	40.50	31	
16	*Normalograptus gnaurus* (Chen & Lin)	39.59	16a	
17	*Korenograptus lanpherei* (Churkin & Carter)	46.00	AAA	1
18	*Normalograptus gnaurus* (Chen & Lin)	39.59	xyz	
19	*Neodiplograptus* sp. 1	40.50	15	

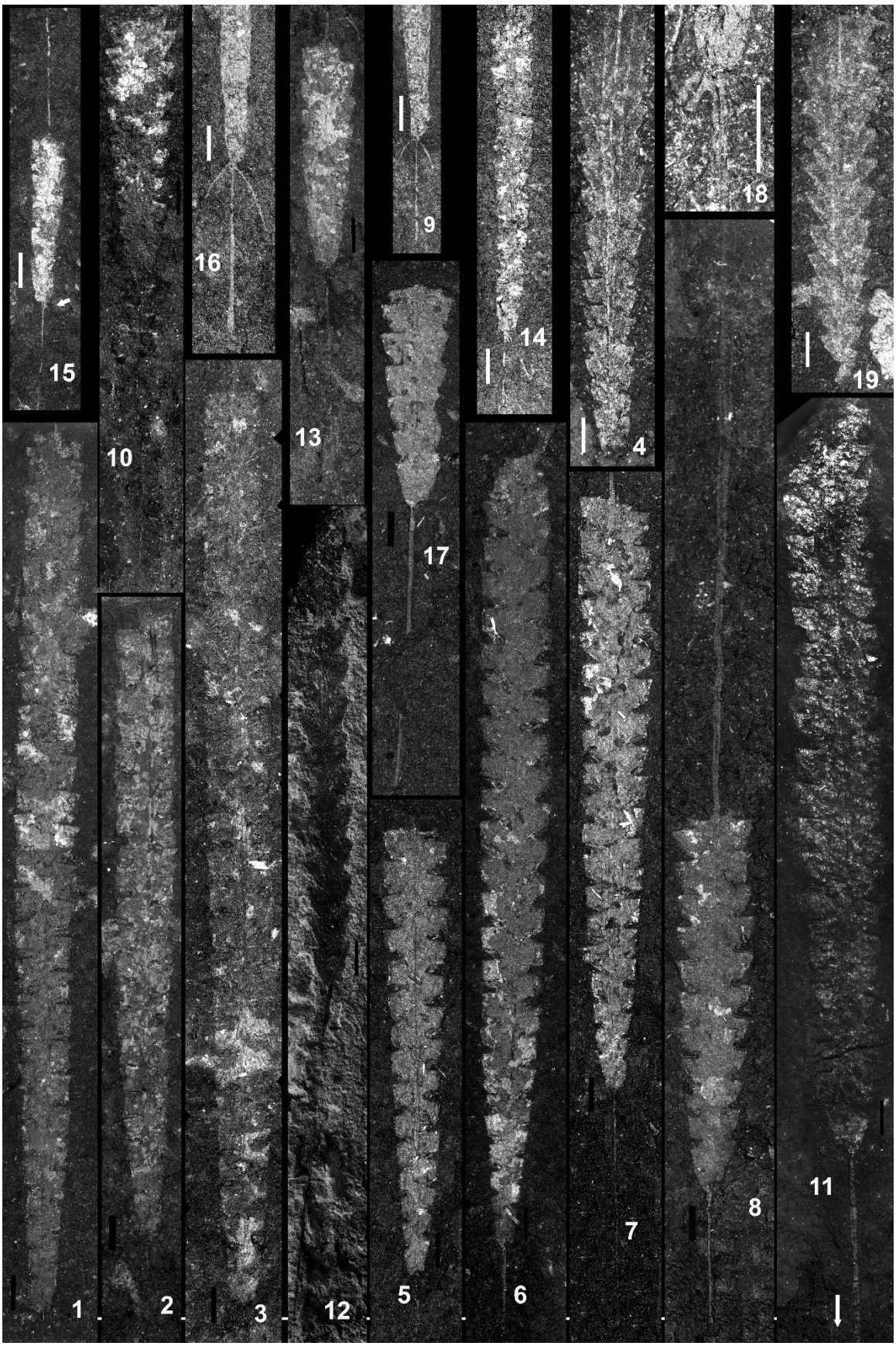
15
16
9
14
18
19
10
13
17
4
1
2
3
12
5
6
7
8
11

Plate 46

Figures 1-3 x5; all other figures x6

Fig.	Species	Level (m)	Slab	#
1	*Neodiplograptus* sp. 1	41.66	057b	
2	*Neodiplograptus* sp. 1	41.66	047x	
3	*Neodiplograptus* sp. 1	41.66	010a	1
4	*Paraclimaco. obesus* (Churkin & Carter)	46.00	AAA	10
5	*Korenograptus* sp. 3	44.02	44	
6	*Korenograptus* sp. 3	49.17	076b	
7	*Korenograptus* sp. 3	49.19	34c	
8	*Korenograptus* sp. 3	49.17	018a	
9	*Korenograptus* sp. 1	39.19	36a	
10	*Neodiplograptus* sp. 1?	37.00 (ISO)		
11	*Paraclimaco. obesus* (Churkin & Carter)	46.00	AAA	7
12	*Paraclimaco. obesus* (Churkin & Carter)	47.00	AAA	1
13	*Paraclimaco. obesus* (Churkin & Carter)	46.00	9	2
14	*Paraclimaco. obesus* (Churkin & Carter)	46.00	9	1

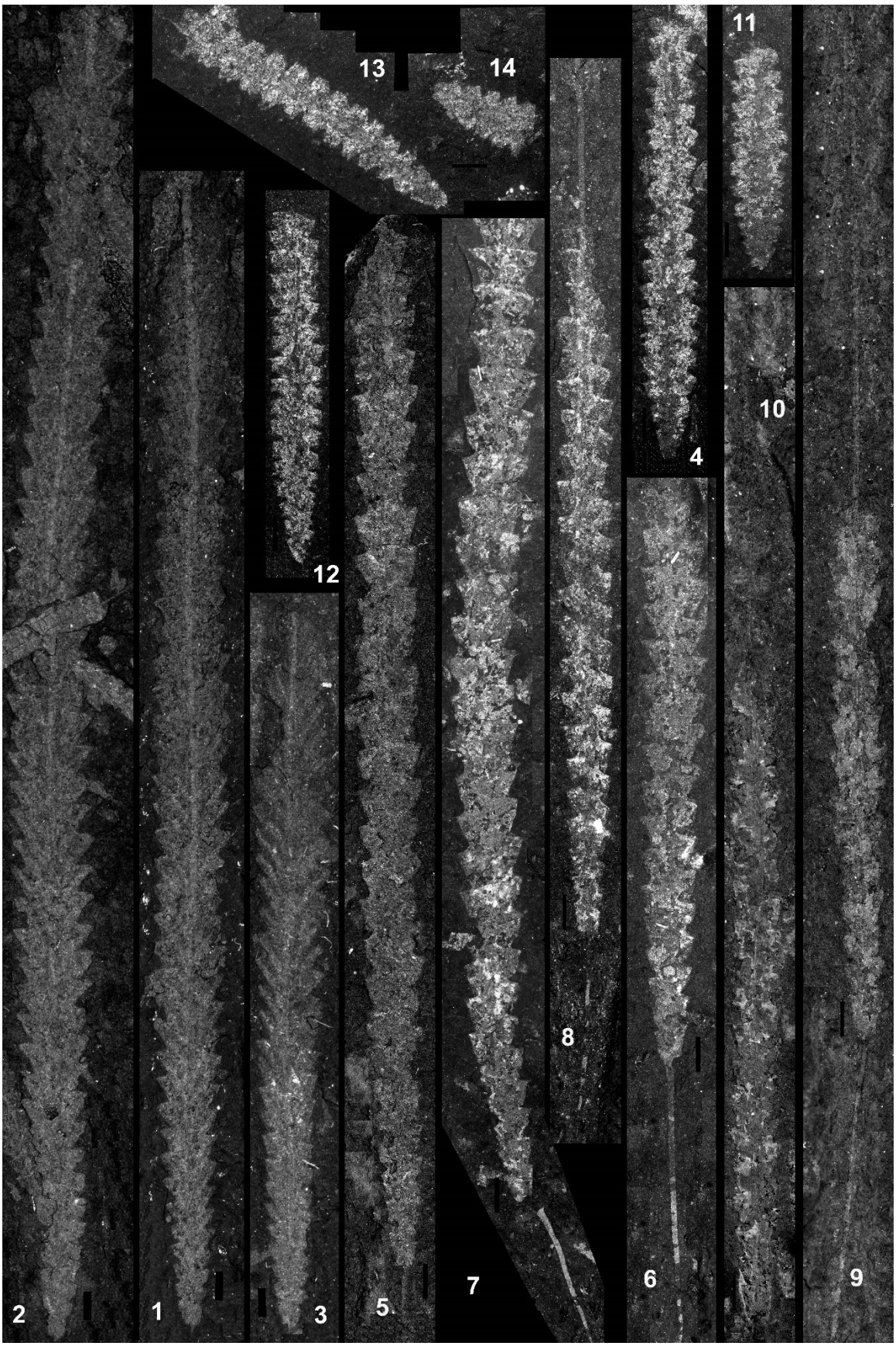
13
14
11
12
10
4
8
2
1
3
5
7
6
9

Plate 47

All figures x6

Fig.	Species	Level (m)	Slab	#
1	*Rickardsograptus magnus* (Churkin & Carter)	49.17	76b	
2	*Rickardsograptus magnus* (Churkin & Carter)	49.17	26b	
3	*Rickardsograptus magnus* (Churkin & Carter)	49.17	16b	
4	*Rickardsograptus magnus* (Churkin & Carter)	49.17	32a	
5	*Rickardsograptus magnus* (Churkin & Carter)	49.17	046b	
6	*Normalograptus rectangularis* (McCoy)	49.17	39b	
7	*Normalo.*? aff. *nanjingensis* (Chen & Lin)	41.66	29a	1
8	*Normalo.*? aff. *nanjingensis* (Chen & Lin)?	45.38	18	1
9	*Normalograptus ajjeri* (Legrand) Form A	45.38	1000	1
10	*Hirsutograptus* sp.	Arctic	C 905 5.2-5.3	
11	*Hirsutograptus jinyangensis* (Ye)	Arctic	C 905 5.2-5.3	
12	*Korenograptus* sp. 3	49.17	YYY	
13	*Normalograptus*? *radicatus* (Chen & Lin)?	38.19	003b	
14	*Cystograptus ancestralis* Štorch	Peel	455.4	
15	*Rickardsograptus* aff. *lautus*	45.38	10	


13
10
11
14
7
12
1
2
3
4
5
6
8
9
15

Plate 48

Figures 8, 21-22 x10; 4, 6-7, 11-12 x12; all other figures x6

Fig.	Species	Level (m)	Slab	#
1	*Normalograptus gnaurus* (Chen & Lin)	39.59	YYY	
2	*Normalograptus gnaurus* (Chen & Lin)	39.59?		
3	*Normalograptus gnaurus* (Chen & Lin)	39.59	022b	
4	*Cystograptus* cf. *ancestralis* Štorch	46.00	48	
5	"*Songxigraptus elongatus*" Fang et al.	37.43	29	
6	*Normalograptus* cf. *ajjeri* (Legrand)	41.66	021b	
7	*Normalograptus* cf. *ajjeri* (Legrand)	41.66	054b	
8	*Normalo.*? aff. *melchini* (Koren' & Rickards)	49.17	DINO	
9	*Cystograptus* cf. *ancestralis* Štorch	45.30 (06)		
10	*Cystograptus* cf. *ancestralis* Štorch	46.00	48	
11	*Korenograptus* sp. 1	38.19?	ABC	
12	*Paramplexograptus paucispinus* (Li)	38.19	087a	2
13	*Paramplexograptus paucispinus* (Li)	38.19	003b	
14	*Korenograptus ugurensis* (Koren' and Melchin)	38.19	084_3	
15	*Korenograptus ugurensis* (Koren' and Melchin)	38.19	020b	
16	*Korenograptus ugurensis* (Koren' and Melchin)	38.19	084_2	
17	*Paramplexograptus wuningensis* (Fang et al.)	37.43		
18	*Korenograptus* sp. 1	38.19	081b	
19	*Normalo. mirnyensis* (Obut & Sobolevskaya)?	38.19	87a	
20	*Koreno. ugurensis* (Koren' and Melchin)?	39.30	29b	
21	*Normalo. skeliphrus* (Koren' & Melchin)	39.59	025c	
22	*Normalo. skeliphrus* (Koren' & Melchin)	39.30	17b	
23	*Hirsutograptus tuberculatus* (Nicholson)	39.59	003a	1
24	*Hirsutograptus tuberculatus* (Nicholson)	39.59	BBB	1
25	*Hirsutograptus tuberculatus* (Nicholson)	39.59	27	

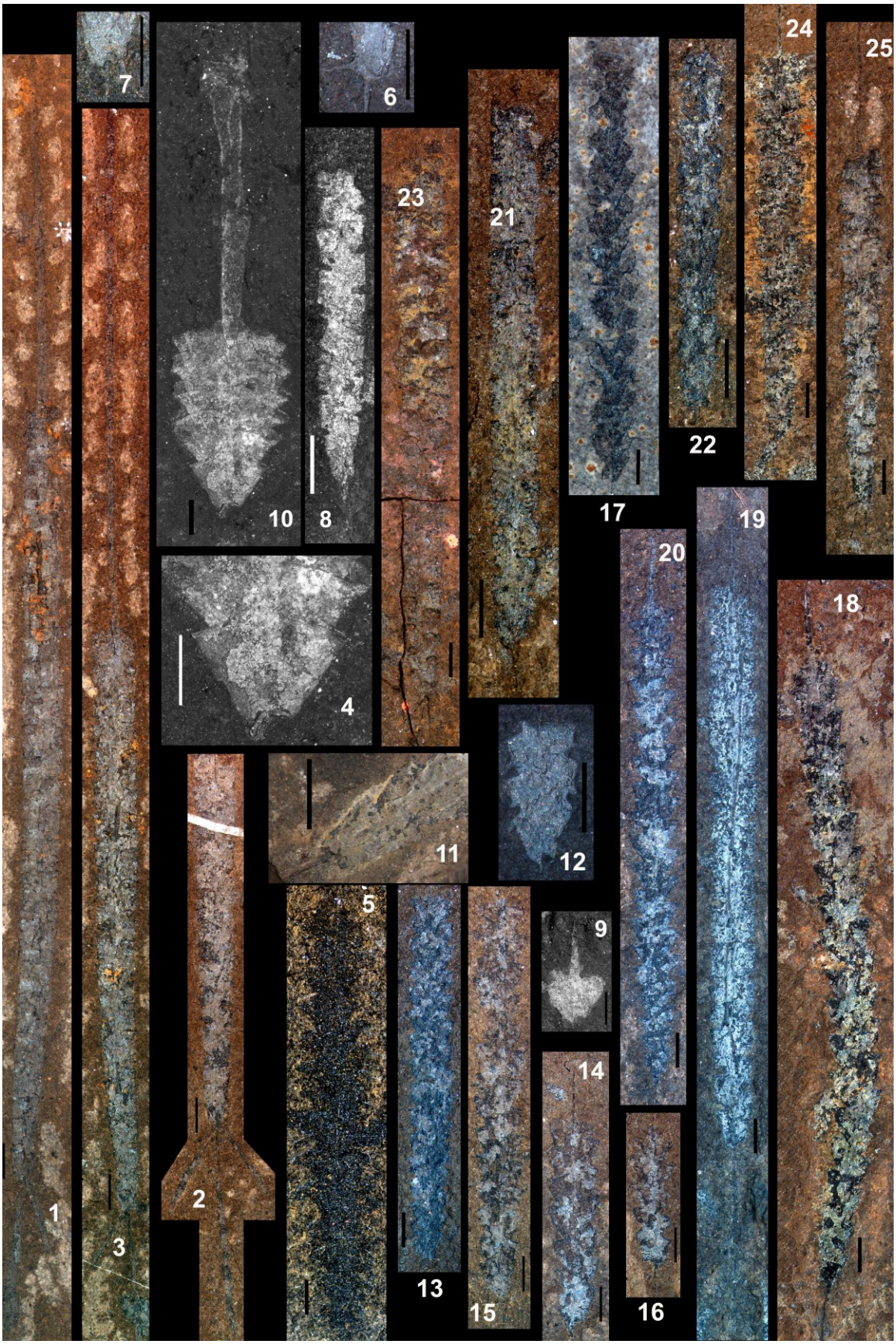
1
2
3
4
5
6
7
8
9
10
11
12
13
14
15
16
17
18
19
20
21
22
23
24
25

Plate 49

Figure 23 x10; all other figures x6

Fig.	Species	Level (m)	Slab	#
1	*Koreno. ugurensis* (Koren' and Melchin)	46.00	AAA	
2	*Koreno. ugurensis* (Koren' and Melchin)	46.00	021a	
3	*Koreno. ugurensis* (Koren' and Melchin)?	38.19	3	
4	*Normalo.*? aff. *nanjingensis* (Chen & Lin)	41.66	34	
5	*Normalo.*? aff. *nanjingensis* (Chen & Lin)	41.66	018b	
6	*Normalo.*? aff. *nanjingensis* (Chen & Lin)	41.66	029a	2
7	*Normalo.*? aff. *nanjingensis* (Chen & Lin)	41.66	AAA	
8	*Normalo.*? *nanjingensis* (Chen & Lin)	37.43	EEE	
9	*Korenograptus*? *diminutus* (Elles & Wood)	42.83	48	
10	*Paraclimacograptus obesus* (Churkin & Carter)	44.02	14	
11	*Paraclimacograptus obesus* (Churkin & Carter)	44.02	100	
12	*Paraclimacograptus obesus* (Churkin & Carter)	44.02	35b	
13	*Korenograptus*? *diminutus?* (Elles & Wood)	41.66	18	
14	*Normalo.*? *nanjingensis* (Chen & Lin)?	41.66	028b	
15	*Normalograptus imperfectus* (Legrand)?	41.66	043a1	
16	*Normalograptus imperfectus* (Legrand)?	41.66	27.3	
17	*Normalograptus imperfectus* (Legrand)?	41.66	043 b 1	
18	*Normalograptus imperfectus* (Legrand)?	41.66	027 1	
19	*Normalograptus imperfectus* (Legrand)?	41.66	059d1	
20	*Metaclimacograptus hughesi* (Nicholson)	49.17	032b	
21	*Paraclimacograptus obesus* (Churkin & Carter)	49.17	046a	
22	*Paraclimacograptus obesus* (Churkin & Carter)	46.00	002b_5	
23	*Atavograptus primitivus* (Li)	40.50	007b	
24	*Paraclimacograptus obesus* (Churkin & Carter)	49.17	028a	
25	*Paraclimacograptus obesus* (Churkin & Carter)	44.02	14	
26	*Paraclimacograptus obesus* (Churkin & Carter)	49.17?	OWL	
27	*Metaclimacograptus hughesi* (Nicholson)	49.17	004b	
28	*Paramplexograptus paucispinus* (Li)	38.62	33b	
29	*Paramplexograptus paucispinus* (Li)	38.19	087a	1
30	*Paramplexograptus paucispinus* (Li)	38.19	31a	
31	*Korenograptus ugurensis* (Koren' and Melchin)	48.10	009b	
32	*Korenograptus ugurensis* (Koren' and Melchin)	45.38	59	
33	*Paramplexograptus kiliani* (Legrand)	37.43	1	
34	*Paramplexograptus kiliani* (Legrand)	37.43	34	1
35	*Paramplexograptus wuningensis* (Fang et al.)	37.43		
36	*Paramplexograptus wuningensis* (Fang et al.)	37.43		
37	*Paraclimacograptus obesus* (Churkin & Carter)	47.00	001b	1
38	*Paraclimacograptus obesus* (Churkin & Carter)	49.17	042a	2
39	*Normalograptus imperfectus*? (Legrand)	41.66	47	
40	*Korenograptus*? *diminutus* (Elles & Wood)	42.83	005a	1

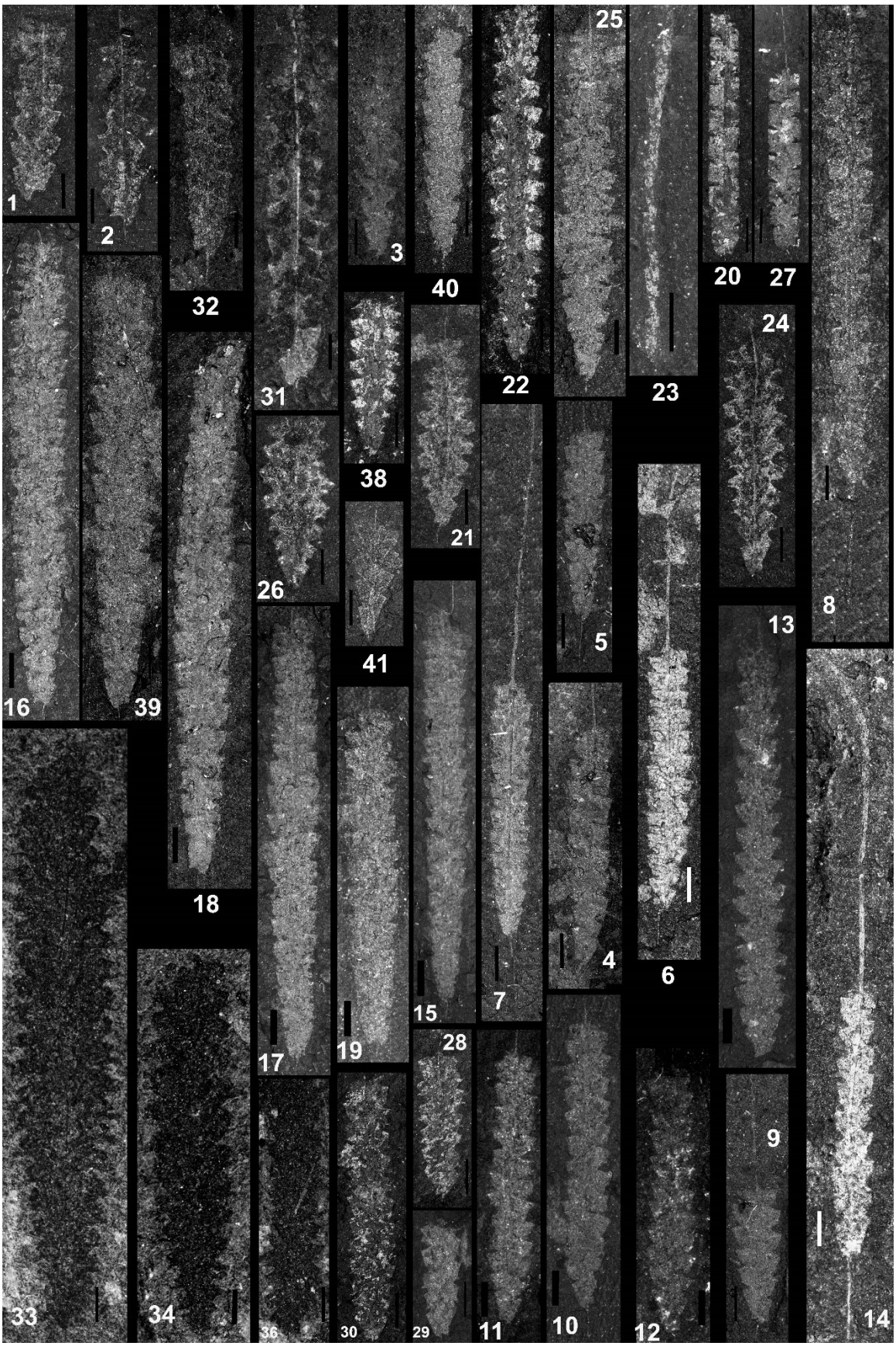
1
2
32
31
3
40
22
25
23
20
27
24
8
16
39
18
26
38
21
41
5
13
17
19
15
7
4
6
28
9
33
34
36
30
29
11
10
12
14

Plate 50

All figures x6

Fig.	Species	Level (m)	Slab	#
1	*Normalograptus* cf. *ajjeri* (Legrand)	45.38	"b"	
2	*Normalograptus* cf. *ajjeri* (Legrand)	41.66	021b	
3	*Normalograptus* cf. *ajjeri* (Legrand)	41.66	054B	
4	*Normalograptus ajjeri* (Legrand) Form A	45.00	107b	
5	*Neodiplograptus* sp. 2	48.10	031a	
6	*Normalograptus*? *radicatus* (Chen & Lin)	?		
7	*Normalograptus*? *radicatus* (Chen & Lin)	39.30	046b3	
8	*Normalograptus*? *radicatus* (Chen & Lin)	39.30	047b	
9	*Normalograptus* sp.	49.17	014a	1
10	*Normalograptus* sp.	49.17	014a	2
11	*Neodiplograptus* sp. 2	48.10	33b	
12	*Neodiplograptus* sp. 2	48.10	030a	
13	*Neodiplograptus* sp. 2	48.10	22	
14	*Rickardsograptus magnus* (Churkin & Carter)?	49.17	17	
15	*Normalograptus* aff. *rhizinus* (Lee & Yang)	41.66	34	
16	*Neodiplograptus* sp. 2	48.10	931a	
17	*Korenograptus* sp. 3?	48.10	040b	2
18	*Neodiplograptus* sp. 2?	48.10	040b	1

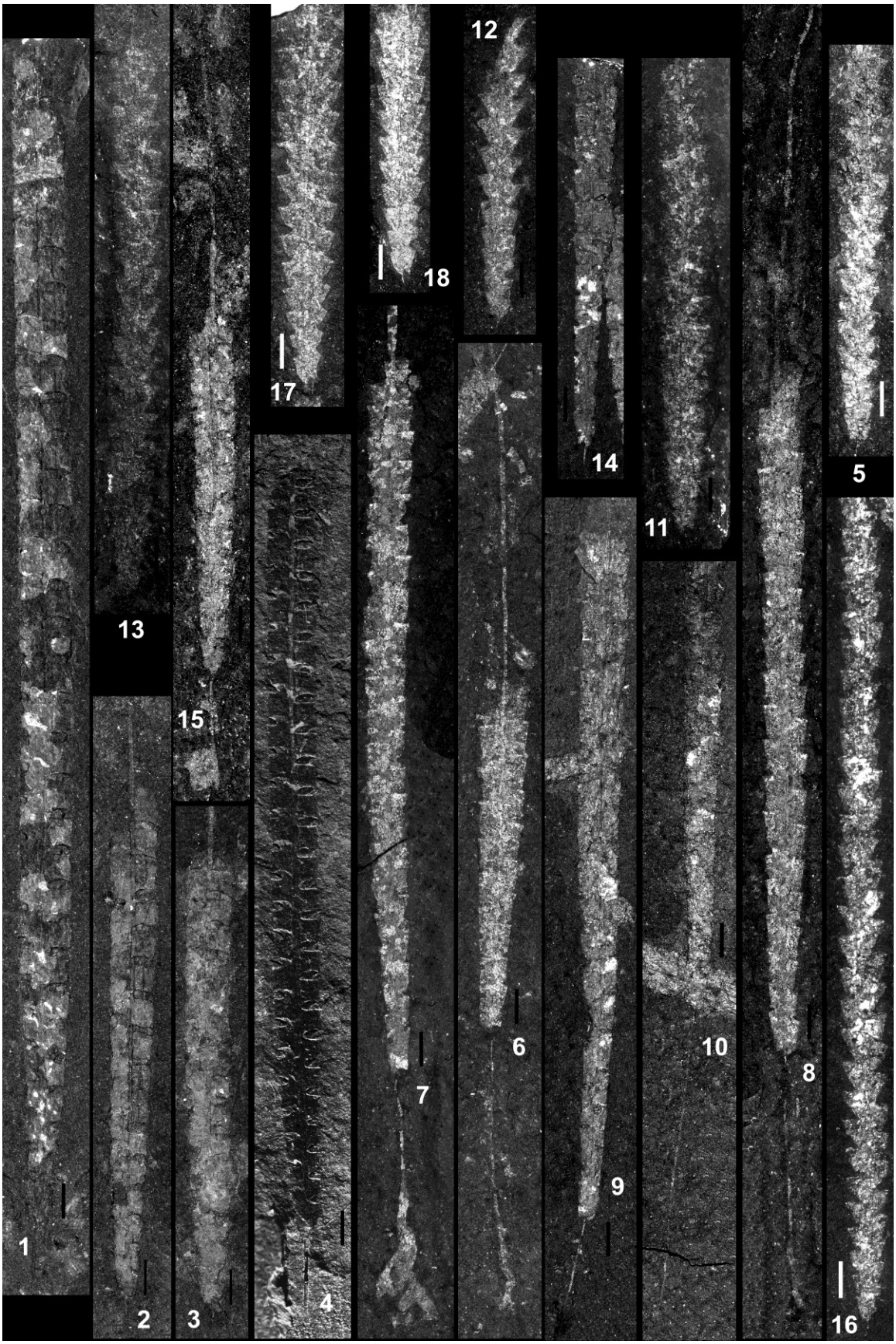
1
2
3
4
5
6
7
8
9
10
11
12
13
14
15
16
17
18

Plate 51

All figures x10

Fig.	Species	Level (m)	Slab	#
1	*Metaclimacograptus*? sp.	38.62	030b	
2	*Metaclimacograptus*? sp.	38.62	21	
3	*Metaclimacograptus*? sp.	38.62	13a	
4	*Normalo. skeliphrus* (Koren' & Melchin)	37.43	7	
5	*Normalo. skeliphrus* (Koren' & Melchin)	37.43	17	
6	*Normalo. skeliphrus* (Koren' & Melchin)	37.43	EEE	1
7	*Normalograptus* aff. *angustus* (Perner)	39.30	049b	1
8	*Normalograptus* aff. *angustus* (Perner)	39.30	48	1
9	*Normalograptus* aff. *angustus* (Perner)	39.30	049b	5
10	*Normalograptus* aff. *angustus* (Perner)	39.30	049b	4
11	*Normalograptus* aff. *angustus* (Perner)	39.30	40	1 & 2
12	*Normalograptus* aff. *angustus* (Perner)	39.30	40	1 & 2
13	*Normalograptus* aff. *angustus* (Perner)	39.30	040x	1
14	*Normalograptus* aff. *angustus* (Perner)	39.30	049b	3
15	*Normalo.*? aff. *melchini* (Koren' & Rickards)	46.00	035E	
16	*Normalo. mirnyensis* (Obut & Sobolevskaya)	39.59	6	
17	*Normalo. mirnyensis* (Obut & Sobolevskaya)	38.19	64a	
18	*Normalo. mirnyensis* (Obut & Sobolevskaya)	45.38	049b	
19	*Normalo.* aff. *mirnyensis* (Obut & Sobolevskaya)	37.43	7	
20	*Normalograptus* aff. *angustus* (Perner)	39.30	049b	2
21	*Metaclimacograptus hughesi* (Nicholson)	49.17	005b	
22	*Metaclimacograptus hughesi* (Nicholson)	49.17	032b 2	
23	*Metaclimacograptus*? sp.	38.90	003a	
24	*Metaclimacograptus hughesi* (Nicholson)	47.17	040a	
25	*Normalo. mirnyensis* (Obut & Sobolevskaya)	41.66	QQQ	

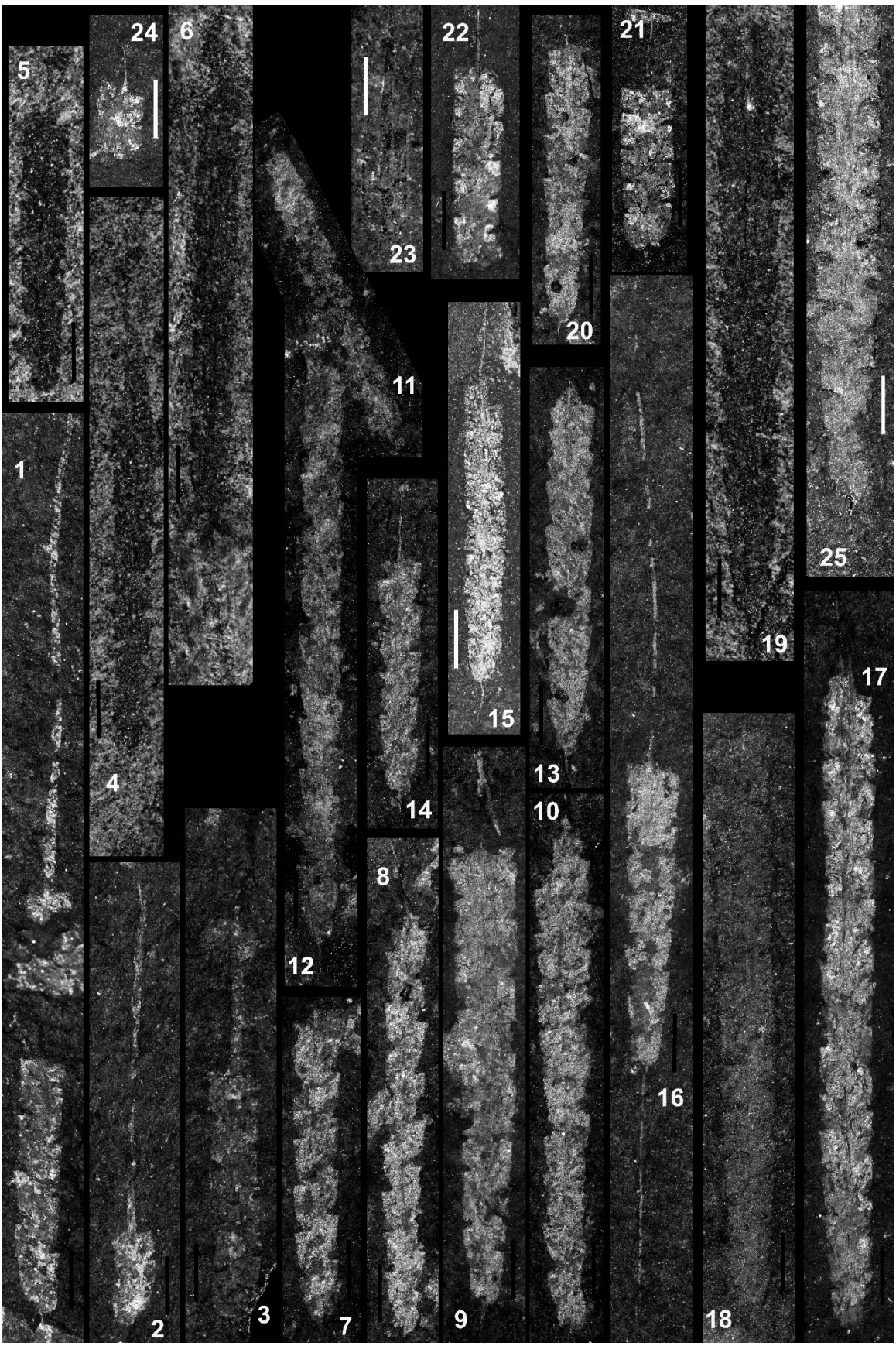
1
2
3
4
5
6
7
8
9
10
11
12
13
14
15
16
17
18
19
20
21
22
23
24
25

Plate 52

Figures 10 & 20 x10; 3-5, 7-8, & 19 x20; all other figures x6

Fig.	Species	Level (m)	Slab	#
1	*Normalograptus* aff. *rhizinus* (Lee & Yang)	42.83	48	
2	*Normalo.*? aff. *melchini* (Koren' & Rickards)	49.17	008b	
3	*Hirsutograptus jinyangensis* (Ye)	Arctic		
4	*Hirsutograptus* sp.	Arctic	1	
5	*Hirsutograptus* sp.	Arctic	2	
6	*Hirsuto. longispinosus* Koren' & Rickards	42.65	1	
7	*Hirsuto. longispinosus* Koren' & Rickards	42.65	1	
8	*Hirsutograptus sinitzini* (Chaletzkaya)	42.83	31	2
9	*Hirsutograptus comantis* (Chaletzkaya)	42.83	040a	
10	*Hirsutograptus comantis* (Chaletzkaya)	42.83	002a	
11	*Hirsutograptus comantis* (Chaletzkaya)	42.83	43	1
12	*Hirsutograptus comantis* (Chaletzkaya)	42.83	23a	1
13	*Hirsutograptus sinitzini*? (Chaletzkaya)	42.83	005b	1
14	*Hirsutograptus comantis*? (Chaletzkaya)	42.83	005b	2
15	*Hirsutograptus sinitzini* (Chaletzkaya)	42.83	49	
16	*Hirsutograptus comantis* (Chaletzkaya)	42.83	002b	
17	*Hirsutograptus sinitzini* (Chaletzkaya)	42.83	55	
18	*Hirsutograptus sinitzini* (Chaletzkaya)	42.83	064a	
19	*Paramplexograptus paucispinus* (Li)	38.90	6	
20	*Normalo.*? aff. *melchini* (Koren' & Rickards)	46.00	035E	

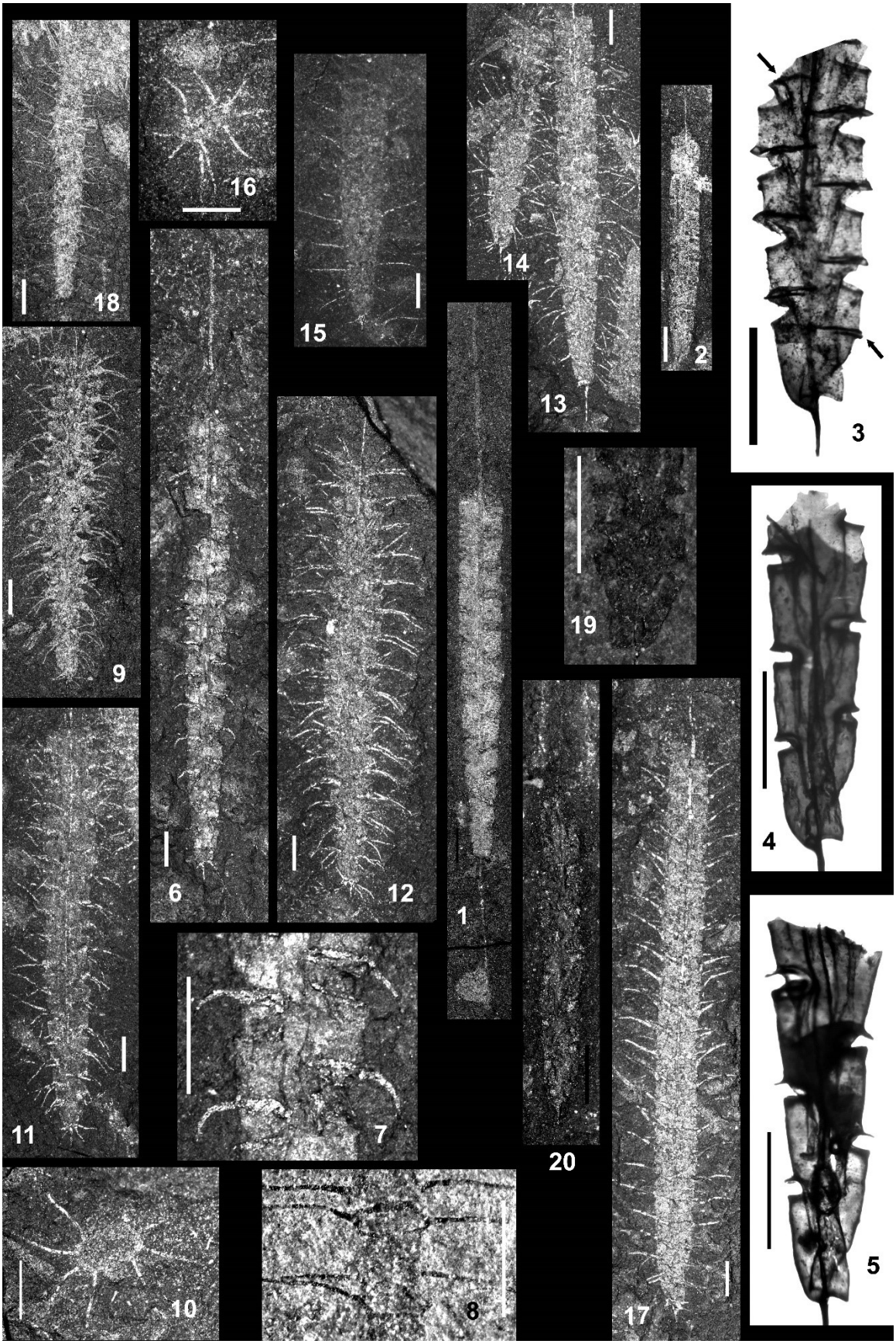
18
16
15
14
2
3
9
6
12
13
19
1
4
11
7
20
5
10
8
17

Plate 53

Figure 23 x15; all other figures x6

Fig.	Species	Level (m)	Slab	#
1	*Hirsutograptus* sp.	40.5 or 39.59	unlabeled	
2	*Hirsutograptus* sp.	41.66	39	
3	*Hirsutograptus* sp.	40.50	5	
4	*Hirsutograptus* sp.	41.66	44a	
5	*Hirsutograptus* sp.	Dob's Linn[1]	25	
6	*Hirsutograptus* sp.	40.50	2	
7	*Hirsutograptus* sp.	40.50	17	
8	*Hirsutograptus* sp.	41.66	048a	
9	*Hirsutograptus* sp.	CPS96 32.9[2]	4	
10	*Hirsutograptus* sp.	CPS96 36.3[2]	13	1
11	*Hirsutograptus sinitzini* (Chaletzkaya)	42.83	31	2
12	*Hirsutograptus comantis* (Chaletzkaya)	42.83	030b	1
13	*Hirsutograptus sinitzini* (Chaletzkaya)	42.83	002b	
14	*Hirsutograptus* sp.	40.5 or 39.59	3000	
15	*"Songxigraptus elongatus"* Fang et al.	37.43	22	
16	*"Songxigraptus elongatus"* Fang et al.	37.43	NNN	
17	*Hirsutograptus jinyangensis* (Ye)	40.50	004a	3
18	*Hirsutograptus jinyangensis* (Ye)	40.50	004a	1
19	*Hirsutograptus jinyangensis* (Ye)	40.50	004b	1
20	*Hirsutograptus* sp.?	41.66	28a	
21	*Paramplexo. wuningensis* (Fang et al.)	38.19	069a	1
22	*Paramplexo. wuningensis* (Fang et al.)	38.19	077B	1
23	*Hirsutograptus jinyangensis* (Ye)	40.50	004a	
24	*Akidograptus cuneatus* Chaletzkaya	46.00	BBC	

[1]Long Burn Trench: 4.95-5.05 m

[2]Arctic Canada

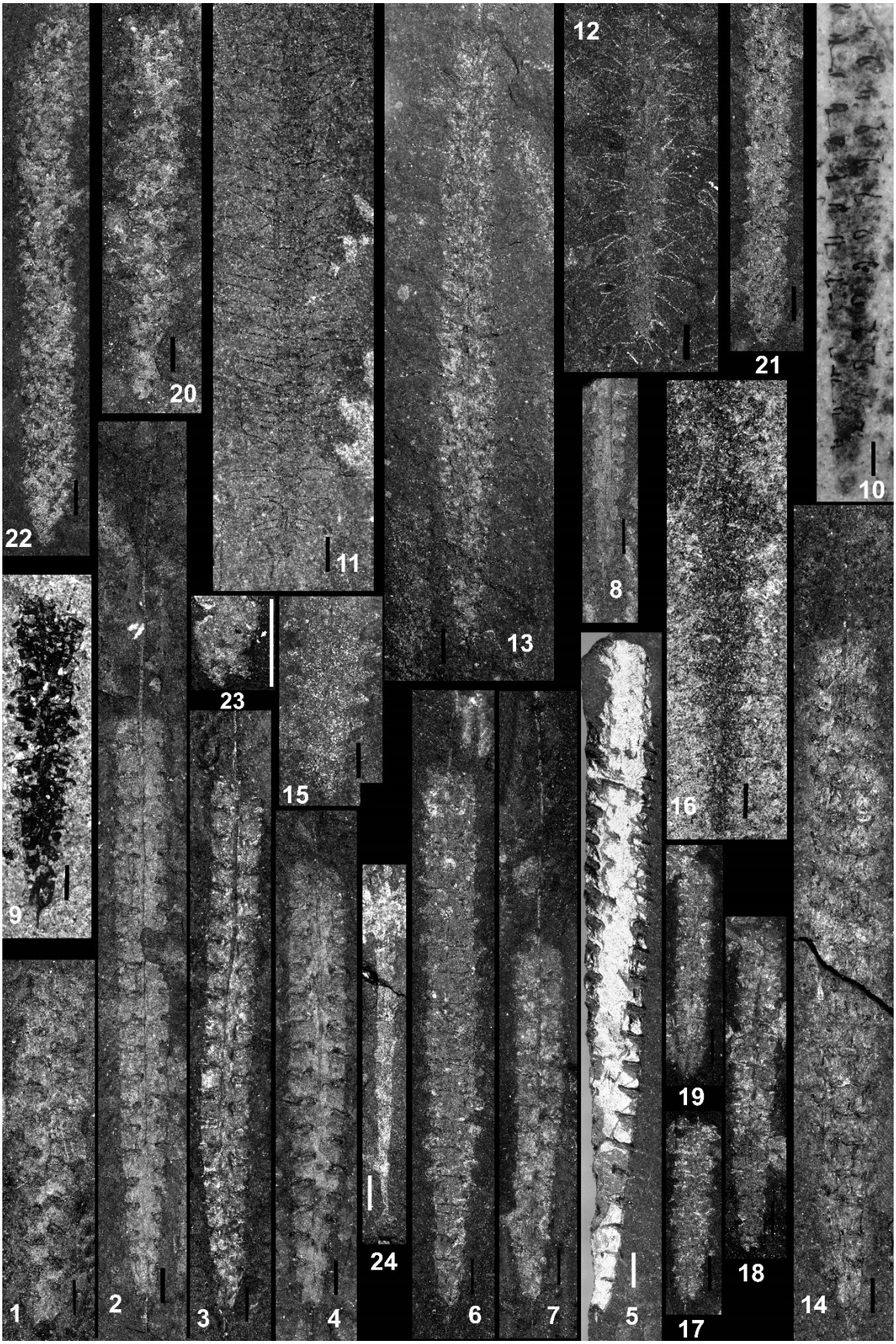
1
2
3
4
24
6
7
5
17
18
19
14
9
22
20
11
23
15
13
12
21
10
8
16

Plate 54

Figure 24 & 26 x10; 25 & 30 x15; 31 x20; all other figures x6

Fig.	Species	Level (m)	Slab	#
1	*Rickardsograptus* aff. *lautus* (Štorch & Feist)	45.38	1000	2 & 3
2	*Rickardsograptus* aff. *lautus* (Štorch & Feist)	45.38	1000	2 & 3
3	*Parakidograptus acuminatus* (Nicholson)	45.38?	?	3
4	*Parakidograptus acuminatus* (Nicholson)	45.38?	?	2
5	*Parakidograptus acuminatus* (Nicholson)	41.66	16	1
6	*Akidograptus ascensus* Davies	38.62	15b	
7	*Akidograptus ascensus* Davies	44.02	19b	1
8	*Akidograptus ascensus* Davies	44.02	19b	2
9	*Parakidograptus acuminatus* (Nicholson)	45.38?	?	1
10	*Parakidograptus acuminatus* (Nicholson)	45.38	81	
11	*Parakidograptus acuminatus* (Nicholson)	45.30 (06)	108	
12	*Akidograptus ascensus* Davies	45.38	46	
13	*Akidograptus cuneatus* Chaletzkaya	45.38?	?	1
14	*Korenograptus* sp. 2	45.30 (06)	100/103	1
15	*Koreno. ugurensis* (Koren' and Melchin)	45.30 (06)	100/103	
16	*Korenograptus* sp. 2	45.30 (06)	102	
17	*Korenograptus* sp. 2	45.30 (06)	101	
18	*Korenograptus* sp. 2	45.30 (06)	104	1
19	*Korenograptus lanpherei* (Churkin & Carter)	44.02	019b	
20	*Neodiplograptus* sp. 1?	38.90	039a	
21	*Neodiplograptus* sp. 1?	38.90	44	
22	*Neodiplograptus* sp. 1?	38.90	34b	
23	*Normalograptus* aff. *angustus* (Perner)	39.59	LC01	1
24	*Korenograptus* sp. 2	49.17	019 frag	
25	*Normalograptus anjiensis* (Yang)	39.30	777	
26	*Normalograptus anjiensis* (Yang)	37.43	14	
27	*Paramplexograptus kiliani* (Legrand)	37.43	6	
28	*Normalo. mirnyensis* (Obut & Sobolevskaya)	39.30	058a	
29	*Normalograptus* sp.	49.17	008bx	
30	*Hirsutograptus* sp.	41.66	044a	
31	*Normalograptus* aff. *angustus* (Perner)	39.30	48	1

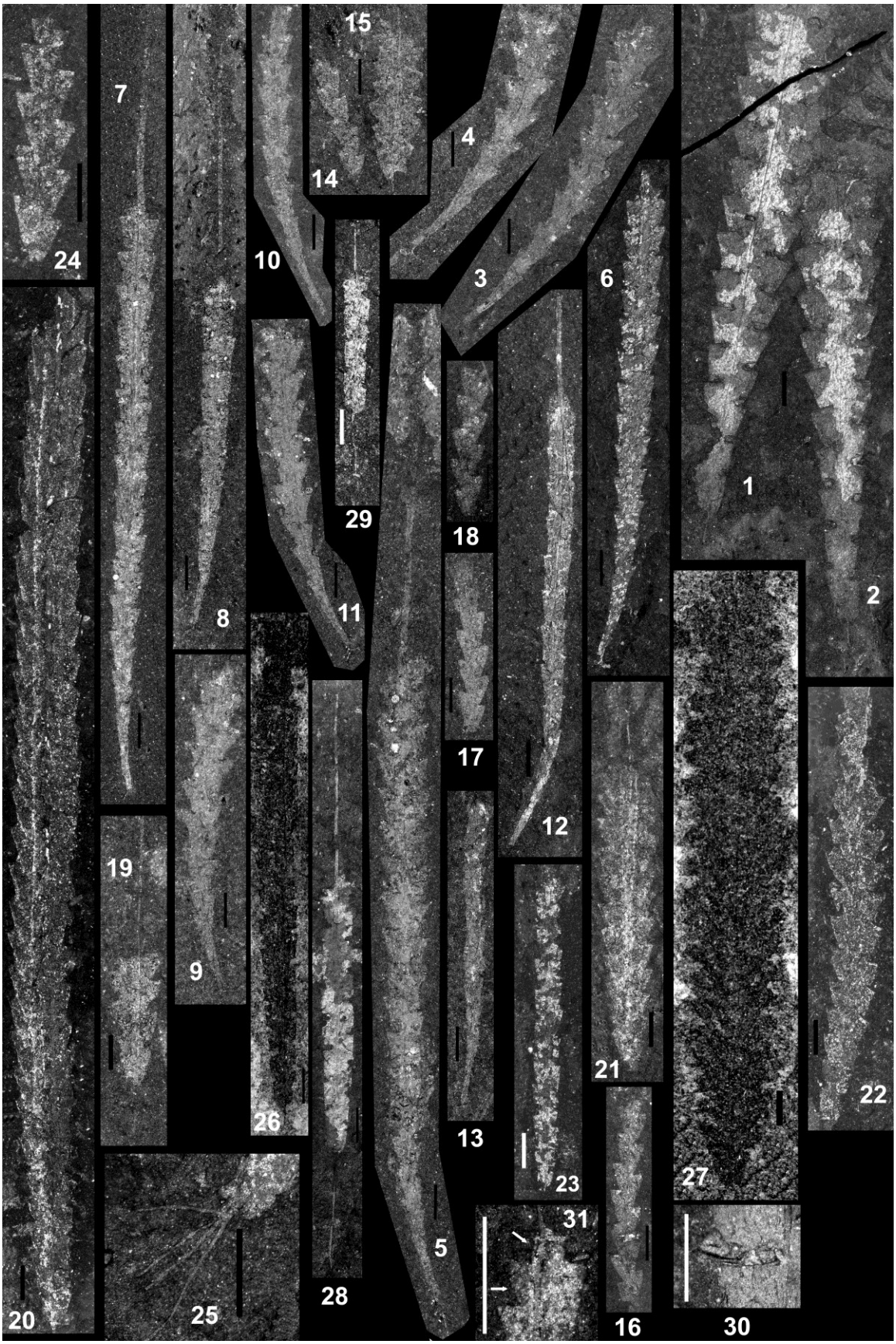
1
2
3
4
5
6
7
8
9
10
11
12
13
14
15
16
17
18
19
20
21
22
23
24
25
26
27
28
29
30
31

Plate 55

All figures x6

Fig.	Species	Level (m)	Slab	#
1	*Normalograptus ajjeri* (Legrand) Form A	45.38	79	
2	*Normalograptus ajjeri* (Legrand) Form A	45.00	11	
3	*Normalograptus ajjeri* (Legrand) Form A	44.02	LOBSTER	
4	*Normalograptus ajjeri* (Legrand) Form A	44.02	020b	5
5	*Normalograptus ajjeri* (Legrand) Form A	44.02	020a	1
6	*Normalograptus ajjeri* (Legrand) Form A	44.02	020b	1
7	*Normalograptus ajjeri* (Legrand) Form B	39.59	10000	
8	*Normalograptus ajjeri* (Legrand) Form B	39.59	034b	
9	*Normalograptus ajjeri* (Legrand) Form B	39.59	32	
10	*Normalograptus ajjeri* (Legrand) Form B	39.30	XXX	
11	*Normalograptus*? *radicatus* (Chen & Lin)?	38.62	15b	
12	*Normalograptus ajjeri* (Legrand) Form B	41.66	52	
13	*Normalograptus* cf. *ajjeri* (Legrand)	39.59	29	
14	*Normalograptus* aff. *rhizinus* (Lee & Yang)	41.66	044a	1
15	*Normalograptus* aff. *rhizinus* (Lee & Yang)	41.66	032a	1
16	*Paraclimacograptus obesus* (Churkin & Carter)	47.00	001b	10 & 11
17	*Paraclimacograptus obesus* (Churkin & Carter)	49.17	046a	
18	*Paraclimacograptus obesus* (Churkin & Carter)	46.00	038a	4
19	*Paraclimacograptus obesus* (Churkin & Carter)	49.17	042a	1
20	*Paraclimacograptus obesus* (Churkin & Carter)	46.00	017a	4
21	*Paraclimacograptus obesus* (Churkin & Carter)	43.50	1	
22	*Paraclimacograptus obesus* (Churkin & Carter)	45.38	6	2
23	*Paraclimacograptus obesus* (Churkin & Carter)	45.38	6	1

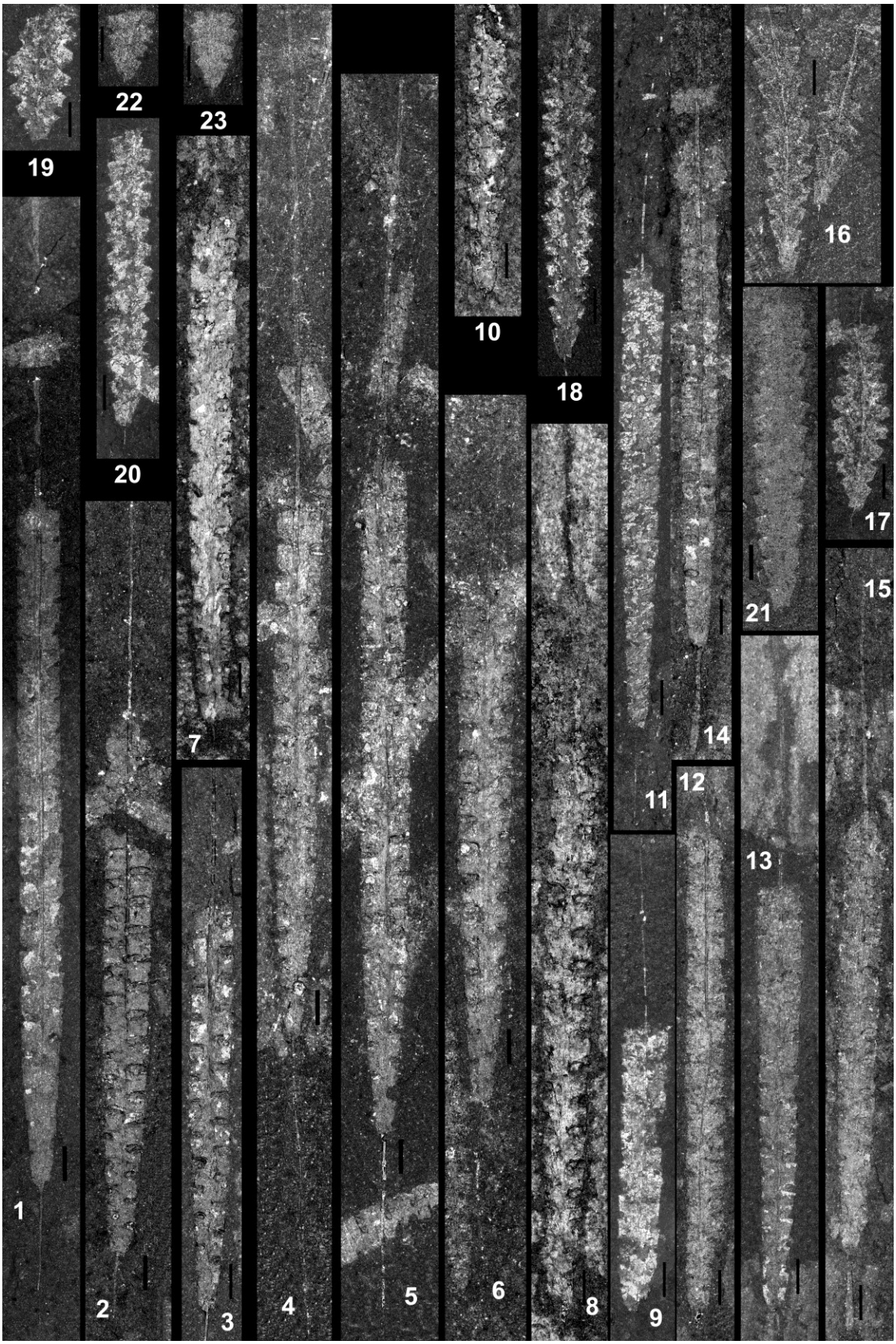
1
2
3
4
5
6
7
8
9
10
11
12
13
14
15
16
17
18
19
20
21
22
23

Plate 56

Figures 10-15 & 33 x10; 22, 29, & 32 x15; 23 x20; all other figures x6

Fig.	Species	Level (m)	Slab	#
1	*Paraclimacograptus obesus* (Churkin & Carter)	46.00	019b	2
2	*Cystograptus* cf. *ancestralis* Štorch	?		
3	*Paraclimacograptus obesus* (Churkin & Carter)	49.17	46c	
4	*Paraclimacograptus obesus* (Churkin & Carter)	46.00	019b	2
5	*Korenograptus*? *diminutus* (Elles & Wood)?	43.50	AY	2
6	*Paraclimacograptus obesus* (Churkin & Carter)	44.02	004a-2	1
7	*Paraclimacograptus obesus* (Churkin & Carter)	44.02	004a-2	2
8	*Akidograptus cuneatus* Chaletzkaya	46.00	004c3	2
9	*Akidograptus cuneatus* Chaletzkaya	46.00	004c3	1
10	*Normalo.*? aff. *melchini* (Koren' & Rickards)	46.00	004c3	
11	*Metaclimacograptus hughesi* (Nicholson)	48.10	901a	
12	*Metaclimacograptus hughesi* (Nicholson)	48.10	902a	
13	*Normalo*.? aff. *melchini* (Koren' & Rickards)	46.00	AAA	
14	*Metaclimacograptus hughesi* (Nicholson)	48.10	900a	
15	*Normalo*.? aff. *melchini* (Koren' & Rickards)	46.00	35e	
16	*Rickardsograptus* aff. *lautus* (Štorch & Feist)	45.30 (06)	700	
17	*Normalograptus* cf. *transgrediens* (Waern)	38.62	4	
18	*Normalograptus* cf. *transgrediens* (Waern)	38.62	11b	
19	*Normalograptus* cf. *transgrediens* (Waern)	38.62	56b	1
20	*Normalograptus* cf. *transgrediens* (Waern)	38.62	56b	2
21	*Normalograptus gnaurus* (Chen & Lin)	40.50	Z1	
22	*Normalograptus gnaurus* (Chen & Lin)	40.50	Z1	
23	*Parakidograptus acuminatus* (Nicholson)	45.30 (06)	108	
24	*Korenograptus*? *diminutus* (Elles & Wood)	41.66	009b	
25	*Akidograptus cuneatus*? Chaletzkaya	41.66	66a	
26	*Atavograptus atavus* (Jones)	49.50	XXX	
27	*Akidograptus cuneatus* Chaletzkaya	47.00	411	
28	*Normalograptus medius* (Törnquist)	48.10	009a	
29	*Normalograptus medius* (Törnquist)	48.10	009a	
30	*Normalograptus medius* (Törnquist)	48.10	004a	2
31	*Normalograptus medius* (Törnquist)	48.10	004a	1
32	*Normalograptus medius* (Törnquist)	48.10	009a	
33	*Metaclimacograptus hughesi* (Nicholson)	49.17	32b	2
34	*Huttagraptus* sp.	49.50	002b	

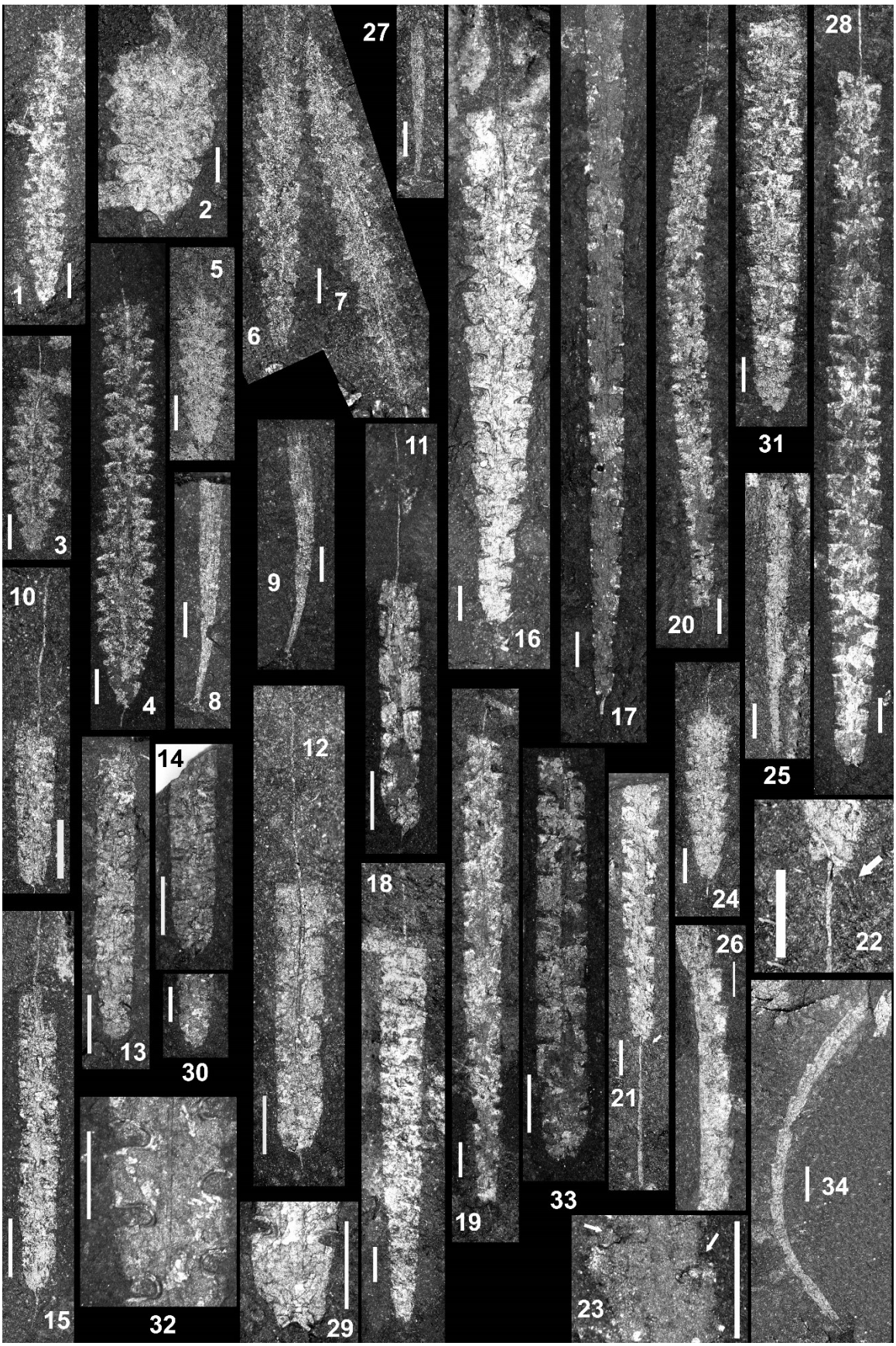
1
2
3
4
5
6
7
8
9
10
11
12
13
14
15
16
17
18
19
20
21
22
23
24
25
26
27
28
29
30
31
32
33
34

Plate 57

Figure 16 x15; all other figures x6

Fig.	Species	Level (m)	Slab
1	*Normalograptus rectangularis* (McCoy)?	45.38	009b
2	*Normalograptus rectangularis* (McCoy)?	45.38	009b
3	*Rickardsograptus lautus* (Štorch and Feist)	47.00	23_1
4	*Rickardsograptus lautus* (Štorch and Feist)	47.00	23_1
5	*Rickardsograptus lautus* (Štorch and Feist)	49.17	44b
6	*Rickardsograptus lautus* (Štorch and Feist)	49.17	44b
7	*Rickardsograptus lautus* (Štorch and Feist)	47.00	39d
8	*Rickardsograptus* aff. *lautus* (Štorch & Feist)	45.38	MUTANT
9	*Rickardsograptus* aff. *lautus* (Štorch & Feist)	45.38	10
10	*Rickardsograptus* aff. *lautus* (Štorch & Feist)	45.30 (06)	TT
11	*Rickardsograptus* aff. *lautus* (Štorch & Feist)	45.38	6
12	*Rickardsograptus* aff. *lautus* (Štorch & Feist)	45.38	15
13	*Rickardsograptus lautus* (Štorch and Feist)	49.17	35
14	*Rickardsograptus lautus* (Štorch and Feist)	49.17	23_1x
15	*Rickardsograptus lautus* (Štorch and Feist)	49.17	25b
16	*Metaclimacograptus*? sp.	38.90	56


1
2
3
11
14
15
12
5
6
16
9
13
4
7
8
10

Appendix A. Sample Descriptions for Counted Samples

Sample 0.1-0.2 m (*D. ornatus* Zone)

Black calcareous shale (22% $CaCO_3$). Splits to 0.5-2.5 mm thick slabs. Specimens often fragmentary, but well preserved as flattened, silver films. Quality poor to very good. Specimens mostly randomly oriented, but some lag deposit style clusters. Graptolite material low density compared to higher samples. No accessory fauna. No evidence of deformation. Sample counted.

Sample 0.17- m (*D. ornatus* Zone):

Dark grey, brown-weathering, silty calcareous shale to mudstone. Splits with effort. Well-preserved graptolites as silver films. Some current alignment. Specimens mostly intact. Dominated by *A. lata* (53%), with abundant *A. supernus, C. hastatus,* and *R. abbreviatus*. Collected as a conodont sample originally, so much smaller than other counted samples. Sample counted.

Sample 1.3-1.42 m (*P. pacificus* Zone)

Black calcareous shale to limey mudstone. Strong acid reaction. Splits are 0.5-4 cm. Graptolites fragmentary to well-preserved and sparse to abundant, depending on slab. Slabs dominated by large intact *Anticostia lata* show some alignment, but those with gregarious *Paraorthograptus* are randomly oriented. Quality poor to good. Sample dominated by *Paraorthograptus*. Specimens preserved as flattened silver films. No evidence of deformation. Uncommon phosphatic brachiopods and rare articulated trilobites (*Triarthrus*). Sample counted.

Sample 5.3-5.4 m (*P. pacificus* Zone)

Black calcareous shale (strong acid reaction). Splits to ca. 0.5 mm thick slabs. Common patches of euhedral crystals of mica(?). Graptolites preserved as flattened silver films. Graptolites relatively sparse, mostly mature *Rectograptus abbreviatus* and *Anticostia lata*. Very rare articulate brachiopods. Some specimens aligned. Some slabs possibly slightly deformed. Sample counted.

Sample 5.5-5.6 m (*P. pacificus* Zone)

Black calcareous shale (48% $CaCO_3$). No evidence of deformation. Sample counted. Patches of euhedral crystals of mica common, and cover some bedding surfaces entirely. Graptolites preserved as flattened silver films. Preservation quality moderate. Clear evidence of current alignment and sorting, with large specimens, mostly *Rectograptus abbreviatus* and *Dicellograptus ornatus,* dominant. Patches of some slabs offset along jagged, mineralized planes. Accessory fauna absent (one possible nautiloid). Some slabs possibly slightly deformed. Sample counted.

Sample 8.80-8.90 m (*P. pacificus* Zone)

Black calcareous shale (strong acid reaction). Splits to ca. 0.5 mm thick slabs. Some patches of euhedral crystals of mica. Graptolites preserved as flattened silver films, sometimes overprinted by calcite(?). Preservation poor to excellent. Graptolite abundance patchy, with many slabs only containing fragmentary material, sometimes with clusters of larger material on portions of the slab. Fragments of trilobites present on two slabs (disarticulated spines and thoracic segments, probably from *Pugilator.*

yukonensis), along with rare impressions of straight-shelled nautiloids. Moderate deformation clearly present (especially clear in asymmetrical dicellos). Sample counted.

Sample 12.67 m (*P. pacificus* Zone)

Black calcareous shale (strong acid reaction). Splits readily to 0.5-1 mm slabs. Graptolites preserved as flattened silver films. Graptolites very rare and mostly damaged or fragmentary, but some exquisitely preserved. *Rectograptus* dominates sample, but well-preserved mature dicellograptids also occur, along with other *pacificus* Zone taxa. Trilobites common, both fragments and articulated specimens (*Triarthrus* and *Pugilator*). Rare orthocone nautiloids and articulate brachiopods also present. Patches of euhedral crystals of mica common, and cover some bedding surfaces entirely. No evidence of deformation. Sample counted, but small. (Unlike other samples, only slabs with graptolites collected at locality, with majority of material rejected as non-graptolitic.)

Sample 14.15-14.25 m (*mirus* Subzone)

Black calcareous shale (strong acid reaction). Splits readily to 0.5-1 mm slabs. Graptolites preserved as flattened silver films. Graptolites abundant, and vary from very well-preserved mature specimens to common fragments. Dicellograptids dominate sample. Large specimens of *A. lata,* which often occur in clusters, show current alignment, but much of the broken graptolite 'hash' that covers slabs is randomly oriented. Rare specimen of a trilobite (articulated *Triarthrus* n =1) and a straight-shelled nautiloid (n =1) are present. No evidence of deformation. Sample counted.

Sample 15.65-15.77 m (*mirus* Subzone)

Black calcareous shale (strong acid reaction). Splits at 0.75-2 cm. Graptolites preserved as flattened silver films. Graptolites abundance highly variable: some surfaces are nearly devoid of graptolites and other surfaces completely covered in a mixture of complete specimens and fragments. Preservation is moderate to poor for most of the sample. *Paraorthograptus pacificus* dominates (66% of sample). Some large specimens are clustered or aligned, whereas fragments are randomly oriented. Very rare accessory fauna: a single inarticulate brachiopod and some fragments of trilobite segments. Parts of slabs offset by small faults. Some surfaces show signs of slickensides and or heavy mineralization. No obvious evidence of deformation, but structures and some odd measurements suggest subtle deformation may be present. Sample counted.

Sample 16.03-16.18 m (*mirus* Subzone)

Black calcareous shale (strong acid reaction). Splits readily into large slabs at 0.5-1 mm. Graptolites preserved as flattened silver films. Graptolite abundance variable, but many surfaces highly abundant, with some so covered in large overlapping specimens (mostly of *A. lata*) that counting is difficult. Large specimens often current aligned or present in lag-style clusters. Preservation excellent, with lots of very mature material. Sample dominated by *P. pacificus* and *A. lata,* which make up 82% of specimens. All other species make up less 6% of sample, and most species <1%. Rare accessory fauna: two partial *Pugilator* specimens and a possible nautiloid. No evidence of deformation. Sample counted.

Sample 17.20-17.30 m (*mirus* Subzone)

Black, brown-weathering, calcareous shale (strong acid reaction). Graptolites abundant and very well-preserved. Preservation excellent, with lots of very mature material. Large specimens often current aligned or present in lag deposit style clusters. Sample dominated by *R. abbreviatus* (53% of sample), with abundant *A. supernus* and *A. lata* (ca. 19% each). *P. pacificus* and dicellograptids almost completely absent. Rare accessory fauna: one specimen of *Triarthrus* and one brachiopod. No evidence of deformation. Sample counted.

Sample 18.05-18.16 m: 2007 sample (*mirus* Subzone)

Black, calcareous shale/bedded limestone (carbonate fraction of isotope sample is 56%). Beds split between 0.5 and 2 cm. Graptolites preserved as flattened silver films. Graptolites abundant. Preservation variable, with majority of material fragmentary, but some very well-preserved mature specimens. Some current alignment of larger specimens, but fragmentary material mostly randomly arranged or in densely overlapping clusters. Some surfaces covered by mineralization. Slickensides present on some surfaces. Sample dominated by *P. pacificus* (65%) and *A. supernus* (27%). All other species minor components. Very rare accessory fauna (1 brachiopod). Specimens do not appear to be deformed, but presence of slickensides on some surfaces suggests possibility. Sample collected and counted. Additional sample from very similar level (18.06 m in 2006 survey) scanned for additional species, but not counted because of poor preservation.

Sample 18.83-18.95 m (*mirus* Subzone)

Sample scanned, but not counted.

Sample 18.95-19.0 m (*mirus* Subzone)

Black, calcareous shale/bedded limestone (carbonate fraction of isotope sample at 19 m = 66%). Graptolites preserved as flattened silver films. Graptolites abundant. Preservation variable, with majority of material fragmentary or poorly preserved. Some current alignment of larger specimens, but fragmentary material mostly randomly arranged. Some mineralization present on surfaces, as well as calcite-filled fracture surfaces. Sample dominated by *P. pacificus* (57%) and *A. supernus* (26%), with *A. lata* and *R. abbreviatus* common (7% each). All other species minor components. Rare accessory fauna (at least a dozen calcareous brachiopods, plus possible fragments of trilobites). Sample may be deformed. Sample counted.

Sample 19.0-19.05 m (*mirus* Subzone)

Black, highly-fissible, calcareous shale/bedded limestone (carbonate fraction isotope sample at 19 m is 66%). Graptolites preserved as flattened silver films. Graptolite abundance patchy: many surfaces contain only rare graptolites or scattered broken material. Preservation is highly variable, but is excellent where complete specimens are preserved. Some current alignment of larger specimens, but fragmentary material mostly randomly arranged. Sample dominated by *P. pacificus* (43%) and specimens of *Appendispinograptus.* (Note: Count records 30% *A. supernus* vs. 5% *A.* pogrebovi, however, this represents the count before *A.* pogrebovi was recognized as an

independent species; as the sample was heavily resplit post-count in the process of trying to find sufficient material to confirm rare taxa, selectively destroying more common taxa, an unbiased recount was not possible. As a result, only specimens that exhibited high thecal spacing, which were binned into a questionable category during the original count, are included in the *A. pogrebovi* number; its actual abundance in the sample is likely underestimated). Accessory fauna consists of relatively common, very small (ca. 2 mm), nearly round, phosphatic brachiopods, and rare calcareous brachiopods. The sample does not appear to be deformed. Sample counted.

Sample 19.05-19.10 m (*mirus* Subzone)

Black calcareous (strong acid reaction), friable shale. Splits readily into slabs at 0.5-1 cm. Graptolites preserved as flattened silver films. Graptolites very poorly to moderately preserved. Graptolite abundance variable, but mostly low, with some slabs containing only two or three specimens. Sample strongly dominated by *Anticostia uniformis* (81% of sample). Small (1.5-3.0 mm) inarticulate brachiopods cover most slabs, and are more common than graptolites. Small articulated brachiopods, larger inarticulate brachiopods (bivalves?), and possible nautiloids and bryozoans also occur. Some evidence of minor deformation. Sample counted.

Sample 19.10-19.15 m (*mirus* Subzone)

Black calcareous (strong acid reaction), friable shale. Splits readily into slabs at 0.5-1.5 cm. Graptolites preserved as flattened silver films. Graptolites mostly very poorly preserved. Graptolite abundance overall low and patchy, with many large slabs

possessing only a few complete specimens. The sample is dominated by neograptine species (*Metabolograptus ojsuensis* (71%) and *Neodiplogratus charis* (17%)), with common *Appendispinograptus leptothecalis.* All other species are rare, although *Styracograptus mississippiensis* (2.3%) was somewhat likely underrepresented in the count due to the difficulty, given the poor level of preservation, of distinguishing it from the superficially similar *M. ojsuensis.* Accessory fauna consists of common small, round phosphatic brachiopods and rare examples of one or two species of larger calcareous brachiopods. No evidence of deformation, but sample too poorly preserved to be confident. Sample counted.

Sample 19.15-19.20 m (*extraordinarius* Zone)

Black calcareous (strong acid reaction), friable shale. Splits readily into slabs at 0.5-1 cm. Graptolites preserved as flattened silver films. Graptolites poorly to moderately preserved (mixture of very large mature specimens and fragments). Graptolite abundance patchy, but most slabs are covered with mature, current aligned specimens. The sample is nearly 100% neograptine species: *M. extraordinarius* (54%), *M. ojsuensis* (39%), and *Neo. charis* (6%). All other species occur as much less than 1% of the sample. Accessory fauna consists of rare small, round phosphatic brachiopods, calcareous brachiopods, and trilobite fragments. Sample counted.

Sample 19.20-19.25 m (*extraordinarius* Zone)

Black calcareous (strong acid reaction), friable shale. Splits readily into slabs at 0.5-1 cm. Graptolites preserved as flattened silver films and, rarely, as three-dimensional internal

molds. Preservation is poor to good. Graptolite abundance very patchy, with some slabs covered with mature, current aligned specimens, but most slabs containing rare or only fragmentary graptolites. The sample is nearly 100% neograptine species, and dominated by *M. extraordinarius* (71%), with *M. ojsuensis* (14%), and *Neo. charis* (15%) common. Other species occur as much less than 1% of the population. Accessory fauna includes abundant trilobites (representing all growth stages, but mostly disarticulated), and rare brachiopods. No evidence of deformation. Sample counted.

Sample 19.25-19.30 m (*extraordinarius* Zone)

Black calcareous (strong acid reaction), friable shale. Splits readily into slabs at 0.5-1 cm. Graptolites preserved as flattened silver films. Preservation is mostly poor. Graptolite abundance is low, and most specimens are fragmentary; rare slabs contain mature current aligned specimens, but abundance on all slabs is much lower than in previous collections. The sample is nearly 100% *Metabolograptus* (67% *M. extraordinarius* and 22% *M. extraordinarius*). Nine percent of the population was assigned to *S. mississippiensis*, but this represents an approximation: only a small number of specimens were confidently identified as *S. mississippiensis*, with the majority of the count redistributed from the *S. mississippiensis/M. ojsuensis* uncertain bin. Rare slender, mostly scalariform, “climacograptid”, specimens were also assigned to *S. mississippiensis*, as its presence in the sample was confirmed, although it is possible that they actually represented *Appendispinograptus* or thin neograptine species. Trilobite

material is very abundant, but mostly fragmentary. No evidence of deformation, but preservation poor. Sample counted.

Appendix B. Graptolite Counts (Tables and Graphs)

Sample (Meters)	0.10	0.17	1.30	5.30/5.50	8.80	12.67
TOTAL Ided	712	248	1556	993	966	123
Total (exc. sic)	884	357	2031	1247	1531	173
PERCENT Ided	81%	69%	77%	80%	63%	71%
Total sample counted?	Y	Y	Y	Y	Y	Y
Anticostia lata	29	134	126	296	233	1
Anticostia uniformis	0	0	0	0	0	0
Anticostia mcgregorae	0	0	0	0	0	0
Appendi. leptothecalis	0	0	0	0	0	0
Appendi. supernus	419	43	247	18	177	2
A. pogrebovi	0	0	0	0	0	0
Climaco. hastatus	5	24	8	34	4	1
Dicello. minor	0	0	0	0	6	5
Dicello.* cf. *mirabilis	0	0	0	0	0	0
D.* aff. *mirabilis	0	0	0	0	0	0
Dicello. ornatus	20	6	10	200	79	12
Dicello. tenuiculus	0	0	0	0	0	0
Dicello. turgidus	0	0	0	0	2	5
D.* aff. *turgidus	0	0	0	1	0	0
Dicerato. mirus	0	0	0	0	0	0
Diplo. rarithecatus	0	0	0	0	0	15
Neo. charis	0	0	0	0	0	0
M. extraordinarius	0	0	0	0	0	0
Meta. ojsuensis	0	0	0	0	0	0
Paraortho. affinis	0	0	0	0	0	0
Paraorthp. kimi	0	0	1092	19	282	13
Paraortho. pacificus	0	0	0	0	0	0
Parareteo. turgidus	0	0	0	0	0	0
Parareteo. sinensis	7	0	6	0	0	0
Phormo. connectus	6	3	24	38	17	3
Pleuro. lui	13	4	11	1	1	3
Pleuro.? grandis	0	0	0	0	0	0
Recto. abbreviatus	37	34	18	386	148	51
***Styracograptus* sp.**	0	0	0	0	0	0
S. mississippiensis	93	0	3	0	7	11
S. tatianae	83	0	3	0	0	1
Yino. disjunctus	0	0	8	0	10	0

Sample (Meters)	14.15	15.65	16.03	17.20	18.06	18.94
TOTAL Ided	1861	1629	1632	1368	3072	2025
Total (exc. sic)	3809	2054	2471	2142	4786	3310
PERCENT Ided	49%	79%	66%	64%	64%	61%
Total sample counted?	N	N	N	N	N	N
Anticostia lata	390	65	700	270	127	140
Anticostia uniformis	0	4	1	NIC	NIC	0
Anticostia mcgregorae	0	1	0	NIC	0	0
Appendi. leptothecalis	0	7	NIC	25	43	17
Appendi. supernus	167	229	82	253	819	511
A. pogrebovi	0	0	0	0	0	24
Climaco. hastatus	55	0	26	8	19	1
Dicello. minor	0	0	2	NIC	0	2
Dicello.* cf. *mirabilis	0	0	12	NIC	0	1
D.* aff. *mirabilis	0	17	7	7	5	0
Dicello. ornatus	0	0	0	0	0	0
Dicello. tenuiculus	789	11	5	0	2	6
Dicello. turgidus	0	0	0	0	0	0
D.* aff. *turgidus	0	0	0	0	0	0
Dicerato. mirus	NIC	1	1	NIC	1	3
Diplo. rarithecatus	0	100	52	0	0	0
Neo. charis	0	0	0	0	0	0
M. extraordinarius	0	0	0	0	0	0
Meta. ojsuensis	0	0	0	0	0	0
Paraortho. affinis	0	0	0	0	0	0
Paraorthp. kimi	0	0	0	0	0	0
Paraortho. pacificus	449	1073	628	1	1989	1150
Parareteo. turgidus	1	0	0	0	0	0
Parareteo. sinensis	0	0	0	0	0	0
Phormo. connectus	1	4	10	8	2	2
Pleuro. lui	NIC	29	10	2	0	0
Pleuro.*? *grandis	NIC	0	1	0	0	0
Recto. abbreviatus	7	1	95	719	23	147
***Styracograptus* sp.**	0	0	0	0	NIC	0
S. mississippiensis	2	77	1	47	42	9
S. tatianae	0	10	0	25	0	12
Yino. disjunctus	NIC	0	0	3	0	0

NIC = species not captured in the abundances counts, but which were recovered during scans of additional uncounted slabs in a given level.

Sample (Meters)	19.00	19.05	19.10	19.15	19.20	19.25
TOTAL Ided	884	364	306	720	865	329
Total (exc. sic)	1761	645	701	1336	1225	464
PERCENT Ided	50%	56%	44%	54%	71%	71%
Total sample counted?	N	N	N	N	N	N
Anticostia lata	30	0	0	0	0	0
Anticostia uniformis	30	294	0	0	0	0
Anticostia mcgregorae	0	0	0	0	0	0
Appendi. leptothecalis	17	31	20	NIC	0	0
Appendi. supernus	264	0	0	0	0	0
A. pogrebovi	41	0	0	0	0	0
Climaco. hastatus	3	0	0	0	0	0
Dicello. minor	0	0	0	0	0	0
Dicello.* cf. *mirabilis	5	0	0	0	0	0
D.* aff. *mirabilis	0	0	0	0	0	0
Dicello. ornatus	0	0	0	0	0	0
Dicello. tenuiculus	5	0	0	0	0	0
Dicello. turgidus	0	0	0	0	0	0
D.* aff. *turgidus	0	0	0	0	0	0
Dicerato. mirus	9	0	1	0	0	0
Diplo. rarithecatus	0	0	0	0	0	0
Neo. charis	0	0	52	40	129	2
M. extraordinarius	0	0	0	391	614	74
Meta. ojsuensis	0	0	217	282	118	221
Paraortho. affinis	0	0	0	4	1	0
Paraorthp. kimi	0	0	0	0	0	0
Paraortho. pacificus	384	0	6	1	1	1
Parareteo. turgidus	0	0	0	0	0	0
Parareteo. sinensis	0	0	0	0	0	0
Phormo. connectus	16	3	3	1	0	0
Pleuro. lui	0	0	0	NIC	0	0
Pleuro.? grandis	1	0	0	0	0	0
Recto. abbreviatus	58	17	0	0	0	0
***Styracograptus* sp.**	0	0	0	0	0	0
S. mississippiensis	15	6	7	1	2	31
S. tatianae	6	13	0	0	0	0
Yino. disjunctus	0	0	0	0	0	0

NIC = species not captured in the abundances counts, but which were recovered during scans of additional uncounted slabs in a given level.

Sample (Meters)	0.10	0.17	1.30	5.30/5.50	8.80	12.67
TOTAL Ided	712	248	1556	993	966	123
Total (exc. sic)	884	357	2031	1247	1531	173
PERCENT Ided	81%	69%	77%	80%	63%	71%
Total sample counted?	Y	Y	Y	Y	Y	Y
Anticostia lata	4.07%	54.03%	8.10%	29.81%	24.12%	0.81%
Anticostia uniformis						
Anticostia mcgregorae						
Appendi. leptothecalis						
Appendi. supernus	58.85%	17.34%	15.87%	1.81%	18.32%	1.63%
A. pogrebovi						
Climaco. hastatus	0.70%	9.68%	0.51%	3.42%	0.41%	0.81%
Dicello. minor					0.62%	4.07%
D.* cf. *mirabilis						
Dicello.* aff. *mirabilis						
Dicello. ornatus	2.81%	2.42%	0.64%	20.14%	8.18%	9.76%
Dicello. tenuiculus						
Dicello. turgidus					0.21%	4.07%
D.* aff. *turgidus				0.10%		
Dicerato. mirus						
Diplo. rarithecatus						12.20%
Neo. charis						
M. extraordinarius						
Meta. ojsuensis						
Paraortho. affinis						
Paraorthp. kimi			70.18%	1.91%	29.19%	10.57%
Paraortho. pacificus						
Parareteo. turgidus						
Parareteo. sinensis	0.98%		0.39%			
Phormo. connectus	0.84%	1.21%	1.54%	3.83%	1.76%	2.44%
Pleuro. lui	1.83%	1.61%	0.71%	0.10%	0.10%	2.44%
Pleuro.? grandis						
Recto. abbreviatus	5.20%	13.71%	1.16%	38.87%	15.32%	41.46%
***Styracograptus* sp.**						
S. mississippiensis	13.06%		0.19%		0.72%	8.94%
S. tatianae	11.66%		0.19%			0.81%
Yino. disjunctus			0.51%		1.04%	

NIC = species not captured in the abundances counts, but which were recovered during scans of additional uncounted slabs in a given level.

Sample (Meters)	14.15	15.65	16.03	17.20	18.06	18.94
TOTAL Ided	1861	1629	1632	1368	3072	2025
Total (exc. sic)	3809	2054	2471	2142	4786	3310
PERCENT Ided	49%	79%	66%	64%	64%	61%
Total sample counted?	N	N	N	N	N	N
Anticostia lata	20.96%	3.99%	42.89%	19.74%	4.13%	6.91%
Anticostia uniformis		0.25%	0.06%	NIC	NIC	
Anticostia mcgregorae		0.06%		NIC		
Appendi. leptothecalis		0.43%	NIC	1.83%	1.40%	0.84%
Appendi. supernus	8.97%	14.06%	5.02%	18.49%	26.66%	25.23%
A. pogrebovi						1.19%
Climaco. hastatus	2.96%		1.59%	0.58%	0.62%	0.05%
Dicello. minor			0.12%	NIC		0.10%
Dicello.* cf. *mirabilis			0.74%	NIC		0.05%
D.* aff. *mirabilis		1.04%	0.43%	0.51%	0.16%	
Dicello. ornatus						
Dicello. tenuiculus	42.40%	0.68%	0.31%		0.07%	0.30%
Dicello. turgidus						
D.* aff. *turgidus						
Dicerato. mirus	NIC	0.06%	0.06%	NIC	0.03%	0.15%
Diplo. rarithecatus		6.14%	3.19%			
Neo. charis						
M. extraordinarius						
Meta. ojsuensis						
Paraortho. affinis						
Paraorthp. kimi						
Paraortho. pacificus	24.13%	65.87%	38.48%	0.07%	64.75%	56.79%
Parareteo. turgidus	0.05%					
Parareteo. sinensis						
Phormo. connectus	0.05%	0.25%	0.61%	0.58%	0.07%	0.10%
Pleuro. lui	NIC	1.78%	0.61%	0.15%		
Pleuro.? grandis	NIC		0.06%			
Recto. abbreviatus	0.38%	0.06%	5.82%	52.56%	0.75%	7.26%
***Styracograptus* sp.**					NIC	
S. mississippiensis	0.11%	4.73%	0.06%	3.44%	1.37%	0.44%
S. tatianae		0.61%		1.83%		0.59%
Yino. disjunctus	NIC			0.22%		

NIC = species not captured in the abundances counts, but which were recovered during scans of additional uncounted slabs in a given level.

Sample (Meters)	19.00	19.05	19.10	19.15	19.20	19.25
TOTAL Ided	884	364	306	720	865	329
Total (exc. sic)	1761	645	701	1336	1225	464
PERCENT Ided	50%	56%	44%	54%	71%	71%
Total sample counted?	N	N	N	N	N	N
Anticostia lata	3.39%					
Anticostia uniformis	3.39%	80.77%				
Anticostia mcgregorae						
Appendi. leptothecalis	1.92%	8.52%	6.54%	NIC		
Appendi. supernus	29.86%					
A. pogrebovi	4.64%					
Climaco. hastatus	0.34%					
Dicello. minor						
Dicello.* cf. *mirabilis	0.57%					
D.* aff. *mirabilis						
Dicello. ornatus						
Dicello. tenuiculus	0.57%					
Dicello. turgidus						
D.* aff. *turgidus						
Dicerato. mirus	1.02%		0.33%			
Diplo. rarithecatus						
Neo. charis			16.99%	5.56%	14.91%	0.61%
M. extraordinarius				54.31%	70.98%	22.49%
Meta. ojsuensis			70.92%	39.17%	13.64%	67.17%
Paraortho. affinis				0.56%	0.12%	
Paraorthp. kimi						
Paraortho. pacificus	43.44%		1.96%	0.14%	0.12%	0.30%
Parareteo. turgidus						
Parareteo. sinensis						
Phormo. connectus	1.81%	0.82%	0.98%	0.14%		
Pleuro. lui				NIC		
Pleuro.? grandis	0.11%					
Recto. abbreviatus	6.56%	4.67%				
***Styracograptus* sp.**						
S. mississippiensis	1.70%	1.65%	2.29%	0.14%	0.23%	9.42%
S. tatianae	0.68%	3.57%				
Yino. disjunctus						

NIC = species not captured in the abundances counts, but which were recovered during scans of additional uncounted slabs in a given level.

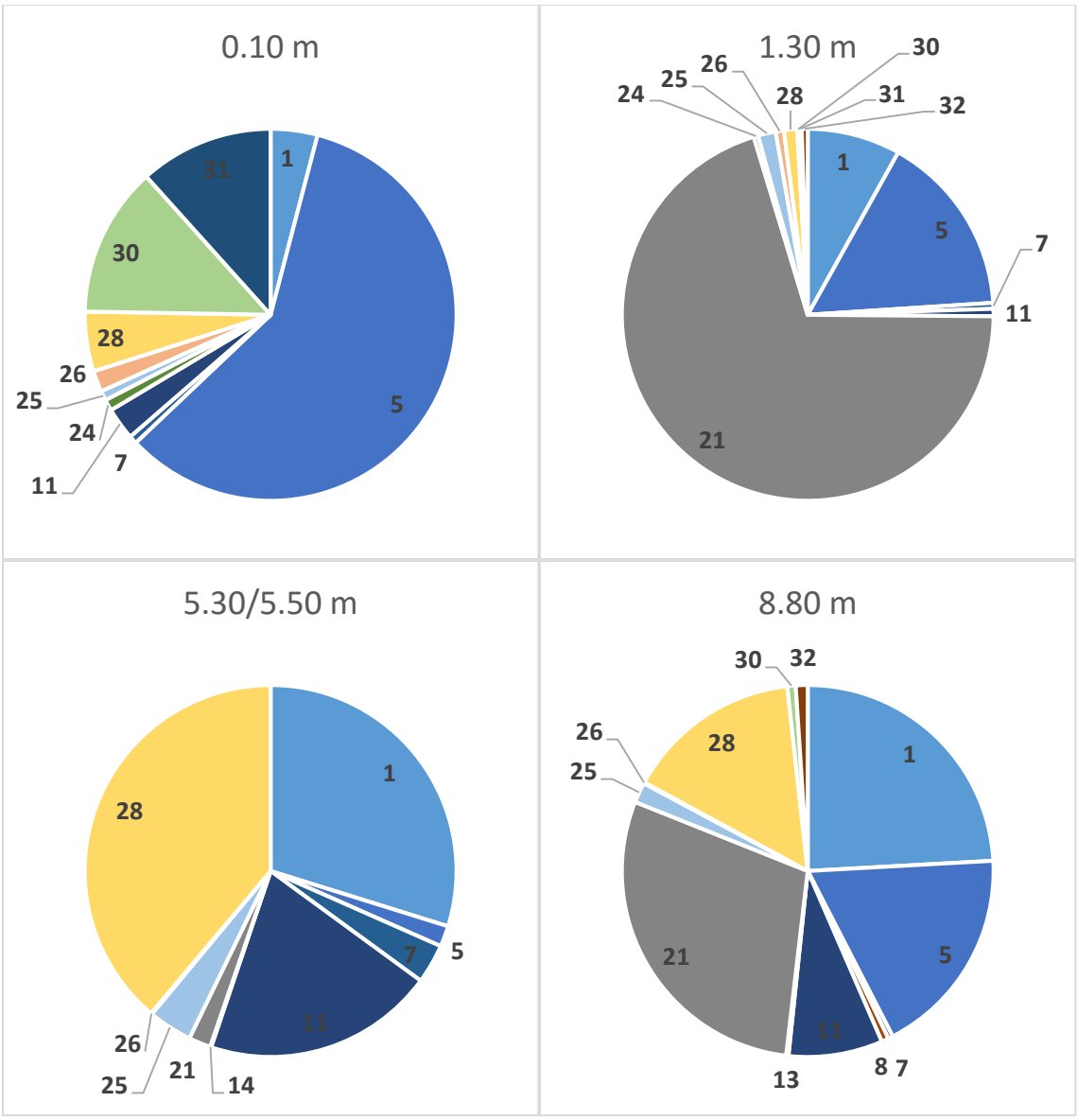

1	*Anticostia lata*	*17*	*Neodiplograptus charis*
2	*Anticostia uniformis*	*18*	*Metabolograptus extraordinarius*
3	*Anticostia mcgregorae*	*19*	*Metabolograptus ojsuensis*
4	*Appendispinograptus leptothecalis*	*20*	*Paraorthograptus affinis*
5	*Appendispinograptus supernus*	*21*	*Paraorthograptus kimi*
6	*Appendispinograptus pogrebovi*	*22*	*Paraorthograptus pacificus*
7	*Climacograptus hastatus*	*23*	*Parareteograptus turgidus*
8	*Dicellograptus minor*	*24*	*Parareteograptus sinensis*
9	*Dicellograptus* cf. *mirabilis*	*25*	*Phormograptus connectus*
10	*Dicellograptus* aff. *mirabilis*	*26*	*Pleurograptus lui*
11	*Dicellograptus ornatus*	*27*	*Pleurograptus? grandis*
12	*Dicelograptus tenuiculus*	*28*	*Rectograptus abbreviatus*
13	*Dicellograptus turgidus*	*29*	*Styracograptus* sp.
14	*Dicellograptus* aff. *turgidus*	*30*	*Styracograptus mississippiensis*
15	*Diceratograptus mirus*	*31*	*Styracograptus tatianae*
16	*Diplograptus rarithecatus*	*32*	*Yinograptus disjunctus*

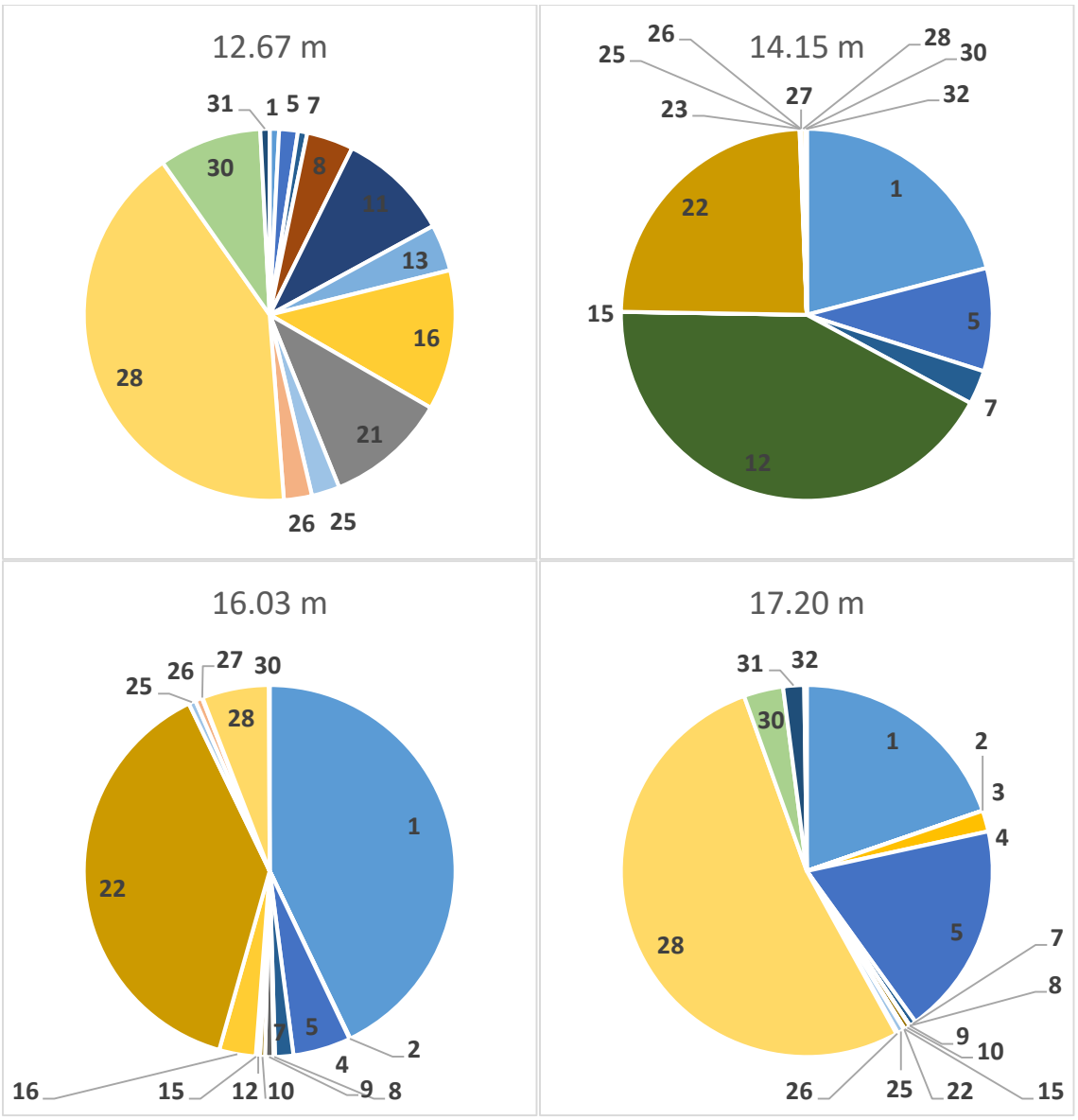

1	*Anticostia lata*	*17*	*Neodiplograptus charis*
2	*Anticostia uniformis*	*18*	*Metabolograptus extraordinarius*
3	*Anticostia mcgregorae*	*19*	*Metabolograptus ojsuensis*
4	*Appendispinograptus leptothecalis*	*20*	*Paraorthograptus affinis*
5	*Appendispinograptus supernus*	*21*	*Paraorthograptus kimi*
6	*Appendispinograptus pogrebovi*	*22*	*Paraorthograptus pacificus*
7	*Climacograptus hastatus*	*23*	*Parareteograptus turgidus*
8	*Dicellograptus minor*	*24*	*Parareteograptus sinensis*
9	*Dicellograptus* cf. *mirabilis*	*25*	*Phormograptus connectus*
10	*Dicellograptus* aff. *mirabilis*	*26*	*Pleurograptus lui*
11	*Dicellograptus ornatus*	*27*	*Pleurograptus? grandis*
12	*Dicelograptus tenuiculus*	*28*	*Rectograptus abbreviatus*
13	*Dicellograptus turgidus*	*29*	*Styracograptus* sp.
14	*Dicellograptus* aff. *turgidus*	*30*	*Styracograptus mississippiensis*
15	*Diceratograptus mirus*	*31*	*Styracograptus tatianae*
16	*Diplograptus rarithecatus*	*32*	*Yinograptus disjunctus*

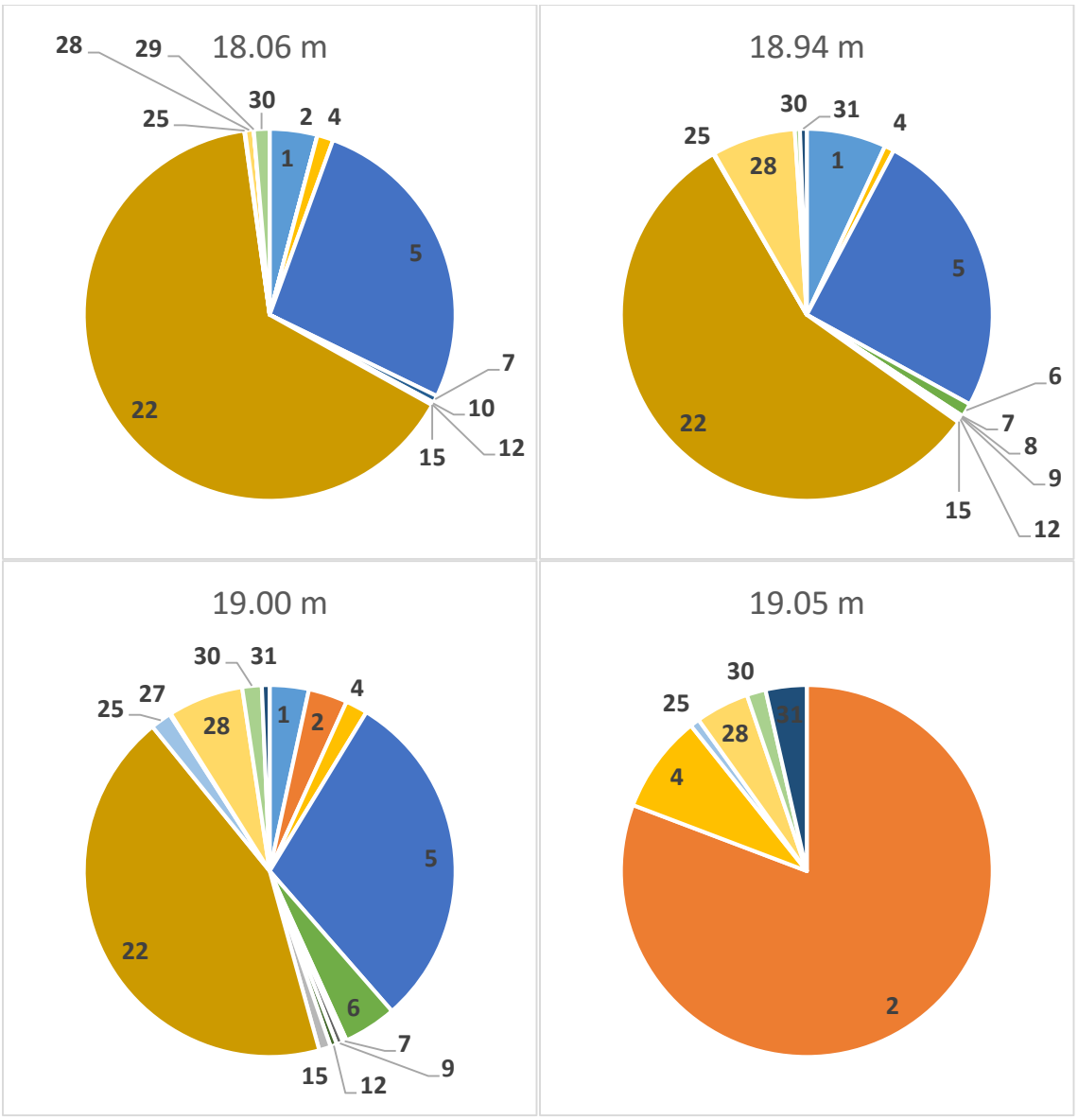

1 *Anticostia lata*
2 *Anticostia uniformis*
3 *Anticostia mcgregorae*
4 *Appendispinograptus leptothecalis*
5 *Appendispinograptus supernus*
6 *Appendispinograptus pogrebovi*
7 *Climacograptus hastatus*
8 *Dicellograptus minor*
9 *Dicellograptus* cf. *mirabilis*
10 *Dicellograptus* aff. *mirabilis*
11 *Dicellograptus ornatus*
12 *Dicelograptus tenuiculus*
13 *Dicellograptus turgidus*
14 *Dicellograptus* aff. *turgidus*
15 *Diceratograptus mirus*
16 *Diplograptus rarithecatus*
17 *Neodiplograptus charis*
18 *Metabolograptus extraordinarius*
19 *Metabolograptus ojsuensis*
20 *Paraorthograptus affinis*
21 *Paraorthograptus kimi*
22 *Paraorthograptus pacificus*
23 *Parareteograptus turgidus*
24 *Parareteograptus sinensis*
25 *Phormograptus connectus*
26 *Pleurograptus lui*
27 *Pleurograptus? grandis*
28 *Rectograptus abbreviatus*
29 *Styracograptus* sp.
30 *Styracograptus mississippiensis*
31 *Styracograptus tatianae*
32 *Yinograptus disjunctus*

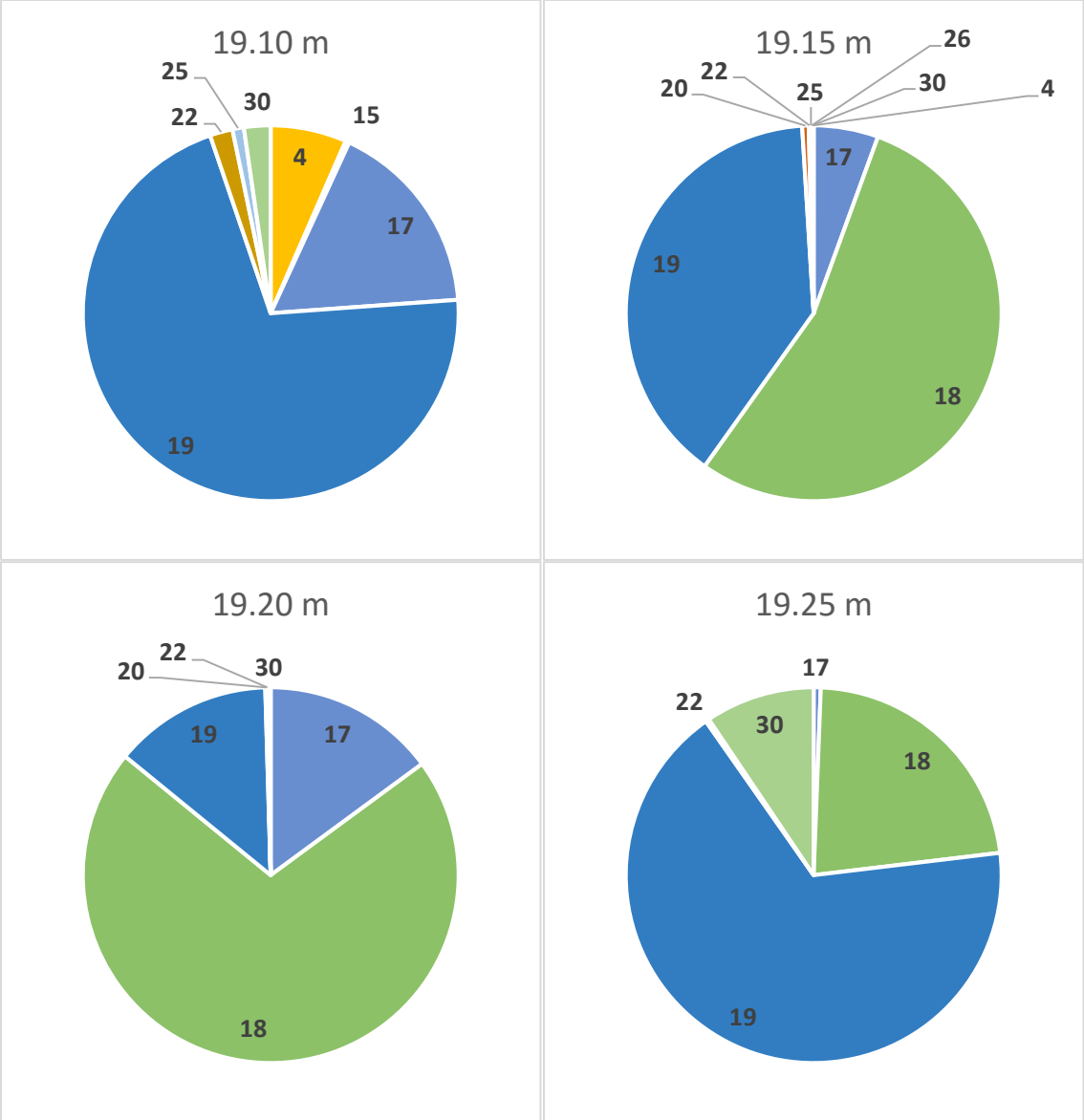

1	*Anticostia lata*	*17*	*Neodiplograptus charis*
2	*Anticostia uniformis*	*18*	*Metabolograptus extraordinarius*
3	*Anticostia mcgregorae*	*19*	*Metabolograptus ojsuensis*
4	*Appendispinograptus leptothecalis*	*20*	*Paraorthograptus affinis*
5	*Appendispinograptus supernus*	*21*	*Paraorthograptus kimi*
6	*Appendispinograptus pogrebovi*	*22*	*Paraorthograptus pacificus*
7	*Climacograptus hastatus*	*23*	*Parareteograptus turgidus*
8	*Dicellograptus minor*	*24*	*Parareteograptus sinensis*
9	*Dicellograptus* cf. *mirabilis*	*25*	*Phormograptus connectus*
10	*Dicellograptus* aff. *Mirabilis*	*26*	*Pleurograptus lui*
11	*Dicellograptus ornatus*	*27*	*Pleurograptus? grandis*
12	*Dicelograptus tenuiculus*	*28*	*Rectograptus abbreviatus*
13	*Dicellograptus turgidus*	*29*	*Styracograptus* sp.
14	*Dicellograptus* aff. *turgidus*	*30*	*Styracograptus mississippiensis*
15	*Diceratograptus mirus*	*31*	*Styracograptus tatianae*
16	*Diplograptus rarithecatus*	*32*	*Yinograptus disjunctus*

Appendix C. Binning Methodology

See Chapter 3.2 for a discussion of the rationale for species assignment during the counting process.

Sample 0.1-0.2 m (*D. ornatus* Zone):

1. All 'UnIDed archios ' assigned to *Phormograptus connectus*
2. All *Dicellograptus* fragments assigned to *D. ornatus*
3. All unidentified *Rectograptus* assigned to *R. abbreviatus*
4. All *Appendispinograptus* assigned to *A. supernus*
4. All *A. lata* categories lumped together
5. '*S. mississippiensis*/*C. hastatus*' split between the two species based on current abundance
6. '*S. mississippiensis*/*S. tatianae'* split between the two species based on current abundance
7. '<1.5 mm climacos' divided between *A. supernus* and *S. tatianae* at present abundances
8. 'UnIDed climaco' divided between *C. hastatus, S. mississippiensis*, *A. lata, A. supernus*, and *S. tatianae* based on relative abundance to this point

Sample 0.17- m (*D. ornatus* Zone):

File corrupted. Methodology lost.

Sample 1.3-1.42 m (*P. pacificus* Zone):

1. All 'archiretiolitids' reexamined and assigned to species if possible
2. All 'UnIDed archios ' assigned to *Phormograptus connectus* or *Yinograptus disjunctus* based on relative abundance
3. All unidentified *Appendispinogratus* assigned to *A. supernus*
4. All unidentified *Paraorthograptus* assigned to *P. kimi*
5. All unidentified *Rectograptus* assigned to *R. abbreviatus*
6. All *Dicellograptus* fragments assigned to *D. ornatus*

7. ‘Wide amplexo’ assigned to *A. lata*

8. ‘Glypto prox. end’ assigned to *A. lata*

9. ‘Climaco >1.5 mm’ divided between *C. hastatus, S. mississippiensis*, and *A. lata* based on relative abundance to this point

10. ‘UnIDed climaco’ divided between *C. hastatus, S. mississippiensis*, *A. lata, A. supernus*, and *S. tatianae* based on relative abundance to this point.

Sample 5.3-5.4 m (*P. pacificus* Zone):

1. All *Appendispinograptus* assigned to *A. supernus*

2. All unidentified *Paraorthograptus* assigned to *P. kimi*

3. All unidentified *Rectograptus* assigned to *R. abbreviatus*

5. Proximal and distal *A. lata* combined

6. All ‘>1.5 climacos’ divided between *C. hastatus* and *A. lata* based on relative abundance at this point

7. All ‘<1.5 mm climacos’ assigned to *A. supernus*

8. All remaining unidentified ‘climaco’ fragments split between *C. hastatus, A. supernus,* and *A. lata* based on relative abundance to this point.

Sample 5.5-5.6 m (*P. pacificus* Zone):

1. All dicello fragments and juvenile specimens assigned to *D. ornatus*

2. All ‘<1.5 mm climacos’ assigned to *A. supernus*

3. All ‘>1.5 climacos’ assigned to *A. lata*

4. All remaining unidentified ‘climaco’ fragments split between *C. hastatus* and *A. lata* based on relative abundance to this point.

5. All unidentified *Paraorthograptus* assigned to *P. kimi*

6. All unidentified *Rectograptus* assigned to *R. abbreviatus*

7. All 'UnIDed archios ' assigned to *Phormograptus connectus*

Sample 8.8 m (*P. pacificus* Zone):

1. All dicello fragments and juvenile specimens assigned to *D. ornatus* (since other species questionable, and mostly identifiable from juvenile/distal fragments)
2. All *Paraorthograptus* in *P. kimi*
3. All *Rectograptus* in *R. abbreviatus*
4. All *Appendispinograptus* in *A. supernus*
5. '*S. mississippiensis*/*C. hastatus*' split between the two species based on current abundance
6. All '<1.5 mm climacos' assigned to *A. supernus*
7. Proximal and distal *A. lata* specimens combined
8. '>1.5 mm climacos' split between *S. mississippiensis*, *C. hastatus,* and *A. lata* based on current abundance
9. All remaining unidentified 'climaco' fragments split between *C. hastatus, S. mississippiensis, A. supernus,* and *A. lata* based on relative abundance to this point.
10. All 'UnIDed archios ' assigned to *Phormograptus connectus* or *Yinograptus disjunctus* based on relative abundance

Sample 12.67 m (*P. pacificus* Zone):

1. All *Paraorthograptus* in *P. kimi*
2. All *Rectograptus* in *R. abbreviatus*
3. All 'UnIDed archios ' assigned to *Phormograptus connectus*
4. Possible *D. tenuiculus* assigned to *D. ornatus*
5. All *Dicellograptus* fragments >0.8 m wide assigned to *D. ornatus*
6. All *Dicellograptus* fragments <0.8 m wide divided between *D. ornatus, D. turgidus,* and *D. minor*
7. Proximal *Dicellograptus* specimens assigned to *D. ornatus*
8. Single 'climaco >1.5 mm' and both unidentified 'climaco' fragments assigned to *S. mississippiensis*
9. Questionable *D. tumidus* specimen assigned to *D. turgidus*

Sample 14.15-14.25 m (*mirus* Subzone)

1. All *Paraorthograptus* in *P. pacificus*

2. All *Rectograptus* in *R. abbreviatus*

3. All *Appendispinograptus* in *A. supernus*

4. '>1.5 mm climacos' split between *S. mississippiensis*, *C. hastatus,* and *A. lata* based on current abundance

5. All '<1.5 mm climacos' assigned to *A. supernus*

6. Proximal and distal *A. lata* specimens combined

Sample 15.65-15.77 m (*mirus* Subzone)

1. All *Paraorthograptus* in *P. pacificus*

2. All *Diplograptus* in *D. rarithecatus*

3. All *Rectograptus* in *Rectograptus abbreviatus*

4. Unidentified *Appendispinograptus* split between *A. supernus* and *A. leptothecalis* based on current abundance

5. '*S. mississippiensis*/*S. tatianae*' split between the two species based on current abundances

6. *Diplograptus/Rectograptus* split between the two species based on current abundances

7. '<1.5 mm climacos' split between *A. supernus* and *A. leptothecalis* based on current abundances

8. '>1.5 mm climacos' split between *S. mississippiensis* and *A. lata* based on current abundances

9. Proximal and distal *A. lata* specimens combined

10. All remaining unidentified 'climaco' fragments split between *S. mississippiensis, S. tatianae, A. supernus, A. leptothecalis,* and *A. lata*
based on current abundances

11. Proximal and distal *Dicellograptus* fragments divided between *D.* aff. *mirabilis* and *D. tenuiculus* at present abudances

12. All 'UnIDed archios ' assigned to *Phormograptus connectus*

Sample 16.03-16.18 m (*mirus* Subzone)

1. All *Paraorthograptus* in *P. pacificus*

2. All *Diplograptus* in *D. rarithecatus*

3. All *Rectograptus* in *Rectograptus abbreviatus*

4. *Diplograptus/Rectograptus* split between the two species based on current abundances

5. '<1.5 mm climacos' assigned to *A. supernus*

8. '>1.5 mm climacos' split between *S. mississippiensis, C. hastatus,* and *A. lata* based on current abundances

9. All remaining unidentified 'climaco' fragments split between *S. mississippiensis, S. tatianae, A. supernus, C. hastatus,* and *A. lata*
based on current abundances

10. Proximal and distal *A. lata* specimens combined

11. Proximal and distal *Dicellograptus* fragments divided between *D.* aff. *mirabilis, D.* cf. *mirabilis* and *D. tenuiculus* at current abundances

12. All 'UnIDed archios ' assigned to *Phormograptus connectus*

Sample 17.20-17.30 m (*mirus* Subzone)

1. Unidentified *Appendispinograptus* split between *A. supernus* and *A. leptothecalis* based on current abundance

2. All *Rectograptus* in *Rectograptus abbreviatus*

3. All *Diplograptus/Rectograptus* assigned to *Rectograptus abbreviatus*

4. All *Dicellograptus* fragments assigned to *D.* aff. *mirabilis*

5. '*S. mississippiensis*/*C. hastatus*' split between the two species based on current abundances

6. '*S. mississippiensis*/*S. tatianae*' split between the two species based on current abundances

7. ‘<1.5 mm climacos’ split between *S. tatianae, A. supernus* and *A. leptothecalis* based on current abundances

8. ‘>1.5 mm climacos’ split between *S. mississippiensis, C. hastatus,* and *A. lata* based on current abundances

9. Proximal and distal *A. lata* specimens combined

10. All remaining unidentified ‘climaco’ fragments split between *S. mississippiensis, C. hastatus, S. tatianae, A. supernus, A. leptothecalis,* and *A. lata* based on relative abundance to this point

11. All 'UnIDed archios ' assigned to *Phormograptus connectus*

Sample 18.05-18.16 m: 2007 sample (*mirus* Subzone)

1. All *Paraorthograptus* assigned to *P. pacificus*

2. All ‘*S. mississippiensis*/*S. tatianae*’ assigned to *S. mississippiensis*

3. ‘*S. mississippiensis*/*C. hastatus*’ split between the two species based on current abundance

4. All *Diplograptus/Rectograptus* assigned to *Rectograptus abbreviatus*

5. Unidentified *Appendispinograptus* split between *A. supernus* and *A. leptothecalis* based on current abundance

6. ‘<1.5 mm climacos’ divided between *A. supernus* and *A. leptothecalis* based on current abundance

7. ‘>1.5 mm climacos’ split between *S. mississippiensis, C. hastatus,* and *A. lata* based on current abundances

8. Proximal and distal *A. lata* specimens combined

9. All remaining unidentified ‘climaco’ fragments split between *S. mississippiensis, C. hastatus, A. supernus, A. leptothecalis,* and *A. lata* based on relative abundance to this point

1. All 'UnIDed archios ' assigned to *Phormograptus connectus*

Note: "*C. trifidis"* and "Fat *tubuliferus*", placeholder catagories that are present in the raw count data werenot to be real species catagories; material assigned to *C. hasatus* and *S. mississippiensis*, respectively.

Sample 18.83-18.95 m (*mirus* Subzone)

Sample scanned, but not counted.

Sample 18.94-19.0 m (*mirus* Subzone)

1. All *Paraorthograptus* assigned to *P. pacificus*

*2. "*Too high 2trd *supernus*" assigned to *A.pogrebovi*

3. Unidentified *Appendispinograptus* split between *A. supernus, A.* pogrebovi*,* and *A. leptothecalis* based on current abundance

3. All '*Diplograptus/Rectograptus'* and unidentified *Rectograptus* assigned to *Rectograptus abbreviatus*

4. '*S. mississippiensis*/*S. tatianae*' divided between two species based on current abundances

5. '>1.5 mm climacos' split between *S. mississippiensis, C. hastatus,* and *A. lata* based on current abundances

6. '<1.5 mm climacos' divided between *A. supernus, A.* pogrebovi*, A. leptothecalis,* and *S. tatianae* based on current abundance

7. Proximal and distal *A. lata* specimens combined

8. All remaining unidentified 'climaco' fragments split between *C. hastatus, S. mississippiensis, S. tatianae*, *A. supernus, A. leptothecalis, A. pogrebovi* and *A. lata* based on relative abundance to this point

9. Unidentified *Dicellograptus* divided among all *Dicellograptus* species present based on current abundance (=all assigned to *D. tenuiculus*).

10. 'UnIDed archio' assigned to *Phormograptus connectus*

Sample 19.0-19.05 m (*mirus* Subzone)

1. All *Paraorthograptus* assigned to *P. pacificus*

2. Unidentified *Appendispinograptus* split between *A. supernus, A. pogrebovi,* and *A. leptothecalis* based on current abundance

3. '*S. mississippiensis*/*S. tatianae*' divided between two species based on current abundances

4. Proximal and distal *A. lata* specimens combined (no '>1.5 mm' category in sample)

5. '<1.5 mm climaco' split between *S. tatianae*, *A. supernus, A. pogrebovi,* and *A. leptothecalis* at present abundances

6. Unidentified climaco fragments split between *S. mississippiensis, A. lata, C. hastatus, S. tatianae*, *A. supernus, A. pogrebovi,* and *A. leptothecalis* at present abundances

7. *A. lata*/*A. uniformis'* split between species at abundances after Step 4

8. *Rectograptus*/*Anticostia* split between species in these genera at their original abundances

9. 'UnIDed archio' assigned to *Phormograptus connectus*

10. Two wide and one thin *Dicellograptus* fragments assigned to *D.* aff. *mirabilis* and *D. tenuiculus*, respectively; remaining unidentified *Dicellograptus* split at current abundances

Sample 19.05-19.10 m (*mirus* Subzone)

1. 'UnIDed archio' assigned to *Phormograptus connectus*

2. All unidentified *Rectograptus* assigned to *R. abbreviatus*

3. All *Appendispinograptus* assigned to *A. leptothecalis*

4. Unidentified climaco fragments split between *S. mississippiensis, S. tatianae*, and *A. leptothecalis* at present abundances

Sample 19.10-19.15 m (*mirus* Subzone)

1. All *Appendispinograptus* assigned to *A. leptothecalis*

2. All unidentified *Paraorthograptus* assigned to *P. pacificus*

3. ‘Proximal end >1.2 mm’ and ‘Normalo frag >2.3 mm’ assigned to *Neodiplograptus charis* at present abundance

4. ‘Proximal end <1.2 mm’ and ‘Normalo frag <2.3 mm’ assigned to *Metabolograptus osjuensus* at present abundance ‘*osjuensus*/*charis’* divided between the two species at present abundances

5. 'UnIDed archio' assigned to *Phormograptus connectus*

6. ‘climaco >1.5 mm’ and ‘climaco <1.5 mm’ divided between *A. leptothecalis* and *S. mississippiensis* at present abundances

7. All unidentified ‘climacos’ divided between *Metabolograptus ojsuensus, Neodiplograptus charis, A. leptothecalis* and *S. mississippiensis* at present abundances

Sample 19.15-19.20 m (*extraordinarius* Zone)

1. All *‘temalaensis*/*ojsuensis*’ in *M. ojsuensis*’

2. ‘*ojsuensis/extraordinarius*’ and ‘*charis*/*extraordinarius*’ divided among each species based on present abundances

3. Unidentified ‘normalograptid’ material divided among *M. ojsuensis*, *M. extraordinarius,* and *Neo. charis* at present abundances

4. Two of three unidentified *Paraorthograptus* assigned to *P. affinis* and remaining specimen assigned to *P. pacificus* (which is present in scans)

5. 'UnIDed archio' assigned to *Phormograptus connectus*

Sample 19.20-19.25 m (*extraordinarius* Zone)

1. ‘*ojsuensis/extraordinarius*’ and ‘*charis*/*extraordinarius*’ divided among each species based on present abundances

2. Thin ‘climaco’ specimens assigned to *S. mississippiensis*

3. Two unidentified *Paraorthograptus* divided between *P. affinis* and *P. pacificus,* which both compellingly occur in the scans

Sample 19.25-19.30 m (*extraordinarius* Zone)

1. Fragments assigned to respective species
2. '*ojsuensis/extraordinarius*' divided among each species based on present abundances
3. All 'skinny' (thinner than *M. ojsuensis*) specimens assigned to *S. mississippiensis*
4. Single unidentified *Paraorthograptus* assigned to *P. pacificus* based on abundance throughout section—do not actually know what species this specimen is
5. 'Unidentified climacos' divided among all species except *P. pacificus* at present abundances

Appendix D. Rarefaction Curves

Rarefaction analysis was conducted using the paleontological statistics software package, PAST (PaleontologicalSTatistics- Hammer et al. 2007). Rarefaction is a statistical technique developed by Sanders (1968) that provides an estimate of the effect of sampling on apparent species richness. Rarefaction curves are created by resampling fractions of an existing sample to determine the impact of sample size on apparent species richness in a population. The results of the resampling runs are plotted as the curves shown below. The central red line represents the average of resampling attempts at a particular sample size, and upper and lower blue lines, represent 95% confidence intervals. The curve of the line is an indication of sampling completeness: the degree to which a curve plateaus indicates the likelihood that a larger sample size would change species abundance (plateaued samples are likely reasonable complete).

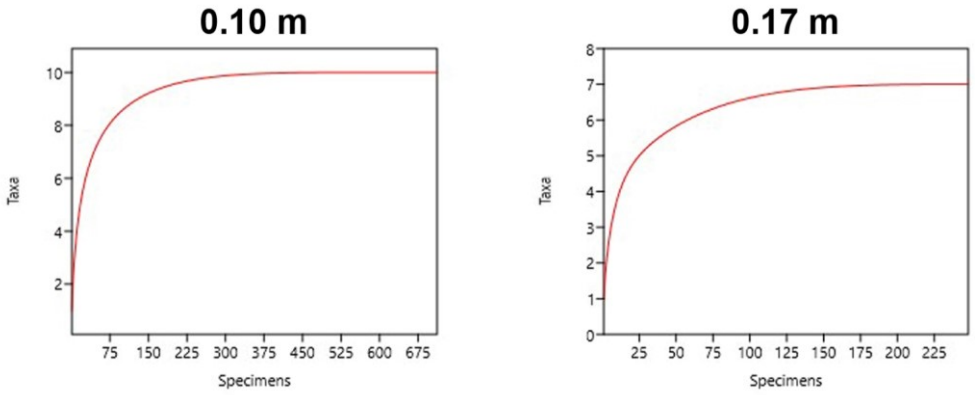

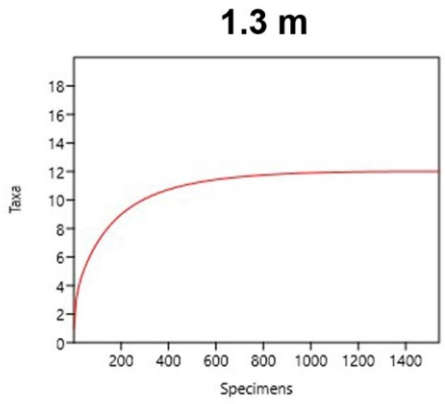
1.3 m
Taxa
Specimens
0 2 4 6 8 10 12 14 16 18
200 400 600 800 1000 1200 1400

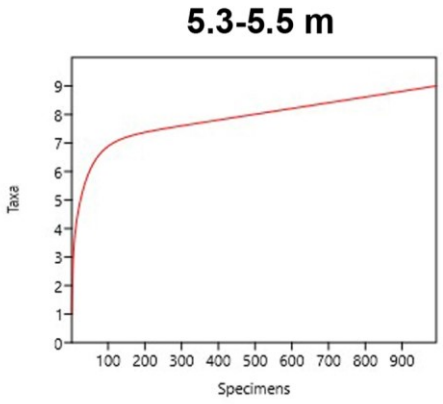
5.3-5.5 m
Taxa
Specimens
0 1 2 3 4 5 6 7 8 9
100 200 300 400 500 600 700 800 900

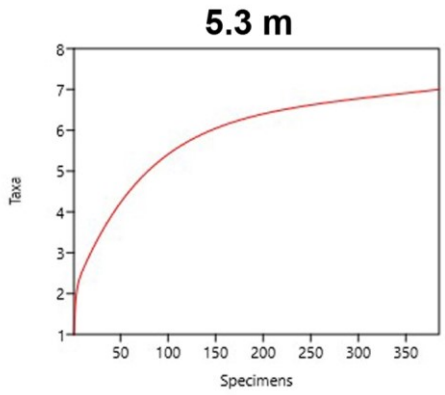
5.3 m
Taxa
Specimens
1 2 3 4 5 6 7 8
50 100 150 200 250 300 350

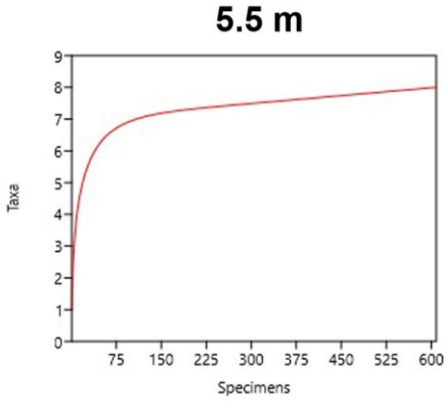
5.5 m
Taxa
Specimens
0 1 2 3 4 5 6 7 8 9
75 150 225 300 375 450 525 600

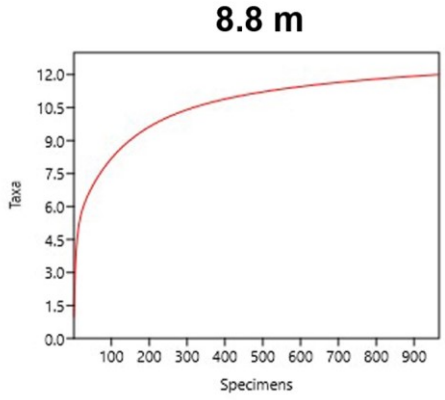
8.8 m
Taxa
Specimens
0.0 1.5 3.0 4.5 6.0 7.5 9.0 10.5 12.0
100 200 300 400 500 600 700 800 900

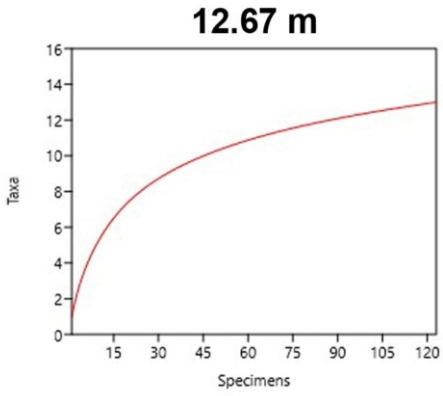
12.67 m
Taxa
Specimens
0 2 4 6 8 10 12 14 16
15 30 45 60 75 90 105 120

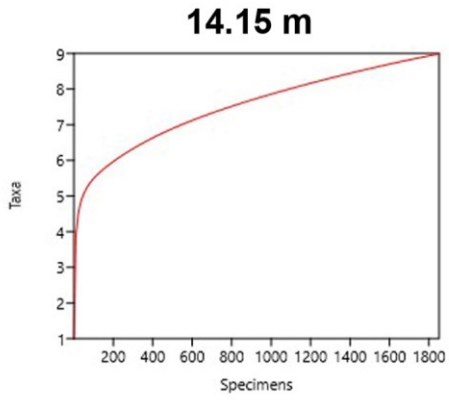
14.15 m
Taxa
Specimens
1 2 3 4 5 6 7 8 9
200 400 600 800 1000 1200 1400 1600 1800

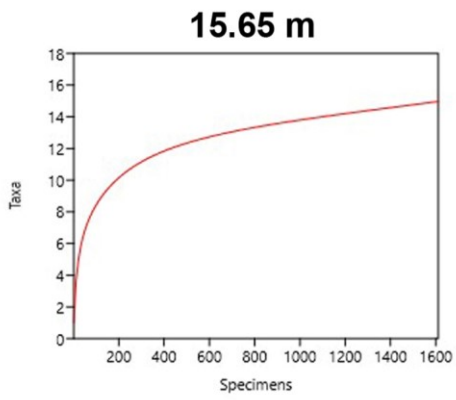
15.65 m
Taxa
Specimens
0 2 4 6 8 10 12 14 16 18
200 400 600 800 1000 1200 1400 1600

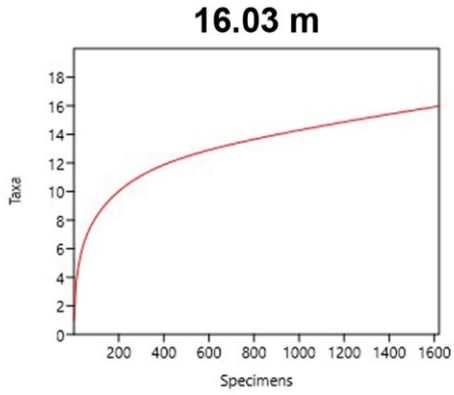
16.03 m
Taxa
Specimens
0 2 4 6 8 10 12 14 16 18
200 400 600 800 1000 1200 1400 1600

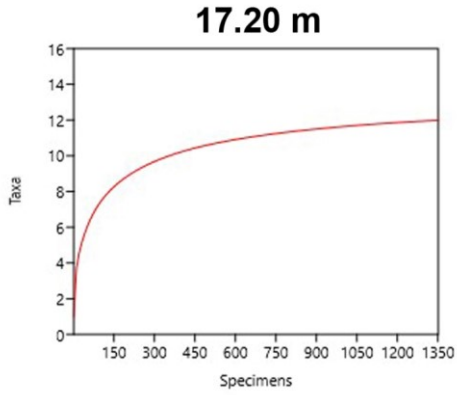
17.20 m
Taxa
Specimens
0 2 4 6 8 10 12 14 16
150 300 450 600 750 900 1050 1200 1350

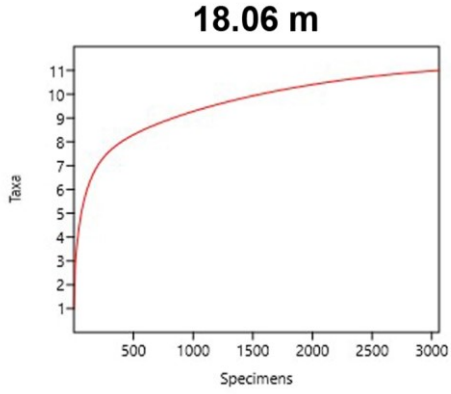
18.06 m
Taxa
Specimens
1 2 3 4 5 6 7 8 9 10 11
500 1000 1500 2000 2500 3000

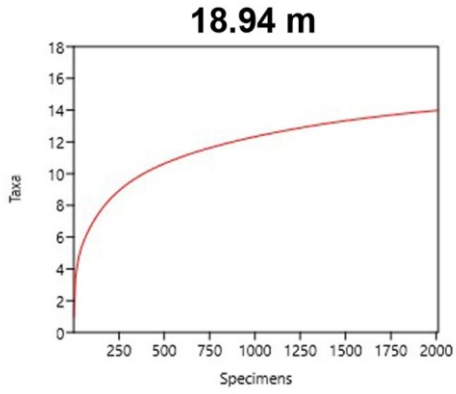
18.94 m
Taxa
Specimens
0 2 4 6 8 10 12 14 16 18
250 500 750 1000 1250 1500 1750 2000

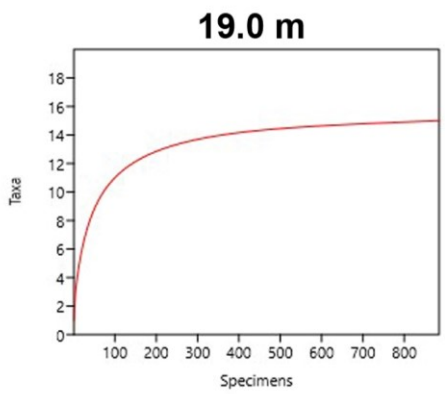
19.0 m
Taxa
0
2
4
6
8
10
12
14
16
18
100 200 300 400 500 600 700 800
Specimens

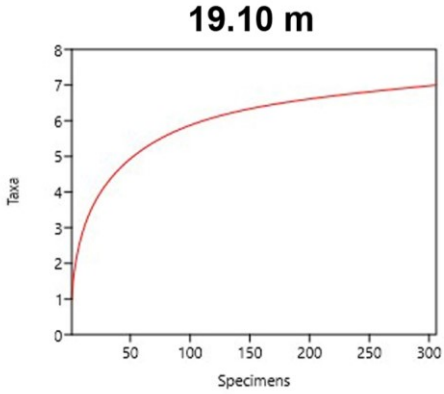
19.10 m
Taxa
0
1
2
3
4
5
6
7
8
50 100 150 200 250 300
Specimens

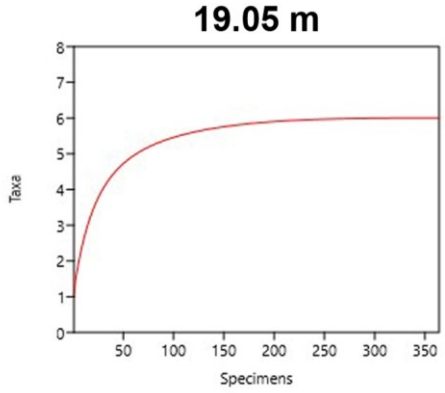
19.05 m
Taxa
0
1
2
3
4
5
6
7
8
50 100 150 200 250 300 350
Specimens

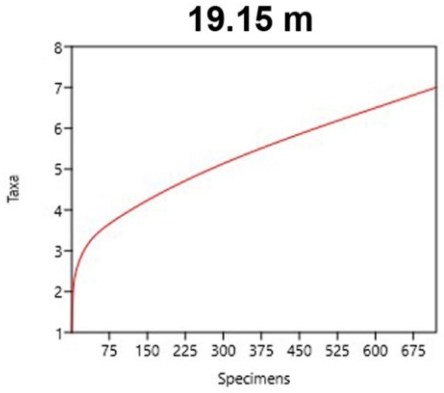
19.15 m
Taxa
1
2
3
4
5
6
7
8
75 150 225 300 375 450 525 600 675
Specimens

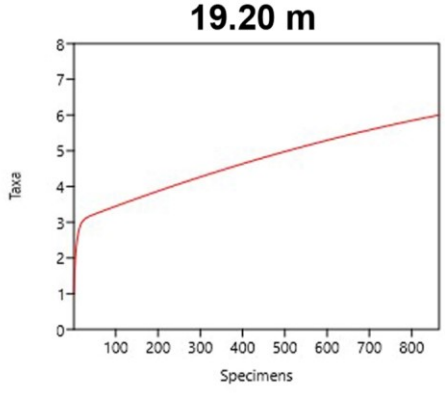
19.20 m
Taxa
0
1
2
3
4
5
6
7
8
100 200 300 400 500 600 700 800
Specimens

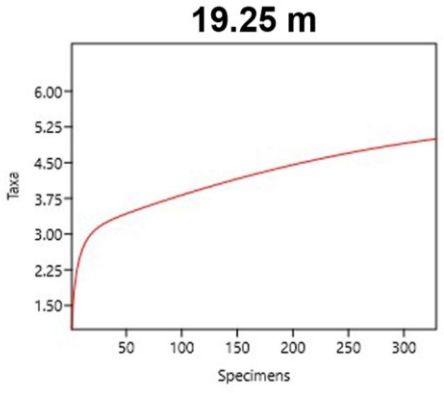
19.25 m
Taxa
1.50
2.25
3.00
3.75
4.50
5.25
6.00
50 100 150 200 250 300
Specimens

Appendix E. Accessory Fauna

Examples of accessory fauna. Photos taken and preliminary identifications made early in the project and not revisited. The material depicted and additional material remains to be studied in depth. Three dimensionally preserved specimen of *M. ojsuensis* included to illustrate a rare mode of preservation.

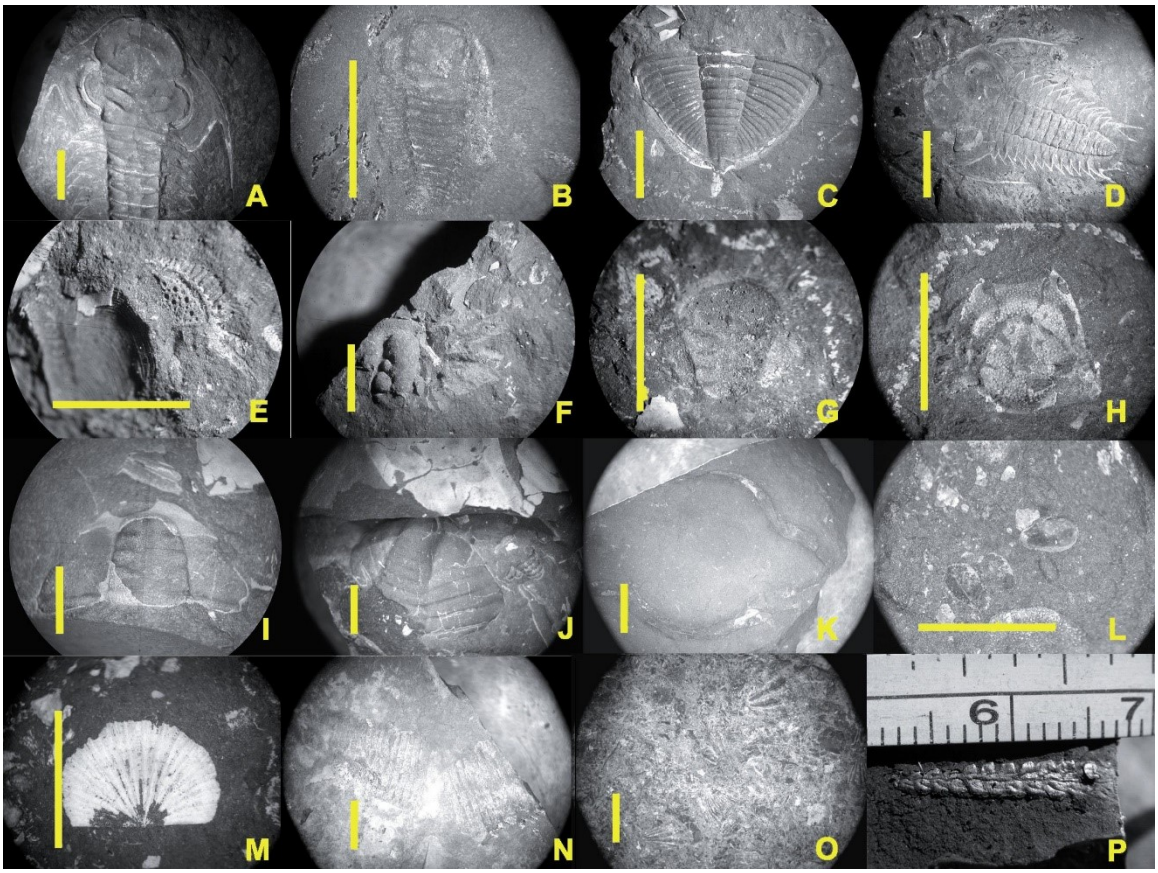

A, D, *Pugilator yukonensis*: (A) 8.27 m*, pacificus* Zone. (D) 12.67-12.77 m*, pacificus* Zone. B, *Triarthrus* sp. 14.15-14.25 m, *pacificus* Zone. C, G, *Mucronaspis* sp. 32.80-32.83 m, *persculptus* Zone. E, *Odontopleura* or *Anacaenaspis* sp. 32.80-32.83 m, *persculptus* Zone. F, *Flexicalymene* sp. 32.80-32.83 m, *persculptus* Zone. H, I J, K, L, unidentified homalonotid: (H) hypostome, (I) thoracic segments, (L) protaspids, all 19.20-19.30 m, *N. extraordinarius* Zone. M, unidentified brachiopod, 32.80-32.83 m, *persculptus* Zone. N, nautiloid, 8.13 m, *pacificus* Zone. O, brachiopod horizon, 31.0 m, *persculptus* Zone, P, *Metabolograptus ojsuensis*, internal mould, 19.20-19.30 m, *extraordinarius* Zone. Vertical bars: 5 mm. Horizontal bars: 10 mm. Ruler scale in cm. Scales approximate.

Appendix F. Comparative Diversity Diagrams

Diversity and extinction/origination curves for South China (A and B) and a diversity curve from Vinini Creek, Nevada (C) (Štorch et al., 2011). Full context and discussion of methodology of each figure is available in the relevant publication. Fig. A and B reproduced from Chen et al., 2005b). Fig. C reproduced from Štorch et al. (2011).

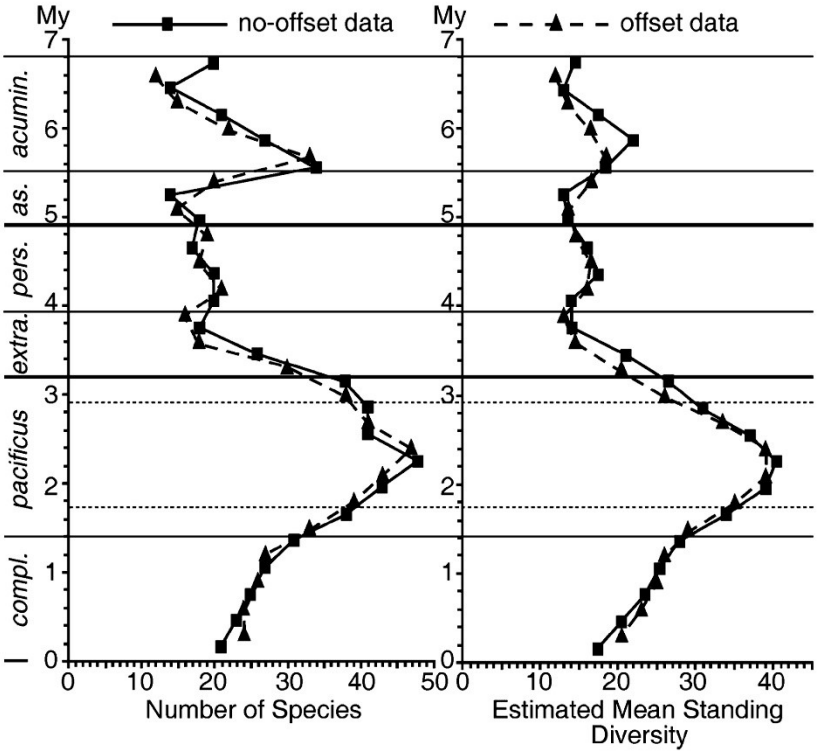

A.

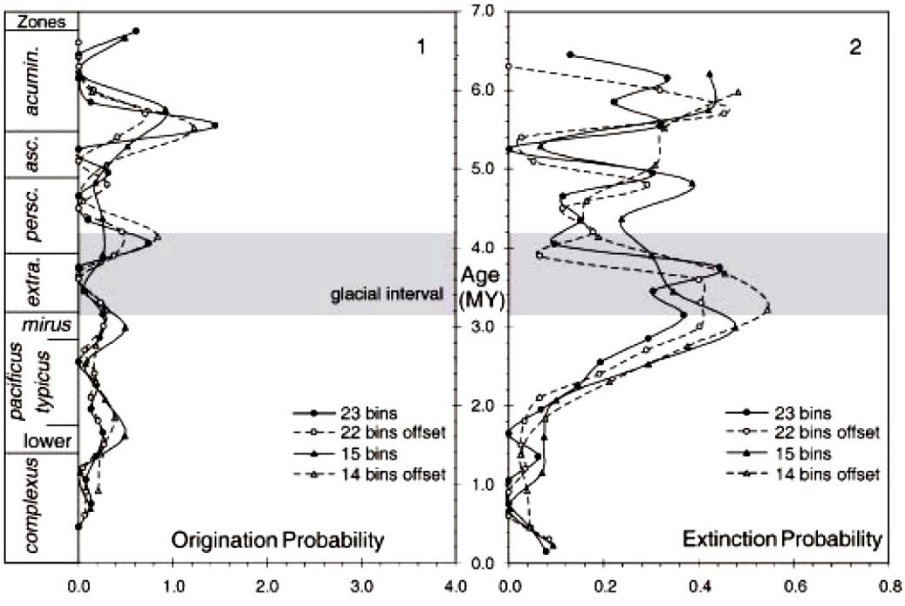

B.

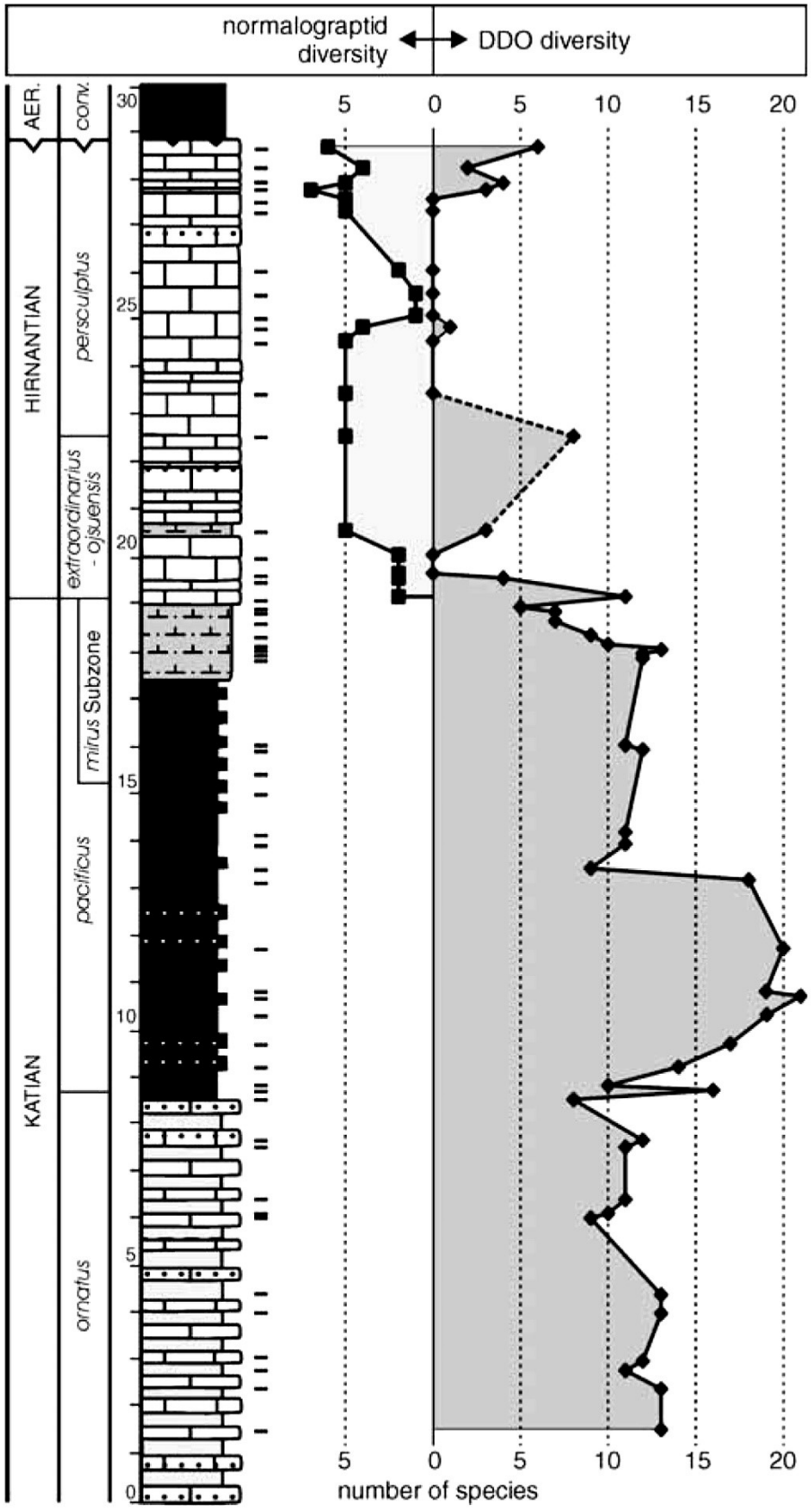
normalograptid diversity
DDO diversity
AER.
HIRNANTIAN
KATIAN
conv.
persculptus
extraordinarius - ojsuensis
mirus Subzone
pacificus
ornatus
30
25
20
15
10
5
0
5
0
5
10
15
20
number of species

C.

Appendix G. Copyright Release

Chapter 7 reproduces a paper that was published in typeset form in the *Proceedings of the Yorkshire Geological Society* (2011: v.58(4), 253–260). It is republished in original manuscript form following the Premissions laid out by the Geological Society of London regarding their copyright (reproduced below):

"Authors may re-use their own material without permission subject to the exceptions listed below. They may include the whole article in a PhD or other thesis provided that it will not be published, and that the original source is fully acknowledged in the standard form. If the thesis is to be included in the institution's electronic repository or other online host, authors must use their own finally accepted version, not the typeset PDF (unless it is Gold Open Access)."

The Geological Society of London, *Permissions,* accessed July 24, 2017. <https://www.geolsoc.org.uk/permissions>